

**Sustainable syntheses and modifications of  
water-stable metal-organic frameworks (MOFs)  
for gas sorption and adsorption-driven  
heat transformation applications**

Inaugural Dissertation

zur Erlangung des Doktorgrades  
Dr. rer. nat.  
der Mathematisch-Naturwissenschaftlichen Fakultät  
der Heinrich-Heine-Universität Düsseldorf

vorgelegt von

**Niels Tannert**  
aus Düsseldorf

Düsseldorf, Juni 2021

aus dem Institut für Anorganische und Strukturchemie I  
der Heinrich-Heine-Universität Düsseldorf

Gedruckt mit der Genehmigung der  
Mathematisch-Naturwissenschaftlichen Fakultät der  
Heinrich-Heine-Universität Düsseldorf

Berichtersteller:

1. Prof. Dr. Christoph Janiak

2. Prof. Dr. Christian Ganter

Tag der mündlichen Prüfung: 20.08.2021



## **Eidesstattliche Erklärung**

Ich versichere an Eides statt, dass die Dissertation von mir selbstständig und ohne unzulässige fremde Hilfe unter der Beachtung der „Grundsätze zur Sicherung guter wissenschaftlicher Praxis“ an der Heinrich-Heine-Universität Düsseldorf erstellt worden ist. Die aus fremden Quellen direkt oder indirekt übernommenen Gedanken sind als solche kenntlich gemacht. Die Arbeit wurde bisher weder im Inland noch im Ausland in gleicher oder ähnlicher Form einer anderen Prüfungsbehörde vorgelegt. Es wurden keine früheren erfolglosen Promotionsversuche unternommen.

Düsseldorf, den 22.06.2021

Ort, Datum

---

Unterschrift

Die vorliegende Dissertation wurde im Rahmen des vom Bundesministerium für Bildung und Forschung (BMBF) geförderten Verbundprojekts „Optimierung von neuartigen Materialien für zyklische Adsorptionsprozesse“ (kurz: OptiMat, 03SF0492A/C) angefertigt. Teilnehmende Projektpartner waren das Fraunhofer-Institut für Solare Energiesysteme (ISE) Freiburg, die DencoHappel GmbH Herne (später FläktGroup) und die Heinrich-Heine-Universität Düsseldorf (HHU). Ziel des Projekts OptiMat war die Entwicklung neuer, hydrothermal stabiler, mikroporöser Adsorbentien, vorwiegend Metallorganischer Gerüstnetzwerke (*engl.: metal-organic frameworks*, kurz: MOFs) für den Einsatz in thermisch angetriebenen Wärmepumpen und Klimaanlage. Neben der Synthese(-optimierung), Charakterisierung und Evaluation neuartiger Hochleistungsadsorbentien waren die Formgebung dieser Materialien sowie Modellsimulationen Grundlage für die erfolgreiche Entwicklung eines funktionsfähigen Demonstrationsmusters in Form einer mit MOF-Komposit beschichteten Wärmeüberträgerstruktur.



*Meinen Eltern*



## Publication List

### First Authorships

---

N. Tannert, S. Gökpınar, E. Hastürk, S. Nießing and C. Janiak, Microwave-assisted dry-gel conversion (MW-DGC) – a new sustainable route for the rapid synthesis of metal-organic frameworks with solvent re-use, *Dalton Trans.*, 2018, **47**, 9850-9860.

N. Tannert, S.-J. Ernst, C. Jansen, S. Nießing, S. K. Henninger, H.-J. Bart and C. Janiak, Evaluation of the highly stable metal-organic framework MIL-53(Al)-TDC (TDC = 2,5-thiophenedicarboxylate) as a new and promising adsorbent for heat transformation applications, *J. Mater. Chem. A*, 2018, **6**, 17706-17712. Part of the themed collection: 2018 J. Mater. Chem. A, HOT Papers.

<https://pubs.rsc.org/en/journals/articlecollectionlanding?sercode=ta&themeid=f7d0c2cb-4131-4611-8a14-f0c78308057d>

N. Tannert, C. Jansen, S. Nießing and C. Janiak, Robust synthesis routes and porosity of Al-based metal-organic frameworks Al-fumarate, CAU-10-H and MIL 160, *Dalton Trans.*, 2019, **48**, 2967-2976.

N. Tannert, Y. Sun, E. Hastürk, S. Nießing and C. Janiak, A Series of New Urea-MOFs Obtained via Post-synthetic Modification of NH<sub>2</sub>-MIL-101(Cr): SO<sub>2</sub>, CO<sub>2</sub> and H<sub>2</sub>O sorption, *Z. Anorg. Allg. Chem.*, 2021, **647** 1124-1130.

### Co-Authorships

---

C. Schlüsener, M. Xhinovci, N. Tannert, A. Schmitz and C. Janiak, Solid-Solution Mixed-Linker-Synthesis of Isorecticular Al-based MOFs for an Easy Hydrophilicity Tuning in Water-Sorption Heat Transformations, *Chem. Mater.*, 2019, **31**, 4051-4062.

T. Matemb Ma Ntep, H. Breitzke, L. Schmolke, C. Schlüsener, B. Moll, S. Millan, N. Tannert, I. El Aita, G. Buntkowsky and C. Janiak, Facile in-situ Halogen Functionalization via Triple-Bond Hydrohalogenation: Enhancing Sorption Capacities through Halogenation to Halofumarate-based Zr(IV)-Metal-Organic Frameworks, *Chem. Mater.*, 2019, **31**, 8629-8638.

S. Gökpınar, S.-J. Ernst, E. Hastürk, M. Möllers, I. El Aita, R. Wiedey, N. Tannert, S. Nießing, S. Abdpour, A. Schmitz, J. Quodbach, G. Földner, S. K. Henninger and C. Janiak, Air-Con Metal-Organic Frameworks in Binder Composites for Water Adsorption Heat Transformation Systems, *Ind. Eng. Chem. Res.*, 2019, **58**, 21493-21503.

Ü. Kökcam-Demir, N. Tannert, M. Bengsch, A. Spieß, C. Schlüsener, S. Nießing and C. Janiak, Improving porosity and water uptake of aluminum metal-organic frameworks (Al-MOFs) as graphite oxide (GO) composites, *Micropor. Mesopor. Mater.*, 2021, submitted.

## **Conferences**

---

09/2020      **7<sup>th</sup> Conference on Metal-Organic Frameworks and Open Framework Compounds (MOF2020<sup>WEB</sup>), Dresden**

### **Participation**

09/2018      **9<sup>th</sup> Seminar Adsorption, Duisburg/Essen**

### **Plenary lecture**

Water sorption behavior of Al-based metal-organic frameworks (MOFs) and their potential for heat transformation application.

04/2018      **Workshop “Dynamic Adsorption”, Leipzig**

### **Poster**

1. Evaluation of metal-organic framework Al-MIL-53-TDC as new adsorbent for heat transformation application.

N. Tannert, S.-J. Ernst, C. Jansen, S. K. Henninger and C. Janiak

2. Shaping of metal-organic frameworks for heat transformation application. – Poster-Award

S. Gökpınar, S.-J. Ernst, N. Tannert, E. Hastürk and C. Janiak

11/2017      **2<sup>nd</sup> EuroMOF Conference, Delft, Niederlande**

### **Poster**

Microwave-assisted dry-gel conversion (MW-DGC) as a novel and environmentally benign tool for the rapid synthesis of MOFs.

N. Tannert, S. Gökpınar, E. Hastürk, S. Nießing and C. Janiak

- 03/2017      **29<sup>th</sup> German Zeolite Conference, Frankfurt**
- Poster**
- Microwave-assisted dry-gel conversion (MW-DGC) as a rapid and green tool for high-yield MOF-synthesis? MIL-100(Fe) as an example.
- N. Tannert, E. Hastürk and C. Janiak
- 09/2016      **International Workshop on Hierarchically Structured Materials: For a Green Environment, Düsseldorf**
- Organization & Execution**
- 02/2016      **28<sup>th</sup> German Zeolite Conference, Gießen**
- Poster**
- A series of new urea-MOFs obtained *via* post-synthetic modification of amino-MIL-101(Cr) for altered water sorption.
- N. Tannert, E. Hastürk and C. Janiak
- 10/2015      **1<sup>st</sup> European Conference on Metal-Organic Frameworks and Porous Polymers (EuroMOF), Potsdam**
- Participation**



## Danksagung

Mein erster Dank gebührt Prof. Christoph Janiak, der mir nicht nur die Gelegenheit zur Promotion in seinem Arbeitskreis geboten hat, sondern es mir darüber hinaus auch ermöglicht hat eigene Ideen auszuarbeiten, umzusetzen und bis zur Publikation zu bringen. Weiterhin bedanke ich mich bei ihm für die Ermöglichung zu vielen Konferenz- und Tagungsbeiträgen, für das Korrekturlesen sowie für die interessante Themenvergabe im Rahmen des Projektes OptiMat. Für die besondere Gelegenheit zur Übernahme von Geräteverantwortung für mehrere Gas- und Dampfsorptionsgeräte und Verantwortung in Koordinationsangelegenheiten im Projekt OptiMat möchte ich mich ebenso bedanken.

Herrn Prof. Dr. Christian Ganter danke ich recht herzlich für die freundliche Übernahme des Koreferates sowie für seine stete Hilfsbereitschaft und äußerst konstruktive Beiträge zu fachlichen und persönlichen Belangen.

Ich bedanke mich besonders bei Emrah Hastürk, den ich bereits im gemeinsamen Bewerbungsgespräch und anschließender Bahnfahrt näher kennenlernen durfte und als wertvollen Kollegen und ehrlichen Freund schätzen lernte. Die enge chemische Zusammenarbeit im Büro, Labor und auf Konferenzen war stets inspirierend, menschlich war er für mich eine Bereicherung. Ich bedanke mich daher auch für spannende und fruchtbare Diskussionen, fachlicher und privater Natur.

Für die enge Zusammenarbeit danke ich außerdem besonders: Sandra Nießing, Tobie Matemb Ma Ntemb, Serkan Gökpınar, Simon Millan, Carsten Schlüsener, Alexander Nuhnen, Ülkü Kökcam-Demir, Anna Goldmann sowie Sebastian-Johannes Ernst (Fraunhofer ISE Freiburg) und Thomas Westerdorf (FläktWoods).

Ich danke meinem Bachelor-Studenten Christian Jansen für sein gewissenhaftes wissenschaftliches Arbeiten und seine Beiträge zu Al-MOF Synthesen. Ebenso danke ich meinem Master-Studenten Simon-Patrick Höfert, mit dem ich zahlreiche Gespräche führte, chemische und lustige. Auch bei meinem Bachelor-Studenten Marco Bengsch möchte ich mich für die Beiträge zu Synthesen von GO-MOF Kompositen bedanken. Ich danke auch Melchior Flügge für seine Arbeiten zu Urea-MOFs und  $\text{NH}_2\text{-MIL-125(Ti)}$ .

Bei meinen weiteren Bürokollegen Annika Herbst, Ilka Simon, Vasily Gvilava möchte ich mich für das angenehme Arbeitsklima, die stete Hilfsbereitschaft und netten Gespräche bedanken.

Vielen Dank an Sebastian Glomb, der mich geduldig an den Sorptionsgeräten angelernt hat und täglich seine Positivität zum Ausdruck brachte.

Mein Dank gilt auch Birgit Tommes, die für mich zahlreiche IR-Messungen angefertigt hat und immer eine gute Ansprechpartnerin war, wie es auch Annette Ricken, Dietmar Frunzke und Marcell Demandt waren.

Bei Claudia Schäfer bedanke ich mich für Ihre souveräne und gelassene, stets empathische und patente Aufttrittsweise sowie Ihre Hilfe bei organisatorischen Fragen.

Martin Wickenheisser (3P Instruments) danke ich für die Unterstützung bei Sorptionsanalytik sowie im Anschaffungsprozess und bei der Inbetriebnahme von verschiedenen Geräten. Für die Übernahme der Kosten zu mehreren Workshops bedanke ich mich in diesem Zusammenhang auch bei Dietmar Klank (3P Instruments).

Ich bedanke mich bei Christian Krebs, Udo Jung und Heike Fischer von der Glasbläserei der HHU für die enorme Hilfbereitschaft und ihre technischen Fähigkeiten sowie bei Sonja Schiller und Corell Spöringer der Feinmechanik der HHU für die Fertigung von sämtlichen Reaktorteilen für DGC- und MW-DGC-Synthesen.

Dem ganzen Arbeitskreis möchte ich für die angenehme Arbeitsatmosphäre danken. Die Kreierung von Grilladen, spaßigen Karnevals- und Weihnachtsfeiern, ausschweifenden Promotionsfeiern und wieder Grilladen, bei zeitgleichen Gesprächen über die aktuellen Forschungsfronten von MOFs, war einfach belebend.

Ich bedanke mich aufrichtig bei der Gesellschaft Deutscher Chemiker (GDCh), die mich sowohl bei Konferenzen finanziell unterstützt hat, mir aber darüber hinaus auch Stipendien für die Fortbildungen zum Geprüften Wirtschaftschemiker und Geprüften Qualitätsexperten GxP gewährt hat. Ganz besonders bedanke ich mich dafür bei Anke Moosbauer und Lena Rubner, aber auch bei allen Mitgliedern des Gremiums.

Ebenso fand ich finanzielle Unterstützung und inhaltliche Fortbildungen bei der Graduiertenakademie Interdisciplinary Graduate and Research Academy Düsseldorf (iGRAD) und Heine Research Academies (HeRA) der HHU. Für die äußerst gelungenen und informativen Workshops sowie den Reisekostenzuschuss für die EuroMOF Konferenz in Delft möchte ich mich herzlich bedanken.

Abschließend danke ich ganz besonders meiner Familie. Insbesondere meinen Eltern Marita und Hans-Peter Tannert kann ich für die unermüdlichen seelischen und enormen finanziellen Unterstützungen, die ich nicht nur im Verlauf meiner Promotionszeit genossen habe, nicht genug danken. Meinem Vater danke ich hier auch für die interessanten chemischen Fachgespräche. Ebenso unterstützt hat mich meine Schwester Nora Langner, in zahlreichen ermutigenden Gesprächen, mit einem offenen Ohr, aber auch mit Korrekturlesen.

Ich danke meiner Ehefrau Lena, die mir, zu meinem großen Glück, im Verlauf der Promotionszeit das Ja-Wort gegeben und mir am 05.11.2019 unsere wundervolle Tochter Jara geschenkt hat. Für die absolut bedingungslose Unterstützung zu allen Zeiten bedanke ich mich von ganzem Herzen.

Danke.

Allen denen, die an dieser Stelle eigentlich hätten stehen müssen, danke ich ebenso.



## Zusammenfassung

Die vorliegende kumulative Thesis hat, wie der Titel vermuten lässt, mehrere miteinander zusammenhängende Schwerpunktthemen. Sie befasst sich zunächst mit der Syntheseoptimierung von wasserstabilen Metall-organischen Gerüstnetzwerken (engl. metal-organic frameworks, kurz: MOFs) vor dem Hintergrund der Nachhaltigkeit sowie darüber hinaus mit dem Einsatz solcher MOFs in umweltrelevanten Anwendungen. Ziel der Arbeit ist demnach sowohl die (Weiter-) Entwicklung neuartiger und umweltschonender Synthesemethoden für wasserstabile MOFs als auch deren anwendungsorientierte Modifizierung und Charakterisierung als Adsorbentien für den Einsatz in Adsorptionskältemaschinen und möglichen weiteren umweltrelevanten Anwendungen.

Dabei sind bei den Syntheseoptimierungen wasserstabiler MOFs primär im Fokus:

- (Weiter-)Entwicklung von nachhaltigen MOF-Synthesen und Prozessen
- Reduzierung der Syntheszeiten
- Reduzierung des nötigen Energieeintrags
- Reduzierung der Lösemittelmengen

Bei den Optimierungen sollen dabei als einheitliche Bewertungskriterien sowohl die Syntheseausbeuten, die Kristallinität der erhaltenen MOFs, deren Porositätsparameter, insbesondere BET-Oberfläche, Porenvolumen und Wassersorptionskapazität dienen. Insbesondere der letztgenannte Stichpunkt der Lösemittelreduzierung ist eine der grundlegenden Motivation der Arbeit, da Standard-MOF-Synthesen von wasserstabilen MOFs fast immer enorm hohe Mengen an Lösemitteln/Wasser beinhaltet. Das Schwerpunktthema der MOF-Syntheseoptimierungen soll demnach einen Beitrag zu deutlich ökonomisch und ökologisch optimierten MOF-Synthesen leisten und Potentiale aufzeigen. Die hierbei eingesetzten Methoden Trockengelsynthese (engl. dry-gel conversion, kurz: DGC) und die im Rahmen dieser Thesis entwickelte und für MOFs neuartige Mikrowellenunterstützte Trockengelsynthese (MW-DGC) lieferten MOFs, welche alle die gesetzten Qualitätskriterien erfüllen und darüber hinaus drastische Einsparungen in den genannten Punkten erreichen. Diese Einsparungen werden sowohl durch verringerte Lösemittelmengen in den Synthesen erreicht als auch durch die bei allen MOFs belegte, mehrfache Wiederverwendung des Lösemittels im nächsten Syntheselauf. MW-DGC erwies sich dabei vorteilhafterweise als einzigartige Methode für die Herstellung eines hierarchisch mikro-meso-porösen Aluminiumfumarats (Alfum). Die Integration der genannten Methoden in den Kontext aller Literatur-bekannten Synthesen fand zusätzlich tabellarisch und durch Rechnungen zu Lösemiteleinsparungen statt.

Das Schwerpunktthema der Bewertung von neuartigen MOFs als Adsorbentien in Adsorptionskältemaschinen beinhaltete vorwiegend:

- Die Bestimmung von hydrothormaler Stabilität mittels Zyklisierungen
- Die Bestimmung von Wassersorptionskapazität und Lage des Wendepunkts der Wasserdampfsorptionsisotherme bezüglich des Partialdrucks bzw. relativer Feuchte und in Abhängigkeit der Temperatur
- Die Kennzahlenbestimmung in entsprechenden Energietransferprozessen, wie Adsorptionseenthalpie und Temperaturlevel von prozessbeteiligten Kompartments

Das neuartige MOF MIL-53(Al)-TDC war dabei das MOF der Wahl, da es im genannten Anwendungszusammenhang bis dato weitgehend nicht charakterisiert war, aber bereits eine vielversprechende Wasseraufnahme und hydrothermale Zyklenstabilität berichtet war. Die erstmalige Bewertung verschiedener Al-Quellen in der MOF-Synthese sowie die Überprüfung der Produkteigenschaften lieferte ca.  $1100 \text{ m}^2 \text{ g}^{-1}$  BET-Oberfläche und bis zu  $0.35 \text{ g g}^{-1}$  Wassersorptionskapazität. Hydrothermale Stabilitätsuntersuchungen belegten die Robustheit des metallorganischen Gerüsts und damit die Eignung für die spezifische Anwendung. Im Verlauf der Untersuchungen konnte auch gezeigt werden, dass MIL-53(Al)-TDC einen einzigartigen Arbeitsbereich für Adsorbentien in Adsorptionskältemaschinen bietet.

Bei der anwendungsbezogenen Modifizierung von wasserstabilen MOFs fiel die Wahl auf das äußerst stabile und hochporöse Plattform-MOF MIL-101(Cr), für welches ausgehend von  $\text{NH}_2\text{-MIL-101(Cr)}$  bereits eine Vielzahl von post-synthetischen Modifizierungen (engl. post-synthetic modification, kurz: PSM) beschrieben wurden. Die hochaktuellen Entwicklungen von  $\text{SO}_2$ -Sorption in MOFs gaben den Anlass zur Überprüfung der These, dass die beiden MOFs MIL-101(Cr) und  $\text{NH}_2\text{-MIL-101(Cr)}$  gute  $\text{SO}_2$ -Sorptionskapazitäten besitzen sollten. Die zusätzliche Herstellung und Charakterisierung von neuartigen PSM-modifizierten Produkten mittels Umsetzung von  $\text{NH}_2\text{-MIL-101(Cr)}$  mit geeigneten Isocyanaten lieferte die gewünschten Urea-modifizierten Substrate in guten Ausbeuten, Kristallinitäten und Porositätsparametern. Darüber hinaus konnten die MOFs MIL-101(Cr) und  $\text{NH}_2\text{-MIL-101(Cr)}$  als gute  $\text{SO}_2$ -Adsorbentien bestätigt werden und am *p*-Toluol-sulfonyl-substituierten Urea-MOF UR3-MIL-101(Cr) die zweithöchste  $\text{SO}_2$ -Sorptionskapazität überhaupt nachgewiesen werden. Die zusätzliche Einordnung aller Ergebnisse in die  $\text{SO}_2$ -Sorptionsliteratur fand dabei in tabellarischer Form statt.

## Abstract

The present cumulative thesis contains several interrelated focus topics, as the title indicates. Initially the thesis addresses the synthesis optimizations of water-stable metal-organic frameworks (MOFs) amid sustainability and in addition the use of such MOFs in environmentally relevant applications. Accordingly the objective of this work is the (further) development of novel and environmentally friendly synthesis routes for water-stable MOFs as well as their application-oriented modification and characterization as adsorbents for the utilization in adsorption heat pumps (AHPs) and other possible environmentally relevant applications.

Regarding synthesis optimizations of water-stable MOFs primarily in focus are:

- (Further) Development of sustainable MOF syntheses and processes
- Reduction of synthesis time
- Reduction of needed energy input
- Reduction of solvent amounts

Within the optimizations there should be consistent assessment criteria: yields, crystallinity of obtained MOF samples, their porosity parameters, particularly BET surface area, pore volume and water sorption capacity. Especially the last key point of solvent reduction is one of the main motivations of this work, as standard syntheses of water-stable MOFs incorporate in most cases enormous amounts of solvent/water. The focus topic of MOF synthesis optimizations should consist in contributing to economically and ecologically optimized MOF syntheses and point up potentials. The applied methods dry-gel conversion (DGC) and microwave-assisted dry-gel conversion (MW-DGC), which have been developed within this thesis, resulted in MOFs that all meet the set quality criteria and advantageously achieve enormous savings in the points stated. These savings can be achieved by reduced solvent amounts in the syntheses and with the repeated re-use of solvent in the next synthesis run. Advantageously MW-DGC turns out to be a unique method to produce hierarchically micro-meso-porous aluminum fumarate (Alfum). The integration of the named methods into the context of all literature known syntheses was done tabularly and by solvent savings calculations.

The focus topic of assessment of MOFs as adsorbents in adsorption heat pumps (AHPs) mainly contains:

- The determination of hydrothermal stability using cycling experiments.
- The determination of water sorption capacity and inflection point of the water vapor sorption isotherm concerning partial pressure, respectively relative humidity depending on a change on temperature.
- The determination of key figures in related energy transfer processes like isosteric heat of adsorption and temperature levels of process-affiliated compartments.

The new MOF MIL-53(Al)-TDC was the MOF of choice, as it had not been characterized within the given application context to a large content. However, it was reported to exhibit a promising water loading and hydrothermal cycle stability. The first evaluation of Al-sources in this MOF synthesis throughout a review of product properties resulted in ca. 1100 m<sup>2</sup> g<sup>-1</sup> BET surface area and up to 0.35 g g<sup>-1</sup> water sorption capacity. Hydrothermal stability experiments proved the robustness of the metal-organic framework and, hence, its suitability for the specific application. During the investigations it could be demonstrated that MIL-53(Al)-TDC offers a unique working window for adsorbents in thermally driven chillers (TDCs).

Within the course of application-oriented modification of water-stable MOFs the stable and highly porous platform MOF MIL-101(Cr) was chosen, for which starting from NH<sub>2</sub>-MIL-101(Cr) many post-synthetic modifications (PSMs) have already been reported. The highly topical developments of SO<sub>2</sub> sorption in MOFs gave rise to check the hypothesis that both MOFs MIL-101(Cr) and NH<sub>2</sub>-MIL-101(Cr) should exhibit good SO<sub>2</sub> sorption capacities. The additional syntheses and characterizations of novel PSM-derived products by conversion of NH<sub>2</sub>-MIL-101(Cr) with suitable isocyanates resulted in the desired urea-modified substrates with good yields, crystallinities and porosity parameters. Furthermore, the MOFs MIL-101(Cr) and NH<sub>2</sub>-MIL-101(Cr) could be confirmed as good SO<sub>2</sub> adsorbents and the *p*-toluenesulfonyl-substituted urea-MOF UR3-MIL-101(Cr) exhibited the second highest SO<sub>2</sub> sorption capacity in general. The additional classification of all results into the SO<sub>2</sub> sorption literature is done tabularly.





## List of abbreviations and symbols

AC	Activated Carbon
ac	Acetate
AcN	Acetonitrile
AHP	Adsorption Heat Pump
AHT	Adsorption Heat Transformation
Alfum	Aluminum fumarate
Al-MOF	Aluminum-Based MOF
a.u.	Arbitrary Unit
BA	Benzoic Acid
bar	Unit of Pressure: Bar(s) (1 bar = 100000 Pa)
BASF	Badische Anilin und Soda Fabrik Aktiengesellschaft
bdc	1,4-Benzenedicarboxylate, also: Terephthalate
BET	Brunauer-Emmett-Teller
bipy	4,4'-bipyridine
BJH	Barrett-Joyner-Halenda
BMBF	Bundesministerium für Bildung und Forschung
btc	1,3,5-Benzenetricarboxylate, also: Trimesate
ca.	Circa
calc.	Calculated
CAU	Christian-Albrechts-Universität
CD-MOF	Cyclodextrin-MOF
CE-DGC	Commonly Electric-Heated DGC
cf.	<i>Latin: confer</i> – compare
COF	Covalent Organic Framework
conc.	Concentrated
cm	Unit of Length: Centimeter(s)
CPL	Coordination Pillared-Layer
CSD	Cambridge Structural Database
CUS	Coordinatively Unsaturated (Metal) Sites
CVD	Chemical Vapor Deposition

d	Unit of Time: Day(s)
<i>d</i>	Diameter
DCM	Dichloromethane
DGC	Dry-Gel Conversion
DMF	<i>N,N'</i> -Dimethylformamide
DoE	Design of Experiments
DUT	Dresden University of Technology
DVS	Dynamic Vapor Sorption
EDX	Energy-Dispersive X-Ray Spectrometry
e.g.	<i>Latin: exempli gratia</i> – for example
engl.	English
eq.	Equivalent(s)
eqn	Equation
ESI	Electronic Supporting Information
et al.	<i>Latin: et alii</i> (male), <i>et aliae</i> (female) – and others
EtOH	Ethanol
eV	Unit of Energy: Electronvolt(s) ( $1\text{ eV} = 1.602 \cdot 10^{-19}\text{ J}$ )
exp.	Experimentally
fdc	2,5-Furandicarboxylate
Fig.	Figure(s)
FMOF	Fluorous MOF
FT-IR	Fourier Transformed IR
g	Unit of Weight: Gram(s)
GO	Graphite Oxide
h	Unit of Time: Hour(s)
HEMA	2-Hydroxyethylmethacrylate
HHU	Heinrich-Heine-Universität
HIPE	High Internal Phase Emulsion
HKUST	Hong Kong University of Science and Technology
HoA	(Isosteric) Heat of Adsorption
HOF	Hydrogen-Bonded Organic Framework

HoV	Heat of Vaporization
<i>i</i>	Intercept of BET Plot
IAST	Ideal Adsorbed Solution Theory
i.e.	<i>Latin: id est</i> – that is to say
IL	Ionic Liquid
IR	Infrared (Spectroscopy)
IRMOF	Isorecticular Metal-Organic Framework
ISE	Fraunhofer-Institut für Solare Energiesysteme, Freiburg, Germany
IUPAC	International Union of Pure and Applied Chemistry
K	Unit of Temperature: Degree(s) Kelvin
<i>K</i>	Langmuir Constant
<i>k<sub>Ads</sub></i>	Rate Constant of Adsorption
<i>k<sub>Des</sub></i>	Rate Constant of Desorption
KAUST	King Abdullah University of Science and Technology
keV	Unit of Energy: Kiloelectronvolt(s)
kJ	Unit of Energy: Kilojoule(s) ( $1\text{ J} = 1\text{ Nm} = 1\text{ kg m}^2\text{ s}^{-2}$ )
kPa	Unit of Pressure: Kilopascal(s) ( $1\text{ Pa} = 1\text{ N m}^{-2}$ )
kV	Unit of Voltage: Kilovolt(s) ( $1\text{ V} = 1\text{ W A}^{-1}$ )
L	Unit of Volume: Liter(s)
nm	Unit of Length: Nanometer(s) ( $1\text{ nm} = 10^{-9}\text{ m}$ )
NMR	Nuclear Magnetic Resonance
<i>M<sub>w</sub></i>	Molar Weight
mA	Unit of Electric Current: Milliampere(s) ( $1\text{ A} = 1\text{ W V}^{-1}$ )
mbar	Unit of Pressure: Millibar(s)
MFM	Manchester Framework Material
MIL	Matériau de l'Institut Lavoisier
min	Unit of Time: Minute(s)
mg	Unit of Weight: Milligram(s)
mL	Unit of Volume: Milliliter(s)
mm	Unit of Volume: Millimeter(s)
MMM	Mixed-Matrix Membrane

mmol	Unit of Amount of Substance: Millimole(s) $\text{mol} \triangleq 6.022 \cdot 10^{23}$ particles)	(1
MOA	Metal-Organic Aerogel	
MOF	Metal-Organic Framework	
MTV	Multivariate	
mult.	Multiple	
MW	Microwave	
MW-DGC	Microwave-Assisted DGC	
$N_A$	Avogadro Constant ( $6.02214086 \cdot 10^{23} \text{ mol}^{-1}$ )	
NLDFT	Non-Linear Density Functional Theory	
NOTT	University of Nottingham	
NMR	Nuclear Magnetic Resonance	
No.	Number(s)	
NP	Nanoparticle	
p	Pressure	
p.a.	<i>Latin: pro analysi</i> – analytically pure	
PCN	Porous Coordination Network	
PCP	Porous Coordination Polymer	
PET	Polyethylene terephthalate	
$p_{p_0}^{-1}$	Partial Pressure	
ppm	Parts per Million	
PSM	Post-Synthetic Modification	
PTFE	Polytetrafluoroethylene	
PU	Polyurethane	
PXRD	Powder X-Ray Diffractometry	
$Q_{\text{ads}}$	Heat of Adsorption	
$Q_{\text{cond}}$	Heat of Condensation	
$Q_{\text{des}}$	Desorption Heat ( <i>i.e.</i> heat for desorption of a specific adsorbent)	
$Q_{\text{evap}}$	Evaporation Heat	
$r$	Standard Deviation	
ref.	Reference	

RH	Relative Humidity
RT	Room Temperature
s	Unit of Time: Second(s)
s	Slope of BET Plot
S <sub>BET</sub>	BET Surface Area
S <sub>BET(micro)</sub>	Micropore BET Surface Area
SBU	Secondary Building Unit
SCD	Supercritical Drying
SEM	Scanning Electrode Microscope
S <sub>t</sub>	Total Surface Area
STP	Standard Temperature and Pressure
STY	Space-Time-Yield
T	Temperature
Tab.	Table(s)
TBAF	Tetrabutylammonium fluoride
TDC	2,5-Thiophenedicarboxylate
TDC	Thermally Driven Chiller
TEM	Transmission Electron Microscopy
TGA	Thermogravimetric Analysis
TMAOH	Tetramethylammonium hydroxide
UiO	Universitetet i Oslo
UNAM	Universidad Nacional Autónoma de México
UR	Urea
V <sub>micro</sub>	Micropore Volume
V <sub>pore</sub>	Pore Volume
V <sub>total</sub>	Total Pore Volume
VOC	Volatile Organic Compound
vs.	versus
W	Unit of Energy: Watt(s) (1 W = 1 J s <sup>-1</sup> )
W <sub>m</sub>	Weight of Adsorbed Monolayer of Adsorptive
wDSL	Weighted Dual-Site Langmuir

wt%	Weight Percentage
ZIF	Zeolitic Imidazolate Framework

---

$\alpha$	Alpha (stands for inflection point of water sorption isotherm)
$\text{\AA}$	Ångström (length scale, $1 \text{ \AA} = 0.1 \text{ nm} = 10^{-10} \text{ m}$ )
$\Delta_{ads}H$	Heat of Adsorption
$\Delta_{evap}H$	Heat of Evaporation
$\Delta_{vap}H$	Heat of Vaporization
$\Delta$	Delta (stands for difference)
$\delta$	Delta (stands for chemical shift in NMR spectra)
$\lambda$	Lambda (stands for wavelength)
$\mu\text{m}$	Unit of Length: Micrometer(s) ( $1 \mu\text{m} = 10^{-6} \text{ m}$ )
$\Theta$	Theta (stands for a specific angle in the Bragg equation)
$\Theta$	Surface Coverage Rate of Change During Adsorption

## Table of content

Publication List .....	VII
Danksagung .....	X
Zusammenfassung .....	XIV
Abstract .....	XVI
List of abbreviations and symbols.....	XIX
Table of content.....	XXV
1. Introduction .....	27
1.1. Metal-Organic Framework Materials.....	27
1.1.1. Structural Properties .....	29
1.1.2. Synthesis Routes of MOFs .....	32
1.1.3. Tuning the Chemical Properties of MOFs .....	35
1.1.4. Analytical Characterizations of MOFs .....	38
1.2. Fundamentals of Adsorption.....	40
1.2.1. Principles and Theory of Physisorption in Micro-/Mesoporous Adsorbents.....	40
1.2.2. Gas Adsorption in MOFs.....	45
1.2.3. Water Vapor Adsorption in MOFs .....	48
1.3. Potential applications of MOFs.....	50
1.3.1. Gas Storage and Separation.....	50
1.3.2. Adsorption-Driven Heat Transformation.....	51
1.3.3. Other Potential Applications of MOFs .....	54
1.3.3.1. MOF Composites .....	54
1.3.3.2. Heterogeneous Catalysis .....	55
1.3.3.3. Electronic Devices and Chemical Sensing .....	56
1.3.3.4. Water Purification .....	56
2. Assignment of Tasks.....	57
3. Cumulative Part .....	59



3.1.	Microwave-Assisted Dry-Gel Conversion (MW-DGC) – A New Sustainable Route for the Rapid Synthesis of Metal-Organic Frameworks with Solvent Re-Use .....	60
3.2.	Evaluation of the Highly Stable Metal-Organic Framework MIL-53(Al)-TDC (TDC = 2,5-Thiophenedicarboxylate) as a New and Promising Adsorbent for Heat Transformation Applications .....	100
3.3.	Robust Synthesis Routes and Porosity of Al-based Metal-Organic Frameworks Al-fumarate, CAU-10-H and MIL 160 .....	124
3.4.	A Series of New Urea-MOFs Obtained <i>via</i> Post-synthetic Modification of NH <sub>2</sub> -MIL-101(Cr): SO <sub>2</sub> , CO <sub>2</sub> and H <sub>2</sub> O Sorption .....	167
4.	Unpublished Results .....	197
4.1.	Unravelling Gas Sorption in Microporous Al-MOF CAU-23 – N <sub>2</sub> , Ar, CO <sub>2</sub> , H <sub>2</sub> , CH <sub>4</sub> , SO <sub>2</sub> and H <sub>2</sub> O Sorption and Mixed-Adsorptive Calculations .....	197
4.2.	Evaluation of Al-sources in The Syntheses of MIL-53-type MOFs With [Al(OH)(linker)]-Structure .....	198
4.3.	MOF composites .....	201
4.3.1.	Stabilized HIPEs with High MOF Fraction .....	201
4.3.2.	Composites Obtained from Aerosil® and Aeroperl® with CAU-10-H .....	203
4.4.	Hydrothermal Long-term Cycling (6000 cycles) of NH <sub>2</sub> -MIL-125(Ti) .....	205
5.	Conclusions .....	208
6.	Outlook .....	210
6.1.	Sustainable Syntheses of MOFs .....	210
6.2.	Water Sorption Applications .....	211
7.	Experimental Part .....	212
7.1.	Instrumentation and Equipment .....	212
7.2.	General Working Methods .....	216
7.3.	List of Chemicals and Solvents .....	217
8.	References .....	219

# 1. Introduction

## 1.1. Metal-Organic Framework Materials

Metal-organic frameworks (MOFs) display a subclass of coordination polymers that are potentially porous for gases and other guest molecules. MOFs originate from coordination chemistry and, generally, consist of metal ion or metal ion cluster *nodes*, connected by at least ditopic organic ligands (*linkers*), generating a network with permanent 1D, 2D or 3D porosity. According to IUPAC classification (*International Union of Pure and Applied Chemistry*), porous materials are divided into three groups (*cf.* Figure 1). While macroporous materials have bigger pores than 50 nm, mesopores are in the subrange of 2–50 nm; smaller pores with a diameter less than 2 nm are categorized as microporous adsorbents. MOFs can typically be allocated in the micro- to mesoporous range. They have received considerable attention in the scope of porous materials due to their outstanding properties within the last decades. The denomination “metal-organic framework” was invented by Prof Omar Yaghi, one of the pioneers in MOF-chemistry, in 1995. Initially, he described two microporous 3D-coordination polymers, namely Cu-bipy and Co-btc.<sup>1,2</sup> Two years later, another pioneer of MOF chemistry, Prof Susumo Kitagawa, demonstrated that the inherent microporosity of frameworks of the type  $\{[M_2(4,4'\text{-bipy})_3(\text{NO}_3)_4](\text{H}_2\text{O})_x\}_n$  with M = Co, Ni, Zn makes such frameworks generally accessible for gases like N<sub>2</sub>, O<sub>2</sub> and CH<sub>4</sub>. In the following Yaghi *et al.* proved the concept of reticular chemistry (lat. *reticulum* = small net) as a powerful and most versatile tool in coordination chemistry, so that the field has been named as such by Yaghi *et al.* in his introductory works of a conceptual approach to design predetermined structures.<sup>3,4</sup> The synthesis of highly microporous zinc terephthalate “MOF-5” by Yaghi *et al.* was one milestone in the history of MOFs, also because a series of structurally similar compounds with increasing pore sizes (*isoreticular* MOFs, short: IR-MOFs) could be obtained using elongated linker molecules.<sup>5</sup> Thereby the flexibility of the modular cluster-linker concept was exploited to prove the feasibility of synthetic generation of various novel MOF structures and open the field for pore geometry design and chemical design of MOFs. Reticular chemistry, yet in the form of purely inorganic and non-porous compounds, has been known since at least the beginning of the 18<sup>th</sup> century, when the German chemist Georg Stahl published the synthesis procedure for Prussian Blue ( $\text{Fe}^{\text{III}}_4[\text{Fe}^{\text{II}}(\text{CN})_6]_3 \cdot 14 \text{ H}_2\text{O}$ ).<sup>6</sup> However, its crystal structure was resolved 250 years later.<sup>7,8</sup> Without being termed as MOF, the first metal-organic coordination polymer maintaining porosity upon removal of the solvent molecule was first reported in 1965.<sup>9,10</sup>

The umbrella term porous coordination networks (PCNs) include MOFs, covalent organic frameworks (COFs), hydrogen-bonded organic frameworks (HOFs), porous coordination polymers (PCPs) and several related or subordinated compounds.

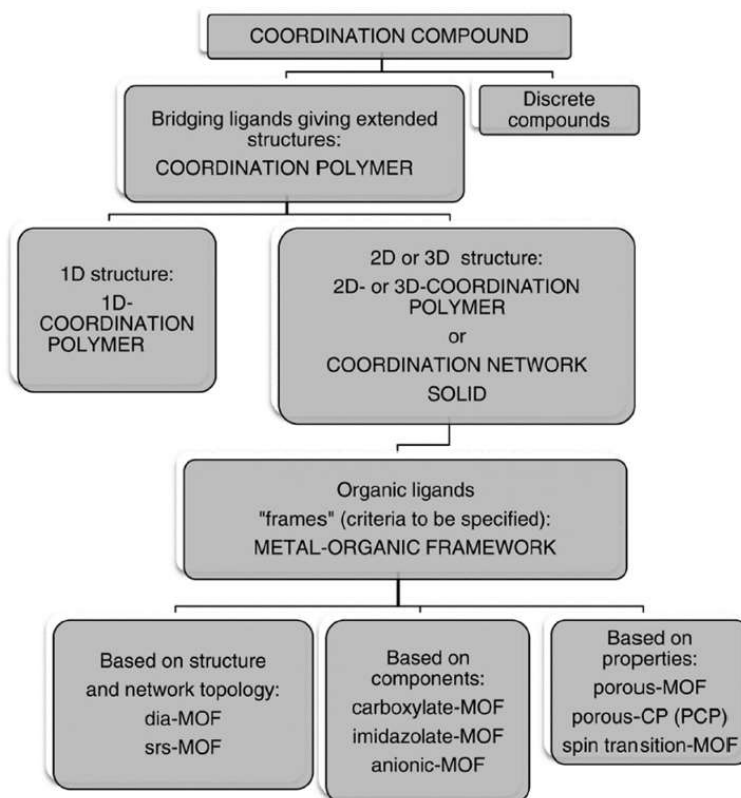


**Figure 1: Classifications of coordination compounds, coordination polymers and metal-organic frameworks.** Reprinted from ref. 11 with permission, © 2012, The Royal Society of Chemistry (RSC).

The rather wide-ranging IUPAC definition is: “Metal-Organic Framework, abbreviated to MOF, is a Coordination Polymer with an open framework containing potential voids.”<sup>11,12</sup> This definition comprises materials with dynamic porosity – *i.e.* materials that change properties upon external stimuli like pressure, temperature or even in dependency of presence/absence of guest molecules. Consequently, the criterion crystallinity is not stated in this definition. Moreover, a general nomenclature and systematic classification of metal-organic frameworks and the uniform use of termini have neither been established nor been defined by the IUPAC until to date. This is also true, because the vast variety of potential combinations of bridging multidentate organic linkers and cations give rise to millions of distinct MOFs, of which at least 500.000 structures have been predicted so far, and already min. 90.000 structures have been synthesized until today.<sup>13</sup>

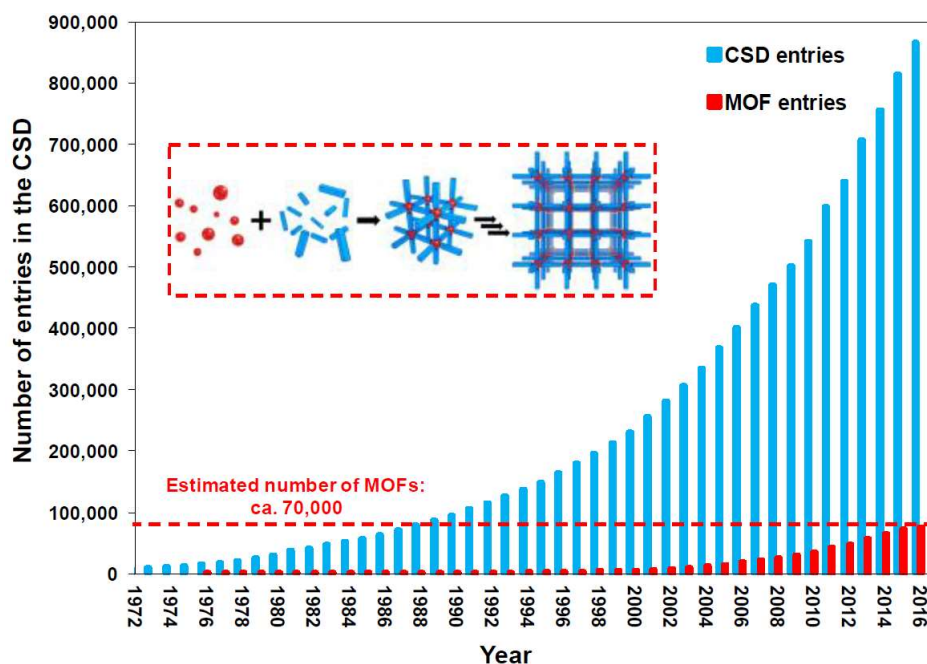


**Figure 2: Increase of the CSD and MOF entries in total numbers since 1972. The inset shows the self-assembly process from building blocks: metals (red spheres) and organic ligands (blue struts). Reprinted from ref. 14 with permission, © 2017, American Chemical Society (ACS).**

As a consequence, in the group of Yaghi MOFs were designated as MOF-5 and ascending numbers, while other groups use abbreviations of their research facility or university, such as for famous MOF families like MIL-101 (*Materieaux de l'Institut Lavoisier*), HKUST-1 (*Hong Kong University of Science and Technology*), CAU-10-H (*Christian-Albrechts-Universität*) or HHU-1 (*Heinrich-Heine-Universität*), sometimes followed by the element symbol of the respective ion (e.g. MIL-100(Fe) with iron-based nodes).

### 1.1.1. Structural Properties

Metal ions in MOFs are usually from the transition metal or d-block elements, such as (not accredited to completeness)  $\text{Ti}^{4+}$ ,  $\text{Zr}^{4+}$ ,  $\text{Hf}^{4+}$ ,  $\text{V}^{3+}$ ,  $\text{Cr}^{3+}$ ,  $\text{Fe}^{3+}$ ,  $\text{Mn}^{2+}$ ,  $\text{Ni}^{2+}$ ,  $\text{Cu}^{2+}$ ,  $\text{Zn}^{2+}$ ,  $\text{Cd}^{2+}$ , but also from main-group elements, such as  $\text{Ca}^{2+}$ ,  $\text{Mg}^{2+}$ ,  $\text{Al}^{3+}$ ,  $\text{Ga}^{3+}$ ,  $\text{In}^{3+}$ , additionally from the lanthanoid and even actinoid block, like  $\text{La}^{3+}$ ,  $\text{Eu}^{3+}$ ,  $\text{Yb}^{3+}$ ,  $\text{Tb}^{3+}$ ,  $\text{Th}^{3+}$ ,  $\text{Pu}^{3+}$ ,  $\text{U}^{3+}$  and others.<sup>15,16</sup> Metal ions or dimers can act as nodes, but tend to form tri- to octanuclear clusters, which commonly contain bridging oxido or hydroxido anions. In combination with carboxylate groups from the linkers (or any other bridging donors), these oligonuclear metal nodes are classified as inorganic secondary building units (SBUs),<sup>17</sup> an expression adapted from zeolite chemistry. The underlying principles of structurally related clusters can be comprehended in Figure 3 and in acute works by Yaghi *et al.*<sup>18</sup> However, any coordination geometry known from regular metal complexes has successfully been applied to MOFs in the last decade (for details see p. 133 f. in ref. 19).

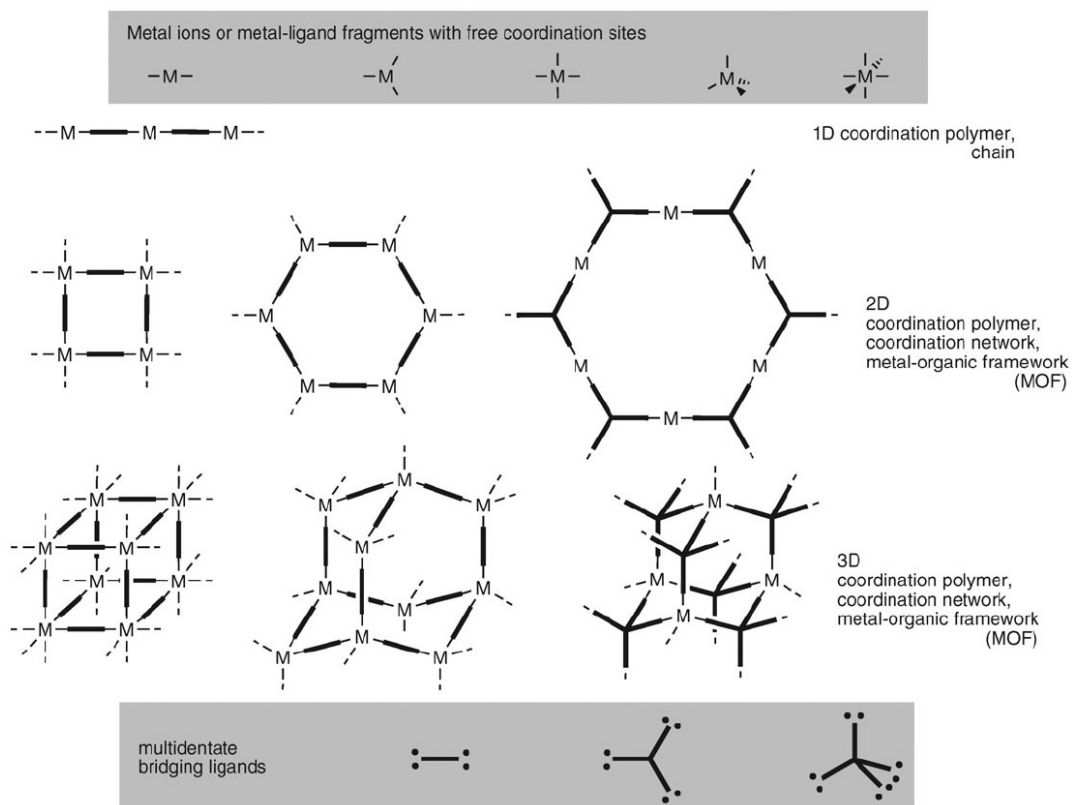


**Figure 3: Schematic representation of the construction of coordination polymers and MOFs from molecular building blocks. Reprinted from ref. 20 with permission, © 2010, The Royal Society of Chemistry (RSC).**

The most popular linkers are rigid (mostly aromatic or olefinic) multitopic ligands, such as di-, tri- or tetracarboxylates. Sulfonates and phosphonates, as well as heterocycles with N-donor function, can also be used. The rigidity of the linker ensures a structurally stable, crystalline network with persisting porosity upon solvent removal. Figure 4 gives a selective overview of typical linker molecules of MOFs.

Until today the use of multiple organic linker ligands together with varying metal cations has provided more than 75000 MOFs.<sup>21</sup> Generally, MOFs are characterized by their high inner surface areas and pore volumes, which exceed those of the known commercial adsorbents such as active carbons (ACs), silica gels or zeolites. Thus, MOFs outperform all other porous materials with experimentally determined Brunauer-Emmet-Teller (BET) surface areas of  $S_{BET} > 7000 \text{ m}^2 \text{ g}^{-1}$  (e.g. NU-110E with  $S_{BET} = 7140 \text{ m}^2 \text{ g}^{-1}$  and DUT-60 with  $S_{BET} = 7839 \text{ m}^2 \text{ g}^{-1}$ ), and pore volumes of  $V_{pore} > 5 \text{ cm}^3 \text{ g}^{-1}$  (DUT-60 with  $5.02 \text{ cm}^3 \text{ g}^{-1}$ ) have been reported.<sup>22,23</sup> Researchers have also shown that the theoretical upper limit for MOF surface areas is  $14600 \text{ m}^2 \text{ g}^{-1}$  (that equals to a surface of 2.7 American football fields per gram of MOF), possibly even higher.<sup>22</sup>

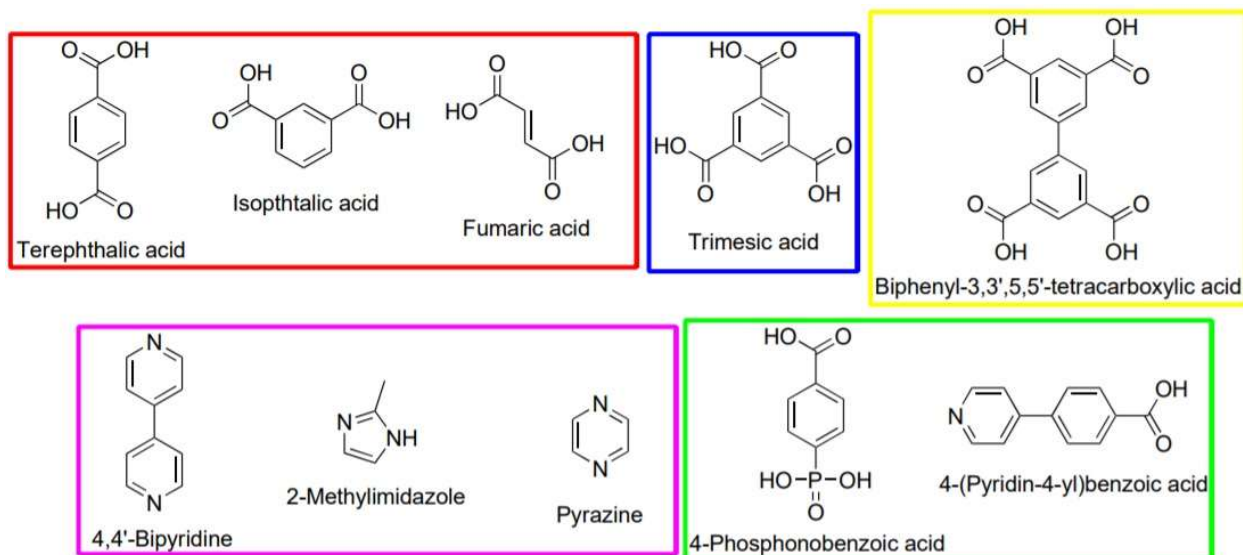


**Figure 4: Selection of typical MOF linkers: Bidentate carboxylate-based (red), tridentate carboxylate-based (blue), tetradentate carboxylate-based (yellow), nitrogen-based (purple), bifunctional (green).**

Different MOF structures can be obtained from the same reactants, so that depending on the external conditions (*i.e.* concentrations, heating rates, reaction times and other parameters) one structure may be generated favorably (*polymorphism*, *cf.* chapter 1.1.3). MIL-101, for instance, is the kinetically favored product, while MIL-53 may precipitate under prolonged reaction duration and can be designated as the thermodynamically favored product.

The narrow pore size distributions of MOFs arise from their crystalline nature. Bimodal pore size distribution can also be found in MOFs, *e.g.* in MIL-100 and MIL-101. Crystal structures and pore sizes/shapes of MOFs are known to vary upon input/removal of guest molecules reversibly. MIL-53 is a prominent example, with channels changing from square-like to rhombic upon adsorption of water.

When the pores of MOFs are large compared to the sterically demand of the molecular building blocks, one or more networks may entangle and cause *interpenetration* in a MOF structure. This attribute is mostly undesired for applications, as the porosity of the framework is reduced. On the other hand the stability of interpenetrated counterpart can be higher than that of the non-interpenetrated.

Breathing of MOFs is the phenomenon of pore size change upon guest molecule incorporation and release.<sup>24</sup> While upmost MOF structures remain rigid upon ad-/desorption, some show structural changes that can be observed by different analysis techniques, such as powder X-ray diffraction (PXRD). One more facet of MOF structures is flexibility that can be guest-dependent (*e.g.* presence of water in the pore) or triggered by external stimuli.<sup>25</sup>

Coordinatively unsaturated (metal) sites (CUS) as for example present in the prototypic MOF HKUST-1 are even one more structural feature that can generally determine the attributes of a MOF. First published in 1999 by Williams *et al.*, HKUST-1 is built up by Cu(II) paddle-wheel SBUs with btc ligands.<sup>26</sup> Upon dehydration terminal solvent molecules, that are present in the Cu(II) paddle-wheels, are removed and leave unsaturated Cu metal sites. The latter are then accessible for guest molecules like gases or vapors. CUS can also be used to attach other molecules in a modification approach (*cf.* chapter 1.1.3).

### 1.1.2. Synthesis Routes of MOFs

The directional growth of the crystallized frameworks and their crystallites is mainly determined by the coordination geometry of the metal nodes, steric properties of the linker and thermodynamics of each reaction pair. Generally MOF growth is a self-organized crystallization process, in which the solvent may serve as a template. The latter may be used in MOF syntheses, however, dedicated template additives are not generally required for the synthesis. On the contrary, synthetic modulators, such as benzoic acid (BA), oxalic acid, amino acids, ionic liquids (ILs) and other mostly acidic modulators, play crucial roles in the synthesis of defective/defect-free MOFs (*i.e.* MOF structures with missing linker connections inside of the framework or even missing clusters).<sup>27,28</sup> Foremost group IV MOFs (*i.e.* Ti, Zr, Hf) apply customarily modulators, especially Zr-MOFs,<sup>29,30</sup> but also Al-MOFs and their crystallinity enhancement have been investigated in this realm.<sup>31</sup>

Metal-organic frameworks can be described as salt and as such they can be prepared in an acid-base reaction. As an example the commercially available microporous aluminum fumarate (short: Alfum, tradename: Basolite® A520) can be precipitated straightforwardly from aqueous solutions of aluminum sulfate and disodium fumarate. The formation of MOFs commonly requires elevated temperatures, due to entropic reasons or solubility issues. Thus they are most often being synthesized in solvothermal or hydrothermal approaches, starting from metal salts and organic linkers, mostly in form of carboxylic acids. The most facile approach for the synthesis of a MOF is common conventional heating of the starting materials in solution in an autoclave. Numerous coordination polymers from such solutions maintain their porosity after activation (*i.e.* after removal of solvent and guest molecules throughout reduced pressure and/or elevated temperature) and can only then be designated as MOFs. Consequently, researchers have not only systematically investigated combinations of metal ions with all types of bridging organic anions including IR-MOFs, but also searched for effective synthetic strategies and chemically elegant protocols to promote their commercialization. MOFs that appear to be promising for applications, hence economically and ecologically increased effective synthesis routes are required. The challenges and prospects of the production of MOFs at affordable costs and in an environmentally benign way should include non-toxic and inexpensive chemicals, water as

solvent (or at least omission of harsh organic solvents), faster reaction times and decreased energy input. Organic linkers like fumaric acid may also be obtained by conversion of biomass or by recycling (e.g. terephthalic acid from PET waste) and thereby contribute to augmented sustainable MOF syntheses. All these factors determine the costs of MOFs, respectively their prospective commercialization. At the same time, each of these factors display both a challenge and an opportunity to boost the sustainability and affordability of MOFs by minimizing their production costs and ecological impact.<sup>32,33</sup>

Ordered crystallization of MOFs can be obtained by gradually supplying the linker anion to the metal ion solution or the other way round. One approach to achieve slow, controlled deprotonation was presented by Dinča *et al.*, who obtained MOF-5 *via* cathodic deprotonation of the linker acid.<sup>34</sup> Moreover, a series of MOFs were obtained by anodic oxidation of metallic electrodes with the respective linker being dissolved in the electrolyte, resulting in electrodeposition of MOFs onto surfaces.<sup>35</sup> Also thermal gradient coating can produce highly oriented MOF thin films.<sup>36</sup> The synthesis of MOF thin films facilitates the fabrication of surface-supported devices and thereby generally simplifies utilization of MOFs by direct linkage to substrates and surfaces (see also chapter 1.3.2. and 1.3.3. for polycrystalline nature of MOFs and along going challenges).<sup>37</sup>

Ambient pressure syntheses of MOFs render pressurized and potentially explosive autoclaves unnecessary, hence they can be designated as sophisticated and safer.<sup>38</sup> Continuous flow-reactors combine solvothermal approaches with continuous production by flow chemistry. Microwave methods can be used to synthesize MOFs, concurrently increasing induction time, hence the reaction speed and nucleation rate dramatically.<sup>39,40,41</sup>

At the same time, microwave techniques enable chemists to produce MOFs with both reduced process energy consumption and reaction time, moreover facilitating large-scale production to thin film approaches.<sup>40,42,43</sup> The combination of microwave heating with continuous flow synthesis poses an effective approach for rapid and steady production of MOFs.<sup>40,44</sup> Mechanochemical conversions of starting materials, for instance *via* ball-milling or extrusion techniques, allow for the synthesis of MOFs in a sustainably upgraded fashion, as such methods diminish or even omit reaction solvent.<sup>45,46</sup> This approach can also be designated as a route for prospective production of MOFs on pilot-scale. Additionally sonochemical syntheses (*i.e.* by energy input *via* ultrasound) have frequently been demonstrated and contribute to environmentally benign routes for the same reasons.<sup>47,48</sup> Chemical vapor-deposition (CVD) was proven to be an elegant tool to derive highly ordered MOF thin films, while coincidentally omitting solvent use.<sup>49</sup> Electrochemical deposition is the synthesis of adherent layers of MOFs onto conductive surfaces or substrates.<sup>50,51</sup> Spray-drying of MOFs can be executed continuously and get in line with environmentally benign methods.<sup>52,53</sup>



Figure 5 depicts a synopsis of MOF synthesis methods.

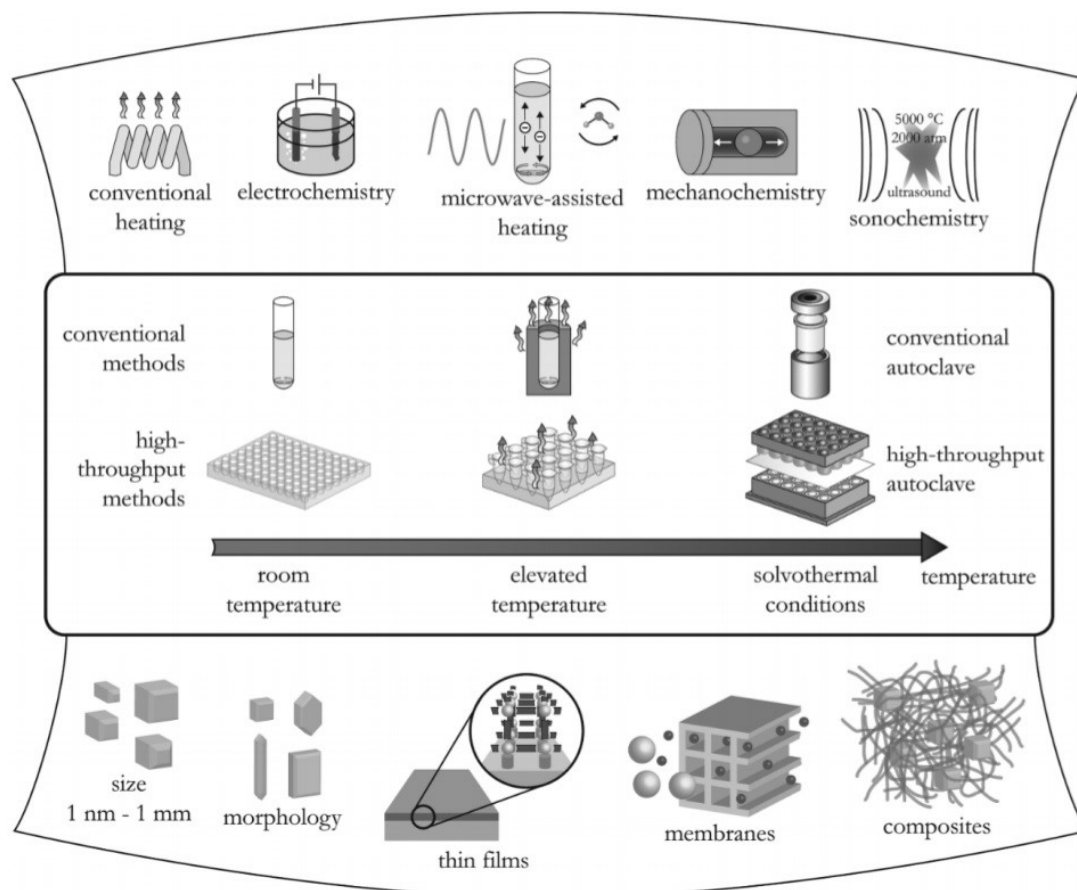


**Figure 5: Top: Schematic representation of synthesis methods for MOFs. Middle: Applied reaction temperatures and vessels. Bottom: Potentially resulting products. Reprinted from ref. 54 with permission, © 2012, American Chemical Society (ACS).**

Details on all presented methods and other concepts and techniques, which are not primarily within the scope of this work, can be found in the comprehensive reviews by N. Stock,<sup>54</sup> by S. Kumar *et al.*,<sup>55</sup> and by Y. Li,<sup>56</sup> both last-mentioned contributions in conjunction with greening the MOF synthesis process.

The present thesis focuses on dry-gel conversion (DGC), which has been only rarely used in MOF chemistry since 2011.<sup>57</sup> Figure 6 illustrates the working principle of DGC and a novel microwave-assisted dry-gel conversion (MW-DGC, *cf.* chapter 3.1) that has been developed for MOFs for the first time during this thesis. The starting materials, placed on a sieve or porous support at the top of an autoclave container, are converted in a chemical reaction upon microwave (or electric heating in a common DGC), while a small amount of solvent is placed at the bottom of this vessel. By separation of solvent and reactant mixture the solvent can be recovered and used again for further reaction runs (*cf.* chapter 3.1 and 3.2). H. Reinsch stated that the accessibility of MOFs will always be limited by the sustainability of the synthesis procedure,<sup>58,59</sup> as a result of that few synthetic protocols of MOFs deliberately follow principles and design methods that correspond with *Green Chemistry* and *Green Engineering* at the very same time.<sup>60,61,62</sup>

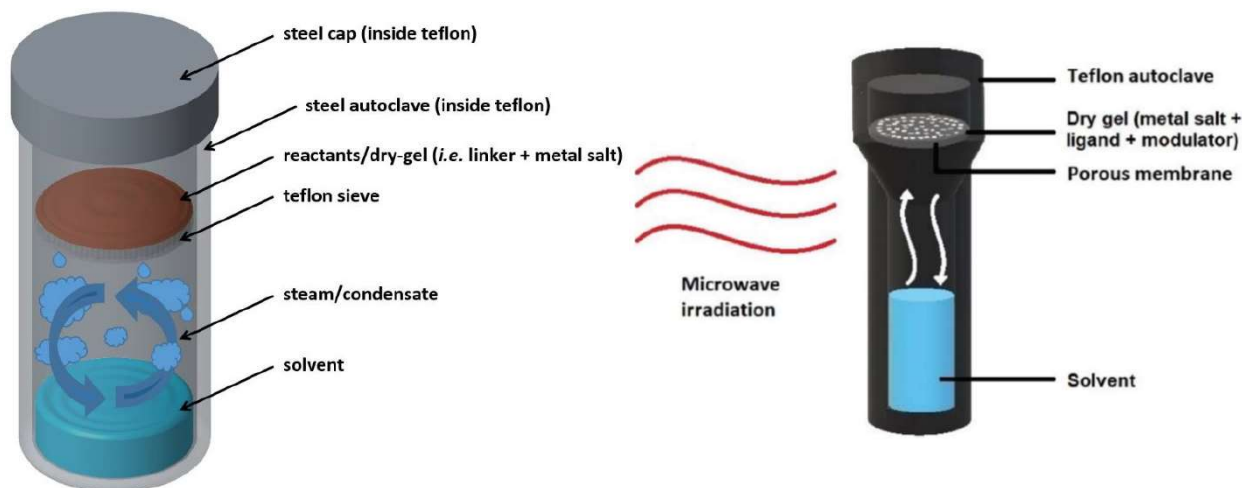


**Figure 6: Schematic depiction of DGC (left) and MW-DGC (right) for the environmentally benign synthesis of MOFs with solvent re-use.**

The author's contribution to MW-DGC (*cf.* chapter 3.1) focuses on both issues: reduced reaction times/energy input and solvent reduction/re-use, concurrently displaying an alternative technique of novel synthetic microwave setup for MOFs. Another recent contribution to optimized MOF synthesis claims that economic and sustainable strategies are imperative for promoting MOF materials into large scale industrial use.<sup>63</sup> Thus continuous methods and scale-up in MOF chemistry challenges MOF researchers and chemical industry. Coevally start-up companies for MOF production at scale sprang up in the last years constantly.<sup>64,65</sup> Although aluminum fumarate (trade name: Basolite® A520) has a most facile synthetic procedure in aqueous media, which has been patented by the company BASF, the economically feasible production on a ton-scale is still not existent and apparently no routine process.

In conclusion, MOFs can be synthesized in multifarious manners always in dependency of the specific formation reaction of linker and metal (salt) and each underlying physical-chemical formation process. Differing synthesis strategies for the very same MOF will most likely result in different product qualities as to crystallinity, porosity, and other MOF product properties.

### 1.1.3. Tuning the Chemical Properties of MOFs

As mentioned in the beginning the pore sizes of MOFs can be adjusted by choosing appropriate linkers, even more by elongation of the linker (*e.g.* terephthalate to 4,4'-biphenylenedicarboxylate, *i.e.* reticular chemistry) and sensible use of SBUs.<sup>66</sup> Upon these changes, however, not only pore size and lattice parameters differ, but also other physical and chemical properties of the MOF derive therefrom. As one simple, yet very specific example of chemical variety within MOF structures, with variation from one metal ion to another in the same MOF structure (*e.g.* in MIL-100(Al), MIL-100(Fe) and MIL-100(Cr) cages respectively), crystallite sizes, pore sizes, gas and vapor affinities and several other chemical properties of the pore vary.<sup>43,67</sup> The resulting

possibilities of chemical variations is well beyond cation or ligand exchange, first of all due to the innumerable quantity of possible linker structures (*cf.* Figure 4). In addition to common *de novo* exchange of metal ion or linker in the synthetic protocol to yield one specific MOF (e.g. MIL-100(Cr) or MIL-100(Fe) by use Cr or Fe salt in the MOF synthesis), various mixed-metal approaches have successfully been demonstrated.<sup>68,69</sup> These possibilities are further extended by post-synthetic (partial) cation exchange, called transmetalation.<sup>70</sup> On the other hand mixed-linker MOFs are constantly being investigated to tailor chemical attributes on demand and for specific targeted application.<sup>71,72</sup> Pre- and post-synthetic approaches of linker substitutions and additional partial functionalization are feasible.<sup>73</sup>

Accordingly, starting as early as 2002, numerous MOF structures with two or more incorporated linker molecules have been reported for several potential applications.<sup>74</sup> Multiple functional groups of varying ratios have been realized, very instructively by prototypical MOF-5 and eight different linkers, disembodying in first real multivariate (MTV) MOFs in 2010.<sup>75,76</sup> By introducing manifold heterogeneity in MOF materials concurrently maintaining high order, profound implications occurred, as they typically possess properties that do not arise from facile linear combinations of the pure constituents.<sup>76</sup> To bring such modifications to a head, Eddaoudi *et al.* expanded reticular chemistry in MOFs by merged nets approaches for the rational design of intricate mixed-linker MOFs.<sup>77</sup> It now becomes obvious that the sheer infinite chemical flexibility of MOFs gives room for tailoring adsorbents on demand and in a highly application-oriented fashion. Figure 7 depicts a representative of chronological development of MTV-MOFs and exemplary formation process. Even more possibilities arise by a facile attachment of amino-, methyl-, ethyl-, or any other group to one linker, resulting once again in altered chemical attributes and further chemical variegations. The latter tool is named post-synthetic modification (PSM) and it displays an ancillary useful tool for tailoring the surface chemistry of MOFs on demand (see chapter 3.4 for more information). Most PSM approaches modify the chemical attributes of the MOF, more precisely the incorporated linker molecules, by a chemical reaction and attachment of certain moieties to the linker. Nevertheless, any modification after MOF synthesis is called PSM, including the previously mentioned (partial) exchange of linker or cation. The review by Zeng *et al.* focuses on recent advances in PSMs.<sup>78</sup>

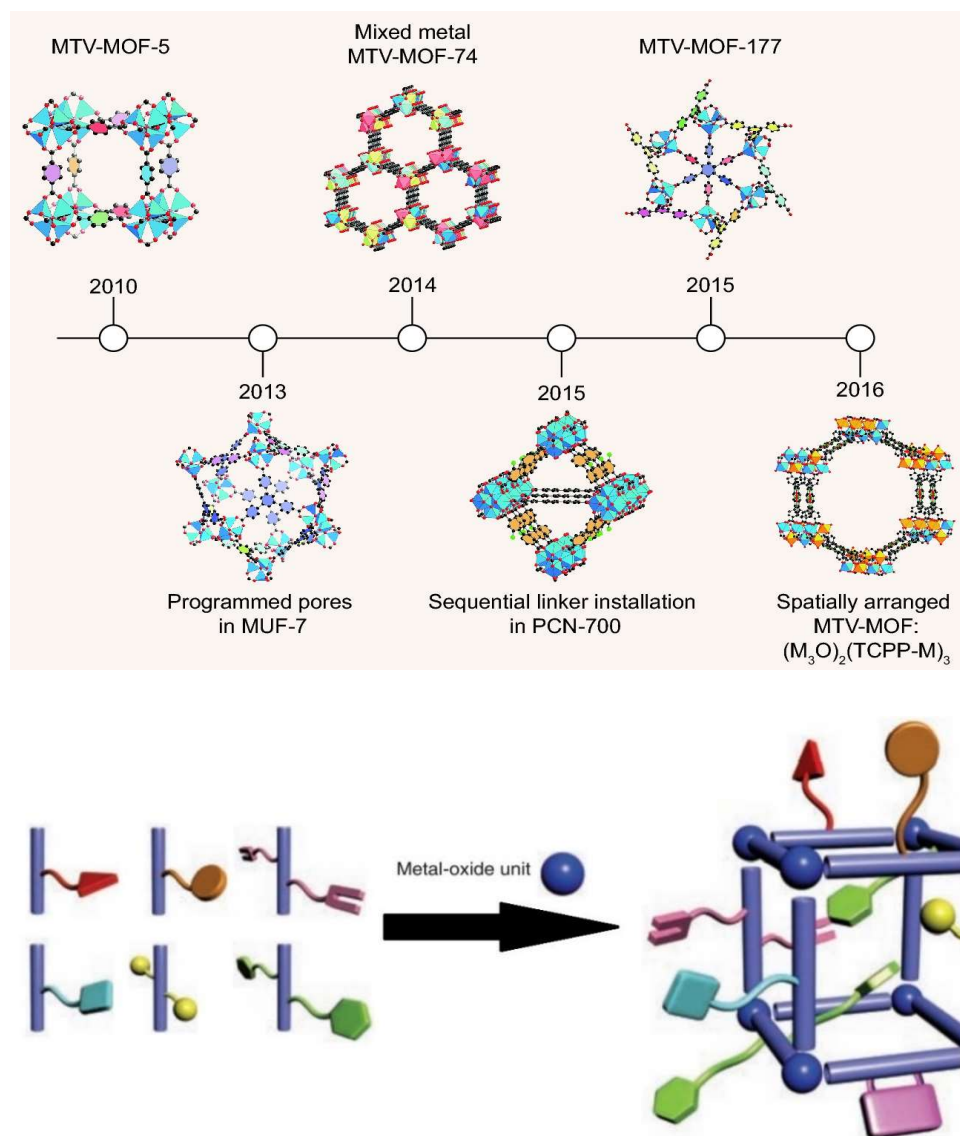


**Figure 7:** Top: Representative discoveries of the multivariate approach for introducing heterogeneity within ordered MOFs. Reprinted from ref. 76 with permission, © 2017, Oxford University Press on behalf of China Science Publishing & Media Ltd.; Bottom: Formation of differently substituted linkers with metal (oxide) unit to an MTV-MOF. Adapted by ref. 75 with permission, © 2010, AAAS.

Crystallite size matters as well, especially regarding ad-/desorption phenomena like kinetics, but also in terms of any other physical-chemical property influencing the adsorption process. Hence nanoparticle (NP) MOFs can significantly differ from bulk materials with order of magnitude varying crystallite sizes.<sup>79</sup>

Isocompositional MOFs (*i.e.* same linker and cation) may show polymorphism, most often in dependence on outer influence factors such as synthesis temperature.<sup>80</sup> Polymorphism is most likely to take place, when both reactants form either the thermodynamic or kinetic product (*e.g.* MIL-101 and MIL-53). The resulting phases may show distinctive differences in chemical properties. Further variegations within MOFs are given by defective MOFs and defect engineering (*cf.* chapter 1.1.2.), extending the infinite chemical playground of MOF compounds even more.

Grafting of MOFs is a tool to alter chemical attributes of MOF crystallite surfaces.<sup>81</sup> Intentional creation of CUS and potentially even selectively saturating CUS with donor molecules in MOFs have been reported, especially for the inclusion of catalytic moieties into MOF (*cf.* Figure 8).

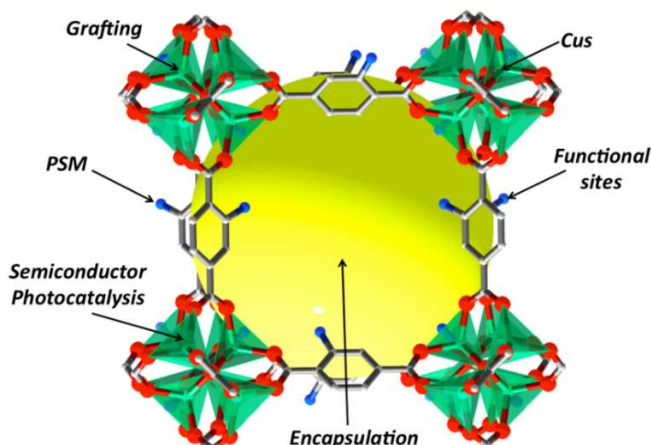


**Figure 8: Different strategies for the inclusion of catalytic moieties into a MOF scaffold. Reprinted from ref. 82 with permission, © 2014, American Chemical Society (ACS).**

Details of chemical variations and other concepts of MOF materials, which are not primarily within the scope of this work, specifically regarding MOF composites (*cf.* chapter 1.3.3), hierarchically structured MOF materials including core-shell composites and many more, can be found in the comprehensive reviews by N. Stock *et al.*, F. Huo *et al.* and by Q. Xu *et al.*<sup>54,83,84</sup> Particularly more promising new class of MOF materials, which may be highlighted, are the rather new class of liquid MOFs, MOF glasses and gels.<sup>85,86</sup> For convenience only it can be concluded that several additional concept and variegations of MOFs are exploited by researchers to tailor MOF properties selectively.

#### 1.1.4. Analytical Characterizations of MOFs

As MOFs are investigated in manifold potential applications (*cf.* chapter 1.3 for more information on applications and accompanied analyses), the analytics of MOFs strongly depend on the utilized property in an intended application. Therefore various chemical analysis techniques have been applied until today. In the following the most important MOF analytics, that were also used within this work, will be highlighted.

PXRD is a common technique of all solid materials that are not amorphous but rather crystalline. Due to the crystalline nature of most MOFs, PXRD is the standard to identify the desired phase after synthesis and generally used as the first instrument in MOF analytics. MOFs can also be semi-amorphous or even amorphous.<sup>85</sup> It may be noted that crystallographic analysis and Rietveld refinement is the most applied tool to resolve crystallographic structures of MOFs, as single crystals of MOFs are most often unattainable due to their polycrystalline nature. PXRD

techniques offer further opportunities such as observation of structural changes upon ad-/desorption of guest molecules or upon other external stimuli like temperature or pressure (*cf.* chapter 1.1.). Additionally PXRD enables the observation of phase transformations, crystallite size dependent reflections and other structural parameters.

Thermogravimetric aalysis (TGA) can be used to determine the behavior of MOFs upon constant heating by measuring mass loss, which is evoked by loss of adsorbed solvent molecules at lower temperatures and structural decomposition at higher temperatures. TGA allows for determination of thermal stability, which typically ranges up to  $T = 200\text{--}450\text{ }^{\circ}\text{C}$  for MOFs, sometimes even higher.<sup>87</sup> TGA can also be used to quantify gas and vapor ad-/desorption by gain/loss of weight upon the corresponding sorption process. The latter process can further be applied in a cyclic fashion to rapidly analyze cycle stability.

Infrared (IR) spectroscopy is generally used to identify molecular elements in terms of their IR vibrational modes and IR absorbance. Hence IR spectroscopy in MOFs can be utilized to, *inter alia*, verify the presence of PSM derived MOF functionalities or trace residual solvent, generally any formed chemical bonds that exhibit distinctive IR absorbance. IR spectroscopy is therefore a useful tool in MOF analytics.

Other analytics used in MOF chemistry are elemental analysis, imaging techniques like scanning electron microscopy (SEM) or transmission electron microscopy (TEM), also Mößbauer spectroscopy (*e.g.* in MOFs with Fe, Ni, Zn). Several more analytics are applied frequently in MOF literature. Whenever expedient, nuclear magnetic resonance (NMR) techniques of several nuclei (*e.g.*  $^1\text{H}$ ,  $^{13}\text{C}$ ,  $^{15}\text{N}$ ) and Raman techniques are commonly utilized in MOFs. Energy-dispersive X-ray spectrometry (EDX) mapping allows for spatially resolved quantification of elements in MOFs and their composites.

Due to the innumerable variety of MOFs together with often unintelligible terminology various approaches of setting up MOF databases,<sup>14,88,89</sup> applying high throughput computational screening,<sup>90,91</sup> further introducing machine learning techniques and prediction models have been described in the literature.<sup>92,93</sup>

Since the key feature of MOFs is their inherent porosity, most important analyses of MOFs are gas and vapor sorption techniques. Such techniques can generally be subdivided in static volumetric methods (*e.g.* determination of isotherms, *cf.* Figure 10) and dynamic measurements (*i.e.* breakthrough experiments). Both methods can be regarded as unique and irreplaceable by each other (*cf.* chapter 1.2.2.). Static volumetric gas sorption, specifically nitrogen sorption ( $T = 77.36\text{ K}$ ; *i.e.* the boiling point of nitrogen and therefore the temperature with no specific thermodynamic force for adsorption or desorption), plays a key role in MOF analytics, as it enables the determination of porosity parameters: specific surface area, pore volume, pore size

distribution and other important key figures of porous materials. The following chapter 1.2 deals with analytical characterization of MOFs utilizing gas and vapor sorption techniques.

## 1.2. Fundamentals of Adsorption

The IUPAC published a technical report on physisorption of gases including classifications of isotherm types in 2015 stating: “Major advances in recent years have made it necessary to update the 1985 IUPAC manual on Reporting Physisorption Data for Gas/Solid Systems”,<sup>94</sup> mainly owed to MOFs and related porous materials.

### 1.2.1. Principles and Theory of Physisorption in Micro-/Mesoporous Adsorbents

The following terms define essential notions within the given thematic area:

*Adsorptive:* Gaseous or liquid molecules, which have not been adsorbed onto the surface yet, hence, can be considered as ‘free’ molecules that only interact with themselves.

*Adsorbent:* Porous, solid phase with external and/or internal surface.

*Adsorbate:* Two component system, consisting of adsorbent and adsorbed molecules

Figure 9 schematically depicts an ad-/desorption process and defines the given terms graphically.

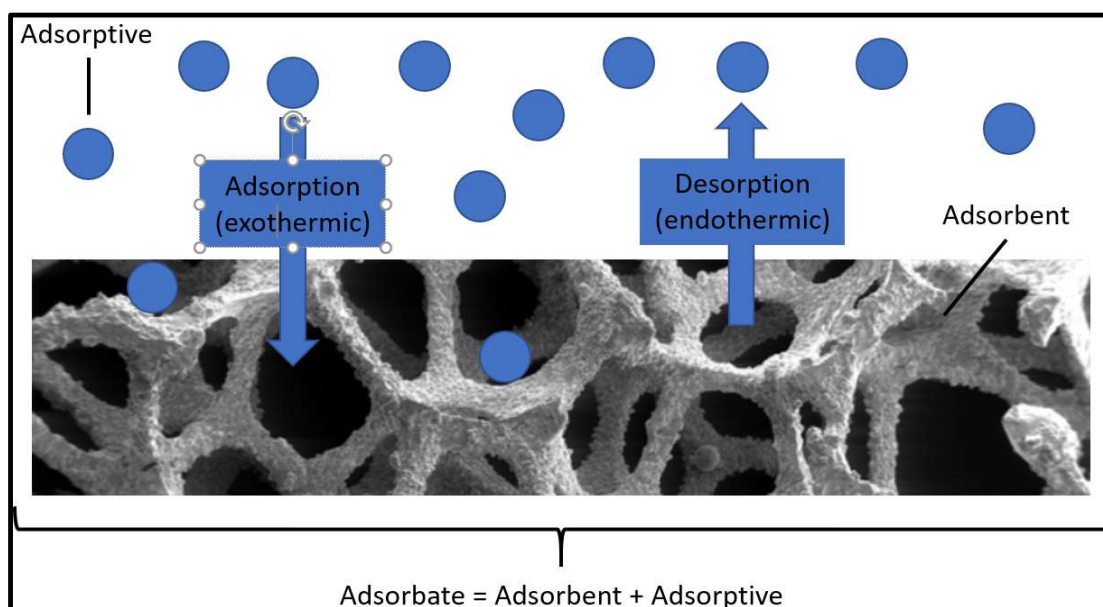


**Figure 9: Ad-/Desorption of a gas (adsorptive) on the surface of a porous media (adsorbent), forming an adsorbate (note: gas molecules and surface depiction not in scale). The adsorbate consists of surface-placed adsorptive molecules, held in place by intermolecular interactions. Adsorption is an exothermic process, desorption an endothermic process.**

In general, gas adsorption can be subdivided into physisorption and chemisorption, additionally by capillary condensation. The fundamental interactive forces of physisorption are determined by van der Waals interactions. Hence, the chemical nature of the adsorbent surface and the adsorptive species remain inert upon the sorption process. Even though the corresponding interaction energies are comparatively low (0.5 eV per adsorbed species or  $< 50 \text{ kJ mol}^{-1}$ ), physisorption plays an important role in nature. Chemisorption often requires activation energy and is mostly going along with irreversibility. Thus, the latter is typically associated with higher binding forces (mostly with formation of new chemical bonds) and significantly higher binding energies of  $50\text{--}450 \text{ kJ mol}^{-1}$ .

For the gas phase it can be assessed that:<sup>95</sup>

Physisorption: binding energy  $\approx 1.5$  enthalpy of evaporation of adsorptive.

Chemisorption: binding energy  $> 2\text{--}3$  enthalpy of evaporation of adsorptive.

Capillary condensation: binding energy  $\approx$  enthalpy of evaporation of adsorptive.

The following paragraphs describe essential terms that must be defined for clarity reasons and comprehensibility of the thesis' scope.

#### *Classification of physisorption isotherms*

Gas adsorption experiments display an import tool for the characterisation of porous solids (see also chapter 1.2.2.). The collection of data within an adsorption process by plotting the partial pressure vs. the gas uptake per adsorbent mass results in isotherms (*cf.* Figure 10). Different pores structures, adsorbent-adsorptive interactions and other factors influence the adsorption process so that different isotherm types can be observed in dependency of the applied adsorbent-adsorptive pair (also in dependency of the temperature). The IUPAC defined the principles and theory of physisorption with respect to gas adsorption and isotherms and offered interpretation of physisorption experimental results in 2015.<sup>94</sup>



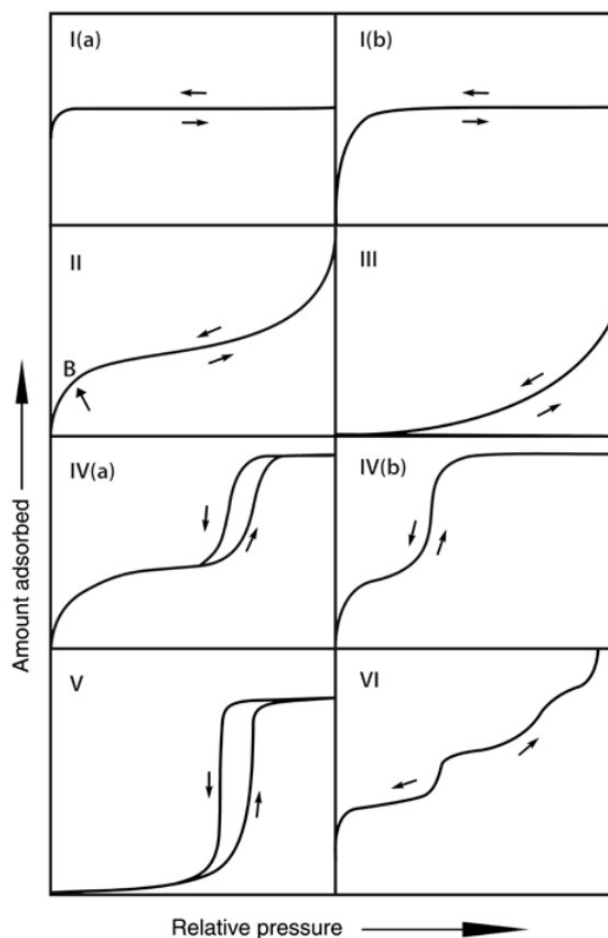


**Figure 10: Classification of physisorption isotherms. Reprinted from ref. 94 with permission, © 2015, De Gruyter.**

The IUPAC states that: Reversible type I isotherms are evoked by microporous solids with relatively small external surfaces. Type I(b) isotherms can be found in materials having pore size distributions over a broader range including wider micropores and possibly narrow mesopores ( $< 2.5$  nm). Reversible Type II isotherms are given by the physisorption of most gases on nonporous or macroporous adsorbents. In the case of a Type III isotherm, the adsorbent-adsorbate interactions are relatively weak, and the adsorbed molecules are clustered around the most favorable sites on the surface of a nonporous or macroporous solid. Type IV isotherms are found for mesoporous adsorbents. In the case of a Type IVa isotherm, capillary condensation is accompanied by hysteresis. This phenomenon occurs when the pore width exceeds a certain critical width, which is dependent on the adsorption system and temperature (*e.g.* for nitrogen and argon adsorption in cylindrical pores at 77 K and 87 K, respectively, hysteresis starts to occur for pores wider than  $\sim 4$  nm). With adsorbents having mesopores of smaller width, completely reversible Type IVb isotherms are observed. In the low partial pressure range, the Type V isotherm shape is very similar to that of Type III and this can be attributed to relatively weak adsorbent-adsorbate interactions. Type V isotherms are observed for water adsorption on

hydrophobic microporous and mesoporous adsorbents. The reversible stepwise Type VI isotherm is representative of layer-by-layer adsorption on a highly uniform nonporous surface.<sup>94</sup>

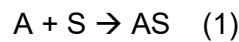
Since the adsorption process and collection of different isotherms required adequate interpretation of physisorption data, researchers developed models to exploit physisorption experiments for surface area assessment, pore size analysis and much more. In the following standard adsorption models implicated assumptions and basic thermodynamics of the process will be explained.

### *Langmuir isotherms and Langmuir surface area*

The Langmuir model, named after American physicist Irvine Langmuir (1881–1957), is the simplest theoretical description of an adsorption isotherm, using the following idealizations:

1. The surface is homogeneous with a large number of identical adsorption sites  $N$ .
2. The adsorbate forms a monolayer on the adsorbent.
3. There is no interaction between adsorbate particles.

The adsorption equilibrium is described with the reactants A (adsorptive) and S (surface adsorption site):



The surface coverage rate of change  $\theta$  for the adsorption process is directly proportional to the partial pressure of A  $p_A$  and to the degree of free adsorption sites  $N(1-\theta)$  on the surface S in the adsorption case, whereas in the desorption case  $\theta$  is proportional to the number of adsorbed gas molecules  $N\theta$ . The rate constants for ad- and desorption are given by  $k_{Ad}$  and  $k_{Des}$  in the respective equations (2) and (3).

$$\frac{d\theta}{dt} = k_{Ad}p_A N(1 - \theta) \quad (2)$$

$$\frac{d\theta}{dt} = -k_{Des}N\theta \quad (3)$$

In the equilibrium case of  $\theta_{ads} = \theta_{des}$  the Langmuir equation can be expressed as:

$$\theta = \frac{1+Kp_A}{Kp_A} \text{ with } K = \frac{k_{Ad}}{k_{Des}} \quad (4)$$

The constant  $K$  is named *Langmuir constant*.

Type I sorption isotherms can be described by the Langmuir equation. A more sophisticated model, which takes multi-layer adsorption into account, is given by the BET model.

### *BET isotherms and BET surface area*

Stephen Brunauer, Paul Emmett and Edward Teller developed in 1938 the BET model in order to take multilayer adsorption into account. The model is based on idealizations of Langmuir, additionally postulating that not only the substrate adsorption site S, but also the adsorbate AS can serve as a site for further adsorbate molecules – in other words: BET takes multilayer formation into account.

The linearized BET equation is given in Formula (5):

$$\frac{1}{W(\frac{p_0}{p}-1)} = \frac{1}{W_m} + \frac{C-1}{W_m C} \frac{p}{p_0} \quad (5)$$

The BET equation requires a linear plot of  $1/[W(p_0/p - 1)]$  against  $p/p_0$  usually in the linear region of  $0.05 < p/p_0 < 0.30$ . The weight of gas molecules in the monolayer  $W_m$  can be calculated from the slope  $s$  and the intercept  $i$  of the linear BET plot:

$$s = \frac{C-1}{W_m C} ; i = \frac{C-1}{W_m C} \quad (6)$$

Consequently, by addition of  $s + i$ , the weight of the monolayer  $W_m$  can be obtained as follows:

$$W_m = \frac{1}{s+i} \quad (7)$$

From  $W_m$  the total surface area  $S_t$  can be calculated with the *Avogadro constant*  $N_A$  and the molar mass  $M$  of the adsorbate (nitrogen):

$$S_t = \frac{W_m N_A A_{CS}}{M} \quad (8)$$

The specific surface area  $S_{BET}$  of the material can be derived by division of  $S_t$  by the weight of the sample  $w$ :

$$S_{BET} = \frac{S_t}{w} \quad (9)$$

Although BET theory for microporous adsorbents can be utilized in the pressure range from  $0.1 < p/p_0 < 0.3$ , it may also be appropriate to calculate surface areas in lower partial pressure regions, especially when microporous adsorbents are characterized (typically calculated in the range from  $0.005 < p/p_0 < 0.1$ ).

### *Pore size distributions and micropore volume*

From adsorption isotherms of comparatively weakly interacting adsorbents like  $N_2$ , Ar or  $CO_2$ , adsorption models can enable to calculate also pore size distributions and micropore volume of

microporous solids by using various models, e.g. the models of Freundlich, Dubinin-Raduskhevich, Dubinin-Astakhov, Barrett-Joyner-Halenda (BJH), or Temkin. The pore-size distributions of mesoporous materials can be obtained by BJH method, which was proposed by E. P. Barrett, L. G. Joyner and P. P. Halenda in 1951.<sup>96</sup>

### *Determination of the Differential Heats of Adsorption*

To gain deeper insights into the ad-/desorption process and underlying energy transfers that occur upon both ad- and desorption, it may be advisable to determine the differential heat of adsorption (HoA)  $\Delta_{ads}H$  from at least two experimentally collected isotherms. Thereby,  $\Delta_{ads}H$  is defined as the energy difference between the state of the system before and after the adsorption of a differential number of particles on that surface, tantamount to the heat that is released, when the adsorptive binds to the adsorbent (*i.e.* exothermic process). Hence,  $\Delta_{ads}H$  can be understood as the molar energy quantity that is released upon the exothermic adsorption process. This method of determining the value of  $\Delta_{ads}H$  enables for exact assessment of released/required heat in adsorption heat transformation (AHT) applications, also in any other ad-/desorption-based device that either rejects  $\Delta H_{ads}$  in the form of heat to the environment or utilizes it (*cf.* chapter 3.2). The attractive interactions within the ad-/desorption process are comparatively weak van-der Waals interactions, hence, typical values of HoA are  $\Delta_{ads}H \leq 50 \text{ kJ mol}^{-1}$ , strongly depending on chemical attributes of adsorptive, adsorbent and temperature boundary conditions. Logically, the most energy will be released at zero coverage of adsorptive, synonymous to *zero coverage*  $\Delta_{ads}H$  which may possibly be  $\Delta_{ads}H > 50 \text{ kJ mol}^{-1}$ , even for gases like  $\text{CO}_2$ .<sup>97</sup> A thorough and comprehensive practical guidance for this calculation of isosteric heat/enthalpy of adsorption from adsorption isotherm branches was very recently provided by colleagues.<sup>98</sup> Summarizing, two – for more precise calculation also three or even more – adsorption branches of experimentally collected isotherms at different but close temperatures with  $\Delta T \leq 20 \text{ K}$  can be fitted with suitable theoretical models. Subsequent mixed-adsorptive calculations by Ideal Adsorbed Solution Theory (IAST) enables to characterize adsorbents energetically more distinctively.

### **1.2.2. Gas Adsorption in MOFs**

Besides nitrogen, several other gases are constantly being investigated as adsorptive in MOFs for various reasons and targeted applications. The following gases are the most used adsorptives in gas storage or gas separation investigations with MOFs (*cf.* chapter 1.3.1).

It may be noted that several gases like Nitrogen,  $\text{CO}_2$  or Argon are typically being measured at its boiling temperature. This is due to the reason that at this point neither thermal force for

adsorption (*i.e.* cold) nor for desorption (*i.e.* heat) affect the ad-/desorption process during isotherm collection. However, it may also be insightful to collect isotherms at elevated and application-oriented temperatures. Both types can be found frequently in the literature.

Interestingly, MOFs can also display exotic and counterintuitive negative gas adsorption, which goes along with desorption upon partial pressure increase.<sup>99</sup> General network design criteria, *e.g.* micromechanics engineering of soft porous crystals,<sup>100,101</sup> furthermore temperature and adsorbate dependencies, have been thoroughly evaluated in this realm.<sup>102,103</sup>

The standard technique for determination of BET surface area and pore volume of micro-mesoporous MOFs is nitrogen sorption at boiling temperature ( $T = 77.36$  K). The principles described within previous chapter 1.2.3. conform to the requirements for calculation of the named porosity parameters from nitrogen ad-/desorption isotherms.

The collection of Argon isotherms requires either liquid Argon, which is rather expensive, or a cryo-cooler that adjusts the boiling temperature of Ar ( $T = 87.3$  K) reliably. While the latter solution is also costly, both display a sound analytic for MOF characterization, as Ar may result in more precise values for microporous adsorbents than Nitrogen sorption.

The collection of CO<sub>2</sub> isotherms is typically performed at its boiling temperature ( $T = 194.7$  K) or at application-oriented elevated temperatures in either ambient range or at higher temperatures that are typically present in gas streams. Not only that CO<sub>2</sub> is a suitable molecule for the fast characterization of microporous adsorbents, CO<sub>2</sub> separation and storage have been main objectives in gas adsorption research of MOFs ever since. The selective adsorption of CO<sub>2</sub> from air or exhaust gases in combination with low regeneration energy input offers a remarkably easy, yet efficient strategy to negative carbon emissions. Quiet logically, there is a constant research effort in the adsorption science related with MOFs and CO<sub>2</sub> separation (*cf.* chapter 1.3.1).

Since the boiling temperature of hydrogen ( $T = 20.28$  K) is significantly lower than those of commonly applied gases, it is not usual to measure hydrogen sorption isotherms at its boiling point. Instead, hydrogen sorption is typically performed at elevated temperatures like  $T = 77.36$  K or even  $T = 0$  °C. Hydrogen storage in MOFs has become a great field of research interest, since, from the beginning of gas adsorption in MOFs, researchers have proven the outstanding potential.<sup>104,105</sup> As a potential energy source like hydrogen, methane has been investigated from the early days of gas adsorption in MOFs.<sup>106,107</sup> CH<sub>4</sub> has to be separated from gas streams which is eventually ambitious, due to elevated temperatures and low adsorbing molecules like CO<sub>2</sub>, ethane, propene or other typical cooperatively adsorbing molecules. CH<sub>4</sub> may also be stored in MOFs at significantly lower pressures in comparison with hydrogen (*cf.* chapter 1.3.1).

The adsorption of other gases like O<sub>2</sub>,<sup>108,109,110</sup> CO,<sup>111,112</sup> NO,<sup>113,114</sup> NO<sub>2</sub>,<sup>113,115,116</sup> SO<sub>2</sub>,<sup>117</sup> NH<sub>3</sub>,<sup>118,119,120</sup> H<sub>2</sub>S,<sup>117,121,122</sup> Xe,<sup>123,124</sup> Kr,<sup>123,125</sup> or SF<sub>6</sub>,<sup>126,127</sup> as well as several other gases, have been reported, nevertheless each single one of these adsorptives display either a rather minor or quiet new part of adsorption research of MOFs. Foremost toxic and harmful gases are in the focus of the gas separation and gas storage research community, due to obvious reasons.<sup>128,129,130,131</sup> In this context, both NO<sub>x</sub> (*i.e.* the sum of nitrogen oxides like NO<sub>2</sub> and NO) and SO<sub>x</sub> (*i.e.* the sum of sulfur oxides SO<sub>2</sub> and SO<sub>3</sub>) may be emphasized in this paragraph, since these gases are combustion products that are emitted into the atmosphere within flue gas, therewith environmentally relevant. Especially NO<sub>2</sub> is recently gaining more attraction, as it is one interesting pollutant adsorptive, that forms in any flame and combustion process, and for a better air quality it needs to be filtrated as such. MOFs have been proven to withstand multiple NO<sub>2</sub> ad-/desorption cycles, also to separate NO<sub>2</sub> from CO<sub>2</sub>, N<sub>2</sub> and SO<sub>2</sub> selectively, even under humid conditions. These attributes render, once again, the subclass of MOFs as very promising material class and, moreover, as alternative to common NO<sub>2</sub> filtration and capture techniques, which often convert NO<sub>2</sub> into nitric acid and mostly require agents like urea or impregnated activated carbons. Accordingly, MOFs nowadays come to the fore of gas pollutant separation, especially by chemical separation of SO<sub>2</sub> and NO<sub>2</sub>. Gaseous pollutants possess a potential risk for humans and aquatic life, but also to sensitive applications like fuel cells, where the membranes and catalyst need to be protected from such molecules. One future application that requires highest standards in air quality is the fuel cell vehicle, because of the sensitivity of membranes and electrode catalysts. MOFs could well play a role in such a sophisticated gas separation application, but they will have to prove their potential in gaseous pollutant abatement at highly dynamic conditions (*e.g.* high air volume flows, varying pollutant molecules and concentrations, varying humidity, pollutant peaks *e.g.* in a tunnel or traffic jam).

In this context, it is obvious that co-adsorption of different gas molecules in an exhaust stream, in air or any other gaseous media, is the key factor for appropriate separation. The high chemical flexibility of MOFs paired with suitable pore sizes have brought various researchers to innumerable experiments and valuable insights into gas/gas separation and co-adsorption.<sup>132</sup>

### *Dynamic measurements*

The adsorption process does not necessarily have to be carried out in a static volumetric fashion. Contrary to the isotherm measurements explained above, alternative breakthrough experiments give further insights into gas and vapor sorption processes of MOFs. Breakthrough measurements result in material-specific properties as well. It must be highlighted that the dynamic adsorption process is influenced multifactorial in principle. The influencing factors from isotherm measurements are mainly adsorbent-adsorptive interactions (*cf.* chapter 1.2.1: HoA)

temperature, pressure and adsorbent grain size (meaning kinetic accessibility of adsorptive, *i.e.* diffusivity). However, additional factors influence dynamic adsorption. These are, *inter alia*, volumetric flow, humidity, adsorptive concentration(s) (*i.e.* partial pressure(s)), co-adsorption of other molecules present in the adsorptive mixture, dwell time of adsorptive, all directly influencing diffusion, kinetics and ultimately also uptake capacities, just to name a few. Consequently, material properties determined by isotherms do not exigently have to coincide with those from breakthrough experiments.

Since most gas or vapor adsorption applications utilize MOFs in a flow through manner, for example in a filter, breakthrough experiments can be designated as highly practically relevant.

### 1.2.3. Water Vapor Adsorption in MOFs

Besides gas sorption, MOFs are gaining notable attention in the field of vapor sorption, superficially water vapor sorption. The steep and stepwise uptake at low relative pressures with high uptake capacity make MOFs eligible for humidity control, desiccant tasks, heat reallocation, air conditioning, water harvesting from atmospheric humidity and related techniques.<sup>133</sup> MOFs easily outperform common water adsorbents in their uptake and there is no end in sight. The latest record uptake with ca. 200 wt.% water in the MOF cavities, corresponding to 1.95 g g<sup>-1</sup>, was set in 2018 by highly porous chromium-based MOF with *soc*-topology, namely Cr-*soc*-MOF-1.<sup>134</sup> Governing parameters in this realm is mainly accessible void volume, additionally hydrophilicity of linker and metal centres, for instance CUS, play a role.

One crucial adsorbent attribute that comes with water sorption is hydrothermal stability. Before any MOF can be considered for adsorbent in a practical water sorption application, it must be assessed as hydrothermally robust. Multi-cyclic water sorption measurements that consist of repeated and subsequent collection of single data points for adsorption and desorption reveal possible fading in adsorption capacity. Cyclic *in-situ* PXRD measurements that subsequently apply dry and humid conditions are a valuable tool to monitor structural changes both upon ad-/desorption, but also due to structural degradation upon cycling. It could be shown that upmost MOFs degrade upon exposure of varying degree of moisture. The underlying degradation mechanisms are most often dominated by hydrolysis of the metal-ligand bond, as carboxylate-metal bonds appear to be vulnerable for this reaction. One strategy to strengthen the metal ion-ligand bond and obtain highly hydrolytically stable MOFs, simply by increasing electrostatic interactions between linker and metal node, is the use of high-valence metal ions like Al<sup>3+</sup> (*e.g.* Al<sub>3</sub>MOF-2, CAU-10-H, MIL-100, MIL-160), Cr<sup>3+</sup> (*e.g.* MIL-100, MIL-101, Cr-*soc*-MOF-1), Fe<sup>3+</sup> (*e.g.* MIL-100, MIL-88A, MIL-88B), Ti<sup>4+</sup> (*e.g.* NH<sub>2</sub>-MIL-125, MIL-125) or Zr<sup>4+</sup> (*e.g.* UiO-66, MOF-801 (*i.e.* zirconium fumarate), MOF-808). However, it should be ascertained that no liker-

or cluster-defects are apparent in the MOF structure. Defects may and may not result in increased liability of the MOF structure and they are especially present in MOFs with cations from group IV (as in the case of Zr- or Ti-MOFs),<sup>135,136</sup> but also in other MOFs.<sup>137</sup>

Concludingly, MOFs can serve as simple desiccants, equating to task fields that are typically conquered by drying agents made of silica materials. In this context, they can also be applied in more complex desiccant devices like a desiccant rotor.<sup>138</sup> Alternatively, MOFs exhibit promising properties as heat-transforming adsorbents (*cf.* chapter 1.3.2.) and can therefore be implemented into AHT devices.

Since this thesis does not tackle any vapor sorption except for water, the paragraph solely sums up the most interesting and typically applied vapor sorption adsorptives. These imply most common alcohols like methanol and ethanol, both also in the AHT context (*cf.* chapter 1.3.2.).<sup>139</sup> Moreover, there are reports on several other organic vapors and volatile organic compounds (VOCs), such as toluene, xylene and other. Dynamic Vapor Sorption (DVS) enables for energetic, kinetic, and cyclic characterization of adsorbents.



### 1.3. Potential applications of MOFs

The conceivable range of applications of MOFs is wide-ranging (*cf.* Figure 11). Although MOFs have been proven to display various advantages over crystalline materials and carbon-based porous matters, their industrial utilization has been impeded for years. This deceleration of MOF implementation into commonplace devices and industrial applications is attributed to several drawbacks. While the properties of MOFs can be claimed as highly auspicious, their synthetic conditions, stabilities, production efforts, along with production costs and several other factors retard their utilizations lastingly.

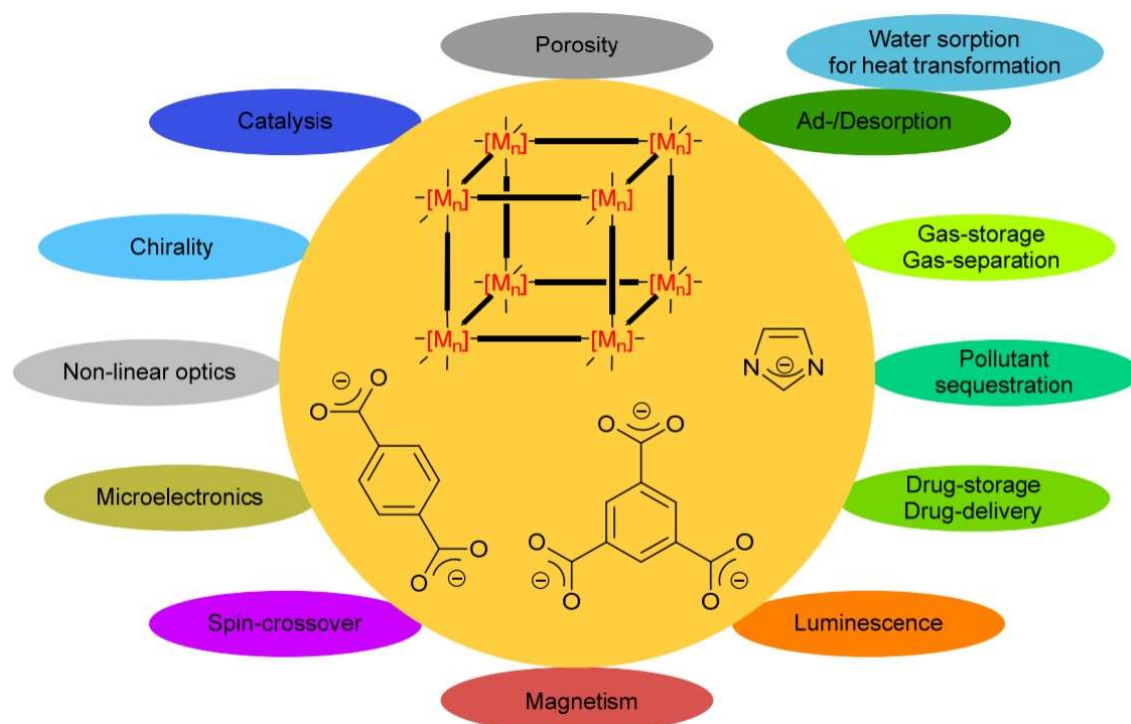


**Figure 11: Outer sphere: Thematic fields of potential applications of MOFs. Inner circle: Prototypic linker molecules and exemplary schematic representation of MOF structure. Adapted by ref. 20 with permission, © 2012, Royal Society of Chemistry.<sup>140</sup>**

In the following subchapters practical applications with most promising chances for prospective utilization are illuminated comprehensively, consistent with the thesis' thematic focus.

#### 1.3.1. Gas Storage and Separation

Since separation efficiencies of these developing technologies depend on internal porosity and surface properties of adsorbents, MOFs display a flourishing class for gas separation and purification.<sup>141,142</sup> Membrane-based separation techniques like mixed-matrix membranes (MMMs) and surface-assisted membranes have the potential to drastically decrease the global energy use, emissions, pollution and ultimately carbon footprint and sustainability within such industrialized processes like gas/gas separation techniques.<sup>143,144</sup> Hence, MOF-based MMMs, but

also adsorber chambers filled with MOF or liquid MOFs can contribute to such ambitious gas separation targets.<sup>86,145</sup>

In general, the previously mentioned separations of pollutants like SO<sub>2</sub> and NO<sub>2</sub>, moreover CO, NO, NH<sub>3</sub> and other exhaust gases from combustion processes remain in the focus of gas separation research within the MOF community. Particularly CO<sub>2</sub> is an adsorptive of modern interest and MOF materials are one class of adsorbents that nowadays already compete with industrial performance materials. Potential candidates for CO<sub>2</sub> separation are amine-based CO<sub>2</sub> ad-/desorption techniques like aminated cellulose, aminated silica, Lewatit® VP OC 1065 (LANXESS AG) and porous amine-based materials in general. Especially moisture displays an additional challenge, as water is a rather good candidate for co-adsorption with CO<sub>2</sub>.<sup>146</sup> As mentioned before, one other adsorptive of interest with respect to separation and storage is methane. On the one hand the presence of CH<sub>4</sub> in gas streams of biomass upgrading, natural gas or exhaust gases requires sufficient separation, on the other hand CH<sub>4</sub> is of interest as a valuable energy carrier. Additionally, CH<sub>4</sub> is one main greenhouse gas which needs to be filtered/separated properly. It may not be overlooked that also other industrially relevant binary gas separations, for instance N<sub>2</sub>/O<sub>2</sub>, N<sub>2</sub>/CO<sub>2</sub>, H<sub>2</sub>/CH<sub>4</sub>, CH<sub>4</sub>/CO<sub>2</sub>, and many others are investigated constantly.

Conclusively, adsorptive removal is a most elegant, at the same time facile method to segregate two or more gas components from each other and MOFs beneficially enable researchers to tailor their adsorption properties. Though gas/vapor separations are widely foregone herein, they are also a viable part of present research activities in the MOF community.

Of high industrial relevance and specifically in the focus of researchers are the gas/gas separations of acetylene/ethylene,<sup>147,148</sup> ethane/ethylene,<sup>149,150</sup> propane/propylene,<sup>151,152</sup> and other hydrocarbon mixtures.<sup>153,154</sup> Each one of these separations displays a great challenge to both chemical engineers and adsorbents. Since the chemical nature of the named gases is very close, such gas mixtures are generally hard to segregate. However, MOFs once again prove to be one superior material in numerous gas/gas and gas/vapor separations.

### 1.3.2. Adsorption-Driven Heat Transformation

The exploitation of heat of adsorption (HoA)  $\Delta_{ads}H$  as usable heat, respectively cold in the reverse desorption process, gives rise to various heating and cooling applications. MOFs can reliably function as adsorbents in several thinkable AHT devices and are constantly being evaluated within this realm. Once again, MOFs compete with other commercially available porous materials like zeolites.<sup>155</sup> Wide-ranging overviews on advances in AHT applications utilizing MOFs as

adsorbents have exemplarily been provided by C. Janiak *et al.*,<sup>156</sup> by F. Kapteijn *et al.*,<sup>139,157</sup> by K. S. Walton *et al.*<sup>158</sup>

Figure 12 depicts a typical 2-step process applied in adsorption heat pumps (AHPs) or thermally driven chillers (TDCs).

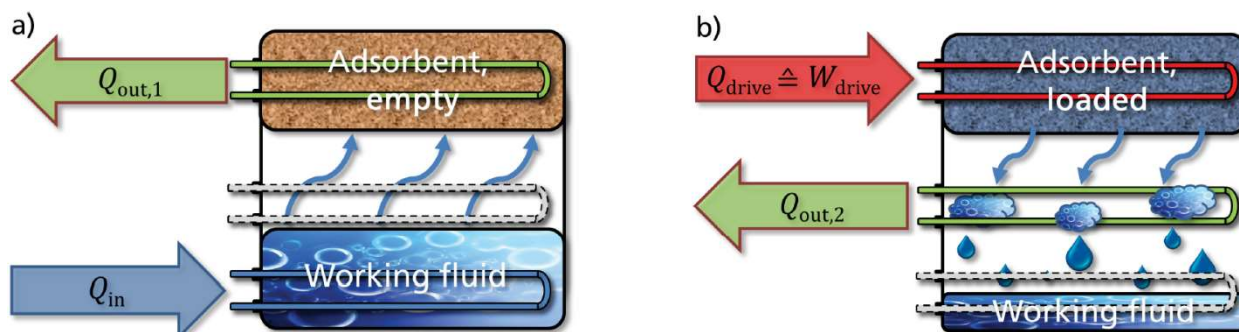


**Figure 12: Working scheme of a sorption heat pump during the working step (a) and the regeneration step (b).** The amounts of energy assigned to each sub-process are in accordance with the labelling of Figure 2. Temperature levels are transliterated using different colors (cold, medium, and hot). Adapted from ref. 67 with permission, © 2012, Royal Society of Chemistry.<sup>159</sup>

Such a device can serve both as a heat pump and as a chiller, depending on the way it is utilized. The heat flows are specified in Table 1.

**Table 1: Heat sources for sorption-based heat pumps and chillers.**

Symbol in Figure 12	Heat of...	Heat pump mode	Chiller mode
$Q_{in}$	vaporization	from environment	useful cold
$Q_{out,1}$	adsorption	useful heat	rejected to environment
$Q_{drive}$	desorption	driving heat, externally supplied (solar, waste, gas...)	
$Q_{out,2}$	condensation	useful heat	rejected to environment

Due to obvious reasons like toxicology, availableness and many more, the most suitable refrigerant in an AHT device will be water. Beneficially, water possesses a comparably high heat of vaporization (HoV,  $\Delta_{vap}H = 40.8$  kJ/mol or 2.26 kJ/kg) amongst eligible refrigerants. Nevertheless, MOFs are also in the focus as adsorbents in AHT applications that apply alcohols as adsorptive, foremost methanol ( $\Delta_{vap}H = 35.2$  kJ/mol) and ethanol ( $\Delta_{vap}H = 38.6$  kJ/mol).<sup>139,160</sup>



**Figure 13: Experimental setup for the illustration of the working cycle in a TDC or AHP. Left: Picture of the apparatus before opening the manual valve. Right: Infrared photograph after opening the manual valve, indicating temperatures of  $T < -5\text{ }^{\circ}\text{C}$  in the water reservoir and  $T > 40\text{ }^{\circ}\text{C}$  in the sorption material. Reprinted from ref. 161 with permission, © 2013, Schweizerische Chemische Gesellschaft.**

Also, the water harvesting capability of MOFs has been proposed and investigated.<sup>162</sup> The proof of concept (*i.e.* that MOFs can trap water from low-RH air in a real environmental setup and ultimately obtain liquid water) has been demonstrated with a simple device by Yaghi *et. al.* in 2017.<sup>163,164</sup> Since then, manifold contributions tackled this topic predominantly under low-RH condition respectively in arid regions by creation and evaluation of novel materials for water harvesters.<sup>165,166,167,168,169</sup> Very recently, Yaghi *et. al.* vividly reported on MOF harvesters and presented a solution to the global water challenge utilizing MOFs “for water harvesting from air, anywhere, anytime”.<sup>170,171</sup>

It is obvious that in any AHT or dehumidification device like a desiccant rotor, the MOF adsorbents need to possess high HoA, hydrothermal stability, abundancy and non-toxicity of metal and linker, scalability and sustainability of MOF synthesis, finally affordability. Prototypic MOFs that meet these requirements are aluminum fumarate (Alfum),<sup>172,173</sup> CAU-10-H,<sup>174</sup> MIL-53-TDC,<sup>175,176</sup> CAU-23,<sup>177</sup> MIL-100,<sup>67</sup> MIL-101,<sup>178,179</sup> NH<sub>2</sub>-MIL-125,<sup>180,181</sup> and other high-valent Al-, Cr-, Fe-, Ti-, or Zr-based di/tricarboxylic acid-MOFs (*cf.* chapter 1.2.3).

In this context, the sufficient transport of mass (here: water) *and* heat is widely unlighted until today, yet incredibly important for applications, since occurring/applied heat needs to be reallocated fast enough to not hinder the adsorption process, respectively facilitate desorption properly.<sup>133</sup> Essential rate determining factors are primarily the thickness of MOF layer on a heat exchanger, thermal transport coefficients (*e.g.* thermal conductivity or technical connection to the heating/cooling plate) and kinetics of the underlying processes.

### 1.3.3. Other Potential Applications of MOFs

Details of all potential applications of MOF materials which are not primarily within the scope of this work can be found in various literature contributions on MOF applications. Comprehensive reviews are given for example by O. M. Yaghi *et al.*,<sup>182</sup> by H.-C. Zhou *et al.*,<sup>183</sup> by G. Z. Chen *et al.*,<sup>184</sup> and by C. Janiak *et al.*.<sup>20</sup> The following section highlights miscellaneous promising MOF applications. It may be noted that MOF applications are gaining increasing attention within the last years, also due to major research progress. Nevertheless, it has in turns to be recorded that for more than ten years the breakthrough of MOFs in real technical applications has not been seen. Obviously, the promising attributes of inherent porosity of MOFs with near infinite scope of flexibility in tailoring material properties strengthen researchers' aspirations towards MOF applications. Some potential market segments for MOFs appear to be more suitable than others. Figure 14 depicts a risk analysis of different MOF market segments published in a position paper in Germany in 2013.

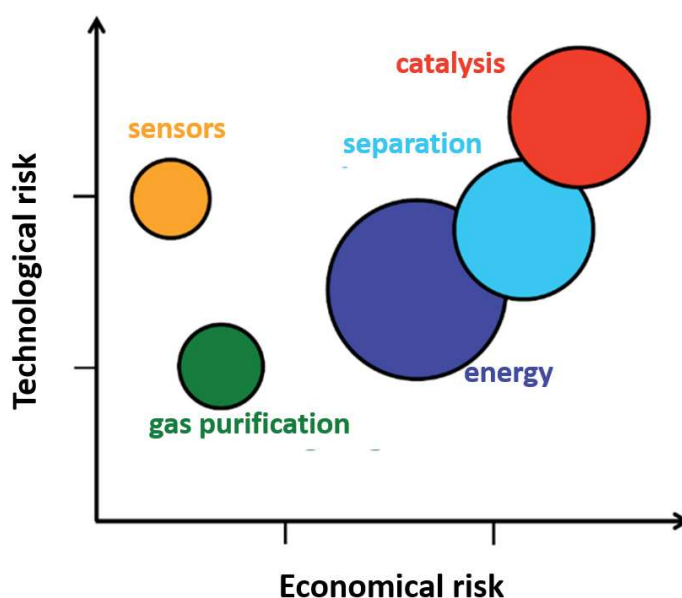


**Figure 14: Risk analysis of different market segments (results from German expert workshop 2013, sizes of circles should correlate to the size of potential market segments). Adapted by ref. 185.**

#### 1.3.3.1. MOF Composites

The polycrystalline nature of MOFs results in powder-like materials after most MOF syntheses, so that a shaping process may be inevitable for utilization. MOF-polymer hybrid materials can solve the problem of inherently crystalline MOF materials and their powdery appearance, which typically goes along with bad processability.<sup>186</sup> Efforts towards the shaping of MOFs are extensively being investigated and they may lead to monolithic structures, granules, coated surfaces, and other moldings. To clarify the umbrella term MOF composite, it must be stated that not only hybrid polymer-MOF materials but any combination of MOF with another material is

denoted as MOF composite: nanoparticle-MOF,<sup>187</sup> quantum dots-MOF,<sup>188</sup> (inorganic) salt-MOF,<sup>189</sup> IL-MOF,<sup>190</sup> carbon-based (e.g. graphene or graphene oxide, nanorods and nanotubes etc.) composites,<sup>191</sup> fiber-MOF composites,<sup>192</sup> core-shell composites like MOF@COF,<sup>193</sup> MOF@MOF,<sup>194</sup> NP@MOF,<sup>195</sup> and several more combinations of guest@MOF and MOF@host. To complete, not only the presented binary composites have been investigated but also multicomponent composites (e.g. PU/GO/MOF composite)<sup>196,197</sup>

As one general example that fits well in the context of this thesis, the application AHT (*cf.* chapter 1.3.2.) demands for coating of heat exchangers with active material.<sup>172,198,199</sup> Moreover, the combination of two porous materials with porosity on different scales (e.g. the combination of a microporous MOF with a macroporous polymer) results in *hierarchically porous* materials.<sup>200</sup> Such composite materials may also incorporate additional beneficial properties for the targeted application. The prospects for water sorption applications by means of MOF shaping and development of adsorbent materials were constantly reported by colleagues in the last years as well as by an unmanageable number of other researchers.<sup>201,202,203,204,205</sup> Another remarkably interesting example is the use of MOF composites in batteries and supercapacitors,<sup>206,207,208</sup> where they were composites were introduced to exploit porosity of MOFs, coincidentally to mitigate the disadvantageous intrinsically poor electrical conductivity of MOFs.<sup>209</sup>

Overarching reviews on all types of MOF composites can scarcely be found in the literature, simply since this area is too wide-ranging and MOFs are combined with various other materials for research purposes. Nevertheless, lately reviews to be recommended are from S. M. Cohen *et al.*,<sup>186</sup> Q. Xu *et al.*,<sup>210</sup> and also from Y. Wu and co-authors.<sup>211</sup> Reviews with focus on MMMs are given by C. Janiak *et al.*,<sup>212</sup> likewise by Z. P. Smith and co-authors.<sup>213</sup>

### 1.3.3.2. Heterogeneous Catalysis

MOFs can be used for various catalytic purposes and show catalytic function in manifold organic reactions like C1 conversion reactions (*i.e.* conversion of CO, CO<sub>2</sub>, CH<sub>4</sub> etc.),<sup>214</sup> C-H-bond activation,<sup>215</sup> cyanosilylation,<sup>216</sup> polymerization,<sup>217</sup> aqueous azide-alkyne cycloaddition,<sup>218</sup> just to name a few. Multiple other organic reactions that need to be catalyzed have been investigated thoroughly and such investigations remain flourishing, because most standard catalysts are composed of expensive noble-metals and/or their chemical compounds. Enantioselectivity and reversal chemical formations are just two of many aspects in this wide-ranging research area.<sup>219,220</sup> Highly topical is photocatalytic hydrogen evolution with MOFs,<sup>221</sup> as well as photocatalytic CO<sub>2</sub> reduction,<sup>222</sup> as such applications pose enormous challenges and opportunities for mankind that cannot be overstated. Oxygen reduction reaction enqueues in this seminal research,<sup>223</sup> just like water splitting does.<sup>224,225</sup> In the context of sustainability, MOF catalysts have been evaluated

in biomass upgrading towards value-added fine chemicals.<sup>226,227,228</sup> Timely and comprehensive reviews on heterogeneous catalysis performed with MOFs and MOF-derived materials can be found for example by Q. Wang *et al.*,<sup>229</sup> by S. H. Jung *et al.*,<sup>230</sup> by Y. Li *et al.*<sup>231</sup>

#### 1.3.3.3. Electronic Devices and Chemical Sensing

MOFs can serve both as electronic and/or chemical sensors, either by detection or by the transmission of (electro-) chemical signals. Numerous sensing implementations of MOFs can be thought of and have vividly been proposed in the literature. For example, lanthanide MOFs were repeatedly shown to be highly versatile in luminescent sensing and photocatalytic applications.<sup>232,233</sup> Detections of various chemical analytes *via* fluorescence in MOF materials have been proposed for manifold purposes.<sup>234,235, 236</sup> Also real-time humidity sensors,<sup>237</sup> pH and temperature sensors,<sup>238</sup> gas and vapor sensors,<sup>239,240</sup> cation sensors,<sup>241</sup> anion sensors,<sup>242</sup> biomolecule sensors,<sup>243,244</sup> and many more have been reported. Synoptically, the sensing of inconceivable amounts of inorganic and organic substances have been described in literature, including numerous gases, multiple vapors, metal ions, organic ions, (bio-) macromolecules and many more. This fact emphasizes once again the enormous versatility of MOFs for extremely specific tasks, arising from their chemical multiplicity. Just to name a few more very promising fields of interest selectively, proton conductivity,<sup>245</sup> electrical conductivity and magnetism are parts of tremendously more intentional MOF applications.<sup>246,247</sup> Extensive reviews focusing on sensing applications are given by J. Li *et al.*,<sup>248</sup> by V. Safarifard *et al.*,<sup>249</sup> and by R. Ameloot and co-authors.<sup>250</sup>

#### 1.3.3.4. Water Purification

The adsorptive removal of hazardous substances is basically resting upon the same interactions in liquid and gaseous phase (*cf.* chapters 1.2.2. and 1.3.1.).<sup>130</sup> MOFs are under constant investigation as adsorbents for several kinds of wastewater treatment and water quality surveillance, for example in detection of antibiotics.<sup>236,251</sup> Especially MOFs for removal of pollutants and contaminants are gaining increasingly attention.<sup>252,253,254</sup> Water filtration membranes display one elegant way to achieve the desired purification performances in desalination and related processes.<sup>255</sup> Further industrially relevant areas may also include oil/water emulsion separation,<sup>256</sup> wastewater treatment or abatement of dissolved/dispersed nuclear species.<sup>257</sup> Recent reviews on water purification and remediation with MOFs are given by C. Beller *et al.*,<sup>258</sup> by A. El-Shazly *et al.*,<sup>259</sup> furthermore by Y. Yoon and co-authors.<sup>260</sup>

## 2. Assignment of Tasks

Since this thesis is carried out within the course of the project OptiMat, the following subsection sums up the specific targets and tasks of the subprojects from the group of Prof Janiak. The main duties of HHU within the project OptiMat are:

- Synthesis and evaluation of new materials
- Further development of direct coating methods
- Development of MOF composites
- Stability investigations
- Technical syntheses
- Transfer of results
- Project organization and steering

The specific objectives of this thesis are determined by the following:

The synthesis of MOFs can be multifaceted. While a predominant portion of MOFs is synthesized under solvothermal conditions, there are also reports on various other techniques (*cf.* chapter 1.1.2. for detailed information). Descriptions of sustainable MOF syntheses, however, are quite rare in literature and MOF-typical solvothermal routes imply huge amounts of solvent waste, when upscaling the procedures and projecting them to industrial scale. Consequently a growing demand for upscaled synthesis along with sustainable procedures can be registered. The fact that there has only been one MOF synthesized on a large industrial scale, namely aluminum fumarate (Alfum), is ample proof for the obstacles that arise during the upscaling procedures of MOFs. That seems even more true as MOFs and their physical-chemical attributes have been praised in manifold ways and have been proposed for various applications for more than two centuries until now. Accordingly, one rate-determining step for the prospective utilization of MOFs is upscaling and sustainability of MOF syntheses. In this context hydrothermally stable MOFs shall be in the focus of synthesis optimizations in order to promote the intended applications of MOF-based AHT. Within the scope of the present thesis it is intended to find solvent- and energy-saving synthesis routes for water-stable/hydrothermally stable MOFs. After identification of hydrothermally stable platform-MOFs, nominal the three Al-based MOFs Alfum, CAU-10-H and MIL-160, and moreover mesoporous MIL-100(Fe), it is targeted to drastically decrease the amount of solvent needed in their syntheses and to decrease both energy input and time required. These efforts shall result in highly sustainable syntheses for the three prominent representatives of hydrothermally stable Al-MOFs as well as for mesoporous MIL-100(Fe).

Several metal-organic frameworks have been evaluated for their water (vapor) stability. It turned out that probably the upmost MOFs do not exhibit sufficient water stability (more exactly hydrothermal stability) for many intended applications, because nearly all applications contain a



cyclic use of the adsorbent. Hence, even air humidity may cause severe damage to MOF structures and thereby also for the touted porosity properties, consequently for performance. Especially for water-based sorption applications, such as AHT or water harvesting from air humidity, the adsorbent needs to withstand thousands of water vapor ad-/desorption cycles. Therefore, novel hydrothermally stable MOFs have been created by chemical researchers and described in literature. Additionally, the evaluation of novel MOFs for their hydrothermal stability, cyclability and their energy related material properties is an ongoing research in the community. Both factors, finding new materials and evaluating their potential utilization as water vapor adsorbents, play a crucial role for the successful implementation of MOFs in cyclic water sorption applications. Conclusively, one main objective of the present work is the synthesis novel MOF materials and their thorough evaluation for water sorption and heat transformation applications. Therefore, water sorption isotherms shall be collected and considered for both water sorption capacity and energy-related attributes like isosteric heat of adsorption (HoA). The latter shall be deduced by taking isotherms at three different temperatures into account, facilitating a precise characterization of thermal conditions in the intended AHT process. The assessment of MOF materials towards cyclic heat transformation shall also include dependencies of temperature levels under AHP operational conditions and the visualization thereof, valuation of both structural integrity and porosity parameters upon cycling as well as determination of water loading lift and inflection point.

The ongoing research with MOFs in focus as SO<sub>2</sub> adsorbents is quite a young research field, nevertheless constantly increasing. This fact is based on a couple of reasons. For example SO<sub>2</sub> adsorption studies and collection of SO<sub>2</sub> isotherms require specially sealed and equipped gas sorption devices, since SO<sub>2</sub> is highly corrosive. The latter is also one reason why this field is rather underdeveloped: MOFs may decay when exposed to SO<sub>2</sub>, especially under humid conditions that appear in a real environmental application and even more with their cyclic usage. Hence, the potential to create valuable contributions to SO<sub>2</sub> sorption is promising and wide-ranged. Therefore, it is intended to determine sorption capacities of the two highly porous MOFs MIL-101(Cr) and NH<sub>2</sub>-MIL-101(Cr). In addition, the amino-moiety of NH<sub>2</sub>-MIL-101(Cr) is targeted for a PSM to create urea-substituted MIL-101(Cr) with different substituents. Thereby, the influence of substituents on SO<sub>2</sub> sorption shall be investigated and reveal possible trends or benefits of PSMs. The comparison of porosity parameters shall be evaluated and taken into consideration regarding total SO<sub>2</sub> sorption capacity. To thoroughly characterize the materials all MOFs shall be measured at two different temperatures and by two CO<sub>2</sub> ad-/desorption isotherms each. The assessment of water vapor ad-/desorption isotherms shall reveal additional trends in hydrophilicity.

The results are presented in the following chapter 3 of this thesis. The chapter contains a cumulative of peer-reviewed scientific articles from international journals.

### 3. Cumulative Part

The cumulative part with the following chapters 3.1–3.4. lists up the main results of this dissertation in chronological order of appearance. Each subchapter is dedicated to one peer-reviewed publication, all published in international journals. Each publication is equipped with a short introductory statement, outlining the scope of the specific research, relating it to the present thesis and specifying the author's contribution of work. Additional results that have not been published in peer-reviewed journals until today are presented in chapter 4.

*Note:* All numbers of citations, figures, tables and page numbers in the chapters 3.1–3.4 do not follow the ones given in the rest in this thesis, as the manuscripts are reprints.

The literature contributions that are presented within the scope of this thesis are:

#### 3.1. Microwave-Assisted Dry-Gel Conversion (MW-DGC) – A New Sustainable Route for the Rapid Synthesis of Metal-Organic Frameworks with Solvent Re-Use

N. Tannert, S. Gökpınar, E. Hastürk, S. Nießing and C. Janiak

*Dalton Trans.*, 2018, 47, 9850-9860.

#### 3.2. Evaluation of the Highly Stable Metal-Organic Framework MIL-53(Al)-TDC (TDC = 2,5-Thiophenedicarboxylate) as a New and Promising Adsorbent for Heat Transformation Applications

N. Tannert, S.-J. Ernst, C. Jansen, S. Nießing, S. K. Henninger, H.-J. Bart and C. Janiak

*J. Mater. Chem. A*, 2018, 6, 17706-17712

#### 3.3. Robust Synthesis Routes and Porosity of Al-based Metal-Organic Frameworks Al-fumarate, CAU-10-H and MIL 160

N. Tannert, C. Jansen, S. Nießing and C. Janiak

*Dalton Trans.*, 2019, 48, 2967-2976

#### 3.4. A Series of New Urea-MOFs Obtained *via* Post-Synthetic Modification of NH<sub>2</sub>-MIL-101(Cr): SO<sub>2</sub>, CO<sub>2</sub> and H<sub>2</sub>O Sorption

N. Tannert, Y. Sun, E. Hastürk, S. Nießing and C. Janiak

*Z. Anorg. Allg. Chem.*, 2021, 647, 1124-1130

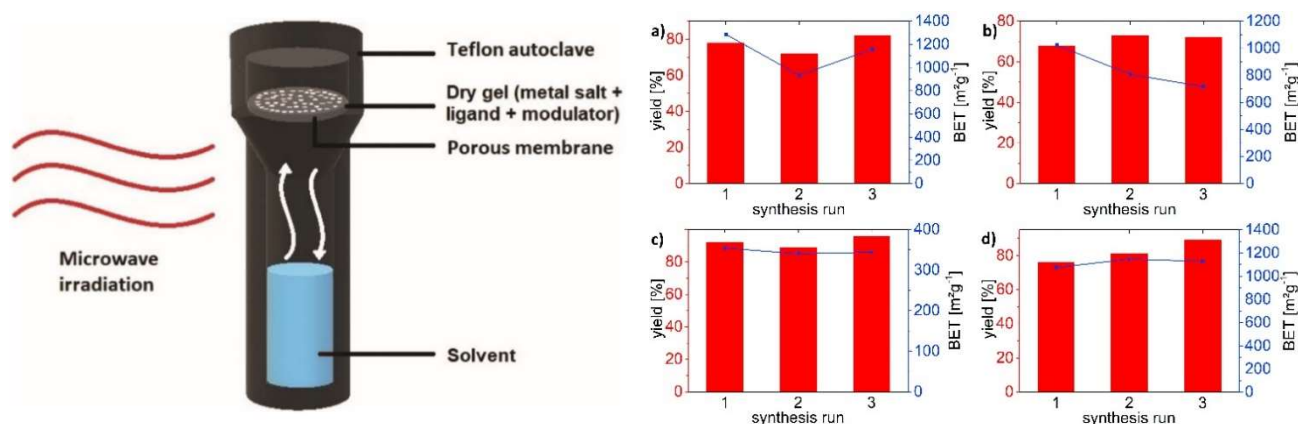
### 3.1. Microwave-Assisted Dry-Gel Conversion (MW-DGC) – A New Sustainable Route for the Rapid Synthesis of Metal-Organic Frameworks with Solvent Re-Use

N. Tannert, S. Gökpınar, E. Hastürk, S. Nießing and C. Janiak

*Dalton Trans.*, 2018, **47**, 9850-9860

DOI: 10.1039/c8dt02029a

Impact factor 2018: 4.052



Author's contribution of work:

- Development of reactors and methods with MIL-100(Fe) for DGC and MW-DGC (with E. Hastürk), transfer of both methods to Al<sub>2</sub>Fu<sub>3</sub> and solvent re-use for both MOFs, all analytical characterizations except for collection of SEM images (done by S. Nießing) and except for the MOFs UiO-66 and MIL-140A (done by S. Gökpınar).
- Writing of the manuscript and drawing of the figures, graphs and tables, except for the MOFs UiO-66 and MIL-140A (done by S. Gökpınar).
- Editing of the manuscript regarding the reviewers' comments, except for the MOFs UiO-66 and MIL-140A (done by S. Gökpınar) with C. Janiak.

Reproduced by permission of The Royal Society of Chemistry.

The following publication describes a novel and sustainable synthesis route for the rapid production of MOFs, namely microwave-assisted dry-gel conversion (MW-DGC). The term MW-DGC was therefore newly introduced to literature in the course of this manuscript. The method was developed by a novel combination of DGC with microwave heating instead of the commonly applied thermal heating. This facile combination was proven to drastically decrease the amount of solvent needed for the synthesis of the four important MOFs MIL-100(Fe) (trade name: Basolite® F300), UiO-66, MIL-140A and aluminum fumarate (Alfum, Basolite® A520). The method allowed the repeated recovery and re-use of the mostly uncontaminated reaction solvent after each MW-DGC synthesis run. Thereby, significant reduction of solvent was proposed and supported by solvent savings calculations in a comparison with the patented Alfum synthesis procedure. The potential of solvent waste savings is visualized by 84 555 L of mother liquor coming from a space – time yield (STY) of  $3615 \text{ kg m}^{-3} \text{ day}^{-1}$  in the patent. For a continuous-flow UiO-66 synthesis with an STY of  $2053 \text{ kg m}^{-3} \text{ day}^{-1}$ , the amount of mother liquor will at least sum up to 59 000 L and amounts to 289 000 L if washing solvents are included. Furthermore, MW-DGC allowed for decreased reaction times and temperatures, correlating with less amount of energy needed. Accordingly, MW-DGC can be claimed as a highly sustainable MOF synthesis method.

In specific, all four MOFs could be synthesized three times each in a MW-DGC setup, while using the same solvent repeatedly. Therefore, the product was replaced with fresh reactant precursor at the head of the container, leaving unchanged solvent left in the bottom of the Teflon vessel. The given quality criteria BET-surface areas, crystallinity (by PXRD) and yields varied within acceptable limits in each case. The comparison of synthesized MOF materials obtained by MW-DGC with commercially available MOFs (Basolite® F300 and Basolite® A520), also with MOFs obtained in a standard solvothermal procedure and moreover with MOFs out of a commonly electric-heated DGC (CE-DGC) synthesis. Especially the latter comparison revealed that MW-DGC holds the potential to drastically decrease reaction times and reaction temperatures, hence, also decrease energy input needed. The method also shows up a path towards control for the selective synthesis of the two isomorphous MOFs MIL-140A and UiO-66. Additionally, MW-DGC offers one step towards safer synthesis conditions in the case of MIL-100(Fe).

Noteworthy, MW-DGC also reproducibly leads to a hierarchical micro-/mesoporous Alfum material, making it unique and different to those from any other synthesis method described. This attribute of porosity across the micro- and mesoporous regime is termed hierarchical porosity and has not been described for Alfum before. The hierarchical porosity could be demonstrated by a comparative nitrogen sorption and pore size analysis of Alfum materials, revealing a prominent hysteresis loop in the region  $pp_0^{-1} > 0.7$ . While the latter is typically going along with mesoporous characteristics, the found bimodal isotherm has supportively been described in the literature for the gel-like formation of MOFs. Consequently, the highly reproducible pore width distribution for

Alfum products from MW-DGC showed a pronounced and narrow mesoporous contribution of 5 – 11 nm. However, typical syntheses of hierarchical porous MOFs include addition of surfactants or templates, while hierarchically porous Alfum was solely derived by the MW-DGC synthesis method and without such modifiers in this case.


In conclusion, MW-DGC was proven synthesize MOFs in an extremely fast, safe, good-yield and energy-reduced procedure and in qualities comparable to the literature or commercial MOF materials. The environmentally and economically optimized syntheses of the selected prototypical MOFs give rise to the expanding the synthesis technique towards other MOFs, upscaling experiments and sustainable MOF syntheses in general. The reproducibly obtainable and unique hierarchical porosity of Alfum from MW-DGC give rise to porosity modulations of Alfum substrates in general.

## PAPER



Cite this: *Dalton Trans.*, 2018, **47**, 9850  
 Accepted 29th June 2018  
 DOI: 10.1039/c8dt02029a  
 rsc.li/dalton

## Microwave-assisted dry-gel conversion-a new sustainable route for the rapid synthesis of metal–organic frameworks with solvent re-use†

Niels Tannert,‡ Serkan Gökpinar,‡ Emrah Hastürk, Sandra Nießing and Christoph Janiak  \*

Microwave-assisted dry-gel conversion (MW-DGC) combines the advantages of concentrated reactants in DGC with fast heating by microwave irradiation. This novel combination allows drastically decreasing the amount of solvent needed for synthesis and reaction times with the energy needed. Furthermore, MW-DGC allows for the recovery and re-use of the reaction solvent and thereby can significantly reduce the overall solvent waste in the syntheses of the four important MOFs MIL-100(Fe) (*Basolite F300*), UiO-66, MIL-140A and aluminium fumarate (Alfum, *Basolite A520*). All the MOF products obtained from MW-DGC showed satisfying yields, crystallinity and porosity in comparison with the industrial benchmarks *Basolite F300* and *Basolite A520*. Moreover, MW-DGC also advantageously leads to a hierarchical micro-mesoporous Alfum material different to that from other synthesis methods.

Received 18th May 2018,  
 Accepted 29th June 2018  
 DOI: 10.1039/c8dt02029a  
 rsc.li/dalton

## Introduction

Metal–organic frameworks (MOFs) have gained considerable attention in recent years due to their high and designable inner surface as permanently porous, crystalline materials, built up by metal ions and bridging organic ligands (“linkers”).<sup>1</sup> MOFs have been investigated for potential applications in the field of catalysis,<sup>2,3</sup> sensing,<sup>4</sup> gas separation<sup>5,6</sup> and storage,<sup>7</sup> drug delivery,<sup>8</sup> cyclic adsorption processes,<sup>9</sup> and many more. MOFs are ascribed to be easily tunable by the choice of metal<sup>10</sup> and linker<sup>11</sup> to modulate their properties.<sup>12,13</sup>

Still, some major challenges for the preparation of MOFs remain: faster, scaled-up syntheses and easier purification/activation procedures that are accompanied by sustainability.<sup>14–21</sup> Recently, Reinsch stated that the accessibility of MOFs will always be limited by the sustainability of the synthesis procedure.<sup>22</sup> The stated space–time yields in the literature do not take into account the economic and ecological aspects of the enormous amounts of mother liquor needed and solvent waste

produced. Another recent contribution to optimized MOF synthesis claims that economic and sustainable strategies are imperative for promoting MOF materials for large-scale industrial use.<sup>23</sup>

The synthetic conditions often appear to be quite harsh (*i.e.* solvo/hydrothermal, use of hydrofluoric acid (HF) or other acidic modulators) and time- and energy-consuming. While mechano-chemical<sup>24,25</sup> or supercritical processing<sup>26</sup> as well as continuous-flow<sup>17,27</sup> methods can be considered as already established in the synthesis of MOFs, the research towards achieving optimized synthetic procedures is still growing rapidly. In order to improve the energy-related issues and further reduce the environmental impacts,<sup>28</sup> while obtaining materials with the maximized performance and minimized undesirable implications,<sup>29</sup> we chose dry-gel conversion (DGC) as an interesting solvent-saving synthesis method for MOFs.

Scheme 1 illustrates the working principle of DGC under microwave irradiation (MW-DGC). The starting materials were placed on a sieve or porous support at the top of an autoclave container, and a small amount of solvent is placed at the bottom of this vessel.<sup>30</sup> By separation of the solvent and reactant mixture, the solvent can be recovered with little contamination and then used again for further reaction runs.<sup>31</sup> Solvent re-use is a very important aspect, since industry generally prefers such environmental and economic improvements in product syntheses. Other advantages of DGC techniques are the reduced solvent amounts, high yields and minimized reactor size.<sup>32</sup>

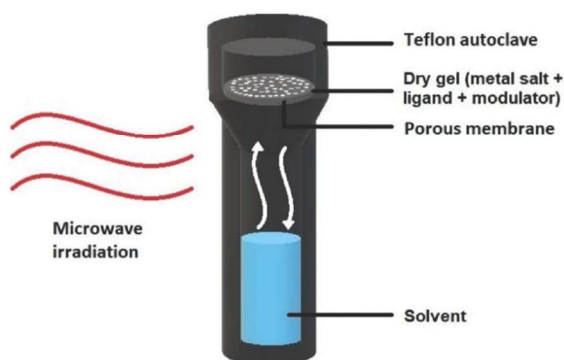
Institut für Anorganische Chemie und Strukturchemie, Heinrich-Heine-Universität Düsseldorf, Universitätsstr. 1, 40204 Düsseldorf, Germany.

E-mail: janiak@uni-duesseldorf.de

† Electronic supplementary information (ESI) available: Details of materials and methods, syntheses, optimizations, work-up procedures, additional PXRDs, nitrogen sorption analyses, SEM, TGA. See DOI: 10.1039/c8dt02029a

‡ These authors contributed equally.





**Scheme 1** Schematic drawing of the reactor set-up for microwave-assisted dry-gel conversion (MW-DGC).

To date, there are only a few reports for MOF synthesis using the DGC-concept.<sup>31–38</sup> These reports point to the advantages of DGC regarding the reduced reaction time<sup>32</sup> and solvent re-use,<sup>31</sup> compared to a conventionally heated solvothermal synthesis.

Microwave-assisted syntheses can further overcome time and energy issues and they are already well-established in synthetic chemistry but are still emerging for MOF syntheses.<sup>39–41</sup> In contrast to conductive heating, microwave radiation directly heats the reaction mixture and not primarily the vessel; hence, it is the reaction mixture that absorbs the microwave energy. This leads to localized superheating with very fast and efficient heating rates so that the desired temperatures are reached within seconds.<sup>42–45</sup> To the best of our knowledge, there has been no report yet on the production of MOFs using DGC in a microwave, with the original concept coming from zeolite synthesis.<sup>14,46</sup>

For the synthesis of MOFs in a microwave oven, the induction times are shortened and the rate constants are substantially increased.<sup>20</sup> In their 2012 review, Stock and Biswas list 25 MOFs prepared through microwave-assisted synthesis.<sup>14</sup> The combination of microfluidics with *e.g.* microwave synthesis may be an interesting efficient method for the large-scale production of MOFs.<sup>47</sup> HKUST-1, UiO-66 and MIL-53(Al) were already prepared in larger amounts and with a high space-time yield also through microwave-assisted heating.<sup>48</sup> Thereby, a continuous-flow microwave synthesis of MOFs as a potential highly efficient method for large-scale production was presented.<sup>48</sup> Furthermore, a recent review points out that microwave MOF synthesis can be considered extremely promising, as being associated with reduced reaction time and reduced process energy consumption, being also able to influence the MOF phase, crystal size, morphology and surface area, as well as being amenable to post-synthetic modifications of MOFs and scale up towards industrial-size microwave reactors.<sup>49</sup>

Besides extensive synthesis optimizations, one challenge was to ensure that microwave heating of the two compartments in the container (*i.e.* the reactants/dry-gel and solvent) occurs equally. However, the microwave absorption efficiency of organic solvents<sup>50</sup> is different from inorganic salts. As a conse-

quence, overheating of the solid salt/linker reactants with decomposition occurred initially at higher pre-set temperatures in our hands, because the organic solvent was not heated to evaporation. We show here that this problem could be overcome by the addition of an ionic liquid (IL). ILs have a high absorption efficiency of microwave energy due to their ionic character, high polarity and high dielectric constant.<sup>51</sup>

In the following, we report the first syntheses of four MOFs by DGC under microwave irradiation with solvent re-use.

## Experimental

### Materials and instrumentation

All the chemicals were used as received by suppliers. For further information about all the materials see section S1 in the ESI†.

Powder X-ray diffractometry (PXRD) was performed at ambient temperature on a *D2 Phaser* (Bruker, Billerica, US) using Cu-K $\alpha$  radiation ( $\lambda = 1.54182 \text{ \AA}$ ) in the range  $5^\circ < 2\theta < 50^\circ$  with a scanning rate of  $0.0125^\circ \text{ s}^{-1}$  (300 W, 30 kV, 10 mA). Analyses of the diffractograms were carried out with *Match 3.11* software.

Thermogravimetric analysis (TGA) was carried out on a *Netzsch TG209 F3 Tarsus* (Netzsch, Selb, Germany) device under a synthetic air atmosphere, ramping at  $5 \text{ K min}^{-1}$  to  $600^\circ \text{C}$ .

SEM images were acquired on a *JEOL JSM-6510 Advanced electron microscope* (Jeol, Akishima, Japan) with a LaB $_6$  cathode at 5–20 keV. The microscope was equipped with a *Xflash 410* (Bruker, Billerica, US) silicon drift detector.

Surface areas (BET) were determined by nitrogen (purity 99.999%, 5.0) sorption experiments at 77 K using liquid nitrogen and *ca.* 20–50 mg of the sample, performed on a *Quantachrome NOVA-4000e* (Quantachrome, Odelzhausen, Germany) instrument within a partial pressure range of  $\text{pp}_0^{-1} = 10^{-3}$ –1 bar. Each sample was degassed under vacuum ( $<10^{-2}$  mbar) at  $150^\circ \text{C}$  for *ca.* 3 h prior to measurement. All the surface areas (BET) were calculated from five adsorption points applying Roquerol plots ( $r > 0.998$ ). For the pressure ranges of each MOF, see chapter S7 (ESI†). Total pore volumes were calculated from the  $\text{N}_2$  sorption isotherm at  $\text{pp}_0^{-1} = 0.95$ . NLDFT calculations for the pore size distributions were done with *NovaWin 11.03* software using the ' $\text{N}_2$  at 77 K on carbon, slit pore, as per the NLDFT equilibrium' model.

### General

In a typical synthetic procedure, we prepared the reactant mixture of the metal salts and linker by pre-grinding them in the molar ratio according to the MOF formula. Microwave-assisted (MW) and, for comparison, conventional electric (CE)-heated DGC reactions were performed in a Teflon reactor using a *CEM MARS-5* microwave or a temperature programmable oven. Detailed information and pictures of the DGC reactors, synthesis information, work-up procedures and characterization are given in the ESI†. Product phase identity was veri-



fied by PXRD. For detailed information of the PXRD measurements with the suppression of X-ray fluorescence of iron, see section S6 (ESI†). Surface areas (Brunauer, Emmett, Teller, BET<sup>52</sup>) were determined by N<sub>2</sub> sorption at 77 K (cf. section S7 in the ESI†) and used as criteria for the porosity quality of the products.

#### MW-DGC of MIL-100(Fe)

Fe(NO)<sub>3</sub>·9H<sub>2</sub>O (77.2 mg, 0.19 mmol) or FeCl<sub>3</sub>·6H<sub>2</sub>O (52.0 mg, 0.19 mmol) and benzene-1,3,5-tricarboxylic acid (40.1 mg, 0.19 mmol) were placed on a MW-DGC sieve (cf. Fig. S1, ESI†) with water or an acidic solution (5 mL) at the bottom of the Teflon reactor, which was tightly closed and heated to 150 °C for 180 min by applying 800 W, using a CEM MARS-5 microwave. The orange-brownish (from Fe(NO)<sub>3</sub>·9H<sub>2</sub>O) or reddish (from FeCl<sub>3</sub>·6H<sub>2</sub>O) solid products were washed with water and ethanol three times (10 mL each) and dried under vacuum (80 °C, 24 h). The amounts of starting materials for the repeat runs and the yields in the already optimized syntheses are given in Table S2 (ESI†).

#### MW-DGC of UiO-66

ZrCl<sub>4</sub> (88 mg, 0.38 mmol), terephthalic acid (H<sub>2</sub>BDC) (63 mg, 0.38 mmol) and benzoic acid (BA) (100 mg, 0.82 mmol) were mixed, ground in a mortar and placed on the sieve. Dimethylformamide, DMF (10 mL) and HCl (1 mL, 37%) were placed at the bottom of the Teflon tube. The Teflon tube was capped and heated to 180 °C (10 min heating to 180 °C, 50 min, cooling) by applying 600 W, using a CEM MARS-5 microwave. After the tube was cooled down to room temperature, the product was soaked in DMF (2 × 5 mL, 24 h each) and ethanol (5 mL, 24 h). The solvent was exchanged every 24 h. After a total time of 3 d of soaking, the solids were centrifuged and dried under vacuum (80 °C, 24 h).

#### MW-DGC of MIL-140A

ZrCl<sub>4</sub> (88 mg, 0.38 mmol), H<sub>2</sub>BDC (63 mg, 0.38 mmol) and BA (100 mg, 0.82 mmol) were mixed, ground in a mortar and placed on the sieve. DMF solvent (10 mL) was placed at the bottom of the Teflon tube, which was capped and heated to 160 °C (10 min heating to 160 °C, 80 min, cooling) by applying 600 W, using a CEM MARS-5 microwave. After the tube was cooled down to room temperature, the product was soaked in DMF (2 × 5 mL, 24 h each) and ethanol (5 mL, 24 h). The solvent was exchanged every 24 h. After 3 d of soaking, the solids were centrifuged and dried under vacuum (80 °C, 24 h).

#### MW-DGC of aluminium fumarate (Alfum)

Al<sub>2</sub>(SO<sub>4</sub>)<sub>3</sub>·18H<sub>2</sub>O (188 mg, 0.28 mmol), fumaric acid (65 mg, 0.56 mmol) and NaOH (44.8 mg, 1.12 mmol) were mixed and placed on a MW-DGC sieve with water (5 mL) at the bottom of a Teflon reactor. Conversion was carried out at 100 °C (60 min) by applying 800 W using a CEM MARS-5 microwave. The white products were washed three times with water (10 mL each), and dried under vacuum (80 °C, 24 h).

## Results and discussion

#### MIL-100(Fe)

In the case of MIL-100(Fe) (see section S2 in the ESI† for a brief description of this MOF, tradename *Basolite F300*), it was concluded that concentrated reactants may help achieve fast crystallization.<sup>32,53</sup> Hence, vapour-assisted methods, such as DGC and MW-DGC, should be advantageous.

For simplification, we do not list each experiment that was carried out within the synthesis optimizations. A lot of experiments yielded unsatisfying products, thereby, leading us to the eventually chosen – optimized – conditions. The synthesis optimization with the varying synthetic conditions for MIL-100(Fe) was done as follows: in a first approach towards MW-DGC of MIL-100(Fe), we optimized the DGC as described by Ahmed *et al.*<sup>32</sup> with respect to the reactants (using Fe<sup>III</sup> salts instead of Fe<sup>0</sup> metal), a lower temperature (150 °C instead of 165 °C) and a significantly shorter reaction time (24 h instead of 4 d). So far in the literature report on the DGC of MIL-100(Fe), iron metal (Fe<sup>0</sup>) was used in combination with HF.<sup>32</sup> Both for the CE-DGC and subsequent MW-DGC syntheses, the use HF or other fluoride sources, such as tetrabutylammonium fluoride (TBAF), as modulators did not increase the crystallinity or enhance the surface areas. Moreover, we found that the use of iron(III) salts with water only, *i.e.* without the use of HF or nitric acid, allowed reducing the reaction time from 96 h (ref. 32) to 24 h in the CE-DGC set-up and even further down to 3 h using MW-DGC. Water as a single solvent can help to overcome safety issues and environmental concerns, which are typically associated with strong acids in the synthesis of MIL-100(Fe).<sup>19,32,54,55</sup> Also, the use of iron(III) salts in CE-DGC seems to yield products with an increased porosity and enhanced BET areas compared to CE-DGC data from the literature (cf. Table 1).

MIL-100(Fe) was synthesized by MW-DGC and CE-DGC from a 1 : 1 mixture of Fe(NO)<sub>3</sub>·9H<sub>2</sub>O or FeCl<sub>3</sub>·6H<sub>2</sub>O and trimesic acid with water in good yields and in a significantly reduced time (cf. Table 1).

The crystallinity of all the obtained products by PXRD was at least equal, but often superior, to the commercially available, semi-amorphous product *Basolite F300* (cf. Fig. 1).

Fig. 2 shows the nitrogen sorption isotherms (from which the BET surface areas and pore volumes were derived) of the MIL-100(Fe) samples obtained *via* different synthetic approaches in comparison to *Basolite F300*.

MW-DGC yielded BET surface areas of MIL-100(Fe) ranging from 1000–1100 m<sup>2</sup> g<sup>−1</sup>, while CE-DGC syntheses formed products with values of *ca.* 1800–1900 m<sup>2</sup> g<sup>−1</sup> (cf. Table 1).

Admittedly, MW-DGC yielded only MIL-100(Fe) products with a lower crystallinity and porosity than CE-DGC, albeit still comparable to the commercial *Basolite F300*. The lower crystallinity and porosity of MIL-100(Fe) can be traced to the xerogel-like or semi-amorphous formation of MIL-100(Fe),<sup>19,59,73</sup> when prepared in water only, *i.e.* without the use of strong mineral acids or other mineralizing agents. Also MW implies fast



**Table 1** Comparison of BET surface areas and yields of MIL-100(Fe) from different synthesis routes

Synthesis route (reactant)	Time <sup>a</sup>	BET area <sup>b</sup> [m <sup>2</sup> g <sup>-1</sup> ]	Pore volume <sup>c</sup> [cm <sup>3</sup> g <sup>-1</sup> ]	Yield [%]
MW-DGC (Fe-chloride)	3 h	1002	0.43	78
MW-DGC (Fe-nitrate)		1105	0.48	81
CE-DGC (Fe-chloride)	24 h	1776	0.83	69
CE-DGC (Fe-nitrate)		1876	0.97	80
CE-DGC (Fe <sup>0</sup> , ref. 32)	4 d	1340	0.63	Not specified
Solution-based (Fe <sup>0</sup> or Fe <sup>III</sup> ) <sup>d</sup>	6 min, <sup>41</sup> 10 d(ref. 32)	356, <sup>56</sup> 2320 <sup>57</sup>	0.39, <sup>58</sup> 1.30 <sup>59</sup>	8, <sup>60</sup> 98 <sup>61</sup>
Solvent-free(Fe <sup>III</sup> and Fe <sup>0</sup> ) <sup>e</sup>	1 min–6 d	849–2492	0.69–0.96	17–99
Basolite F300(not specified)	Not specified	865–1252 <sup>f</sup>	0.28–0.52 <sup>f</sup>	Not specified
		365–1001 <sup>g</sup>	0.15–0.60 <sup>g</sup>	

<sup>a</sup> Reaction time includes any heating time needed to reach the set reaction temperature. <sup>b</sup> BET surface areas were obtained from five adsorption points in the pressure range  $pp_0^{-1} = 0.05$ – $0.20$ . <sup>c</sup> Calculated using the NLDFT model for carbon (slit pore). <sup>d</sup> Lowest and highest values found in the literature.<sup>32,41,53,55,57,59,62–65</sup> A short synthesis correlates with a low BET surface area.<sup>41</sup> <sup>e</sup> Range of solvent-free approaches, which include MW, oven heating and grinding.<sup>66,67</sup> <sup>f</sup> Range of five individual measurements from the same batch (this work, cf. section S7 in the ESI†). <sup>g</sup> Range in the literature,<sup>53,56,58,59,68–70</sup> where it is also noted that the BET given by the supplier (1300–1600 m<sup>2</sup> g<sup>-1</sup>)<sup>71</sup> could not be verified. Values are rounded.

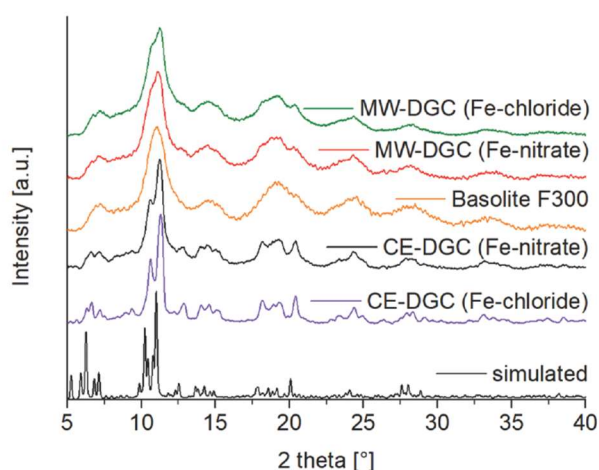


**Fig. 1** PXRDs of CE- and MW-DGC products in comparison with the industrial benchmark *Basolite F300* and the simulated pattern. Simulated pattern was calculated using CSD-Refcode CIGXIA.<sup>72</sup>

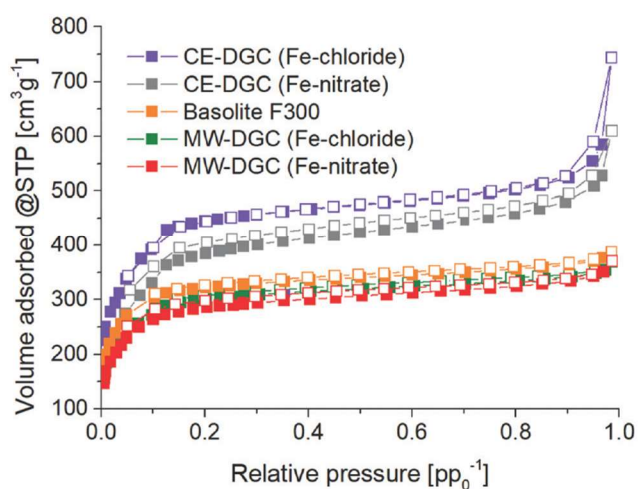


**Fig. 2** Nitrogen sorption isotherms (77 K) of MIL-100(Fe) obtained via different synthetic routes in comparison to *Basolite F300*. Filled symbols: adsorption, empty symbols: desorption.

heating rates, which was found to be detrimental, particularly for highly porous MIL-100(Fe) products.<sup>55,66</sup>

The MIL-100(Fe) particle morphology, which was controlled via scanning electron microscopy (SEM), was similar for the DGC syntheses and commercial *Basolite F300*, with MW-DGC giving the largest particles (cf. section S8 in the ESI† for the SEM images).

#### UiO-66 and MIL-140A

We transferred our previously reported DGC procedure of UiO-66 into a microwave set-up.<sup>31</sup> Depending on the synthesis conditions we obtained two products, namely UiO-66 and MIL-140A (see section S2 in the ESI† for a brief description of these MOFs). In a typical MW-DGC synthesis of UiO-66, ZrCl<sub>4</sub> and H<sub>2</sub>BDC were mixed in a 1 : 1 ratio and DMF was used as the reaction solvent at 180 °C with a 1 h reaction time. Additionally, two modulators (HCl/H<sub>2</sub>O to DMF<sup>74</sup> and BA to ZrCl<sub>4</sub>/H<sub>2</sub>BDC<sup>86</sup>) were added. For synthesis of the polymorph MIL-140A, only BA was used and the temperature was set to 160 °C for 1.5 h (see section S4 in the ESI†). We noted that the reaction temperatures for the conventional solvothermal syntheses of the two polymorphs were reversed, in that UiO-66 was formed at only 120 °C in 24 h,<sup>75</sup> while for MIL-140A, 220 °C and 16 h were needed.<sup>76</sup> Fig. 3 shows the PXRD patterns of UiO-66 and MIL-140A products, verifying the crystallinity and phase purity by positive matching with the simulated patterns.

Fig. 4 shows the nitrogen sorption isotherms and Table 2 lists the porosity parameters derived therefrom. The obtained UiO-66 and MIL-140A product porosities were highly comparable with the results from the solution synthesis in the literature. The BET surface area of solvothermally synthesized UiO-66 varied between 769 (ref. 77) and 1777 m<sup>2</sup> g<sup>-1</sup>.<sup>78</sup> Microwave-assisted synthesis delivered Langmuir surface areas of 888 up to 1661 m<sup>2</sup> g<sup>-1</sup>.<sup>79</sup> The comparable BET surface areas obtained for UiO-66 via MW-DGC varied between 1194 m<sup>2</sup> g<sup>-1</sup> (HCl/BA modulated) and 1023 m<sup>2</sup> g<sup>-1</sup> (IL assisted). The BET surface area of MIL-140A from MW-DGC (354 m<sup>2</sup> g<sup>-1</sup>) corresponds to the literature (335 m<sup>2</sup> g<sup>-1</sup>).<sup>80</sup>

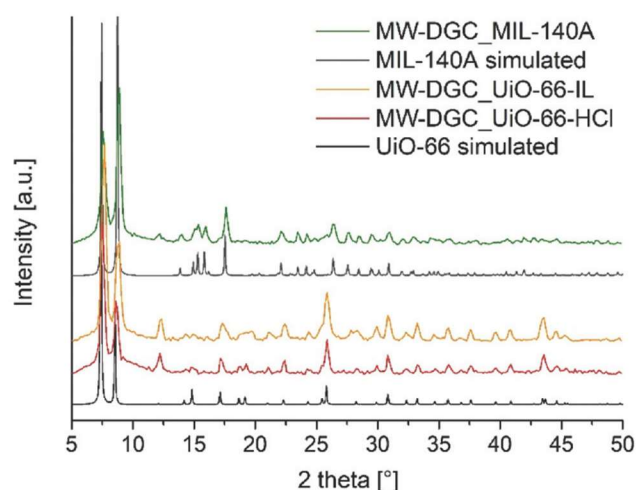


Fig. 3 PXRDs of simulated UiO-66, as-synthesized UiO-66-HCl (MW-DGC) and UiO-66-IL (MW-DGC), simulated MIL-140A and as-synthesized MIL-140A (MW-DGC). Simulated pattern of UiO-66 was calculated using CSD-Refcode RUBTAK02,<sup>75</sup> while the simulated pattern of MIL-140A was calculated using CSD-Refcode ZONBAH.<sup>76</sup>

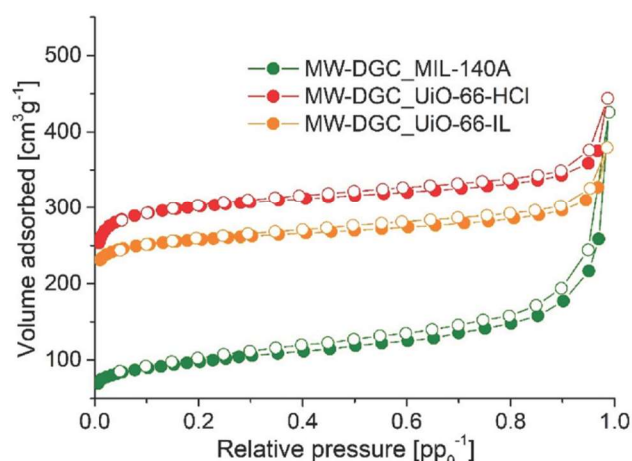


Fig. 4 Nitrogen sorption isotherms (77 K) of MW-DGC products of UiO-66 and MIL-140A. Filled symbols: adsorption, empty symbols: desorption.

The use of BA as a modulator in the reactant mixture ensured the formation of a dry-gel with a stable and thick consistency.  $\text{ZrOCl}_2 \cdot 8\text{H}_2\text{O}$  was proven to allow gel-based morphological control, *e.g.* preparation as monolithic xerogels.<sup>83</sup> Without BA (but with  $\text{HCl}/\text{H}_2\text{O}$ ) as a modulator, the reactants fell through the sieve.  $\text{HCl}$  as a modulator is often used to increase the defects in the framework to reach higher surface areas.<sup>74</sup> Here, the addition of aqueous  $\text{HCl}$  proved necessary to increase the microwave-energy absorption in DMF with the temperature set to 180 °C for sufficient evaporation to wet the reactants. Without  $\text{HCl}/\text{H}_2\text{O}$ , the reactants often decomposed partially due to the enhanced microwave irradiation needed to reach the set temperature of 180 °C. It has to be noted here that the IR temperature sensor of the microwave was placed below the bottom of the Teflon vessel, hence, it measured the temperature of the solvent part. Thus, reproducible preparation of UiO-66 at 180 °C was only successful when adding  $\text{HCl}/\text{H}_2\text{O}$  or an ionic liquid to DMF. For the synthesis of MIL-140A, the addition of  $\text{HCl}/\text{H}_2\text{O}$  proved not necessary as the set temperature of 160 °C did not induce decomposition in the reactants.

However, the use of aqueous  $\text{HCl}$  led to the decomposition of DMF to dimethylamine and formic acid,<sup>84</sup> which prevented the desired solvent re-use. This was the reason why  $\text{HCl}/\text{H}_2\text{O}$  was replaced by the ionic liquid to ensure the microwave absorption in the DMF akin to an IL-assisted synthesis.<sup>85</sup> As an IL, we used 1-*n*-butyl-3-methylimidazolium bis(trifluoromethylsulfonyl)imide,  $[\text{BMIm}][\text{NTf}_2]$ .

Recently we reported that CE-DGC delivers crystals of UiO-66 with a size range of 90–200 nm.<sup>31</sup> The MW-DGC of UiO-66-HCl led to relatively uniform-sized particles in a range of *ca.* 100 to 200 nm, which appear agglomerated. In comparison, solution synthesis delivered UiO-66 crystals with a particle size ranging from *ca.* 200 to 500 nm, as demonstrated by Pullen *et al.* (*cf.* section S8 in the ESI† for SEM images).<sup>86</sup> The MW-DGC of MIL-140A showed also agglomerated particles with a wide particle size ranging from 50 to 250 nm.

For Zr-based MOFs, it is recommended to perform thermogravimetric analysis (TGA) for defect analysis (*cf.* Fig. 5).<sup>78</sup> In the case of UiO-66, typically three weight losses were observed. At the beginning, solvent residues were degassed in a tempera-

Table 2 Results of MW-DGC synthesis of UiO-66 and MIL-140A with different modulators

Product(synthesis route)	Reaction time <sup>a</sup>	BET area <sup>b</sup> [ $\text{m}^2 \text{g}^{-1}$ ]	Pore volume <sup>c</sup> [ $\text{cm}^3 \text{g}^{-1}$ ]	Yield [%]
UiO-66-HCl (MW-DGC) <sup>d</sup>	1 h	1195	0.53	76
UiO-66-IL (MW-DGC) <sup>d</sup>	1 h	1023	0.46	68
UiO-66(CE-DGC, ref. 31)	27 h	1242–1461	0.55–0.69	65–83
UiO-66(solution-based) <sup>e</sup>	5 min, <sup>48</sup> 72 h (ref. 78)	769, <sup>77</sup> 1777 <sup>78</sup>	0.44, <sup>78</sup> 0.69 <sup>78</sup>	94 <sup>48</sup>
UiO-66(solvent-free)	30 (ref. 81)–90 min (ref. 82)	730 <sup>82</sup> –1217 <sup>81</sup>	0.40 <sup>81</sup>	
MIL-140A (MW-DGC) <sup>d</sup>	1.5 h	354	0.35	92
MIL-140A(solution-based) <sup>f</sup>	17 min, <sup>80</sup> 16 h (ref. 76)	337, <sup>80</sup> 415 <sup>76</sup>	0.18 <sup>76</sup>	91 <sup>76</sup>

<sup>a</sup> Reaction time includes any heating time needed to reach the set reaction temperature. <sup>b</sup> BET surface areas were obtained from five adsorption points in the pressure range  $\text{pp}_0^{-1} = 0.01$ –0.05 for UiO-66 and  $\text{pp}_0^{-1} = 0.01$ –0.10 for MIL-140A. <sup>c</sup> Calculated using the NLDFT model for carbon (slit pore). <sup>d</sup> This work. <sup>e</sup> Lowest and highest values found in the literature on UiO-66.<sup>48,77,78</sup> <sup>f</sup> Lowest and highest values found in the literature on MIL-140A.<sup>76,80</sup> Values are rounded.



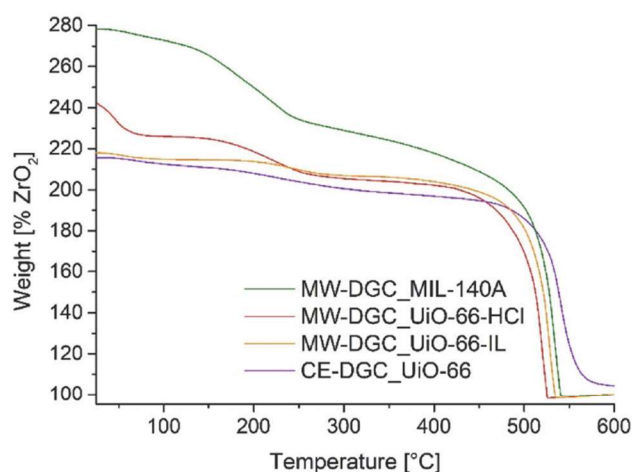


Fig. 5 TGA results of UiO-66-HCl (CE-DGC), UiO-66-IL (MW-DGC), UiO-66-HCl (MW-DGC) and MIL-140A (MW-DGC); end weights are normalized to 100%.

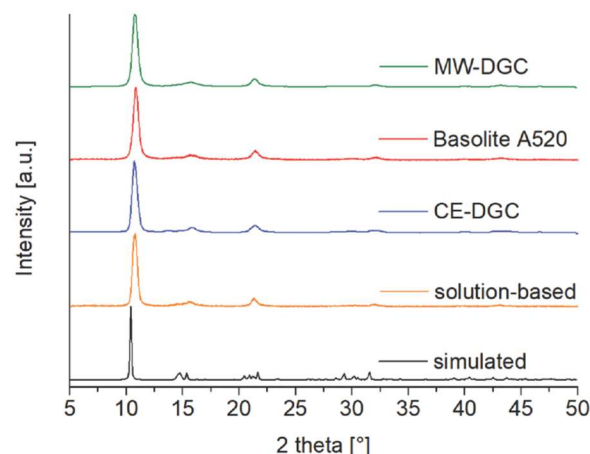


Fig. 6 PXRDs of CE- and MW-DGC products in comparison with solution-based synthesis, the industrial benchmark *Basolite A520* and the simulated pattern. Simulated pattern was calculated using CSD-Refcode DOYBEA.<sup>89</sup>

ture interval between 25 °C and 100 °C. Second, the decomposition of monocarboxylate ligands (*i.e.* BA) and the dihydroxylation of the  $\{Zr_6O_4(OH)_4\}$  secondary building units (SBUs) occur in a similar temperature range of *ca.* 180–300 °C,<sup>78</sup> such that  $\{Zr_6O_6\}$  SBUs are built.<sup>75</sup> Finally, the linker and framework decomposition occur above *ca.* 350–550 °C. In conclusion, we determined the linker defects per SBU unit according to Shearer *et al.*<sup>78</sup> An assumption for this method is that the residue in each TGA experiment is pure  $ZrO_2$ , which is set to 100% (*cf.* Fig. 5). A similar method to determine the defects was applied for MIL-140A.

The defect parameters for UiO-66 and MIL-140A calculated from thermogravimetric analyses are summarized in Table 3. For comparison, the TGA and defect analysis of UiO-66 obtained *via* CE-DGC is added. The number of defects per SBU were in the range of 1.16 to 1.36, which is in the same range of linker deficiencies reported by Shearer *et al.*<sup>78</sup> Detailed information about the calculation of defects is outlined in section S9 in the ESI.

### Aluminium fumarate (Alfum)

We were able to transfer a solution-based synthesis of aluminium fumarate (see section S2 in the ESI† for a brief

description of this MOF, tradename *Basolite A520*)<sup>87,88</sup> into a microwave autoclave for the first time. Alfum was obtained from a precursor mixture of  $Al_2(SO_4)_3 \cdot 18H_2O$ , fumaric acid and NaOH (molar ratio 1 : 2 : 4) with water. The MW-DGC products were compared to CE-DGC products and products from conventional solution-based synthesis. Detailed synthesis information is given in section S5 in the ESI.†

Since the stoichiometric ratio had already been optimized in the BASF patent,<sup>87</sup> we only varied the conversion times. The crystallinity of all the obtained products by PXRD was about equal, including the commercial *Basolite A520* product (*cf.* Fig. 6).

Therefore, the BET surface areas were again used as the main quality criterion for evaluation of all the obtained aluminium fumarate products and were found to be in good agreement with each other, independent of the synthesis method (*cf.* Table 4).

There was a significant difference in the shape of the nitrogen sorption isotherms between the MW-DGC and the other Alfum materials (*cf.* Fig. 7). At very low  $p/p_0$ , all the isotherms showed a steep increase in nitrogen uptake, characteristic of a Type I isotherm for microporous materials.<sup>52</sup> Different from a Type I isotherm, which has a limiting uptake governed by the

Table 3 Determination of defects from TGA under synthetic air atmosphere

Product(synthesis route)	No. of defects per SBU( <i>x</i> ) <sup>a</sup>	Molecular formula $Zr_6O_{6+x}(BDC)_{6-x}$ <sup>b</sup> and $ZrO_{1+x}(BDC)_{1-x}$	Exp. molecular weight [g mol <sup>-1</sup> ]
UiO-66 (CE-DGC, ref. 31)	1.36	$Zr_6O_{7.36}(BDC)_4$ <sup>64</sup>	1435.92
UiO-66-HCl (MW-DGC)	1.17	$Zr_6O_{7.17}(BDC)_4$ <sup>73</sup>	1447.83
UiO-66-IL (MW-DGC)	1.16	$Zr_6O_{7.16}(BDC)_4$ <sup>74</sup>	1449.34
MIL-140A (MW-DGC)	0.03	$ZrO_{1.03}(BDC)_0$ <sup>97</sup>	268.85

<sup>a</sup> Calculation of defect-numbers per SBU *x* are presented in the ESI (section S9). Values are rounded to one decimal digit. <sup>b</sup> Determination of defects from TGA are similar to those in the work of Shearer *et al.*,<sup>78</sup> where the molecular formula and experimental molecular weight were also given without modulator units in place of missing BDC linkers.

**Table 4** Comparison of the porosity parameters and yields of Al<sub>2</sub>Fe from different aqueous synthesis routes

Synthesis route	Time <sup>a</sup>	BET area <sup>b</sup> [m <sup>2</sup> g <sup>-1</sup> ]	Pore volume [cm <sup>3</sup> g <sup>-1</sup> ] <sup>c</sup>	Yield [%]
MW-DGC <sup>d</sup>	1 h	1075–1150	0.72–0.94	76–89
CE-DGC <sup>d</sup>	6 h	1037–1188	0.43–0.61	58–71
Solution-based <sup>d</sup>	>3 h	780–1254	0.36–0.72	73–85
Solution-based <sup>e</sup>		925, <sup>90</sup> 1212 <sup>91</sup>	0.44, <sup>91</sup> 0.65 <sup>90</sup>	88, <sup>90</sup> 90 <sup>92</sup>
Basolite A520	>5 h	723–1333 <sup>f,h</sup>	0.47 <sup>89</sup>	76–98 <sup>e</sup>
		999–1040 <sup>g</sup>	0.51–0.63 <sup>g</sup>	

<sup>a</sup> Reaction time includes any heating time needed to reach the set reaction temperature. <sup>b</sup> BET surface areas were obtained from five adsorption points in the pressure range  $pp_0^{-1} = 0.001$ –0.05. <sup>c</sup> Calculated using the NLDFT model for carbon (slit pore); contributions from micropores are given in Table S7 (ESI). <sup>d</sup> This work, range of six samples. <sup>e</sup> Lowest and highest values found in the literature.<sup>89–94</sup> <sup>f</sup> Stated in the patent.<sup>88</sup> <sup>g</sup> Range of five individual measurements from the same batch (this work, cf. section S7 in the ESI) and in good agreement with ranges given in the literature.<sup>87–89</sup> <sup>h</sup> Langmuir surface area. Values are rounded.

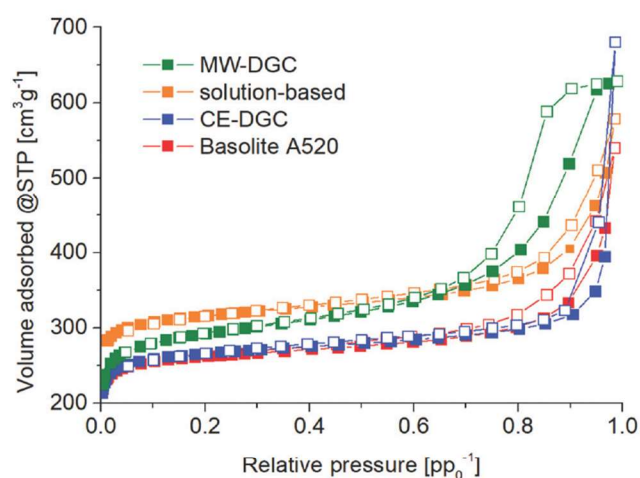


**Fig. 7** Nitrogen sorption isotherms (77 K) of Al<sub>2</sub>Fe obtained via different synthetic routes in comparison to Basolite A520. Filled symbols: adsorption, empty symbols: desorption.

accessible microporous volume, the isotherms showed an increase in N<sub>2</sub> uptake at elevated partial pressure. For the Al<sub>2</sub>Fe materials from CE-DGC, solution synthesis and for Basolite A520, this increase corresponds to a Type II or III isotherm together with an H4 hysteresis. Thus, the overall adsorption isotherms of Al<sub>2</sub>Fe materials from CE-DGC, solution synthesis and for Basolite A520 were a composite of Type I and II/III.

H4 loops go along with composite adsorption branches of Types I and II, and are often found with aggregated crystals of microporous materials. Thus, the microporous Al<sub>2</sub>Fe materials from CE-DGC, solution synthesis and Basolite A520 featured macropores (>50 nm diameter) from the interparticle voids of aggregated microparticles (cf. Fig. S12 in the ESI† for the SEM images).<sup>90</sup> Interparticle condensation typically appears at pressures  $pp_0^{-1} > 0.4$  for N<sub>2</sub> sorption (77 K).<sup>95</sup>

Al<sub>2</sub>Fe obtained by MW-DGC exhibited an adsorption isotherm with an increase at higher partial pressure to a final saturation plateau, which is typical for a Type IV isotherm. Type IV isotherms are given by mesoporous adsorbents. Also, H2(b) hysteresis is seen for mesoporous materials with complex pore

structures and large size distribution of neck widths.<sup>52</sup> Overall, the adsorption isotherm for MW-DGC Al<sub>2</sub>Fe was bimodal as a combination of Type I (due to the known microporosity of Al<sub>2</sub>Fe) and Type IV. This bimodal Type I + IV feature is common and was highly reproducible for all the MW-DGC samples we prepared, as shown in Fig. S7 in the ESI.† Bimodal isotherms are in the literature described for the gel-like formation of MOFs.<sup>96</sup>

By principle, N<sub>2</sub> sorption isotherms and BET theory cannot probe macropores. Thus, the subsequent pore size distribution based on non-linear density functional theory (NLDFT) calculations showed only (micro- and) mesopores (2–50 nm). The pore size distributions for the different Al<sub>2</sub>Fe materials (cf. Fig. S8 and S9 and further porosity details in Table S7 in the ESI†) reflect the aforementioned differences in the sorption isotherms and hystereses between the MW-DGC and the three others. The highly reproducible pore width distribution for Al<sub>2</sub>Fe batches from MW-DGC (cf. Fig. 8) showed a pronounced and unique narrow mesopore contribution of 5–11 nm in comparison with Al<sub>2</sub>Fe obtained via other syntheses methods (cf. Fig. S8 and S9 in the ESI†). Porosity across the micro- and mesoporous regime is termed hierarchical porosity. We noted that the hierarchical porous Al<sub>2</sub>Fe material from MW-DGC

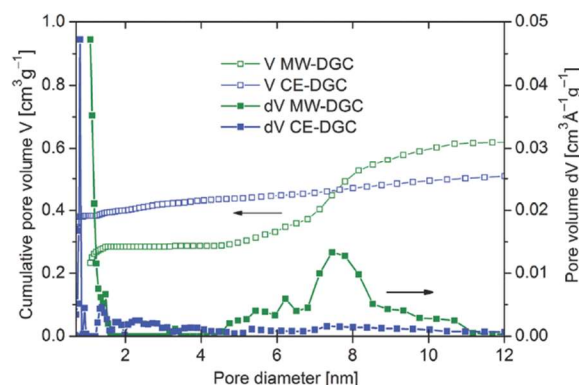


**Fig. 8** Comparative pore size distributions as cumulative (left) and incremental pore volume (right) from N<sub>2</sub> sorption isotherms (77 K) of Al<sub>2</sub>Fe obtained via MW-DGC (green) and CE-DGC (blue). See ESI† for pore size distributions of solution-based Al<sub>2</sub>Fe and Basolite A520.



was achieved solely by the synthesis method, that is without the addition of surfactants or templates, as are typically used for the synthesis of hierarchical porous MOFs.<sup>97–99</sup>

It would not be reasonable to assume that particle aggregation leads to such a narrow mesopore range. Other gel-like micro-mesoporous MOFs exhibit much broader mesopore distribution over at least a 20 nm range, which is then interpreted as an interparticle void.<sup>83</sup> Instead we propose that the Al<sub>2</sub>MOF material made from MW-DGC features mesopores (together with micropores) within the framework due to defects. As such, MW-DGC advantageously leads to a different, namely, hierarchical micro-mesoporous Al<sub>2</sub>MOF material compared to the other synthesis methods (Table S7, ESI†).

### Solvent re-use

The separation of the reaction products and solvent in DGC enables the solvent to be recovered largely uncontaminated and re-used, as was recently shown.<sup>31</sup> Hence, we performed repeated synthesis runs with re-use of the solvent and fresh precursors in the realm of sustainable MOF synthesis.<sup>14,22,28</sup> Thereby, we were able to prove that the re-use of solvent is generally possible in MW-DGC for at least three synthesis runs (*cf.* section S10 in the ESI†). The four MOFs MIL-100(Fe), UiO-66, MIL-140A and Al<sub>2</sub>MOF could be prepared by replacing the product with fresh precursor at the head of the container and then repeating the reaction with the same, unchanged solvent left in the bottom of the Teflon vessel. For UiO-66 the precursor also included the BA modulator. The quality criteria BET surface areas, crystallinity (PXRD, *cf.* Fig S14–S17 ESI† for 3 runs of each MOF) and yields varied, but within acceptable limits (*cf.* Fig. 9).

For MIL-100(Fe), the yield varied between 72% and 82%, the BET surface area between 935 and 1287 m<sup>2</sup> g<sup>−1</sup>.

For MIL-140A, the yields were in the range from 89% to 96% and the BET surface areas from 354 to 340 m<sup>2</sup> g<sup>−1</sup>.

For UiO-66, a solvent re-use was not possible in the presence of HCl/H<sub>2</sub>O due to decomposition of DMF. Alternatively,

the synthesis of UiO-66 with re-use of the solvent-mixture of DMF and IL was successful. Then, the UiO-66 yield varied between 68% and 73% and the BET surface areas between 717 and 1023 m<sup>2</sup> g<sup>−1</sup>.

For Al<sub>2</sub>MOF, we obtained yields between 76% and 89% and BET surface areas between 1075 and 1148 m<sup>2</sup> g<sup>−1</sup>.

When comparing DGC synthesis to seemingly simple and sometimes also fast solution synthesis routes, it should be noted that such solution syntheses involve large amounts of solvents. For example, in the patented and most effective aluminium fumarate synthesis, a space-time yield (STY) of 3615 kg m<sup>−3</sup> day<sup>−1</sup> goes along with the use of at least 84 555 L of mother liquor.<sup>87</sup> For a continuous-flow UiO-66 synthesis with an STY of 2053 kg m<sup>−3</sup> day<sup>−1</sup>, the amount of reaction mother liquor seems to be at least 59 000 L, and amounts to 289 000 L if washing solvents are included (*cf.* section S11 in the ESI† for details of the calculation).<sup>48</sup>

## Conclusion

We demonstrated that the novel technique MW-DGC holds the potential to synthesize MOFs in a fast, safe, good-yield and energy-reduced procedure in qualities comparable to the literature or commercial MOF materials. The reaction times and therefore energy input could be drastically shortened, compared to conventional electric-heated dry-gel conversion or solvothermal synthesis. In addition, MW-DGC is a step towards sustainable MOF synthesis due to the ability of solvent re-use (*cf.* Fig. 10).

Noteworthy, MW-DGC can also give rise to a unique, hierarchical Al<sub>2</sub>MOF material with mesoporosity built into the otherwise microporous framework. This was shown through a comparative N<sub>2</sub> sorption and pore size analysis of Al<sub>2</sub>MOF materials from different synthesis methods. The prominent hysteresis

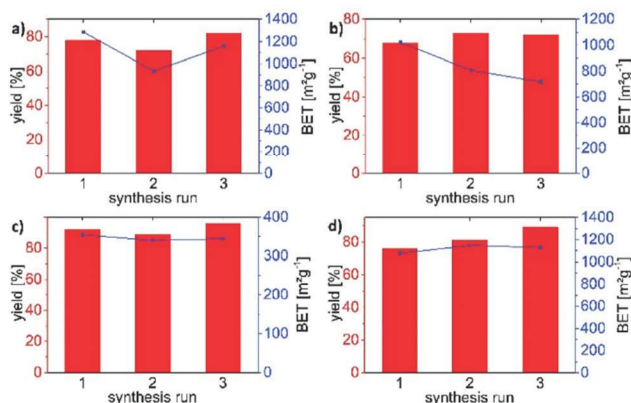


Fig. 9 Solvent re-use over three synthesis runs in the case of: (a) MIL-100(Fe), (b) UiO-66-IL, (c) MIL-140A and (d) Al<sub>2</sub>MOF. Data can be found in Tables S8–S11 in the ESI†.

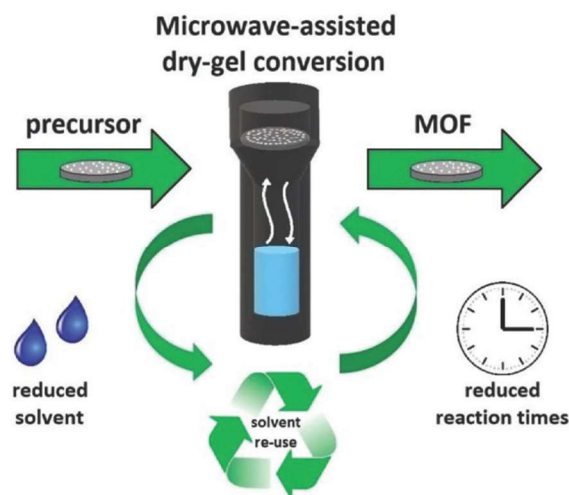


Fig. 10 Schematic summary of the advantages of MW-DGC with respect to reduced reaction times, reduced solvent amount and solvent re-use.

loop in the region  $pp_0^{-1} > 0.7$  with mesopore characteristics was reproducibly obtained for the MW-DGC products of Al<sub>2</sub>O<sub>3</sub>.

The recovery of solvent shown here for the MW-DGC technique allows reducing the solvent use in MOF synthesis drastically, as is otherwise only possible with mechano-chemistry. Accordingly, we hope that we can contribute to the environmentally and economically optimized syntheses of selected prototypical MOFs, since the technique should be clearly expandable to most MOF syntheses.

## Conflicts of interest

There are no conflicts of interest to declare.

## Acknowledgements

The authors gratefully acknowledge the financial support of the Federal German Ministry of Education and Research (BMBF) in the project Optimat under grant no. 03SF0492C.

## References

- 1 G. Maurin, C. Serre, A. Cooper and G. Férey, *Chem. Soc. Rev.*, 2017, **46**, 3104–3107.
- 2 Y.-B. Huang, J. Liang, X.-S. Wang and R. Cao, *Chem. Soc. Rev.*, 2017, **46**, 126–157.
- 3 A. Herbst and C. Janiak, *CrystEngComm*, 2017, **19**, 4092–4117.
- 4 W. P. Lustig, S. Mukherjee, N. D. Rudd, A. V. Desai, J. Li and S. K. Ghosh, *Chem. Soc. Rev.*, 2017, **46**, 3242–3285.
- 5 J.-R. Li, R. J. Kuppler and H.-C. Zhou, *Chem. Soc. Rev.*, 2009, **38**, 1477–1504.
- 6 J. Dechnik, J. Gascon, C. J. Doonan, C. Janiak and C. J. Sumby, *Angew. Chem., Int. Ed.*, 2017, **56**, 9292–9310.
- 7 K. Adil, Y. Belmabkhout, R. S. Pillai, A. Cadiau, P. M. Bhatt, A. H. Assen, G. Maurin and M. Eddaoudi, *Chem. Soc. Rev.*, 2017, **46**, 3402–3430.
- 8 P. Horcajada, R. Gref, T. Baati, P. K. Allan, G. Maurin, P. Couvreur, G. Férey, R. E. Morris and C. Serre, *Chem. Rev.*, 2012, **112**, 1232–1268.
- 9 F. Jeremias, D. Fröhlich, C. Janiak and S. K. Henninger, *New J. Chem.*, 2014, **38**, 1846–1852.
- 10 J. Zhou, H. Li, H. Zhang, H. Li, W. Shi and P. Cheng, *Adv. Mater.*, 2015, **27**, 7072–7077.
- 11 F. A. Almeida Paz, J. Klinowski, S. M. F. Vilela, J. P. C. Tome, J. A. S. Cavaleiro and J. Rocha, *Chem. Soc. Rev.*, 2012, **41**, 1088–1110.
- 12 R. Haldar and T. K. Maji, *CrystEngComm*, 2013, **15**, 9276–9295.
- 13 C. R. Wade, T. Corrales-Sanchez, T. C. Narayan and M. Dincă, *Energy Environ. Sci.*, 2013, **6**, 2172–2177.
- 14 N. Stock and S. Biswas, *Chem. Rev.*, 2012, **112**, 933–969.
- 15 J. Chen, K. Shen and Y. Li, *ChemSusChem*, 2017, **10**, 3165–3187.
- 16 M. Gaab, N. Trukhan, S. Maurer, R. Gummaraju and U. Müller, *Microporous Mesoporous Mater.*, 2012, **157**, 131–136.
- 17 P. A. Bayliss, I. A. Ibarra, E. Pérez, S. Yang, C. C. Tang, M. Poliakoff and M. Schröder, *Green. Chem.*, 2014, **16**, 3796–3802; C. Avci-Camur, J. Troyano, J. Pérez-Carvajal, A. Legrand, D. Farrusseng, I. Imaz and D. Maspocho, *Green Chem.*, 2018, **20**, 873–878.
- 18 J. Ren, X. Dyosiba, N. M. Musyoka, H. W. Langmi, M. Mathe and S. Liao, *Coord. Chem. Rev.*, 2017, **352**, 187–219.
- 19 K. Guesh, C. A. D. Caiuby, Á. Mayoral, M. Díaz-García, I. Díaz and M. Sanchez-Sanchez, *Cryst. Growth Des.*, 2017, **17**, 1806–1813.
- 20 H. Reinsch and N. Stock, *Dalton Trans.*, 2017, **46**, 8339–8349.
- 21 Z. Hu and D. Zhao, *Dalton Trans.*, 2015, **44**, 19018–19040.
- 22 H. Reinsch, *Eur. J. Inorg. Chem.*, 2016, **27**, 4290–4299; H. Reinsch, S. Waitschat, S. M. Chavan, K. P. Lillerud and N. Stock, *Eur. J. Inorg. Chem.*, 2016, 4490–4498.
- 23 G. Zhan and H. C. Zheng, *Chem. Commun.*, 2017, **53**, 72–81.
- 24 T. Friščić, S. L. Childs, S. A. A. Rizvi and W. Jones, *CrystEngComm*, 2009, **11**, 418–426.
- 25 D. Crawford, J. Casaban, R. Haydon, N. Giri, T. McNally and S. L. James, *Chem. Sci.*, 2015, **6**, 1645–1649.
- 26 K. Matsuyama, *J. Supercrit. Fluid*, 2018, **134**, 197–203.
- 27 P. W. Dunne, E. Lester and R. I. Walton, *React. Chem. Eng.*, 2016, **1**, 352–360.
- 28 P. A. Julien, C. Mottillo and T. Friščić, *Green Chem.*, 2017, **19**, 2729–2747.
- 29 L. M. Gilbertson, J. B. Zimmermann, D. L. Plata, J. E. Hutchinson and P. T. Anastas, *Chem. Soc. Rev.*, 2015, **44**, 5758–5777.
- 30 M. Matsukata, M. Ogura, T. Osaki, P. R. H. P. Rao, M. Nomura and E. Kikuchi, *Top. Catal.*, 1999, **9**, 77–92.
- 31 S. Gökpınar, T. Diment and C. Janiak, *Dalton Trans.*, 2017, **46**, 9895–9900.
- 32 I. Ahmed, J. Jeon, N. A. Khan and S. H. Jung, *Cryst. Growth Des.*, 2012, **12**, 5878–5881.
- 33 H. Zhang, J. Zhong, G. Zhou, J. Wu, Z. Yang and X. Shi, *J. Nanomater.*, 2016, 9648386.
- 34 Q. Shi, Z. Chen, Z. Song, J. Li and J. Dong, *Angew. Chem., Int. Ed.*, 2011, **50**, 672–675.
- 35 J. Kim, Y.-R. Lee and W.-S. Ahn, *Chem. Commun.*, 2013, **49**, 7647–7649.
- 36 N. D. McNamara and J. C. Hicks, *ACS Appl. Mater. Interfaces*, 2015, **7**, 5338–5346.
- 37 A. K. Das, R. S. Vemuri, I. Kutnyakov, B. P. McGrail and R. K. Motkuri, *Sci. Rep.*, 2016, **6**, 28050.
- 38 P. Tan, X.-Y. Xie, X.-Q. Liu, T. Pan, C. Gu, P.-F. Chen, J.-Y. Zhou, Y. Pan and L.-B. Sun, *J. Hazard. Mater.*, 2017, **321**, 344–352.
- 39 Z. Ni and R. I. Masel, *J. Am. Chem. Soc.*, 2006, **128**, 12394–12395.



- 40 S. H. Jhung, J.-H. Lee, J. W. Yoon, C. Serre, G. Férey and J.-S. Chang, *Adv. Mater.*, 2007, **19**, 121–124.
- 41 A. G. Márquez, A. Demessence, A. E. Platero-Prats, D. Heurtaux, P. Horcajada, C. Serre, J.-S. Chang, G. Férey, V. A. de la Peña-O'Shea, C. Boissière, D. Grosso and C. Sanchez, *Eur. J. Inorg. Chem.*, 2012, 5165–5174.
- 42 M. F. Groh, M. Heise, M. Kaiser and M. Ruck, *Nachr. Chem.*, 2013, **61**, 26–29.
- 43 A. L. Buchachenko and E. L. Frankevich, *Chemical Generation and Reception of Radio- and Microwaves*, Wiley-VCH, Weinheim, Germany 1993, pp. 41–56.
- 44 V. K. Ahluwalia, *Alternative Energy Processes in Chemical Synthesis*, Alpha Science International LTD, Oxford, United Kingdom, 2008.
- 45 I. Bilecka and M. Niederberger, *Nanoscale*, 2010, **2**, 1358–1374.
- 46 C. S. Cundy and P. A. Cox, *Chem. Rev.*, 2003, **103**, 663–702.
- 47 C. Echaide-Górriz, C. Clément, F. Cacho-Bailo, C. Téllez and J. Coronas, *J. Mater. Chem. A*, 2018, **6**, 5485–5506.
- 48 M. Taddei, D. A. Steitz, J. A. van Bokhoven and M. Ranocchiari, *Chem. – Eur. J.*, 2016, **22**, 3245–3249.
- 49 I. Thomas-Hillmann, A. Laybourn, C. Dodds and S. W. Kingman, *J. Mater. Chem. A*, 2018, **6**, 11564–11581.
- 50 A. de la Hoz, A. Diaz-Ortiz and A. Moreno, *Chem. Soc. Rev.*, 2005, **34**, 164–178.
- 51 M. Larhed, C. Moberg and A. Hallberg, *Acc. Chem. Res.*, 2002, **35**, 717–727.
- 52 M. Thommes, K. Kaneko, A. V. Neimark, J. P. Olivier, F. Rodriguez-Reinoso, J. Rouquerol and K. S. Sing, *Pure Appl. Chem.*, 2015, **87**, 1051–1069.
- 53 Y.-K. Seo, J. W. Yoon, J. S. Lee, U.-H. Lee, Y. K. Hwang, C.-H. Jun, P. Horcajada, C. Serre and J.-S. Chang, *Microporous Mesoporous Mater.*, 2012, **157**, 137–145.
- 54 G. Férey, C. Serre, C. Mellot-Draznieks, F. Millange, S. Surblé, J. Dutour and I. Margiolaki, *Angew. Chem.*, 2004, **116**, 6456–6461.
- 55 F. Jeremias, S. K. Henninger and C. Janiak, *Dalton Trans.*, 2016, **45**, 8637–8644.
- 56 G. Majano, O. Ingold, M. Yulikov, G. Jeschke and J. Pérez-Ramírez, *CrystEngComm*, 2013, **15**, 9885–9892.
- 57 J. W. Yoon, Y.-K. Seo, Y. K. Hwang, J.-S. Chang, H. Leclerc, S. Wuttke, P. Bazin, A. Vimont, M. Daturi, E. Bloch, P. L. Llewellyn, C. Serre, P. Horcajada, J. M. Grèneche, A. E. Rodrigues and G. Férey, *Angew. Chem.*, 2010, **122**, 6085–6088.
- 58 M. Piloni, F. Padella, G. Ennas, S. Lai, M. Bellusci, E. Rombi, F. Sini, M. Pentimalli, C. Delitala, A. Scano, *et al.*, *Microporous Mesoporous Mater.*, 2015, **213**, 14–21.
- 59 M. Sanchez-Sanchez, I. de Asua, D. Ruano and K. Diaz, *Cryst. Growth Des.*, 2015, **15**, 4498–4506.
- 60 E. Bellido, M. Guillevis, T. Hidalgo, M. J. Santander-Ortega, C. Serre and P. Horcajada, *Langmuir*, 2014, **30**, 5911–5920.
- 61 A. García Márquez, A. Demessence, A. E. Platero-Prats, D. Heurtaux, P. Horcajada, C. Serre, J.-S. Chang, G. Férey, V. A. de la Peña-O'Shea, C. Boissière, D. Grosso and C. Sanchez, *Eur. J. Inorg. Chem.*, 2012, **30**, 5165–5174.
- 62 M. Wickenheisser, T. Paul and C. Janiak, *Microporous Mesoporous Mater.*, 2015, **215**, 258–269.
- 63 M. Wickenheisser, A. Herbst, R. Tannert, B. Milow and C. Janiak, *Microporous Mesoporous Mater.*, 2016, **220**, 143–153.
- 64 F. Jeremias, S. K. Henninger and C. Janiak, *J. Mater. Chem.*, 2012, **22**, 1014810151.
- 65 H. Tian, J. Peng, Q. Du, X. Hui and H. He, *Dalton Trans.*, 2018, **47**, 3417–3424.
- 66 M. Lanchas, S. Arcediano, A. T. Aguayo, G. Beobide, O. Castillo, J. Cepeda, D. Vallejo-Sánchez and A. Luque, *RSC Adv.*, 2014, **4**, 60409–60412.
- 67 L. Han, H. Qi, D. Zhang, G. Ye, W. Zhou, C. Hou, W. Xu and Y. Sun, *New J. Chem.*, 2017, **41**, 13504–13509.
- 68 A. Dhakshinamoorthy, M. Alvaro, P. Horcajada, E. Gibson, M. Vishnuvarthan, A. Vimont, J.-M. Grèneche, C. Serre, M. Daturi and H. Garcia, *ACS Catal.*, 2012, **2**, 2060–2065.
- 69 A. Dhakshinamoorthy, M. Alvaro, H. Chevreau, P. Horcajada, T. Devic, C. Serre and H. Garcia, *Catal. Sci. Technol.*, 2012, **2**, 324–330.
- 70 G. Blanco-Brieva, J. M. Campos-Martin, S. M. Al-Zahrani and J. L. G. Fierro, *Global NEST J.*, 2010, **12**, 296–304.
- 71 <http://www.sigmaaldrich.com/catalog/product/aldrich/690872>; 28.06.2017, 16:03 h.
- 72 P. Horcajada, S. Surble, C. Serre, D.-Y. Hong, Y.-K. Seo, J.-S. Chang, J.-M. Grèneche, I. Margiolaki and G. Férey, *Chem. Commun.*, 2007, **27**, 2820–2822.
- 73 S. Xiang, L. Li, J. Zhang, X. Tan, H. Cui, J. Shi, Y. Hu, L. Chen, C.-Y. Su and S. L. James, *J. Mater. Chem.*, 2012, **22**, 1862–1867.
- 74 M. J. Katz, Z. J. Brown, Y. J. Colón, P. W. Siu, K. A. Scheidt, R. Q. Snurr, J. T. Hupp and O. K. Farha, *Chem. Commun.*, 2013, **49**, 9449–9451.
- 75 L. Valenzano, B. Civalleri, S. Chavan, S. Bordiga, M. H. Nilsen, S. Jakobsen, K. P. Lillerud and C. Lamberti, *Chem. Mater.*, 2011, **23**, 1700–1718.
- 76 V. Guillermin, F. Ragon, M. Dan-Hardi, T. Devic, M. Vishnuvarthan, B. Campo, A. Vimont, G. Clet, Q. Yang, G. Maurin, G. Férey, A. Vittadini, S. Gross and C. Serre, *Angew. Chem., Int. Ed.*, 2012, **51**, 9267–9271.
- 77 Z. Hu, Y. Peng, Z. Kang, Y. Qian and D. Zhao, *Inorg. Chem.*, 2015, **54**, 4862–4868.
- 78 G. C. Shearer, S. Chavan, S. Bordiga, S. Svelle, U. Olsbye and K. P. Lillerud, *Chem. Mater.*, 2016, **28**, 3749–3761.
- 79 Y. Li, Y. Liu, W. Gao, L. Zhang, W. Liu and J. Lu, *CrystEngComm*, 2014, **16**, 7037–7042.
- 80 W. Liang and D. M. D'Alessandro, *Chem. Commun.*, 2013, **49**, 3706–3708.
- 81 P. Hu, X. Liang, M. Yaseen, X. Sun, Z. Tong, Z. Zhao and Z. Zhao, *Chem. Eng. J.*, 2018, **332**, 608–618.
- 82 K. Užarević, T. C. Wang, S.-Y. Moon, A. M. Fidelli, J. T. Hupp, O. K. Farha and T. Friščić, *Chem. Commun.*, 2016, **52**, 2133–2136.
- 83 B. Bueken, N. Van Velthoven, T. Willhammar, T. Stassin, I. Stassen, D. A. Keen, G. V. Baron, J. F. M. Denayer, R. Ameloot, S. Bals, D. De Vos and T. D. Bennett, *Chem. Sci.*, 2017, **8**, 3939–3948.

- 84 H.-P. Kruse, Key word 'Dimethylformamide', in *Römpch Lexikon Chemie*, ed. J. Falbe and M. Regitz, Georg Thieme Verlag, Stuttgart, Germany, 10th edn, 1997.
- 85 B. Floris, F. Sabuzi, P. Galloni and V. Conte, *Catalysts*, 2017, **7**, 261; A. K. Pathak, C. Ameta, R. Ameta and P. B. Punjabi, *J. Heterocycl. Chem.*, 2016, **53**, 1697–1705.
- 86 S. Pullen, H. Fei, A. Orthaber, S. M. Cohen and S. Ott, *J. Am. Chem. Soc.*, 2013, **135**, 16997–17003.
- 87 C. Kiener, U. Müller and M. Schubert, Method of using a metal organic frameworks based on aluminum fumarate, *U.S. Patent*, 8518264, BASF SE, 27 Aug. 2013.
- 88 E. Leung, U. Müller, N. Trukhan, H. Mattenheimer, G. Cox and S. Blei, Process for preparing porous metal-organic frameworks based on aluminum fumarate, *U.S. Patent*, 8524932, BASF SE, 3 Sep. 2013.
- 89 E. Alvarez, N. Guillou, C. Martineau, B. Bueken, B. Van de Voorde, C. Le Guillouzer, P. Fabry, F. Nouar, F. Taulelle, D. de Vos, J.-S. Chang, K. H. Cho, N. Ramsahye, T. Devic, M. Daturi, G. Maurin and C. Serre, *Angew. Chem., Int. Ed.*, 2015, **54**, 3664–3668.
- 90 L. Zhou, X. Zhang and Y. Chen, *Mater. Lett.*, 2017, **197**, 224–227.
- 91 E. Elsayed, R. AL-Dadah, S. Mahmoud, P. A. Anderson, A. Elsayed and P. G. Youssef, *Desalination*, 2017, **406**, 25–36.
- 92 F. Jeremias, D. Fröhlich, C. Janiak and S. K. Henninger, *RSC Adv.*, 2014, **4**, 24073–24082.
- 93 M. Rubio-Martinez, T. D. Hadley, M. P. Batten, K. Constanti-Carey, T. Barton, D. Marley, A. Mönch, K.-S. Lim and M. R. Hill, *ChemSusChem*, 2016, **9**, 938–941.
- 94 S. Karmakar, J. Dechnik, C. Janiak and S. De, *J. Hazard. Mater.*, 2016, **303**, 10–20.
- 95 S. J. Gregg and K. S. W. Sing, *Adsorption, Surface Area and Porosity*, Academic Press, London, 1982.
- 96 L. Li, S. Xiang, S. Cao, J. Zhang, G. Ouyang, L. Chen and C.-Y. Su, *Nat. Commun.*, 2013, **4**, 1774.
- 97 D. Bradshaw, S. El-Hankari and L. Lupica-Spagnolo, *Chem. Soc. Rev.*, 2014, **43**, 5431–5443.
- 98 M.-H. Pham, G.-T. Vuong, F.-G. Fontaine and T.-O. Do, *Cryst. Growth Des.*, 2012, **12**, 1008–1013.
- 99 B. Seoane, A. Dikhtiarenko, A. Mayoral, C. Tellez, J. Coronas, F. Kapteijn and J. Gascon, *CrystEngComm*, 2015, **17**, 1693–1700.



## *ELECTRONIC SUPPLEMENTARY INFORMATION (ESI)*

### **Microwave assisted dry-gel conversion - a new sustainable route for the rapid synthesis of metal-organic frameworks with solvent re-use**

Niels Tannert<sup>a</sup>, Serkan Gökpınar<sup>a</sup>, Emrah Hastürk<sup>a</sup>, Sandra Nießing<sup>a</sup> and Christoph Janiak<sup>a\*</sup>

<sup>a</sup> Institut für Anorganische Chemie und Strukturchemie, Heinrich-Heine-Universität Düsseldorf, Universitätsstraße 1, 40225 Düsseldorf, Germany. \*E-mail: [janiak@uni-duesseldorf.de](mailto:janiak@uni-duesseldorf.de)

<sup>b</sup> These authors contributed equally.

#### **Keywords**

Metal-Organic Frameworks, MIL-100(Fe), UiO-66, MIL-140A, Aluminum fumarate, Microwave, Dry-Gel Conversion, Synthesis Optimization, Sustainability, Solvent re-use

Emails: [niels.tannert@hhu.de](mailto:niels.tannert@hhu.de); [serkan.goekpinar@hhu.de](mailto:serkan.goekpinar@hhu.de); [emrah.hastuerk@hhu.de](mailto:emrah.hastuerk@hhu.de); [sandra.niessing@hhu.de](mailto:sandra.niessing@hhu.de)

#### **Table of Contents**

Section S1.	Materials and equipment
Section S2.	Brief description of synthesized metal-organic frameworks
Section S3.	Syntheses of MIL-100(Fe)
Section S4.	Syntheses of UiO-66 and MIL-140A
Section S5.	Syntheses of aluminum fumarate
Section S6.	PXRD measurements
Section S7.	Nitrogen sorption experiments (T = 77 K)
Section S8.	Scanning electron microscopy (SEM)
Section S9.	Thermogravimetric analysis (TGA)
Section S10.	Results of three synthesis runs with solvent re-use
Section S11.	Calculation of solvent amounts
Section S12.	References

## **S1. Materials and equipment**

All chemicals were used as received from supplier (cf. Table S1).

**Table S1** *Used chemicals, supplier and purities.*

Chemical	Supplier	Purity
$\text{Al}(\text{SO})_4 \cdot 18\text{H}_2\text{O}$	AppliChem	not specified
<i>Basolite™ A520</i>	Sigma Aldrich	not specified
<i>Basolite™ F300</i>	Sigma Aldrich	not specified
Benzene-1,4-dicarboxylic acid	Sigma Aldrich	≥98.0%
Benzene-1,3,5-tricarboxylic acid	Sigma Aldrich	95%
Benzoic acid	Riedel de Haen	99.5%
Dimethylformamide	Fischer Chemicals	99.99%
Ethanol	Sigma Aldrich	>99.8%
$\text{FeCl}_3 \cdot 6\text{H}_2\text{O}$	Sigma Aldrich	97%
$\text{Fe}(\text{NO})_3 \cdot 9\text{H}_2\text{O}$	Sigma Aldrich	98%
Fumaric acid	Alfa Aesar	99%
Hydrochloric acid, 37%	Sigma Aldrich	p.a.
Hydrofluoric acid, 48%	Sigma Aldrich	p.a.
NaOH (microgranulate)	Chem Solute	not specified
Nitric acid, 65%	VWR Chemicals	p.a.
Sodium fluoride	Sigma Aldrich	99.99%
Tetrabutylammonium fluoride, hydrate	Sigma Aldrich	96%
Zirconium chloride	Alfa Aesar	≥99.5%

Powder X-ray diffraction (PXRD) patterns were obtained out at ambient temperature on a *D2 phaser* (BRUKER, Billerica, US) using Cu-K $\alpha$  radiation ( $\lambda = 1.54182 \text{ \AA}$ ) between  $5^\circ < 2\theta < 50^\circ$  with a scanning rate of  $0.0125^\circ/\text{s}$  (300 W, 30 kV, 10 mA). The diffractograms were obtained on a flat “low background sample holder”, in which at low angle the beam spot is strongly broadened so that only a fraction of the reflected radiation reaches the detector, hence the low relative intensities measured at  $2\theta < 7^\circ$ . Analyses of the diffractograms were carried out with *Match 3.11* software.

Thermogravimetric analysis (TGA) was performed with a *TG209 F3 Tarsus* (NETZSCH, Selb, Germany). Samples were placed in alumina pans and heated at a rate of  $5 \text{ Kmin}^{-1}$  from 25–600 °C under synthetic air atmosphere.

Nitrogen (purity 99.9990%, 5.0) physisorption isotherms were carried out on a *Nova 4000e* (QUANTACHROME, Odelzhausen, Germany) at  $T = 77 \text{ K}$ . Before measuring of the isotherms, the products were transferred into glass tubes capped with septa, which were weighted out before. These tubes were attached to the corresponding degassing port of the sorption analyzer, degassed under vacuum at 120 °C for 3 h, weighted out again and then transferred to the analysis port of the sorption analyzer. BET surface areas were calculated from the  $\text{N}_2$  adsorption isotherms in an individual  $p/p_0$  range for each MOF (cf. Section S7). Total pore volumes were calculated from the  $\text{N}_2$  sorption isotherm at  $p/p_0 = 0.95$ . NLDFT calculations for the pore size distribution curves were done with the native *NovaWin 11.03* software using the ‘ $\text{N}_2$  at 77 K on carbon, slit pore, NLDFT equilibrium’ model.

Scanning electron microscopy (SEM) images were recorded with a *JSM-6510LV QSEM Advanced electron microscope* (JEOL, Akishima, Japan) with a LaB $_6$  cathode at 5–20 keV. The microscope was equipped with a *Xflash 410* (BRUKER, Billerica, US) silicon drift detector.

The microwave for MW-DGC syntheses was a *MARS-5* (CEM, Matthews, US).

DGC inlays were self-built, made of Teflon. The holes in the DGC sieves had 0.5 mm diameter. The ring inlays, shown in Figure S1, can have various heights for adjustment. We thank the precision mechanics workshop of Heinrich-Heine-University.



**Figure S1** Top: Full autoclave set for MW-DGC with microwave tube, lid and screw-cap, three ring inlays for height-adjustment of sieve and DGC sieve, given also at bottom left in close-up view. Bottom right: Close-up view of a CE-DGC sieve with inlay ring for height adjustment.

## S2. Brief description of synthesized metal-organic frameworks

### S2.1. MIL-100(Fe)

Metal-organic frameworks with MIL-100 topology (*Matériaux de l'Institut Lavoisier*) were first described by the group of G. Férey in 2004.<sup>1</sup> Figure S2 shows the structural features of MIL-100(Fe) with respect to bonding situations and cavities.

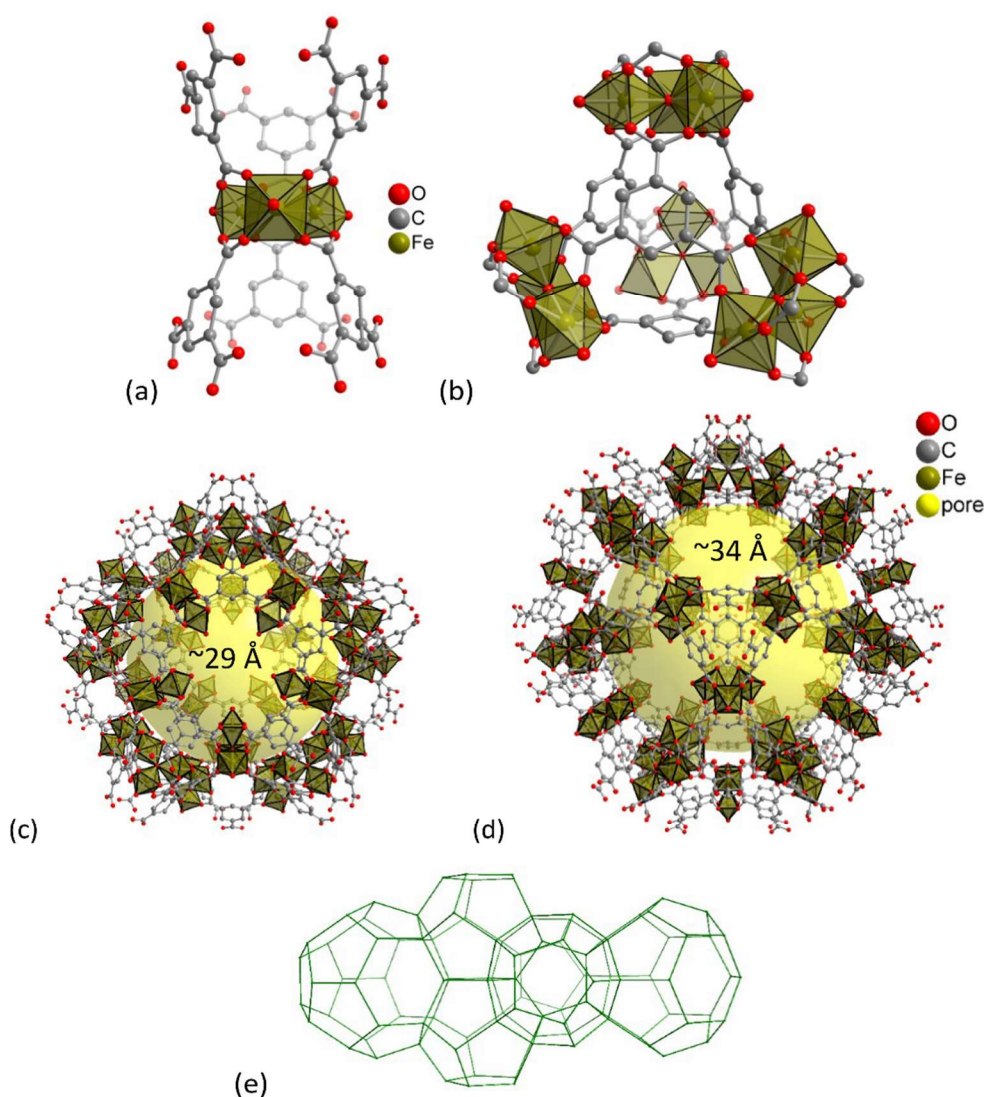


**Figure S2** Structural features of MIL-100(Fe). (a) secondary building unit (SBU), (b) supertetrahedra, (c) small S cage, (d) large L cage and (e) topology of the mesoporous network (objects are not drawn to scale). Hydrogen atoms and solvent molecules are not shown. The yellow spheres in the mesoporous cages with the indicated diameters take into account the van-der-Waals radii of the framework walls. Hydrogen atoms and solvent molecules of crystallization are not shown. Graphics have been drawn with the software DIAMOND<sup>2</sup> from the deposited cif-file under CCDC no. 640536 for Fe.<sup>3</sup>

MIL-100(Fe) consists of hybrid supertetrahedra with oxocentered trimers of trivalent metal octahedra connected by trimesate anions (benzene-1,3,5-tricarboxylate – short: BTC).<sup>1,4</sup> MIL-100(Fe) with the chemical formula  $[\text{Fe}^{\text{III}}_3(\mu_3\text{-O})(\text{X})(\text{BTC})_2 \cdot n\text{H}_2\text{O}]_m$  (with X = F, OH; depending on synthetic conditions) exhibit zeolite MTN topology, mesoporous cages of 25 and 29 Å with microporous (i.e. <2



nm) windows of 5.5 and 8.6 Å and an inner specific surface area of 356-2320 m<sup>2</sup>g<sup>-1</sup> (Brunauer-Emmett-Teller, BET area), highly depending on synthetic conditions.<sup>5-6</sup>

MIL-100 is studied for gas storage and sequestration,<sup>11-7</sup> in composites,<sup>8,9</sup> as sorption material for heating/cooling applications,<sup>10-11,12,13</sup> mixed-matrix membranes,<sup>14</sup> many-sided synthesis optimizations,<sup>5,8,10,15,16</sup> drug delivery and more.<sup>17-18</sup> Notably, MIL-100 materials were shown to be highly versatile and tunable in terms of crystallinity, morphology and particle size.<sup>19-20</sup> This in turn allows their preparation as xerogels and aerogels, what expands applicability even further.<sup>21-22</sup> Moreover, MIL-100 proved to be suitable as heterogeneous catalyst in several organic reactions.<sup>3,20,22,23-24</sup> Low toxicity, biocompatibility and abundance of iron are key-factors for utilization of MIL-100(Fe) in application-oriented research.<sup>3</sup>

MIL-100(Fe) can as well be prepared continuously with a space-time yield (STY) of 20 kg m<sup>-3</sup> day<sup>-1</sup>.<sup>25</sup> STY is hereby defined as the amount of produced MOF (kg) per unit volume of reactor (m<sup>3</sup>) per day of synthesis (alternatively: per unit volume of reaction mixture (m<sup>3</sup>) per day of synthesis<sup>26</sup>).<sup>27</sup>

Exemplarily, Figure S3 depicts MIL-100(Fe) products, obtained by DGC.



**Figure S3** Left: Autoclave with DGC sieve, with MIL-100(Fe) product on top. Right: Products obtained from Fe(NO<sub>3</sub>)<sub>3</sub>·9H<sub>2</sub>O (left), FeCl<sub>3</sub>·6H<sub>2</sub>O (right).

## S2.2. UiO-66 and MIL-140A

Zirconium MOFs represent a subclass of frameworks, which gets more and more attention, due to their excellent stability in thermal, aqueous and acid conditions.<sup>28,29</sup> Among these Zr-MOFs is UiO-66 (*Universitetet i Oslo*), which was first synthesized by Lillerud and co-workers<sup>30</sup> and MIL-140A synthesized by Serre and co-workers.<sup>31</sup> UiO-MOFs have a  $\{\text{Zr}_6\text{O}_4(\text{OH})_4\}$ -SBU, which is an octahedral  $\text{Zr}_6$ -cluster of six edge-sharing  $\text{ZrO}_8$  square-antiprism and which is 12 coordinated by the linker molecules to 12 neighboring SBUs in a face-centered cubic (fcc) packing arrangement.<sup>44</sup> Depending on used dicarboxylate linker it can be obtained UiO-66 (linker = 1,4-benzenedicarboxylic acid), UiO-67 (linker = 4,4'-biphenyldicarboxylic acid) or UiO-68 (4,4''-terphenyldicarboxylic acid) with an isorecticular framework. Figure S4 shows the crystal structure of zirconium terephthalate UiO-66.

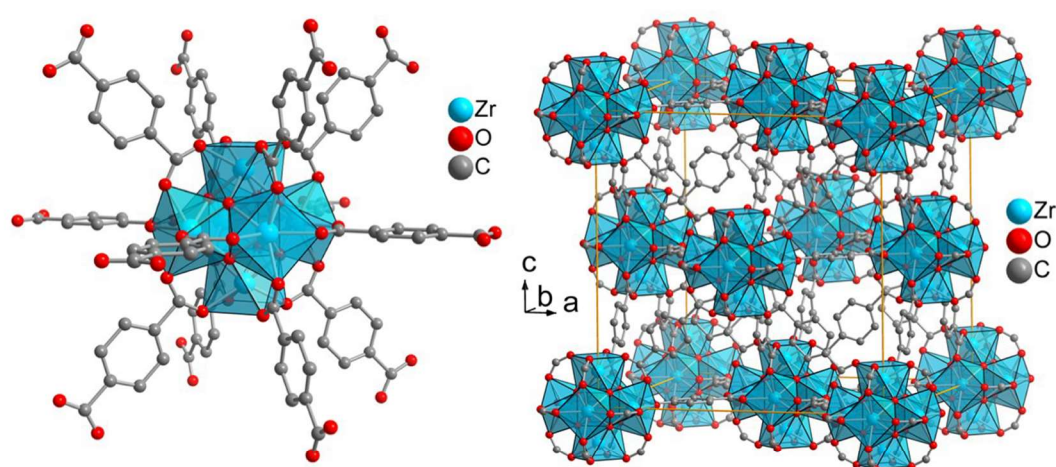


**Figure S4** Crystal structure of zirconium terephthalate UiO-66.<sup>44</sup> Hydrogen atoms and solvent molecules are not shown. The UiO-66 structure is drawn with the software Diamond<sup>2</sup> from the deposited cif-file under CCDC no. 837796.<sup>32</sup>

The properties of these UiO-MOFs are interesting for gas storage,<sup>33</sup> separation,<sup>34</sup> water sorption,<sup>35,36</sup> sensing<sup>37</sup> and catalysis.<sup>38,39</sup> UiO-66 can be synthesized solvothermally, *via* mechanochemistry<sup>40</sup> or DGC<sup>41</sup> and also continuously with a space-time yield (STY) of  $4,899 \text{ kg d}^{-1} \text{ m}^{-3}$ .<sup>42</sup>

Figure S5 shows the crystal structure of zirconium terephthalate MIL-140A. The MIL-140 series are polymorphs of the UiOs with the general formula  $[\text{ZrO}(\text{linker})]$ , while MIL-140A has a BDC linker. MIL-140s consist of one dimensional zirconium oxide chains (along the c-axis), which are linked to six other chains through dicarboxylate linkers, thereby obstructing one-dimensional channels.<sup>45</sup>

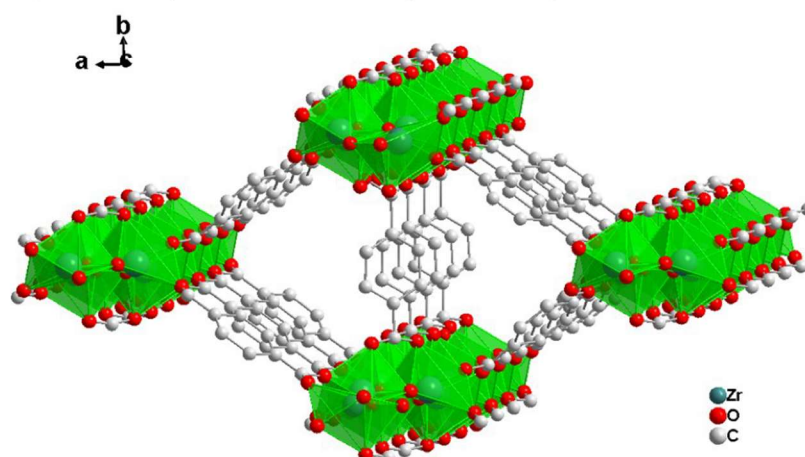


**Figure S5** Crystal structure of zirconium terephthalate MIL-140A. The MIL-140A structure is drawn with the software Diamond<sup>2</sup> from the deposited cif-file under CCDC no. 905026.<sup>45</sup>

### S2.3. Aluminum fumarate (Alfum)

Aluminum fumarate (Alfum) was first described in the patent literature.<sup>43,44</sup> Figure S6 shows the structural features of aluminum fumarate with respect to bonding situations and cavities.

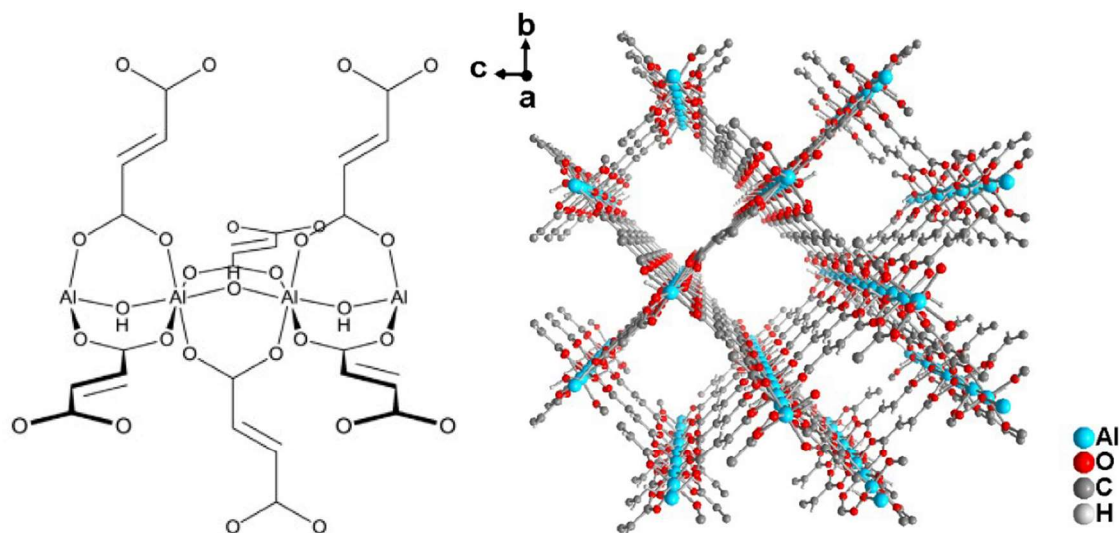


**Figure S6** Left: Building block of Alfum, in analogy to the structure of MIL-53. The illustration was taken from ref. <sup>45</sup> Right: Crystal structure of aluminum fumarate. Graphic produced by software Diamond <sup>2</sup> from cif-file for Basolite A520 (CSD-Refcode DOYBEA, CCDC no. 1051975).<sup>46</sup>

Alfum resembles the monoclinic MIL-53(Al) structure (i.e. with benzene-1,4-dicarboxylate as linker) with infinite Al-OH-Al chains connected by fumarate linkers. It has the chemical formula  $[\text{Al}(\text{OH})(\text{O}_2\text{C}-\text{CH}=\text{CH}-\text{CO}_2)]_n$  and displays microporous, rhombohedral channels with circa  $5.7 \times 6.0 \text{ \AA}^2$  free dimensions.<sup>60,47</sup>

Aluminum fumarate is one of the most promising MOFs for application,<sup>59,60,48</sup> due to its hydrothermal stability and an environmentally friendly synthesis route with water as single solvent, inexpensive and benign metal cation, moreover, a “green” linker from renewable biomass,<sup>49</sup> besides possible large scale production with a high STY of  $>3615 \text{ kg m}^{-3} \text{ day}^{-1}$ .<sup>57,58,50</sup> Gaab *et al.* proved its applicability as storage container for natural gas, used as fuel in a vehicle, by 40% increased cruising distance.<sup>64</sup> Moreover, Alfum was proven to represent suitable water sorption characteristics and cyclic stability for heat transformation application,<sup>59</sup> it is applicable as super adsorbent for removal of fluoride from water <sup>51</sup> and in desalination processes <sup>52</sup> and it was proposed to be the best porous solid for mechanical energy storage.<sup>53</sup> It can as well be prepared *via* (potentially continuously operable) mechanochemical techniques, such as extrusion.<sup>54</sup> Thereby,  $27000 \text{ kg m}^{-3} \text{ day}^{-1}$  STY were calculated to be feasible.<sup>55</sup> Continuous flow methods achieved even STYs up to  $97\,159 \text{ kg m}^{-3} \text{ day}^{-1}$  at  $5.6 \text{ kg h}^{-1}$  and ca.  $1000\text{--}1100 \text{ m}^2\text{g}^{-1}$ .<sup>40</sup>



### S3. Syntheses of MIL-100(Fe)

In a typical synthetic procedure, the metal salts  $\text{Fe}(\text{NO})_3 \cdot 9\text{H}_2\text{O}$  and  $\text{FeCl}_3 \cdot 6\text{H}_2\text{O}$  were ground with  $\text{H}_3\text{BTC}$  in a molar ratio of 1:1 (2-4 mmol of each reactant) *via* ball-milling (20 Hz, 20 Min) using a *Retsch MM301* (RETSCH, Haan, Germany). However, simple grinding in a mortar yielded the desired phase too.

#### S3.1. Microwave-assisted dry-gel conversion (MW-DGC)

The precursor mixture of around 100 mg combined mass was placed on a MW-DGC sieve (cf. Fig. S1) with water or acidic solutions (5 mL) at the bottom of the Teflon-reactor, which was tightly closed and heated to 150 °C for 180 min by applying 800 W, using a *CEM MARS-5* microwave. The orange-brownish (from  $\text{Fe}(\text{NO})_3 \cdot 9\text{H}_2\text{O}$ ) or reddish (from  $\text{FeCl}_3 \cdot 6\text{H}_2\text{O}$ ) solid products were washed with water and ethanol three times (10 mL each) and dried (80 °C, 24 h). Amounts of starting materials and yields in already optimized syntheses are given in Table S2.

**Table S2** Synthesis details of different MIL-100(Fe) samples obtained via MW-DGC.

Fe source	Solvent (5 mL)	$m_{\text{Fe-salt}}$ [mg]	$m_{\text{H}_3\text{BTC}}$ [mg]	$n_{\text{Fe}} = n_{\text{BTC}}$ [mmol]	Yield [g]	Yield [%] <sup>a</sup>	BET [ $\text{m}^2\text{g}^{-1}$ ]
Fe-chloride	neat $\text{H}_2\text{O}$	50.0	38.9	0.185	0.045	78	1002
	$\text{H}_2\text{O} + \text{HNO}_3$ (1:1)	49.5	38.4	0.183	0.046	81	460
	$\text{H}_2\text{O}/\text{EtOH}$ (4:1)	53.0	41.2	0.196	0.037	61	922
Fe-nitrate	neat $\text{H}_2\text{O}$	77.2	40.1	0.191	0.047	81	1105
	$\text{H}_2\text{O} + \text{HNO}_3$ (1:1)	78.0	41.3	0.193	0.046	78	526
	$\text{H}_2\text{O}/\text{EtOH}$ (4:1)	84.8	45.0	0.210	0.050	78	1180

<sup>a</sup> Based on the amount of Fe-salt and on the MIL-100(Fe) formula of  $[\text{Fe}^{\text{III}}_3(\mu_3\text{-O})(\text{H}_2\text{O})_2(\text{Cl})(\text{BTC})_2 \cdot 14.5 \text{H}_2\text{O}]_m$  and  $M_w = 930.47 \text{ g mol}^{-1}$  for MIL-100(Fe) products of Fe-chloride based synthesis, respectively  $[\text{Fe}^{\text{III}}_3(\mu_3\text{-O})(\text{H}_2\text{O})_2(\text{OH})(\text{BTC})_2 \cdot 14.5 \text{H}_2\text{O}]_m$  and  $M_w = 912.02 \text{ g mol}^{-1}$  for MIL-100(Fe) products of Fe-nitrate based synthesis. The amount of crystal water after drying was estimated to be  $x = 14.5$  per formula unit in accordance to earlier reports.<sup>9,11</sup>

#### S3.2. Conventionally heated dry-gel conversion (CE-DGC)

Synthetic conversions of precursors were performed on top of a DGC sieve holder with water or acidic solutions (20 mL) on the bottom of a Teflon-lined steel autoclave at 150 °C (2 h heating to 150 °C, 24 h, 2 h cooling) using electrical heating ovens. The orange-brownish (from  $\text{Fe}(\text{NO})_3 \cdot 9\text{H}_2\text{O}$ ) or reddish (from  $\text{FeCl}_3 \cdot 6\text{H}_2\text{O}$ ) solid products were washed with water and ethanol three times (each 40 mL), dried and finally activated (80 °C, 24 h). Initial weights of precursor mixtures and yields in already optimized syntheses are given in Table S3.

**Table S3** Synthesis details of different MIL-100(Fe) samples obtained via CE-DGC.

Fe source	Solvent (20 mL)	$m_{\text{Fe-salt}}$ [mg]	$m_{\text{H}_3\text{BTC}}$ [mg]	$n_{\text{Fe}} = n_{\text{BTC}}$ [mmol]	Yield [g]	Yield [%] <sup>a</sup>	BET [ $\text{m}^2\text{g}^{-1}$ ]
Fe-chloride	neat $\text{H}_2\text{O}$	205.4	159.7	0.760	0.162	69	1776
	$\text{H}_2\text{O} + \text{HNO}_3$ (1:1)	203.8	158.4	0.754	0.146	62	1469
	$\text{H}_2\text{O}/\text{EtOH}$ (4:1)	197.0	153.2	0.729	0.101	45	1287
Fe-nitrate	neat $\text{H}_2\text{O}$	444.0	230.9	1.099	0.267	80	1876
	$\text{H}_2\text{O} + \text{HNO}_3$ (1:1)	248.0	129.0	0.614	0.166	89	1550
	$\text{H}_2\text{O}/\text{EtOH}$ (4:1)	190.7	99.2	0.472	0.138	96	1561

<sup>a</sup> Based on the amount of Fe-salt and on the MIL-100(Fe) formula of  $[\text{Fe}^{\text{III}}_3(\mu_3\text{-O})(\text{H}_2\text{O})_2(\text{Cl})(\text{BTC})_2 \cdot 14.5 \text{H}_2\text{O}]_m$  and  $M_w = 930.47 \text{ g mol}^{-1}$  for MIL-100(Fe) products of



Fe-chloride based synthesis, respectively  $[\text{Fe}^{\text{III}}_3(\mu_3\text{-O})(\text{H}_2\text{O})_2(\text{OH})(\text{BTC})_2 \cdot 14.5 \text{ H}_2\text{O}]_m$  and  $M_w = 912.02 \text{ g mol}^{-1}$  for MIL-100(Fe) products of Fe-nitrate based synthesis. The amount of crystal water after drying was estimated to be  $x = 14.5$  per formula unit in accordance to earlier reports.<sup>9,11</sup>

During our work we have carried out synthesis optimization for the MW-DGC approach for MIL-100(Fe): We varied the molar ratio of reactants, reaction time and temperature, respectively microwave irradiation power. Additionally, we performed syntheses with fluoride sources such as tetrabutylammonium fluoride (TBAF) and sodium fluoride, by adding 2 wt.% to the precursor mixture. Aqueous HF was added to the solvent (1: 10 by vol.). The addition of any fluoride source did not lead to improved products. Also other ratios of water/ethanol and water/ $\text{HNO}_3$  were applied, but did not yield improved products. Thus, we describe only the optimized syntheses above.

## **S4. Syntheses of UiO-66 and MIL-140A**

### **S4.1. UiO-66**

#### **S4.1.1. Microwave-assisted dry-gel conversion (MW-DGC)**

For the synthesis of UiO-66-HCl *via* MW-DGC,  $\text{ZrCl}_4$  (88 mg, 0.38 mmol, 1.0 eq),  $\text{H}_2\text{BDC}$  (63 mg, 0.38 mmol, 1.0 eq) and benzoic acid (BA) (100 mg, 0.82 mmol, 2.1 eq) were mixed, ground in a mortar and placed on the sieve. DMF solvent (10 mL) and 1 mL of HCl (37%) was placed at the bottom of the Teflon tube. The sieve, which was filled with precursor mixture was placed above the solvent-mixture and the Teflon tube was capped and heated to 180 °C (10 min heating to 180 °C, 50 min, cooling) by applying 600 W, using a CEM MARS-5 microwave. After the tube was cooled down to room temperature, the obtained as-synthesized product was soaked in DMF (2 x 5 mL, 24 h each) and ethanol (5 mL, 24 h). The solvent was exchanged every 24 h. After a total time of 3 d of soaking, the solids were centrifuged and dried under vacuum. For UiO-66-IL a DMF/[BMIm]NTf<sub>2</sub> (9:1 by vol.) solvent mixture was used.

#### **S4.1.2. Synthesis of ionic liquid (IL) [BMIm]NTf<sub>2</sub>**

The ionic liquid was synthesized according to a modified procedure of Deetlefs *et al.*<sup>56</sup> For microwave synthesis of [BMIm]Cl a mixture of 1-methylimidazole (150 mmol) and 1-chlorobutane (153 mmol) was placed in a Teflon vessel equipped with a magnetic stirrer. The temperature was raised to 160 °C over the course of 20 min, and microwave irradiation continued for a further 60 min. The anion of [BMIm]Cl was exchanged by reaction with LiNTf<sub>2</sub> (150 mmol) in H<sub>2</sub>O to give the [BMIm]NTf<sub>2</sub> according to the procedure by Wegner *et al.*<sup>57</sup>

### **S4.2. MIL-140A**

#### **S4.2.1. Microwave-assisted dry-gel conversion (MW-DGC)**

For the synthesis of MIL-140A *via* MW-DGC,  $\text{ZrCl}_4$  (88 mg, 0.38 mmol, 1 eq),  $\text{H}_2\text{BDC}$  (63 mg, 0.38 mmol, 1 eq) and benzoic acid (100 mg, 0.82 mmol, 2.1 eq) were mixed, ground in a mortar and placed on the sieve. The DMF solvent (10 mL) was placed at the bottom of the Teflon tube and the sieve, filled with precursor mixture, was placed above the solvent. The Teflon tube was capped and heated to 160 °C (10 min heating to 160 °C, 80 min, cooling) by applying 600 W, using a CEM MARS-5 microwave. After the tube was cooled down to room temperature, the obtained as-synthesized product was soaked in DMF (2 x 5 mL, 24 h each) and ethanol (5 mL, 24 h). The solvent was exchanged every 24 h. After 3 d of soaking, the solids were centrifuged and dried under vacuum.

Yields, BET areas and pore volumes for UiO-66 and MIL-140A from MW-DGC synthesis are given in Table 2 in the full manuscript, in comparison with literature values for CE-DGC and solution synthesis.

## S5. Syntheses of aluminum fumarate

The compounds  $\text{Al}_2(\text{SO}_4)_3 \cdot 18\text{H}_2\text{O}$ , fumaric acid and NaOH were mixed at a molar ratio of 1:2:4 by rapid grinding in a mortar. Thereupon, the precursor mixture was quickly placed on top of a DGC sieve holder, quickly placed in the Teflon container for the reaction in the microwave or CE oven.

### S5.1. Microwave-assisted dry-gel conversion (MW-DGC)

Synthetic conversions of precursors were performed on top of a MW-DGC sieve holder with water (5 mL) at the bottom of a Teflon-reactor at 100 °C (60 Min) by applying 800 W using a CEM MARS-5 microwave. The white products were washed three times with water (10 mL each), and dried under vacuum (80 °C, 24 h). Initial weights of precursor mixtures and yields are given in Table S4.

**Table S4** Synthesis details of different aluminum fumarate samples obtained via repeated MW-DGC.

Precursor [g]	$m_{\text{Al-salt}}$ [g]	$m_{\text{fumaric acid}}$ [g]	$n_{\text{Al}}$ [mmol]	$n_{\text{fumaric acid}}$ [mmol]	Yield [g]	Yield [%] <sup>a</sup>	BET [ $\text{m}^2\text{g}^{-1}$ ]
0.273	0.172	0.060	0.52	0.52	0.062	76	1075
0.252	0.159	0.055	0.48	0.48	0.060	81	1150
0.298	0.188	0.065	0.56	0.56	0.079	89	1128

<sup>a</sup> Based on the amount of Al-salt and on the product formula  $[\text{Al}(\text{OH})(\text{O}_2\text{C}-\text{CH}=\text{CH}-\text{CO}_2)]_n$  and  $M_w = 158.045 \text{ g mol}^{-1}$  for Alfum.

### S5.2. Conventionally electric-heated dry-gel conversion (CE-DGC)

Synthetic conversions of precursors were performed on top of a DGC sieve holder with water (2 mL) at the bottom of a Teflon-reactor inside a stainless-steel autoclave at 100 °C (6-24 h) in an electrically heated oven. The white products were washed three times with water (50 mL each) and dried under vacuum (80 °C, 24 h). Initial weights of aluminum sulfate and yields are given in Table S5.

**Table S5** Synthesis details of different aluminum fumarate samples obtained via CE-DGC.

$m_{\text{Al-salt}}$ [g]	$m_{\text{fumaric acid}}$ [g]	$n_{\text{Al}}$ [mmol]	$n_{\text{fumaric acid}}$ [mmol]	Yield [g]	Yield [%] <sup>a</sup>	BET [ $\text{m}^2\text{g}^{-1}$ ]	Time [h]
0.159	0.111	0.48	0.96	0.0435	58	1284	6
0.157	0.109	0.47	0.94	0.0500	67	1037	6
0.159	0.111	0.48	0.96	0.0532	71	1129	24

<sup>a</sup> Based on the amount of Al-salt and on the product formula  $[\text{Al}(\text{OH})(\text{O}_2\text{C}-\text{CH}=\text{CH}-\text{CO}_2)]_n$  and  $M_w = 158.045 \text{ g mol}^{-1}$  for Alfum.

### S5.3. Conventional solution-based synthesis

According to the patent by BASF,<sup>57,58</sup> we performed solution-based syntheses at 60 °C under aqueous reflux conditions in a round-bottom flask. Aluminum sulfate-octadecahydrate (1.1710 g, 1.76 mmol, 1 eq), sodium hydroxide (0.2803 g, 7.01 mmol, 4 eq) and fumaric acid (0.3863 g, 3.33 mmol, 2 eq) yielded 74% of product (0.4104 g; after vacuum, 80 °C, 24 h).

## S6. PXRD measurements

Crystallinity and phase purity was examined with powder X-ray diffractometry (PXRD), using a *D2 Phaser* (BRUKER, Billerica, US) diffractometer with a flat silicon, low background sample holder and Cu-K $\alpha$  radiation ( $\lambda = 1.54184 \text{ \AA}$ ) at 30 kV and  $0.04 \text{ }^\circ\text{s}^{-1}$  in the  $2\theta = 5\text{--}50^\circ$  range. In the case of MIL-100(Fe) samples detector limits were 0.18 and 0.25 V, in order to suppress the X-ray-fluorescence of iron. Analyses of the diffractograms were carried out with *Match 3.11* software.

Relevant PXRD plots are given in the full paper.

## S7. Nitrogen sorption experiments (T = 77 K)

Surface areas (BET) were determined by nitrogen (purity 99.999%, 5.0) sorption experiments at T = 77 K using a *NOVA-4000e* (QUANTACHROME, Odelzhausen, Germany) instrument within a partial pressure range of  $p/p_0 = 10^{-3}\text{--}1$  bar. Each sample (20–50 mg each) was degassed under vacuum ( $< 10^2$  mbar) at 100 °C (MIL-100(Fe)), 120 °C (UiO-66, MIL-140A) and 150 °C (Alfum) for ca. 3 h, prior to measurement.

All surface areas (BET) were calculated from five adsorption points in the pressure range  $p/p_0 = 0.05\text{--}0.2$  for samples of MIL-100(Fe),  $p/p_0 = 0.01\text{--}0.05$  for UiO-66,  $p/p_0 = 0.01\text{--}0.10$  for MIL-140A and  $p/p_0 = 0.001\text{--}0.05$  for Alfum. This range is suitable for microporous materials.<sup>58</sup> Full isotherms were collected exemplarily and are given in the full paper in Fig. 2, Fig. 4 and Fig. 7.

Table S6 summarizes repeated N<sub>2</sub> sorption results of the industrial benchmarks *Basolite F300* and *Basolite A520* using the same batch, but not the same sample.

**Table S6** Repeated determination of BET surface areas of *Basolite F300* and *Basolite A520* using nitrogen sorption (T = 77 K).

Benchmark	No. of measurement	BET [m <sup>2</sup> g <sup>-1</sup> ]
<i>Basolite F300</i>	1	1140
	2	1252
	3	847
	4	1100
	5	1024
<i>Basolite A520</i>	1	1030
	2	1038
	3	999
	4	1040
	5	1026

All relevant nitrogen isotherm plots are given in the full paper.

Figure S7 exemplarily depicts four N<sub>2</sub> sorption isotherms of Alfum obtained *via* MW-DGC, proving reproducibility of the composite Type I + Type IV isotherm, caused by micro-mesoporous structure (cf. Fig. S8 and S9).

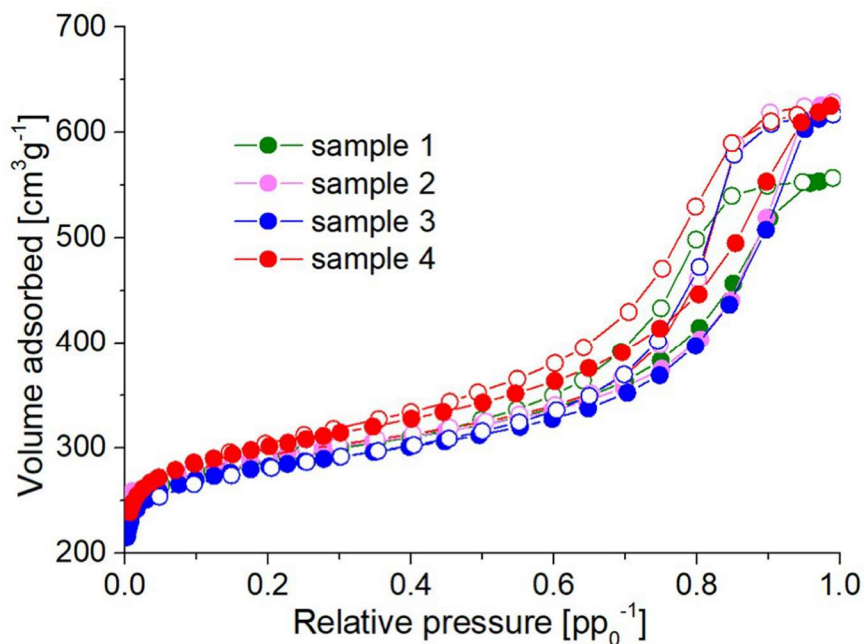


**Figure S7** Examples of nitrogen sorption isotherms (77 K) of four Alfum samples obtained via MW-DGC, revealing reproducibility of adsorption behavior, i.e. composite Type I + Type IV isotherm.

### S7.1. Pore size distributions of Alfum samples

Figures S8 and S9 depict the pore size distributions (NLDFT equilibrium model, carbon, slit pore, N<sub>2</sub> at 77 K) of Alfum samples obtained by different synthesis methods. All pore size distribution curves were calculated with the native *NovaWin 11.03* software using the 'N<sub>2</sub> at 77 K on carbon, slit pore, NLDFT equilibrium' model.

The images visualize the different porosity properties of Alfum samples obtained by different synthesis methods including *Basolite A520*.

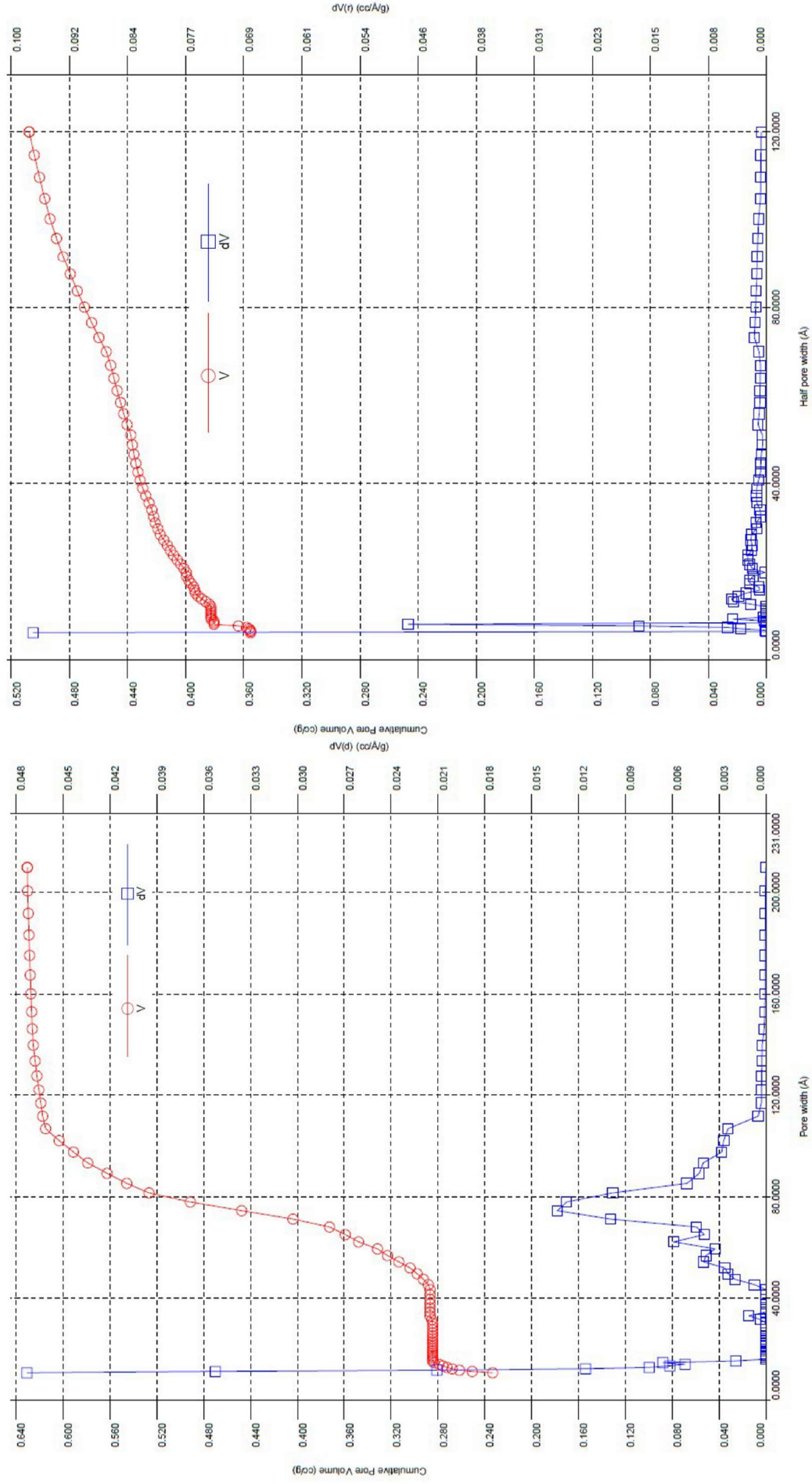


**Figure S8** Pore size distributions (NLDFT equilibrium model, carbon, slit pore, N<sub>2</sub> sorption at 77 K) of Al<sub>2</sub>O<sub>3</sub> samples obtained by MW-DGC (left) and CE-DGC (right). The images shown here are representative examples out of more than 10 determined pore size distributions for the Al<sub>2</sub>O<sub>3</sub> materials.



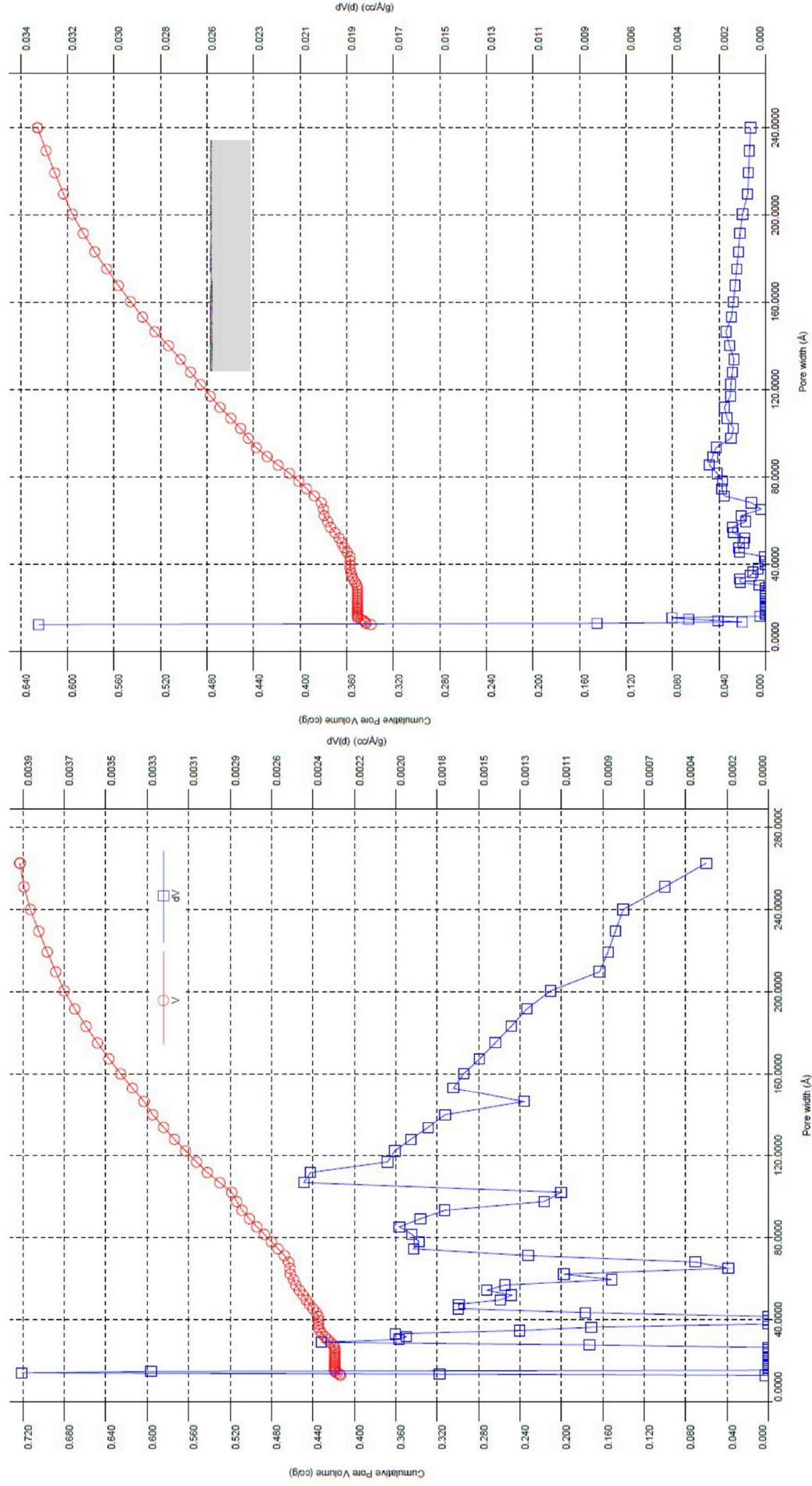


**Figure S9** Pore size distributions (NLDFT equilibrium model, carbon, slit pore,  $N_2$  sorption at 77 K) of Alftum samples obtained by solution-based synthesis (left) and Basolite A520 (right). The images shown here are representative examples out of 6 determined pore size distributions for the Alftum materials.

## S7.2. Comparison of porosity parameters of Alfum samples

Table S7 summarizes the ranges from at least six samples from each synthesis method for Alfum within this work, described in Section S5. All values were derived from N<sub>2</sub> sorption isotherms using the native *NovaWin 11.03* software.

**Table S7** Ranges of porosity parameters from different Alfum samples obtained via MW-DGC, CE-DGC and solution-based synthesis in comparison with Basolite A520. At least six samples of each synthesis method were measured and taken into account.

	$S_{BET}$ [m <sup>2</sup> g <sup>-1</sup> ] <sup>a</sup>	$S_{micro-BET}$ [m <sup>2</sup> g <sup>-1</sup> ] <sup>b</sup>	$S_{Ext}$ [m <sup>2</sup> g <sup>-1</sup> ] <sup>c</sup>	$V_{pore (total)}$ [cm <sup>3</sup> g <sup>-1</sup> ] <sup>d</sup>	$V_{pore (NLDFT)}$ [cm <sup>3</sup> g <sup>-1</sup> ] <sup>e</sup>	$V_{pore (micro)}$ [cm <sup>3</sup> g <sup>-1</sup> ] <sup>f</sup>
MW-DGC	1015-1148	781-912	216-307	0.67-0.96	0.72-0.94	0.27-0.36
CE-DGC	1037-1188	941-1089	86-118	0.43-0.72	0.43-0.61	0.37-0.42
Solution-based	780-1254	654-1120	126-134	0.49-0.72	0.36-0.72	0.26-0.43
Basolite A520	999-1040	885-930	109-114	0.58-0.63	0.51-0.63	0.31-0.36

<sup>a</sup> BET surface areas ( $S_{BET}$ ) were obtained from five adsorption points in the pressure range  $pp_0^{-1}=0.001-0.05$ . <sup>b</sup> Micropore areas ( $S_{micro-BET}$ ) were obtained by t-plot and V-t-method. <sup>c</sup> External area ( $S_{Ext}$ ) refers to all area that does not originate from micropores and it includes meso- and macropores, i.e. pores > 2nm. Obtained by t-plot and V-t-method. <sup>d</sup> Total pore volumes ( $V_{pore (total)}$ ) were derived at  $pp_0^{-1} = 0.95$  for pores ≤20 nm. <sup>e</sup> Pore volumes from NLDFT ( $V_{pore (NLDFT)}$ ) were calculated using 'N<sub>2</sub> at 77 K on carbon, slit pore, NLDFT equilibrium' model. <sup>f</sup> Micropore volume ( $V_{pore (micro)}$ ) refers to volume that originates only from micropores, obtained by V-t-method with thickness method 'DeBoer'.

All correlation coefficients (r) within calculations were >0.999.

### **S8. Scanning electron microscopy (SEM)**

The morphology was imaged by SEM using a *JSM-6510 advanced electron microscope* (JEOL, Akishima, Japan) with a  $\text{LaB}_6$  cathode at 5-20 keV. Figures S10-S12 display obtained products at different scales.

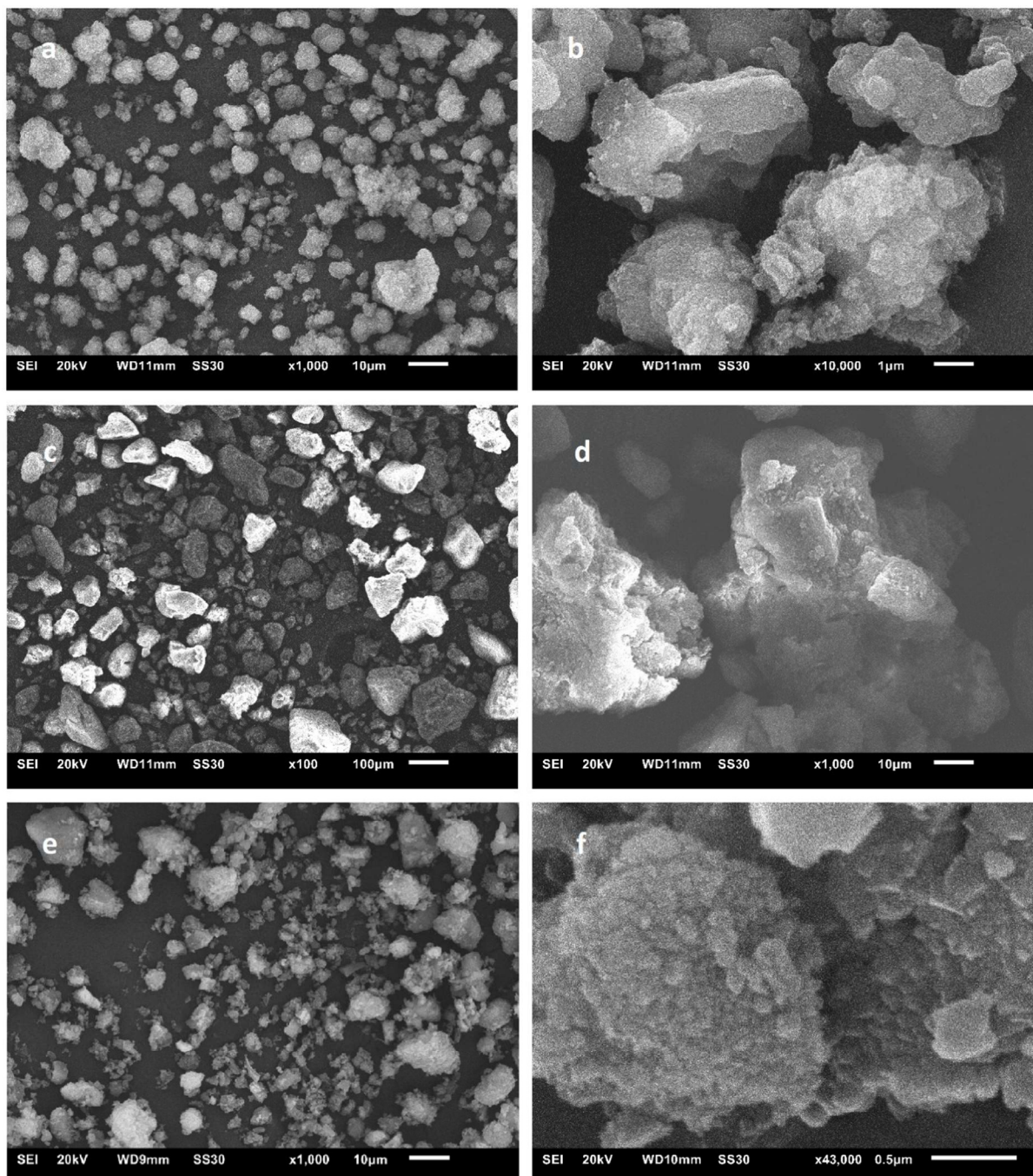


**Figure S10** SEM images of MIL-100(Fe) (left: overview, right: close-up): Basolite F300 (a, b), MW-DGC product (c, d) and CE-DGC product (e, f).



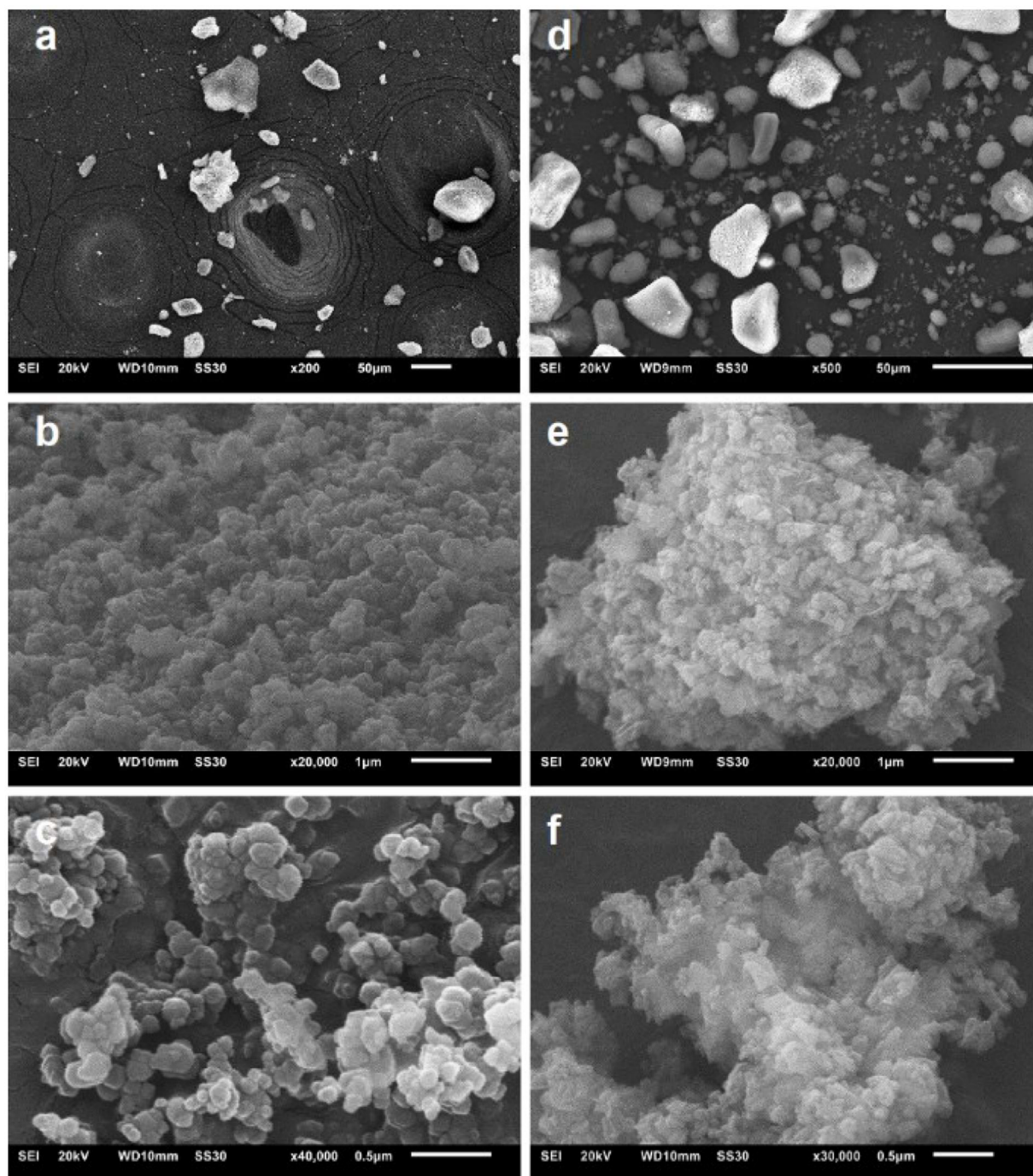


**Figure S11** SEM images of UiO-66-HCl (a, b and c) and MIL-140A (d, e and f) obtained via MW-DGC.



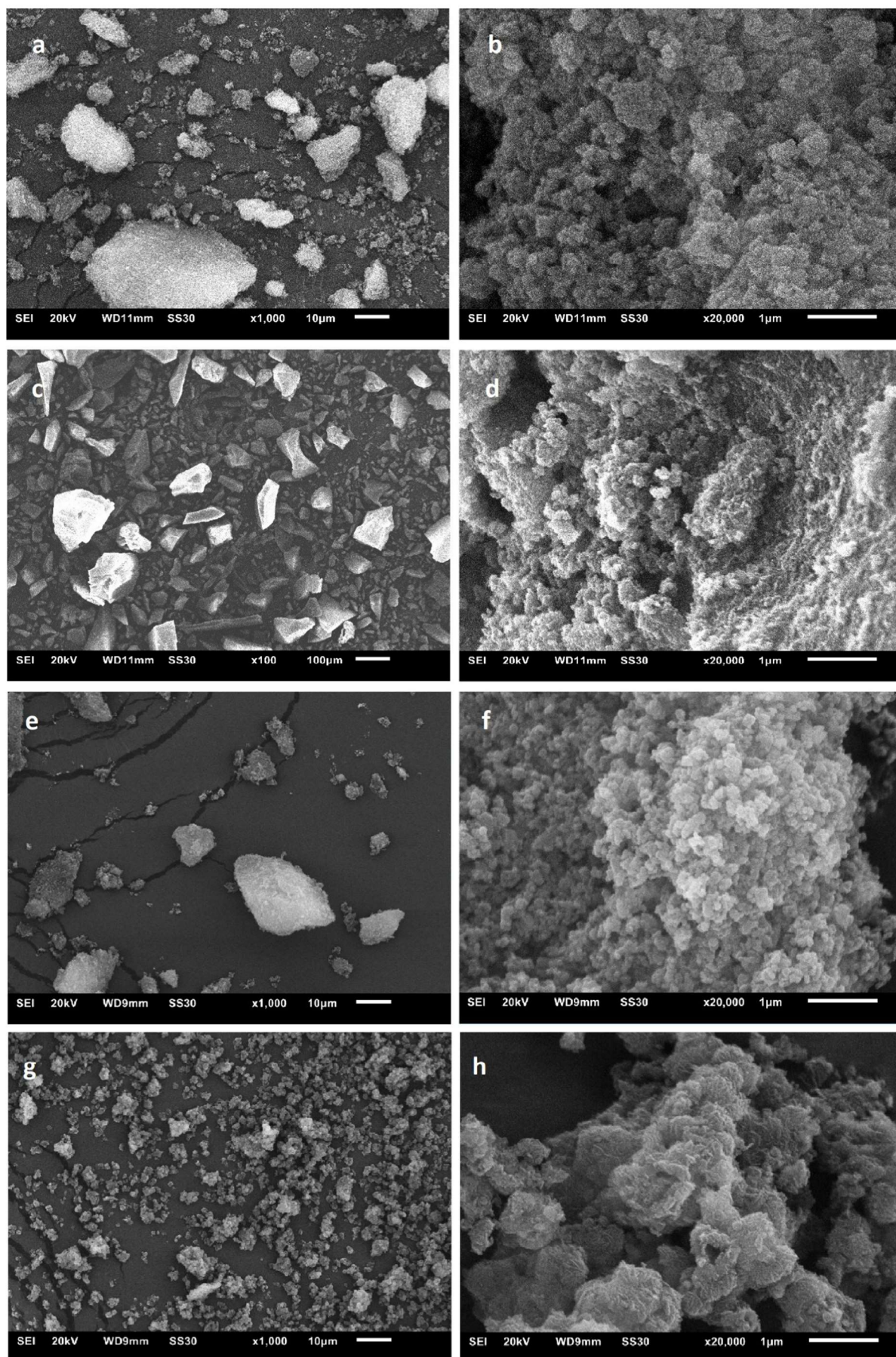
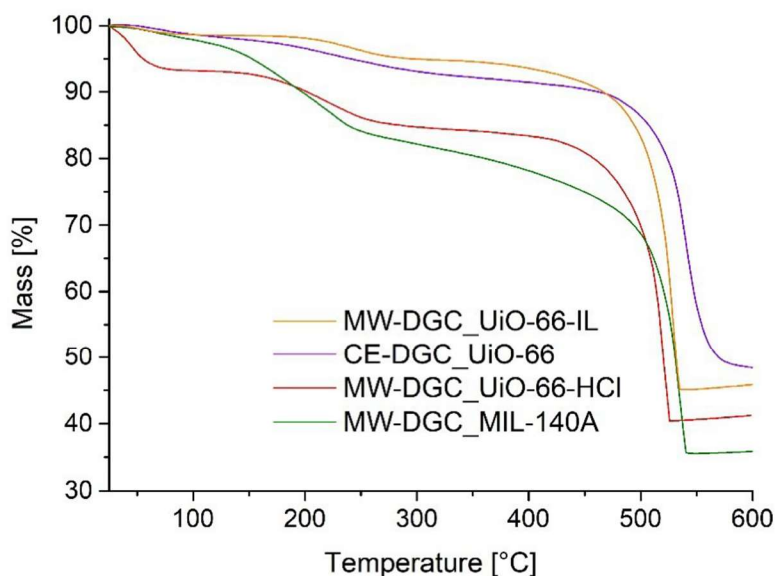


**Figure S12** SEM images of aluminum fumarate (left: overview, right: close-up): Basolite A520 (a, b), MW-DGC product (c, d), CE-DGC product (e, f) and conventional solution-based product (g, h).

### S9. Thermogravimetric Analysis (TGA)

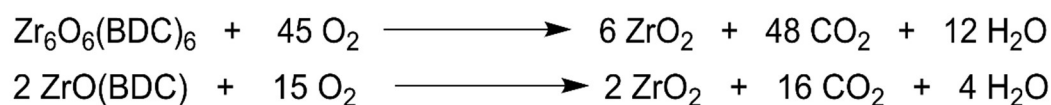
TGA measurements were carried out on a *TG209 F3 Tarsus* (NETZSCH, Selb, Germany) device under synthetic air atmosphere, ramping with 5 Kmin<sup>-1</sup> to target temperature (600 °C).

Figure S13 shows the TGA curves of MW-DGC products of UiO-66 and MIL-140A in comparison to the CE-DGC product of UiO-66 from ref. 55.



**Figure S13** TGA results of MW-DGC products UiO-66 and MIL-140A.

**Determination of defects per SBU** was done similar to the procedure of Shearer *et. al.*<sup>43</sup> An assumption of this method is that the residue in each TGA experiment is ZrO<sub>2</sub>. The reaction of decomposition for both MOFs UiO-66 (Zr<sub>6</sub>O<sub>6</sub>(BDC)<sub>6</sub> (defect-free and dehydroxylated) and MIL-140A ZrO(BDC) can be described as follows:



The determination can be parted in three steps:

1) Determine the theoretical plateau weight **W<sub>Theo.Plat</sub>** :

$$W_{\text{Theo.Plat}} = (M_{\text{Comp}}/M_{6\text{xZrO}_2}) \cdot W_{\text{End}}$$

$$W_{\text{Theo.Plat}} = (M_{\text{Comp}}/M_{\text{ZrO}_2}) \cdot W_{\text{End}}$$

with  $M_{\text{Comp}}$  (UiO-66; dehydroxylated, defect-free) = 1628.03 g/mol,  $M_{\text{Comp}}$  (MIL-140A) = 271.22 g/mol,  $M_{6\text{xZrO}_2}$  = 739.34 g/mol,  $M_{\text{ZrO}_2}$  = 123.22 g/mol and  $W_{\text{End}}$  = 100%, which is the end weight of the TGA run (=normalized to 100%).

We obtain  $W_{\text{Theo.Plat}}$  values of UiO-66 and MIL-140A:

$$W_{\text{Theo.Plat}} (\text{UiO-66}) = 220.20\%$$

$$W_{\text{Theo.Plat}} (\text{MIL-140A}) = 220.20\%$$

2) Determination of the weight contribution per BDC linker **Wt.PL<sub>Theo</sub>**:

$$Wt.PL_{Theo} = (W_{Theo.Platt} - W_{End})/NL_{Ideal}$$

$$Wt.PL_{Theo} (UiO-66) = (220.20-100)/6 = 20.03\%$$

$$Wt.PL_{Theo} (MIL-140A) = (220.20-100)/1 = 120.20\%$$

, while  $NL_{Ideal}$  is the number of linkers (1 or 6) in *ideal* Zr/Zr<sub>6</sub>-SBU.

3) Calculation of number of linkers per *defective* Zr/Zr<sub>6</sub> unit  $NL_{Exp}$ :

$$NL_{Exp} = (6-x) = (W_{Exp.Platt} - W_{End}) / Wt.PL_{Theo} \text{ or } NL_{Exp} = (1-x) = (W_{Exp.Platt} - W_{End}) / Wt.PL_{Theo}$$

, while  $W_{Exp.Platt}$  is the experimental TGA plateau. The value can be taken from **Figure S13**.  $x$  is the number of linker deficiencies per Zr<sub>6</sub> SBU. We used following equations to calculate:

$$x = 6 - NL_{Exp} = 6 - [(W_{Exp.Platt} - W_{End}) / Wt.PL_{Theo}]$$

$$x = 1 - NL_{Exp} = 1 - [(W_{Exp.Platt} - W_{End}) / Wt.PL_{Theo}]$$

$$x (CE-DGC-UiO-66) = 6 - 4.643 = 6 - ((193.0 - 100\%) / 20.03\%) = 1.357 \cong 1.36^{55}$$

$$x (MW-DGC-UiO-66-HCl) = 6 - 4.833 = 6 - ((196.8 - 100\%) / 20.03\%) = 1.167 \cong 1.17$$

$$x (MW-DGC-UiO-66-IL) = 6 - 4.843 = 6 - ((197.0 - 100\%) / 20.03\%) = 1.157 \cong 1.16$$

$$x (MW-DGC-MIL-140A) = 1 - 0.970 = 1 - ((216.5 - 100\%) / 120.2\%) \cong 0.03$$



### **S10. Results of three synthesis runs with solvent re-use**

The MW-DGC synthesis procedures described in Section S3 were exemplarily performed with solvent re-use, that is, using the same solvent, but fresh precursor on top of the DGC sieve each time.

Figures S14-S17 show PXRD patterns of all four presented MOFs, each proving maintaining crystallinity over three repeated synthesis runs with solvent re-use.

According to the data given in the Tables S8-S11 (cf. Fig. 8 in the full manuscript), we were able to prove the re-use of solvent with good yields and high specific surface areas (BET).

#### **S10.1 MIL-100(Fe)**

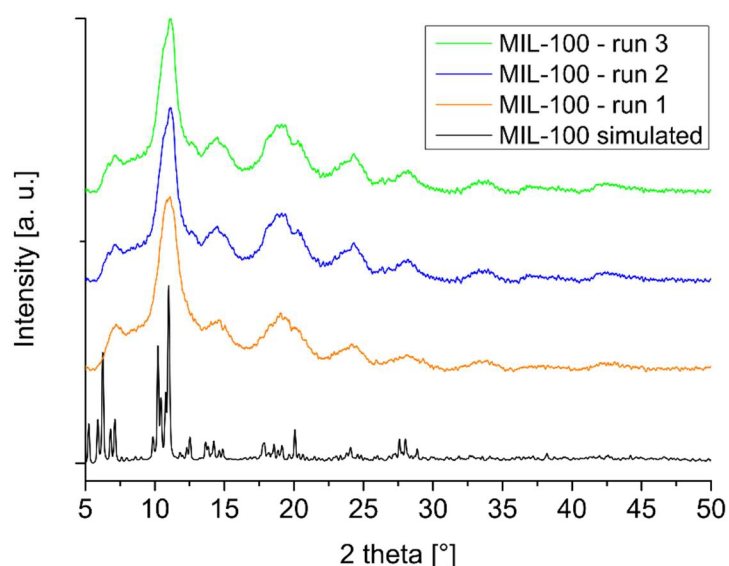


**Figure S14** PXRD patterns of MIL-100(Fe) samples from repeated synthesis runs with solvent re-use.

**Table S8** Results of three repeated synthesis runs with re-use of solvent for MIL-100(Fe).

Run	BET [m <sup>2</sup> g <sup>-1</sup> ]	Yield [%]
1	1287	78
2	935	72
3	1158	82

### S10.2. UiO-66-IL

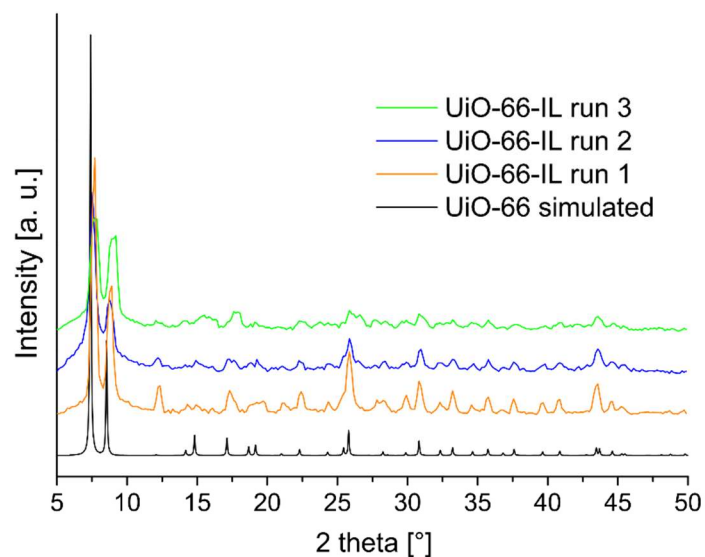


**Figure S15** PXRD patterns of UiO-66-IL samples from repeated synthesis runs with solvent re-use.

**Table S9** Results of three repeated synthesis runs with re-use of solvent for UiO-66-IL.

Run	BET [m <sup>2</sup> g <sup>-1</sup> ]	Yield [%]
1	1023	68
2	807	73
3	717	72

### S10.3. MIL-140A

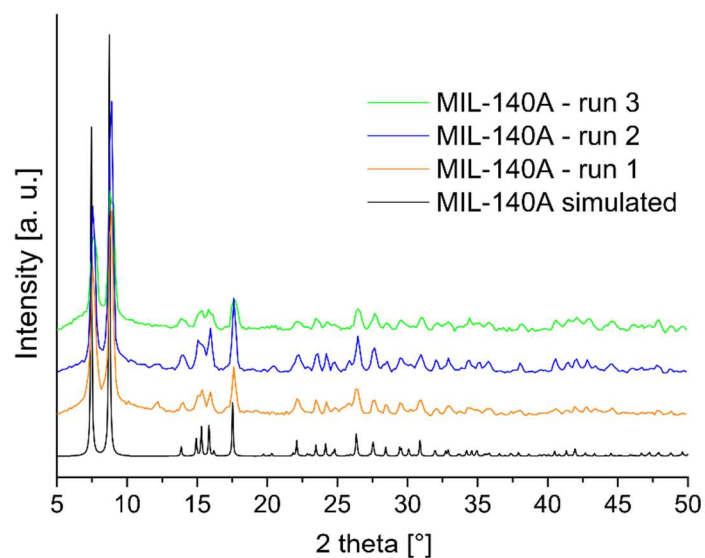


**Figure S16** PXRD patterns of MIL-140A samples from repeated synthesis runs with solvent re-use.

**Table S10** Results of three repeated synthesis runs with re-use of solvent for MIL-140A.

Run	BET [m <sup>2</sup> g <sup>-1</sup> ]	Yield [%]
1	354	92
2	340	89
3	344	96

#### S10.4. Aluminum fumarate

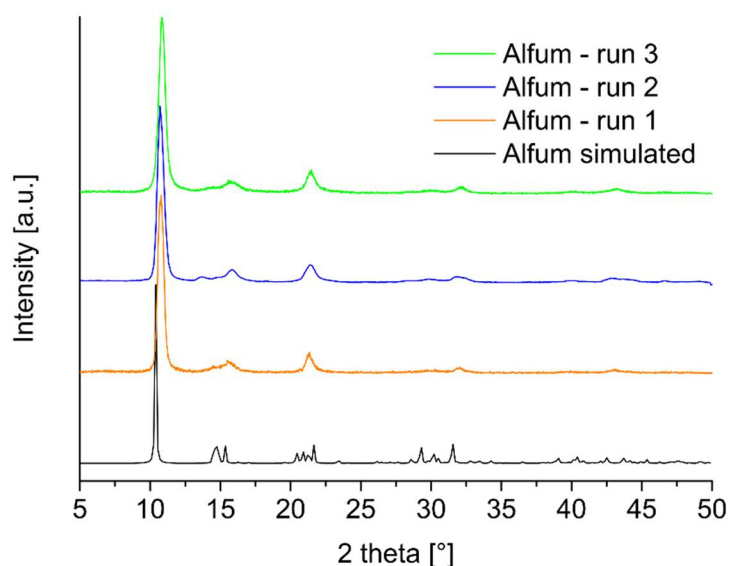


**Figure S17** PXRD patterns of AlFum samples from repeated synthesis runs with solvent re-use.

**Table S11** Results of three repeated synthesis runs with re-use of solvent for aluminum fumarate.

Run	BET [m <sup>2</sup> g <sup>-1</sup> ]	Yield [%]
1	1075	76
2	1148	81
3	1128	89

#### S11. Calculation of solvent amounts

##### - for aluminum fumarate

The patented synthesis procedure for continuous production of AlFum demonstrates different methods with varying STYs from 2032-5339 kg m<sup>-3</sup> day<sup>-1</sup>. The most effective one (i.e. 3615 kg m<sup>-3</sup> day<sup>-1</sup>) yields 97.5 mol-% based on Al, achieving 4.1 wt.% product in solution.<sup>57</sup>

$$3615 \text{ kg m}^{-3} \text{ day}^{-1} = 4.1 \text{ wt.}\% \text{ of product in solution}$$

$$\rightarrow 95.9 \text{ wt.}\% \text{ mother liquor} = 84555.73 \text{ kg} = \underline{84.55 \text{ tons}}$$

##### - for UiO-66

The continuous flow synthesis procedure reports STY = 7163 kg m<sup>-3</sup> day<sup>-1</sup> with a concentration of 0.1 mol L<sup>-1</sup> Zr in solution, 94% yield (i.e. 0.094 mol L<sup>-1</sup> product in solution), a flow of 1.23 mL min<sup>-1</sup>. Specifically it is stated that from 20 mL processed a yield of 0.696 g (94%) of desolvated MOF in 24.4 min total run time was obtained.

$$\text{This amounts to } 0.696 \text{ g} / [(0.020 \text{ L} / 10^{-3} \text{ L/m}^3) \times (24.4 \text{ min} / 1440 \text{ min/day})] = 2054 \text{ kg m}^{-3} \text{ day}^{-1}.$$

There is an additional solvent amount of 8 mL + 10 mL and 60 mL for washing, that is in total apparently 98 mL for the STY of 2053 kg m<sup>-3</sup> day<sup>-1</sup>

From only the 20 mL = 0.02 L and STY of 2054 kg m<sup>-3</sup> day<sup>-1</sup> the solvent volume per day is estimated as  

$$x = 2053 \cdot 10^3 \text{ g} / 0.696 \text{ g} \times 0.02 \text{ L} = \underline{59\,000 \text{ L}}$$

From the total of 98 mL = 0.098 L and STY of 2054 kg m<sup>-3</sup> day<sup>-1</sup> the solvent volume per day is estimated:

$$x = 2053 \cdot 10^3 \text{ g} / 0.696 \text{ g} \times 0.098 \text{ L} = \underline{289\,000 \text{ L}}$$

## **S12. References**

- 1 G. Férey, C. Serre, C. Mellot-Draznieks, F. Millange, S. Surblé, J. Dutour and I. Margiolaki, *Angew. Chem.*, 2004, **116**, 6456-6461.
- 2 K. Brandenburg, Diamond 4.3.1, Crystal and Molecular Structure Visualization, Crystal Impact - K. Brandenburg & H. Putz GbR, Bonn, Germany, 2009.
- 3 P. Horcajada, S. Surblé, C. Serre, D.-Y. Hong, Y.-K. Seo, J.-S. Chang, J.-M. Grèneche, I. Margiolaki and G. Férey, *Chem. Commun.*, 2007, **27**, 2820-2822.
- 4 L. Sciortino, A. Alessi, F. Messina, G. Buscarino and F. M. Gelardi, *J. Phys. Chem. C*, 2015, **119**, 7826-7830.
- 5 F. Jeremias, S. K. Henninger and C. Janiak, *Dalton Trans.*, 2016, **45**, 8637-8644.
- 6 J. W. Yoon, Y.-K. Seo, Y. K. Hwang, J.-S. Chang, H. Leclerc, S. Wuttke, P. Bazin, A. Vimont, M. Daturi, E. Bloch P. L. Llewellyn, C. Serre, P. Horcajada, J.-M. Grenèche, A. E. Rodrigues and G. Férey, *Angew. Chem.*, 2010, **122**, 6085-6088.
- 7 P. L. Llewellyn, S. Bourrelly, C. Serre, A. Vimont, M. Daturi, L. Hamon, G. de Weireld, J.-S. Chang, D.-Y. Hong, Y. K. S. H. Jhung and G. Férey, *Langmuir*, 2008, **24**, 7245-7250.
- 8 I. Ahmed and S. H. Jhung, *Mater. Today*, 2014, **17**, 136-146.
- 9 C. Petit and T. J. Bandoz, *Adv. Funct. Mater.*, 2011, **21**, 2108-2117.
- 10 F. Jeremias, A. Khutia, S. K. Henninger and C. Janiak, *J. Mater. Chem.*, 2012, **22**, 10148-10151.
- 11 S. K. Henninger, F. Jeremias, H. Kummer, P. Schossig and H.-M. Henning, *Energy Proced.*, 2012, **30**, 279-288.
- 12 S. K. Henninger, F. Jeremias, H. Kummer and C. Janiak, *Eur. J. Inorg. Chem.*, 2012, **16**, 2625-2634.
- 13 A. Rezk, R. Al-Dadah, S. Mahmoud and A. Elsayed, *Int. J. Heat Mass Tran.*, 2012, **55**, 7366-7374.
- 14 S. Kovačič, M. Mazaj, M. Ješelnik, D. Pahovnik, E. Žagar, C. Slugovc and N. Z. Logar, *Macromol. Rapid Comm.*, 2015, **36**, 1605-1611.
- 15 A. G. Márquez, A. Demessence, A. E. Platero-Prats, D. Heurtaux, P. Horcajada, C. Serre, J.-S. Chang, G. Férey, V. A. de la Peña-O'Shea, C. Boissière, D. Grosso and C. Sanchez, *Eur. J. Inorg. Chem.*, 2012, 5165-5174.
- 16 M. Pilloni, F. Padella, G. Ennas, S. Lai, M. Bellusci, E. Rombi, F. Sini, M. Pentimalli, C. Delitala, A. Scano, V. Cabras and I. Ferino, *Micropor. Mesopor. Mater.*, 2015, **213**, 14-21.
- 17 S. Rojas, F. J. Carmona, C. R. Maldonado, E. Barea and J. A. R. Navarro, *New J. Chem.*, 2016, **40**, 5690-5694.
- 18 E. Bellido, M. Guillevis, T. Hidalgo, M. J. Santander-Ortega, C. Serre and P. Horcajada, *Langmuir*, 2014, **30**, 5911-5920.
- 19 A. García Márquez, A. Demessence, A. E. Platero-Prats, D. Heurtaux, P. Horcajada, C. Serre, J.-S. Chang, G. Férey, de la Peña-O'Shea, Victor Antonio, C. Boissière, D. Grosso and C. Sanchez, *Eur. J. Inorg. Chem.*, 2012, 5165-5174.
- 20 F. Tan, M. Liu, K. Li, Y. Wang, J. Wang, X. Guo, G. Zhang and C. Song, *Chem. Eng. J.*, 2015, **281**, 360-367.
- 21 L. Li, S. Xiang, S. Cao, J. Zhang, G. Ouyang, L. Chen and C.-Y. Su, *Nat. Commun.*, 2013, **4**, article



---

number 1774.

- 22 B. Zhang, J. Zhang, C. Liu, L. Peng, X. Sang, B. Han, X. Ma, T. Luo, X. Tan and G. Yang, *Sci. Rep.*, 2016, **6**, article number 21401.
- 23 F. Vermoortele, R. Ameloot, L. Alaerts, R. Matthessen, B. Carlier, E. V. R. Fernandez, J. Gascon, F. Kapteijn and D. E. de Vos, *J. Mater. Chem.*, 2012, **22**, 10313-10321.
- 24 J.-W. Zhang, G.-P. Lu and C. Cai, *Green Chem.*, 2017, **19**, 4538-4543.
- 25 A. U. Czaja, N. Trukhan and U. Müller, *Chem. Soc. Rev.*, 2009, **38**, 1284-1293.
- 26 M. Rubio-Martinez, T. D. Hadley, M. P. Batten, K. Constanti-Carey, T. Barton, D. Marley, A. Mönch, K.-S. Lim and M. R. Hill, *ChemSusChem*, 2016, **9**, 938-941.
- 27 M. Rubio-Martinez, C. Avci-Camur, A. W. Thornton, I. Imaz, D. Maspoch and M. R. Hill, *Chem. Soc. Rev.*, 2017, **46**, 3453-3480.
- 28 M. J. Katz, Z. J. Brown, Y. J. Colón, P. W. Siu, K. A. Scheidt, R. Q. Snurr, J. T. Hupp and O. K. Farha, *Chem. Commun.*, 2013, **49**, 9449-9451.
- 29 G. C. Shearer, S. Chavan, S. Bordiga, S. Svelle, U. Olsbye and K. P. Lillerud, *Chem. Mater.*, 2016, **28**, 3749-3761.
- 30 J. H. Cavka, S. Jakobsen, U. Olsbye, N. Guillou, C. Lamberti, S. Bordiga and K.P. Lillerud, *J. Am. Chem. Soc.*, 2008, **130**, 13850-13851.
- 31 V. Guillerme, F. Ragon, M. Dan-Hardi, T. Devic, M. Vishnuvarthan, B. Campo, A. Vimont, G. Clet, Q. Yang, G. Maurin, G. Férey, A. Vittadini, S. Gross and C. Serre, *Angew. Chem. Int. Ed.*, 2012, **51**, 9267-9271.
- 32 L. Valenzano, B. Civalieri, S. Chavan, S. Bordiga, M. H. Nilsen, S. Jakobsen, K. P. Lillerud and C. Lamberti, *Chem. Mater.*, 2011, **23**, 1700-1718.
- 33 H. Wu, Y. S. Chua, V. Krungleviciute, M. Tyagi, P. Chen, T. Yildirim and W. Zhou, *J. Am. Chem. Soc.*, 2013, **135**, 10525-10532.
- 34 M. W. Anjum, F. Vermoortele, A. L. Khan, B. Bueken, D. E. De Vos and I. F. J. Vankelecom, *ACS Appl. Mater. Interfaces*, 2015, **7**, 25193-25201.
- 35 F. Jeremias, V. Lozan, S. K. Henninger and C. Janiak, *Dalton Trans.*, 2013, **42**, 15967-15973.
- 36 F. Jeremias, D. Fröhlich, C. Janiak and S. Henninger, *New J. Chem.*, 2014, **38**, 1846-1852.
- 37 A. Shahat H. M. A. Hassan and H. M. E. Azzazy, *Analyt. Chim. Acta*, 2013, **793**, 90-98.
- 38 F. Vermoortele, B. Bueken, G. Le Bars, B. Van de Voorde, M. Vandichel, K. Houthoofd, A. Vimont, M. Daturi, M. Waroquier, V. Van Speybroeck, C. Kirschhock and D. E. De Vos, *J. Am. Chem. Soc.*, 2013, **135**, 11465-11468.
- 39 W. Cao, W. Luo, H. Ge, Y. Su, A. Wang and T. Zhang, *Green Chem.*, 2017, **19**, 2201-2211.
- 40 K. Užarević, T. C. Wang, S.-Y. Moon, A. M. Fidelli, J. T. Hupp, O. K. Farha and T. Friščić, *Chem. Commun.*, 2016, **52**, 2133-2136.
- 41 S. Gökpınar, T. Diment and C. Janiak, *Dalton Trans.*, 2017, **46**, 9895-9900.
- 42 M. Taddei, D. A. Steitz, J. A. van Bokhoven and M. Ranocchiari, *Chem. Eur. J.*, 2016, **22**, 3245-3249.
- 43 E. Leung, U. Müller, N. Trukhan, H. Mattenheimer, G. Cox and S. Blei, *Process for preparing porous metal-organic frameworks based on aluminum fumarate*, U.S. Patent No. 8,524,932, BASF SE, 3 Sep. 2013.
- 44 C. Kiener, U. Müller and M. Schubert, *Method of using a metal organic frameworks based on aluminum fumarate*, U.S. Patent No. 8,518,264, BASF SE, 27 Aug. 2013.
- 45 F. Jeremias, D. Fröhlich, C. Janiak and S. K. Henninger, *RSC Adv.*, 2014, **4**, 24073-24082.
- 46 E. Alvarez, N. Guillou, C. Martineau, B. Bueken, B. Van de Voorde, C. Le Guillouzer, P. Fabry, F. Nouar, F. Taulelle, D. de Vos, J.-S. Chang, K. H. Cho, N. Ramsahye, T. Devic, M. Daturi, G. Maurin and C. Serre, *Angew. Chem. Int. Ed.*, 2015, **54**, 3664-3668.
- 47 T. Loiseau, C. Volkringer, M. Haouas, F. Taulelle and G. Férey, *C. R. Chim.*, 2015, **18**, 1350-1369.
- 48 B. Yilmaz, N. Trukhan and U. Müller, *Chin. J. Catal.*, 2012, **33**, 3-10.
- 49 J. Chen, K. Shen and Y. Li, *ChemSusChem*, 2017, **10**, 3165-3187.
- 50 M. Gaab, N. Trukhan, S. Maurer, R. Gummaraju and U. Müller, *Micropor. Mesopor. Mater.*, 2012, **157**, 131-136.
- 51 S. Karmakar, J. Dechnik, C. Janiak and S. De, *J. Hazard. Mater.*, 2016, **303**, 10-20.

- 
- 52 E. Elsayed, R. Al-Dadah, S. Mahmoud, P. A. Anderson, A. Elsayed and P. G. Youssef, *Desalination*, 2017, **406**, 25-36.
- 53 P. G. Yot, L. Vanduyfhuys, E. Alvarez, J. Rodriguez, J.-P. Itié, P. Fabry, N. Guillou, T. Devic, I. Beurroies, P. L. Llewellyn V. Van Speybroek, C. Serre and G. Maurin, *Chem. Sci.*, 2016, **7**, 446-450.
- 54 D. E. Crawford and J. Casaban, *Adv. Mater.*, 2016, **28**, 5747-5754.
- 55 D. Crawford, J. Casaban, R. Haydon, N. Giri, T. McNally and S. L. James, *Chem. Sci.*, 2015, **6**, 1645-1649.
- 56 M. Deetlefs and K. R. Seddon, *Green Chem.*, 2003, **5**, 181-186.
- 57 S. Wegner, C. Rutz, K. Schette, J. Barthel and A. Bushmelev, *Chem. Eur. J.*, 2017, **23**, 6330-6340.
- 58 M. Thommes, K. Kaneko, A. V. Neimark, J. P. Olivier, F. Rodriguez-Reinoso, J. Rouquerol and K. S. Sing, *Pure Appl. Chem.*, 2015, **87**, 1051-1069.

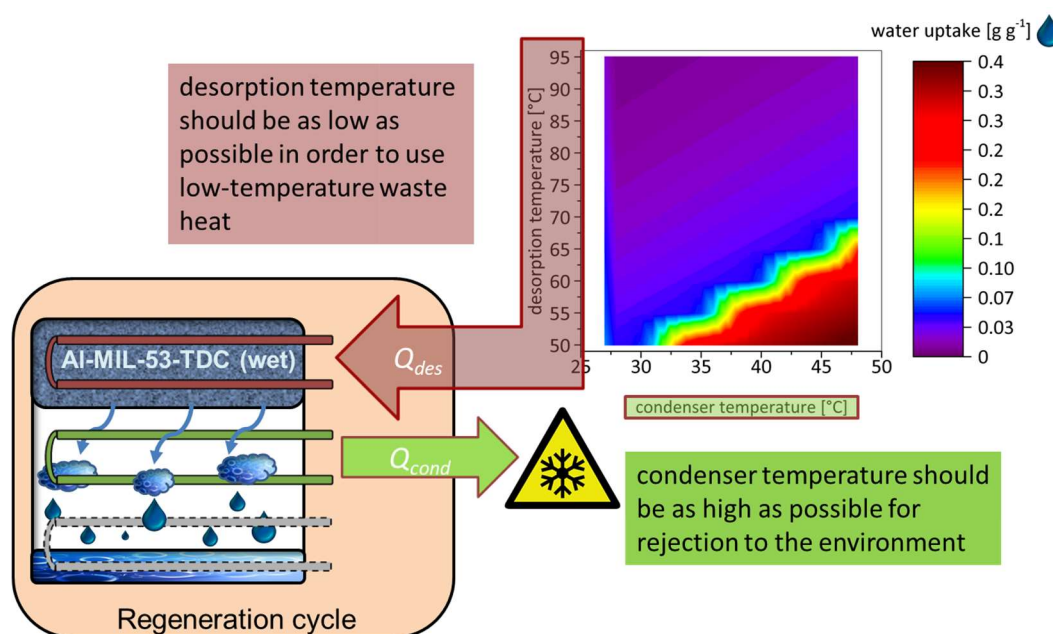
### 3.2. Evaluation of the Highly Stable Metal-Organic Framework MIL-53(Al)-TDC (TDC = 2,5-Thiophenedicarboxylate) as a New and Promising Adsorbent for Heat Transformation Applications

N. Tannert, S.-J. Ernst, C. Jansen, S. Nießing, S. K. Henninger, H.-J. Bart and C. Janiak

*J. Mater. Chem. A*, 2018, **6**, 17706-17712

DOI: 10.1039/c8ta04407d

Impact factor 2018: 11.301



Author's contribution of work:

- Reflux synthesis development for MIL-53(Al)-TDC and optimization (with C. Jansen).
- All analytical characterizations except for water sorption and hydrothermal cycling experiments (done by S.-J. Ernst) and SEM images (done by S. Nießing).
- Writing of the manuscript (partly with S.-J. Ernst) and drawing of figures, graphs and tables except for Figures 3-7 (done by S.-J. Ernst).
- Editing of the manuscript regarding the reviewers' comments with S.-J. Ernst and C. Janiak.

Reproduced by permission of The Royal Society of Chemistry.

The MOF MIL-53(Al)-TDC was described in literature shortly before the appearance of the following contribution. Due to the fact, that related Al-MOFs like aluminum fumarate and CAU-10-H have thoroughly been investigated towards adsorption-driven heat transformation, while also their outstanding capabilities have been demonstrated vividly, an evaluation of this lately described material seemed obvious.

Since the only report on the synthesis of MIL-53(Al)-TDC applied a solvothermal route, and, in order to find a reliable ambient pressure synthesis, a reflux synthesis optimization was carried out. The investigation towards the Al-source in the MOF formation reaction with different Al-salts ( $\text{Al}_2(\text{SO}_4)_3 \cdot 18 \text{ H}_2\text{O}$ ,  $\text{AlCl}_3 \cdot 6\text{H}_2\text{O}$ ,  $\text{Al}(\text{OH})(\text{acetate})_2 \cdot x \text{ H}_2\text{O}$  and  $\text{NaAlO}_2$ ) was performed, as it remained somehow unclear what Al-reagent may be advantageous in Al-MOF syntheses in general (*cf.* also chapter 4.4.), but also in the special case of MIL-53(Al)-TDC. It was found that basic aluminum acetate and aluminum sulphate are superior Al-reagents when water vapor sorption capacity was considered. However, all materials except for the one obtained from sodium aluminate  $\text{NaAlO}_2$  exhibited comparable porosities around  $S_{\text{BET}} = 1100 \text{ m}^2 \text{ g}^{-1}$ . As the utilization of  $\text{Al}(\text{OH})(\text{acetate})_2 \cdot x \text{ H}_2\text{O}$  went along with comparably highest yields of MOF, the thereby obtained material was implemented in the following characterization and evaluation.

The investigated material exhibited high thermal stability and good stability towards chemical solvents including high/low pH values. Hydrothermal cycling experiments over 40 cycles proved excellent stability and therefore a good suitability for water vapor sorption applications, including AHPs and TDCs. Supportive *in-situ* PXRD measurements showed high structural integrity of the material upon cycling for at least 12 cycles. The further characterizations towards such purpose included the collection of water vapor isotherms at three different temperatures ( $T = 20, 40, 60 \text{ }^\circ\text{C}$ ), to determine isosteric heat of adsorption  $\Delta_{\text{ads}}H$  for the adsorbent/adsorptive pair MIL-53(Al)-TDC/water over a typical temperature range. The fitted isotherms delivered an average isosteric heat of adsorption of  $\Delta_{\text{ads}}H = 2.6 \text{ kJ g}^{-1}$ , which renders the material as ideal candidate for adsorptive cooling applications. In such case, the released heat corresponds to waste heat, in comparison to the reverse process, which is the heat-pump mode. Additionally, the low desorption temperature below  $T = 65 \text{ }^\circ\text{C}$  and a desirably high condenser temperature of around  $T = 40 \text{ }^\circ\text{C}$  in combination with  $0.35 \text{ g g}^{-1}$  water vapor ad-/desorption per cycle offers an ideal working window for the intended application. The dependencies of applied temperature levels in the application were visualized in 3D graphical representations.

In summary, MIL-53(Al)-TDC could be characterized as valuable candidate for adsorption-driven heat transformation processes, especially for adsorptive cooling applications.

## PAPER



Cite this: *J. Mater. Chem. A*, 2018, 6, 17706

## Evaluation of the highly stable metal–organic framework MIL-53(Al)-TDC (TDC = 2,5-thiophenedicarboxylate) as a new and promising adsorbent for heat transformation applications†

Niels Tannert,<sup>†a</sup> Sebastian-Johannes Ernst,<sup>†bc</sup> Christian Jansen,<sup>id a</sup> Hans-Jörg Bart,<sup>id b</sup> Stefan K. Henninger<sup>c</sup> and Christoph Janiak<sup>id \*a</sup>

The recently reported Al-based metal–organic framework MIL-53(Al)-TDC (TDC = 2,5-thiophenedicarboxylate) shows desirable water sorption properties towards adsorption-driven heat transformation applications with high thermal and solvent/pH stability as well as hydrothermal stability over 40 cycles. Water vapor sorption measurements at 25, 40 and 60 °C yielded an advantageous isosteric heat of adsorption of only 2.6 kJ g<sup>−1</sup>, favoring the use of MIL-53(Al)-TDC in sorption based chilling where the released heat of adsorption corresponds to waste heat. The good cooling performance of MIL-53(Al)-TDC comes from desirable low desorption temperatures below 65 °C, with also desirable high condenser temperatures of around 40 °C and corresponding water exchange of almost 0.35 g g<sup>−1</sup>. The thereby offered working window cannot be provided by common adsorbents and renders the material an ideal candidate for adsorption cooling applications.

Received 11th May 2018  
Accepted 22nd August 2018

DOI: 10.1039/c8ta04407d

rsc.li/materials-a

## Introduction

Metal–organic frameworks (MOFs) receive continuous attention due to their unsurpassed porosity and chemical variability, which originate from the inherent modular cluster–linker concept.<sup>1</sup> The organic linkers in MOFs are typically bi-, tri- or tetradentate carboxylates.<sup>2</sup> Linker modulation enables tailoring of the properties of a MOF towards applications<sup>3,4</sup> and has yielded thousands of MOFs with a broad range of properties to date.<sup>5,6</sup>

Of recent interest is the application of MOFs in the field of water sorption/harvesting<sup>7,8</sup> and related sorption heat transformation processes.<sup>9–11</sup> Fig. 1 illustrates the underlying principle of heat transformation that can be separated into two stages: a working cycle and a regeneration cycle. During the working cycle, a working fluid is evaporated taking up ambient heat for the evaporation ( $Q_{\text{evap}}$ ), while the adsorbent adsorbs the

working fluid, releasing the heat of adsorption ( $Q_{\text{ads}}$ ). As soon as the adsorbent is sufficiently loaded, the regeneration cycle is started by applying heat to the adsorbent ( $Q_{\text{des}}$ ). The desorbed working fluid is condensed releasing heat of condensation ( $Q_{\text{cond}}$ ).

Typically, two types of applications arise from this principle: adsorption heat pumps and adsorption chillers. In heat pumps, the released  $Q_{\text{ads}}$  and  $Q_{\text{cond}}$  provide a heating system at a medium temperature level, e.g. floor heating at 40 °C, whereas  $Q_{\text{evap}}$  comes from the environment at typically 10 °C. In the chilling mode,  $Q_{\text{evap}}$  is the amount of heat that can be used to

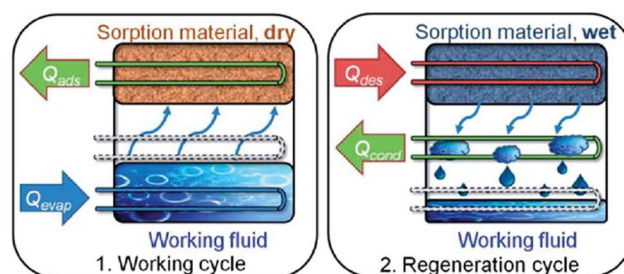


Fig. 1 In the working cycle, a working fluid (favorably water due to its high evaporation enthalpy and no toxicity) is evaporated, taking up evaporation heat  $Q_{\text{evap}}$ . During incorporation into a porous material, adsorption heat  $Q_{\text{ads}}$  is released. In the regeneration cycle, driving heat  $Q_{\text{des}}$  for desorption is applied, and further condensation takes place at a medium temperature level and releases condensation heat  $Q_{\text{cond}}$ . The device can be used as a chiller or a heat pump. The image was taken with permission from ref. 13.

<sup>a</sup>Institut für Anorganische Chemie und Strukturchemie, Heinrich-Heine-Universität Düsseldorf, 40204 Düsseldorf, Germany. E-mail: janiak@uni-duesseldorf.de

<sup>b</sup>Chair of Separation Science and Technology, TU Kaiserslautern, Postfach 3049, 67653 Kaiserslautern, Germany

<sup>c</sup>Fraunhofer Institute for Solar Energy Systems (ISE), Heidenhofstr. 2, 79110 Freiburg, Germany

† Electronic supplementary information (ESI) available: Synthesis details, further (*in situ*) PXRD and TGA, nitrogen (77 K), argon (87 K) and water (20 °C) sorption isotherms, multicycle stability tests, SEM images and more information on methods and devices. See DOI: 10.1039/c8ta04407d

‡ These authors contributed equally.



chill, e.g., an industrial process, whereas  $Q_{\text{ads}}$  and  $Q_{\text{cond}}$  can be considered waste heat, which is dissipated to the environment. In both cases,  $Q_{\text{des}}$  is the amount of heat that has to be provided to drive the process. Desorption temperatures below 100 °C are mostly favored, since they can easily be reached by solar thermal heat or industrial waste heat. Utilization of the energies  $Q_{\text{evap}}$  or  $Q_{\text{ads}}$  and  $Q_{\text{cond}}$  occurs by continuous cycling of the adsorbent.<sup>12,13</sup>

Sorption heat transformation is gaining more and more attention, as the proof of concept has already been demonstrated on a pre-industrial scale.<sup>14–16</sup> Thermally driven heat transformation is a promising approach towards energy efficient heating and cooling,<sup>17</sup> since both the efficiency and cost effectiveness of such processes are critically governed by the performance of the applied adsorbents. Therefore, many MOFs have been investigated with respect to application in thermally driven heat transformation, looking mainly at water sorption and stability characteristics.<sup>18–22</sup>

Since MOFs can show a significant loss of retention of surface area and crystallinity after water sorption,<sup>23</sup> hydro-thermal cycle stability is one key factor for utilization of MOF materials in such applications.<sup>9,13,24–26</sup>

There is a rising demand for adsorbents with tailor-made water sorption properties,<sup>27,28</sup> which is underlined by the ongoing research towards both new materials<sup>15,29–31</sup> and pre-industrial scale applications.<sup>9,12,16</sup>

An important performance indicator for the evaluation of porous materials in heat transformation applications is the working fluid uptake capacity together with adsorption and desorption within the possible temperature boundaries for heat of evaporation ( $Q_{\text{evap}}$ ), driving heat ( $Q_{\text{des}}$ ) and heat dissipation or useful heat in the heat pumping mode ( $Q_{\text{ads}}$  and  $Q_{\text{cond}}$ ). For cooling applications the material must be capable of evaporating the working fluid from as low as possible reservoir temperatures and still showing an uptake when itself reaches as high as possible temperatures through  $Q_{\text{ads}}$ . The latter is more effectively dissipated to the environment from an as high as possible temperature level. For regeneration, an as low as possible temperature level for  $Q_{\text{des}}$  is desirable together with an as high as possible temperature level for the dissipation of  $Q_{\text{cond}}$ .

In particular Al-based MOFs proved to be highly thermally and hydrolytically stable and therefore most suitable for heat transformation applications,<sup>9,13,26,32</sup> and furthermore Al is an abundant, inexpensive light metal with low toxicity.

The most investigated Al-MOFs for sorption heat transformation are MIL-100 (linker = trimesate, MIL = Matériaux de l'Institut Lavoisier),<sup>13,33,34</sup> Al-fumarate (linker = fumarate, trade name Basolite A520),<sup>35</sup> CAU-10 (linker = isophthalate, CAU = Christian-Albrechts-Universität)<sup>36</sup> and MIL-160 (linker = 2,5-furandicarboxylate).<sup>18</sup> These Al-MOFs exhibit pore sizes in the microporous region, yielding pore filling with water vapor at relative pressures around  $0.1 < p/p_0 < 0.4$ , which is an ideal range for sorption heating and cooling.<sup>10,37,38</sup>

In 2017 Maurin and co-workers presented theoretical calculations for promising water sorption properties of ligand functionalized MIL-160 materials, including the linker 2,5-

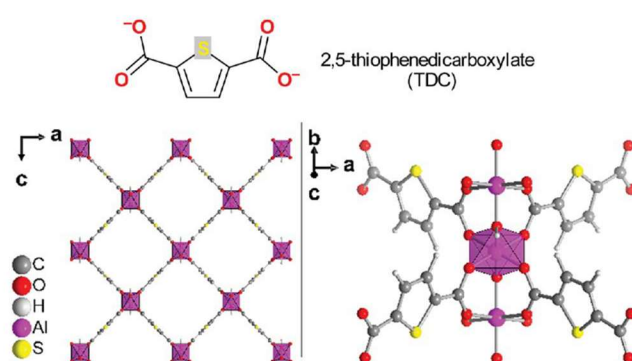


Fig. 2 (Top) The linker 2,5-thiophenedicarboxylate (TDC). (Bottom, left) Section of the packing diagram of MIL-53(Al)-TDC viewed along the channels with a cross-section of approximately  $8 \times 8.2$  Å. (Bottom, right) Extended secondary building unit (SBU) with *trans* corner-sharing  $\text{AlO}_6$  octahedra. The graphics were produced from a cif-file that was generously provided by Serre and co-workers.

thiophenedicarboxylate (TDC) (Fig. 2).<sup>39</sup> In this case, they predicted an isotherm with an inflection point of  $\alpha = 0.19$  and an uptake of  $0.44 \text{ g g}^{-1}$ . Recently, Stock *et al.* published a new Al-based MOF with the MIL-53 topology (Fig. 2).<sup>40</sup> It was denoted as MIL-53(Al)-TDC and proven to exhibit  $0.469 \text{ g g}^{-1}$  water uptake at  $\alpha = 0.19$ , displaying the formula  $[\text{Al}(\mu\text{-OH})(\text{TDC})]$  and comprising lozenge-shaped pores with a diameter of  $8 \times 8.2$  Å.

MIL-53(Al)-TDC was found to exhibit porosity parameters of  $\text{BET} = 1150 \text{ m}^2 \text{ g}^{-1}$  ( $\text{BET} = \text{Brunauer-Emmett-Teller}$ ), a micropore volume of  $0.48 \text{ cm}^3 \text{ g}^{-1}$  and a maximum water vapor uptake of  $469 \text{ mg g}^{-1}$ .<sup>40</sup> Parallel to our study, MIL-53(Al)-TDC was evaluated for  $\text{CO}_2$  capture.<sup>41</sup> Stock and co-workers suggested its applicability in the field of heat transformation processes due to the desirable S-shape of the water isotherm, relatively high water uptake in a good pressure region, and high thermal stability.<sup>40</sup> Herein we thoroughly characterize MIL-53(Al)-TDC towards cyclic water sorption heat transformation applications.

## Experimental

### Materials and instrumentation

All chemicals were used as received from suppliers. For further information about all materials see Section S1 in the ESI.†

Powder X-ray diffractometry (PXRD) was performed at ambient temperature on a D2 phaser (Bruker, Billerica, US) using  $\text{Cu-K}\alpha$  radiation ( $\lambda = 1.54182$  Å) in the range of  $5^\circ < 2\theta < 50^\circ$  with a scan rate of  $0.0125^\circ \text{ s}^{-1}$  (300 W, 30 kV, 10 mA). Analyses of the diffractograms were carried out with Match 3.11 software.

Thermogravimetric analysis (TGA) was carried out on a Netzsch TG209 F3 Tarsus (Netzsch, Selb, Germany) device under a nitrogen atmosphere and heating at a ramp rate of  $5 \text{ K min}^{-1}$  to the target temperature (600 °C).

Elemental analysis was performed on a vario MICRO cube (Elementar Analysensysteme, Langenselbold, Germany).

Infrared spectra were acquired on a Bruker Tensor 37 FT-IR device. SEM images were acquired on a JEOL JSM-6510



advanced electron microscope (Jeol, Akishima, Japan) with a LaB<sub>6</sub> cathode at 5–20 keV. The microscope was equipped with an Xflash 410 (Bruker, Billerica, US) silicon drift detector.

Surface areas (BET) were determined by nitrogen (purity 99.999%, 5.0) sorption experiments at 77 K using liquid nitrogen with a Quantachrome NOVA-4000e (Quantachrome, Odelzhausen, Germany) instrument within a partial pressure range of  $p/p_0 = 10^{-3}$  to 1 bar. Each sample was degassed under vacuum ( $<10^{-2}$  mbar) at 150 °C for *ca.* 3 h, prior to measurement. All surface areas (BET) were calculated from five adsorption points in the pressure range  $p/p_0 = 0.005$ –0.05 by applying Roquerol plots ( $r > 0.998$ ). This range is indeed not recommended by IUPAC (International Union of Pure and Applied Chemistry) for BET surface area determination, but is also suitable for microporous materials.<sup>42</sup> Total pore volumes were calculated from the N<sub>2</sub> sorption isotherm at  $p/p_0 = 0.95$ . NLDFT calculations for the pore size distribution curves were performed with the native NovaWin 11.03 software using the 'N<sub>2</sub> at 77 K on carbon, slit pore, NLDFT equilibrium' model. Argon (purity 99.999%, 5.0) sorption experiments were done at 87 K using a Quantachrome cryocooler (Quantachrome, Odelzhausen, Germany) for appropriate adjustment of  $T = 87$  K on a Quantachrome Autosorb iQ MP (Quantachrome, Odelzhausen, Germany) instrument within a partial pressure range of  $p/p_0 = 10^{-7}$  to 1 bar. All water sorption isotherms (25, 40, and 60 °C) were measured with a Quantachrome VStar4 (Quantachrome, Odelzhausen, Germany) within a partial pressure range of  $p/p_0 = 10^{-3}$  to 0.9 bar.

Water cycling stabilities were examined with a Setaram<sup>TM</sup> TGA-DSC-111 (Setaram, Caluire, France) on powdered samples. A humidified argon gas flow (40 °C, 76.3% relative humidity) was generated by a Setaram<sup>TM</sup> WetSys (Setaram, Caluire, France) humidity controller and passed through the sample chamber, while the temperature of the sample was varied and the mass of the adsorbent was monitored. For the multi-cycle adsorption/desorption experiments, the temperature of the sample was varied between 40 °C and 140 °C with a cycle time of 5 h.

More detailed information on analytical procedures is given in the ESI.<sup>†</sup>

### Reflux synthesis optimization

In order to find a reliable ambient pressure synthesis instead of the only reported solvothermal route for MIL-53(Al)-TDC, we performed synthesis optimization according to Tschense *et al.* in mixtures of water and dimethylformamide (DMF) (4 : 1).<sup>40</sup>

Generally, Al-MOFs are synthesized using various Al reagents and it remains somehow unclear what source of Al is advantageous for the formation of [Al(OH)(linker)]-type MOFs. Therefore, we developed a reflux synthesis (135 °C, 24 h) with varying Al sources (Table 1 and Section S2 in the ESI<sup>†</sup>) and obtained the desired product as a microcrystalline powder in each case. Formation of the desired phase already took place within a few hours; however, we carried out the reaction for 24 h to ensure the completeness of the reaction and superior porosity. Structural verification was performed by PXRD (Fig. S1<sup>†</sup>) and nitrogen sorption studies (Table 1 and Fig. S13 in the ESI<sup>†</sup>).

Table 1 Synthesis results of MIL-53(Al)-TDC with different starting materials

Al source	BET <sup>a</sup> [m <sup>2</sup> g <sup>-1</sup> ]	Pore volume <sup>b</sup> [cm <sup>3</sup> g <sup>-1</sup> ]	Yield [%]
Al(OH)(ac) <sub>2</sub> ·xH <sub>2</sub> O	885, 1092	0.41, 0.52	95, 91
NaAlO <sub>2</sub>	395	0.37	39
Al <sub>2</sub> (SO <sub>4</sub> ) <sub>3</sub> ·18H <sub>2</sub> O	1102	0.46	88
AlCl <sub>3</sub> ·6H <sub>2</sub> O	1096	0.49	83
Ref. 40 <sup>c</sup>	1150	0.48	84

<sup>a</sup> Determined by five adsorption points of nitrogen isotherms in the range  $0.005 < p/p_0 < 0.05$ . <sup>b</sup> Determined using the NLDFT method (carbon, slit pore, nitrogen, 77 K) at  $p/p_0 = 0.9$ . <sup>c</sup> Micropore volume at  $p/p_0 = 0.5$ .

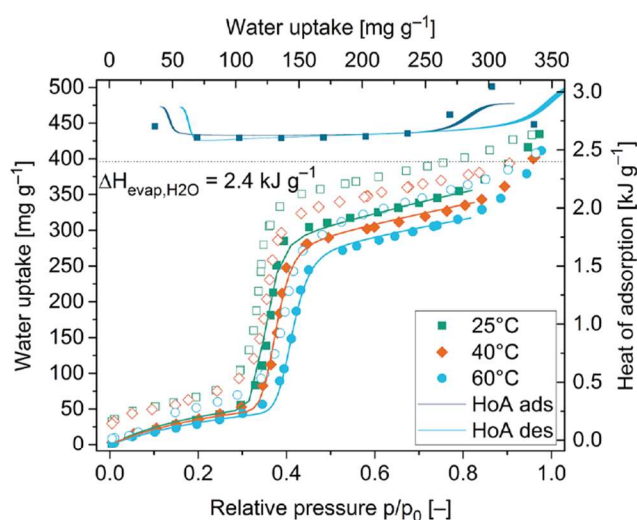


Fig. 3 Water sorption isotherms at three different temperatures (filled symbols: adsorption and open symbols: desorption) and differential heat of adsorption determined from the adsorption (dark blue line) and desorption (light blue line) branches of the isotherm. The solid lines in the adsorption isotherms symbolize simulations with a weighted dual site Langmuir (wDSL) approach (see Section S13, ESI<sup>†</sup>). The dotted line with  $\Delta H_{\text{evap,H}_2\text{O}} = 2.4 \text{ kJ g}^{-1}$  marks the heat of vaporization of water at 25 °C.

## Results and discussion

### Synthesis optimization

Within the described optimization towards a reflux-based synthesis we tested the following Al reagents: AlCl<sub>3</sub>, Al(OH)(acetate)<sub>2</sub>, Al<sub>2</sub>(SO<sub>4</sub>)<sub>3</sub> and NaAlO<sub>2</sub>. All products were characterized by PXRD and nitrogen sorption. The PXRD patterns of all MIL-53(Al)-TDC compounds showed similar crystallinity, revealing the robustness of the formation of the MOF phase (Fig. S1 in the ESI<sup>†</sup>).

From scanning electron microscopy images the products were microcrystalline agglomerates (Fig. S8–S11 in the ESI<sup>†</sup>). Except for NaAlO<sub>2</sub> as the Al source, all obtained products were in the same range of crystallinity and porosity (Table 1 and Fig. 1, see also ESI<sup>†</sup>).

Besides the difference in porosity, the Al source shows influence on the water sorption performance, mostly in terms of



uptake, which in turn directly correlates with the pore volume (nitrogen sorption: Fig. S12† and water sorption: Fig. S14 in the ESI†). More information can be found in the ESI.†

### Stability tests

Additionally, we performed solvent stability tests by dispersing *ca.* 10 mg of MIL-53(Al)-TDC into 3 mL of different solvents and stirring the dispersion for 24 h. By PXRD, no loss of crystallinity was apparent in any solvent. At least partial decomposition and loss of crystallinity occurred within 24 h in aqueous solutions with pH 12 and pH 1 (Fig. S3 and S4 in the ESI†).

Further characterization with infrared spectroscopy (IR), and thermogravimetric analysis (TGA), scanning electron microscopy (SEM), and argon (87 K), nitrogen (77 K) and water (20 °C) sorption isotherms of MIL-53(Al)-TDC products from synthesis optimization are provided in the ESI.†

All further analyses were carried out with the material synthesized from Al(OH)(ac)<sub>2</sub> (BET = 885 m<sup>2</sup> g<sup>-1</sup> from nitrogen sorption, *i.e.* 827 m<sup>2</sup> g<sup>-1</sup> from argon sorption, see Section S11 in the ESI†). This approach showed the highest yield and satisfactory porosity.

### Water sorption characteristics

In order to evaluate the potential of MIL-53(Al)-TDC for thermally driven heat transformation, water sorption isotherms were measured at 25, 40 and 60 °C. Prior to the measurements, each sample was activated at 150 °C under reduced pressure. Fig. 3 shows the water adsorption isotherms, where the solid lines represent thermodynamic fits. The adsorption isotherms show an S-shaped type-V isotherm according to the IUPAC classification,<sup>42</sup> with a steep increase of the uptake at relative pressures in the range 0.35 < *p/p*<sub>0</sub> < 0.4. This uptake is correlated with filling of the micropores. The maximum uptake is about 434 mg<sub>H<sub>2</sub>O</sub> g<sup>-1</sup>. Such an adsorption characteristic is comparable to that of aluminium fumarate, but slightly less hydrophilic, allowing desorption at higher relative pressures, synonymous with lower desorption temperatures.

Furthermore, the isotherms show a slight hysteresis at all temperatures, especially for the uptake after the steep rise that has been attributed to kinetic inhibition.<sup>40</sup> However, hysteresis behaviour occurs on different scales. Yet, a water sorption hysteresis is undesired for the targeted application, because it decreases the usable range of the working fluid exchange within the cycle.<sup>13</sup> Only MIL-53(Al)-TDC obtained from aluminium sulfate and from basic aluminium acetate showed water desorption with almost absence of hysteresis (Fig. S14 in the ESI†). The absence of hysteresis is explained by a lower number of defects. Defects in the form of missing linkers and terminal Al–OH and Al–OH<sub>2</sub> groups will provide stronger binding sites and mesoporous cavities with kinetically delayed desorption, *i.e.* hysteresis.

The isosteric heat of adsorption was determined directly from the adsorption isotherms using the Clausius–Clapeyron equation (Fig. 3, filled squares).<sup>43,44</sup> Also depicted in Fig. 3 is the heat of adsorption calculated according to Van't Hoff (eqn (1)) using the fitted thermodynamic model.<sup>45</sup>

$$\frac{\Delta H_{\text{ads}}(X, T)}{RT^2} = -\left(\frac{\partial \ln p}{\partial T}\right)_{X(p, T)} \quad (1)$$

For the largest adsorbed amount, the heat of adsorption  $\Delta H_{\text{ads}}$  remains constant around 2.6 kJ g<sup>-1</sup>, corresponding to 46.8 kJ mol<sup>-1</sup>. This value is comparable to those of other Al-based MOFs like aluminium fumarate<sup>9</sup> or CAU-10-H<sup>21</sup> and is only a few percent higher than the heat of vaporization of water.<sup>46</sup> Other  $\Delta H_{\text{ads}}$  reports for MOFs determined mostly higher values.<sup>9,10,13,21,28,43,47</sup> In combination with the water adsorption characteristic, this low value favors the use of MIL-53(Al)-TDC in sorption based chilling, where the released heat of adsorption is tantamount to waste heat.

### Multicycle hydrothermal stability and cooling performance

Multicycle stability towards water is a very crucial point when it comes to the envisioned application. Therefore, the sample has been tested in a thermogravimetric setup exposing the sample to a humidified argon flow. Adsorption and desorption are induced by switching the temperature between 40 °C and 140 °C. Prior to and after 20 cycles an equilibrium desorption and adsorption segment was performed. The plot of mass, temperature and water uptake in g g<sup>-1</sup> over time for 2 × 20 hydrothermal cycles is shown in Fig. 4. Over the first 20 cycles a slight decrease of dry mass ( $\Delta m = 1.3\%$ ) as well as equilibrium water uptake ( $\Delta X = 3.7\%$ ) occurred. This behaviour has been observed before for aluminium fumarate and can be explained by post-synthesis activation of the MOF by the desorbed water comparable to steam distillation.<sup>9</sup> In order to further confirm the stability, a second run of 20 cycles was performed on the same sample. Over these cycles no further decrease in dry mass and just a slight decrease in the equilibrium uptake ( $\Delta X = 2.7\%$ ) were observed which is on the order of the balance drift. Conclusively, the material can be suggested to be stable towards cyclic water adsorption and desorption within the test procedure and even more under application related conditions.

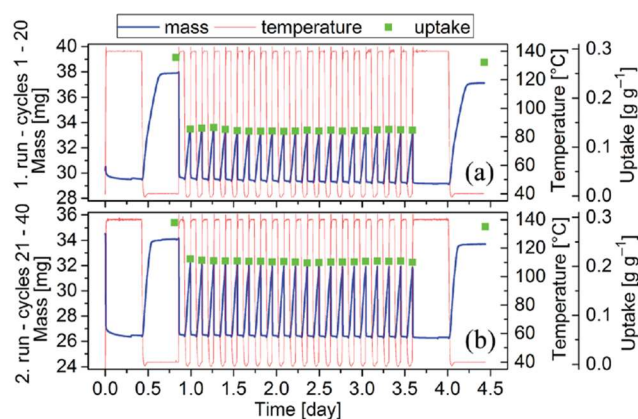


Fig. 4 First (a) and second (b) 20 cycles of adsorption and desorption of MIL-53(Al)-TDC in a thermogravimetric analyzer. Red curve: temperature, blue curve: sample mass, and green dots: uptake.

For additional stability investigations, a fresh sample of the material was investigated with PXRD over 12 cycles at 40 °C with varying humidities. Within the first and the last cycle a complete isotherm ( $0 < p/p_0 < 0.8$ ) was recorded, followed by PXRD (Fig. S1 and S2 in the ESI†), whereas all other cycles only consisted of adsorption at  $p/p_0 = 0.8$  and desorption at  $p/p_0 = 0.02$ .

MIL-53 is known for its breathing effect, that is, a network adapting to guest molecules yielding a wide-pore or narrow pore form.<sup>48</sup> For MIL-53(Al)-TDC we have not observed any reversible or irreversible structural changes upon (repeated) water sorption measurements with *in situ* powder X-ray diffraction. As can be seen from the diffractograms depicted in Fig. 5 (Fig. S2 and S3 in the ESI†), only the height of the peaks reproducibly decreased during adsorption (increasing humidity) and increased during desorption (decreasing humidity). During these cycles no loss in crystallinity and no phase change, which would be marked by additional peaks, can be observed. This result supports MIL-53(Al)-TDC to be structurally stable towards water.

Up to this point, the general suitability of MIL-53(Al)-TDC for adsorption heat transformation has been proven in terms of the demanded S-shaped isotherm, a high maximum water uptake and a good hydrothermal stability. The low heat of adsorption favors MIL-53(Al)-TDC for cooling applications. To further assess the suitability, experimental data were fit using a recently proposed dual-site Langmuir approach,<sup>49,50</sup> which is stated in detail in Section S13 in the ESI.†

During desorption, driving heat ( $Q_{\text{des}}$ ) has to be provided at the adsorbent and heat of condensation ( $Q_{\text{cond}}$ ) has to be discharged at the condenser (cf. Fig. 1). The sensitivity of the sample towards these two temperature levels is shown in Fig. 6. As can be seen from this plot, MIL-53(Al)-TDC can almost completely be desorbed at low temperatures between 50 and 70 °C, depending on the condenser temperature. Even at a high condenser temperature of 40 °C a desorption temperature of about 60 °C is sufficient to dry the material, enabling the possibility to dissipate the heat of condensation to the

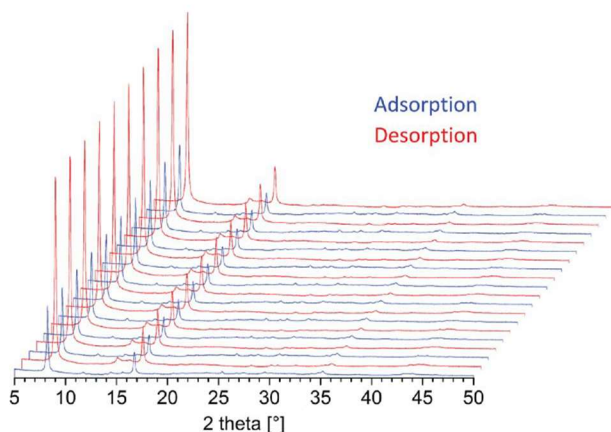


Fig. 5 Ten adsorption (blue)/desorption (red) cycles of MIL-53(Al)-TDC with *in situ* XRD observation, confirming its structural stability upon hydrothermal cycling.

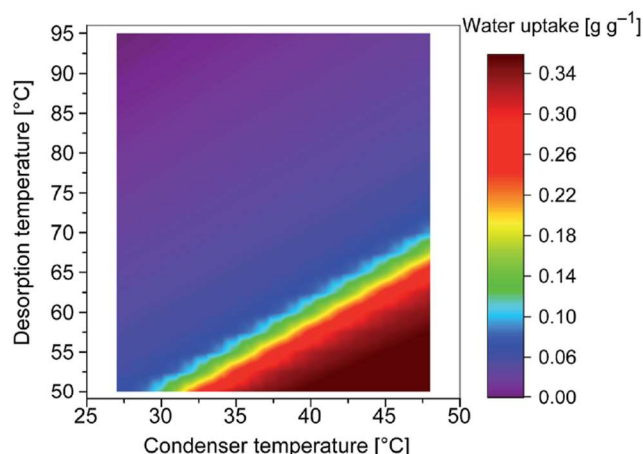


Fig. 6 Sensitivity of uptake capacity towards desorption temperature and condenser temperature, showing that MIL-53(Al)-TDC can be desorbed even at very high condenser temperatures with desorption temperatures below 70 °C.

environment *via* heat exchangers. Thus, low temperature waste heat can be utilized that cannot be used for other processes for desorption (see ref. 51 for an overview of waste heat temperature levels).

For the investigation of the adsorption stage, the desorption temperature was fixed at 65 °C, and the water uptake was calculated depending on the evaporation temperature and the heat rejection temperature corresponding to the adsorption temperature (Fig. 7). A desirable high water uptake of  $0.35 \text{ g g}^{-1}$  can be achieved for comparably high evaporation temperatures of above 15 °C and/or heat rejection below 30 °C. These findings recommend MIL-53(Al)-TDC for thermally driven cooling in industrial processes, as it can work at evaporation temperatures (providing the cooling) above 10 °C on one hand and can be regenerated with waste or solar thermal heat at around 65 °C on the other hand. Thereby, a working window is offered that is not accessible for conventional adsorbents with the corresponding water loading lift.

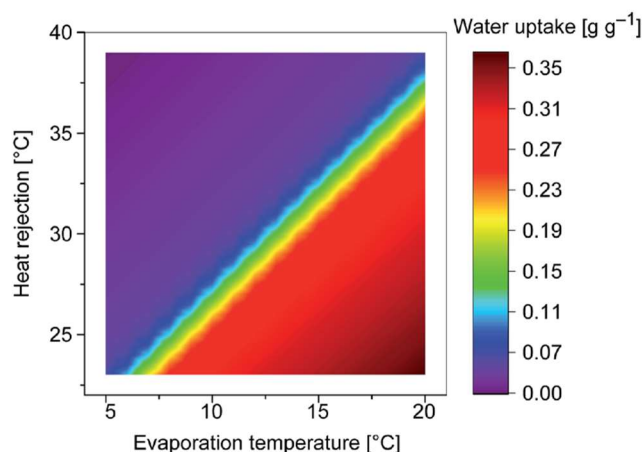


Fig. 7 Water uptake capacity as a function of heat rejection temperature and evaporation temperature, showing a broad plateau for different temperature settings. Drying conditions were set at 65 °C.



## Conclusion

MIL-53(Al)-TDC is preferably synthesized from aluminium sulfate or from basic aluminum acetate as water hysteresis is not observed in these cases, which renders this material advantageous for water sorption applications. Extensive water sorption studies followed by *in situ* PXRD and mass balance demonstrated the stability of MIL-53(Al)-TDC during hydro-thermal cycling for at least 40 cycles. Besides the technically feasible water uptake of  $0.3 \text{ g g}^{-1}$ , the low heat of adsorption ( $2.6 \text{ kJ g}^{-1}$ ) favors the use of MIL-53(Al)-TDC in chilling processes, since this heat must be rejected to the environment and is waste heat. The thermodynamic evaluation gives good low desorption temperatures at comparably good high condenser temperatures and sufficient water uptake capacities (cf. Fig. S17, ESI†) at medium evaporator temperatures. In combination with the previously reported MOFs based on  $\text{Al}^{3+}$ , like aluminum fumarate or CAU-10-H that show similar stability towards water, the assumption of Al-based MOFs being the most promising MOF adsorbents for application in thermally driven heat transformation can be sustained.

## Conflicts of interest

There are no conflicts of interest to declare.

## Acknowledgements

The authors gratefully acknowledge the financial support of the Federal German Ministry of Education and Research (BMBF) within the project Optimat under grant no. 03SF0492A/C.

## Notes and references

- 1 H.-C. Zhou, J. R. Long and O. M. Yaghi, *Chem. Rev.*, 2012, **112**, 673–674.
- 2 M. Eddaoudi, D. B. Moler, H. Li, B. Chen, T. M. Reineke, M. O’Keeffe and O. M. Yaghi, *Acc. Chem. Res.*, 2001, **34**, 319–330.
- 3 G. Akiyama, R. Matsuda, H. Sato, A. Hori, M. Takata and S. Kitagawa, *Microporous Mesoporous Mater.*, 2012, **157**, 89–93.
- 4 H. Furukawa, K. E. Cordova, M. O’Keeffe and O. M. Yaghi, *Science*, 2013, **341**, 1230444.
- 5 N. Stock and S. Biswas, *Chem. Rev.*, 2012, **112**, 933–969.
- 6 G. Maurin, C. Serre, A. Cooper and G. Férey, *Chem. Soc. Rev.*, 2017, **46**, 3104–3107.
- 7 M. J. Kalmutzki, C. S. Diercks and O. M. Yaghi, *Adv. Mater.*, 2018, 1704304.
- 8 F. Fathieh, M. J. Kalmutzki, E. A. Kapustin, P. J. Waller, J. Yang and O. M. Yaghi, *Sci. Adv.*, 2018, **4**, eaat3198.
- 9 F. Jeremias, D. Fröhlich, C. Janiak and S. K. Henninger, *RSC Adv.*, 2014, **4**, 24073–24082.
- 10 M. F. de Lange, K. J. F. M. Verouden, T. J. H. Vlugt, J. Gascon and F. Kapteijn, *Chem. Rev.*, 2015, **115**, 12205–12250.
- 11 J. Canivet, A. Fateeva, Y. Guo, B. Coasne and D. Farrusseng, *Chem. Soc. Rev.*, 2014, **43**, 5594–5617.
- 12 F. Jeremias, D. Fröhlich, C. Janiak and S. K. Henninger, *New J. Chem.*, 2014, **38**, 1846–1852.
- 13 F. Jeremias, A. Khutia, S. K. Henninger and C. Janiak, *J. Mater. Chem.*, 2012, **22**, 10148–10151.
- 14 H. Kummer, F. Jeremias, A. Warlo, G. Földner, D. Fröhlich, C. Janiak, R. Gläser and S. K. Henninger, *Ind. Eng. Chem. Res.*, 2017, **56**, 8393–8398.
- 15 D. Lenzen, P. Bendix, H. Reinsch, D. Fröhlich, H. Kummer, M. Möllers, P. P. C. Hügenell, R. Gläser, S. Henninger and N. Stock, *Adv. Mater.*, 2017, **6**, 1705869.
- 16 M. F. de Lange, T. Zeng, T. J. H. Vlugt, J. Gascon and F. Kapteijn, *CrystEngComm*, 2015, **17**, 5911–5920.
- 17 A. A. Askalany, M. Salem, I. M. Ismael, A. H. H. Ali, M. G. Morsy and B. B. Saha, *Renewable Sustainable Energy Rev.*, 2013, **19**, 565–572.
- 18 A. Cadiou, J. S. Lee, D. Damasceno Borges, P. Fabry, T. Devic, M. T. Wharmby, C. Martineau, D. Foucher, F. Taulelle, C.-H. Jun, Y. K. Hwang, N. Stock, M. F. De Lange, F. Kapteijn, G. Gascon, G. Maurin, J.-S. Chang and C. Serre, *Adv. Mater.*, 2015, **27**, 4775–4780.
- 19 J. Canivet, J. Bonnefoy, C. Daniel, A. Legrand, B. Coasne and D. Farrusseng, *New J. Chem.*, 2014, **38**, 3102–3111.
- 20 H. Furukawa, F. Gandara, Y.-B. Zhang, J. Jiang, W. L. Queen, M. R. Hudson and O. M. Yaghi, *J. Am. Chem. Soc.*, 2014, **136**, 4369–4381.
- 21 D. Fröhlich, E. Pantatosaki, P. D. Kolokathis, K. Markey, H. Reinsch, M. Baumgartner, M. A. van der Veen, D. E. de Vos, N. Stock, G. K. Papadopoulos, S. K. Henninger and C. Janiak, *J. Mater. Chem. A*, 2016, **4**, 11859–11869.
- 22 S.-I. Kim, T.-U. Yoon, M.-B. Kim, S.-J. Lee, Y. K. Hwang, J.-S. Chang, H.-J. Kim, H.-N. Lee, U.-H. Lee and Y.-S. Bae, *Chem. Eng. J.*, 2016, **286**, 467–475.
- 23 P. M. Schoenecker, C. G. Carson, H. Jasuja, C. J. J. Flemming and K. S. Walton, *Ind. Eng. Chem. Res.*, 2012, **51**, 6513–6519.
- 24 S. K. Henninger, G. Munz, K.-F. Ratzsch and P. Schossig, *Renew. Energ.*, 2011, **36**, 3043–3049.
- 25 A. Khutia, H. U. Rammelberg, T. Schmidt, S. Henninger and C. Janiak, *Chem. Mater.*, 2013, **25**, 790–798.
- 26 D. Fröhlich, S. K. Henninger and C. Janiak, *Dalton Trans.*, 2014, **43**, 15300–15304.
- 27 M. F. de Lange, C. P. Ottevanger, M. Wiegman, T. J. H. Vlugt, J. Gascon and F. Kapteijn, *CrystEngComm*, 2015, **17**, 281–285.
- 28 F. Jeremias, V. Lozan, S. K. Henninger and C. Janiak, *Dalton Trans.*, 2013, **42**, 15967–15973.
- 29 A. Permyakova, O. Skrylnyk, E. Courbon, M. Affram, S. Wang, U.-H. Lee, A. H. Valekar, F. Nouar, G. Mouchaham, T. Devic, G. D. Weireld, J.-S. Chang, N. Steneou, M. Frère and C. Serre, *ChemSusChem*, 2017, **10**, 1419–1426.
- 30 N. Ko, P. G. Choi, J. Hong, M. Yeo, S. Sung, K. E. Cordova, H. J. Park, J. K. Yang and J. Kim, *J. Mater. Chem. A*, 2015, **3**, 2057–2064.
- 31 S. K. Henninger, S.-J. Ernst, L. Gordeeva, P. Bendix, D. Fröhlich, A. D. Grekova, L. Bonaccorsi, Y. Aristov and J. Jaenchen, *Renew. Energ.*, 2017, **110**, 59–68.
- 32 A. Samokhvalov, *Coord. Chem. Rev.*, 2018, **374**, 236–253.

- 33 G. Férey, C. Serre, C. Mellot-Draznieks, F. Millange, S. Surblé, J. Dutour and I. Margiolaki, *Angew. Chem.*, 2004, **116**, 6456–6461.
- 34 C. Volkringer, D. Popov, T. Loiseau, G. Férey, M. Burghammer, C. Riekel, M. Haouas and F. Taulelle, *Chem. Mater.*, 2009, **21**, 5695–5697.
- 35 E. Alvarez, N. Guillou, C. Martineau, B. Bueken, B. Van de Voorde, C. Le Guillouzer, P. Fabry, F. Nouar, F. Taulelle, D. de Vos, J.-S. Chang, K. H. Cho, N. Ramsahye, T. Devic, M. Daturi, G. Maurin and C. Serre, *Angew. Chem., Int. Ed.*, 2015, **54**, 3664–3668.
- 36 H. Reinsch, M. A. van der Veen, B. Gil, B. Marszalek, T. Verbiest, D. de Vos and N. Stock, *Chem. Mater.*, 2013, **25**, 17–26.
- 37 M. H. Bagheri and S. N. Schiffres, *Langmuir*, 2018, **34**, 1908–1915.
- 38 N. C. Burtch, H. Jasuja and K. S. Walton, *Chem. Rev.*, 2014, **114**, 10575–10612.
- 39 D. D. Borges, G. Maurin and D. S. Galvão, *MRS Adv.*, 2017, **2**, 519–524.
- 40 C. W. L. Tschense, N. Reimer, C.-W. Hsu, H. Reinsch, R. Siegel, W.-J. Chen, C.-H. Lin, A. Cadiau, C. Serre, J. Senker and N. Stock, *Z. Anorg. Allg. Chem.*, 2017, **21**, 1600–1608.
- 41 G. A. González-Martínez, T. Jurado-Vázquez, D. Solís-Ibarra, B. Vargas, E. Sánchez-González, A. Martínez, R. Vargas, E. González-Zamora and I. A. Ibarra, *Dalton Trans.*, 2018, **47**, 9459–9465.
- 42 M. Thommes, K. Kaneko, A. V. Neimark, J. P. Olivier, F. Rodriguez-Reinoso, J. Roquerol and K. S. W. Sing, *Pure Appl. Chem.*, 2015, **87**, 1051–1069.
- 43 H. Kim, H. J. Cho, S. Naranayan, S. Yang, H. Furukawa, S. Schiffres, X. Li, Y.-B. Zhang, J. Jiang, O. M. Yaghi and E. N. Wang, *Sci. Rep.*, 2016, **6**, 19097.
- 44 R. Krishna, *Chem. Eng. Sci.*, 2015, **123**, 191–196.
- 45 D. M. Ruthven, *Principles of Adsorption and Adsorption Processes*, Wiley, New York, 1984.
- 46 (a) N. S. Osborne, H. F. Stimson and G. C. Ginnings, *J. Res. Natl. Bur. Stand.*, 1939, **23**, 197–260; (b) J. A. Dean, *Lange's Handbook of Chemistry*, McGraw-Hill Handbooks, New York, 15th edn, 1998; (c) National Institute of Standards and Technology Chemistry WebBook: <https://webbook.nist.gov/chemistry/>, accessed April 06th, 2018.
- 47 S. K. Henninger, F. Jeremias, H. Kummer and C. Janiak, *Eur. J. Inorg. Chem.*, 2012, **16**, 2625–2634.
- 48 C. Serre, F. Millange, C. Thouvenot, M. Noguès, G. Marsolier, D. Louër and G. Férey, *J. Am. Chem. Soc.*, 2002, **124**, 13519–13526.
- 49 M. Hefti, L. Joss, Z. Bjelobrk and M. Mazzotti, *Faraday Discuss.*, 2016, **192**, 153–179.
- 50 S.-J. Ernst, M. Baumgartner, D. Fröhlich, H.-J. Bart and S. K. Henninger, *Chem. Ing. Tech.*, 2017, **89**, 1650–1660.
- 51 S. Brueckner, S. Liu, L. Miró and E. Laevemann, *Appl. Energy*, 2015, **151**, 157–167.

## ELECTRONIC SUPPLEMENTARY INFORMATION

### Evaluation of the highly stable metal-organic framework MIL-53(Al)-TDC (TDC = 2,5-thiophenedicarboxylate) as a new and promising adsorbent for heat transformation applications

Niels Tannert,<sup>a,x</sup> Sebastian-Johannes Ernst,<sup>b,c,x</sup> Christian Jansen,<sup>a</sup> Hans-Jörg Bart,<sup>b</sup> Stefan K. Henninger<sup>c</sup> and Christoph Janiak<sup>a,\*</sup>

<sup>a</sup> *Institut für Anorganische Chemie und Strukturchemie, Heinrich-Heine-Universität Düsseldorf, Universitätsstraße 1, 40225 Düsseldorf, Germany.*

<sup>b</sup> *Chair of Separation Science and Technology, TU Kaiserslautern, Postfach 3049, 67653 Kaiserslautern, Germany.*

<sup>c</sup> *Fraunhofer Institute for Solar Energy Systems (ISE), Heidenhofstr. 2, 79110 Freiburg, Germany.*

*x These authors contributed equally.*

*\*E-mail: [janiak@uni-duesseldorf.de](mailto:janiak@uni-duesseldorf.de)*

further Emails: [Niels.Tannert@uni-duesseldorf.de](mailto:Niels.Tannert@uni-duesseldorf.de); [sebastian-johannes.ernst@ise.fraunhofer.de](mailto:sebastian-johannes.ernst@ise.fraunhofer.de); [christian.jansen@hhu.de](mailto:christian.jansen@hhu.de); [bart@mv.uni-kl.de](mailto:bart@mv.uni-kl.de); [stefan.henninger@ise.fraunhofer.de](mailto:stefan.henninger@ise.fraunhofer.de)

#### **Keywords**

Metal-Organic Frameworks, MIL-53(Al)-TDC, Synthesis Optimization, Water Sorption, Isothermic Heat of Adsorption, Cooling Performance, Multicycle stability, Hydrothermal stability, Chemical stability, Thermal stability, Heat transformation application

#### **Table of Contents**

Section S1.	Chemicals
Section S2.	Synthesis optimization
Section S3.	Karl-Fischer titrations
Section S4.	PXRD measurements
Section S5.	Solvent and pH stability
Section S6.	Thermogravimetric analysis (TGA)
Section S7.	Elemental analysis
Section S8.	Infrared spectroscopy (IR)
Section S9.	Scanning electron microscopy (SEM)
Section S10:	Nitrogen sorption experiments (T = 77 K)
Section S11.	Argon sorption experiments (T = 87 K)
Section S12:	Water sorption and isosteric heat of adsorption
Section S13:	Multicycle stability tests
Section S14.	References



## S1. Chemicals

All chemicals were used as received by supplier (cf. Table S1).

**Table S1** Used chemicals, supplier and purities.

Chemical	Supplier	Purity
Acetone	Sigma Aldrich	>99.5%
$\text{AlCl}_3 \cdot 6 \text{H}_2\text{O}$	Janssen Chimica	99%
$\text{Al}(\text{SO})_4 \cdot 18\text{H}_2\text{O}$	AppliChem	not specified
$\text{Al}(\text{OH})(\text{acetate})_2 \cdot x \text{H}_2\text{O}$	AlfaAesar	not specified
Diethylether	Riedel de Haën	99.8%
Dimethylformamide	Fischer Chemicals	99.99%
Ethanol	Chem Solute	99.9%
2,5-Furandicarboxylic acid	OxChem	95%
Hydrochloric acid, 37%	Sigma Aldrich	37%
$\text{NaAlO}_2$	VWR Chemicals	not specified
NaOH (microgranulate)	Chem Solute	not specified
Nitric acid, 65%	VWR Chemicals	not specified
Tetrahydrofuran	Riedel de Haën	p.a.
2,5-thiophenedicarboxylic acid	Sigma Aldrich	99%

## S2. Synthesis optimization

The syntheses were following a modified protocol of Tschense *et al.*<sup>1</sup>

Approximately 5.0 mmol of 2,5-thiophenedicarboxylic acid ( $\text{H}_2\text{TDC}$ ) and 5.7 mmol of either  $\text{AlCl}_3 \cdot 6 \text{H}_2\text{O}$ ,  $\text{Al}_2(\text{SO}_4)_3 \cdot 18 \text{H}_2\text{O}$ ,  $\text{Al}(\text{OH})(\text{ac})_2 \cdot x \text{H}_2\text{O}$  or  $\text{NaAlO}_2$  were refluxed (24 h, 135 °C) with 32 mL of water and 8 mL of dimethylformamide (DMF). The precipitate was recovered by centrifugation, consecutively washed and re-dispersed in water (three times, 100 mL each). A fourth washing step was applied by further stirring in water (100 mL, 24 h). After final centrifugation and decantation, the product was dried under reduced pressure (24 h, 80 °C, 50 mbar). All products were obtained as white powders. Table S2 summarizes the synthesis results.

**Table S2** Synthesis results of MIL-53(Al)-TDC syntheses using different aluminum sources.

Al-source	Reactant [g] <sup>a</sup>	Yield [g]	Yield [%]	BET [ $\text{m}^2\text{g}^{-1}$ ] <sup>b</sup>
$\text{Al}(\text{OH})(\text{ac})_2 \cdot x \text{H}_2\text{O}$	1.027	0.983	95, 91	885, 1092
$\text{NaAlO}_2$	0.469	0.482	39	394
$\text{Al}(\text{SO})_4 \cdot 18\text{H}_2\text{O}$	3.798	0.946	88	1102
$\text{AlCl}_3 \cdot 6 \text{H}_2\text{O}$	1.376	0.889	83	1096
ref. [1]	1.158	0.880	84	1150

<sup>a</sup> The weighted amounts of  $\text{Al}(\text{OH})(\text{ac})_2 \cdot x \text{H}_2\text{O}$  and  $\text{NaAlO}_2$  were adjusted in terms of water content per formula unit (cf. Section S3). <sup>b</sup> Determined by five adsorption points of nitrogen sorption isotherms.

## S3. Karl-Fischer titrations

In order to weigh out the proper stoichiometric amounts of  $\text{Al}(\text{OH})(\text{ac})_2 \cdot x \text{H}_2\text{O}$  and  $\text{NaAlO}_2$ , which was suspected to contain water of crystallization, we carried out Karl-Fischer-titrations. Both experiments were carried out on an ECH AQUA 40.00 (ECH, Halle (Saale), Germany) with repeated

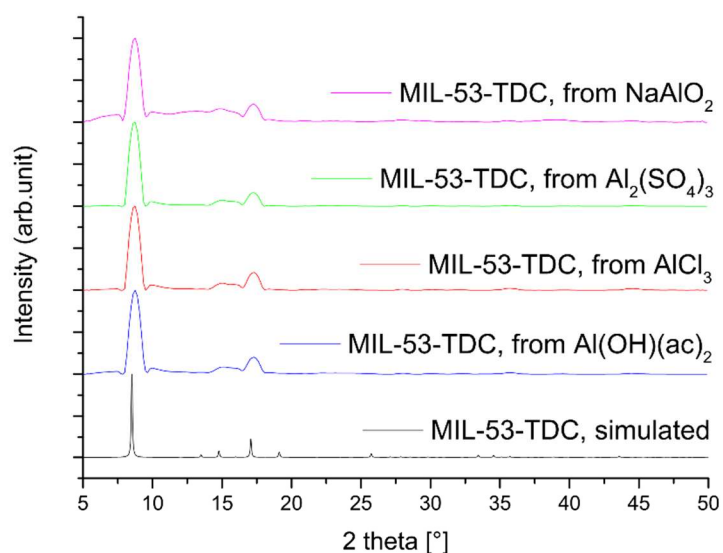
determinations. Therefore,  $\text{Al}(\text{OH})(\text{ac})_2 \cdot x \text{H}_2\text{O}$  (12.90 mg) and  $\text{NaAlO}_2$  (11.00 mg) were analyzed. The water contents were determined to be 9.82% for  $\text{Al}(\text{OH})(\text{ac})_2 \cdot x \text{H}_2\text{O}$  and 3.21% for  $\text{NaAlO}_2$ , correlating to formulas of approximately  $\text{Al}(\text{OH})(\text{ac})_2 \cdot \text{H}_2\text{O}$  and  $\text{NaAlO}_2 \cdot 0.2 \text{H}_2\text{O}$ . Hence, both molar weights were adjusted and taken into account for calculation of reactant ratios during synthesis optimizations.

#### S4. PXRD measurements

Powder X-ray diffraction (PXRD) patterns were obtained at ambient temperature on a *D2 phaser* (BRUKER, Billerica, US) using  $\text{Cu-K}\alpha$  radiation ( $\lambda = 1.54182 \text{ \AA}$ ) between  $5^\circ < 2\theta < 50^\circ$  with a scanning rate of  $0.0125^\circ/\text{s}$  (300 W, 30 kV, 10 mA). The diffractograms were obtained on a flat “low background sample holder”, in which at low angle the beam spot is strongly broadened so that only a fraction of the reflected radiation reaches the detector, hence the low relative intensities measured at  $2\theta < 7^\circ$ . Analyses of the diffractograms were carried out with *Match 3.11* software.

X-ray diffractograms under humid conditions were acquired *in-situ* on a *Bruker D8 Advance* with *DaVinci™* (BRUKER, Billerica, US), using a Cu anode tube at 40 kV/40 mA, with a Ni filter and constant sample illumination spot size (broadness: 12 mm); step size  $0.02^\circ$ , 1.0 s/step,  $\text{Cu-K}\alpha$  radiation. *MRI Humidity Stage* (BRUKER AXS, Karlsruhe, Germany) was used for controlled humidity, where a humidified  $\text{N}_2$  gas flow was passed over the sample at atmospheric pressure. Before each scan, the sample was allowed to equilibrate for 90 min.

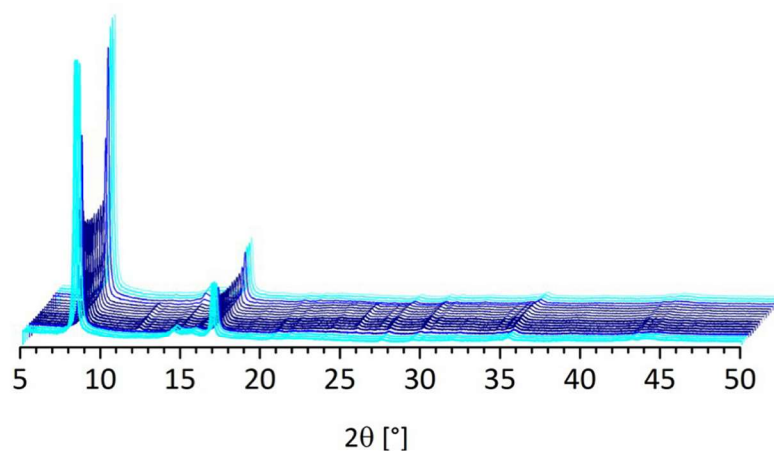
All relevant PXRD plots of synthesis optimization are given in the full paper in Figure S1.



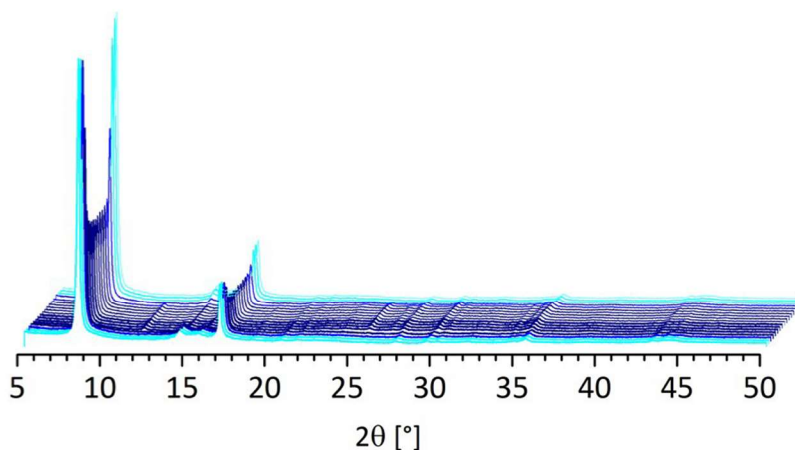
**Figure S1** PXRD patterns of different MIL-53(Al)-TDC samples obtained by varying aluminum salt sources. The theoretical powder pattern was calculated from a cif-file that was generously provided by Serre and co-workers.

Figure S2 and Figure S3 show the PXRD patterns of an adsorption-desorption isotherm at  $40^\circ\text{C}$ . Before and after ten cycles performed in an *in-situ* PXRD humidity chamber. As can be seen from the diffractograms, the reflexes decrease in the presence of humidity but increase reproducibly during desorption.





**Figure S2** Complete adsorption-desorption in-situ PXRD at 40 °C **before** the performed multicycling. Light blue represent desorbed state, whereas dark blue indicates adsorbed state.



**Figure S3** Complete adsorption-desorption in-situ PXRD at 40 °C **after** the performed multicycling. Light blue represent desorbed state, whereas dark blue indicates adsorbed state.

### **S5. Solvent and pH stability**

In order to check the chemical stability of MIL-53(Al)-TDC towards different solvents and pH 1/pH 12 solutions, approximately 10 mg of MIL-53(Al)-TDC was suspended in 3 mL solvent each. After 24 h of stirring, the solid was recovered by centrifugation and dried (80 °C, 50 mbar). Subsequent PXRD analyses are illustrated in the Figures S4 and S5.

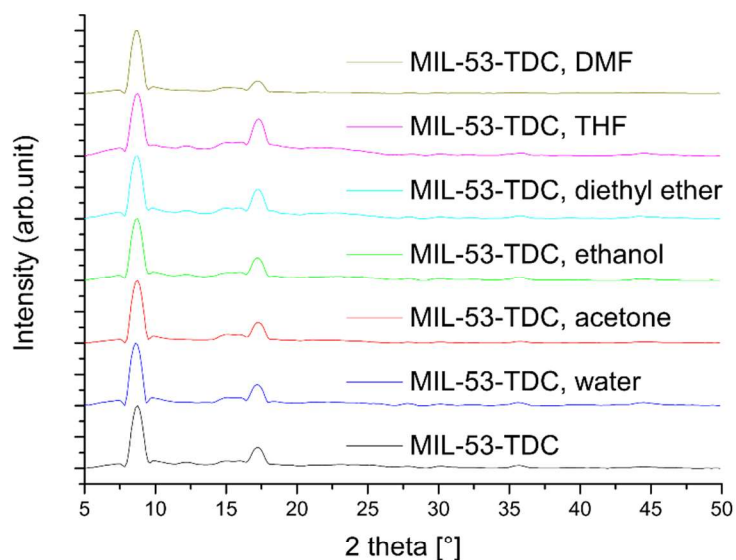


**Figure S4** PXRDs of MIL-53(Al)-TDC before and after 24 h of stirring in the stated solvent.

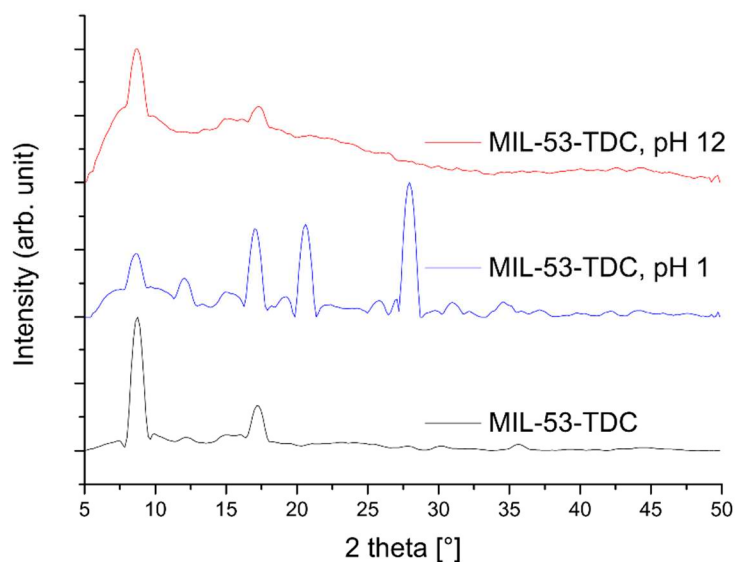


**Figure S5** PXRDs of MIL-53(Al)-TDC before and after 24 h of stirring in pH 1/pH 12 solutions ( $\text{HNO}_3$  and NaOH used for pH adjustment).

MIL-53(Al)-TDC seems to be highly stable towards organic solvents. None of the applied solvents seem to affect the crystallinity of the MIL-53(Al)-TDC phase. Figure S5 reveals that the compound loses crystallinity in pH 12, as the amorphous ratio in the pattern arises. After treatment in a pH 1 solution, MIL-53(Al)-TDC seems to be still present in the sample. However, the powder diffractogram shows various additional reflexes.

## **S6. Thermogravimetric Analysis (TGA)**

TGA measurements were carried out on a *Netzsch TG209 F3 Tarsus* (NETZSCH, Selb, Germany) device under nitrogen atmosphere, ramping with 5 Kmin<sup>-1</sup> to target temperature (600 °C). Figure S6 shows the TGA curve of MIL-53(Al)-TDC obtained from Al(OH)(ac)<sub>2</sub>.

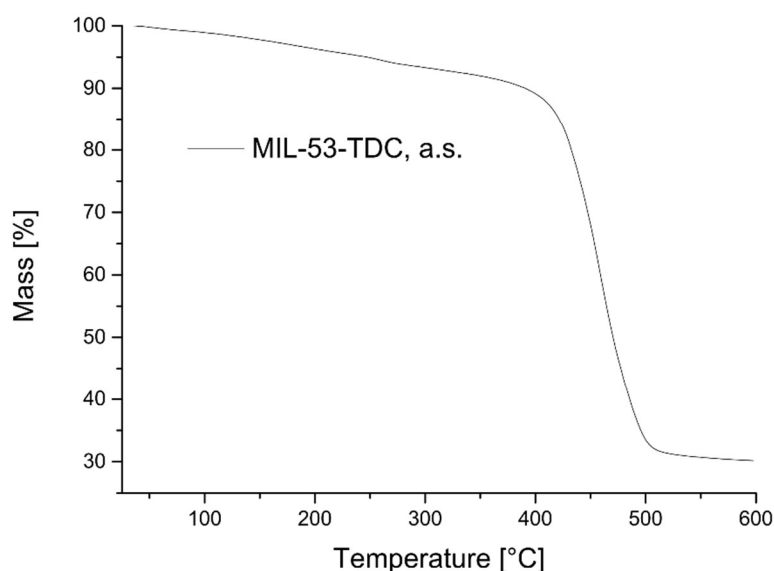


**Figure S6** TGA curve of MIL-53(Al)-TDC, revealing thermal stability up to at least 400 °C.

The curve reveals thermal stability of the compound up to at least 400 °C, which is in very good accordance to Stock and co-workers, who reported the same value (cf. ESI<sup>†</sup> of Tschense *et al.*).<sup>1</sup>

## **S7. Elemental analysis**

Elemental analysis was acquired on a *vario MICRO cube* (ELEMENTAR ANALYSENSYSTEME, Langenselbold, Germany).

Elemental analysis confirmed the composition of the as-synthesized product:

- **C** (meas.: 31.14%, calc. 31.04)
- **H** (meas.: 1.50%, calc. 2.17%)
- **S** (meas.: 13.21, calc. 13.81%)

The results are in good agreement with the thermogravimetric analysis.

### S8. Infrared (IR) spectral analysis

Infrared spectra were acquired on a *Bruker Tensor 37 FT-IR* device. Figure S7 depicts the IR spectra of MIL-53(Al)-TDC and the linker H<sub>2</sub>TDC.

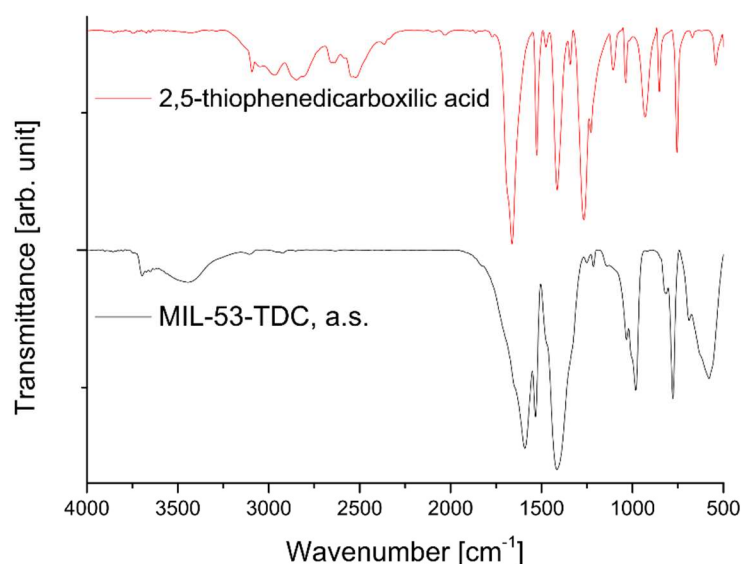


**Figure S7** Infrared spectra of MIL-53(Al)-TDC (black) and free linker 2,5-thiophenedicarboxylic acid (red).

The IR spectrum of MIL-53(Al)-TDC is in very good accordance to Tschense *et al.*<sup>1</sup>, who reported 1589 cm<sup>-1</sup> and 1408 cm<sup>-1</sup> for symmetric and asymmetric coordinating carboxylate groups. Stretching vibrations of the aromatic ring were consistently reported at  $\nu_{C=C}$  = 1651 cm<sup>-1</sup>,  $\nu_{C=C}$  = 1531 cm<sup>-1</sup> and  $\nu_{C-S}$  = 690 cm<sup>-1</sup>. That is good accordance to the prior report (cf. 1668 cm<sup>-1</sup> for DMF, 1589 cm<sup>-1</sup> and 1408 cm<sup>-1</sup> for symmetric and asymmetric vibrations of carboxylate, and  $\nu_{C=C}$  = 1651 cm<sup>-1</sup>, 1531 cm<sup>-1</sup> and  $\nu_{C-S}$  = 690 cm<sup>-1</sup> for the aromatic vibrations.<sup>1</sup>

Ancillary, a broad band around 3500 cm<sup>-1</sup> can be observed, indicating H-bonds and incorporated water molecules inside the cavities. The band around 3685 cm<sup>-1</sup> more pronounced than reported lately.<sup>1</sup> It is affected by  $\mu$ -OH groups of the framework and therefore another distinctive band for the product. Additionally, we provide the IR spectrum of H<sub>2</sub>TDC, which proves absence of unreacted linker molecules by absence of corresponding IR absorbance bands (e.g. absence of prominent band around 1280 cm<sup>-1</sup>, present in the linker H<sub>2</sub>BDC).

### S9. Scanning electron microscopy (SEM)

For control of morphology we recorded SEM images using a *JEOL JSM-6510 Advanced electron microscope* (JEOL, Akishima, Japan) with a LaB<sub>6</sub> cathode at 5-20 keV. The microscope was equipped with a *Xflash 410* (BRUKER, Billerica, US) silicon drift detector. Figures S8-S11 show selected images of obtained samples out of varying Al-sources.

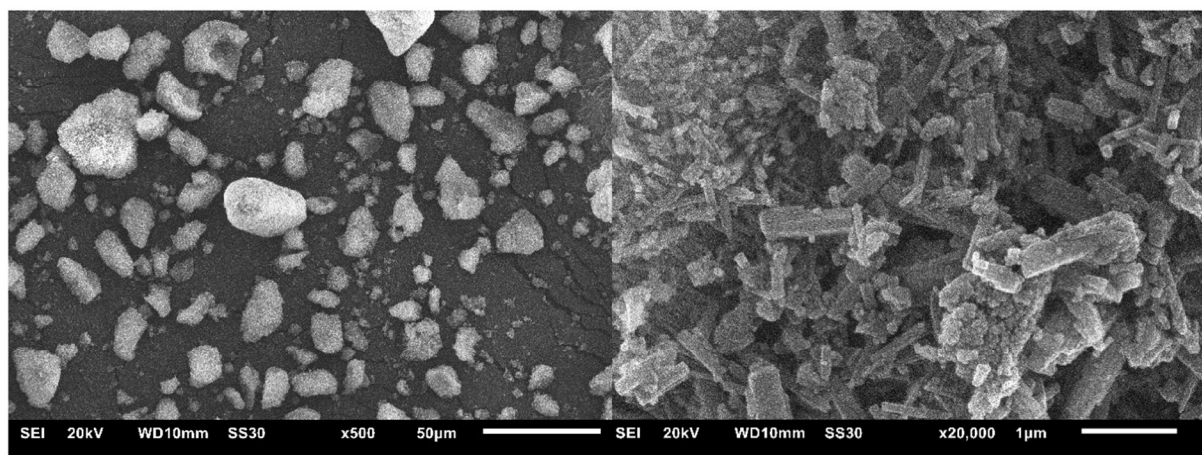


**Figure S8** SEM images of MIL-53(Al)-TDC obtained out of  $\text{Al}(\text{OH})(\text{ac})_2$ , left: overview of agglomerates, right: close-up.

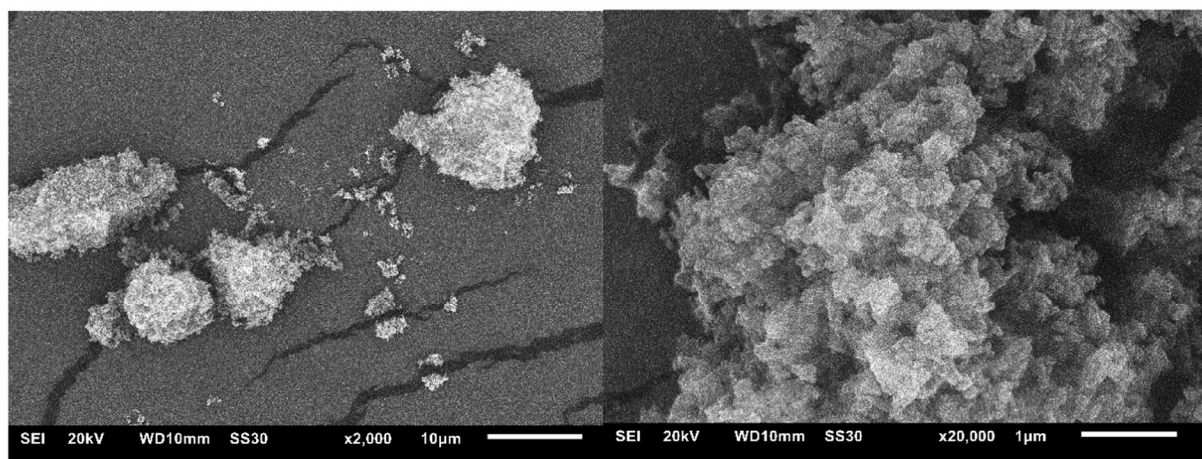


**Figure S9** SEM images of MIL-53(Al)-TDC obtained out of  $\text{AlCl}_3$ , left: overview of agglomerates, right: close-up.

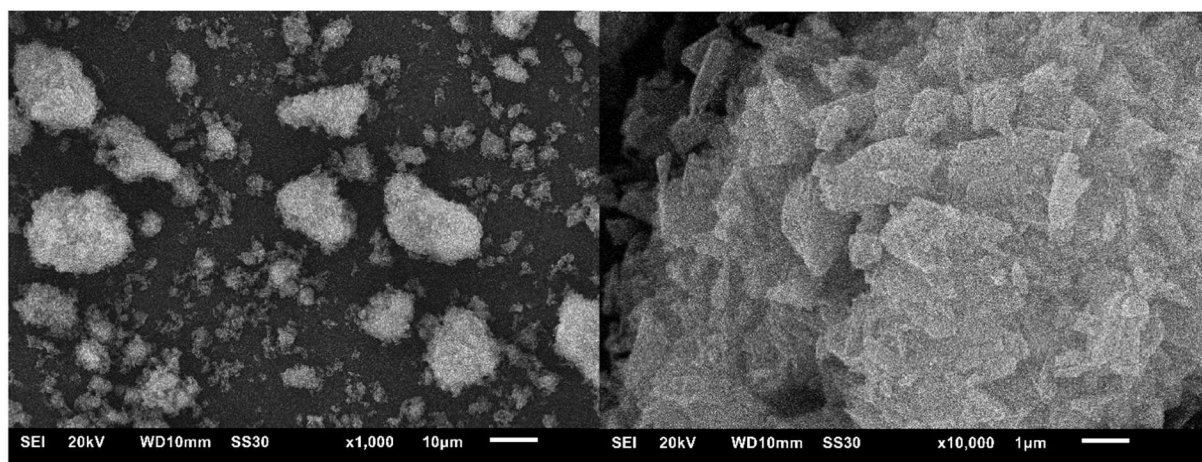


**Figure S10** SEM images of MIL-53(Al)-TDC obtained out of  $\text{Al}_2(\text{SO}_4)_3$ , left: overview of agglomerates, right: close-up.



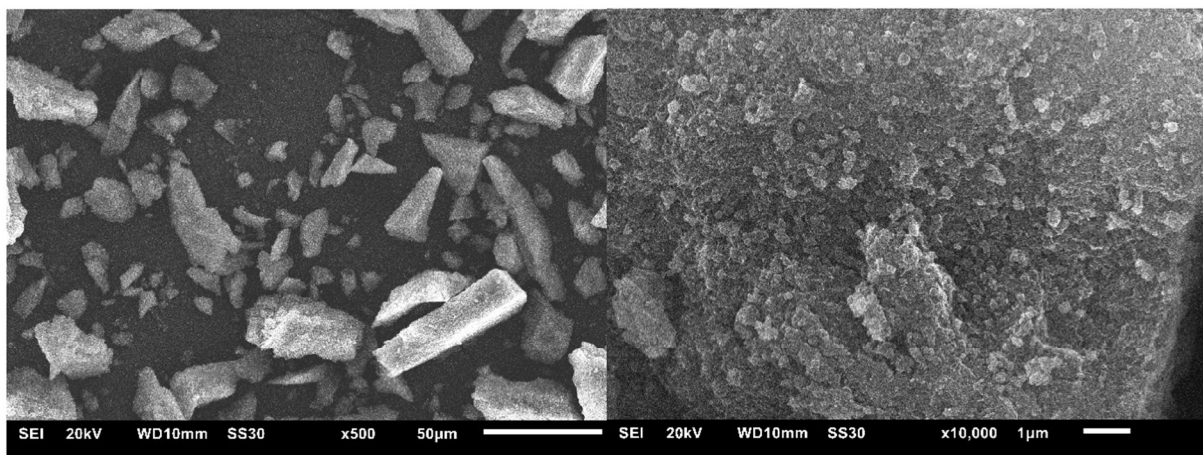


**Figure S11** SEM images of MIL-53(Al)-TDC obtained out of  $\text{NaAlO}_2$ , left: overview of agglomerates, right: close-up.

All samples appear to be composed as agglomerates, which is typical for Al-based MOFs. The observation of different crystallite morphologies with the same PXRD pattern and comparable degree of crystallinity is evident. Certainly, all samples can be designated as uniform homogeneous MIL-53(Al)-TDC materials, nevertheless crystallite morphologies variegate with the applied Al-source. In comparison to the picture shown in the ESI<sup>†</sup> of Stock and co-workers,<sup>1</sup> the morphology of our material obtained from  $\text{Al}(\text{OH})(\text{ac})_2$  seems to be most alike. Yet, morphology may also vary due to reflux syntheses in the present cases shown above, compared to microwave solvothermal synthesis in the literature.

#### **S10. Nitrogen sorption experiments (T = 77 K)**

Surface areas (BET) were determined by nitrogen (purity 99.999%, 5.0) sorption experiments at 77 K using liquid nitrogen and performing on a *Quantachrome NOVA-4000e* (QUANTACHROME, Odelzhausen, Germany) instrument within a partial pressure range of  $p/p_0 = 10^{-3}$ -1 bar.

Each sample was degassed under vacuum ( $<10^{-2}$  mbar) at 150 °C for ca. 3 h, prior to measurement.

All surface areas (BET) were calculated from five adsorption points in the pressure range  $p/p_0 = 0.005$ -0.05 by applying Roquerol plots ( $r > 0.998$ ). This range is indeed not recommended by IUPAC (International Union of Pure and Applied Chemistry) for BET surface determination, but rather suitable for microporous materials.<sup>2</sup>

Total pore volumes were calculated from the  $\text{N}_2$  sorption isotherm at  $p/p_0 = 0.95$ . NLDFT calculations for the pore size distribution curves were done with the native *NovaWin 11.03* software using the 'N<sub>2</sub> at 77 K on carbon, slit pore, NLDFT equilibrium' model.

Figure S12 depicts the nitrogen sorption isotherm of MIL-53(Al)-TDC obtained out of  $\text{Al}(\text{OH})(\text{ac})_2$  (that is the material used for multicycle stability experiments and further water sorption experiments, including affiliated calculations.).



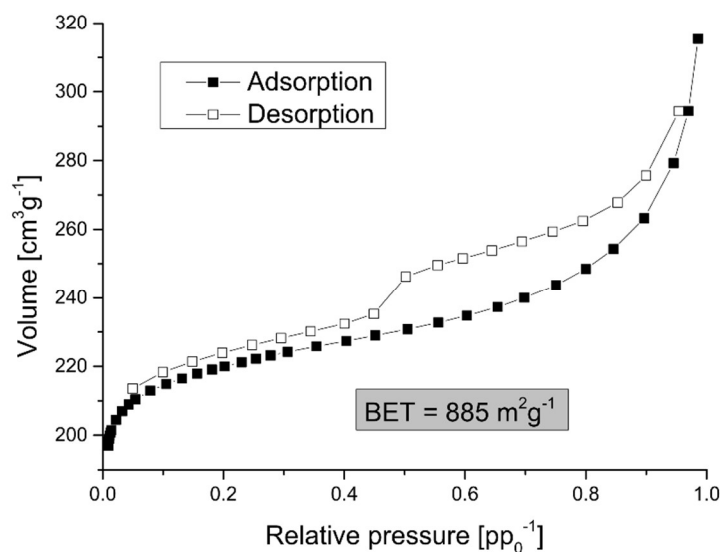


**Figure S12** Nitrogen sorption isotherms of MIL-53(Al)-TDC obtained out of  $\text{Al}(\text{OH})(\text{ac})_2$ .

Figure S13 shows the isotherms collected from the samples derived from different Al-sources.

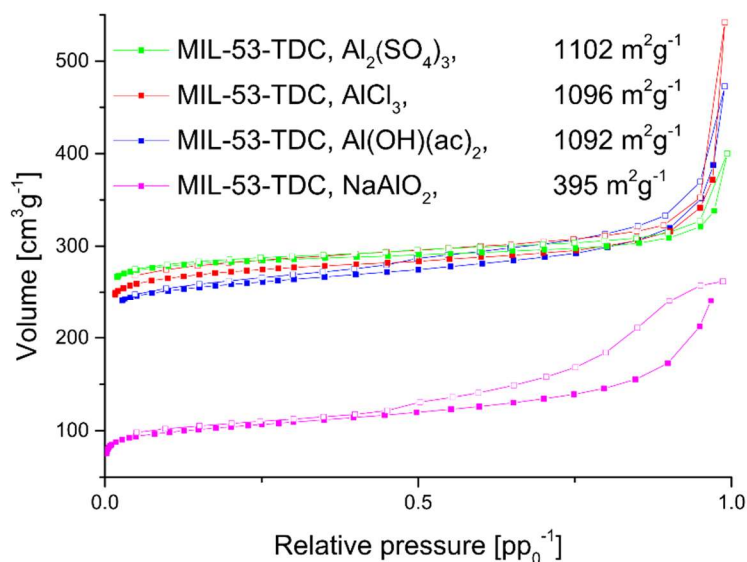


**Figure S13** Nitrogen sorption isotherms of MIL-53(Al)-TDC samples obtained out of varying Al-sources.

The results show that although MIL-53(Al)-TDC was synthesized free from phase shift in all cases of Al-sources (cf. PXRD patterns in Figure S1), porosity varied. The reactant  $\text{NaAlO}_2$  cannot compete with the other three starting materials, which seem to be more or less in the same range of porosity. Table S3 concludes the porosity parameters derived from nitrogen sorption isotherms (cf. Figure S13) of MIL-53(Al)-TDC samples obtained out of varying Al-sources.

**Table S3** Porosity parameters of different MIL-53(Al)-TDC samples obtained out of varying Al-sources, determined with nitrogen sorption (77 K) and stated calculation methods.

Al-source	$S_{\text{BET}}$ [m <sup>2</sup> g <sup>-1</sup> ] <sup>a</sup>	$S_{\text{BET (micro)}}$ [m <sup>2</sup> g <sup>-1</sup> ] <sup>b</sup>	$V_{\text{total}}$ [cm <sup>3</sup> g <sup>-1</sup> ] <sup>c</sup>	$V_{\text{micro}}$ [cm <sup>3</sup> g <sup>-1</sup> ] <sup>d</sup>
Al(OH)(ac) <sub>2</sub> · x H <sub>2</sub> O	885, 1092	800, 965	0.41, 0.52	0.30, 0.43
NaAlO <sub>2</sub>	395	275	0.37	0.11
Al(SO) <sub>4</sub> · 18H <sub>2</sub> O	1102	1041	0.46	0.41
AlCl <sub>3</sub> · 6 H <sub>2</sub> O	1096	1002	0.49	0.38
AlCl <sub>3</sub> , ref. [1] *	1150	Not specified	Not specified	0.48

<sup>a</sup> Specific surface areas ( $S_{\text{BET}}$ ) were determined by five adsorption points of nitrogen sorption isotherms in the range  $0.005 < pp_0^{-1} < 0.05$ . <sup>b</sup> Micropore areas were determined by t-plot method with De Boer model in the range  $0.2 < pp_0^{-1} < 0.4$ . <sup>c</sup> Total pore volumes ( $V_{\text{total}}$ ) were calculated at  $pp_0^{-1} = 0.9$ . <sup>d</sup> Micropore volumes ( $V_{\text{micro}}$ ) were calculated by NLDFT method (carbon, slit pore, nitrogen, 77 K). \* Determined at  $pp_0^{-1} = 0.5$ .

### **S11. Argon sorption experiments (T = 87 K)**

Argon (purity 99.999%, 5.0) sorption experiments were performed at 87 K using a *Quantachrome CryoCooler* (QUANTACHROME, Odelzhausen, Germany) for appropriate adjustment of T = 87 K and performing on a *Quantachrome Autosorb iQ MP* (QUANTACHROME, Odelzhausen, Germany) instrument with within a partial pressure range of  $p/p_0 = 10^{-7}$ -1 bar.

Each sample was degassed under vacuum ( $<10^{-5}$  mbar) at 150 °C for ca. 3 h, prior to measurement. All surface areas (BET) were calculated from five adsorption points in the pressure range  $0.005 < pp_0^{-1} < 0.05$

Additionally, we carried out argon sorption measurements (87 K) which is rather rare, but recommended for microporous materials.<sup>2</sup> While nitrogen sorption (cf. Figure S11) often overestimates BET areas of (especially micro- to mesoporous) MOFs,<sup>2,3,4</sup> it determined a specific surface area of  $BET = 885 \text{ m}^2\text{g}^{-1}$  and  $0.41 \text{ cm}^3\text{g}^{-1}$  pore volume (NLDFT, carbon, slit pore, nitrogen, 77 K). Argon sorption revealed a surface area of  $BET = 827 \text{ m}^2\text{g}^{-1}$  and  $0.35 \text{ cm}^3\text{g}^{-1}$  pore volume (NLDFT, carbon, slit pore, argon, 87 K) and  $0.27 \text{ cm}^3\text{g}^{-1}$  micropore volume (t-plot method, De Boer model). It has to be noted that BET calculation is usually performed in a pressure range  $0.05 < pp_0^{-1} < 0.3$ , but its applicability also works for microporous materials in a lower range (here:  $0.005 < pp_0^{-1} < 0.05$ ).<sup>3,5</sup>

Argon sorption was carried out exemplarily for a sample obtained out of Al(OH)(ac)<sub>2</sub>, from which the isotherm is depicted in Figure S14. The shape of isotherm is typical for microporous material, a Type-I isotherm with steep increase at relative pressures of  $pp_0^{-1} < 0.1$ .

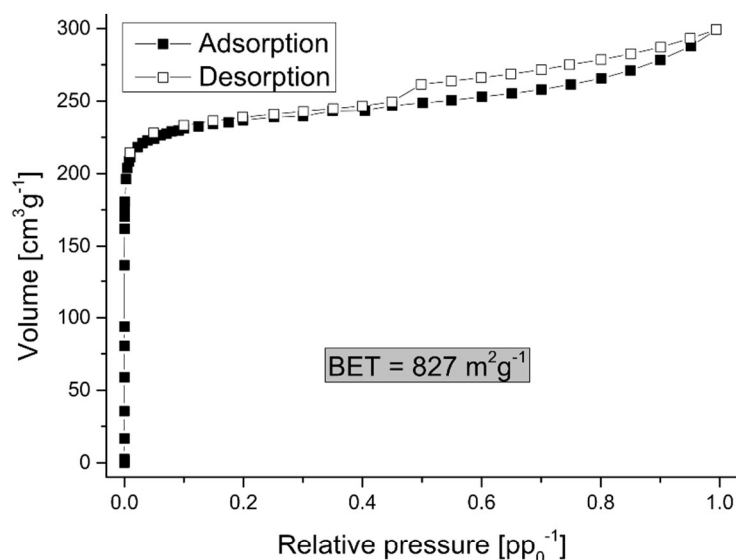


**Figure S14** Argon sorption isotherm (87 K), exhibiting typical isotherm Type-I appearance for microporous materials.

### **S12. Water sorption and isosteric heat of adsorption**

All water sorption isotherms (25, 40, 60 °C) were measured with a *Quantachrome VStar4* (QUANTACHROME, Odelzhausen, Germany) within a partial pressure range of  $p/p_0 = 10^{-3}$ -0.9 bar. Each sample was degassed under vacuum ( $<10^{-5}$  mbar) at 150 °C for ca. 3 h, prior to measurement. The acquired data were fit with native *VersaWin™ 1.0* software.

Figure S15 illustrates the water sorption isotherms of different samples MIL-53(Al)-TDC.

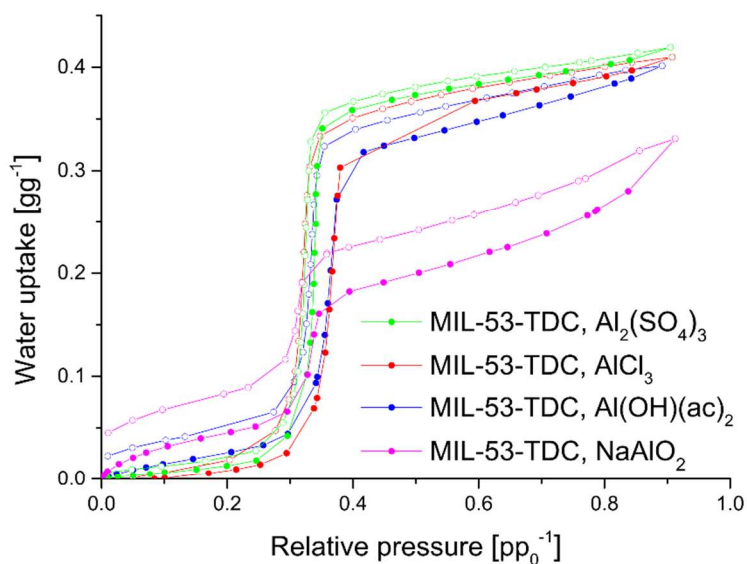


**Figure S15** Water sorption isotherms of MIL-53(Al)-TDC samples obtained out of varying Al-sources.

Obviously, the influence of the Al-source occurs on smaller scales for three of the four tested Al-sources (i.e.  $\text{Al}_2(\text{SO}_4)_3$ ,  $\text{Al}(\text{OH})(\text{acetate})_2$  and  $\text{AlCl}_3$ ), which correlates with  $\text{N}_2$  sorption results (cf. Table S3). However, hystereses differ even among the named materials, indicating probably residual or coordinated anions of the Al-sources that bias during ad- and desorption.

The isosteric heat of adsorption was determined directly from the measurements at 25 °C, 40 °C and 60 °C (Figure 3 in the full paper), and this data was fitted by a thermodynamic model according to *Van't Hoff* (eqn (1)).<sup>6</sup>

$$\frac{\Delta H_{\text{ads}}(X,T)}{RT^2} = - \left( \frac{\partial \ln p}{\partial T} \right)_{X(p,T)} \quad (1)$$

For the broadest range of adsorbed amount, the heat of adsorption is constant at around 2.6 kJ g<sup>-1</sup>.

Water uptake capacity as a function of heat rejection can be seen in Figure 6 in the full paper. Sensitivity of uptake capacity towards desorption temperature and condenser temperature is also given in the full paper in Figure 7.

### S13. Multicycle stability tests

Water cycling stabilities were examined in a *Setaram*<sup>TM</sup> TGA-DSC-111 (SETARAM, Caluire, France) on powdered samples. A humidified argon gas flow (40 °C, 76.3% relative humidity) was generated by a *Setaram*<sup>TM</sup> WetSys (SETARAM, Caluire, France) humidity controller and passed through the sample chamber, while the temperature of the sample was varied and the mass of the adsorbent was monitored. For the multi-cycle ad-/desorption experiments, the temperature of the sample was varied between 40 °C and 140 °C with a cycle time of 5 h.

The cycling results of the first 40 cycles are depicted in Figure S16.

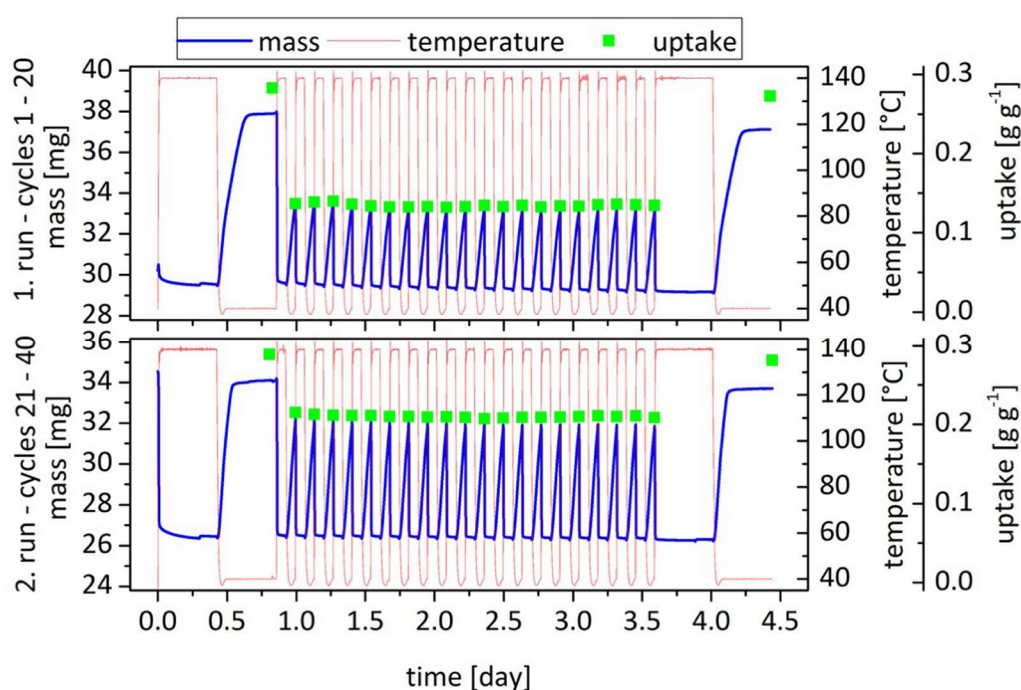


**Figure S16** Multicycle water stability tests (40 cycles). Blue: sample mass [mg], red: temperature [°C], green: uptake [g g<sup>-1</sup>].

To fit the experimental data, a recently proposed <sup>7,8</sup> weighted Dual-Site Langmuir (wDSL) approach was used:

$$X(p,T) = X_L(1 - w(p,T)) + X_U(p,T)w(p,T) \quad (2)$$

$$X_L(p,T) = X_{L,\infty} \frac{b_L p}{1 + b_L p} \quad (3)$$

$$X_U(p,T) = X_{U,\infty} \frac{b_U p}{1 + b_U p} + b_H p \quad (4)$$

$$b_\alpha = b_{\alpha,\infty} \exp\left(\frac{E_\alpha}{RT}\right), \alpha = L, U, H \quad (5)$$

$$w(p,T) = \left( \frac{\exp\left(\frac{\ln(p) - \ln(p_{step}(T))}{\sigma(T)}\right)}{1 + \exp\left(\frac{\ln(p) - \ln(p_{step}(T))}{\sigma(T)}\right)} \right)^\gamma \quad (6)$$

$$\sigma(T) = \chi_1 \exp\left(\chi_2 \left(\frac{1}{T_0} - \frac{1}{T}\right)\right) \quad (7)$$

$$p_{step}(T) = p_{step,0} \exp\left(\frac{-H_{Step}}{R} \left(\frac{1}{T_0} - \frac{1}{T}\right)\right) \quad (8)$$

, wherein the water uptake at a certain pressure and temperature  $X(p,T)$  is calculated from two Langmuir-terms ( $X_L$  and  $X_U$ ), representing the adsorption before and after the step in the uptake.  $w(p,T)$  is a weighting function that depends on the pressure  $p$ , the temperature  $T$  and the pressure  $p_{step}$  at which the uptake step occurs. Further symbols  $X_\infty$ ,  $b_\alpha$ ,  $E_\alpha$  and  $\chi_{1,2}$  represent fit parameters.



Figure S17 gives a graphical illustration of thermodynamic evaluation of MIL-53(Al)-TDC (cf. Fig. 1).

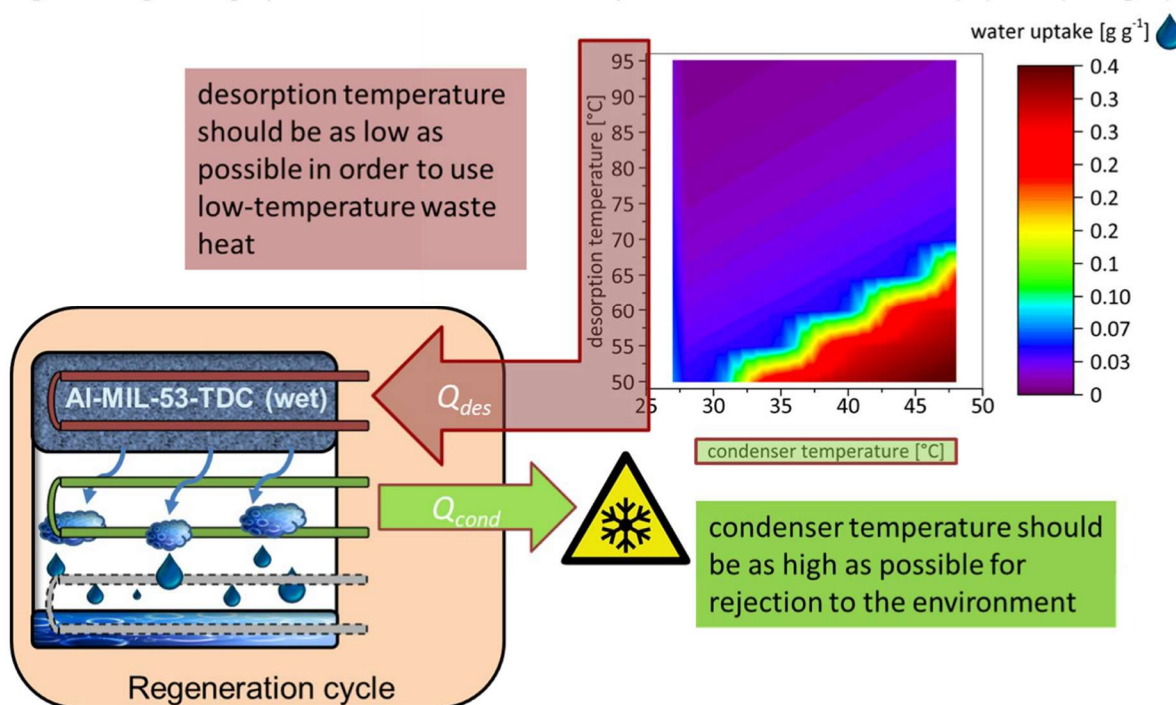


**Figure S17** Illustration of the thermodynamic evaluation of MIL-53(Al)-TDC, which yields preferably low desorption temperatures at comparably good high condenser temperatures and reasonable water uptake capacities of  $\sim 0.3 \text{ g g}^{-1}$ .

#### S14. References

- 1 C. W. L. Tschense, N. Reimer, C.-W. Hsu, H. Reinsch, R. Siegel, W.-J. Chen, C.-H. Lin, A. Cadiau, C. Serre, J. Senker and N. Stock, *Z. Anorg. All. Chem.*, 2017, **21**, 1600-1608.
- 2 M. Thommes, K. Kaneko, A. V. Neimark, J. P. Olivier, F. Rodríguez-Reinoso, J. Rouquerol and K. S. Sing, *Pure Appl. Chem.*, 2015, **87**, 1051-1069.
- 3 D. A. Gómez-Gualdrón, P. Z. Moghadam, J. T. Hupp, O. K. Farha and R. Q. Snurr, *J. Am. Chem. Soc.*, 2016, **138**, 215-224.
- 4 T. C. Wang, W. Bury, D. A. Gómez-Gualdrón, N. A. Vermeulen, J. E. Mondloch, P. Deria, K. Zhang, P. Z. Moghadam, A. A. Sarjeant, R. Q. Snurr, J. F. Stoddart, J. T. Hupp and O. K. Farha, *J. Am. Chem. Soc.*, 2015, **137**, 3585-3591.
- 5 K. S. Walton and R. Q. Snurr, *J. Am. Chem. Soc.*, 2007, **129**, 8552-8556.
- 6 D. M. Ruthven, *Principles of adsorption and adsorption processes*, Wiley, New York, 1984.
- 7 M. Hefti, L. Joss, Z. Bjelobrk and M. Mazzotti, *Faraday Discuss.*, 2016, **192**, 153-179.
- 8 S.-J. Ernst, M. Baumgartner, D. Fröhlich, H.-J. Bart and S. K. Henninger, *Chem-Ing-Tech.*, 2017, **89**, 1650-1660.



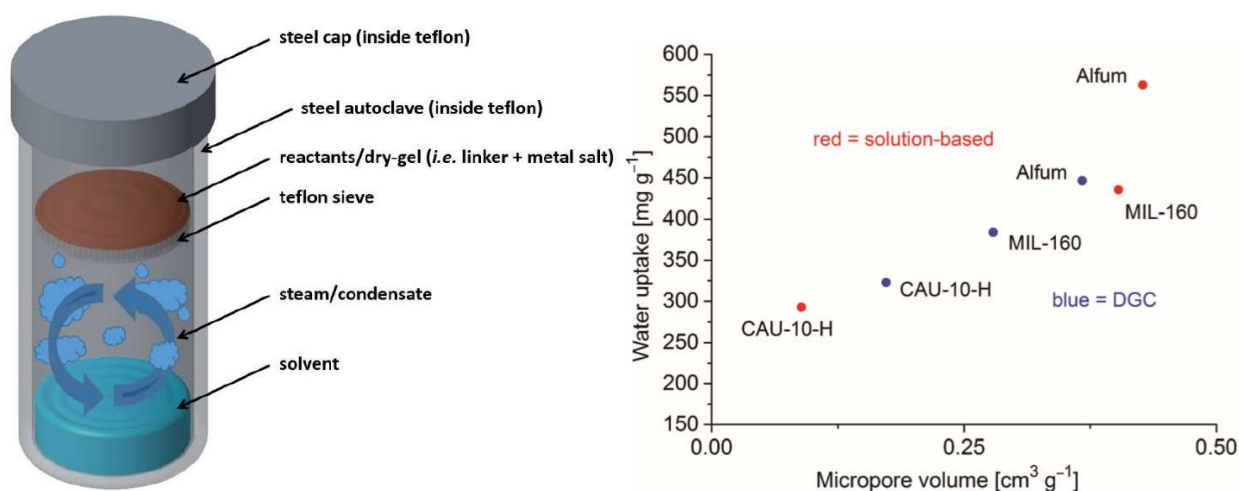
### 3.3. Robust Synthesis Routes and Porosity of Al-based Metal-Organic Frameworks Al-fumarate, CAU-10-H and MIL 160

N. Tannert, C. Jansen, S. Nießing and C. Janiak

*Dalton Trans.*, 2019, **48**, 2967-2976

DOI: 10.1039/c8dt04688c

Impact factor 2019: 4.174



Author's contribution of work:

- Development of DGC reactors and methods (with C. Jansen).
- All analytical characterizations except for SEM images (done by S. Nießing). PXRD, nitrogen sorption and water vapor sorption experiments were done with C. Jansen.
- Writing of the manuscript and drawing of all figures, graphs and tables except for Table 1 and Figure 6 (done by C. Jansen).
- Editing of the manuscript regarding the reviewers' comments with C. Jansen and C. Janiak.

Reproduced by permission of The Royal Society of Chemistry.

The following publication was carried out since aluminum-based metal–organic frameworks have developed into one of the most promising MOFs for potential applications. This fact is owed to their high hydrothermal stability and comparatively easy syntheses, the availability of abundant, inexpensive and non-poisonous metal and due to several other advantages. Three prominent representatives of hydrothermally stable Al-MOFs with a good water loading and an inflection point of (*i.e.* where the water vapor isotherm shows a steep uptake) that is in a feasible pressure region are Al<sub>fum</sub>, CAU-10-H and MIL-160. Consequently, the three MOFs were synthesized in a standard aqueous route and for comparison in a dry-gel conversion (DGC) synthetic setup.

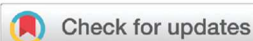
DGC was introduced to the landscape of synthesis routes for Al-MOFs in the literature contribution presented in chapter 3.1. for the first time. Hence, the following publication can be regarded as a consistent continuation and systematic investigation of synthetic parameters of structurally related Al-MOFs. All DGC container parts were self-built, each synthesis protocol was developed *via* variegations such as (non-)wetting of the precursor mixture, conversion time and temperature. The optimized DGC syntheses yielded Al-MOFs with satisfying crystallinities and microporosities in the range of solution-based materials, and notably, BET surface areas that reached or even outperformed solution-based products.

Additionally, a tabular overview of all syntheses with respect to porosities and yields (including continuous, extrusion-based and microwave syntheses and in comparison to employed Al-source and synthetic conditions like temperature and conversion times) could be presented for the three MOFs. Obtained samples of Al<sub>fum</sub> were additionally compared to commercially available Basolite® A520. It was found that DGCs of Al-MOFs reproducibly led to products with higher total pore volumes due to the inherent aggregate formation under DGC synthesis conditions. The latter promotes water-filled voids within the gel and agglomeration that result in large interparticle volumes after activation, that is, removal of solvent.

DGC syntheses can already be regarded as sustainable MOF synthesis, as they afforded less energy input, conversion time, decreased solvent amounts. Nevertheless, the possibility of solvent-reuse was evaluated for all three MOFs, envisaged to increase the sustainability of the method even more drastically. Thereby, it could be shown that solvent re-use is generally possible for all three MOFs, ultimately leading to ecologically beneficial synthesis protocols.

In conclusion, DGC syntheses were proven to be an ecologically and economically valuable alternative to common solution-based production. Not only both decreased energy input and conversion times are attributed to optimized syntheses in this realm. Especially the possibility of recovering the widely uncontaminated reaction solvent and re-utilize it in a subsequent synthesis run can be regarded as a step towards sustainable syntheses of potentially industrially relevant Al-MOFs.

## PAPER



Cite this: *Dalton Trans.*, 2019, **48**, 2967

## Robust synthesis routes and porosity of the Al-based metal–organic frameworks Al-fumarate, CAU-10-H and MIL-160†

Niels Tannert,  ‡ Christian Jansen,  ‡ Sandra Nießing and Christoph Janiak  \*

Aluminum-based metal–organic frameworks, Al-MOFs, have developed into one of the most promising MOFs for potential applications because of, *inter alia*, their hydrothermal stability and comparatively easy synthesis, and the availability of abundant, inexpensive and non-poisonous metal. Here, we evaluate the synthesis and porosity properties of the three MOFs aluminum fumarate (Alfum), CAU-10-H and MIL-160 involving the commercially readily available ligands fumaric, isophthalic and furandicarboxylic acid, respectively. The three Al-MOFs exhibit proven hydrothermal stability and water uptake to make them eligible for heat transformation applications. At the same time, it is important for applications that the synthesis and porous properties of these MOFs are robust, that is readily reproducible within certain limits. The typical solution synthesis of these MOFs was carried out with slight variations and compared with the literature to check if indeed the reported porosity data can readily be reproduced. Furthermore, dry-gel conversion (DGC) was implemented here for the synthesis of these MOFs and yielded products with higher total pore volumes due to the inherent aggregate formation under dry-gel synthesis conditions. The evaluation and our added syntheses ascertain that these Al-MOFs can be reproducibly synthesized with robust porosity properties, which are independent of the synthesis method, underscoring the potential of these MOFs for applications.

Received 27th November 2018,

Accepted 28th January 2019

DOI: 10.1039/c8dt04688c

rsc.li/dalton

## Introduction

Metal–organic frameworks (MOFs) are crystalline coordination networks, built up by metal nodes<sup>1</sup> and bridging organic ligands (“linkers”)<sup>2</sup> that are receiving steady attention as porous materials, owing to their high specific surface areas<sup>3</sup> and chemical variability to modulate their properties.<sup>4</sup> MOFs appear to be interesting in a wide range of potential applications, such as catalysis,<sup>5,6</sup> sensing,<sup>7</sup> gas separation<sup>8,9</sup> and storage,<sup>10</sup> drug delivery<sup>11</sup> and heat transformation processes.<sup>12,13</sup>

The diversity of synthesis methods for MOFs<sup>14</sup> has steadily increased within the last few years.<sup>15–17</sup> Besides the first solvothermal methods,<sup>18</sup> there are now syntheses under ambient pressure and even ambient temperature.<sup>19</sup> There are electro-<sup>20</sup> and sonochemical,<sup>21</sup> microwave,<sup>22</sup> flow reactor,<sup>18,23</sup> mechanochemical,<sup>24</sup> dry-gel conversion (DGC) syntheses<sup>25</sup> and combinations thereof.<sup>26</sup>

At the same time, it is now becoming clear that the synthesis method of a MOF may lead to material variations, which in turn can have stark effects on the MOF properties, such as porosity and gas uptake.<sup>27–29</sup>

Aluminum-based MOFs like MIL-53,<sup>30</sup> Al-fumarate (Alfum, Basolite A520),<sup>31,32</sup> CAU-10-H,<sup>33</sup> and MIL-160<sup>34</sup> can be considered among the most promising MOFs with regard to applications. Al-MOFs typically display (helical) chains with either *trans*- (MIL-53 and Alfum) or *cis*- (CAU-10-H and MIL-160) corner-sharing AlO<sub>6</sub> octahedra, in which the shared corners are OH-anions or oxygen atoms from the carboxylate groups of the organic linker molecules (Fig. 1, see the ESI† for further structure images and details).

Al-MOFs display microporous, narrow pore size distributions originating from parallel one-dimensional square-to-rhombus-shaped channels. One advantage of Al-MOFs is their high chemical and hydrothermal stability,<sup>35–38</sup> which makes them prone to realistic applications where water content or humidity cannot be avoided. Alfum and CAU-10-H have demonstrated stability over 4500 and 10 000 water adsorption and desorption cycles, respectively.<sup>36,38</sup> Both exhibit the desired steep s-shaped water sorption isotherm with uptake in a relatively low partial pressure range.<sup>36,38</sup> Besides, aluminum is considered non-toxic and is one of the most abundant (8.3% by weight in the Earth’s crust) and inexpensive metals.

Institut für Anorganische Chemie und Strukturchemie, Heinrich-Heine-Universität Düsseldorf, 40204 Düsseldorf, Germany. E-mail: janiak@uni-duesseldorf.de

† Electronic supplementary information (ESI) available: The background of the presented MOFs, details of materials and methods, synthesis protocols and optimizations, work-up procedures, additional PXRDs, nitrogen and water sorption analyses, SEMs, and TGAs. See DOI: 10.1039/c8dt04688c

‡ These authors contributed equally.



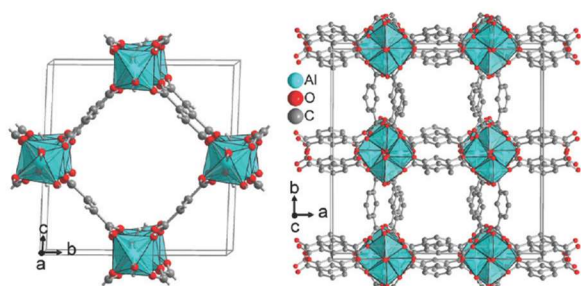


Fig. 1 Unit-cell content of Alfum (left) and CAU-10-H (right, corresponding to MIL-160) with the Al atoms in polyhedral presentation. See Fig. S2–S4 in the ESI† for further information.

Al-MOFs have received attention in hierarchical porosity,<sup>39</sup> gas storage and gas separation,<sup>40</sup> adsorption of organics,<sup>41</sup> catalysis,<sup>42</sup> mechanical energy storage,<sup>43</sup> water and air purification/remediation,<sup>44</sup> water harvesting,<sup>45</sup> desalination,<sup>46</sup> sensing,<sup>47</sup> proton conductivity,<sup>48</sup> mixed-matrix membranes (MMMs)<sup>49</sup> and in heat transformation applications.<sup>36,38,50–55</sup> In the last few years, Alfum and CAU-10-H have therefore moved from basic research materials to adsorbents in pre-industrial full-scale devices.<sup>50,54,55</sup>

In view of the importance of Al-MOFs, it seems crucial that the material properties are robust, within certain limits to variations in syntheses. Here we critically assess the different synthesis methods together with the porosity properties of Alfum, CAU-10-H and MIL-160 for their robustness. We carried out the typical solution synthesis of these MOFs with a slight variation compared to the literature to check if the reported data can be readily reproduced.

We also extended the syntheses towards more novel dry-gel conversion (DGC) in order to try minimizing the often high solvent consumption in MOF syntheses following our earlier work on this technique<sup>26,56</sup> towards more sustainable MOF synthesis procedures.<sup>57</sup> DGC is attributed to the reduced amounts of solvent used and waste due to the physical separation of the solvent and reactant mixture.<sup>26,58</sup> This separation results in the advantage of DGC that only enough solvent for the wetting of the reactants is needed and that after the reaction, the solvent can be recovered largely uncontaminated and could be used for further reaction runs. Hence, DGCs result in drastically reduced amounts of contaminated solvent which need to be disposed of.<sup>26,59</sup>

To the best of our knowledge, this is the first wider testing of DGC in Al-MOF synthesis, following our recent DGC synthesis report of Alfum (see Fig. 1 in the ESI† for details on the DGC apparatus).<sup>26</sup>

## Experimental

### Materials and instrumentation

All chemicals were used as received from the suppliers (see section S1 in the ESI†).

Powder X-ray diffraction (PXRD) was performed at ambient temperature on a D2 phaser (Bruker, Billerica, US) using Cu-K $\alpha$

radiation ( $\lambda = 1.54182 \text{ \AA}$ ) between  $5^\circ < 2\theta < 50^\circ$  at a scanning rate of  $0.0125^\circ \text{ s}^{-1}$  (300 W, 30 kV, 10 mA). Analyses of the diffraction patterns were carried out with Match 3.11 software. All PXRD patterns are obtained in section S6 in the ESI†.

Thermogravimetric analysis (TGA) was performed on a Netzsch TG209 F3 Tarsus (Netzsch, Selb, Germany) device under a synthetic air atmosphere, ramping with  $5 \text{ K min}^{-1}$  from  $25^\circ \text{C}$  to  $600^\circ \text{C}$ . TGA curves are given in section S7 in the ESI†.

SEM images were acquired on a JEOL JSM-6510 advanced electron microscope (Jeol, Akishima, Japan) with a LaB<sub>6</sub> cathode at 5–20 keV. The microscope was equipped with an Xflash 410 (Bruker, Billerica, US) silicon drift detector. SEM images are obtained in section S8 in the ESI†.

The surface area (Brunauer–Emmett–Teller,<sup>60</sup> BET) was determined by nitrogen (purity 99.999%, 5.0) sorption experiments at  $T = 77 \text{ K}$ , using liquid nitrogen and ca. 20–50 mg of the sample and performing on a Quantachrome NOVA-4000e (Quantachrome, Odelzhausen, Germany) instrument within the partial pressure range of  $pp_0^{-1} = 10^{-3}$ –1 bar. Each sample was degassed under vacuum ( $<10^{-2}$  mbar) at  $150^\circ \text{C}$  for ca. 3 h prior to measurement. All surface areas (BET) were calculated from five adsorption points by applying Roquerol plots ( $r > 0.998$ ). For the pressure ranges of five-point-BET calculations of each MOF, see section S9 in the ESI†. Total pore volumes were calculated from the N<sub>2</sub> sorption isotherm at  $pp_0^{-1} = 0.95$ . NLDFT calculations for pore size distributions were done with NovaWin 11.03 software using the ‘N<sub>2</sub> at 77 K on carbon, slit pore, NLDFT equilibrium’ model. All N<sub>2</sub> sorption isotherms are shown in section S9 in the ESI†.

Water sorption experiments were carried out on a Quantachrome VStar4 (Quantachrome, Odelzhausen, Germany) instrument within the partial pressure range of  $pp_0^{-1} = 10^{-3}$ –1 bar. Each sample was degassed under vacuum ( $<10^{-3}$  mbar) at  $150^\circ \text{C}$  for ca. 3 h prior to measurement, using a FloVac (Quantachrome, Odelzhausen, Germany) degasser. All water sorption isotherms are depicted in section S10 in the ESI†.

### Solution syntheses

In brief, the solution synthesis of Alfum was carried out as described in the patented route. The solution of fumaric acid and NaOH was added dropwise to the aluminum sulfate solution at  $60^\circ \text{C}$  (further details in section S3, ESI†).<sup>31</sup>

The solution synthesis of CAU-10-H was carried out in accordance with a report by Reinsch *et al.*<sup>33</sup> Aluminum sulfate and isophthalic acid were reacted in an autoclave in a water/dimethylformamide (DMF) mixture (further details in section S3, ESI†).

The solution synthesis of MIL-160 was carried out following a modified protocol of Cadiau *et al.*,<sup>34</sup> who used 1 eq. of NaOH, whereas we used 2 eq. of NaOH for full deprotonation of 1 eq. of the dicarboxylate linker. To the deprotonated acid solution, dissolved aluminum chloride was added and then the mixture was refluxed (further details in section S3, ESI†).

### Dry-gel conversion (DGC)

In brief, DGC syntheses were performed in a Teflon reactor using a temperature programmable oven (see Fig. S1† for



images of the reactor and section S4 for details of the experimental setup).

In a typical synthetic procedure, we rapidly ground aluminum sulfate octadecahydrate ( $\text{Al}_2(\text{SO}_4)_3 \cdot 18\text{H}_2\text{O}$ ) or aluminum chloride hexahydrate ( $\text{AlCl}_3 \cdot 6\text{H}_2\text{O}$ ) (1 eq.), with fumaric acid (2 eq.), isophthalic acid (1 eq.) or 2,5-furandicarboxylic acid (1 eq.) and sodium hydroxide ( $\text{NaOH}$ ) (4, 0 or 2 eq.) in a mortar and placed the mixture on a DGC sieve with water (2 mL) or water/DMF (4:1, 2 mL) at the bottom of a Teflon reactor. DGCs were carried out at varying temperatures and conversion times. The white products were washed three times with water (10 mL each), recovered by centrifugation each time and finally dried under vacuum (80 °C, 24 h).

From both synthesis routes, the product crystallinity together with phase identification was verified by PXRD (section S6, ESI†), surface areas with pore volumes (BET) were determined by  $\text{N}_2$  sorption at 77 K (section S9, ESI†) and water sorption isotherms were measured at 20 °C (section S10, ESI†).

## Results and discussion

Table 1 summarizes the synthesis conditions, porosity properties and yields of Al<sub>2</sub>MOF, CAU-10-H and MIL-160 given in the literature, supplemented by our modified solution and dry-gel conversion synthesis.

There are synthesis routes in solution using beakers, Pyrex tubes, round bottom flasks, Teflon-lined autoclaves, or even a flow reactor as stated in the literature protocols. In a singular case, an extruder was used for Al<sub>2</sub>MOF albeit no pore volume of the product was reported.<sup>74</sup>

The BET surface area, (micro)pore volume and yield were chosen to assess the product quality and synthesis conditions. We note that the pore volume was not always given and the yield was missing frequently. Thus, a consistent comparison of pore volumes and yields is difficult. For the pore volume it was noted whenever possible if the value refers to the micropore volume calculated from the  $\text{N}_2$  adsorption isotherm at  $pp_0^{-1} = 0.1$  for pores with  $d \leq 2$  nm (20 Å) or the total pore volume at  $pp_0^{-1} = 0.95$  for pores  $\leq 20$  nm.

There are even synthesis reports stating neither surface area nor pore volume nor yield.<sup>50,61–65</sup> These reports are not included in Table 1.

For Al<sub>2</sub>MOF and CAU-10-H aluminum sulfate,  $\text{Al}_2(\text{SO}_4)_3$  is mostly used as the Al source, while for MIL-160 aluminum trichloride,  $\text{AlCl}_3$  is chosen. We see no special reasoning for this choice of aluminum starting material as  $\text{AlCl}_3$  or  $\text{NaAlO}_2$  for Al<sub>2</sub>MOF and basic aluminum acetate  $\text{Al}(\text{OH})(\text{CH}_3\text{COO})_2$  for MIL-160 gave similar results. For Al<sub>2</sub>MOF with  $\text{AlCl}_3$ , the solvent DMF apparently had to be used. It is evident that Al<sub>2</sub>MOF synthesis with  $\text{AlCl}_3$  did not yield very high surface areas.

For Al<sub>2</sub>MOF and MIL-160, deprotonation of the dicarboxylic acid is achieved with added  $\text{NaOH}$ . The reaction of  $\text{Al}_2(\text{SO}_4)_3$  with isophthalic acid to CAU-10-H works without the addition of a base, but with the use of DMF.

The syntheses are mostly carried out in aqueous solution at temperatures ranging from 60 °C to reflux (100 °C) and with DMF up to 135 °C. Reaction times can be as short as 1 min for Al<sub>2</sub>MOF in a continuous reactor system,<sup>66</sup> but also last about 100 or more hours. A special or beneficial effect of long reaction times is not evident.

For Al<sub>2</sub>MOF there is a particular wide range of surface areas reported between 723 and 1333  $\text{m}^2 \text{g}^{-1}$ . For CAU-10-H and MIL-160, the range is more narrow with 525 to 656  $\text{m}^2 \text{g}^{-1}$  and 1070 to 1150  $\text{m}^2 \text{g}^{-1}$ , respectively.

In general, the degree of crystallinity of the Al-MOFs as observed by powder X-ray diffractometry is comparable to that in the literature. The same accounts for the SEM images of Al-MOFs, which typically show intergrown agglomerates of varying sizes independent of the synthesis method. Al-MOFs do not tend to grow larger crystallites, so that no single-crystal X-ray structures have been obtained until today. The reported structures of Al<sub>2</sub>MOF, CAU-10-H and MIL-160 are based on Rietveld refinements.<sup>32–34</sup>

### Al<sub>2</sub>MOF

As shown in Table 1, the synthesis literature on aluminum fumarate is extensive. Furthermore, the MOF is commercially available, which underlines the importance of aluminum fumarate.<sup>67</sup> Different aluminum salts and both water (with  $\text{NaOH}$ ) and DMF as the solvent were used. Temperature and reaction time were varied widely, from 60 to 150 °C and from one minute to four days. A difference from other MOFs is the large-scale synthesis of aluminum fumarate as was patented by BASF. This is related to the simple method of preparation, which makes it possible to also produce the MOF in a flow reactor or an extruder.<sup>66,74</sup>

The patent of commercial Basolite A520 stated only the Langmuir surface area.<sup>31</sup> We drew four samples from the same commercial batch to obtain the BET surface area of  $1033 \pm 7 \text{ m}^2 \text{g}^{-1}$ , which is in very good accordance with that in other reports.<sup>31,32</sup> We could readily obtain Al<sub>2</sub>MOF with a very similar yield, surface area and pore volume when we repeated the synthesis protocol from the BASF patent, except that stirring was continued for a further 2 hours after combining the solutions (details in section S3, ESI†).

Within the DGC synthesis (see section S4.1, ESI† for detailed information) we found 100 °C and 6 h to be the optimal conditions. Wetting of the precursor mixture was not necessary because of the good solubility of fumaric acid with  $\text{NaOH}$ . With DGC, the surface areas and pore volumes were consistent with the other synthesis literature. The yields of the DGC are lower, because of the loss of the starting material or product through the sieve to the bottom of the autoclave.

When comparing the Al<sub>2</sub>MOF DGC synthesis with the continuous solution synthesis route, it should be noted that such continuous solution syntheses involve large amounts of solvents. The patented synthesis procedure for continuous production of Al<sub>2</sub>MOF demonstrates different methods with varying space-time-yields (STYs) from 2032 to 5339  $\text{kg m}^{-3} \text{day}^{-1}$ .<sup>31</sup>

Table 1 Synthesis, porosity parameters and yields of Alfum, CAU-10-H and MIL-160

Al-MOF	Reactants	Conditions	BET surface area <sup>a</sup> [m <sup>2</sup> g <sup>-1</sup> ]	Pore volume [cm <sup>3</sup> g <sup>-1</sup> ]	Yield [%] for STY [kg m <sup>-3</sup> day <sup>-1</sup> ]	Ref.
Alfum	Al <sub>2</sub> (SO <sub>4</sub> ) <sub>3</sub> , fumaric acid, NaOH	65 °C, 1 min residence time (continuous)	1054	n.a.	STY: 97159	18
	Al <sub>2</sub> (SO <sub>4</sub> ) <sub>3</sub> , fumaric acid, NaOH	65 °C, 1 min residence time (continuous)	1015–1084	n.a.	74–85	66
	Al <sub>2</sub> (SO <sub>4</sub> ) <sub>3</sub> , fumaric acid, NaOH	60 °C, 3 h (solution)	1156	n.a.	74	44b
	Purchased from MOF Technologies <sup>67</sup>	Purchased from MOF Technologies <sup>67</sup>	1021	0.44	Purchased	46
	AlCl <sub>3</sub> , fumaric acid, DMF	130 °C, 4 d (solution)	894	n.a.	Purchased	68
	AlCl <sub>3</sub> , fumaric acid, DMF	130 °C, 4 d (solution)	1021	0.48	90	36
	AlCl <sub>3</sub> , fumaric acid, DMF	130 °C, 96 h (solution)	792	0.93 (total)	n.a.	69
	AlCl <sub>3</sub> , fumaric acid, DMF	130 °C, 96 h (solution)	792	0.43	n.a.	70
	AlCl <sub>3</sub> , fumaric acid, DMF	130 °C, 96 h (solution)	792	0.48	n.a.	71
	Al <sub>2</sub> (SO <sub>4</sub> ) <sub>3</sub> , fumaric acid, NaOH	60 °C, 30 min (solution)	1025	0.47	96	32
	Al <sub>2</sub> (SO <sub>4</sub> ) <sub>3</sub> , fumaric acid, NaOH	90 °C, 60 min (solution)	821	0.44	n.a.	71
	NaAlO <sub>2</sub> , fumaric acid	90 °C, 30 min (solution)	925	0.65 (total)	74	72
	Al <sub>2</sub> (SO <sub>4</sub> ) <sub>3</sub> , fumaric acid, NaOH	150 °C, (twin screw extrusion)	980	1.42 (total)	n.a.	73
	Al <sub>2</sub> (SO <sub>4</sub> ) <sub>3</sub> , fumaric acid, NaOH	150 °C, (twin screw extrusion)	1010	n.a.	STY: 27000	74
	Al <sub>2</sub> (SO <sub>4</sub> ) <sub>3</sub> , fumaric acid, NaOH (1 : 2 : 4)	100 °C, 1 h, 800 W (MW-DGC), 6 h (DGC)	983–1189	0.43–0.61 (micropore)	58–71	26
	Al <sub>2</sub> (SO <sub>4</sub> ) <sub>3</sub> , fumaric acid, NaOH (1 : 2 : 4)	RT, 60 °C, 0.17, 0.27, 0.5 h (solution)	723–1333 <sup>d,L</sup>	0.47 (micropore) <sup>32</sup>	76–98	31
	Basolite A520				STY: 2032–5339 <sup>d</sup>	
			880 (Argon)	n.a.	n.a.	75
			965–971	0.85–0.91/0.38 (micropore)	Purchased	76
			999–1040 <sup>e</sup>	0.51–0.63 (micropore) <sup>b,e</sup>	n.a.	This work
	Al <sub>2</sub> (SO <sub>4</sub> ) <sub>3</sub> , fumaric acid, NaOH (1 : 2 : 4)	60 °C, 150 min (solution)	780–1254	0.36–0.72 (micropore) <sup>b</sup>	73–85	This work
	Al <sub>2</sub> (SO <sub>4</sub> ) <sub>3</sub> , fumaric acid, NaOH (1 : 2 : 4)	80, 100, 120 °C, 6, 12, 24 h (DGC)	983–1189 <sup>c</sup>	0.51–0.61 <sup>b</sup>	23–53	This work
CAU-10-H	Al <sub>2</sub> (SO <sub>4</sub> ) <sub>3</sub> , isophthalic acid (1 : 1)	Reflux, 117 h (solution)	564	0.26	91	38
	NaAlO <sub>2</sub> , Al <sub>2</sub> (SO <sub>4</sub> ) <sub>3</sub> , sodium isophthalate (1 : 1, 5 : 4)	Reflux, 10 h (solution)	n.a.	n.a.	93	54
	Al <sub>2</sub> (SO <sub>4</sub> ) <sub>3</sub> , isophthalic acid (1 : 1), DMF	135 °C, 12 h (solution in autoclave)	635	0.25 (micropore)	60–70	48 and 33
			525	0.27	n.a.	37
			656	0.25 (micropore)	n.a.	42a
			640	0.25 (micropore)	n.a.	77
			615	n.a.	89	78
	Al <sub>2</sub> (SO <sub>4</sub> ) <sub>3</sub> , isophthalic acid (1 : 1), DMF	135 °C, 12 h (solution in autoclave)	415–484	0.25–0.27 <sup>b</sup>	35–42	This work
	Al <sub>2</sub> (SO <sub>4</sub> ) <sub>3</sub> , isophthalic acid (1 : 1), DMF	115, 135, 155 °C, 6, 12, 24 h (DGC)	285–560 <sup>c</sup>	0.24–0.47 <sup>b</sup>	22–44	This work
MIL-160	Al(OH)(CH <sub>3</sub> COO) <sub>2</sub> , 2,5-furandicarboxylic acid (1 : 1)	Reflux, 24 h (solution)	1150	0.48	93	79
	AlCl <sub>3</sub> , 2,5-furandicarboxylic acid, NaOH (1 : 1 : 1)	Reflux, 24 h (solution)	1070	0.40 (micropore)	n.a.	34
	Al(OH)(CH <sub>3</sub> COO) <sub>2</sub> , 2,5-furandicarboxylic acid (1 : 1)	100 °C, 96 h (solution in Pyrex tube)	1098	0.41 (micropore)	n.a.	83
	AlCl <sub>3</sub> , 2,5-furandicarboxylic acid, NaOH (1 : 1 : 1)	Reflux, 24 h (solution)	1148	0.46 (total)	n.a.	80
	AlCl <sub>3</sub> , 2,5-furandicarboxylic acid, NaOH (1 : 1 : 2)	Reflux, 24 h (solution)	1178	0.42 <sup>b</sup>	55	This work
	AlCl <sub>3</sub> , 2,5-furandicarboxylic acid, NaOH (1 : 1 : 1 or 2)	80, 100, 120 °C, 12, 24, 48 h (DGC)	968–1180 <sup>c</sup>	0.54–0.56 <sup>b</sup>	22–50	This work

<sup>a</sup> BET surface areas were obtained from five adsorption points in the individual MOF pressure range (section S9, ESI). <sup>b</sup> This work: Calculated using the NLDFT model for carbon (slit pore), with  $pp_0^{-1} = 0.95$  for total pore volume and  $pp_0^{-1} = 0.5$  for micropore volume. <sup>c</sup> This work; the range of at least three samples. <sup>d</sup> Stated in the patent. <sup>31</sup> <sup>e</sup> Range of five individual measurements from the same batch (this work, Table S9, ESI) and in good agreement with values in the literature.<sup>31,32</sup> <sup>L</sup> Langmuir surface area. All values are rounded.

The most effective STY of 3615 kg m<sup>-3</sup> day<sup>-1</sup> achieves 4.1 wt% of the product in the dispersion/solution, which in turn means 95.9 wt% of the mother liquor. Thus, 3615 kg Alfum

product per day from a 4.1 wt% dispersion would go along with 3615 × 100/4.1 = 88 170 kg (= 88.17 tons) mother liquor waste per day.



Fig. 2a depicts the exemplary PXRD patterns of Al<sub>3</sub>MOF samples obtained *via* our solution synthesis, by optimized DGC, from commercial Basolite A520 and the theoretical pattern.

Fig. 2b shows the N<sub>2</sub> sorption isotherms of different Al<sub>3</sub>MOF samples, underscoring the similar porosity properties of the samples from solution synthesis, DGC and commercial Basolite A520 (Table 1). The observed steep rise at high partial pressures ( $pp_0^{-1} > 0.9$ ) in the DGC product can be attributed to a larger inter-particle volume of aggregated crystallites, which result in the dry-gel formation. The latter promotes (meso-) to macroporous cavities,<sup>26</sup> as the residual water in the DGC

process forms such voids in the gel.<sup>81</sup> This property is a common feature within our presented DGC results, since it could be observed in any DGC isotherm of all three presented Al-MOFs and can therefore be declared as highly reproducible and a unique feature of DGC for Al-MOFs. Therefore, the total pore volume at  $pp_0^{-1} = 0.95$  will always be superior in DGC syntheses compared to solution-based approaches.

The SEM images of Al<sub>3</sub>MOF (Fig. S14, ESI†) show the typical intergrown agglomerates of varying sizes independent of the synthesis method.

Thermogravimetric analysis (TGA) of the Al<sub>3</sub>MOF samples (Fig. S11, ESI†) revealed mostly comparable thermal stability to over 400 °C among all samples, which is in agreement with the literature, where around 400 °C is typically given as thermal stability.<sup>32</sup>

Water uptake capacities correlate with the porosity of the sample, and it is worth noting that the DGC product has a higher uptake than commercial Basolite A520 (Fig. 1c).

### CAU-10-H

CAU-10-H syntheses are mainly carried out in autoclaves and under reflux. The most commonly followed synthesis route was first published by Reinsch *et al.*,<sup>33</sup> which used an autoclave at 135 °C for 12 h and provided surface areas of 525 to 656 m<sup>2</sup> g<sup>-1</sup>. For the reflux synthesis yield, over 90% can be reached albeit at very long reaction times of up to 117 h.

We repeated here the synthesis in solution from the work of Reinsch *et al.* using an autoclave at 135 °C for 12 h. The surface areas and yields from our syntheses are below the literature values. For the DGC synthesis (see section S4.2, ESI† for detailed information), 155 °C and 12 h were found to be the optimal conditions. Wetting of the precursor mixture with a small amount of DMF was necessary to ensure proper phase formation since the linker isophthalic acid possesses poor solubility in water.<sup>82</sup> The DGC surface areas and pore volumes were consistent with those mentioned in the literature. The yields of the DGC are lower due to the loss of the starting material or product when falling through the sieve.

The PXRDs show no crystallinity differences between the products from solution synthesis and moistened DGC (Fig. 3a).

The nitrogen sorption isotherm of the CAU-10-H samples obtained by DGC again indicates the more pronounced inter-particle volume (Fig. 3b). Nitrogen sorption further revealed comparable BET surface areas from both routes, however with higher values and a wider range within DGC (Table 1). TGA showed comparable stability (~380 °C) for both CAU-10-H samples (Fig. S12, ESI†) which agrees with the thermal stability values mentioned in the literature from TGA at around 400 °C.<sup>33</sup> The SEM images confirm the formation of seemingly macroporous agglomerates by DGC (Fig. S15, ESI†). The water uptake capacity correlates with the porosity of the individual sample with the expected S-shaped isotherms below  $pp_0^{-1} = 0.2$ .<sup>37,38</sup>

### MIL-160

MIL-160 is a new Al-MOF whose first published synthesis dated from 2015.<sup>34</sup> Only two different sources of aluminum

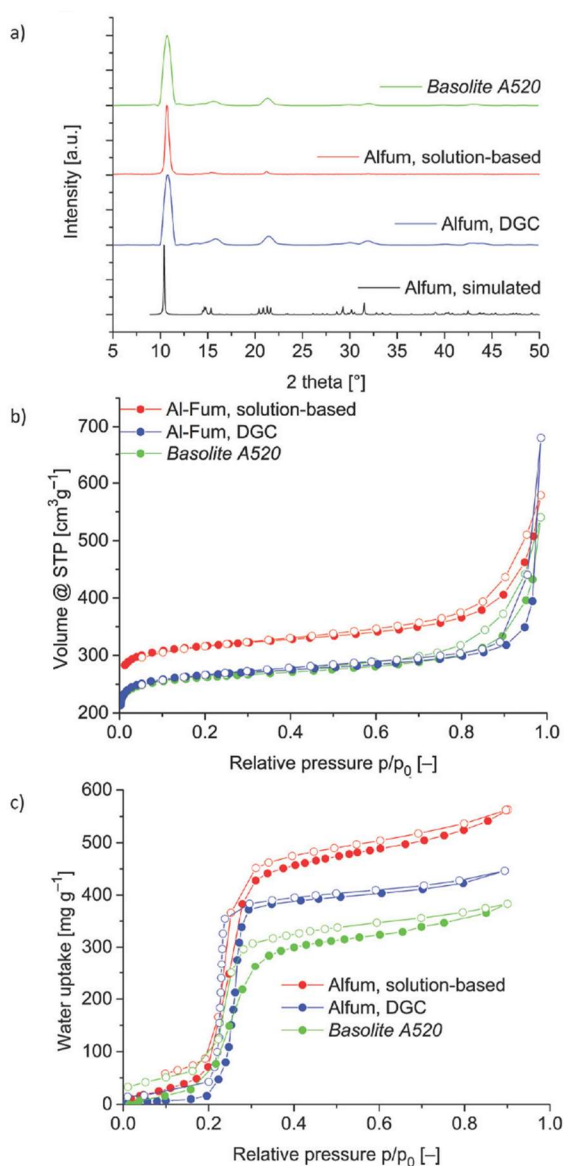


**Fig. 2** Comparison of Al<sub>3</sub>MOF from solution synthesis, DGC and commercial Basolite A520: (a) PXRDs. The simulated pattern was calculated using CSD-Refcode DOYBEA.<sup>32</sup> (b) Nitrogen sorption isotherms ( $T = 77$  K). (c) Water sorption isotherms ( $T = 20$  °C). Filled circles depict adsorption; unfilled circles indicate desorption.

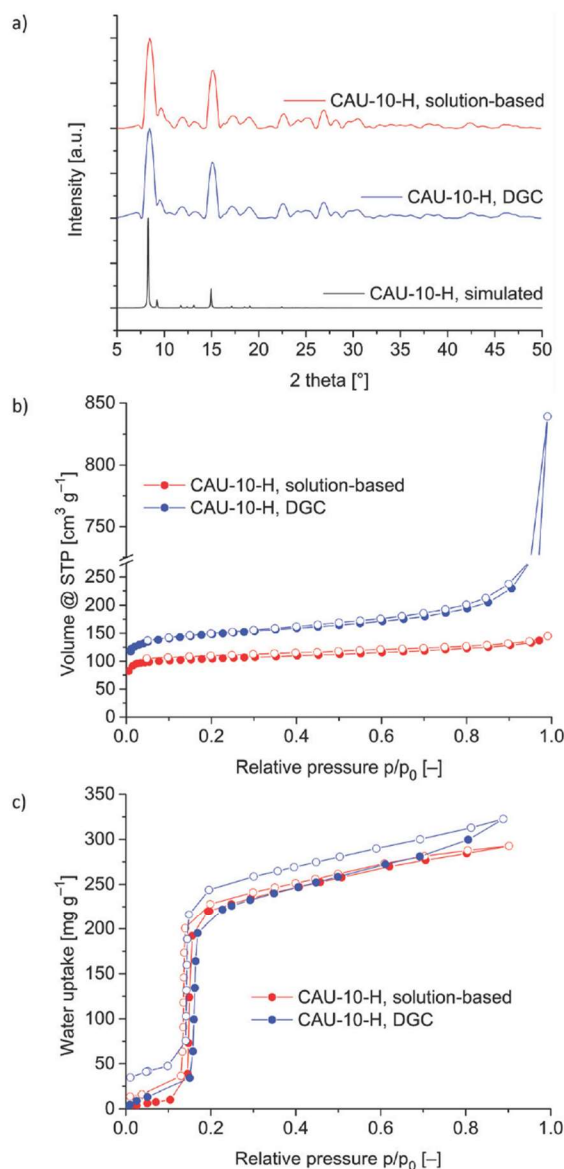


Fig. 3 Comparison of CAU-10-H from solution and DGC synthesis: (a) PXRDs. The simulated pattern was calculated using CSD-Refcode QQOBT.<sup>36</sup> (b) Nitrogen sorption isotherms ( $T = 77$  K). (c) Water sorption isotherms ( $T = 20$  °C). Filled circles depict adsorption; unfilled circles indicate desorption.

were used and the conditions of synthesis appear to have not differed much or even systematically investigated. Most publications use the reflux synthesis by Cadiau *et al.*<sup>34</sup> Only one publication reported the production of MIL-160 in a Pyrex tube at 100 °C for 96 h.<sup>83</sup>

In our work, the solution synthesis is also based on the work by Cadiau *et al.*, but we used twice the molar amount of NaOH to achieve the complete deprotonation of the acid. With this synthesis modification, we achieved the same results as Cadiau *et al.* The use of only 1 mol NaOH for 1 mol of furandicarboxylic acid gave considerably lower surface areas of 135–451 m<sup>2</sup> g<sup>-1</sup> (moistened).

DGC synthesis (see section S4.3, ESI† for details) gave optimum samples at 100 °C and 48 h reaction time. Wetting of the precursor mixture showed no particular improvement. The use of 2 mol NaOH for each mol of linker yielded a higher surface area.

From the typical PXRD patterns given in Fig. 4a, MIL-160 samples obtained from the solution synthesis gave a better match to the simulated pattern, while samples from DGC showed additional reflections.

Fig. 4b shows the N<sub>2</sub> sorption isotherms of MIL-160 samples obtained by DGC and a solution-based approach.

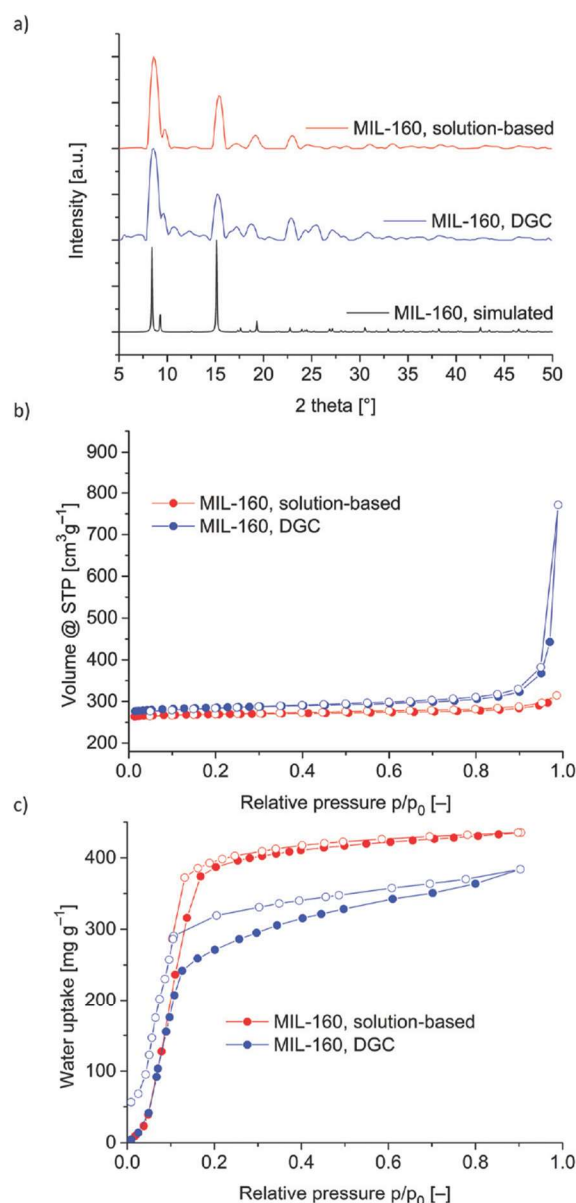


Fig. 4 Comparison of MIL-160 from solution and DGC synthesis: (a) PXRDs. Simulated pattern was calculated using CSD-Refcode PIBZOS.<sup>83</sup> (b) Nitrogen sorption isotherms ( $T = 77$  K). (c) Water sorption isotherms ( $T = 20$  °C). Filled circles depict adsorption; unfilled circles indicate desorption.



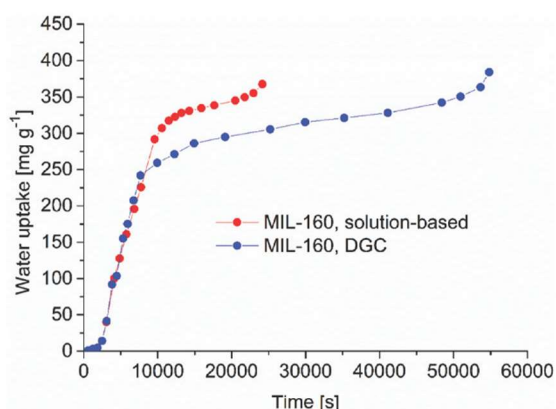


Fig. 5 Water uptake versus equilibration time for each data point for MIL-160 from solution and DGC synthesis.

Once again, the steep uptake at  $pp_0^{-1} > 0.9$  is evident for the DGC product and, consequently, total pore volumes of DGC syntheses are reproducibly higher than from the solution synthesis. Other than this, DGC surface areas and pore volumes were consistent with the literature. Water sorption isotherms are depicted in Fig. 4c.

The additional pore volume in MIL-160-DGC is due to mesopores. The  $V-t$ -plot method determined the micropore versus total pore volume to be 0.40/0.42 for MIL-160-solution and 0.28/0.54 for MIL-160-DGC. It can be assumed that the meso-microporosity should also affect the water sorption kinetics, such that a hierarchical macro-meso-microporosity may be expected to lead to fast adsorption into the micropores. We have exemplarily plotted the water uptake versus time for the two MIL-160 probes to check for a kinetic water adsorption effect in view of the increased total pore volume and higher mesopore content for MIL-160-DGC (Fig. 5). Yet, and maybe in contrast to expectation, the smaller micropore filling occurs at the same rate. The filling of the larger micropores requires more time but is still faster in the overall microporous

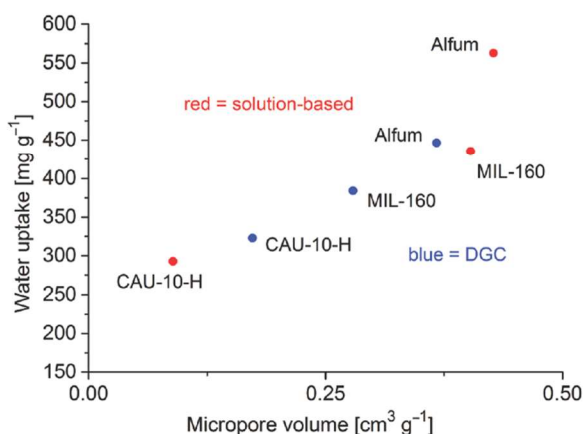


Fig. 6 Water uptake versus micropore volume (by  $V-t$ -plot method) for solution and DGC samples.

MIL-160-solution sample. The mesopore filling in MIL-160-DGC then becomes very time consuming. This may be rationalized by a non- or even inverse-hierarchical nature of the micro-mesopores. Internal mesopores, which are only accessible by micropores leading to them, will require extended equilibration times.

TGA revealed comparable stability for both samples ( $>300$  °C), with the DGC product decomposing at slightly lower temperatures (Fig. S13, ESI†). According to the literature, MIL-160 is temperature stable up to 400 °C.<sup>34</sup> SEM images (Fig. S16, ESI†) show the typical morphology with intergrown crystallites in samples of both synthesis routes.

## Conclusion

Al-MOFs present a most promising class of MOFs for diverse applications due to their ease of synthesis and hydrothermal stability. Their synthesis procedures and porosity properties appear to be rather robust, that is, BET surface areas were rather independent of the synthesis route and readily reproducible from standard literature synthesis protocols. The same can be seen for the pore volume and yield for CAU-10-H and MIL-160, which can be traced to essentially one primary synthesis procedure. For Alfum, the pore volume and yield (if given) varied widely due to the large differences in the synthesis conditions concerning starting materials, solvent, temperature, time and method.

Dry-gel conversion could be introduced as an alternative synthesis procedure for Al-MOFs, where as an ecological benefit, only low amounts of solvent are needed. The crystallinity and microporosity of all optimized DGC products were in the range of solution-based materials (Table 1), while the BET surface areas of DGC products reached or even outperformed those of solution-based products. We found that DGCs of Al-MOFs reproducibly led to products with higher total pore volumes due to the inherent aggregate formation in the dry-gel synthesis process. The latter promotes water-filled voids within the gel and agglomeration that results in large interparticle volumes after activation. Depending on the literature source, water uptake may be correlated with total pore volume (calculated at  $pp_0^{-1} = 0.95$ ).<sup>84</sup> When plotting the water uptake at  $pp_0^{-1} = 0.95$  versus the total pore volume at  $pp_0^{-1} = 0.95$  (Fig. S20, ESI†), it is evident that for MIL-160 the trend is reversed; that is, the solution-based MIL-160 product with a lower pore volume has a higher water uptake. However, from our experience the micropore volume (Table S10, ESI†) has a more decisive role in determining the water uptake. A plot of the water uptake versus micropore volume indeed presents a more convincing trend: for chemically identical MOFs a higher micropore volume is followed by a higher water uptake (Fig. 6).

In conclusion, DGC was proven to be a sustainable alternative for the robust syntheses of sorption-active Al-MOFs. In the future, attention should be paid to developing continuous (non-autoclave) processes for the Al-MOFs CAU-10-H and MIL-160, as exist already for Alfum.

## Conflicts of interest

There are no conflicts of interest to declare.

## Acknowledgements

The authors gratefully acknowledge the financial support from the Federal German Ministry of Education and Research (BMBF) for the project Optimat under grant no. 03SF0492C.

## References

- 1 J. Zhou, H. Li, H. Zhang, H. Li, W. Shi and P. Cheng, *Adv. Mater.*, 2015, **27**, 7072–7077.
- 2 F. A. Almeida Paz, J. Klinowski, S. M. F. Vilela, J. P. C. Tome, J. A. S. Cavaleiro and J. Rocha, *Chem. Soc. Rev.*, 2012, **41**, 1088–1110.
- 3 G. Maurin, C. Serre, A. Cooper and G. Férey, *Chem. Soc. Rev.*, 2017, **46**, 3104–3107.
- 4 R. Haldar and T. K. Maji, *CrystEngComm*, 2013, **15**, 9276–9295.
- 5 Y.-B. Huang, J. Liang, X.-S. Wang and R. Cao, *Chem. Soc. Rev.*, 2017, **46**, 126–157.
- 6 A. Herbst and C. Janiak, *CrystEngComm*, 2017, **19**, 4092–4117.
- 7 W. P. Lustig, S. Mukherjee, N. D. Rudd, A. V. Desai, J. Li and S. K. Ghosh, *Chem. Soc. Rev.*, 2017, **46**, 3242–3285.
- 8 J.-R. Li, R. J. Kuppler and H.-C. Zhou, *Chem. Soc. Rev.*, 2009, **38**, 1477–1504.
- 9 J. Dechnik, J. Gascon, C. J. Doonan, C. Janiak and C. J. Sumby, *Angew. Chem., Int. Ed.*, 2017, **56**, 9292–9310.
- 10 K. Adil, Y. Belmabkhout, R. S. Pillai, A. Cadiau, P. M. Bhatt, A. H. Assen, G. Maurin and M. Eddaoudi, *Chem. Soc. Rev.*, 2017, **46**, 3402–3430; C. Petit, *Curr. Opin. Chem. Eng.*, 2018, **20**, 132–142.
- 11 P. Horcajada, R. Gref, T. Baati, P. K. Allan, G. Maurin, P. Couvreur, G. Férey, R. E. Morris and C. Serre, *Chem. Rev.*, 2012, **112**, 1232–1268.
- 12 F. Jeremias, D. Fröhlich, C. Janiak and S. K. Henninger, *New J. Chem.*, 2014, **38**, 1846–1852.
- 13 M. F. de Lange, K. J. F. M. Verouden, T. J. H. Vlugt, J. Gascon and F. Kapteijn, *Chem. Rev.*, 2015, **115**, 12205–12250.
- 14 N. Stock and S. Biswas, *Chem. Rev.*, 2012, **112**, 933–969.
- 15 J. Ren, X. Dyosiba, N. M. Musyoka, H. W. Langmi, M. Mathe and S. Liao, *Coord. Chem. Rev.*, 2017, **352**, 187–219.
- 16 T. Ogawa, K. Iyoki, T. Fukushima and Y. Kajikawa, *Materials*, 2017, **10**, 1428–1448; S. Barman, H. Furukawa, O. Blacque, K. Venkatesan, O. M. Yaghi, G.-X. Jin and H. Berke, *Chem. Commun.*, 2011, **47**, 11882–11884.
- 17 H. Reinsch and N. Stock, *Dalton Trans.*, 2017, **46**, 8339–8349.
- 18 M. Rubio-Martinez, C. Avci-Camur, A. W. Thornton, I. Imaz, D. MasPOCH and M. R. Hill, *Chem. Soc. Rev.*, 2017, **46**, 3453–3480.
- 19 M. Sánchez-Sánchez, N. Getachew, K. Díaz, M. Díaz-García, Y. Chebude and I. Díaz, *Green Chem.*, 2015, **17**, 1500–1509; F. Jeremias, S. K. Henninger and C. Janiak, *Dalton Trans.*, 2016, **45**, 8637–8644.
- 20 R. Ameloot, L. Stappers, J. Fransaer, L. Alaerts, B. F. Sels and D. E. de Vos, *Chem. Mater.*, 2009, **21**, 2580–2582.
- 21 W.-J. Son, J. Kim, J. Kim and W.-S. Ahn, *Chem. Commun.*, 2008, **47**, 6336–6338; N. Abdollahi, M. Y. Masoomi, P. C. Junk and J. Wang, *Ultrason. Sonochem.*, 2018, **45**, 50–56; N. A. Khan and S. H. Jhung, *Coord. Chem. Rev.*, 2015, **285**, 11–23.
- 22 I. Thomas-Hillman, A. Laybourn, C. Dodds and S. W. Kingman, *J. Mater. Chem. A*, 2018, **6**, 11564–11581; M. Taddei, D. A. Steitz, J. A. van Bokhoven and M. Ranocchiari, *Chem. – Eur. J.*, 2016, **22**, 3245–3249.
- 23 P. A. Bayliss, I. A. Ibarra, E. Pérez, S. Yang, C. C. Tang, M. Poliakoff and M. Schröder, *Green Chem.*, 2014, **16**, 3796–3802.
- 24 K. Užarević, T. C. Wang, S.-Y. Moon, A. M. Fidelli, J. T. Hupp, O. K. Farha and T. Frišćić, *Chem. Commun.*, 2016, **52**, 2133–2136.
- 25 Q. Shi, Z. Chen, Z. Song, J. Li and J. Dong, *Angew. Chem., Int. Ed.*, 2011, **123**, 698–701; A. K. Das, R. S. Vemuri, I. Kutnyakov, B. P. McGrail and R. K. Motkuri, *Sci. Rep.*, 2016, **6**, 28050; J. Kim, Y.-R. Lee and W.-S. Ahn, *Chem. Commun.*, 2013, **49**, 7647–7649.
- 26 N. Tannert, S. Gökpınar, E. Hastürk, S. Nießing and C. Janiak, *Dalton Trans.*, 2018, **47**, 9850–9860.
- 27 M. Peplow, *Chem. World*, 2018, **13**; S. Goldie, *Chem. World*, 2018, **5**.
- 28 J. Park, J. D. Howe and D. S. Sholl, *Chem. Mater.*, 2017, **29**, 10487–10495.
- 29 T. Tian, Z. Zeng, D. Vulpe, M. E. Casco, G. Divitini, P. A. Midgley, J. Silvestre-Albero, J.-C. Tan, P. Z. Moghadam and D. Fairen-Jimenez, *Nat. Mater.*, 2018, **17**, 174–180.
- 30 F. Millange, C. Serre and G. Férey, *Chem. Commun.*, 2002, 822–823; T. Loiseau, C. Serre, C. Huguenard, G. Fink, F. Taulelle, M. Henry, T. Bataille and G. Férey, *Chem. – Eur. J.*, 2004, **10**, 1373–1382.
- 31 C. Kiener, U. Müller and M. Schubert, *Germany Pat*, WO2007/118841A2, BASF SE, 2007; C. Kiener, U. Müller and M. Schubert, *US Pat*, 12/297666, BASF SE, 2012; E. Leung, U. Müller, N. Trukhan, H. Mattenheimer and G. Cox, *US Pat*, 13/249943, BASF SE, 2012.
- 32 E. Alvarez, N. Guillou, C. Martineau, B. Bueken, B. Van de Voorde, C. Le Guillouzer, P. Fabry, F. Nouar, F. Taulelle, D. de Vos, J.-S. Chang, K. H. Cho, N. Ramsahye, T. Devic, M. Daturi, G. Maurin and C. Serre, *Angew. Chem., Int. Ed.*, 2015, **54**, 3664–3668.
- 33 H. Reinsch, M. A. van der Veen, B. Gil, B. Marszałek, T. Verbiest, D. de Vos and N. Stock, *Chem. Mater.*, 2013, **25**, 17–26.



- 34 A. Cadiau, J. S. Lee, D. Damasceno Borges, P. Fabry, T. Devic, M. T. Wharmby, C. Martineau, D. Foucher, F. Taulelle, C.-H. Jun, Y. K. Hwang, N. Stock, M. F. De Lange, F. Kapteijn, J. Gascon, G. Maurin, J.-S. Chang and C. Serre, *Adv. Mater.*, 2015, **27**, 4775–4780.
- 35 M. Gaab, N. Trukhan, S. Maurer, R. Gummaraju and U. Müller, *Microporous Mesoporous Mater.*, 2012, **157**, 131–136.
- 36 F. Jeremias, D. Fröhlich, C. Janiak and S. K. Henninger, *RSC Adv.*, 2014, **4**, 24073–24082.
- 37 D. Fröhlich, S. K. Henninger and C. Janiak, *Dalton Trans.*, 2014, **43**, 15300–15304.
- 38 D. Fröhlich, E. Pantatosaki, P. D. Kolokathis, K. Markey, H. Reinsch, M. Baumgartner, M. A. van der Veen, D. E. de Vos, N. Stock, G. K. Papadopoulos, S. K. Henninger and C. Janiak, *J. Mater. Chem. A*, 2016, **4**, 11859–11869.
- 39 W. Liang, L. Li, J. Hou, N. D. Shepherd, T. D. Bennett, D. M. D'Alessandro and V. Chen, *Chem. Sci.*, 2018, **9**, 3508–3516; L. Feng, S. Yuan, L.-L. Zhang, K. Tan, J.-L. Li, A. Kirchon, L.-M. Liu, P. Zhang, Y. Han, Y. J. Chabal and H.-C. Zhou, *J. Am. Chem. Soc.*, 2018, **140**, 2363–2372; U. Betke, M. Klaus, J. G. Eggebrecht, M. Scheffler and A. Lieb, *Microporous Mesoporous Mater.*, 2018, **265**, 43–56.
- 40 D. Damasceno Borges, P. Normand, A. Permiakova, R. Barbaro, N. Heymans, D. S. Galvao, C. Serre, G. de Weireld and G. Maurin, *J. Phys. Chem. C*, 2017, **121**, 26822–26832.
- 41 S. Couck, Y.-Y. Liu, K. Leus, G. V. Baron, P. Van der Voort and J. F. M. Denayer, *Microporous Mesoporous Mater.*, 2015, **206**, 217–225.
- 42 (a) A. Dhakshinamoorthy, N. Heidenreich, D. Lenzen and N. Stock, *CrystEngComm*, 2017, **19**, 4187–4193; (b) L. M. Aguirre-Díaz, D. Reinares-Fisac, M. Iglesias, E. Gutiérrez-Puebla, F. Gándara, N. Snejkó and M. Á. Monge, *Coord. Chem. Rev.*, 2017, **335**, 1–27.
- 43 P. G. Yot, L. Vanduyfhuys, E. Alvarez, J. Rodriguez, J.-P. Itié, P. Fabry, N. Guillou, T. Devic, I. Beurroies, P. L. Llewellyn, V. Van Speybroek, C. Serre and G. Maurin, *Chem. Sci.*, 2016, **7**, 446–450.
- 44 (a) Y. Belmabkhout, R. S. Pillai, D. Alezi, O. Shekhah, P. M. Bhatt, Z. Chen, K. Adil, S. Vaesen, G. de Weireld, M. Pang, M. Suetin, A. J. Cairns, V. Solovyeva, A. Shkurenko, O. E. Talil, G. Maurin and M. Eddaoudi, *J. Mater. Chem. A*, 2017, **5**, 3293–3303; (b) S. Karmakar, J. Dechnik, C. Janiak and S. De, *J. Hazard. Mater.*, 2016, **303**, 10–20; (c) M. Mon, R. Bruno, J. Ferrando-Soria, D. Armentano and E. Pardo, *J. Mater. Chem. A*, 2018, **6**, 4912–4947.
- 45 M. J. Kalmutzki, C. S. Diercks and O. M. Yaghi, *Adv. Mater.*, 2018, **30**, 1704304; H. Kim, S. Yang, S. R. Rao, S. Narayanan, E. A. Kapustin, H. Furukawa, A. S. Umans, O. M. Yaghi and E. N. Wang, *Science*, 2017, **356**, 430–434; F. Trapani, A. Polyzoidis, S. Loebbecke and C. G. Piscopo, *Microporous Mesoporous Mater.*, 2016, **230**, 20–24.
- 46 E. Elsayed, R. Al-Dadah, S. Mahmoud, P. A. Anderson, A. Elsayed and P. G. Youssef, *Desalination*, 2017, **406**, 25–36.
- 47 A. Weiss, N. Reimer, N. Stock, M. Tiemann and T. Wagner, *Phys. Chem. Chem. Phys.*, 2015, **17**, 21634–21642.
- 48 N. Reimer, B. Bueken, S. Leubner, C. Seidler, M. Wark, D. De Vos and N. Stock, *Chem. – Eur. J.*, 2015, **21**, 12517–12524.
- 49 S. Karmakar, S. Bhattacharjee and S. De, *J. Environ. Chem. Eng.*, 2017, **5**, 6087–6097.
- 50 M. F. de Lange, T. Zeng, T. J. H. Vlught, J. Gascon and F. Kapteijn, *CrystEngComm*, 2015, **17**, 5911–5920; M. F. de Lange, C. P. Ottevanger, M. Wiegman, T. J. H. Vlught, J. Gascon and F. Kapteijn, *CrystEngComm*, 2015, **17**, 281–285.
- 51 J. Canivet, A. Fateeva, Y. Guo, B. Coasne and D. Farrusseng, *Chem. Soc. Rev.*, 2014, **53**, 5594–5617.
- 52 N. C. Burtch, H. Jasuja and K. S. Walton, *Chem. Rev.*, 2014, **114**, 10575–10612.
- 53 N. Tannert, S.-J. Ernst, C. Jansen, S. Nießing, H.-J. Bart, S. K. Henninger and C. Janiak, *J. Mater. Chem. A*, 2018, **6**, 17706–17712; M. F. de Lange, B. L. van Velzen, C. P. Ottevanger, K. J. F. M. Verouden, L.-C. Lin, T. J. H. Vlught, J. Gascon and F. Kapteijn, *Langmuir*, 2015, **31**, 12783–12796.
- 54 D. Lenzen, P. Bendix, H. Reinsch, D. Fröhlich, H. Kummer, M. Möllers, P. P. C. Hügenell, R. Gläser, S. Henninger and N. Stock, *Adv. Mater.*, 2017, **30**, 1705869.
- 55 H. Kummer, F. Jeremias, A. Warlo, G. Földner, D. Fröhlich, C. Janiak, R. Gläser and S. K. Henninger, *Ind. Eng. Chem. Res.*, 2017, **56**, 8393–8398.
- 56 S. Gökpınar, T. Diment and C. Janiak, *Dalton Trans.*, 2017, **46**, 9895–9900.
- 57 H. Reinsch, *Eur. J. Inorg. Chem.*, 2016, 4290–4299; H. Reinsch, S. Waitschat, S. M. Chavan, K. P. Lillerud and N. Stock, *Eur. J. Inorg. Chem.*, 2016, 4490–4498.
- 58 I. Ahmed, J. Jeon, N. A. Khan and S. H. Jhung, *Cryst. Growth Des.*, 2012, **12**, 5878–5881.
- 59 N. Yang, M. Yue and Y. Wang, *Prog. Chem.*, 2012, **24**, 253–261.
- 60 M. Thommes, K. Kaneko, A. V. Neimark, J. P. Olivier, F. Rodriguez-Reinoso, J. Rouquerol and K. S. Sing, *Pure Appl. Chem.*, 2015, **87**, 1051–1069.
- 61 Y. Wang, Q. Qu, G. Liu, V. S. Battaglia and H. Zheng, *Nano Energy*, 2017, **39**, 200–210.
- 62 H. Jin, A. Wollbrink, R. Yao, Y. Li, J. Caro and W. Yang, *J. Membr. Sci.*, 2016, **513**, 40–46.
- 63 D. Damasceno Borges, P. Normand, A. Permiakova, R. Babarao, N. Heymans, D. S. Galvao, C. Serre, G. de Weireld and G. Maurin, *J. Phys. Chem. C*, 2017, **121**, 26822–26832.
- 64 D. D. Borges, G. Maurin and D. S. Galvao, *MRS Adv.*, 2017, **2**, 519–524.
- 65 J. Caro, X. Wu, W. Wan, J. Jiang and A. Huang, *Angew. Chem., Int. Ed.*, 2018, **57**, 1–5.
- 66 M. Rubio-Martinez, T. D. Hadley, M. P. Batten, K. Constanti-Carey, T. Barton, D. Marley, A. Mönch, K.-S. Lim and M. R. Hill, *ChemSusChem*, 2016, **9**, 938–941.
- 67 [http://www.moftechnologies.com/products/\(10-12-2018\)](http://www.moftechnologies.com/products/(10-12-2018)).



- 68 E. Elsayed, R. AL-Dadah, S. Mahmoud, A. Elsayed and P. A. Anderson, *Appl. Therm. Eng.*, 2016, **99**, 802–812.
- 69 H. W. B. Teo, A. Chakraborty, Y. Kitagawa and S. Kayal, *Int. J. Heat Mass Transfer*, 2017, **114**, 621–627.
- 70 H. W. B. Teo, A. Chakraborty and S. Kayal, *Microporous Mesoporous Mater.*, 2018, **272**, 109–116.
- 71 S. Kayal, A. Chakraborty and H. W. B. Teo, *Mater. Lett.*, 2018, **221**, 165–167.
- 72 L. Zhou, X. Zhang and Y. Chen, *Mater. Lett.*, 2017, **197**, 224–227.
- 73 R. Kashanaki, H. Ebrahimzadeh and M. Moradi, *New J. Chem.*, 2018, **42**, 5806–5813.
- 74 D. Crawford, J. Casaban, R. Haydon, N. Giri, T. McNally and S. L. James, *Chem. Sci.*, 2015, **6**, 1645–1649.
- 75 B. Bozbiyik, J. Lannoeye, D. E. de Vos, G. V. Baron and J. F. M. Denayer, *Phys. Chem. Chem. Phys.*, 2016, **18**, 3294–3301.
- 76 J. A. Coelho, A. M. Ribeiro, A. F. P. Ferreira, S. M. P. Lucena, A. E. Rodrigues and D. C. S. de Azevedo, *Ind. Eng. Chem. Res.*, 2016, **55**, 2134–2143.
- 77 H. Reinsch, S. Waitschat and N. Stock, *Dalton Trans.*, 2013, **42**, 4840–4847.
- 78 V. B. López-Cervantes, E. Sánchez-González, T. Jurado-Vázquez, A. Tejeda-Cruz, E. González-Zamora and I. A. Ibarra, *Polyhedron*, 2018, **155**, 163–169.
- 79 A. Permyakova, O. Skrylnyk, E. Courbon, M. Affram, S. Wang, U.-H. Lee, A. H. Valekar, F. Nouar, G. Mouchaham, T. Devic, G. de Weireld, J.-S. Chang, N. Steunou, M. Frère and C. Serre, *ChemSusChem*, 2017, **10**, 1419–1426.
- 80 A. Permyakova, S. Wang, E. Courbon, F. Nouar, N. Heymans, P. D'Ans, N. Barrier, P. Billefont, G. de Weireld, N. Steunou, M. Frère and C. Serre, *J. Mater. Chem. A*, 2017, **5**, 12889–12898.
- 81 R. Cai, Y. Liu, S. Gu and Y. Yan, *J. Am. Chem. Soc.*, 2010, **132**, 12776–12777.
- 82 B.-W. Long, L.-S. Wang and J.-S. Wu, *J. Chem. Eng. Data*, 2005, **50**, 136–137.
- 83 M. Wahiduzzaman, D. Lenzen, G. Maurin, N. Stock and M. T. Wharmby, *Eur. J. Inorg. Chem.*, 2018, 3626–3632.
- 84 S. M. T. Abtab, D. Alezi, P. M. Bhatt, A. Shkurenko, Y. Belmabkhout, H. Aggarwal, Ł. J. Weseliński, N. Alsadun, U. Samin, M. N. Hedhili and M. Eddaoudi, *Chem*, 2017, **4**, 94–105.

*ELECTRONIC SUPPORTING INFORMATION (ESI)*

**Robust synthesis routes and porosity of Al-based metal-organic frameworks  
Al-fumarate, CAU-10-H and MIL-160†**

*Niels Tannert, Christian Jansen, Sandra Nießing and Christoph Janiak\**

*Institut für Anorganische Chemie und Strukturchemie, Heinrich-Heine-Universität Düsseldorf,  
Universitätsstraße 1, 40225 Düsseldorf, Germany. \*E-mail: [janjak@uni-duesseldorf.de](mailto:janjak@uni-duesseldorf.de)*

Emails:

[niels.tannert@hhu.de](mailto:niels.tannert@hhu.de); [christian.jansen@hhu.de](mailto:christian.jansen@hhu.de); [sandra.niessing@hhu.de](mailto:sandra.niessing@hhu.de)

**Keywords**

Metal-Organic Frameworks, Synthesis Optimization, Dry-Gel Conversion, Al-MOFs, [Al(OH)(Linker)], Aluminum fumarate (Alfum), CAU-10-H, MIL-160, Solvent Re-use

**Table of Contents**

Section S1.	Materials and equipment
Section S2.	Additional information on Alfum, CAU-10-H and MIL-160
Section S3.	Reflux-based syntheses for comparison
Section S4.	Dry-gel conversions: Synthesis optimizations
Section S4.1.	-- Aluminum fumarate (Alfum)
Section S4.1.1.	-- Aluminium fumarate (Alfum) solvent re-use
Section S4.2.	-- CAU-10-H
Section S4.2.1.	-- CAU-10-H solvent re-use
Section S4.2.2.	-- CAU-10-H solvent re-use (less DMF)
Section S4.3.	-- MIL-160
Section S4.3.1.	-- MIL-160 solvent re-use
Section S5.	Solvent re-use for Alfum, CAU-10-H and MIL-160
Section S6.	PXRD measurements
Section S7.	Thermogravimetric Analysis (TGA)
Section S8.	Scanning electron microscopy (SEM)
Section S9.	Nitrogen sorption experiments solvent re-use (T = 77 K)
Section S10.	Water sorption experiments (T = 20 °C) and microporosity
Section S11.	References

## S1. Materials and equipment

All chemicals were used as received by the supplier (*cf.* Table 1).

Table 1: Used chemicals, supplier and purities.

Chemical	Supplier	Purity
$\text{AlCl}_3 \cdot 6 \text{H}_2\text{O}$	Janssen Chimica	99%
$\text{Al}(\text{SO}_4)_3 \cdot 18 \text{H}_2\text{O}$	AppliChem	not specified
$\text{Al}(\text{OH})(\text{acetate})_2$	AlfaAesar	not specified
Basolite™ A520	Sigma Aldrich	not specified
Dimethylformamide	Fischer Chemicals	99.99
Ethanol	Sigma Aldrich	> 99.8%
Fumaric acid	Alfa Aesar	99%
2,5-furandicarboxylic acid	OxChem	95%
Isophthalic acid	AlfaAesar	99%
NaOH (microgranulate)	Chem Solute	not specified

Dry-gel conversion, DGC inlays were self-built. The full equipment was made of Teflon. The holes in DGC sieves had a diameter of 0.5 mm. The ring inlays, shown in Figure S1, can have various heights for height adjustment. We thank the mechanics workshop of Heinrich-Heine-University Düsseldorf for the manufacturing of the DGC container set.

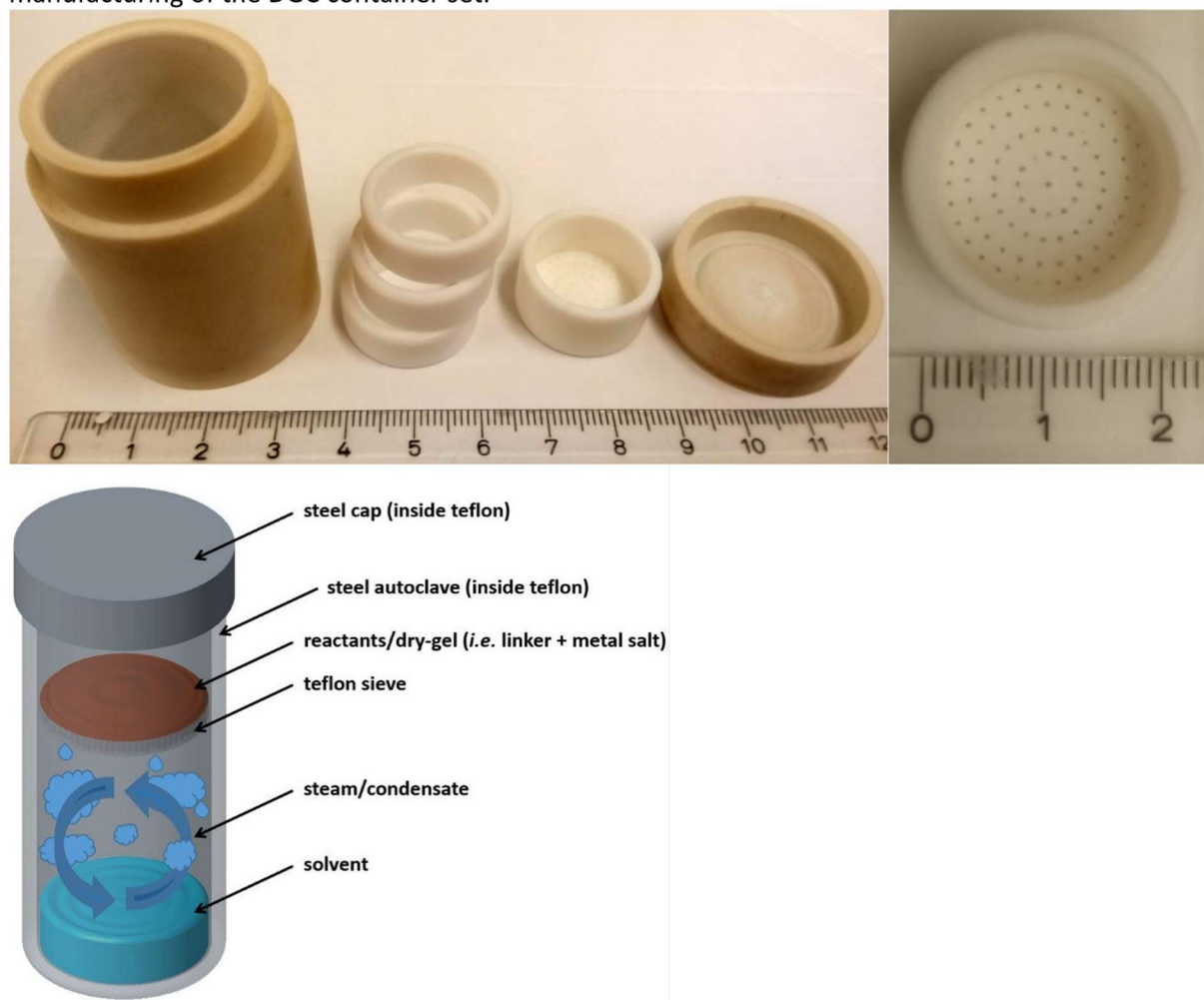


**Figure S1** Top left: Full Teflon autoclave set for DGC with container, three inlay rings for height adjustment, DGC sieve and cap (from left to right). Top right: Close-up view of a DGC sieve. Bottom: Schematic illustration of the working principle of dry-gel conversion.

## S2. Additional information on Alfum, CAU-10-H and MIL-160

### Aluminum fumarate (Alfum)

Aluminum fumarate was first described in the patent literature in 2013.<sup>1,2</sup> It was the first MOF synthesized on a ton scale and it is marketed by BASF under the name *Basolite™* A520. Figure S2 shows the structural features of Alfum.

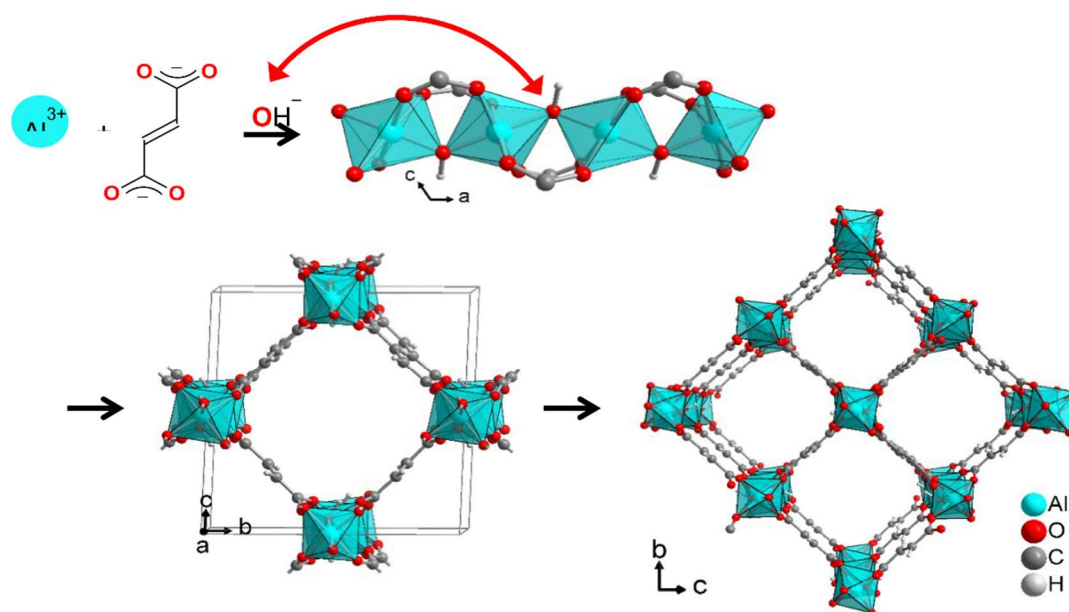


**Figure S2**  $\text{Al}^{3+}$ , hydroxide and fumarate building blocks of Alfum, from which in analogy to the structure of MIL-53 a chain of trans- $\mu$ -OH-connected vertex-bridged  $\{\text{AlO}_6\}$  octahedra is formed. These chains run along the crystallographic  $a$  direction and are connected through the fumarate linkers along the  $bc$  diagonal. Graphic produced by software Diamond<sup>3</sup> from cif-file for Basolite A520 (CSD-Refcode DOYBEA).<sup>4</sup>

Aluminum fumarate resembles the MIL-53 topology with its infinite Al-OH-Al chains, bridged by fumarate linkers. It presents the chemical formula  $[\text{Al}(\text{OH})(\text{O}_2\text{C}-\text{CH}=\text{CH}-\text{CO}_2) \cdot n \text{H}_2\text{O}]_m$  and displays microporous, rhombohedral channels with  $\text{ca. } 5.7 \times 6.0 \text{ \AA}^2$  free dimensions.<sup>4,5</sup> The BET surface area (Brunauer-Emmett-Teller) ranges from 925 to 1212  $\text{m}^2 \text{g}^{-1}$ .<sup>6,7</sup> The material exhibits high hydrothermal stability, which is attributed to its aqueous synthesis route and the good hydrolytic stability of the Al-carboxylate bond.

Besides the patented solution-based route, it can as well be prepared in continuous flow reactors,<sup>8</sup> or *via* mechanochemical procedures such as extrusion.<sup>9</sup> Thereby, 27 000  $\text{kg m}^{-3} \text{day}^{-1}$  space-time-yields (STY) were calculated to be feasible.<sup>10</sup> Continuous flow methods achieved even STYs up to 97 159  $\text{kg m}^{-3} \text{day}^{-1}$  at 5.6  $\text{kg h}^{-1}$  and  $\text{ca. } 1000\text{--}1100 \text{ m}^2 \text{g}^{-1}$ .<sup>8</sup> Other synthetic routes comprise for example spray drying,<sup>11</sup> and our recently proposed technique or microwave assisted-dry gel conversion, MW-DGC.<sup>12</sup>

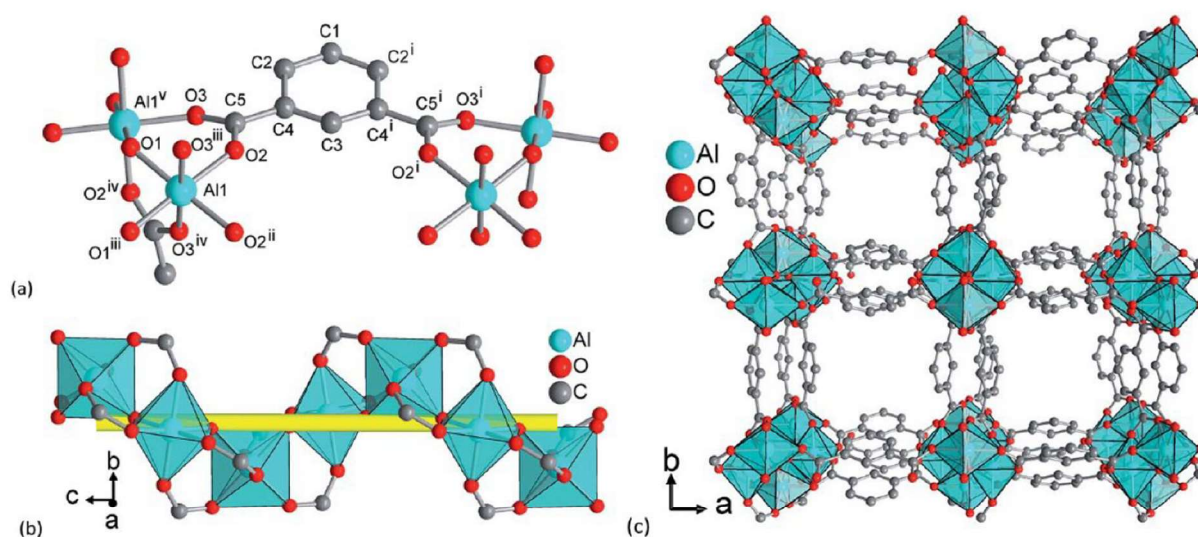
Aluminum fumarate is one of the most promising MOFs for application,<sup>4,13,14</sup> mostly due to its hydrothermal stability and water sorption properties, but also due to an environmentally friendly synthesis route with water as single solvent, inexpensive and abundant metal cation, and a “green” linker from renewable biomass.<sup>15,16</sup> Gaab *et al.* proved its applicability as storage container for natural gas, used as fuel in a vehicle, with 40% increased cruising distance.<sup>16</sup> Moreover, Alfum was proven to be a very promising candidate for implementation as adsorbent in heat transformation applications,<sup>14,17</sup> since it displays suitable water sorption characteristics (desired s-shaped isotherm with steep loading lift, absence of hysteresis, reasonable isosteric heat of adsorption).<sup>4,14</sup> Alfum is applicable as adsorbent for removal of fluoride from water,<sup>18</sup> in desalination processes,<sup>7</sup> in mixed-



matrix-membranes (MMMs)<sup>19</sup> and it was proposed to be the best porous solid for mechanical energy storage.<sup>20</sup> Latest contributions to Al<sub>2</sub>MOFs included defective engineering/modulation,<sup>21</sup> modelling,<sup>22</sup> adsorption of volatile organic compounds,<sup>6</sup> and kinetics of water sorption.<sup>23</sup>

## CAU-10-H

In 2012 Reinsch and co-workers described the synthesis of CAU-10-H (Fig. S3) (CAU = *Christian-Albrechts-Universität*) out of a water-dimethylformamide (DMF) mixture of isophthalic acid and aluminum sulfate, applying solvothermal conditions (135 °C, 12 h).<sup>24</sup>





CAU-10-H is a very good candidate for heat transformation applications,<sup>17</sup> as it represents nearly perfect hydrothermal stability,<sup>35</sup> which is underlined by no structural degradation of the material over 700 repeated adsorption/desorption cycles.<sup>35</sup> It has a higher volumetric adsorption capacity ( $0.38 \text{ cm}^3 \text{ g}^{-1}$  at  $p/p_0 = 0.26$ )<sup>24</sup> and thermodynamic efficiency for water than commercial adsorbents (e.g. SAPO-34),<sup>33,36</sup> possessing an isosteric heat of adsorption of *ca.*  $54 \text{ kJ mol}^{-1}$  (theoretically  $-49 \text{ kJ mol}^{-1}$ , predicted by GCMC simulations.<sup>37</sup> Accordingly, dense coatings of CAU-10-H were employed on different substrates with the purpose of heat transformation.<sup>38</sup> Due to its properties, it was also addressed to be suitable for humidity sensing by impedance spectroscopy,<sup>31</sup> investigated in terms of proton conductivity and catalytic activity,<sup>32</sup> as well as gas adsorption and separation.<sup>39</sup>

### MIL-160

A rather new Al-MOF material is MIL-160 (*Matériaux Institut Lavoisier*), which was described by Cadiau *et al.* in 2015.<sup>27</sup> They obtained the MOF by applying reflux conditions for aqueous solutions of 2,5-furandicarboxylic acid, sodium hydroxide and aluminum chloride. MIL-160 is constructed identical to CAU-10-H by *cis*- $\mu$ -OH-connected, vertex-sharing  $\{\text{AlO}_6\}$  octahedra, that form helical chains, which are then joined by the linker 2,5-furandicarboxylate (Fig. S4).

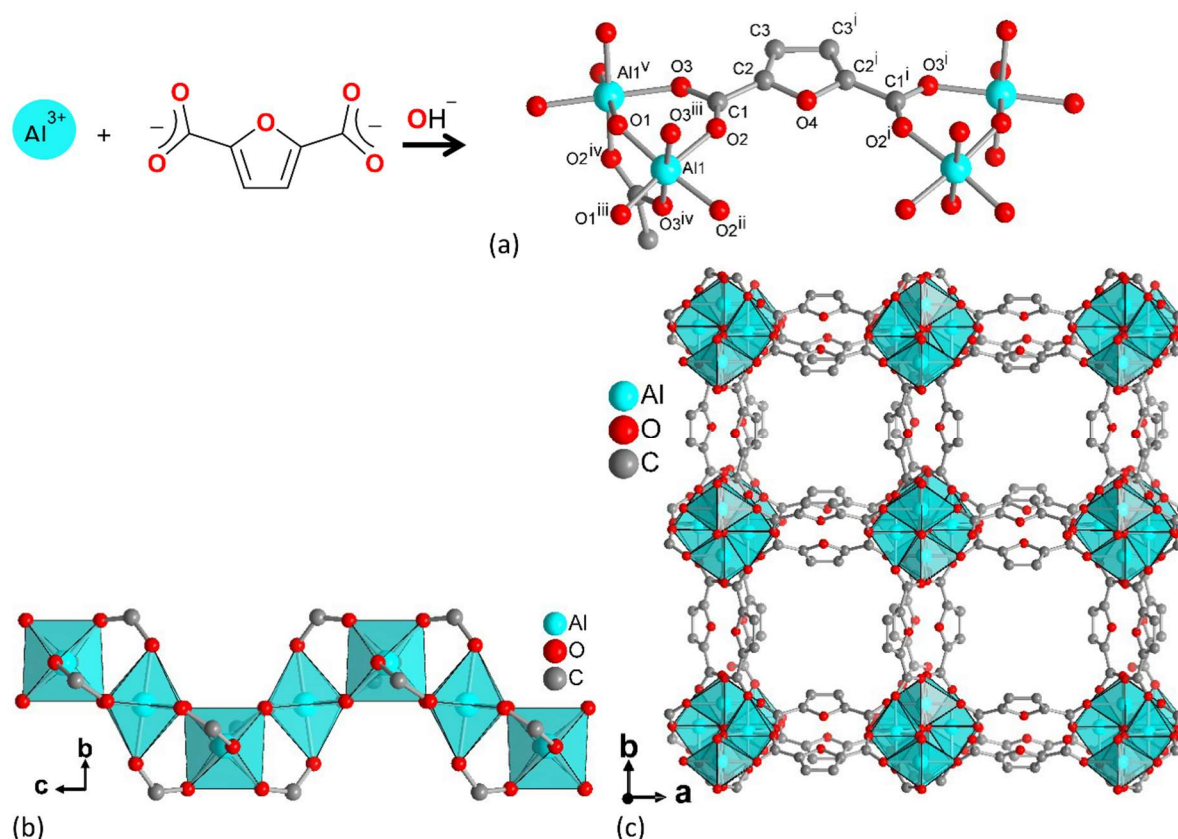


**Figure S4** Structural elements in the framework of MIL-160: (a) Extended asymmetric unit with full Al coordination spheres and full ligand bridging mode. Symmetry transformations  $i = 1-x, y, z$ ;  $ii = x, -y, -z$ ;  $iii = 0.25+y, 0.25-x, -0.25+z$ ;  $iv = 0.25+y, -0.25+x, 0.25-z$ ;  $v = 0.25-y, -0.25+x, 0.25+z$ . (b) Helical chains of *cis* vertex-bridged  $\{\text{AlO}_6\}$ -polyhedra and (c) surrounded by the carboxylate ligands, to yield square-shaped one dimensional channels; compare to the closely related structure of CAU-10-H in Fig. S3. Graphic produced by software Diamond<sup>3</sup> from cif-file for MIL-160 (CSD-Refcode PIBZOS).<sup>40</sup>

MIL-160 is reported to be isostructural to CAU-10-H, having chains of  $\{\text{AlO}_6\}$ -polyhedra that are surrounded by linker molecules.<sup>27</sup> This results in a chemical formula of  $[\text{Al}(\text{OH})(\text{O}_2\text{C}-\text{C}_4\text{H}_2\text{O}-\text{CO}_2) \cdot n \text{ H}_2\text{O}]_m$  and microporous square-shaped channels of  $5 \text{ \AA}$  edge length.<sup>27,41</sup> The material exhibits a surface

area of  $1070 \text{ m}^2 \text{ g}^{-1}$  and a pore volume of  $0.40 \text{ cm}^3 \text{ g}^{-1}$  from  $\text{AlCl}_3$  and  $\text{NaOH}$  (theoretically:  $1250 \text{ m}^2 \text{ g}^{-1}$ ,  $0.48 \text{ cm}^3 \text{ g}^{-1}$ ),<sup>27</sup> respectively  $1150 \text{ m}^2 \text{ g}^{-1}$  and  $0.46 \text{ cm}^3 \text{ g}^{-1}$ , from  $\text{Al}(\text{OH})(\text{CH}_3\text{COO})_2$ ,<sup>41</sup> although very recent theoretical calculations suggested a surface area of  $776 \text{ m}^2 \text{ g}^{-1}$  and a pore volume of  $0.45 \text{ cm}^3 \text{ g}^{-1}$ .<sup>28</sup>

The hydrophilic character of the MOF is also due to the heteroatom in the furan moiety of the linker. This resulted in a highly hydrothermally stable material with promising water sorption characteristics. Very recently, the MOF was advantageously synthesized from basic aluminum acetate (*i.e.*  $\text{Al}(\text{OH})(\text{CH}_3\text{COO})_2$ ) in a scale-up.<sup>41</sup> The synthesis route of MIL-160 is environmentally friendly, since the linker is already on the way to being produced from renewable biomass *via* oxidation of 5-(hydroxymethyl)furfural (5-HMF) on a very large industrial scale and water is the single solvent.<sup>42,43</sup> Hence, the production costs for MIL-160 may decline further within the next years. MIL-160 is quite a new material, there are – to the best of our knowledge – only the aforementioned two reports for different synthesis routes, mainly varying in the aluminum source and scale of synthesis.<sup>27,41</sup> A most recent and third report on MIL-160 focusses on structural refinements and flexibility upon  $\text{N}_2$  and  $\text{H}_2\text{O}$  sorption.<sup>40</sup>

Cadiau *et al.* denoted MIL-160 as the most promising Al-MOF for heat pump applications.<sup>27</sup> In comparison to CAU-10-H, slightly higher desorption temperatures are required; nevertheless, it outperforms both Alfum and CAU-10-H in terms of gravimetric water loadings.<sup>27</sup> In detail, it submits distinctively higher performance in terms of the loading spread (*i.e.* mass of adsorbed water vapor per mass of adsorbent) for the desired lift phase 1 (*i.e.* according to Henninger *et al.*: desired loading at low  $p_{p0}^{-1}$ , depending on driving temperature).<sup>27,44,45,46</sup> Permyakova *et al.* investigated MIL-160 with respect to shaping into granules and heat reallocation.<sup>41</sup> Their report suggests similar properties to the ones reported by Cadiau *et al.* and underlines the suitability of the material for heat transformation application.

### **S3. Reflux-based syntheses for comparison**

**Alfum** was synthesized according to the patented approach:<sup>1,2</sup> for solution 1, sodium hydroxide (0.2803 g, 7.01 mmol, 4 eq) and fumaric acid (0.3863 g, 3.33 mmol, 2 eq) were dissolved in water (6 mL). For solution 2, aluminum sulfate octadecahydrate (1.171 g, 1.76 mmol, 1 eq) was diluted in water (5 mL) at 60 °C. Over the course of 30 min, solution 1 was dropped into solution 2 and further stirred (60 °C, 2 h). The product was centrifuged (2000 U/min, 15 min) and decanted, subsequently washed with water (50 mL). The latter step was repeated. Subsequently, the product was dried overnight (80 °C, 1 - 10 mbar), yielding a white powder (0.4104 g, 74% yield, BET = 1131 m<sup>2</sup> g<sup>-1</sup>).

**CAU-10-H** was synthesized according to a protocol by Reinsch *et al.*: Aluminum sulfate octadecahydrate (0.8005 g, 4.82 mmol, 1 eq) and isophthalic acid (0.2000 g, 5.00 mmol, 1 eq) were transferred into a Teflon-lined autoclave (37 mL reactor volume) with water (4 mL) and DMF (1 mL). After 5 min of stirring, the autoclave was closed and heated (3 h heating, 12 h at 135 °C, 1 h cooling). Afterwards, the reaction mixture was decanted, washed with water three times (30 mL each), centrifuged (2000 U/min, 30 min), decanted and re-dispersed each time. Subsequently, the product was dried overnight (80 °C, 1 - 10 mbar), yielding a white powder (0.2122 g, 42% yield, BET = 435 m<sup>2</sup> g<sup>-1</sup>).

**MIL-160** was synthesized in a modified protocol of Cadiau *et al.*, who used 1 eq NaOH, whereas we used 2 eq NaOH to deprotonate the linker fully: 2,5-furandicarboxylic acid (0.3123 g, 2.0 mmol, 1 eq) and sodium hydroxide (0.1603 g, 4.0 mmol, 2 eq) were converted in water (10 mL, 2 h). Aluminum chloride hexahydrate (0.4826 g, 2.0 mmol, 1 eq) was added and reflux (24 h, 100 °C) was initiated. After decantation, the product was washed with water three times (30 mL each), centrifuged (2000 U/min, 30 min), decanted and re-dispersed each time. Subsequently, the product was dried overnight (80 °C, 1 - 10 mbar), yielding a white powder (0.2184 g, 55% yield, BET = 1178 m<sup>2</sup> g<sup>-1</sup>).

#### **S4. Dry-gel conversions: Syntheses optimizations**

In order to find reliable DGC synthesis routes for the three presented MOFs, we carried out profound synthesis optimizations for each MOF individually: In a first approach, we assumed the stated synthesis temperatures and conversion times according to the reflux-based syntheses described in the literature for each MOF. Subsequently, we varied the temperature to one elevated and one lower level to find an optimal synthesis temperature. By applying the most suitable temperature, we varied time by choosing one longer and one shorter protocol.

The details and results of these time and temperature variations are summarized in Table S2, S4 and S7 for Alfum, CAU-10-H and MIL-160, respectively.

In each synthesis, one approach was carried with dry starting materials, another with wetted reactants. Thereby, we checked if wetting of the precursor mixture before conversion may be supportive for crystallinity and/or BET surface areas of the presented MOFs (*cf.* Figures S5-S12 and Figures S17-S19). Thereby, we were able to assure best and most efficient DGCs of the presented MOFs. The criteria yield, crystallinity, BET surface area and pore volume, as well as water sorption behavior were taken into account for synthesis optimizations towards first DGCs of Al-MOFs in general.

For CAU-10-H the DGC synthesis is based on the autoclave solution synthesis of Reinsch *et al.* using the same molar ratios of aluminum sulfate and isophthalic acid.<sup>24</sup> The reaction conditions of 135 °C for 12 h were taken as a starting point and the time and temperature were systematically varied.

For MIL-160 we have used the reaction conditions of Cadiou *et al.* as a starting point, that is 100 °C and 24 h.<sup>27</sup> From this starting point we have chosen a higher and lower temperature and at the medium temperature we varied the reaction to longer and shorter times than the literature. Furthermore, we investigate the use of 1 or 2 eq NaOH.

PXRD plots and nitrogen sorption isotherms that were taken into account as key-factors for synthesis optimizations are depicted in the respective Sections S4.1, S4.2 and S4.3.

##### **Alfum**

In a typical synthetic procedure, we rapidly ground aluminum sulfate octadecahydrate ( $\text{Al}_2(\text{SO}_4)_3 \cdot 18\text{H}_2\text{O}$ ) (159 mg, 0.24 mmol, 1 eq), fumaric acid ( $\text{H}_2\text{fum}$ ) (53 mg, 0.48 mmol, 2 eq) and sodium hydroxide (NaOH) (40 mg, 1.02 mmol, 4 eq) in a mortar and placed the mixture on a DGC sieve with water (5 mL) at the bottom of a Teflon reactor. DGCs were carried out at varying temperatures and conversion times. The white products were washed three times with water (10 mL each), recovered by centrifugation each time and finally dried under vacuum (80 °C, 24 h).

##### **CAU-10-H**

In a typical synthetic procedure, we rapidly ground aluminum sulfate octadecahydrate ( $\text{Al}_2(\text{SO}_4)_3 \cdot 18\text{H}_2\text{O}$ ) (169 mg, 0.25 mmol, 1 eq), isophthalic acid ( $\text{H}_2\text{BDC}$ ) (42 mg, 0.25 mmol, 1eq) in a mortar and placed the mixture on a DGC sieve with water/DMF (4:1, 5 mL) at the bottom of a Teflon reactor. DGCs were carried out at varying temperatures and conversion times. The white products were washed three times with water (10 mL each), recovered by centrifugation each time and finally dried under vacuum (80 °C, 24 h).

**MIL-160**

In a typical synthetic procedure, we rapidly ground aluminum chloride hexahydrate ( $\text{AlCl}_3 \cdot 6\text{H}_2\text{O}$ ) (144 mg, 0.60 mmol, 1 eq), 2,5-furandicarboxylic acid ( $\text{H}_2\text{FDC}$ ) (93 mg, 0.60 mmol, 1 eq) and sodium hydroxide ( $\text{NaOH}$ ) (1 or 2 eq) in a mortar and placed the mixture on a DGC sieve with water (5 mL) at the bottom of a Teflon reactor. DGCs were carried out at varying temperatures and conversion times. The white products were washed three times with water (10 mL each), recovered by centrifugation each time and finally dried under vacuum (80 °C, 24 h).



#### S4.1. Dry-gel conversions: Synthesis optimizations -- Alfum

Table S2. Listing of DGC synthesis conditions for Alfum with variation of time and temperature.

Aluminum fumarate						
Conditions	Not Moistened					
80 °C; 12 h	Starting Materials	Initial Weight	Molar Amount	Equivalents	Product	
	Aluminum Sulfate	0.1559 g	0.23 mmol	1 eq	Yield	0.0516 g (70 %)
	Fumaric acid	0.0542 g	0.47 mmol	2 eq		
	NaOH	0.0400 g	1.00 mmol	4 eq	Surface	630 m <sup>2</sup> /g
	Water	2 ml	-	-		
100 °C; 12 h	Starting Materials	Initial Weight	Molar Amount	Equivalents	Product	
	Aluminum Sulfate	0.1597 g	0.24 mmol	1 eq	Yield	0.0524 g (69 %)
	Fumaric acid	0.0555 g	0.48 mmol	2 eq		
	NaOH	0.0409 g	1.02 mmol	4 eq	Surface	795 m <sup>2</sup> /g
	Water	2 ml	-	-		
120 °C; 12 h	Starting Materials	Initial Weight	Molar Amount	Equivalents	Product	
	Aluminum Sulfate	0.1571 g	0.24 mmol	1 eq	Yield	0.0609 g (82 %)
	Fumaric acid	0.0546 g	0.47 mmol	2 eq		
	NaOH	0.0403 g	1.01 mmol	4 eq	Surface	749 m <sup>2</sup> /g
	Water	2 ml	-	-		
100 °C; 6 h	Starting Materials	Initial Weight	Molar Amount	Equivalents	Product	
	Aluminum Sulfate	0.1573 g	0.24 mmol	1 eq	Yield	0.0500 g (67 %)
	Fumaric acid	0.0547 g	0.47 mmol	2 eq		
	NaOH	0.0404 g	1.01 mmol	4 eq	Surface	1037 m <sup>2</sup> /g
	Water	2 ml	-	-		
100 °C; 24 h	Starting Materials	Initial Weight	Molar Amount	Equivalents	Product	
	Aluminum Sulfate	0.1590 g	0.24 mmol	1 eq	Yield	0.0532 g (71 %)
	Fumaric acid	0.0553 g	0.48 mmol	2 eq		
	NaOH	0.0408 g	1.02 mmol	4 eq	Surface	1129 m <sup>2</sup> /g
	Water	2 ml	-	-		
Conditions	Moistened					
80 °C; 12 h	Starting Materials	Initial Weight	Molar Amount	Equivalents	Product	
	Aluminum Sulfate	0.1550 g	0.23 mmol	1 eq	Yield	0.0468 g (64 %)
	Fumaric acid	0.0539 g	0.46 mmol	2 eq		
	NaOH	0.0397 g	0.99 mmol	4 eq	Surface	1004 m <sup>2</sup> /g
	Water	1.8 + 0.2 ml	-	-		
100 °C; 12 h	Starting Materials	Initial Weight	Molar Amount	Equivalents	Product	
	Aluminum Sulfate	0.1593 g	0.24 mmol	1 eq	Yield	0.0460 g (61 %)
	Fumaric acid	0.0554 g	0.48 mmol	2 eq		
	NaOH	0.0408 g	1.02 mmol	4 eq	Surface	604 m <sup>2</sup> /g
	Water	1.8 + 0.2 ml	-	-		
120 °C; 12 h	Starting Materials	Initial Weight	Molar Amount	Equivalents	Product	
	Aluminum Sulfate	0.1564 g	0.23 mmol	1 eq	Yield	0.0663 g (89 %)
	Fumaric acid	0.0544 g	0.47 mmol	2 eq		
	NaOH	0.0402 g	1.01 mmol	4 eq	Surface	577 m <sup>2</sup> /g
	Water	1.8 + 0.2 ml	-	-		
100 °C; 6 h	Starting Materials	Initial Weight	Molar Amount	Equivalents	Product	
	Aluminum Sulfate	0.1591 g	0.24 mmol	1 eq	Yield	0.0435 g (58 %)
	Fumaric acid	0.0553 g	0.48 mmol	2 eq		
	NaOH	0.0409 g	1.02 mmol	4 eq	Surface	1284 m <sup>2</sup> /g
	Water	1.8 + 0.2 ml	-	-		
100 °C; 24 h	Starting Materials	Initial Weight	Molar Amount	Equivalents	Product	
	Aluminum Sulfate	0.1590 g	0.24 mmol	1 eq	Yield	0.0280 g (37 %)
	Fumaric acid	0.0553 g	0.48 mmol	2 eq		
	NaOH	0.0408 g	1.02 mmol	4 eq	Surface	575 m <sup>2</sup> /g
	Water	1.8 + 0.2 ml	-	-		

### Section S4.1.1. Dry-gel conversions: Synthesis optimizations -- Alfum solvent re-use

Table S3. Listing of DGC synthesis conditions for Alfum and solvent re-use.

Aluminum fumarate						
Conditions	Not moistened					
100 °C; 6 h	Starting Materials	Initial Weight	Molar Amount	Equivalents	Product	
	Aluminum Sulfate	0.1676 g	0.25 mmol	1 eq	Yield	0.0386 g (49 %)
	Fumaric acid	0.0587 g	0.51 mmol	2 eq		
	NaOH	0.0406 g	1.02 mmol	4 eq	Surface	924 m <sup>2</sup> /g
	Water	2 ml	-	-		
100 °C; 6 h	Starting Materials	Initial Weight	Molar Amount	Equivalents	Product	
	Aluminum Sulfate	0.1670 g	0.25 mmol	1 eq	Yield	0.0326 g (41 %)
	Fumaric acid	0.0579 g	0.50 mmol	2 eq		
	NaOH	0.0423 g	1.06 mmol	4 eq	Surface	1076 m <sup>2</sup> /g
	Water	2 ml	-	-		
100 °C; 6 h	Starting Materials	Initial Weight	Molar Amount	Equivalents	Product	
	Aluminum Sulfate	0.1672 g	0.25 mmol	1 eq	Yield	0.0390 g (49 %)
	Fumaric acid	0.0588 g	0.51 mmol	2 eq		
	NaOH	0.0405 g	1.01 mmol	4 eq	Surface	1045 m <sup>2</sup> /g
	Water	2 ml	-	-		
100 °C; 6 h	Starting Materials	Initial Weight	Molar Amount	Equivalents	Product	
	Aluminum Sulfate	0.1673 g	0.25 mmol	1 eq	Yield	0.0364 g (46 %)
	Fumaric acid	0.0582 g	0.50 mmol	2 eq		
	NaOH	0.0437 g	1.09 mmol	4 eq	Surface	1032 m <sup>2</sup> /g
	Water	2 ml	-	-		
Conditions	Moistened					
100 °C; 6 h	Starting Materials	Initial Weight	Molar Amount	Equivalents	Product	
	Aluminum Sulfate	0.1673 g	0.25 mmol	1 eq	Yield	0.0377 g (48 %)
	Fumaric acid	0.0592 g	0.51 mmol	2 eq		
	NaOH	0.0410 g	1.02 mmol	4 eq	Surface	983 m <sup>2</sup> /g
	Water	1.8 + 0.2 ml	-	-		
100 °C; 6 h	Starting Materials	Initial Weight	Molar Amount	Equivalents	Product	
	Aluminum Sulfate	0.1650 g	0.25 mmol	1 eq	Yield	0.0413 g (53 %)
	Fumaric acid	0.0579 g	0.50 mmol	2 eq		
	NaOH	0.0422 g	1.06 mmol	4 eq	Surface	991 m <sup>2</sup> /g
	Water	1.8 + 0.2 ml	-	-		
100 °C; 6 h	Starting Materials		Molar Amount	Equivalents	Product	
	Aluminum Sulfate	0.1661 g	0.25 mmol	1 eq	Yield	0.0180 g (23 %)
	Fumaric acid	0.0586 g	0.50 mmol	2 eq		
	NaOH	0.0401 g	1.00 mmol	4 eq	Surface	1189 m <sup>2</sup> /g
	Water	1.8 + 0.2 ml	-	-		
100 °C; 6 h	Starting Materials		Molar Amount	Equivalents	Product	
	Aluminum Sulfate	0.1691 g	0.25 mmol	1 eq	Yield	0.0404 g (50 %)
	Fumaric acid	0.0590 g	0.51 mmol	2 eq		
	NaOH	0.0427 g	1.07 mmol	4 eq	Surface	1089 m <sup>2</sup> /g
	Water	1.8 + 0.2 ml	-	-		

## S4.2. Dry-gel conversions: Synthesis optimizations -- CAU-10-H

Table S4. Listing of DGC synthesis conditions for CAU-10-H with variation of time and temperature.

CAU-10-H						
Conditions	Not Moistened					
115 °C; 12 h	Starting Materials	Initial Weight	Molar Amount	Equivalents	Product	
	Aluminum Sulfate	0.2065 g	0.31 mmol	1 eq	Yield	-
	Isophthalic Acid	0.0517 g	0.31 mmol	1 eq		
	N,N-Dimethylformamide	0.4 ml	-	-	Surface	-
	Water	1.6 ml	-	-		
135 °C; 12 h	Starting Materials	Initial Weight	Molar Amount	Equivalents	Product	
	Aluminum Sulfate	0.2001 g	0.30 mmol	1 eq	Yield	0.0362 g (29 %)
	Isophthalic Acid	0.0509 g	0.31 mmol	1 eq		
	N,N-Dimethylformamide	0.4 ml	-	-	Surface	33 m <sup>2</sup> /g
	Water	1.6 ml	-	-		
155 °C; 12 h	Starting Materials	Initial Weight	Molar Amount	Equivalents	Product	
	Aluminum Sulfate	0.1920 g	0.29 mmol	1 eq	Yield	0.0783 g (65 %)
	Isophthalic Acid	0.0481 g	0.29 mmol	1 eq		
	N,N-Dimethylformamide	0.4 ml	-	-	Surface	13 m <sup>2</sup> /g
	Water	1.6 ml	-	-		
135 °C; 6 h	Starting Materials	Initial Weight	Molar Amount	Equivalents	Product	
	Aluminum Sulfate	0.2002 g	0.30 mmol	1 eq	Yield	-
	Isophthalic Acid	0.0502 g	0.30 mmol	1 eq		
	N,N-Dimethylformamide	0.4 ml	-	-	Surface	-
	Water	1.6 ml	-	-		
135 °C; 24 h	Starting Materials	Initial Weight	Molar Amount	Equivalents	Product	
	Aluminum Sulfate	0.1642 g	0.25 mmol	1 eq	Yield	0.0487 g (48 %)
	Isophthalic Acid	0.0411 g	0.25 mmol	1 eq		
	N,N-Dimethylformamide	0.4 ml	-	-	Surface	1 m <sup>2</sup> /g
	Water	1.6 ml	-	-		
Conditions	Moistened					
115 °C; 12 h	Starting Materials	Initial Weight	Molar Amount	Equivalents	Product	
	Aluminum Sulfate	0.2062 g	0.31 mmol	1 eq	Yield	0.0460 g (36 %)
	Isophthalic Acid	0.0517 g	0.31 mmol	1 eq		
	N,N-Dimethylformamide	0.4 ml	-	-	Surface	168 m <sup>2</sup> /g
	Water	1.6 ml	-	-		
135 °C; 12 h	Starting Materials	Initial Weight	Molar Amount	Equivalents	Product	
	Aluminum Sulfate	0.1999 g	0.30 mmol	1 eq	Yield	0.0590 g (47 %)
	Isophthalic Acid	0.0508 g	0.31 mmol	1 eq		
	N,N-Dimethylformamide	0.4 ml	-	-	Surface	398 m <sup>2</sup> /g
	Water	1.6 ml	-	-		
155 °C; 12 h	Starting Materials	Initial Weight	Molar Amount	Equivalents	Product	
	Aluminum Sulfate	0.1690 g	0.25 mmol	1 eq	Yield	0.0552 g (52 %)
	Isophthalic Acid	0.0423 g	0.25 mmol	1 eq		
	N,N-Dimethylformamide	0.4 ml	-	-	Surface	472 m <sup>2</sup> /g
	Water	1.6 ml	-	-		
135 °C; 6 h	Starting Materials	Initial Weight	Molar Amount	Equivalents	Product	
	Aluminum Sulfate	0.2015 g	0.30 mmol	1 eq	Yield	0.0373 g (30 %)
	Isophthalic Acid	0.0506 g	0.30 mmol	1 eq		
	N,N-Dimethylformamide	0.4 ml	-	-	Surface	255 m <sup>2</sup> /g
	Water	1.6 ml	-	-		
135 °C; 24 h	Starting Materials	Initial Weight	Molar Amount	Equivalents	Product	
	Aluminum Sulfate	0.1707 g	0.26 mmol	1 eq	Yield	0.0484 g (45 %)
	Isophthalic Acid	0.0427 g	0.26 mmol	1 eq		
	N,N-Dimethylformamide	0.4 ml	-	-	Surface	250 m <sup>2</sup> /g
	Water	1.6 ml	-	-		

#### S.4.2.1. Dry-gel conversions: Synthesis optimizations -- CAU-10-H solvent re-use

Table S5. Listing of DGC synthesis conditions for CAU-10-H and solvent re-use.

CAU-10-H						
Conditions	Not Moistened					
155 °C; 12 h	Starting Materials	Initial Weight	Molar Amount	Equivalents	Product	
	Aluminum Sulfate	0.1987 g	0.30 mmol	1 eq	Yield	0.0643 g (52 %)
	Isophthalic Acid	0.0502 g	0.30 mmol	1 eq		
	N,N-Dimethylformamide	0.4 ml	-	-	Surface	67 m <sup>2</sup> /g
	Water	1.6 ml	-	-		
155 °C; 12 h	Starting Materials	Initial Weight	Molar Amount	Equivalents	Product	
	Aluminum Sulfate	0.1998 g	0.30 mmol	1 eq	Yield	0.0606 g (49 %)
	Isophthalic Acid	0.0500 g	0.30 mmol	1 eq		
	N,N-Dimethylformamide	0.4 ml	-	-	Surface	23 m <sup>2</sup> /g
	Water	1.6 ml	-	-		
155 °C; 12 h	Starting Materials	Initial Weight	Molar Amount	Equivalents	Product	
	Aluminum Sulfate	0.1982 g	0.30 mmol	1 eq	Yield	0.0387 g (31 %)
	Isophthalic Acid	0.0505 g	0.30 mmol	1 eq		
	N,N-Dimethylformamide	0.4 ml	-	-	Surface	232 m <sup>2</sup> /g
	Water	1.6 ml	-	-		
155 °C; 12 h	Starting Materials	Initial Weight	Molar Amount	Equivalents	Product	
	Aluminum Sulfate	0.1990 g	0.30 mmol	1 eq	Yield	0.0408 g (33 %)
	Isophthalic Acid	0.0503 g	0.30 mmol	1 eq		
	N,N-Dimethylformamide	0.4 ml	-	-	Surface	20 m <sup>2</sup> /g
	Water	1.6 ml	-	-		
Conditions	Moistened					
155 °C; 12 h	Starting Materials	Initial Weight	Molar Amount	Equivalents	Product	
	Aluminum Sulfate	0.2008 g	0.30 mmol	1 eq	Yield	0.0071 g (6 %)
	Isophthalic Acid	0.0503 g	0.30 mmol	1 eq		
	N,N-Dimethylformamide	0.4 ml	-	-	Surface	285 m <sup>2</sup> /g
	Water	1.6 ml	-	-		
155 °C; 12 h	Starting Materials	Initial Weight	Molar Amount	Equivalents	Product	
	Aluminum Sulfate	0.1994 g	0.30 mmol	1 eq	Yield	0.0376 g (30 %)
	Isophthalic Acid	0.0496 g	0.30 mmol	1 eq		
	N,N-Dimethylformamide	0.4 ml	-	-	Surface	348 m <sup>2</sup> /g
	Water	1.6 ml	-	-		
155 °C; 12 h	Starting Materials	Initial Weight	Molar Amount	Equivalents	Product	
	Aluminum Sulfate	0.1974 g	0.30 mmol	1 eq	Yield	0.0362 g (29 %)
	Isophthalic Acid	0.0503 g	0.30 mmol	1 eq		
	N,N-Dimethylformamide	0.4 ml	-	-	Surface	560 m <sup>2</sup> /g
	Water	1.6 ml	-	-		
155 °C; 12 h	Starting Materials	Initial Weight	Molar Amount	Equivalents	Product	
	Aluminum Sulfate	0.2005 g	0.30 mmol	1 eq	Yield	0.0114 g (9 %)
	Isophthalic Acid	0.0515 g	0.31 mmol	1 eq		
	N,N-Dimethylformamide	0.4 ml	-	-	Surface	42 m <sup>2</sup> /g
	Water	1.6 l	-	-		

#### S4.2.2. Dry-gel conversions: Synthesis optimizations -- CAU-10-H solvent re-use (less DMF)

Table S6. Listing of DGC synthesis conditions for CAU-10-H and solvent re-use with less DMF.

CAU-10-H						
Conditions	Not Moistened					
155 °C; 12 h	Starting Materials	Initial Weight	Molar Amount	Equivalents	Product	
	Aluminum Sulfate	0.2023 g	0.30 mmol	1 eq	Yield	0.0706 g (56 %)
	Isophthalic Acid	0.0515 g	0.31 mmol	1 eq		
	N,N-Dimethylformamide	0.4 ml	-	-	Surface	8 m <sup>2</sup> /g
	Water	1.6 ml	-	-		
155 °C; 12 h	Starting Materials	Initial Weight	Molar Amount	Equivalents	Product	
	Aluminum Sulfate	0.2008 g	0.30 mmol	1 eq	Yield	0.0588 g (47 %)
	Isophthalic Acid	0.0492 g	0.30 mmol	1 eq		
	N,N-Dimethylformamide	0.4 ml	-	-	Surface	15 m <sup>2</sup> /g
	Water	1.6 ml	-	-		
155 °C; 12 h	Starting Materials	Initial Weight	Molar Amount	Equivalents	Product	
	Aluminum Sulfate	0.1999 g	0.30 mmol	1 eq	Yield	0.0565 g (45 %)
	Isophthalic Acid	0.0502 g	0.30 mmol	1 eq		
	N,N-Dimethylformamide	0.4 ml	-	-	Surface	0 m <sup>2</sup> /g
	Water	1.6 ml	-	-		
155 °C; 12 h	Starting Materials	Initial Weight	Molar Amount	Equivalents	Product	
	Aluminum Sulfate	0.2004 g	0.30 mmol	1 eq	Yield	0.0547 g (44 %)
	Isophthalic Acid	0.0505 g	0.30 mmol	1 eq		
	N,N-Dimethylformamide	0.4 ml	-	-	Surface	10 m <sup>2</sup> /g
	Water	1.6 ml	-	-		
Conditions	Moistened					
155 °C; 12 h	Starting Materials	Initial Weight	Molar Amount	Equivalents	Product	
	Aluminum Sulfate	0.2000 g	0.30 mmol	1 eq	Yield	0.0547 g (44 %)
	Isophthalic Acid	0.0484 g	0.29 mmol	1 eq		
	N,N-Dimethylformamide	0.4 ml	-	-	Surface	317 m <sup>2</sup> /g
	Water	1.6 ml	-	-		
155 °C; 12 h	Starting Materials	Initial Weight	Molar Amount	Equivalents	Product	
	Aluminum Sulfate	0.2008 g	0.30 mmol	1 eq	Yield	0.0434 g (35 %)
	Isophthalic Acid	0.0496 g	0.30 mmol	1 eq		
	N,N-Dimethylformamide	0.4 ml	-	-	Surface	497 m <sup>2</sup> /g
	Water	1.6 ml	-	-		
155 °C; 12 h	Starting Materials	Initial Weight	Molar Amount	Equivalents	Product	
	Aluminum Sulfate	0.1998 g	0.30 mmol	1 eq	Yield	0.0093 g (7 %)
	Isophthalic Acid	0.0500 g	0.30 mmol	1 eq		
	N,N-Dimethylformamide	0.4 ml	-	-	Surface	10 m <sup>2</sup> /g
	Water	1.6 ml	-	-		
155 °C; 12 h	Starting Materials	Initial Weight	Molar Amount	Equivalents	Product	
	Aluminum Sulfate	0.2026 g	0.30 mmol	1 eq	Yield	0.0277 g (22 %)
	Isophthalic Acid	0.0500 g	0.30 mmol	1 eq		
	N,N-Dimethylformamide	0.4 ml	-	-	Surface	312 m <sup>2</sup> /g
	Water	1.6 l	-	-		



### S4.3. Dry-gel conversions: Synthesis optimizations -- MIL-160

Table S7. Listing of DGC synthesis conditions for MIL-160 with variation of time and temperature.

MIL-160						
Conditions	Not Moistened					
80 °C; 24 h	Starting Materials	Initial Weight	Molar Amount	Equivalents	Product	
	Aluminium Chloride	0.1391 g	0.58 mmol	1 eq	Yield	0.0313 g (27 %)
	2,5-Furandicarboxylic Acid	0.0899 g	0.58 mmol	1 eq		
	NaOH	0.0230 g	0.58 mmol	1 eq	Surface	264 m <sup>2</sup> /g
	Water	2 ml	-	-		
100 °C; 24 h	Starting Materials	Initial Weight	Molar Amount	Equivalents	Product	
	Aluminium Chloride	0.1927 g	0.80 mmol	1 eq	Yield	0.0416 g (26 %)
	2,5-Furandicarboxylic Acid	0.1242 g	0.80 mmol	1 eq		
	NaOH	0.0326 g	0.82 mmol	1 eq	Surface	57 m <sup>2</sup> /g
	Water	2 ml	-	-		
120 °C; 24 h	Starting Materials	Initial Weight	Molar Amount	Equivalents	Product	
	Aluminium Chloride	0.1439 g	0.60 mmol	1 eq	Yield	0.0162 g (14 %)
	2,5-Furandicarboxylic Acid	0.0929 g	0.60 mmol	1 eq		
	NaOH	0.0238 g	0.60 mmol	1 eq	Surface	101 m <sup>2</sup> /g
	Water	2 ml	-	-		
100 °C; 12 h	Starting Materials	Initial Weight	Molar Amount	Equivalents	Product	
	Aluminium Chloride	0.1465 g	0.61 mmol	1 eq	Yield	0.0227 g (19 %)
	2,5-Furandicarboxylic Acid	0.0947 g	0.61 mmol	1 eq		
	NaOH	0.0243 g	0.61 mmol	1 eq	Surface	394 m <sup>2</sup> /g
	Water	2 ml	-	-		
100 °C; 48 h	Starting Materials	Initial Weight	Molar Amount	Equivalents	Product	
	Aluminium Chloride	0.1395 g	0.58 mmol	1 eq	Yield	0.0237 g (21 %)
	2,5-Furandicarboxylic Acid	0.0902 g	0.58 mmol	1 eq		
	NaOH	0.0232 g	0.58 mmol	1 eq	Surface	119 m <sup>2</sup> /g
	Water	2 ml	-	-		
Conditions	Moistened					
80 °C; 24 h	Starting Materials	Initial Weight	Molar Amount	Equivalents	Product	
	Aluminium Chloride	0.1402 g	0.58 mmol	1 eq	Yield	0.0216 g (19 %)
	2,5-Furandicarboxylic Acid	0.0906 g	0.58 mmol	1 eq		
	NaOH	0.0232 g	0.58 mmol	1 eq	Surface	135 m <sup>2</sup> /g
	Water	1.8 + 0.2 ml	-	-		
100 °C; 24 h	Starting Materials	Initial Weight	Molar Amount	Equivalents	Product	
	Aluminium Chloride	0.1931 g	0.80 mmol	1 eq	Yield	0.0765 g (48 %)
	2,5-Furandicarboxylic Acid	0.1244 g	0.80 mmol	1 eq		
	NaOH	0.0327 g	0.82 mmol	1 eq	Surface	354 m <sup>2</sup> /g
	Water	1.8 + 0.2 ml	-	-		
120 °C; 24 h	Starting Materials	Initial Weight	Molar Amount	Equivalents	Product	
	Aluminium Chloride	0.1444 g	0.60 mmol	1 eq	Yield	0.0902 g (76 %)
	2,5-Furandicarboxylic Acid	0.0933 g	0.60 mmol	1 eq		
	NaOH	0.0239 g	0.60 mmol	1 eq	Surface	402 m <sup>2</sup> /g
	Water	1.8 + 0.2 ml	-	-		
100 °C; 12 h	Starting Materials	Initial Weight	Molar Amount	Equivalents	Product	
	Aluminium Chloride	0.1475 g	0.61 mmol	1 eq	Yield	0.0099 g (7 %)
	2,5-Furandicarboxylic Acid	0.0954 g	0.61 mmol	1 eq		
	NaOH	0.0245 g	0.61 mmol	1 eq	Surface	249 m <sup>2</sup> /g
	Water	1.8 + 0.2 ml	-	-		
100 °C; 48 h	Starting Materials	Initial Weight	Molar Amount	Equivalents	Product	
	Aluminium Chloride	0.1391 g	0.58 mmol	1 eq	Yield	0.0066 g (6 %)
	2,5-Furandicarboxylic Acid	0.0899 g	0.58 mmol	1 eq		
	NaOH	0.0231 g	0.58 mmol	1 eq	Surface	451 m <sup>2</sup> /g
	Water	1.8 + 0.2 ml	-	-		

### S4.3.1. Dry-gel conversions: Synthesis optimizations -- MIL-160 solvent re-use

Table S8. Listing of DGC synthesis conditions for MIL-160 and solvent re-use.

MIL-160						
Conditions	Not Moistened					
100 °C; 24 h	Starting Materials	Initial Weight	Molar Amount	Equivalents	Product	
	Aluminum Chloride	0.0980 g	0.41 mmol	1 eq	Yield	0.0336 g (42 %)
	2,5-Furandicarboxylic Acid	0.0637 g	0.41 mmol	1 eq		
	NaOH	0.0332 g	0.83 mmol	2 eq	Surface	438 m <sup>2</sup> /g
	Water	2 ml	-	-		
100 °C; 24 h	Starting Materials	Initial Weight	Molar Amount	Equivalents	Product	
	Aluminum Chloride	0.0993 g	0.41 mmol	1 eq	Yield	0.0294 g (36 %)
	2,5-Furandicarboxylic Acid	0.0646 g	0.41 mmol	1 eq		
	NaOH	0.0343 g	0.85 mmol	2 eq	Surface	435 m <sup>2</sup> /g
	Water	2 ml	-	-		
100 °C; 24 h	Starting Materials	Initial Weight	Molar Amount	Equivalents	Product	
	Aluminum Chloride	0.1005 g	0.42 mmol	1 eq	Yield	0.0413 g (50 %)
	2,5-Furandicarboxylic Acid	0.0622 g	0.40 mmol	1 eq		
	NaOH	0.0323 g	0.81 mmol	2 eq	Surface	370 m <sup>2</sup> /g
	Water	2 ml	-	-		
100 °C; 24 h	Starting Materials	Initial Weight	Molar Amount	Equivalents	Product	
	Aluminum Chloride	0.0988 g	0.41 mmol	1 eq	Yield	0.0295 g (36 %)
	2,5-Furandicarboxylic Acid	0.0624 g	0.40 mmol	1 eq		
	NaOH	0.0315 g	0.79 mmol	2 eq	Surface	891 m <sup>2</sup> /g
	Water	2 ml	-	-		
Conditions	Moistened					
100 °C; 24 h	Starting Materials	Initial Weight	Molar Amount	Equivalents	Product	
	Aluminum Chloride	0.0966 g	0.40 mmol	1 eq	Yield	0.0302 g (38 %)
	2,5-Furandicarboxylic Acid	0.0614 g	0.40 mmol	1 eq		
	NaOH	0.0337 g	0.84 mmol	2 eq	Surface	995 m <sup>2</sup> /g
	Water	1.8 + 0.2 ml	-	-		
100 °C; 24 h	Starting Materials	Initial Weight	Molar Amount	Equivalents	Product	
	Aluminum Chloride	0.0987 g	0.41 mmol	1 eq	Yield	0.0244 g (30 %)
	2,5-Furandicarboxylic Acid	0.0659 g	0.42 mmol	1 eq		
	NaOH	0.0333 g	0.83 mmol	2 eq	Surface	968 m <sup>2</sup> /g
	Water	1.8 + 0.2 ml	-	-		
100 °C; 24 h	Starting Materials	Initial Weight	Molar Amount	Equivalents	Product	
	Aluminum Chloride	0.1010 g	0.42 mmol	1 eq	Yield	0.0379 g (46 %)
	2,5-Furandicarboxylic Acid	0.0625 g	0.40 mmol	1 eq		
	NaOH	0.0344 g	0.86 mmol	2 eq	Surface	1180 m <sup>2</sup> /g
	Water	1.8 + 0.2 ml	-	-		
100 °C; 24 h	Starting Materials	Initial Weight	Molar Amount	Equivalents	Product	
	Aluminum Chloride	0.0989 g	0.41 mmol	1 eq	Yield	0.0177 g (22 %)
	2,5-Furandicarboxylic Acid	0.0631 g	0.40 mmol	1 eq		
	NaOH	0.0321 g	0.80 mmol	2 eq	Surface	980 m <sup>2</sup> /g
	Water	1.8 + 0.2 ml	-	-		

### S5. Solvent re-use for Alfum, CAU-10-H and MIL-160

We carried out solvent re-use experiments over four repeated DGC runs with the same solvent and fresh reactant mixture on the sieve at the head of the DGC autoclave (*cf.* Figure S1).

The details and results of these solvent re-use experiments are summarized in Table S3, S5, S6 and S8 for Alfum, CAU-10-H and MIL-160, respectively.

Figure S5-S8 graphically depict the results of solvent re-use with respect to BET surface area and yield.

#### Alfum

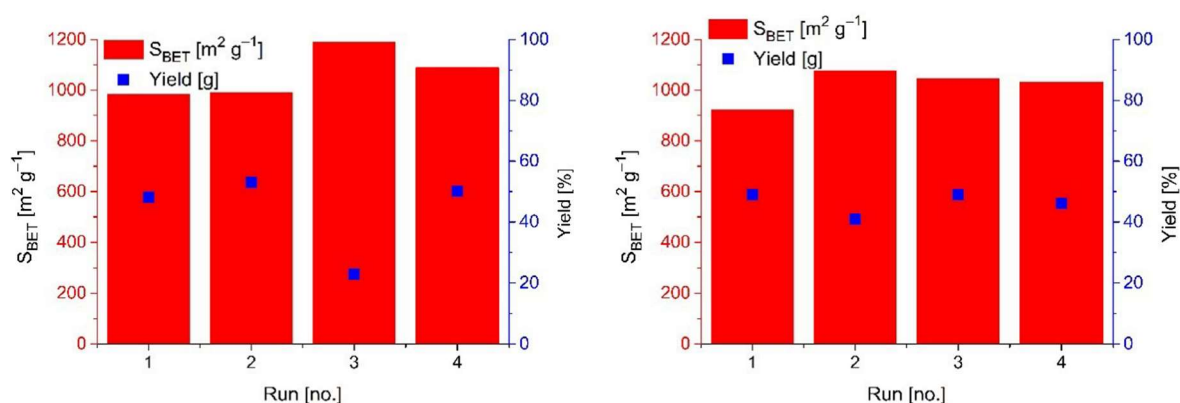


**Figure S5** Solvent re-use over four DGC runs for Alfum, with BET surface area (red bars) and yields (blue squares). Left: wetted precursor mixture, right: dry precursor mixture. Minor yields, e.g. 20% in run 3, due to washing off/falling down of the product during handling of the DGC setup.

#### CAU-10-H, repetition with wetting of neat DMF

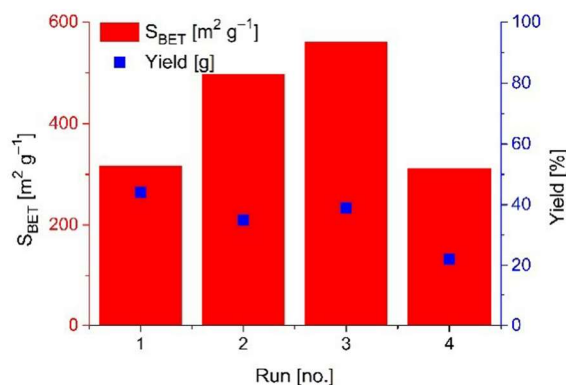


**Figure S6** Solvent re-use over four DGC runs for CAU-10-H, with BET surface area (red bars) and yields (blue boxes). A wetted (neat DMF) precursor mixture was used. Minor yields, due to washing off/falling down of the product during handling of the DGC setup.

## MIL-160

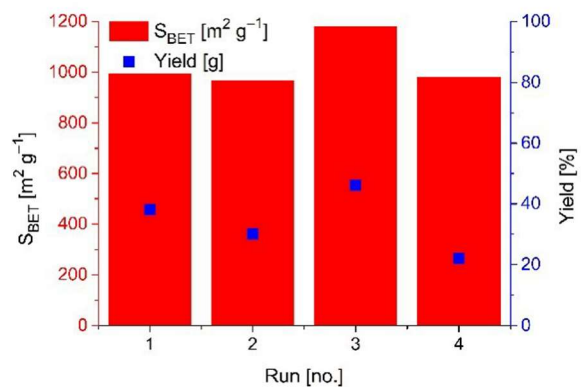


**Figure S7** Solvent re-use over four DGC runs for MIL-160, with BET surface area (red bars) and yields (blue boxes). A wetted precursor mixture was used. Minor yields, due to washing off/falling down of the product during handling of the DGC setup.

## S6. PXRD measurements

Crystallinity was proven with powder X-ray diffractometry (PXRD), using a *Bruker D2 Phaser* diffractometer with a flat silicon, low background sample holder and Cu-K $\alpha$  radiation ( $\lambda = 1.54184 \text{ \AA}$ ) at 30 kV and  $0.04^\circ \text{ s}^{-1}$  in the  $2\theta = 5\text{--}50^\circ$  range.

Figure S8-S12 depict PXRD patterns of all obtained samples Alfum, CAU-10-H and MIL-160 samples within solvent re-use in comparison with each simulated pattern.

### Alfum

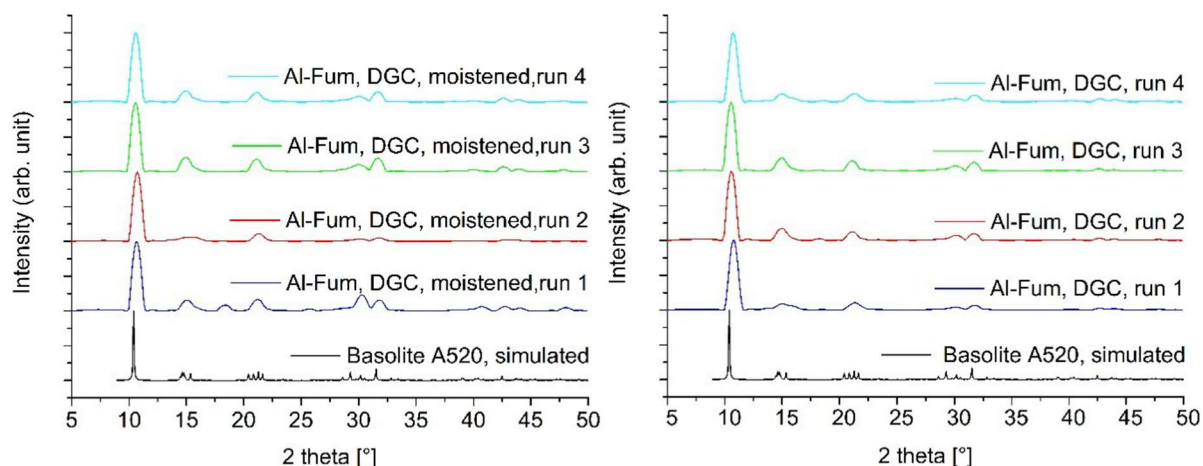


**Figure S8** PXRD patterns of Alfum samples obtained by synthesis runs with solvent re-use, in comparison with simulated pattern (CDS-Refcode DOYBEA).<sup>4</sup> Left: wetted precursor mixture, right: dry precursors. Figure 1 in the main manuscript shows a comparison with the industrial benchmark Basolite A520.

### CAU-10-H, repetition with wetting of neat DMF

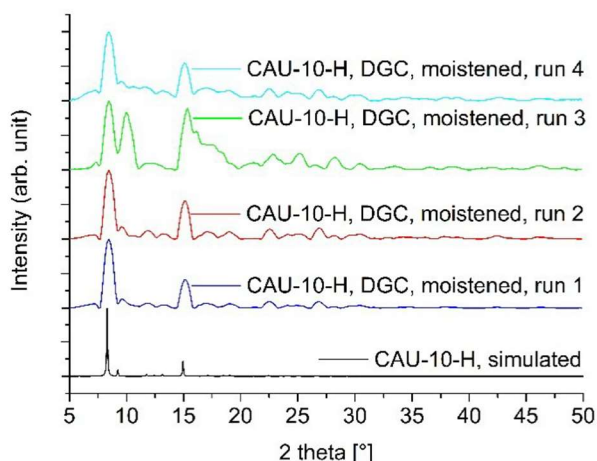


**Figure S9** PXRD patterns of aluminum CAU-10-H samples obtained by synthesis runs with solvent re-use, in comparison with simulated pattern (CCDC CSD-Refcode QQOBUT).<sup>25</sup> A wetted (neat DMF) precursor mixture was used.



## MIL-160

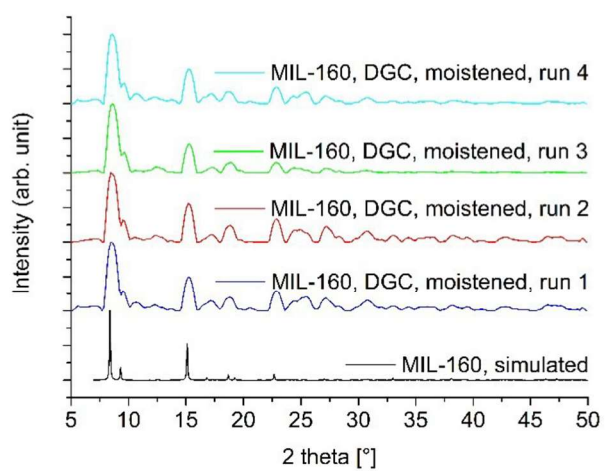


**Figure S10** PXRD patterns of MIL-160 samples obtained by synthesis runs with solvent re-use, in comparison with simulated pattern (CCDC PIBZOS).<sup>40</sup> A wetted precursor mixture was used.

## **S7. Thermogravimetric Analysis (TGA)**

Exemplarily, we performed thermogravimetric analyses (TGA) of samples obtained *via* DGC of each of the presented MOFs. Figure S11-S15 depict TGA curves of Alfum, CAU-10-H and MIL-160 samples.

### **Alfum**

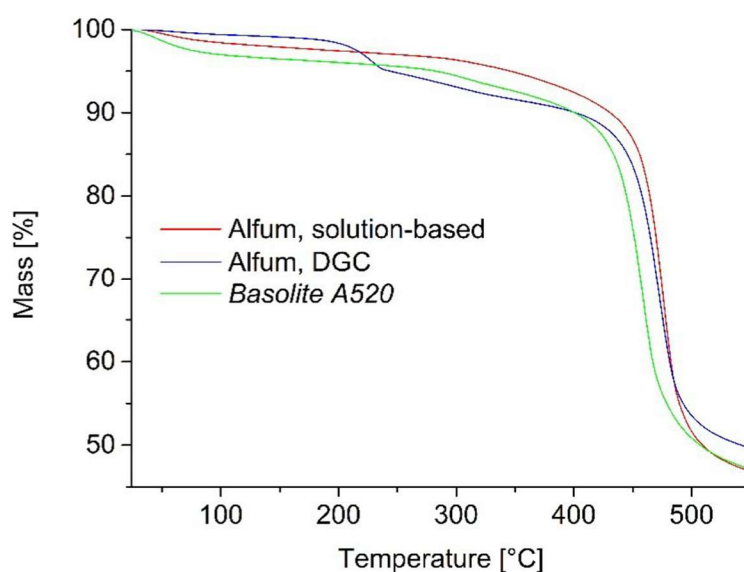


**Figure S11** TG curve of Alfum samples from DGC (blue) and from solution-based synthesis (red) in comparison with industrial benchmark *Basolite A520*.

### **CAU-10-H**

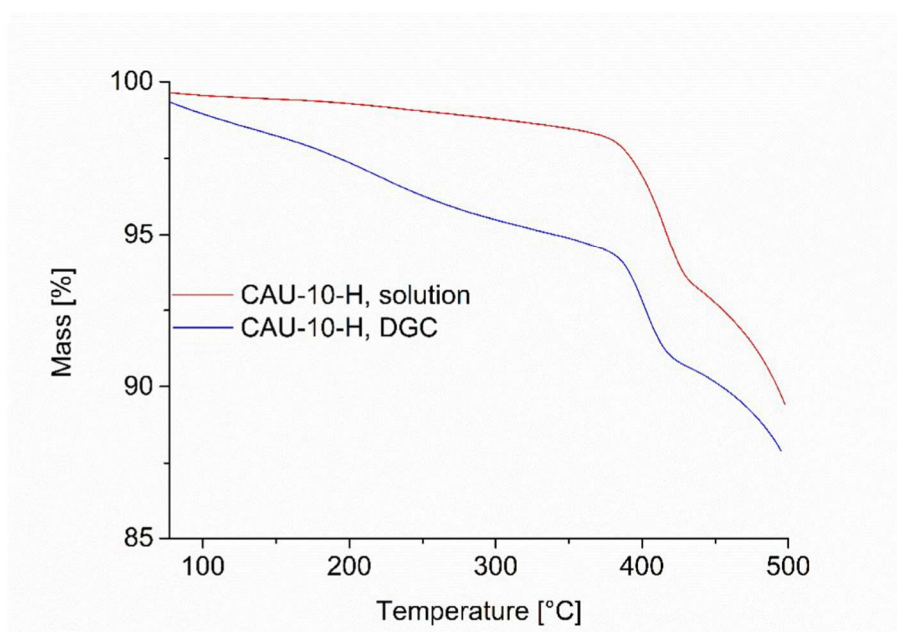


**Figure S12** TG curve of CAU-10-H samples from DGC (blue) and from solution-based synthesis (red).

## MIL-160

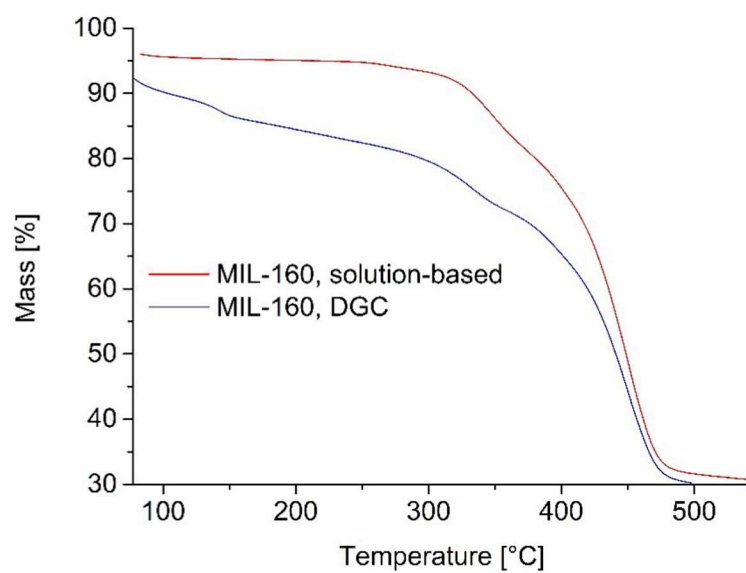


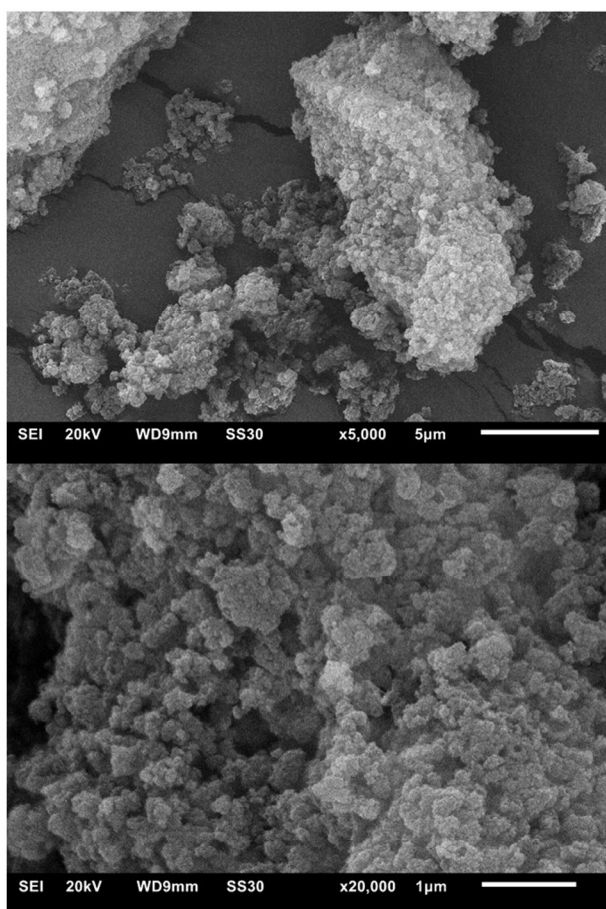
**Figure S13** TG curve of MIL-160 samples from DGC (blue) and from solution-based synthesis (red).

### **S8. Scanning electron microscopy (SEM)**

For control of morphology we recorded SEM images using a *JEOL JSM-6510 advanced electron microscope* with a  $\text{LaB}_6$  cathode at 20 keV.

Figure S14-S18 exemplarily depict SEM images of selected samples of the three presented MOFs.

#### **Alfum**



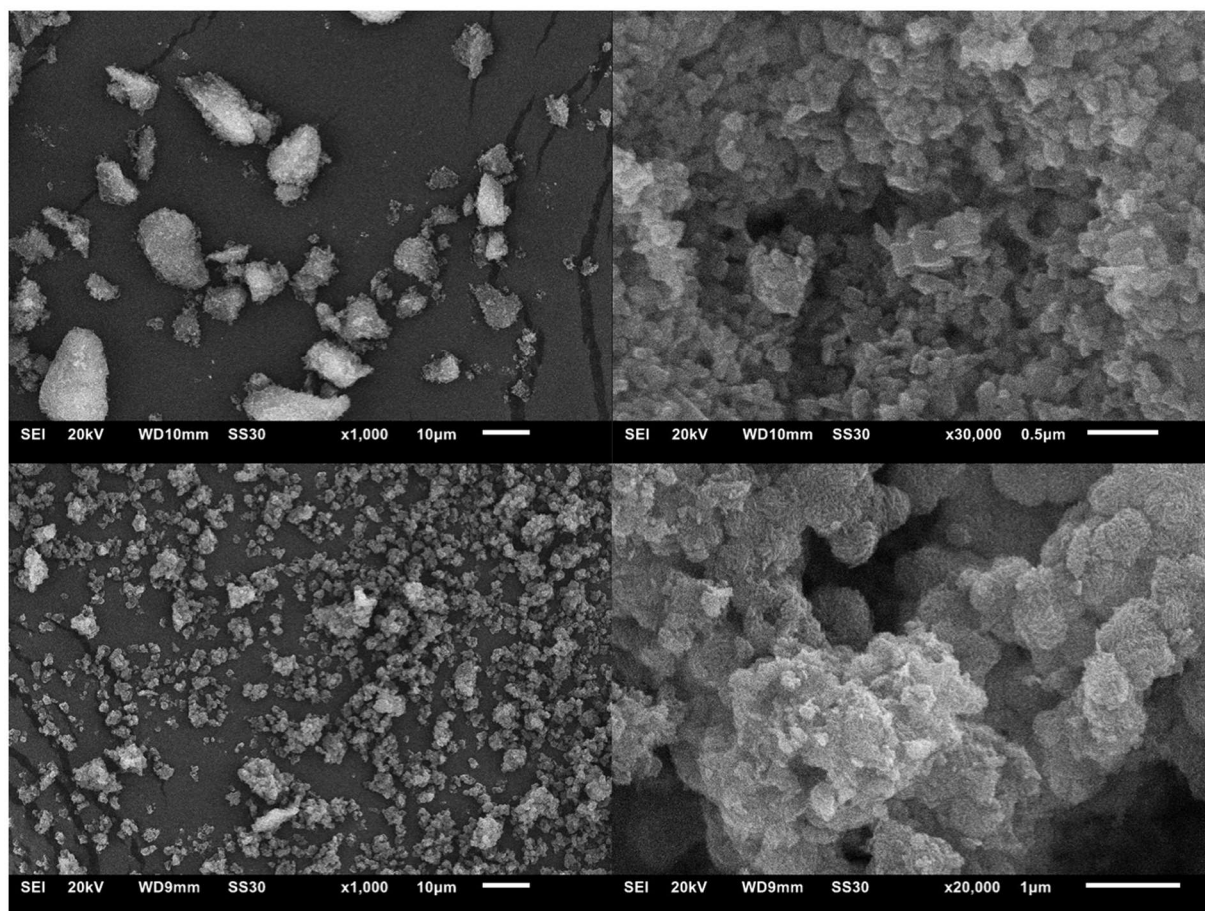


**Figure S14** SEM images of different AlFum samples at different magnifications (left: overview, right: close-up). Top: Basolite A520. Middle: AlFum from DGC. Bottom: AlFum from solution-based synthesis



## CAU-10-H

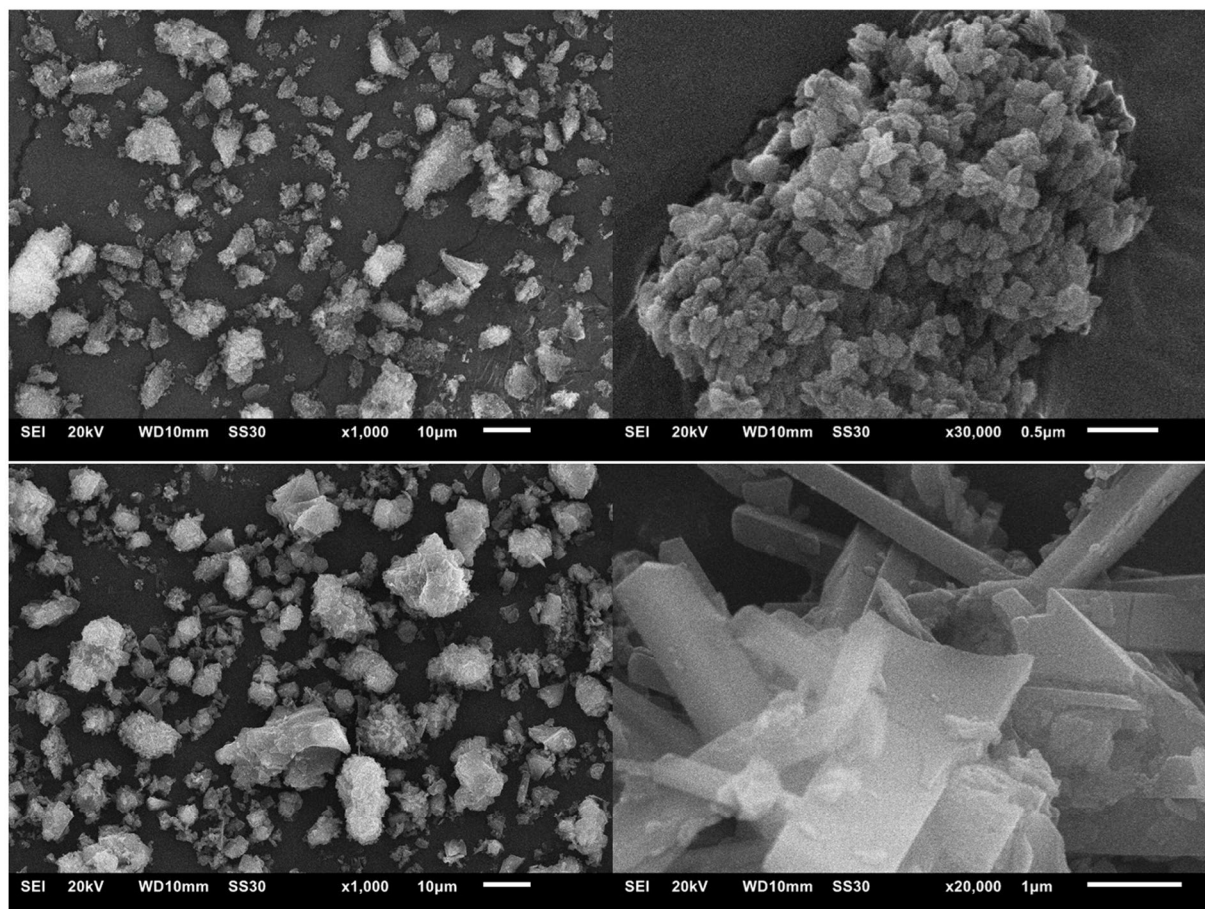


**Figure S15** SEM images of different CAU-10-H samples at different magnifications (left: overview, right: close-up). Top: CAU-10-H from DGC. Bottom: CAU-10-H from solution-based synthesis.

## MIL-160

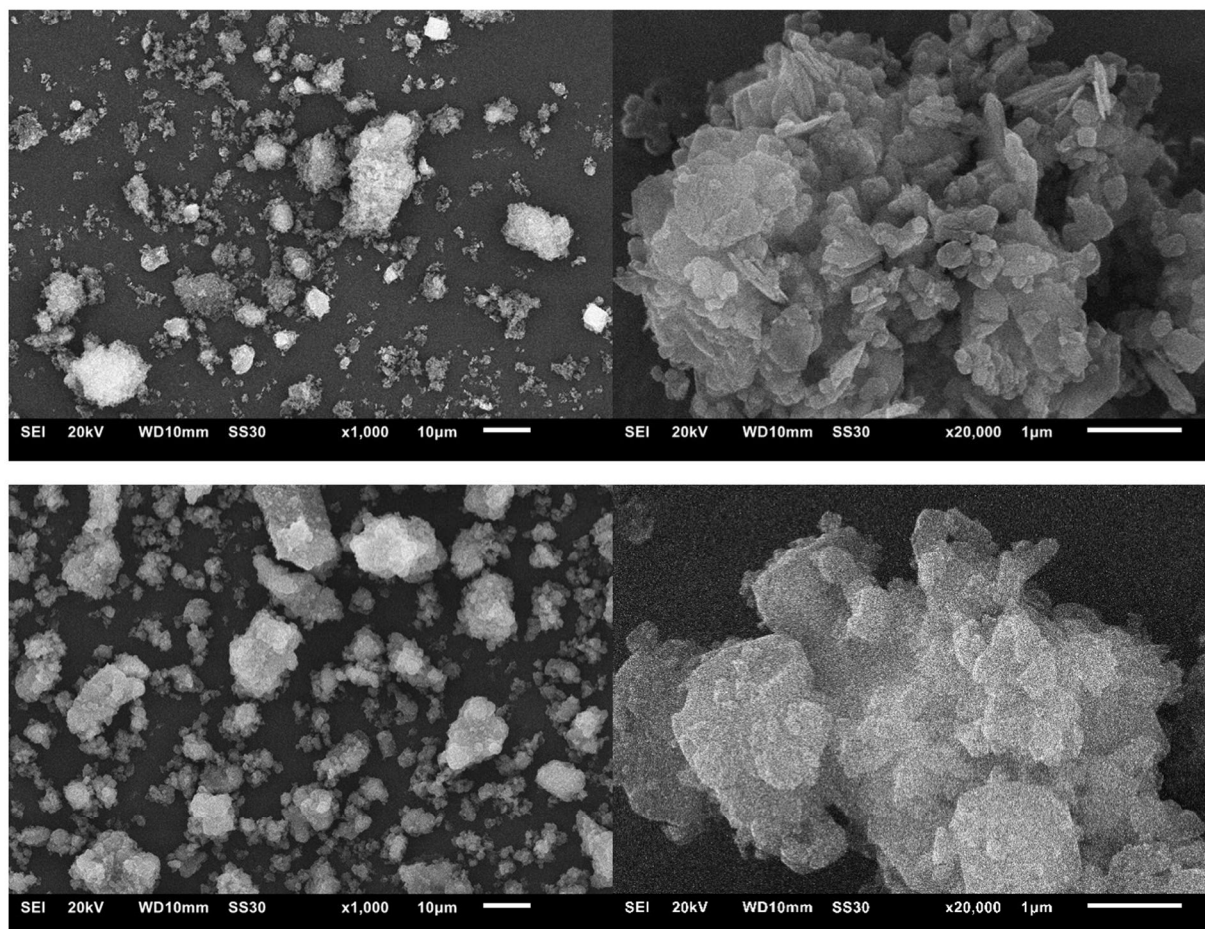


**Figure S16** SEM images of MIL-160 samples at different magnifications (left: overview, right: close-up). Top: MIL-160 from DGC. Bottom: MIL-160 from solution-based synthesis.

### S9. Nitrogen sorption experiments solvent re-use (T = 77 K)

Surface areas (BET) were determined by nitrogen (purity 99.999%) sorption experiments at 77.35 K using a *Quantachrome NOVA-4000e* instrument within a partial pressure range of  $pp_0^{-1} = 10^{-3}$ -1 bar. Each sample was degassed under vacuum ( $< 10^{-2}$  mbar) at 100 °C (MIL-100(Fe)), respectively 150 °C (Alfum) for *ca.* 3 h, prior to measurement. All surface areas (BET) were calculated from five adsorption points in the pressure range  $pp_0^{-1} = 0.009$  - 0.041 bar for samples of Alfum,  $pp_0^{-1} = 0.004$  - 0.125 bar for samples of CAU-10-H and  $pp_0^{-1} = 0.014$  - 0.052 bar for samples of MIL-160. This range is indeed not recommended by IUPAC (International Union of Pure and Applied Chemistry) for BET surface determination, but rather suitable for microporous materials.<sup>47</sup>

Figure S17-S19 depict the nitrogen sorption isotherms of all obtained MOF samples during DGCs with solvent re-use over four DGC runs.

#### Aluminum fumarate

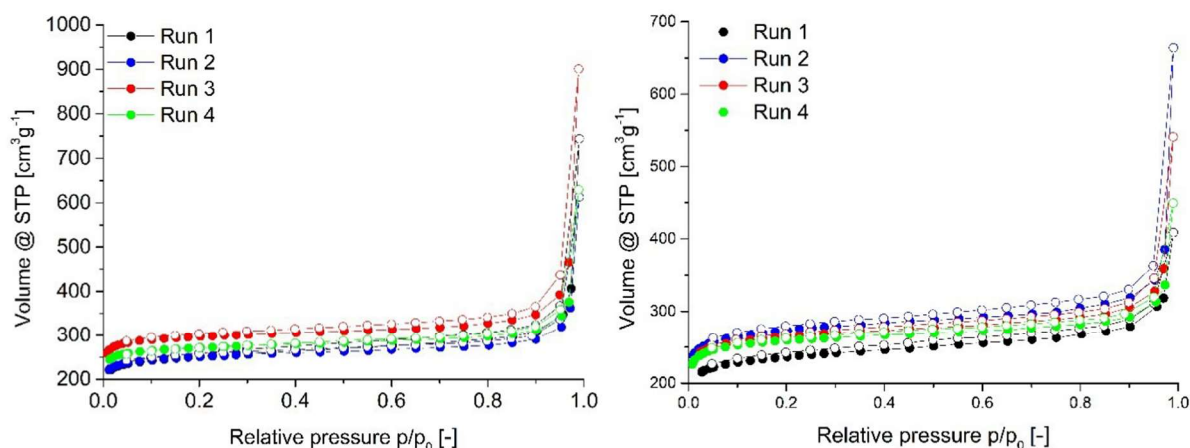


**Figure S17** Nitrogen sorption (77 K) isotherms of aluminum fumarate samples obtained by synthesis runs with solvent re-use. Left: wetted precursor mixture, right: dry precursor mixture.

#### CAU-10-H, repetition with wetting of neat DMF

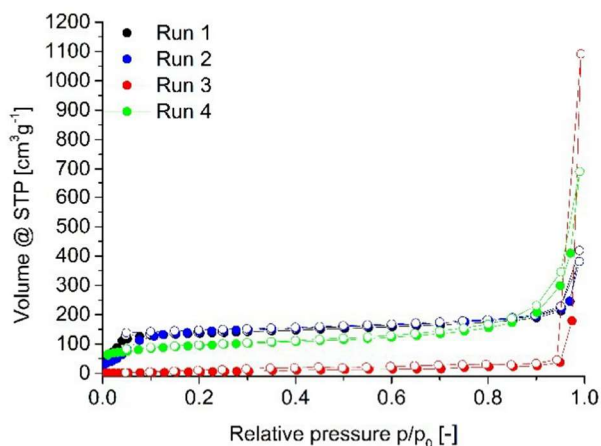


**Figure S18** Nitrogen sorption (77 K) isotherms of CAU-10-H samples obtained by synthesis runs with solvent re-use. A wetted (neat DMF) precursor mixture was used.

## MIL-160

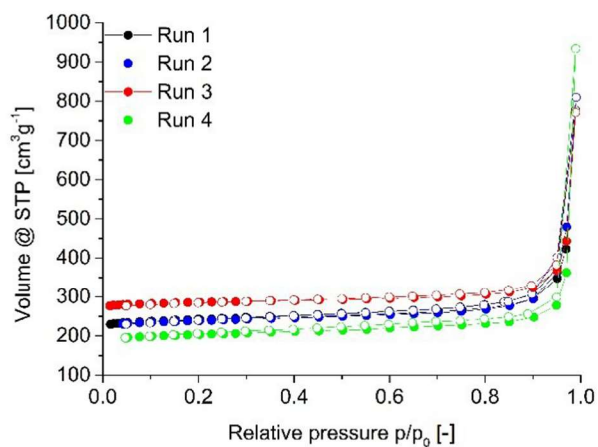


**Figure S19** Nitrogen sorption (77 K) isotherms of MIL-160 samples obtained by synthesis runs with solvent re-use. A wetted (neat DMF) precursor mixture was used.

Table S9 summarizes repeated N<sub>2</sub> sorption results of the industrial benchmark *Basolite A520* using the same batch, but not the same sample.

**Table S9** Repeated determination of BET areas of *Basolite A520* using nitrogen sorption ( $T = 77$  K).

Benchmark	No. of measurement	BET [m <sup>2</sup> g <sup>-1</sup> ]
<i>Basolite A520</i>	1	1030
	2	1038
	3	999
	4	1040
	5	1026



### S10. Water sorption experiments (T = 20 °C)

Water sorption experiments were carried out on a *Quantachrome VStar4* (QUANTACHROME, Odelzhausen, Germany) instrument within a partial pressure range of  $p/p_0 = 10^{-3}$ -1 bar. Each sample was degassed under vacuum ( $< 10^{-3}$  mbar) at 150 °C for *ca.* 3 h prior to measurement, using a *FloVac* (QUANTACHROME, Odelzhausen, Germany) degasser.

All water sorption isotherms are depicted in Figures 2c) ,3c),4c) in the main manuscript.

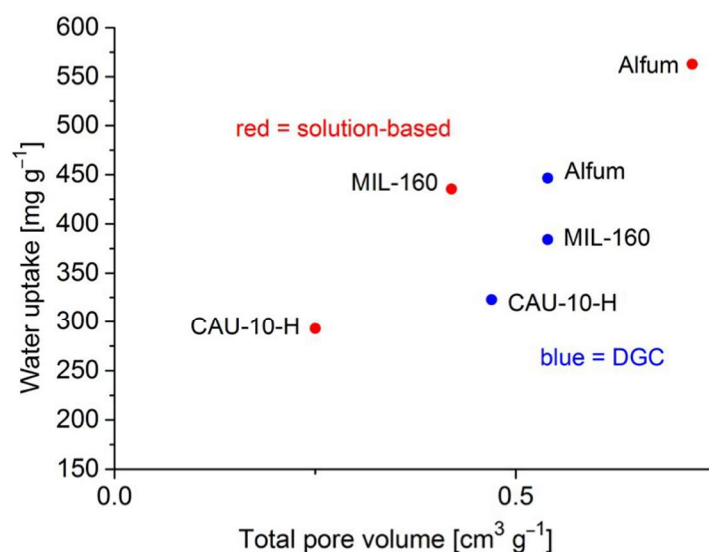


**Fig. S20** Water uptake (at  $p/p_0 = 0.95$ ) versus the total pore volume (at  $p/p_0 = 0.95$ ) for solution and DGC samples.

**Table S10** Microporosity characteristics for solution and DGC samples from V-t-plot method.

Sample	Micropore surface area [m <sup>2</sup> g <sup>-1</sup> ]	External and mesopore surface area [m <sup>2</sup> g <sup>-1</sup> ]	Micropore volume [cm <sup>3</sup> g <sup>-1</sup> ]
Alfum solution-based	1112	141	0.427
DGC	941	104	0.367
CAU-10-H solution-based	378	192	0.089
DGC	437	129	0.173
MIL-160 solution-based	1067	30	0.403
DGC	899	81	0.279



## S11. References

- <sup>1</sup> E. Leung, U. Müller, N. Trukhan, H. Mattenheimer, G. Cox and S. Blei, *Process for preparing porous metal-organic frameworks based on aluminum fumarate*, U.S. Patent No. 8,524,932, BASF SE, 3 Sep. 2013.
- <sup>2</sup> C. Kiener, U. Müller, and M. Schubert, *Method of using a metal organic frameworks based on aluminum fumarate*, U.S. Patent No. 8,518,264, BASF SE, 27 Aug. 2013.
- <sup>3</sup> K. Brandenburg, Diamond 4.3.1, Crystal and Molecular Structure Visualization, Crystal Impact - K. Brandenburg & H. Putz GbR, Bonn, Germany, 2009.
- <sup>4</sup> E. Alvarez, N. Guillou, C. Martineau, B. Bueken, B. Van de Voorde, C. Le Guillouzer, P. Fabry, F. Nouar, F. Taulelle, D. de Vos, J.-S. Chang, K. H. Cho, N. Ramsahye, T. Devic, M. Daturi, G. Maurin and C. Serre, *Angew. Chem. Int. Ed.*, 2015, **54**, 3664-3668.
- <sup>5</sup> T. Loiseau, C. Volkringer, M. Haouas, F. Taulelle and G. Férey, *C. R. Chim.* 2015, **18**, 1350-1369.
- <sup>6</sup> L. Zhou, X. Zhang and Y. Chen, *Mater. Lett.*, 2017, **197**, 224-227.
- <sup>7</sup> E. Elsayed, R. Al-Dadah, S. Mahmoud, P. A. Anderson, A. Elsayed and P. G. Youssef, *Desalination*, 2017, **406**, 25-36.
- <sup>8</sup> M. Rubio-Martinez, T. D. Hadley, M. P. Batten, K. Constanti-Carey, T. Barton, D. Marley, A. Mönch, K.-S. Lim and M. R. Hill, *ChemSusChem*, 2016, **9**, 938-941.
- <sup>9</sup> D. E. Crawford and J. Casaban, *Adv. Mater.*, 2016, **28**, 5747-5754.
- <sup>10</sup> D. Crawford, J. Casaban, R. Haydon, N. Giri, T. McNally and S. L. James, *Chem. Sci.*, 2015, **6**, 1645-1649.
- <sup>11</sup> M. Rubio-Martinez, C. Avci-Camur, A. W. Thornton, I. Imaz, D. Maspoch, M. R. Hill, *Chem. Soc. Rev.* **2017**, **46**, 3453–3480.
- <sup>12</sup> N. Tannert, S. Gökpınar, E. Hastürk, S. Nießing and C. Janiak, *Dalton Trans.*, 2018, **47**, 9850-9860.
- <sup>13</sup> B. Yilmaz, N. Trukhan and U. Müller, *Chin. J. Catal.*, 2012, **33**, 3-10.
- <sup>14</sup> F. Jeremias, D. Fröhlich, C. Janiak and S. K. Henninger, *RSC Adv.*, 2014, **4**, 24073-24082.
- <sup>15</sup> J. Chen, K. Shen and Y. Li, *ChemSusChem*, 2017, **10**, 3165-3187.
- <sup>16</sup> M. Gaab, N. Trukhan, S. Maurer, R. Gummaraju and U. Müller, *Micropor. Mesopor. Mater.*, 2012, **157**, 131-136.
- <sup>17</sup> S. K. Henninger, S.-J. Ernst, L. Gordeeva, P. Bendix, D. Fröhlich, A. D. Grekova, L. Bonaccorsi, Y. Aristov and J. Jaenchen, *Renew. Energ.*, 2017, **110**, 59-69.
- <sup>18</sup> S. Karmakar, J. Dechnik, C. Janiak and S. De, *J. Hazard. Mater.*, 2016, **303**, 10-20.
- <sup>19</sup> S. Karmakar, S. Bhattacharjee and S. De, *J. Env. Chem. Eng.*, 2017, **5**, 6087-6097.
- <sup>20</sup> P. G. Yot, L. Vanduyfhuys, E. Alvarez, J. Rodriguez, J.-P. Itié, P. Fabry, N. Guillou, T. Devic, I. Beurroies, P. L. Llewellyn, V. Van Speybroek, C. Serre and G. Maurin, *Chem. Sci.*, 2016, **7**, 446-450.
- <sup>21</sup> H. W. B. Teo, A. Chakraborty and S. Kayal, *Micropor. Mesopor. Mater.*, 2018, **272**, 109-116.
- <sup>22</sup> T. Splith, D. Fröhlich, S. K. Henninger and F. Stallmach, *J. Magn. Reson.*, 2018, **291**, 40-46.
- <sup>23</sup> H. W. B. Teo, A. Chakraborty, Y. Kitagawa and S. Kayal, *Int. J. Heat Mass Tran.*, 2017, **114**, 621-629.
- <sup>24</sup> H. Reinsch, M. A. van der Veen, B. Gil, B. Marszalek, T. Verbiest, D. de Vos and N. Stock, *Chem. Mater.*, 2012, **25**, 17-26.
- <sup>25</sup> D. Fröhlich, E. Pantatosaki, P. D. Kolokathis, K. Markey, H. Reinsch, M. Baumgartner, M. A. van der Veen, D. E. de Vos, N. Stock, G. K. Papadopoulos, S. K. Henninger and C. Janiak, *J. Mater. Chem. A*, 2016, **4**, 11859-11869.
- <sup>26</sup> H. Reinsch, M. Krüger, J. Wack, J. Senker, F. Salles, G. Maurin and N. Stock, *Micropor. Mesopor. Mater.*, 2012, **157**, 50-55.
- <sup>27</sup> A. Cadiau, J. S. Lee, D. D. Borges, P. Fabry, T. Devic, M. T. Wharmby, C. Martineau, D. Foucher, F. Taulelle, C.-H. Jun, Y. K. Hwang, N. Stock, M. F. De Lange, F. Kapteijn, J. Gascon, G. Maurin, J.-S. Chang and C. Serre, *Adv. Mater.*, 2015, **27**, 4775-4780.
- <sup>28</sup> D. D. Borges, G. Maurin and D. S. Galvao, *MRS Adv.*, 2017, **2**, 519-524.
- <sup>29</sup> M. F. de Lange, C. P. Ottevanger, M. Wiegmann, T. J. H. Vlugt, J. Gascon and F. Kapteijn, *CrystEngComm*, 2015, **17**, 281-285.
- <sup>30</sup> H. Reinsch, S. Waitschat and N. Stock, *Dalton Trans.*, 2013, **42**, 4840-4847.

- 
- <sup>31</sup> A. Weiss, N. Reimer, N. Stock, M. Tiemann and T. Wagner, *Micropor. Mesopor. Mater.*, 2016, **220**, 39-43.
- <sup>32</sup> N. Reimer, B. Bueken, S. Leubner, C. Seidler, M. Wark, D. De Vos and N. Stock, *Chem. Eur. J.*, 2015, **21**, 12517-12524.
- <sup>33</sup> M. F. de Lange, T. Zeng, T. J. H. Vlught, J. Gascon and F. Kapteijn, *CrystEngComm*, 2015, **17**, 5911-5920.
- <sup>34</sup> R. J. Sheehan, *Ullmann's Encyclopedia of Industrial Chemistry*, Wiley-VCH Verlag GmbH & Co., Weinheim, Germany 2000.
- <sup>35</sup> D. Fröhlich, S. K. Henninger and C. Janiak, *Dalton Trans.*, 2014, **43**, 15300-15304.
- <sup>36</sup> M. Goldsworthy, *Micropor. Mesopor. Mater.*, 2014, **196**, 59-67.
- <sup>37</sup> A. Cadiou, J. S. Lee, D. Damasceno Borges, P. Fabry, T. Devic, M. T. Wharmby, C. Martineau, D. Foucher, F. Taulelle, C.-H. Jun et al., *Adv. Mater.* **2015**, **27**, 4775-4780.
- <sup>38</sup> H. Kummer, F. Jeremias, A. Warlo, G. Földner, D. Fröhlich, C. Janiak, R. Gläser and S. K. Henninger, *Ind. Eng. Chem. Res.*, 2017, **56**, 8393-8398.
- <sup>39</sup> A. D. Wiersum, C. Giovannangeli, D. Vincent, E. Bloch, H. Reinsch, N. Stock, J. S. Lee, J.-S. Chang and P. L. Llewellyn, *ACS Comb. Sci.*, 2013, **2**, 111-119.
- <sup>40</sup> M. Wahiduzzaman, D. Lenzen, G. Maurin, N. Stock and M. T. Wharmby, *Eur. J. Inorg. Chem.*, 2018, 3626-3632.
- <sup>41</sup> A. Permyakova, O. Skrylnyk, E. Courbon, M. Affran, S. Wang, U.-H. Lee, A. H. Valekar, F. Nouar, G. Mouchaham, T. Devic, G. De Weireld, J.-S. Chang, N. Steunou, M. Frère and C. Serre, *ChemSusChem*, 2017, **10**, 1419-1426.
- <sup>42</sup> <http://avantium.com/yxy/yxy-technology.html>; accessed 01.08.2017, 01:54 h.
- <sup>43</sup> Press releases: 'Synvina: Jointventure of BASF and Avantium established', 2016.
- <sup>44</sup> S. K. Henninger, H. A. Habib and C. Janiak, *J. Am. Chem. Soc.*, 2009, **131**, 2776-2777.
- <sup>45</sup> S. K. Henninger, F. P. Schmidt and H.-M. Henning, *Appl. Therm. Eng.*, 2010, **30**, 1692-1702.
- <sup>46</sup> S. K. Henninger, F. Jeremias, H. Kummer, P. Schossig and H.-M. Henning, *Energy Proc.*, 2012, **30**, 279-288.
- <sup>47</sup> M. Thommes, K. Kaneko, A. V. Neimark, J. P. Olivier, F. Rodriguez-Reinoso, J. Rouquerol and K. S. Sing, *Pure Appl. Chem.*, 2015, **87**, 1051-1069.

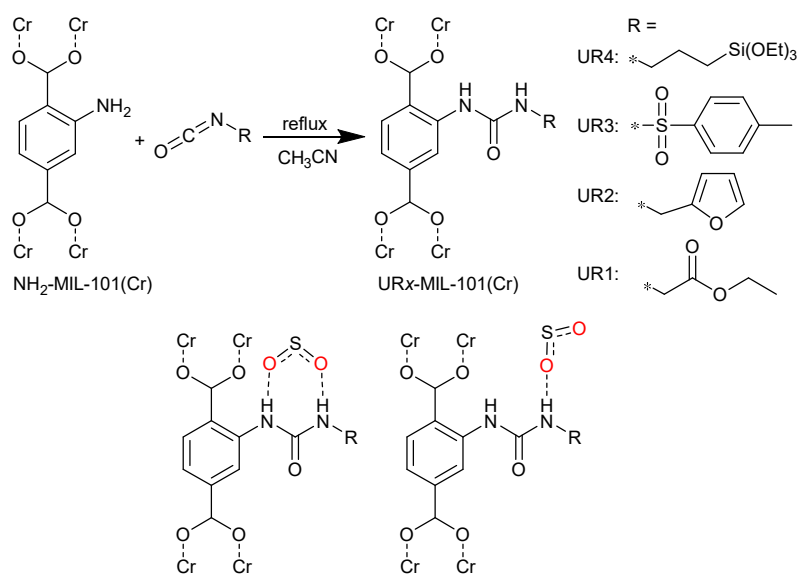
### 3.4. A Series of New Urea-MOFs Obtained *via* Post-synthetic Modification of NH<sub>2</sub>-MIL-101(Cr): SO<sub>2</sub>, CO<sub>2</sub> and H<sub>2</sub>O Sorption

N. Tannert, Y. Sun, E. Hastürk, S. Nießing and C. Janiak

*Z. Anorg. Allg. Chem.*, 2021, **647**, 1124-1130.

DOI: 10.1002/zaac.202100023

Impact factor 2020: 1.240



Author's contribution of work:

- Syntheses and PSMs, including reproduction of all PSMs.
- All analytical characterizations except for SEM images (done by S. Nießing), SO<sub>2</sub> sorption experiments (with E. Hastürk) and three cycles SO<sub>2</sub> of MIL-101(Cr) (done by Y. Sun).
- Writing of the manuscript and drawing of the figures, graphs, and tables.
- Editing of the manuscript regarding the reviewers' comments with C. Janiak.

Reproduced by permission of The Royal Society of Chemistry.

The following literature contribution describes post-synthetic modifications of the MOF NH<sub>2</sub>-MIL-101(Cr) by conversion of the amino-functionality with four different isocyanates into the corresponding urea-MOFs respectively. The four isocyanates employed were ethyl isocyanatoacetate, furfuryl isocyanate, *p*-toluenesulfonyl isocyanate and 3-(triethoxysilyl)propyl isocyanate. The obtained MOF substrates had not been described in the literature before, hence, all four of them can be regarded as novel MOFs. The investigation of their porosity by nitrogen sorption revealed the expectedly lower BET surface areas and slightly decreased crystallinities. Surprisingly, the degree of functionalization (determined by digestion <sup>1</sup>H-NMR spectroscopic investigations) varied with each synthetic conversion (in the range from 18–83%), ultimately leading to varying sorption properties for the adsorptives SO<sub>2</sub>, CO<sub>2</sub> and H<sub>2</sub>O. The four urea-MOFs performed individually regarding the sorption capacities of the named adsorptives and always in dependency of porosities. Nevertheless, the capacities varied even more in dependency of the specific interactions between the integrated functionality attached to the urea and the adsorptive. In specific, the strikingly high uptake of UR3-MIL-101(Cr) for SO<sub>2</sub> (823 cm<sup>3</sup> g<sup>-1</sup> at 0.9 bar and 273 K) was attributed to the introduced sulfonyl groups which are then available for the important SO<sub>2</sub>⋯SO<sub>2</sub> host-guest dipole-dipole interactions. The other capacities for SO<sub>2</sub> at 0.9 bar and 273 K were 218 cm<sup>3</sup> for UR1-, 194 cm<sup>3</sup> for UR2- and 331 cm<sup>3</sup> for UR4-MIL101(Cr), while parental NH<sub>2</sub>-MIL-101(Cr) exhibited 190 cm<sup>3</sup> SO<sub>2</sub> uptake.

In conclusion, the PSM of NH<sub>2</sub>-MIL-101(Cr) with isocyanates led to four new urea-MOFs with decreased porosities compared to the parental NH<sub>2</sub>-MIL-101(Cr) on the one hand. However, at the same time all four urea-MOFs showed increased sorption capacities for SO<sub>2</sub>. In particular, the introduction of sulfonyl groups with the reaction of *p*-toluenesulfonyl isocyanate to yield the derivative UR3-MIL-10(Cr) strongly enhanced the SO<sub>2</sub> adsorption capacity. Noteworthy, the MOF UR3-MIL-101(Cr) outperforms nearly all MOFs in the current literature with its significantly higher uptake of SO<sub>2</sub> (823 cm<sup>3</sup> g<sup>-1</sup> at 0.9 bar and 273 K).

Consequently, it could be demonstrated that the incorporation of sulfonyl moieties into highly porous substrates can be an effective strategy to increase SO<sub>2</sub> sorption capacity.

# A Series of new Urea-MOFs Obtained via Post-synthetic Modification of NH<sub>2</sub>-MIL-101(Cr): SO<sub>2</sub>, CO<sub>2</sub> and H<sub>2</sub>O Sorption

Niels Tannert,<sup>[a]</sup> Yangyang Sun,<sup>[a]</sup> Emrah Hastürk,<sup>[a]</sup> Sandra Nießing,<sup>[a]</sup> and Christoph Janiak<sup>\*,[a]</sup>

*Dedicated to Prof. Dr. Thomas Klapötke on the occasion of his 60th birthday*

The amino group in the MOF NH<sub>2</sub>-MIL-101(Cr) was post-synthetically converted into urea-groups partially using either ethyl isocyanatoacetate, furfuryl isocyanate, *p*-toluenesulfonyl isocyanate or 3-(triethoxysilyl)propyl isocyanate in acetonitrile. The derived four novel urea-MOFs exhibit the expected lower BET surface areas and pore volumes than MIL-101(Cr) and NH<sub>2</sub>-MIL-101(Cr) MOFs but the partially *p*-toluenesulfonyl-urea-modified MOF exhibits an outstanding SO<sub>2</sub> adsorption capacity

of 823 cm<sup>3</sup> g<sup>-1</sup> (corresponding to 36.7 mmol g<sup>-1</sup> or 70 wt.% at T = 0 °C and 0.9 bar), which is the second highest SO<sub>2</sub> uptake of any known material today – surprisingly even better than for highly porous MIL-101(Cr) with an uptake of 645 cm<sup>3</sup> g<sup>-1</sup> SO<sub>2</sub> under the same conditions. The high uptake is linked to the favorable dipole interactions of SO<sub>2</sub> with the sulfonyl group of the *p*-toluenesulfonyl-modified MOF.

## Introduction

Sulfur dioxide (SO<sub>2</sub>) is an invisible gas with sharp smell, good solubility in water and high toxicity. Although the atmospheric concentration of SO<sub>2</sub> is only roughly 1 ppm,<sup>[1]</sup> once in the atmosphere, its end products (e.g. sulfuric acid, H<sub>2</sub>SO<sub>4</sub>) and SO<sub>2</sub> itself pose a threat to vegetation, aquatic life and humans, mostly through photochemical smog and acid rain. The anthropogenic emission of SO<sub>2</sub> was estimated to be 24.4 Mt in 2010 in China only,<sup>[2]</sup> with 87% of this value being caused by coal combustion.<sup>[3]</sup> Worldwide SO<sub>2</sub> emissions drastically account for air pollution and contribute to the greenhouse effect, hence SO<sub>2</sub> is a significant factor for air pollution and climate change.<sup>[4]</sup> As a consequence, manifold strategies to decrease SO<sub>2</sub> emissions have been proposed,<sup>[5,6]</sup> and flue gas desulfurization already resulted in declined emissions within the last decades.<sup>[7]</sup> The still existing demand for removal of SO<sub>2</sub> by several industries must not be underestimated. As one example, CeO<sub>2</sub> is widely used as a catalyst in the automotive industry and severely suffers from even low concentrations of SO<sub>2</sub> in exhaust streams.<sup>[8,9]</sup> Limestone slurry or wet sulfuric acid processes are cost-effective industrial tools for SO<sub>2</sub> removal, yet they can only remove SO<sub>2</sub> in flue gas up to ~95%, with the last 5% still remaining.<sup>[10]</sup> SO<sub>2</sub> emissions in flue gas can be as high as

420 ppm,<sup>[11]</sup> which is 50000 times higher than the WHO recommendation.<sup>[12]</sup> Moreover, residual SO<sub>2</sub> in flue gas can cause permanent loss of catalyst activities and decrease efficiencies of post-combustion processes.<sup>[13]</sup> Even much lower SO<sub>2</sub> concentrations in ambient air can irreversibly poison Pt-based catalysts/electrodes in fuel cells, so that generally cathode air needs to be free of airborne pollutants such as SO<sub>2</sub>.<sup>[14]</sup> However, complete removal of SO<sub>2</sub> is a challenging process, since it requires selective adsorbents with additional stability towards the highly corrosive SO<sub>2</sub>. Amongst the proposed strategies for SO<sub>2</sub> trace removal are selective adsorbents and reversible physisorption.<sup>[13,15]</sup>

Metal-organic frameworks (MOFs) are coordination networks with organic ligands that exhibit potential porosity on a micro- (<2 nm) to lower mesoporous (2–50 nm) scale.<sup>[16,17]</sup> At present, sorption and stability studies of SO<sub>2</sub> in MOFs are still rare compared to H<sub>2</sub>, CO<sub>2</sub> or CH<sub>4</sub> sorption, but are gaining more and more attention.<sup>[13,18–30]</sup> In 2008, Britt *et al.* began investigating several MOFs with respect to SO<sub>2</sub>.<sup>[31]</sup> Subsequent research constantly extended the understanding of SO<sub>2</sub>@MOF and further expanded the limit of SO<sub>2</sub> capacity.<sup>[13,32–38]</sup> Lately, several mixed-gas SO<sub>2</sub> adsorption studies were carried out.<sup>[39–44]</sup> A comprehensive overview on SO<sub>2</sub> adsorption in MOFs and underlying interactions was given recently by Ibarra *et al.*<sup>[20]</sup> Our group showed that MOFs can exhibit significantly more uptake of SO<sub>2</sub> (up to 10.9 mmol g<sup>-1</sup>) using incorporated urea functionalities in the linker,<sup>[45]</sup> which should be well suited for interaction with SO<sub>2</sub> via hydrogen-bonding (Figure 1).<sup>[46,47]</sup> We also observed that MOF-177 exhibited the highest SO<sub>2</sub> capacity (25.7 mmol g<sup>-1</sup>) at room temperature reported until today.<sup>[41]</sup> However, MOF-177 lacks stability towards the corrosive SO<sub>2</sub> gas.<sup>[41]</sup> Therefore, we extended SO<sub>2</sub> sorption studies towards the robust MIL-101(Cr) (see SI for details, MIL = *Matériaux de l'Institut Lavoisier*),<sup>[48]</sup> as this is one of the most hydrothermally stable MOFs, proven to withstand multiple cycles of SO<sub>2</sub> ad- and desorption.<sup>[26,49]</sup> Moreover, the adsorption capacity of MIL-101(Cr) for SO<sub>2</sub> changed very little in the concentration range from

[a] N. Tannert, Y. Sun, E. Hastürk, S. Nießing, Prof. C. Janiak  
Institut für Anorganische Chemie und Strukturchemie  
Heinrich-Heine Universität Düsseldorf  
40204 Düsseldorf, Germany  
E-mail: janiak@uni-duesseldorf.de

Supporting information for this article is available on the WWW under <https://doi.org/10.1002/zaac.202100023>

© 2021 The Authors. Zeitschrift für anorganische und allgemeine Chemie published by Wiley-VCH GmbH. This is an open access article under the terms of the Creative Commons Attribution Non-Commercial NoDerivs License, which permits use and distribution in any medium, provided the original work is properly cited, the use is non-commercial and no modifications or adaptations are made.



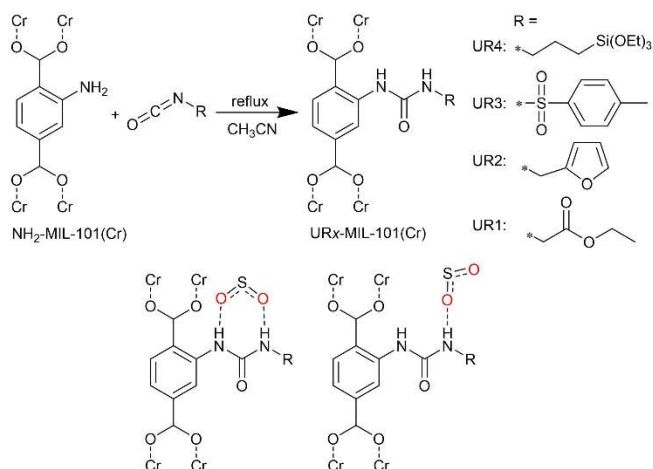


**Figure 1.** Top row: Post-synthetic conversions of  $\text{NH}_2\text{-MIL-101(Cr)}$  with different isocyanates, yielding the urea-functionalized MOFs UR1-, UR2-, UR3- and UR4-MIL-101(Cr). Bottom row: anticipated preferential interactions of  $\text{SO}_2$  with the urea function.

0 to 2000 ppm  $\text{SO}_2$ , when  $\text{CO}_2$  was added to the adsorptive.<sup>[50]</sup> MIL-101(Cr) and its aminoterephthalate-derivative  $\text{NH}_2\text{-MIL-101(Cr)}$  were already shown to be widely modifiable by post-synthetic modification (PSM).<sup>[51–54]</sup>

The PSM approach of converting the amino functionality within  $\text{NH}_2\text{-MIL-101(Cr)}$  into a urea-group by applying isocyanates has also already been exploited thoroughly.<sup>[55–63]</sup> In order to tailor the adsorption properties of MIL-101(Cr) compounds for  $\text{SO}_2$  we synthesized and investigated four novel urea-functionalized MOFs, namely  $\text{UR}_x\text{-MIL-101(Cr)}$  ( $x = 1, 2, 3$  and  $4$ , Figure 1). The four isocyanates were selected, because of their polar functional groups ( $-\text{CO}_2\text{-C-}$ ,  $\text{C-O-C-}$ ,  $-\text{SO}_2\text{-}$  and  $-\text{Si-O-C-}$ ) and due to reasonably priced availability.

## Results and Discussion

The parent MOFs MIL-101(Cr) and  $\text{NH}_2\text{-MIL-101(Cr)}$  were synthesized in good yields and porosities according to slightly adapted protocols given in the literature (see SI for details). The desired urea-MOFs were reproducibly obtained in good yields (75–99%).  $^1\text{H-NMR}$  spectroscopy on digested samples (Section S5, SI) was used to determine the degree of urea-functionalization from the ratio of corresponding functionalized and non-functionalized linker NMR signals (Figure 2, see also Section S5, SI). We note that most other works on urea-functionalized  $\text{NH}_2\text{-MIL-101(Cr)}$  did not investigate the degree of functionalization of the PSM-derived urea-MOFs and PSM-functionalized MIL-101(Cr) in general, but rather focused on other issues. Upon functionalization the crystallinity is partly lost according to the powder X-ray diffractograms (PXRDs) (Figure 3). Already the starting material  $\text{NH}_2\text{-MIL-101(Cr)}$  is of lower crystallinity than MIL-101(Cr) which then deteriorated further upon PSM and the washing steps. The lower degree of crystallinity for  $\text{NH}_2\text{-MIL-101(Cr)}$  and the urea-functionalized MOFs in comparison to non-

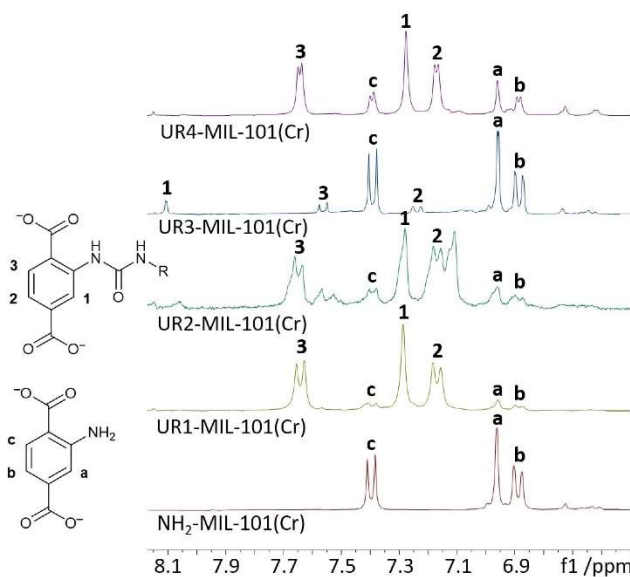


**Figure 2.** Aromatic range from the  $^1\text{H-NMR}$  spectra (300 MHz) of the organic linkers in  $\text{D}_2\text{O/NaOD}$  solution after decomposition (“digestion”) of  $\text{NH}_2\text{-MIL-101(Cr)}$  and the urea-functionalized  $\text{UR}_x\text{-MIL-101(Cr)}$  compounds (see Section S5, Figures S9–S13 in the SI for NMR spectra with integrals and for a discussion of the chemical shift of H-1 in the UR3 linker).

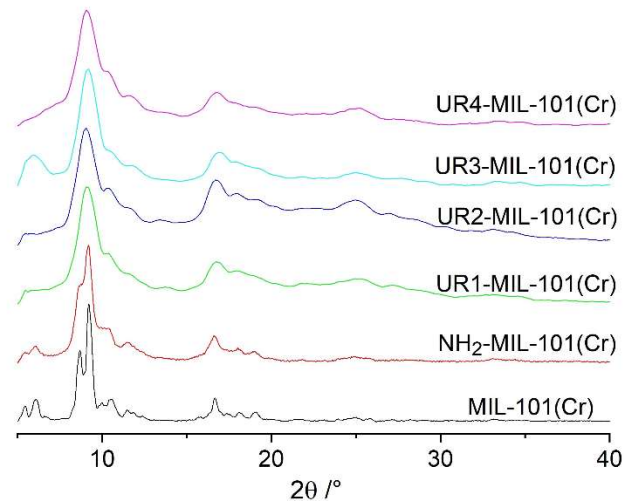


**Figure 3.** Powder X-ray diffractograms of MIL-101(Cr),  $\text{NH}_2\text{-MIL-101(Cr)}$  and the urea-functionalized  $\text{UR}_x\text{-MIL-101(Cr)}$  compounds.

functionalized MIL-101(Cr) is also evident from the scanning electron microscopy (SEM) images (Figure S3–S8, SI).

Nitrogen sorption isotherms (Figure 4) were collected for each material and apparent BET surface areas and pore volumes were derived therefrom. Sulfur dioxide ad-/desorption isotherms of the urea-MIL-101 compounds were measured at 273 K and 293 K (Figure 5). Table 1 lists porosity parameters derived from  $\text{N}_2$  sorption isotherms in comparison to  $\text{SO}_2$  sorption capacities.

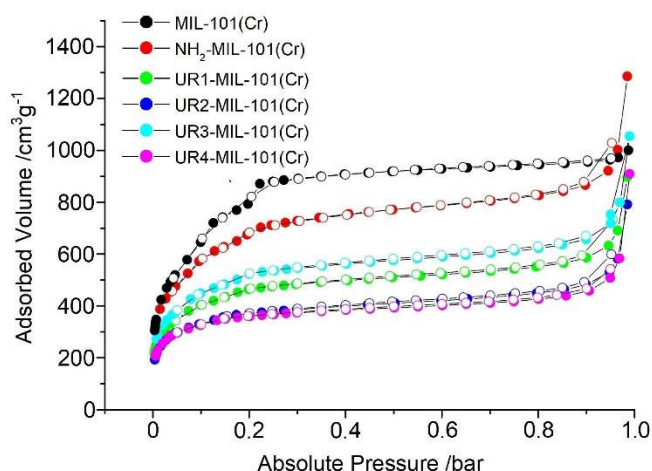


**Figure 4.**  $N_2$  sorption isotherms of urea-MOFs URx-MIL-101(Cr) in comparison to MIL-101(Cr) and  $NH_2$ -MIL-101(Cr) (filled symbols: adsorption, empty symbols: desorption).

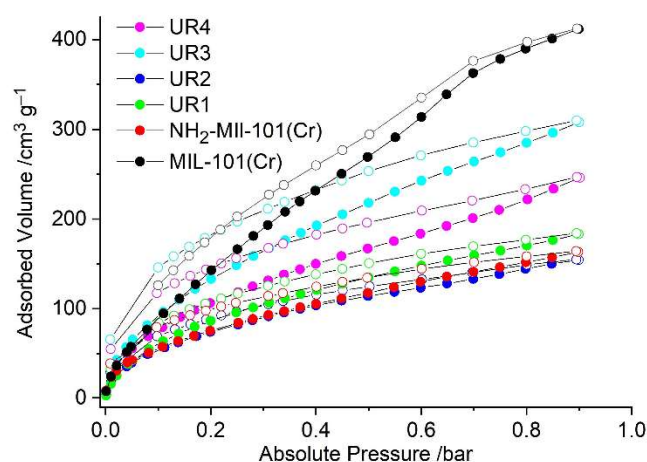
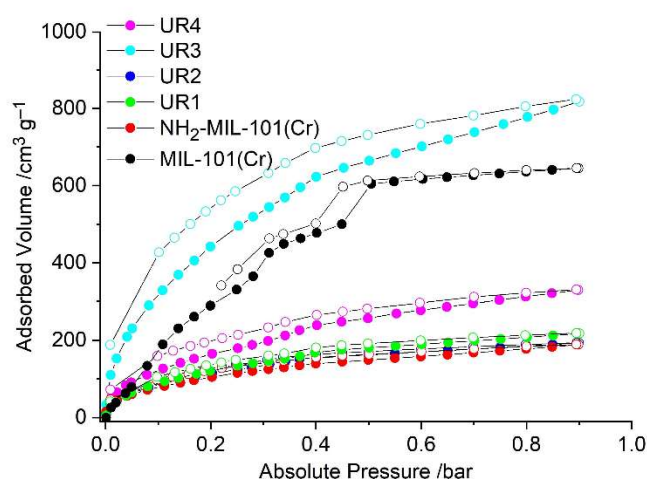


**Figure 5.**  $SO_2$  isotherms at 273 K (top) and at 293 K (bottom) of urea-MOFs URx-MIL-101(Cr) in comparison to MIL-101(Cr) and  $NH_2$ -MIL-101(Cr) (filled symbols: adsorption, empty symbols: desorption).

The  $SO_2$  isotherm of MIL-101(Cr) at  $T=273$  K resolves the two mesoporous apertures of MIL-101(Cr) by displaying two steps as in the  $N_2$  isotherm. This isotherm attribute is well known and has been described for MIL-101(Cr) and  $NH_2$ -MIL-101(Cr) with other gases and also for water vapor isotherms.<sup>[64,65]</sup>

The curvature for MIL-101(Cr) at  $T=293$  K is very similar to the one reported for MIL-101(Cr) and MIL-101(Cr)-4F at 298 K.<sup>[26]</sup> It could be anticipated that the highest  $SO_2$  adsorption capacity is exhibited by MIL-101(Cr) due to its highest pore volume in the compound series (cf. Table 1). This is indeed true at  $T=293$  K, where MIL-101(Cr) has the highest uptake of  $SO_2$  ( $412\text{ cm}^3\text{ g}^{-1}$  at 0.9 bar). A comparison with the urea-MOFs reveals, however, that the simple uptake vs. pore volume correlation does not hold. Remarkably,  $NH_2$ -MIL-101(Cr) with the second largest pore volume, close to MIL-101(Cr), features one of the lowest  $SO_2$  uptakes in the series. Also, the  $SO_2$  uptakes of the ethyl acetate- and furfuryl-functionalized urea-MOFs UR1- and UR2-MIL-101(Cr) are low ( $184\text{ cm}^3\text{ g}^{-1}$  and  $155\text{ cm}^3\text{ g}^{-1}$  at 293 K). Instead, the partially *p*-toluenesulfonyl-urea-functionalized derivative UR3-MIL-101(Cr) has the second highest uptake ( $310\text{ cm}^3\text{ g}^{-1}$  at 293 K) although its pore volume is less than that of  $NH_2$ -MIL-101(Cr). The 3-(triethoxysilyl)propyl function in UR4-MIL-101(Cr) yields the smallest pore volume but a comparatively high  $SO_2$  uptake of  $247\text{ cm}^3\text{ g}^{-1}$  at 293 K.

All the more, at  $T=273$  K the partially *p*-toluenesulfonyl-urea-functionalized derivative UR3-MIL-101(Cr) surpasses the uptake of MIL-101(Cr) ( $823$  vs.  $645\text{ cm}^3\text{ g}^{-1}$ ). UR4-MIL-101(Cr) is third with  $331\text{ cm}^3\text{ g}^{-1}$ . UR1-, UR2- and  $NH_2$ -MIL-101(Cr) remain similarly low with 218, 194 and  $190\text{ cm}^3\text{ g}^{-1}$  respectively. We provide a tabular overview of  $SO_2$  capacities of various MOFs and porous materials from the literature for comparison in Table S2 in the SI. The  $SO_2$  uptake of UR3-MIL-101(Cr) is only superseded by Ni-MOF-74 nanospheres with ca.  $964\text{ cm}^3\text{ g}^{-1}$  at 1 bar, 298 K.<sup>[66]</sup>

UR3-MIL-101(Cr) outperforms its analogs at  $T=273$  K (and most other MOFs at  $T=293$  K, Table S2, SI) with exceptionally high uptake which we link to the strong interactions of  $SO_2$  with the sulfonyl group of UR3. At the same time, the minor degree of functionalization still leaves a high enough pore volume to achieve a high uptake capacity through pore filling by  $SO_2 \cdots SO_2$  dipole-dipole interactions. The intermediate uptake of UR4-MIL-101(Cr), especially in view of its small pore volume, is linked to the formation of  $-Si-OH$  groups through partial hydrolysis of the  $-Si-OEt$  groups at the tri(ethoxy)silane end. The  $-Si-OH$  groups can contribute to  $Si-OH \cdots OSO$  hydrogen bonding. For the low and similar  $SO_2$  uptake of  $NH_2$ -MIL-101(Cr), UR1- and UR2-MIL-101(Cr) we must realize that the amino substitution and the introduced urea group with ethyl acetate and furfuryl moieties obviously destroys or at least hinders  $SO_2$  binding sites, while at the same time they do not make new ones available.

*In situ* inelastic neutron scattering and DFT calculations of  $SO_2$  at MFM-300(Al) indicated a relatively strong  $Al-OH \cdots OSO$  hydrogen bond, complemented by four  $aryl-C-H \cdots OSO$  hydrogen bonds with the adjacent  $C_6$  aryl ligand. To these framework-bound  $SO_2$  molecules, further  $SO_2$  molecules will then bind through  $(MOF-OSO) \cdots OSO$  dipole-dipole interactions, form-



**Table 1.** Porosity parameters (from N<sub>2</sub> sorption isotherms) and SO<sub>2</sub> uptake for MIL-101(Cr), NH<sub>2</sub>-MIL-101(Cr) and the urea-MOFs URx-MIL-101(Cr).

MOF (degree of functionalization)	BET surface	Total pore volume	SO <sub>2</sub> uptake 273, 293 K	
	/m <sup>2</sup> g <sup>-1</sup> <sup>a)</sup>	/cm <sup>3</sup> g <sup>-1</sup> <sup>b)</sup>	/mmol g <sup>-1</sup> <sup>c)</sup>	/cm <sup>3</sup> g <sup>-1</sup> <sup>c)</sup>
MIL-101(Cr) (n.a.) <sup>d)</sup>	3300	1.49	28.8, 18.4	645, 412
NH <sub>2</sub> -MIL-101(Cr) (n.a.) <sup>d)</sup>	2530	1.34	8.5, 7.3	190, 164
UR1-MIL-101(Cr) (83 %) <sup>e)</sup>	1700	0.98	9.7, 8.2	218, 184
UR2-MIL-101(Cr) (71 %)	1360	0.82	8.7, 6.9	194, 155
UR3-MIL-101(Cr) (18 %)	1900	0.96	36.7, 13.9	823, 310
UR4-MIL-101(Cr) (72 %)	1340	0.68	14.8, 11.0	331, 247

<sup>a)</sup> Specific apparent BET surface areas were calculated from five adsorption points of N<sub>2</sub> isotherm within  $0.05 < p/p_0 < 0.2$ . Values were rounded according to the estimated standard deviation of  $\pm 50 \text{ m}^2 \text{ g}^{-1}$ . <sup>b)</sup> Total pore volumes were calculated from experimental N<sub>2</sub> sorption data at  $p/p_0 = 0.95$ . For details see Section S6, SI. <sup>c)</sup> SO<sub>2</sub> uptake values at 0.9 bar. <sup>d)</sup> n.a. = not applicable. <sup>e)</sup> The degree of functionalization was estimated from the ratio of integrals of corresponding functionalized and non-functionalized linker NMR signals, see Section S5, SI.

ing SO<sub>2</sub> chains or clusters.<sup>[34]</sup> *In situ* synchrotron PXRD studies on MFM-601(Zr) supported that the first SO<sub>2</sub> molecules bind by Zr–OH...OSO hydrogen bonds, aryl–C–H...OSO and by aryl- $\pi$ ...SO<sub>2</sub> interactions. These first bound SO<sub>2</sub> molecules interact with following SO<sub>2</sub> guest molecules by OS...OSO dipole-dipole interactions, verifying the important role of the dipole moment of SO<sub>2</sub> in the adsorption process.<sup>[39]</sup>

DFT calculations of SO<sub>2</sub> at MIL-160(Al) with a furan-dicarboxylate linker proposed SO<sub>2</sub> above a plane spanned by two furan units with two O<sub>furan</sub>...SO<sub>2</sub> and simultaneously four O<sub>carboxylate</sub>...SO<sub>2</sub> interactions as the site with highest (negative) binding energy, providing a model for low concentration SO<sub>2</sub> binding. Of next highest, but already substantially lower binding energy were single O<sub>furan</sub>...SO<sub>2</sub> and Al–OH...OSO interactions.<sup>[41]</sup>

Based on a summary of these findings on SO<sub>2</sub> binding sites we reason that the amino substitution in NH<sub>2</sub>-MIL-101(Cr) and the ethyl acetate and furfuryl moieties in UR1- and UR2-MIL-101(Cr) block crucial Cr–OH, Cr–OH<sub>2</sub>, –CO<sub>2</sub> (carboxylate), aryl–C–H and aryl- $\pi$  interactions. A possible blocking can occur by N–H...OC (carboxylate) hydrogen bonding but also by steric constraints (in UR1 and UR2).

At the same time, it is unlikely that the conversion of NH<sub>2</sub>-MIL-101(Cr) with isocyanates to the UR1 and UR2 derivative led to outer surface degradation or pore blocking effects or that the parent NH<sub>2</sub>-MIL-101(Cr) MOF suffered from such effects. In the case of MOF instability towards air or moisture or towards the urea-forming reaction conditions already the N<sub>2</sub> adsorption and subsequent surface area and porosity would have been much lower.

Still, to rule out surface or other kinds of degradation effects or pore-blocking phenomena we collected carbon dioxide and water vapor ad-/desorption isotherms (Figure 6, Figure S16,

uptake values in Table 2). Evidently, the CO<sub>2</sub> uptake shows a quite different trend with MIL-101(Cr) > NH<sub>2</sub>-MIL-101(Cr)  $\approx$  UR4 > UR2 > UR1 > UR3 at 273 K and MIL-101(Cr) > NH<sub>2</sub>-MIL-101(Cr) > UR4 > UR1 > UR2 > UR3 at 293 K. The expected and known effect of amino groups for CO<sub>2</sub> uptake through carbamate formation (R–NH–CO<sub>2</sub><sup>-</sup> together with R–NH<sub>3</sub><sup>+</sup>) now leads to the expected high uptake of NH<sub>2</sub>-MIL-101(Cr).<sup>[67]</sup> The next highest uptake of UR4 is again rationalized through its –Si–OH groups.

Obviously, CO<sub>2</sub> sorption differs from SO<sub>2</sub> capacities for the investigated MOFs, especially regarding UR3-MIL-101(Cr) with highest uptake of SO<sub>2</sub> at 273 K, while displaying the lowest CO<sub>2</sub> capacities at 273 and 293 K. This is remarkable as UR3 still has about 82% of unchanged NH<sub>2</sub> groups (Table S3) and, thus, should follow more the CO<sub>2</sub> uptake behavior of NH<sub>2</sub>-MIL-101(Cr). So, if steric hindrance or gate opening plays a role, their effect would be expected for the CO<sub>2</sub> uptake in UR3 with its bulky *para*-toluenesulfonyl groups. Thus, we assign the low CO<sub>2</sub> uptake of UR3-MIL-101(Cr) to such a kinetic phenomenon. We

**Table 2.** CO<sub>2</sub> and H<sub>2</sub>O uptake for MIL-101(Cr), NH<sub>2</sub>-MIL-101(Cr) and urea-MOFs URx-MIL-101(Cr).

MOF	CO <sub>2</sub> uptake 273 K, 293 K /cm <sup>3</sup> g <sup>-1</sup> <sup>a)</sup>	H <sub>2</sub> O uptake 293 K /g g <sup>-1</sup> <sup>b)</sup>
MIL-101(Cr)	92, 56	n.d.
NH <sub>2</sub> -MIL-101(Cr)	72, 52	0.8
UR1-MIL-101(Cr)	61, 41	0.5
UR2-MIL-101(Cr)	67, 39	0.4
UR3-MIL-101(Cr)	50, 32	0.8
UR4-MIL-101(Cr)	72, 46	0.5

<sup>a)</sup> Uptake values at 0.9 bar; <sup>b)</sup> at  $p/p_0 = 0.95$ .

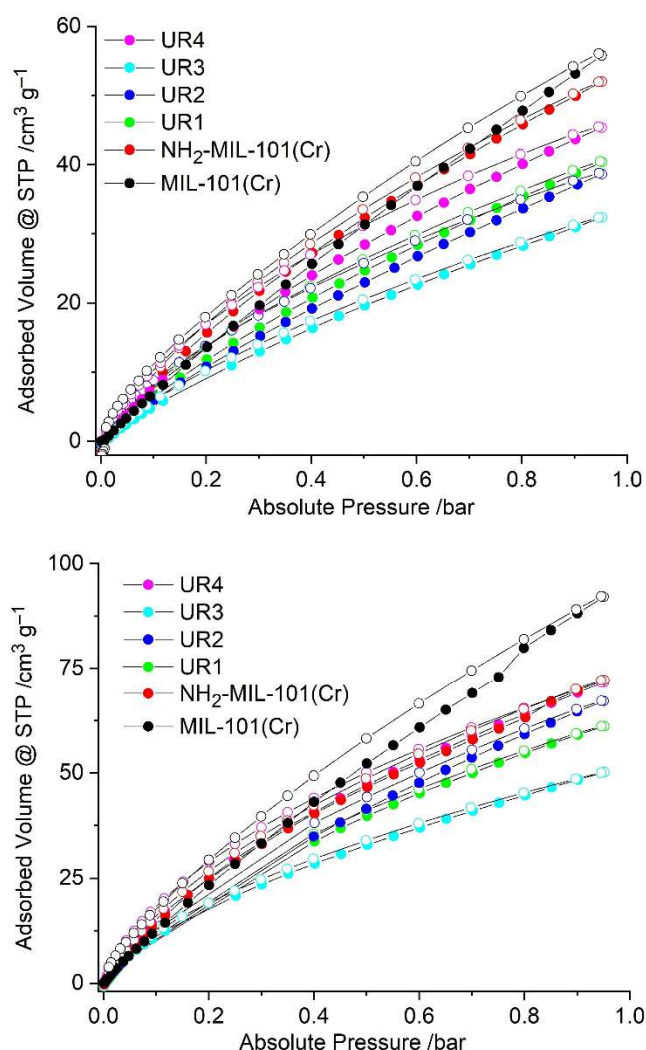


**Figure 6.** CO<sub>2</sub> isotherms at 273 K (top) and at 293 K (bottom) of urea-MOFs UR<sub>x</sub>-MIL-101(Cr) in comparison to MIL-101(Cr) and NH<sub>2</sub>-MIL-101(Cr) (filled symbols: adsorption, empty symbols: desorption).

note that for CO<sub>2</sub> uptake saturation could not be reached for any of the MOFs UR<sub>x</sub>-MIL-101(Cr), MIL-101(Cr) and NH<sub>2</sub>-MIL-101(Cr) due to their micro- and mesoporosity. The CO<sub>2</sub> adsorption isotherms in Figure 6 at 1 bar still have high positive slopes and are far from levelling off, which indicates adsorption curves far from saturation, which will be reached only at higher pressures.

The trend of water uptake in the order of MIL-101(Cr) > NH<sub>2</sub>-MIL-101(Cr) ≈ UR<sub>3</sub> > UR<sub>1</sub> ≈ UR<sub>4</sub> > UR<sub>2</sub> follows roughly the trend of porosity in the samples, modulated through the hydrophilicity/hydrophobicity. In summary, the CO<sub>2</sub> and H<sub>2</sub>O sorption behavior of the MIL derivatives clearly rules out artefacts from degradation or pore-opening effects for the low SO<sub>2</sub> uptake of NH<sub>2</sub>-MIL-101(Cr), UR<sub>1</sub> and UR<sub>2</sub>.

The stability performance of MIL-101(Cr) was checked by performing three SO<sub>2</sub> adsorption-desorption runs. The results showed a significant decline of the SO<sub>2</sub> uptake with only 40% of the initial uptake still being reached in the third run (Figure S14a, SI). This confirms earlier results by Martínez-

Ahumada *et al.* that MIL-101(Cr) gradually loses its crystallinity and surface area after dry SO<sub>2</sub> sorption at 298 K.<sup>[28]</sup>

Similarly, we found in a recent study that NH<sub>2</sub>-MIL-101(Cr) lost porosity after dry and especially after humid SO<sub>2</sub> exposure (Figure S14b, SI).<sup>[68]</sup> The instability of MIL-101(Cr) towards SO<sub>2</sub> was explained by its comparatively hydrophilic nature.<sup>[28]</sup> We suggest that both MIL-101(Cr) and NH<sub>2</sub>-MIL-101(Cr) are unstable because the SO<sub>2</sub> can interact with the chromium-aqua and -hydroxido ligand (Cr–OH<sub>2</sub> and Cr–OH) in the trinuclear secondary building unit (SBU) (Figure S1a, SI). Chemisorption of SO<sub>2</sub> will then form sulfurous acid, H<sub>2</sub>SO<sub>3</sub> or acidic hydrogen sulfite, HSO<sub>3</sub><sup>−</sup> at the chromium sites which can dissociate the adjacent Cr–O<sub>2</sub>C-carboxylate bonds by protonation of the carboxylate ligand. *In situ* IR experiments on MIL-125 upon SO<sub>2</sub> adsorption by Mounfield *et al.* have confirmed the formation of bisulfite species and, together with theoretical simulations, suggested that the degradation of the MIL-125 framework proceeds by reaction with water and the dissociation of water or sulfurous acid.<sup>[36]</sup>

## Conclusions

The facile post-synthetic modification of NH<sub>2</sub>-MIL-101(Cr) with organic isocyanates proved to be a useful tool to modify the adsorption characteristics towards SO<sub>2</sub>. In particular, introduction of sulfonyl groups with the reaction of *p*-toluenesulfonyl isocyanate to give the derivative UR<sub>3</sub>-MIL-101(Cr) strongly enhanced the SO<sub>2</sub> adsorption capacity. UR<sub>3</sub>-MIL-101(Cr) outperforms nearly all MOFs in the current literature with its significantly higher uptake of SO<sub>2</sub> (823 cm<sup>3</sup> g<sup>−1</sup> at 0.9 bar and 273 K). Noteworthy is the higher adsorption compared to MIL-101(Cr) (645 cm<sup>3</sup> g<sup>−1</sup> at 0.9 bar and 273 K), which is counter-intuitive to the pore volume of the two MOFs (0.96 and 1.49 cm<sup>3</sup> g<sup>−1</sup>, respectively). We attribute this good SO<sub>2</sub> sorption behavior to the introduced sulfonyl groups which are then available in UR<sub>3</sub>-MIL-101(Cr) for the important SO<sub>2</sub>...SO<sub>2</sub> host-guest dipole-dipole interactions. To the best of our knowledge such sulfonyl-modified MOFs have not yet been specifically investigated for tailored SO<sub>2</sub> sorption.

## Experimental Section

All chemicals were used as received by suppliers. For further information about all materials see Section S1 in the SI.

Powder X-ray diffractometry (PXRD) was performed at ambient temperature on a Bruker D2 Phaser with a flat silicon, low background sample holder using Cu–K<sub>α</sub> radiation (λ = 1.54182 Å) in the range of 5° < 2θ < 50° with a scan rate of 0.0125° s<sup>−1</sup> (300 W, 30 kV, 10 mA). Analyses of the diffractograms were carried out with Match 3.11 software.

Scanning electron microscopy (SEM) images were acquired on a JEOL JSM-6510 Advanced electron microscope (with a LaB<sub>6</sub> cathode at 5–20 keV. The microscope was equipped with a Bruker Xflash 410 silicon drift detector. Images are depicted in Section S4 in the SI.



$^1\text{H}$ - and  $^{13}\text{C}$ -NMR experiments were carried out on a Bruker FT-NMR AVANCE III – 300 MHz at 300 K. Approximately 15 mg of each sample was dissolved under decomposition in NaOD/D<sub>2</sub>O. The subsequently filtered solution was transferred into an NMR tube and subjected to NMR spectroscopy. NMR spectra are shown in Section S5 in the SI.

Nitrogen sorption experiments for the determination of BET surface areas and pore volumes (Brunauer, Emmett, Teller<sup>69</sup>) were determined at  $T=77\text{ K}$  on a Quantachrome NOVA-4000e instrument within a partial pressure range of  $10^{-3} < p/p_0 < 1$  bar using N<sub>2</sub> gas of purity 99.999% (grade 5.0) and ca. 20–50 mg of sample. Each sample was degassed under vacuum ( $p/p_0 < 10^{-3}$ ) at 150 °C for ca. 3 h prior to measurement. All BET surface areas were calculated from at least five adsorption points applying Roquerol plots ( $r > 0.998$ ). For pressure ranges of five-point-BET calculations of each MOF see Section S6, SI. Total pore volumes were calculated from the N<sub>2</sub> sorption isotherm at  $p/p_0 = 0.95$ .

Sulfur dioxide, carbon dioxide and water vapor sorption experiments were carried out on a Quantachrome iQ MP instrument with all gas option within a partial pressure range of  $10^{-3} < p/p_0 < 1$ . Each sample was degassed under vacuum ( $p/p_0 < 10^{-3}$ ) at 150 °C for ca. 3 h prior to measurement, using a FloVac degasser. For further details see Section S7, SI.

**UR1-, UR2-, UR3- and UR4-MIL-101(Cr):** NH<sub>2</sub>-MIL-101(Cr) (see synthesis in Section S1, SI) (150 mg, 0.2 mmol, 1.0 eq) was dispersed in dehydrated acetonitrile (20 mL). Upon adding the respective isocyanate (9.0 mmol, 45 eq) at room temperature the reaction solution was stirred under reflux conditions and N<sub>2</sub> atmosphere for 6 h and then at room temperature for 12 h. The precipitate was separated by centrifugation and washed with acetonitrile (2 × 25 mL) and acetone (2 × 25 mL). After each washing step the precipitate was separated by centrifugation and decantation of the supernatant liquid. Finally, the raw product was dispersed and boiled in acetone (25 mL) for 24 h and then dried overnight under reduced pressure at 80 °C (yields UR1 204 mg, 99%, UR2 174 mg, 95%, UR3 133 mg, 75%, UR4 205 mg, 99%).

## Supporting Information

(see footnote on the first page of this article): Material sources, information on MIL-101, IR spectra, SEM images, NMR spectra, further details on gas and water vapor sorption.

## Acknowledgements

The work was supported by the German Research Foundation (DFG) through grant Ja-466/29-1. We thank China Scholarship Council (CSC) for funding a PhD fellowship to Y.Y.S. Open access funding enabled and organized by Projekt DEAL.

**Keywords:** Metal-organic frameworks (MOFs) • Post-synthetic modification (PSM) • Urea-MOF • Urea functionalization • SO<sub>2</sub> adsorption

- [1] J. A. Taylor, R. W. Simpson, A. J. Jakeman, *Ecol. Modell.* **1987**, 36, 269–296.

- [2] B. Zhao, S. Wang, J. Wang, J. S. Fu, T. Liu, J. Xu, X. Fu, J. Hao, *Atmos. Environ.* **2013**, 77, 453–463.
- [3] X. Xu, C. Chen, H. Qi, R. He, C. You, G. Xiang, *Fuel Process. Technol.* **2000**, 62, 153–160.
- [4] W. C. Wang, Y. L. Yung, A. A. Lacis, T. Mo, J. E. Hansen, *Science* **1976**, 194, 685–690.
- [5] T. Raju, S. J. Chung, I. S. Moon, *Environ. Sci. Technol.* **2008**, 42, 7464–7469.
- [6] C. Wang, H. Liu, X. Z. Li, J. Y. Shi, G. Ouyang, M. Peng, C. C. Jiang, H. N. Cui, *Environ. Sci. Technol.* **2008**, 42, 8585–8590.
- [7] S. J. Smith, R. Andres, E. Conception, J. Lurz, *Historical Sulfur Dioxide Emissions 1850–2000: Methods and Results*, No. PNNL-14537, Pacific Northwest National Lab. (PNNL), Richland, WA (United States), **2004**.
- [8] a) S. Hilaire, S. Sharma, R. J. Gorte, J. M. Vohs, H. W. Jen, *Catal. Lett.* **2000**, 70, 131–135; b) T. Kolli, M. Huuhtanen, A. Hallikainen, K. Kallinen, R. L. Keiski, *Catal. Lett.* **2009**, 127, 49–54; c) Y. Wang, X. Li, L. Zhan, C. Li, W. Qiao, L. Ling, *Ind. Eng. Chem. Res.* **2015**, 54, 2274–2278; d) E. Park, M. Kim, H. Jung, S. Chin, J. Jurng, *ACS Catal.* **2013**, 3, 1518–1525; e) J. Liu, X. Y. Li, Q. D. Zhao, C. Hao, S. B. Wang, M. Tade, *ACS Catal.* **2014**, 4, 2426–2436.
- [9] W. P. Mounfield III, U. Tumuluri, Y. Jiao, M. Li, S. Dai, Z. Wu, K. S. Walton, *Microporous Mesoporous Mater.* **2016**, 227, 65–75.
- [10] J. H. Gary, G. E. Handwerk, *Petroleum Refining Technology and Economics*, 4th Ed., Marcel Dekker Inc., New York, **2001**.
- [11] X. Xu, C. Song, R. Wincek, J. M. Andresen, B. G. Miller, A. W. Scaroni, *Am. Chem. Soc. Div. Fuel Chem. Prepr.* **2003**, 48, 162–163.
- [12] WHO (World Health Organisation) *Air Quality Guidelines for Particulate Matter, Ozone, Nitrogen Dioxide and Sulfur Dioxide*, Global update **2005**, [http://apps.who.int/iris/bitstream/10665/69477/1/WHO\\_SDE\\_PHE\\_OEH\\_06.02\\_eng.pdf](http://apps.who.int/iris/bitstream/10665/69477/1/WHO_SDE_PHE_OEH_06.02_eng.pdf); retrieved January 7th 2021.
- [13] M. Savage, Y. Cheng, T. L. Easun, J. E. Eyley, S. P. Argent, M. R. Warren, W. Lewis, C. Murray, C. C. Tang, M. D. Frogley, G. Cinque, J. Sun, S. Rudić, R. T. Murden, M. J. Benham, A. N. Fitch, A. J. Blake, A. J. Ramirez-Cuesta, S. Yang, M. Schröder, *Adv. Mater.* **2016**, 28, 8705–8711.
- [14] a) F. N. Jing, M. Hou, W. Y. Shi, J. Fu, H. M. Yu, P. W. Ming, B. L. Yi, *J. Power Sources* **2007**, 166, 172–176; b) P. C. Bruce, J. Tatarchuk, *Chem. Eng. Sci.* **2019**, 201, 157–166; c) X. Wang, X. Ma, C. Song, *Catal. Today* **2020**, <https://doi.org/10.1016/j.cattod.2020.07.068>.
- [15] M. Cantu, E. Lopez-Salinas, J. S. Valente, *Environ. Sci. Technol.* **2005**, 39, 9715–9720.
- [16] H.-C. Zhou, J. R. Long, O. M. Yaghi, *Chem. Rev.* **2012**, 112, 673–674.
- [17] G. Maurin, C. Serre, A. Cooper, G. Férey, *Chem. Soc. Rev.* **2017**, 46, 3104–3107.
- [18] X. Han, S. Yang, M. Schröder, *Nature Rev. Chem.* **2019**, 3, 108–118.
- [19] X. Wang, W. Xu, J. Gu, X. Yan, Y. Chen, M. Guo, G. Zhou, S. Tong, M. Ge, Y. Liu, C. Chen, *Nanoscale* **2019**, 11, 17782–17790.
- [20] E. Martínez-Ahumada, A. López-Olvera, V. Jancik, J. E. Sánchez-Bautista, E. González-Zamora, V. Marzís, D. R. Williams, I. A. Ibarra, *Organometallics* **2020**, 7, 883–915.
- [21] M. H. Alkord, Y. Belmabkhout, A. Cairns, M. Eddaoudi, *iUCr* **2017**, 4, 131–135.
- [22] M. Wittmann, S. Ling, A. Gladysiak, K. C. Stylianou, B. Smit, B. Slater, M. Haranczyk, *J. Phys. Chem. C* **2017**, 121, 1171–1181.
- [23] Y. Lin, C. Kong, Q. Zhang, L. Chen, *Adv. Energy Mater.* **2017**, 7, 1601296.
- [24] A. J. Rieth, A. M. Wright, M. Dinča, *Nat. Rev. Mater.* **2019**, 4, 708–725.



- [25] R. Domínguez-González, I. Rojas-Léon, E. Martínez-Ahumada, D. Martínez-Otero, H. A. Lara-García, J. Balmaseda-Era, I. A. Ibarra, E. G. Percástegui, V. Jancik, *J. Mater. Chem. A* **2019**, *7*, 26812–26817.
- [26] G. L. Smith, J. E. Eyley, X. Han, X. Zhang, J. Li, N. M. Jacques, H. G. W. Godfrey, S. P. Argent, L. J. McCormick, McPherson, S. J. Teat, Y. Cheng, M. D. Frogley, G. Cinque, S. J. Day, C. C. Tang, T. L. Easun, S. Rudić, A. J. Ramirez-Cuesta, S. Yang, M. Schröder, *Nat. Mater.* **2019**, *18*, 1358–1365.
- [27] Z. Chen, X. Wang, R. Cao, K. B. Idrees, X. Liu, M. C. Wasson, O. K. Farha, *ACS Materials Lett.* **2020**, *2*, 1129–1134.
- [28] E. Martínez-Ahumada, M. L. Díaz-Ramírez, H. A. Lara-García, D. R. Williams, V. Martis, V. Jancik, E. Lima, I. A. Ibarra, *J. Mater. Chem. A* **2020**, *8*, 11515–11520.
- [29] J. Carter, C. Morris, H. G. W. Godfrey, S. J. Day, J. Potter, S. P. Thompson, C. Tang, S. Yang, M. Schröder, *ACS Appl. Mater. Interfaces* **2020**, *12*, 42949–42954.
- [30] J. Antonio-Zárate, E. Domínguez-Ojeda, E. Sánchez-González, E. Martínez-Ahumada, V. B. López-Cervantes, D. R. Williams, V. Martis, I. A. Ibarra, J. Alejandro, *Dalton Trans.* **2020**, *49*, 9203–9207.
- [31] D. Britt, D. Tranchemontagne, O. M. Yaghi, *Proc. Natl. Acad. Sci. USA* **2008**, *105*, 11623–11627.
- [32] C. A. Fernandez, P. K. Thallapally, R. K. Motkuri, S. K. Nune, J. C. Sumrak, J. Tian, J. Liu, *Cryst. Growth Des.* **2010**, *10*, 1037–1039.
- [33] T. G. Glover, G. W. Peterson, B. J. Schindler, D. Britt, O. M. Yaghi, *Chem. Eng. Sci.* **2011**, *66*, 163–170.
- [34] S. Yang, J. Sun, A. J. Ramirez-Cuesta, S. K. Callear, W. I. F. David, D. P. Anderson, R. Newby, A. J. Blake, J. E. Parker, C. C. Tang, M. Schröder, *Nat. Chem.* **2012**, *4*, 887–894.
- [35] K. Tan, P. Canepa, Q. Gong, J. Liu, D. H. Johnson, A. Dyevoich, P. K. Thallapally, T. Thonhauser, J. Li, Y. J. Chabal, *Chem. Mater.* **2013**, *25*, 4653–4662.
- [36] W. P. Mounfield III, C. Han, S. H. Pang, U. Tumuluri, Y. Jiao, S. Bhattacharyya, M. R. Dutzer, S. Nair, Z. Wu, R. P. Lively, D. S. Sholl, K. S. Walton, *J. Phys. Chem. C* **2016**, *120*, 27230–27240.
- [37] S. Han, Y. Huang, T. Watanabe, S. Nair, K. S. Walton, D. S. Sholl, J. C. Meredith, *Microporous Mesoporous Mater.* **2013**, *173*, 86–91.
- [38] J. A. Zárate, E. Sánchez-González, D. R. Williams, E. González-Zamora, V. Martis, A. Martínez, J. Balmaseda, G. Maurin, I. A. Ibarra, *J. Mater. Chem. A* **2019**, *7*, 15580–15584.
- [39] J. H. Carter, X. Han, F. Y. Moreau, I. da Silva, A. Nevin, H. G. W. Godfrey, C. C. Tang, S. Yang, M. Schröder, *J. Am. Chem. Soc.* **2018**, *140*, 15564–15567.
- [40] M. R. Tchalala, P. M. Bhatt, K. N. Chappanda, S. R. Tavaréz, K. Adil, Y. Belmabkhout, A. Shkurenko, A. Cadiau, N. Heymans, G. De Weireld, G. Maurin, K. N. Salama, M. Eddaoudi, *Nat. Commun.* **2019**, *10*, 1–10.
- [41] P. Brandt, A. Nuhnen, M. Lange, J. Möllmer, O. Weingart, C. Janiak, *ACS Appl. Mater. Interfaces* **2019**, *11*, 17350–17358.
- [42] L. Xia, Q. Cui, X. Suo, Y. Li, X. Cui, Q. Yang, J. Xu, Y. Yang, H. Xing, *Adv. Funct. Mater.* **2018**, *28*, 1704292.
- [43] Y. Zhang, Z. Chen, X. Liu, Z. Dong, P. Zhang, J. Wang, Q. Deng, Z. Zeng, S. Zhang, S. Deng, *Ind. Eng. Chem. Res.* **2020**, *59*, 874–882.
- [44] H. Wang, J. Q. Bai, Y. Yin, S. F. Wang, *J. Mol. Graphics Modell.* **2020**, *96*, 107533.
- [45] S. Glomb, D. Woschko, G. Makhlofi, C. Janiak, *ACS Appl. Mater. Interfaces* **2016**, *9*, 37419–37434.
- [46] K. Tan, S. Zuluaga, Q. Gong, Y. Gao, N. Nijem, J. Li, T. Thonhauser, Y. J. Chabal, *Chem. Mater.* **2015**, *27*, 2203–2217.
- [47] J. Zhang, P. Zhang, F. Han, G. Chen, L. Zhang, X. Wei, *Ind. Eng. Chem. Res.* **2009**, *48*, 1287–1291.
- [48] G. Férey, C. Mellot-Draznieks, C. Serre, F. Millange, J. Dutour, S. Surblé, I. Margiolaki, *Science* **2005**, *309*, 2040–2042.
- [49] K. Leus, T. Bogaerts, J. De Decker, H. Depauw, K. Hendrickx, H. Vrielinck, V. Van Speybroeck, P. Van Der Voort, *Microporous Mesoporous Mater.* **2016**, *226*, 110–116.
- [50] Q. Liu, L. Ning, S. Zheng, M. Tao, J. Shi, Y. He, *Sci. Rep.* **2013**, *3*, 2916.
- [51] M. Lammert, S. Bernt, F. Vermoortele, D. E. De Vos, N. Stock, *Inorg. Chem.* **2013**, *52*, 8521–8528.
- [52] D. Jiang, L. L. Keenan, A. D. Burrows, K. J. Edler, *Chem. Commun.* **2012**, *48*, 12053–12055.
- [53] A. Klinkebiel, N. Reimer, M. Lammert, N. Stock, U. Lüning, *Chem. Commun.* **2014**, *50*, 9306–9308.
- [54] N. Ko, P. G. Choi, J. Hong, M. Yeo, S. S. Kyle, E. Cordova, H. J. Park, J. K. Yang, J. Kim, *J. Mater. Chem. A* **2015**, *3*, 2057–2064.
- [55] E. Dugan, Z. Wang, M. Okamura, A. Medina, S. M. Cohen, *Chem. Commun.* **2008**, *29*, 3366–3368.
- [56] S. Bernt, V. Guillerme, C. Serre, N. Stock, *Chem. Commun.* **2011**, *47*, 2838–2840.
- [57] X.-W. Dong, T. Liu, Y.-Z. Hu, X.-Y. Liu, C.-M. Che, *Chem. Commun.* **2013**, *49*, 7681–7683.
- [58] T. Wittmann, R. Siegel, N. Reimer, W. Milius, N. Stock, J. Senker, *Chem. Eur. J.* **2015**, *21*, 314–323.
- [59] X. Yang, Y. Xia, *Microchim. Acta* **2016**, *183*, 2235–2240.
- [60] P. W. Seo, N. A. Khan, S. H. Jhung, *Chem. Eng. J.* **2017**, *315*, 92–100.
- [61] D. Feng, Y. Xia, *Sep. Sci.* **2018**, *41*, 732–739.
- [62] A. Modrow, D. Zargarani, R. Herges, N. Stock, *Dalton Trans.* **2012**, *41*, 8690–8696.
- [63] T. Lescouet, J. G. Vitillo, S. Bordiga, J. Canivet, D. Farrusseng, *Dalton Trans.* **2013**, *42*, 8249–8258.
- [64] a) Z. Zhou, B. Cheng, C. Ma, F. Xu, J. Xiao, Q. Xia, Z. Li, *RSC Adv.* **2015**, *5*, 94276–94282; b) M. Saikia, D. Bhuyan, L. Saikian, *New J. Chem.* **2015**, *39*, 64–67.
- [65] J. Canivet, J. Bonnefoy, C. Daniel, A. Legrand, B. Coasne, D. Farrusseng, *New J. Chem.* **2014**, *38*, 3102–3111.
- [66] M. Ranjbar, M. A. Taher, *J. Porous Mater.* **2016**, *23*, 1249–1254.
- [67] A. Khutia, C. Janiak, *Dalton Trans.* **2014**, *43*, 1338–1347.
- [68] P. Brandt, A. Nuhnen, S. Öztürk, G. Kurt, J. Liang, C. Janiak, *Adv. Sust. Mater.* **2021**, in press. <https://doi.org/10.1002/adsu.202000285>.
- [69] M. Thommes, K. Kaneko, A. V. Neimark, J. P. Olivier, F. Rodriguez-Reinoso, J. Rouquerol, K. S. Sing, *Pure Appl. Chem.* **2015**, *87*, 1051–1069.

Manuscript received: January 18, 2021

Revised manuscript received: March 16, 2021

Accepted manuscript online: March 16, 2021

# Zeitschrift für anorganische und allgemeine Chemie

Supporting Information

**A Series of new Urea-MOFs Obtained *via* Post-synthetic  
Modification of NH<sub>2</sub>-MIL-101(Cr): SO<sub>2</sub>, CO<sub>2</sub> and H<sub>2</sub>O Sorption**

Niels Tannert, Yangyang Sun, Emrah Hastürk, Sandra Nießing, and Christoph Janiak\*

## SUPPORTING INFORMATION

### A Series of new Urea-MOFs Obtained *via* Post-synthetic Modification of NH<sub>2</sub>-MIL-101(Cr): SO<sub>2</sub>, CO<sub>2</sub> and H<sub>2</sub>O Sorption

Niels Tannert,<sup>[a]</sup> Yangyang Sun,<sup>[a]</sup> Emrah Hastürk,<sup>[a]</sup> Sandra Nießing,<sup>[a]</sup> Christoph Janiak<sup>\*,[a]</sup>

<sup>a</sup> Institut für Anorganische Chemie und Strukturchemie, Heinrich-Heine-Universität Düsseldorf, Universitätsstraße 1, 40225 Düsseldorf, Germany. \*E-mail: [janiak@uni-duesseldorf.de](mailto:janiak@uni-duesseldorf.de)

Emails: [niels.tannert@hhu.de](mailto:niels.tannert@hhu.de); [Yangyang.Sun@hhu.de](mailto:Yangyang.Sun@hhu.de), [emrah.hastuerk@hhu.de](mailto:emrah.hastuerk@hhu.de); [sandra.niessing@hhu.de](mailto:sandra.niessing@hhu.de)

#### **Table of Contents**

Section S1.	Materials
Section S2.	MIL-101(Cr)
Section S3.	Fourier-transformed infrared spectroscopy (FT-IR)
Section S4.	Scanning electron microscopy (SEM)
Section S5.	Nuclear magnetic resonance experiments ( <sup>1</sup> H-NMR)
Section S6.	Nitrogen sorption experiments (T = 77 K)
Section S7.	SO <sub>2</sub> sorption experiments (T = 0 °C, 20 °C)
Section S8.	CO <sub>2</sub> sorption experiments (T = 0 °C, 20 °C)
Section S9.	H <sub>2</sub> O vapor sorption experiments (T = 20 °C)
Section S10.	References

## S1. Materials

**Table S1.** Used chemicals, suppliers, and purities. All chemicals were used as received. Only acetonitrile was distilled and stored under nitrogen atmosphere with molecular sieve until usage.

Chemical	Supplier	Purity
acetonitrile	Sigma Aldrich	99.8%
acetone	OxChem	99%
2-aminoterephthalic acid	Sigma Aldrich	99%
$\text{Cr}(\text{NO}_3)_3 \cdot 9\text{H}_2\text{O}$	AlfaAesar	99%
ethanol	Sigma Aldrich	>99.8%
ethyl isocyanatoacetate	Sigma Aldrich	95%
furfuryl isocyanate	Sigma Aldrich	97%
nitric acid (65%)	Alfa Aesar	not specified
<i>p</i> -toluenesulfonyl isocyanate	Sigma Aldrich	96%
3-(triethoxysilyl)propyl isocyanate	Sigma Aldrich	95%

**MIL-101(Cr):** Following a procedure of Zhao *et al.*,<sup>[1]</sup>  $\text{Cr}(\text{NO}_3)_3 \cdot 9\text{H}_2\text{O}$  (2006 mg, 5.0 mmol, 1.0 eq) and terephthalic acid (830.0 mg, 5.0 mmol, 1.0 eq) were dispersed in a nitric solution of deionized water (5 mL) and 65% nitric acid (0.35 mL, 5.0 mmol, 1 eq). The suspension was inserted into a PTFE liner that was placed in an autoclave. The autoclave was heated to 220 °C for 8 h and then cooled to room temperature again within 6 h. The resulting raw product was separated from the liquid *via* centrifugation and decantation and then washed with water (25 mL) and DMF (25 mL) consecutively. The precipitate was again dispersed in water (75 mL) and stirred overnight at 70 °C for 16 h. Upon renewed centrifugation, the precipitate was transferred to two centrifuge tubes and the content of each washed with ethanol (25 mL). The supernatant liquid was decanted. The raw product was then stirred in ethanol (75 mL) at 70 °C for 22 h. For the last time the product was isolated by removal of the solvent with centrifugation and then dried at 80 °C under reduced pressure in a vacuum oven for 18 h (yield 790 mg, 66%, Lit.: 82%).<sup>[1]</sup>

**NH<sub>2</sub>-MIL-101(Cr):** Following a protocol of Jiang *et al.*,<sup>[2]</sup> a suspension of  $\text{Cr}(\text{NO}_3)_3 \cdot 9\text{H}_2\text{O}$  (3.571 g, 8.9 mmol, 1.0 eq) and 2-aminoterephthalic acid (1.630 g, 9.0 mmol, 1.0 eq) in water (50 mL) was transferred to a PTFE liner, heated to 130 °C for 24 h and then slowly cooled to room temperature over 6 h. The suspension was apportioned among two centrifuge tubes and each fraction was washed with water (2 × 20 mL). After washing, the suspensions were centrifuged, and the supernatant liquid was decanted. The same washing procedure was repeated using ethanol (2 × 20 mL). The raw product was boiled in ethanol under reflux conditions for 3 d. After centrifugation and decantation of the supernatant liquid, the product dried overnight under reduced pressure at 80 °C (yield 844 mg, 37%, Lit.: 78%).<sup>[3]</sup>

## S2. MIL-101(Cr)

MIL-101(Cr) is a zeotypic network which contains micropores and two types of mesopores with free diameters of ca. 2.9 and 3.4 nm, accessible through two microporous pentagonal and hexagonal windows of ca. 1.2 nm and 1.6 x 1.5 nm (Figure S1).<sup>[4]</sup>

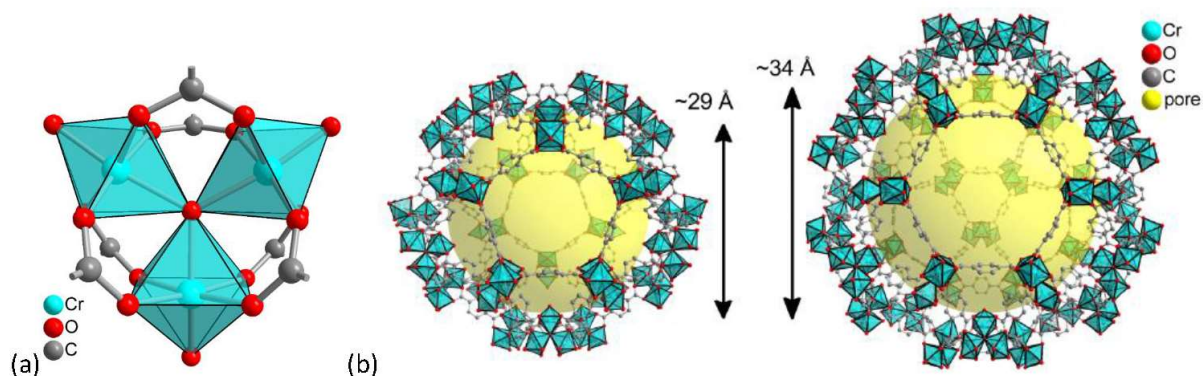


**Figure S1.** (a) Secondary building unit (SBU) of MIL-101(Cr), NH<sub>2</sub>-MIL-101(Cr) and UR<sub>x</sub>-MIL-101(Cr). The outward-oriented three oxygen atoms stand for two aqua ligands (H<sub>2</sub>O) and one hydroxido or fluorido ligand (OH/F), depending on a fluoride-free or fluoride-involving synthesis. The SBU formula is {Cr<sub>3</sub>(μ<sub>3</sub>-O)(H<sub>2</sub>O)<sub>2</sub>(OH,F)(O<sub>2</sub>C-)<sub>6</sub>}.

(b) The two mesoporous cavities of MIL-101(Cr), highlighted as yellow spheres. Left: smaller pore with 2.9 nm diameter and 1.2 nm window. Right: larger pore with 3.4 nm diameter and 1.6 nm window. Graphics have been drawn with the software DIAMOND<sup>[5]</sup> from the deposited cif-files under CCDC no. 605510, Refcode OCUNAK for MIL-101(Cr).<sup>[4]</sup>

MIL-101(Cr) and its analogues are most studied and promising for practical applications, as they feature high surface areas, good thermal and chemical stability and they can be produced on a relatively large scale easily.<sup>[1,4,6,7]</sup> Their uptake for several gases is remarkable,<sup>[8,9,10]</sup> while good gas separation attributes contribute to the interest of researchers.<sup>[11,12,13]</sup> Further factors for prospective utilization of MIL-101(Cr) materials are outstanding (water) vapor capacities with high hydrothermal cycle stability,<sup>[14,15,16]</sup> resulting in a good performance in heat transformation applications,<sup>[17,18,19]</sup> their possible use in catalysis<sup>[7,20,21]</sup> and many more.<sup>[22,23,24,25]</sup>

MIL-101(Cr) and its aminoterephthalate-derivative NH<sub>2</sub>-MIL-101(Cr) were also shown to be widely modifiable by post-synthetic modification (PSM).<sup>[26,27,28,29]</sup> PSM is already a common tool in MOF chemistry,<sup>[30,31,32]</sup> as linker modulation it allows for tailoring the inner surface chemistry of the pores specifically and application oriented.<sup>[33,34]</sup> By attaching a certain organic rest to the organic linker imparted in the MOF (here: urea-functionality), specific interactions for host molecules (here: SO<sub>2</sub>) should result in enhanced sorption properties.



**Table S2.** SO<sub>2</sub> sorption data of porous materials, from the literature and from this work.<sup>a)</sup>

MOF	uptake [mmol g <sup>-1</sup> ]	uptake [cm <sup>3</sup> g <sup>-1</sup> ]	uptake [wt %] <sup>b)</sup>	press. [bar]	temp. [K]	linker functionality	Ref.
Ni(bdc)(ted) <sub>0.5</sub>	9.97	224	39.0	1.13	298	none	35
Zn(bdc)(ted) <sub>0.5</sub>	4.41	99	22.0	1.01	298	none	35
Mg-MOF-74	8.6	193	35.5	1.02	298	(OH) <sub>2</sub>	35
Zn-MOF-74	3.03 <sup>c)</sup>	68	-	0.01	298	(OH) <sub>2</sub>	36
Ni-MOF-74 nanospheres	105.06 (ca. 43)	- (ca. 964)	-	4 (1)	298	(OH) <sub>2</sub>	37
HKUST-1, Cu-btc	0.7 <sup>d)</sup>	-	-	-	273	none	38
MFM-170 <sup>e)</sup>	17.5	-	-	1	298	pyridyl	39
MFM-600 <sup>e)</sup>	8.0	-	-	1	273	pyridyl	40
MFM-601 <sup>e)</sup>	16.9	-	-	1	273	pyridyl	40
NOTT-300 <sup>e)</sup>	8.1	182	29.9	1	273	none	41
MFM-300(In) <sup>e)</sup>	8.28	186	-	1	298	biphenyl	42
MFM-300(Sc) <sup>e)</sup>	9.4	-	-	1	298	biphenyl	43
MFM-305 <sup>e)</sup>	9.05	-	-	1	273	pyridyl	44
MFM-305-CH <sub>3</sub> <sup>e)</sup>	5.16	-	-	-	-	pyridyl/CH <sub>3</sub>	44
NOTT-202a <sup>e),h)</sup>	10.2	229	-	1	298	none	45
UNAM-1	3.5	-	-	1	298	HOF <sup>g)</sup>	46
FMOF-2	2.19	49	13.8	1	298	(CF <sub>3</sub> ) <sub>2</sub>	47
M <sub>3</sub> [Co(CN) <sub>6</sub> ] <sub>2</sub>	2.5	56	-	1	298	none	48
ELM-12	2.5	61.2	-	1	298	CF <sub>3</sub> SO <sub>3</sub> <sup>-</sup>	49
DMOF-1 series	3.5-7.0	-	-	2.5	298	none/(CH <sub>3</sub> ) <sub>x</sub>	50
MOF-801	8.00	195	33.88	1	293	none	51
HHU-2-Cl	9.69	236.19	38.28	1	293	Cl	51
HHU-2-Br	6.07	147.95	28.00	1	293	Br	51
KAUST-7	1.4	-	-	500 ppm	298	pyrazine/F	52
KAUST-8	1.6	-	-	0.97	293	furan	53
MIL-160	7.2	-	-	0.97	293	none	53
MOF-177	25.7	-	-	0.95	293	NH <sub>2</sub>	53
NH <sub>2</sub> -MIL-125(Ti)	10.8	-	-	1	298	pyrazine	54
CPL-1	-	51	-	1	298	azo	55
PCN-250	11.7	-	-	1	298	urea	56
[Zn <sub>4</sub> (μ <sub>4</sub> -O)(L1) <sub>3</sub> ]	2.2	50	12.3	1	293	urea	56
[Zn <sub>2</sub> (L1) <sub>2</sub> (bipy)]	10.9	248	41.2	1	293	urea	56
[Zn <sub>2</sub> (L1) <sub>2</sub> (bpe)]	6.4	146	29.2	1	293	urea	56
InOF-1	ca. 8	-	-	1	298	none	57
CAU-10	4.47	-	-	1	298	none	58
Cr- & Al-aerogels	4.5-6.6	110-147	22-30	1	293	none	59
Na-MnO <sub>x</sub> aerogel	0.6	-	3.7	1	-	none	60
SiN-rGO aerogel	2.19	-	12.3	1	298	none	61
Coconut shell AC <sup>h)</sup>	3.3	75	-	0.46	323	none	62
Coal-based AC <sup>h)</sup>	1.7	-	-	0.5	323	none	62
MFI zeolite	2.7	-	-	-	298	none	63
13X zeolite	2.7	-	-	0.4	323	none	64
5A zeolite	1.7	-	-	0.5	323	none	64
SIFSIX-1 series	2.10-11.01	47-246	-	1	298	SiF <sub>6</sub> <sup>2-</sup> /linker	65
P(TMGA-co-MBA)	4.06	91	-	1	298	mult. organic	66
NiAl-mixed oxides	0.65	15	-	0.1	298	none	67
TMGL@silica	0.6 g g <sup>-1</sup>	-	0.375	-	-	ionic liquid	68
PIL-xerogels	0.516	-	-	-	298	ionic liquid	54
MIL-101(Cr)-4F(1%)	18.4	-	-	1	298	none	69
MIL-101(Cr)	28.8/18.4	645/412	64.9/54.1	0.90	273/293	none	i)
NH <sub>2</sub> -MIL-101(Cr)	8.5/7.3	190/164	35.3/31.9	0.90	273/293	NH <sub>2</sub>	i)
UR1-MIL-101(Cr)	9.7/8.2	218/184	38.3/34.4	0.90	273/293	urea	i)
UR2-MIL-101(Cr)	8.7/6.9	194/154	35.8/30.7	0.90	273/293	urea	i)
UR3-MIL-101(Cr)	36.7/13.9	823/310	70.2/47.1	0.90	273/293	urea	i)
UR4-MIL-101(Cr)	14.8/11.0	331/247	48.7/41.3	0.90	273/293	urea	i)

<sup>a)</sup> Literature values were taken as such (including the stated two decimal digits) and not re-calculated to other units. We note that there are more reports in the literature on SO<sub>2</sub> adsorption in porous host materials,

but most of them tackle only trace gas elimination and/or do not state uptake capacities near 1 bar. Relevant overviews are also given in ref. [67], Fig. 2 therein and in ref. [40], Table 3 therein.

- b) When calculating the  $\text{SO}_2$  as wt%, the mass fraction is equal to  $(\text{mass SO}_2)/(\text{mass MOF} + \text{mass SO}_2)$ . The mass of  $\text{SO}_2$  in the denominator must not be neglected.<sup>[70]</sup>
- c) Dynamic measurement.
- d) Dynamic adsorption capacity.
- e) The MOF-abbreviation NOTT (*University of Nottingham*) from the work of Prof. Martin Schröder was replaced by MFM (*Manchester Framework Material*) with the move of Prof. Schröder from Nottingham to Manchester, so that both terminologies can be found in the literature.
- f) NOTT-202a (NOTT = *University of Nottingham*) undergoes irreversible structural transformation into NOTT-202b upon  $\text{SO}_2$  exposure.<sup>[45]</sup>
- g) HOF stands for hydrogen-bonded organic framework.<sup>[71]</sup>
- h) AC stands for activated carbon.
- i) This work.

### **S3. Fourier-transformed infrared spectroscopy (FT-IR)**

IR spectroscopy measurements were performed with a *Bruker Tensor 37* on KBr pellets.

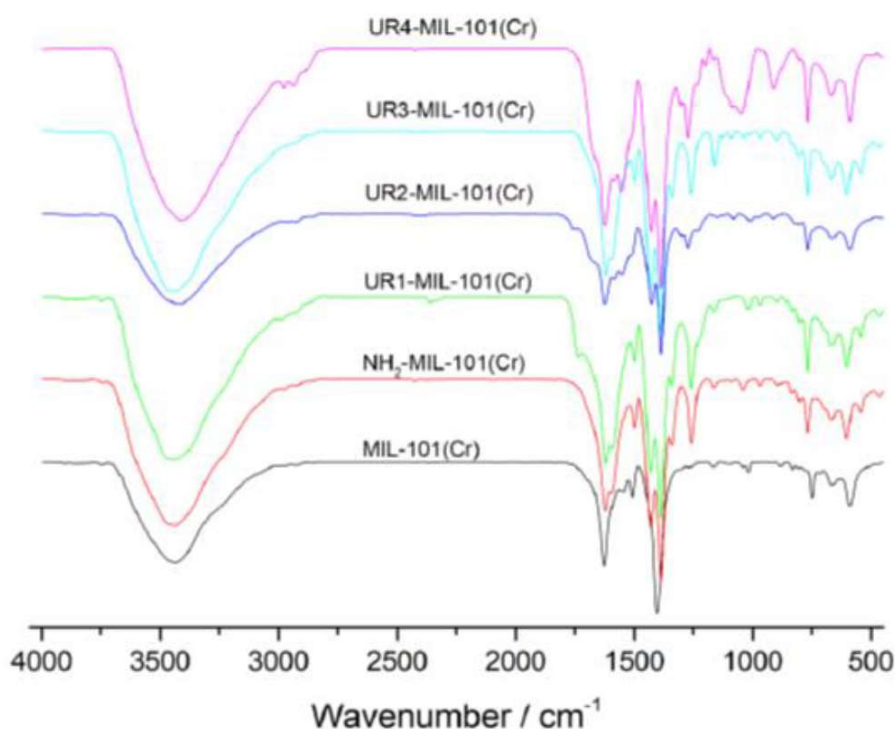


**Figure S2.** FT-IR spectra of urea-MOFs in comparison to MIL-101(Cr) and  $\text{NH}_2$ -MIL-101(Cr).

#### S4. Scanning electron microscopy (SEM)

##### MIL-101(Cr)

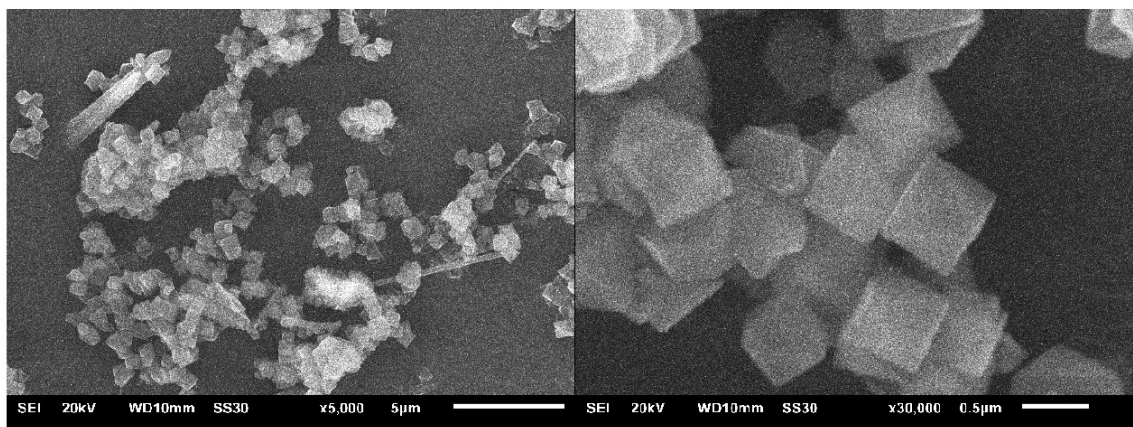


**Figure S3.** SEM images of MIL-101(Cr) at different magnifications. *The left image depicts needle-shaped crystals which are due to remaining unreacted linker.*

##### NH<sub>2</sub>-MIL-101(Cr)

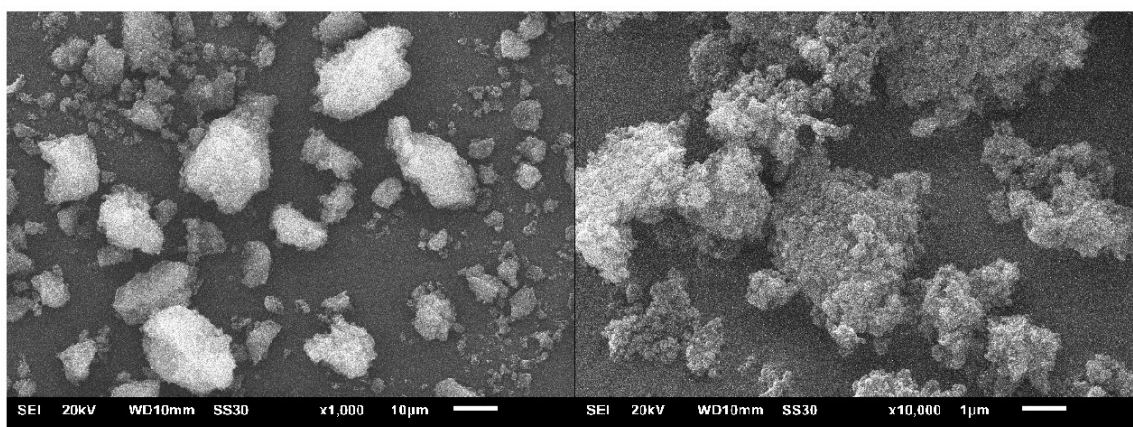


**Figure S4.** SEM images of NH<sub>2</sub>-MIL-101(Cr) at different magnifications.

##### UR1-MIL-101(Cr)

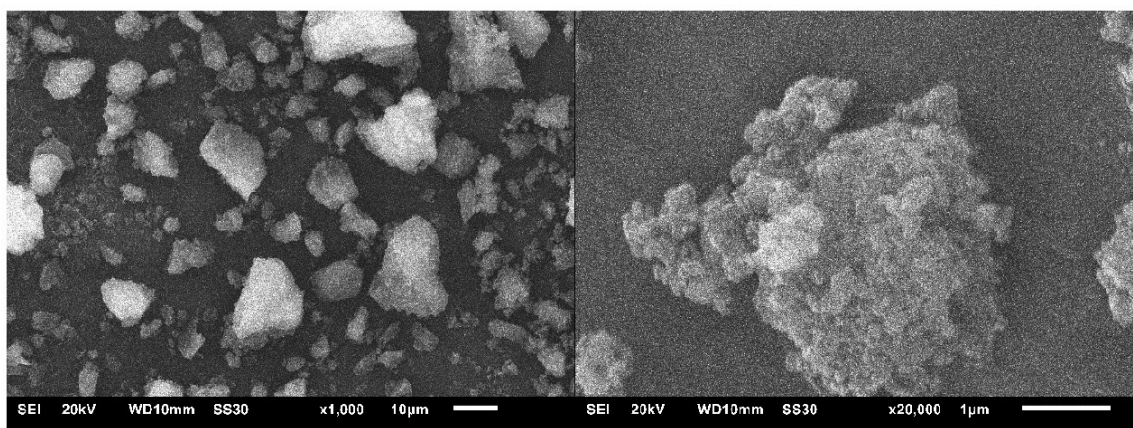


**Figure S5.** SEM images of UR1-MIL-101(Cr) at different magnifications.



#### UR2-MIL-101(Cr)

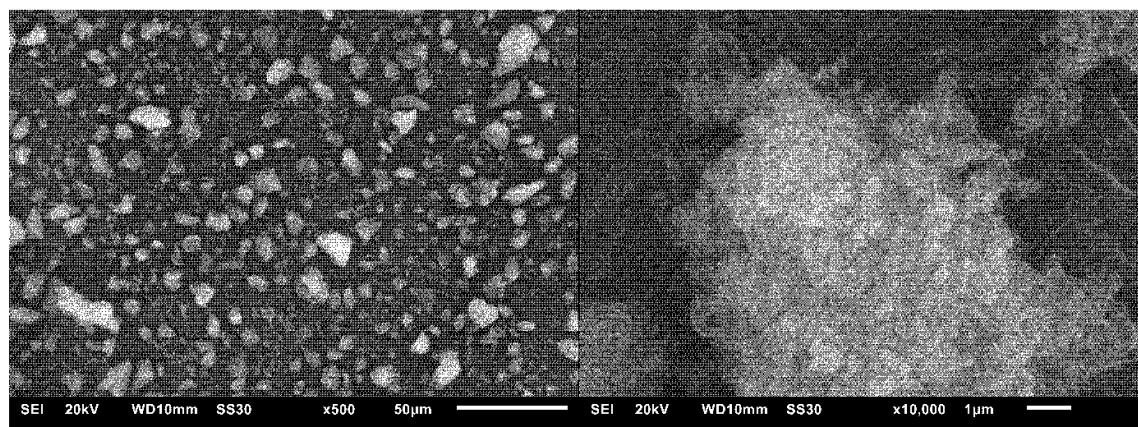


**Figure S6.** SEM images of UR2-MIL-101(Cr) at different magnifications.

#### UR3-MIL-101(Cr)

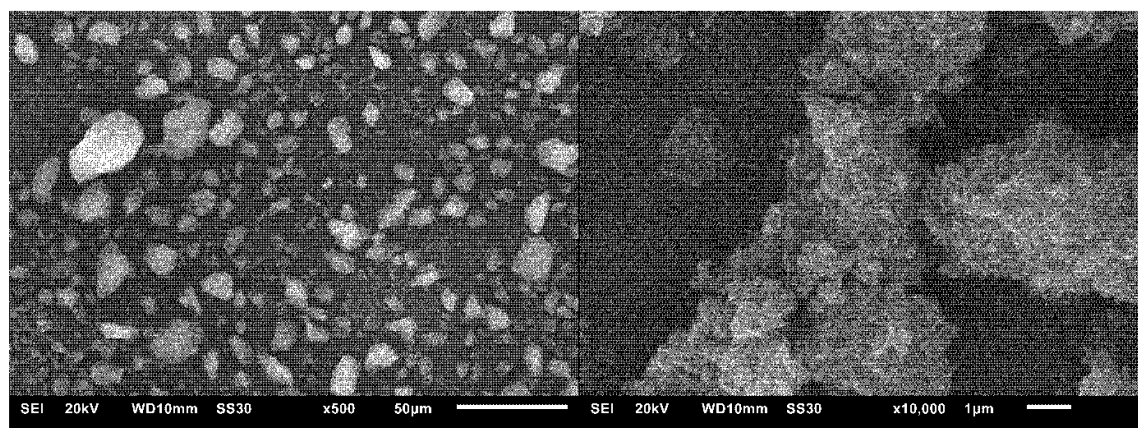


**Figure S7.** SEM images of UR3-MIL-101(Cr) at different magnifications.

#### UR4-MIL-101(Cr)

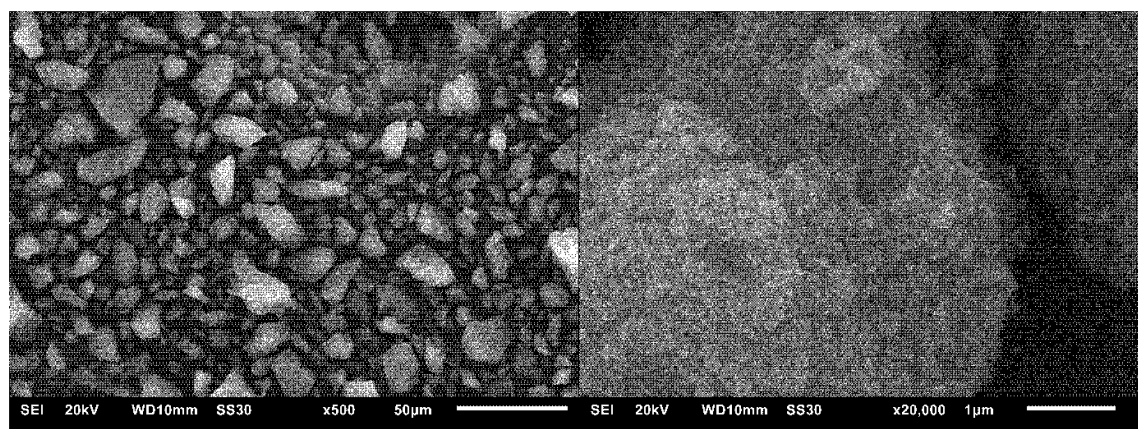


**Figure 8.** SEM images of UR4-MIL-101(Cr) at different magnifications.

## S5. Nuclear magnetic resonance experiments (<sup>1</sup>H-NMR)

All NMR experiments were carried out on a *Bruker FT-NMR AVANCE III – 300 MHz* at 300 K.

Approximately 15 mg of each sample was dissolved under decomposition (“digested”) in NaOD/D<sub>2</sub>O and the filtered solution was transferred into an NMR tube and subjected to NMR spectroscopy.

The degree of functionalization was determined from the ratio of integrals of corresponding functionalized and non-functionalized linker NMR signals. The ortho-H atom to the NH<sub>2</sub>-group in the residual NH<sub>2</sub>-bdc linker which appears as singlet (signal *a* in Fig. S9-S13, Fig. 2 in the main paper) was set to 6.96 ppm in each case.

Figures S9-S13 depict the aromatic region in <sup>1</sup>H-NMR spectra of the linker solution of each digested MOF with the integrals from which the degree of functionalization is determined (Table S3).

**Table S3.** Degree of functionalization of urea-MOFs

MOF	Degree of functionalization [%] <sup>a)</sup>
UR1-MIL-101(Cr)	ca. 83
UR2-MIL-101(Cr)	ca. 71
UR3-MIL-101(Cr)	ca. 18
UR4-MIL-101(Cr)	ca. 72

<sup>a)</sup> Degree of functionalization was estimated from the averaged integrals of the three NMR-signals (1, 2, 3) of the three protons at the aromatic ring, relative to the averaged integrals of the three NMR signals of the unfunctionalized NH<sub>2</sub>-bdc linker (a, b, c); see also Fig. 2 in the main manuscript.

## Spectrum prediction

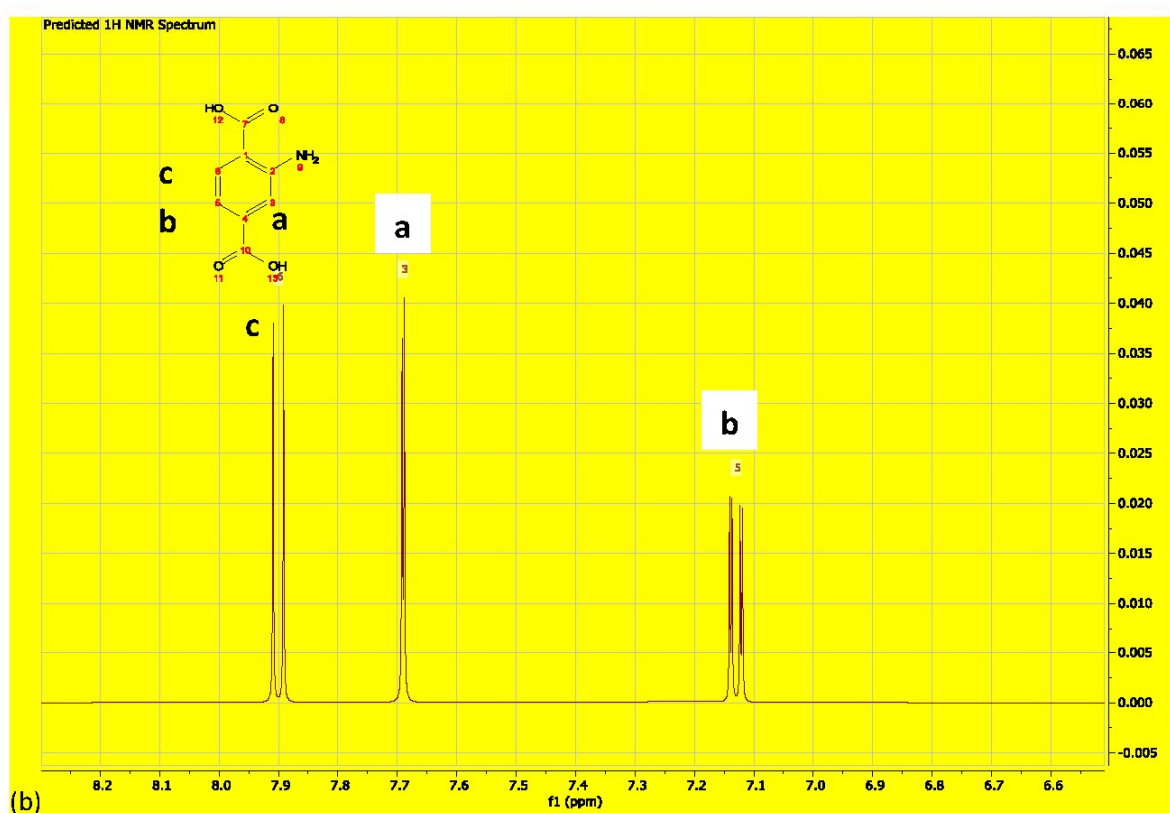
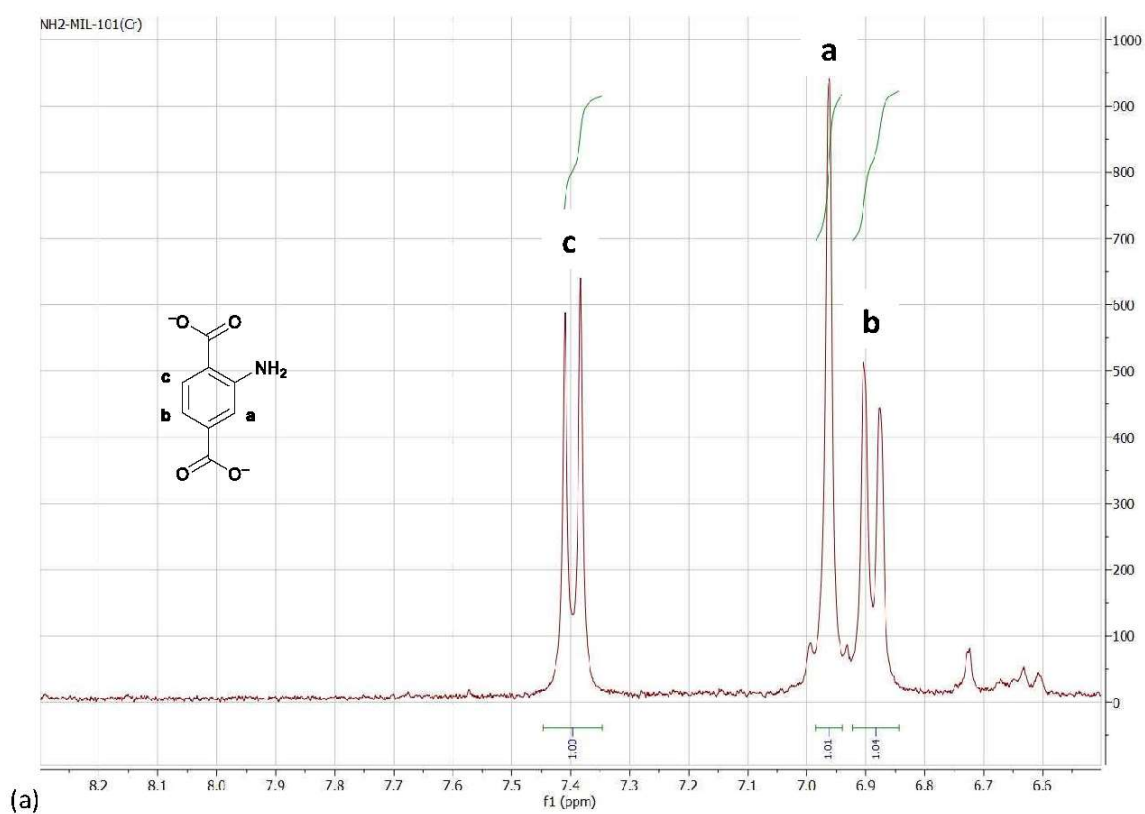
The spectra prediction in Figure S9b for the linker solution from NH<sub>2</sub>-MIL-101(Cr) and in Figure S12b for the linker solution from UR3-MIL-101(Cr), each after decomposition with D<sub>2</sub>O/NaOD were carried out with the program MestReNova, Version 14.1.1-24571, released 2019-12-02, copyright Mestrelab Research S.L.; [www.mestrelab.com](http://www.mestrelab.com)

The comparison between the experimental and predicted spectrum of the linker solution from NH<sub>2</sub>-MIL-101(Cr) in Figure S9a and S9b served as a calibration for the comparison between the experimental and predicted spectrum of the linker solution from UR3-MIL-101(Cr) in Figure S12a and S12b.

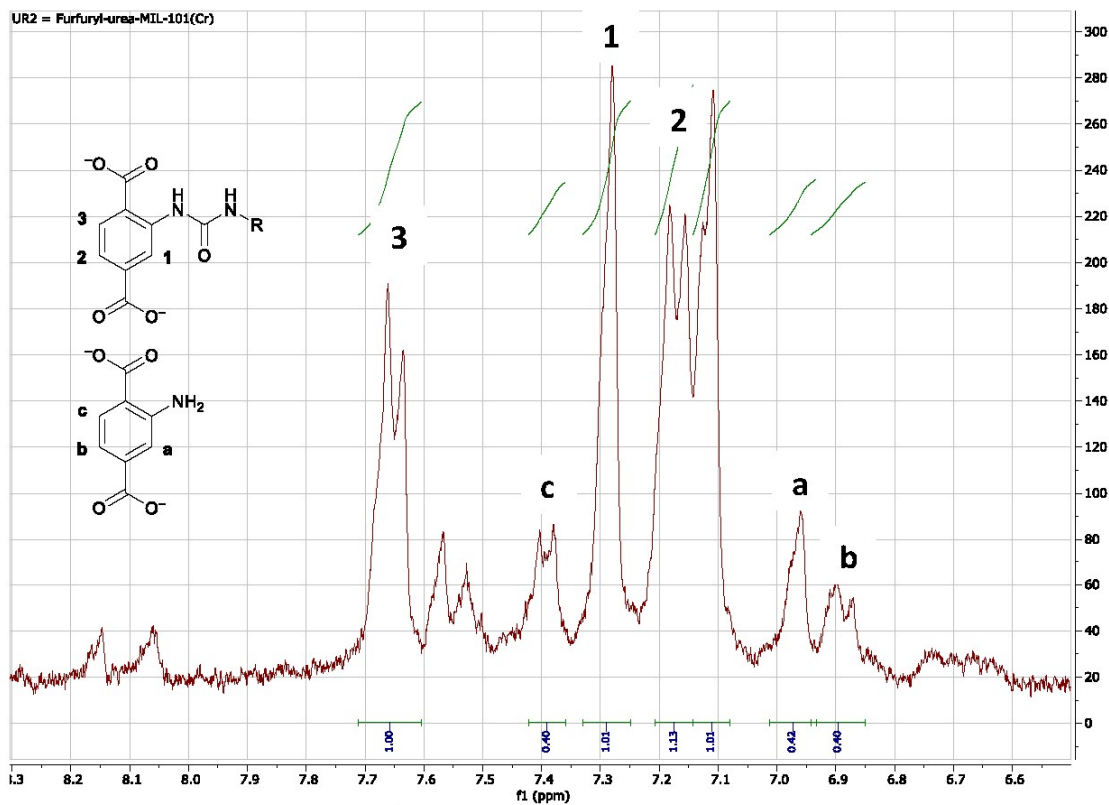
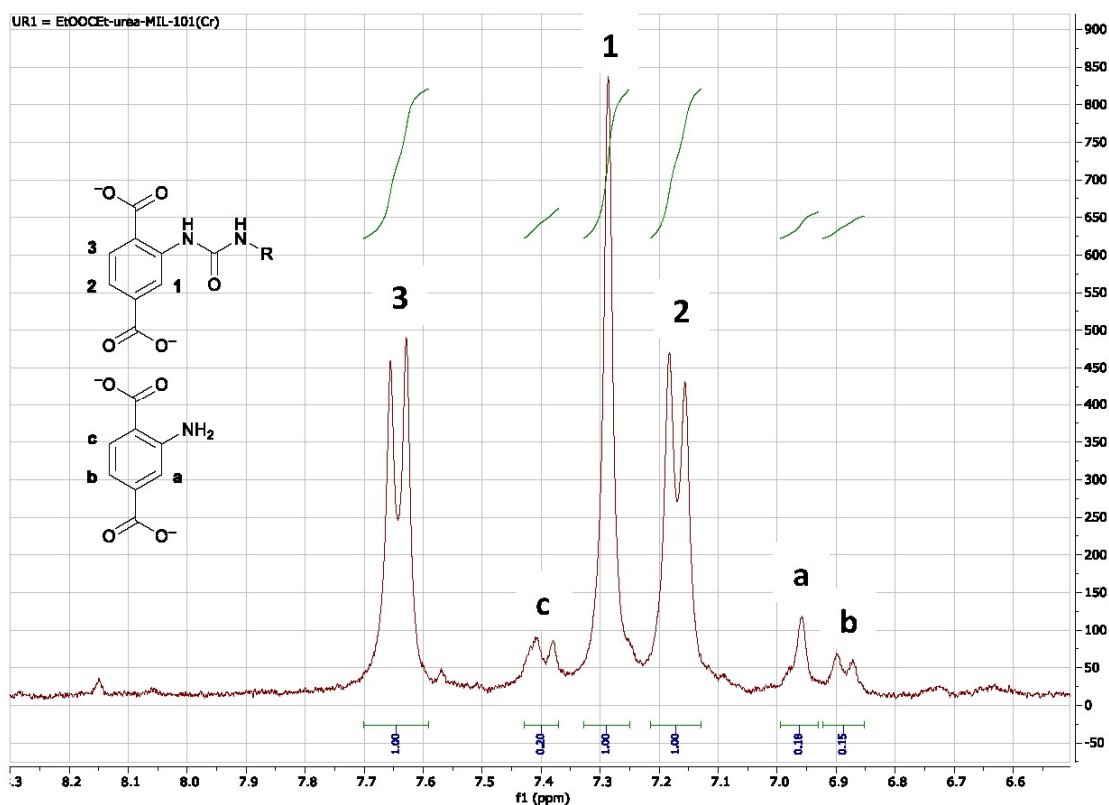
It can be noted from the comparison between the experimental and the predicted spectrum from NH<sub>2</sub>-MIL-101(Cr) in Figure S9a and S9b that the order of the chemical shifts from low to high field as **c – a – b** is reproduced. However, the actual chemical shifts are calculated too high, that is, too far downfield by ~0.5 ppm for **c**, by ~0.7 ppm for **a** and ~0.3 ppm for **b**.

|





**Figure S9.** Aromatic range in the <sup>1</sup>H-NMR spectrum of the linker solution of NH<sub>2</sub>-MIL-101(Cr) after decomposition with D<sub>2</sub>O/NaOD. (a) experimental, (b) predicted spectrum (cf. Fig. S12b for UR3).



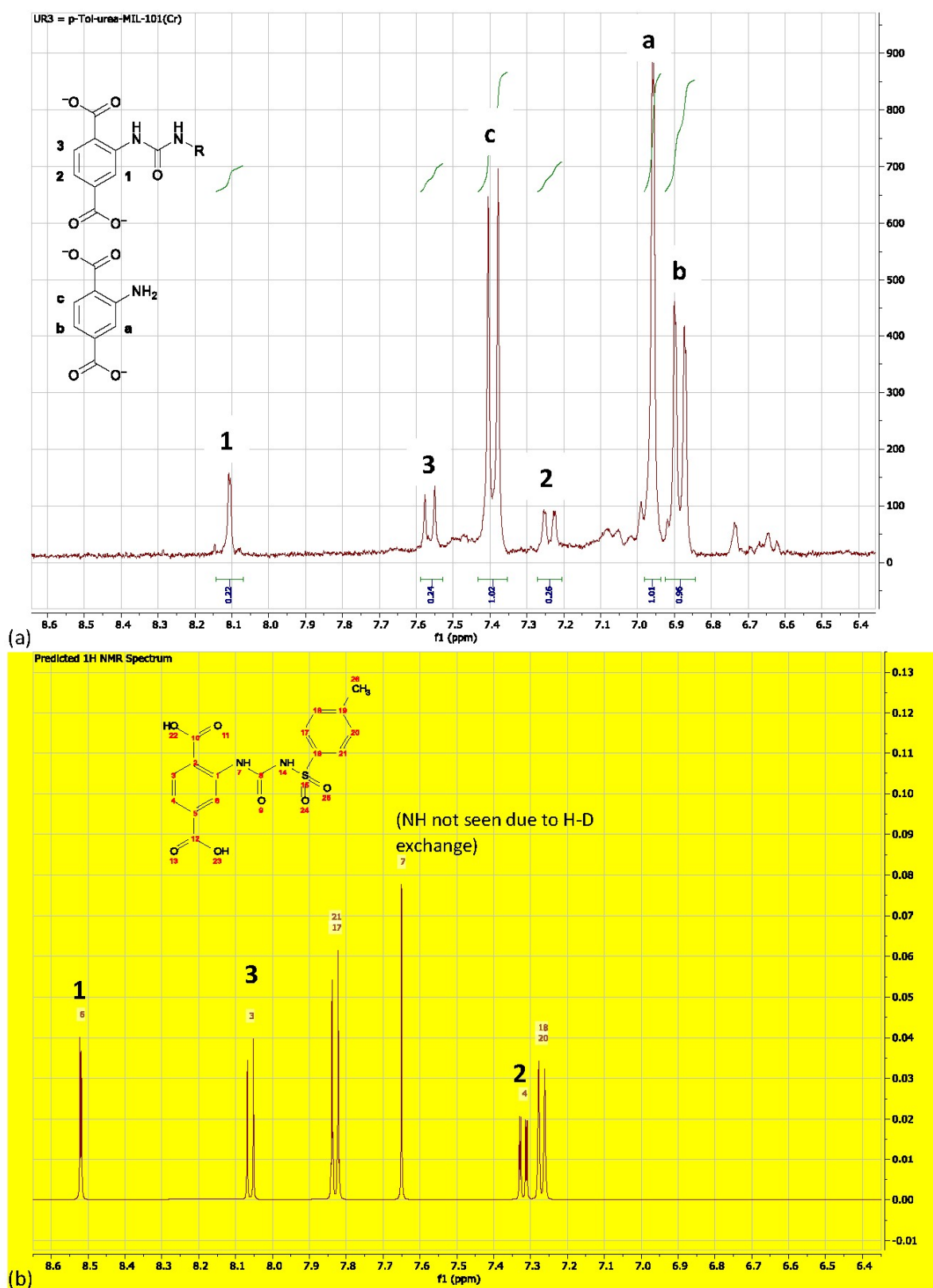


**Figure S12.** Aromatic range in the  $^1\text{H}$ -NMR spectrum of the linker solution of UR3-MIL-101(Cr) after decomposition with  $\text{D}_2\text{O}/\text{NaOD}$ . (a) experimental, (b) predicted spectrum.

We note that the chemical shift of 8.106 ppm of signal H-1 after decomposition ("digestion") of the UR3 derivative deviates significantly with its downfield shift from the chemical shifts of the signals of H-1 in the



UR1, UR2 and UR4 derivative (see Figure 2 and Figures S10, S11 and S13, respectively). The chemical shifts of the signals of H-2 (7.236 ppm) and H-3 (7.565 ppm) in UR3 also deviate from those of UR1, UR2 and -, albeit to a lesser extent from those of the other UR derivatives. At the same time the integrals of H-1, H-2 and H-3 of 0.22, 0.26 and 0.24 indicate the same relative number of H atoms. The coupling constants are

H-1 d,  $J = 1.4$  Hz,

H-2 dd,  $J = 8.1, 1.4$  Hz,

H-3 d,  $J = 8.1$  Hz,

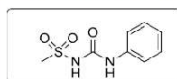
which also indicates that they are part of a 1,2,4-substituted aryl ring as the 2-urea-bound 1,4-dicarboxylate aryl group.

The *p*-toluenesulfonylurea modified linker in UR3 represents a sulfonylurea compound which is a very well investigated compound class. Sulfonylureas are used as a unique group of herbicides for controlling a range of weeds and some grasses in a variety of crops and vegetables. The exact sulfonylurea with the dicarboxyl or even only monocarboxyl substitution pattern as in UR3 appears to be unknown as this compound could not be found in a Scifinder structure search.

In the urea-bound aryl ring of sulfonylureas the ortho-H atoms to the N atom of the urea group appear around 7.3–7.5 ppm in DMSO- $d_6$  and  $CDCl_3$  with obviously little variation due to the substituents on the  $SO_2$  group. See for example in the Supporting Information of J. Zhao, Z. Li, S. Song, M.-A. Wang, B. Fu, Z. Zhang, *Angew. Chem. Int. Ed.* **2016**, *55*, 5545–5549 from where the following two examples were taken.

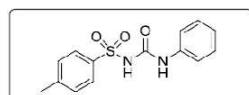
(The chemical shifts of the ortho-H atoms to NH are surrounded by a red rectangle.)

*N*-(phenylcarbamoyl)methanesulfonamide (**3ob**)<sup>[8]</sup>



<sup>1</sup>H NMR (400 MHz, DMSO- $d_6$ )  $\delta$  10.14 (br. s, 1H), 8.88 (s, 1H), 7.42 (dd,  $J = 8.6, 1.1$  Hz, 2H), 7.34–7.28 (m, 2H), 7.08–7.02 (m, 1H), 3.30 (s, 3H). <sup>13</sup>C NMR (100 MHz, DMSO- $d_6$ )  $\delta$  150.16, 138.10, 128.90, 123.27, 119.00, 41.40.

4-methyl-*N*-(phenylcarbamoyl)benzenesulfonamide (**3ab**)<sup>[6]</sup>



<sup>1</sup>H NMR (400 MHz,  $CDCl_3$ )  $\delta$  8.59 (s, 1H), 8.42 (s, 1H), 7.86–7.79 (m, 2H), 7.37 (dd,  $J = 8.6, 1.7$  Hz, 2H), 7.33–7.27 (m, 4H), 7.15–7.09 (m, 1H), 2.41 (s, 3H). <sup>13</sup>C NMR (100 MHz,  $CDCl_3$ )  $\delta$  149.38, 145.33, 136.68, 136.45, 130.24, 129.28, 127.19, 124.96, 120.46, 21.80.

NMR data of sulfonylureas can also be found in M. Hadianawala, A. Shaik, N. Hasija, A. K. Vasu, D. B. Datta, *ChemistrySelect* **2016**, *1*, 2212–2216.

Neither the sulfonyl nor the tolyl group on the sulfonyl side in neutral sulfonylureas exerts strong chemical shifts on the protons of the aromatic ring at the urea group.

Sulfonylureas are known to hydrolyze in aqueous media. (see A. K. Sarmah, J. Sabadie, *J. Agric. Food Chem.* **2002**, *50*, 6253–6365; B. M. Berger, N. L. Wolfe, *Environ. Toxicol. Chem.* **1996**, *15*, 1500–1507.)

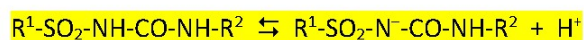
This hydrolysis usually is more rapid in water at an acidic pH and in neutral solutions sulfonylureas remained fairly stable, except for pyridine-2-sulfonylureas where the hydrolysis rates are faster in alkaline conditions than acidic conditions. The main hydrolysis reaction of all sulfonylureas under mildly acidic conditions is the cleavage of the sulfonylurea bridge according to



Hydrolysis occurs through the nucleophilic attack on the carbonyl carbon of the neutral bridge by water, giving carbon dioxide, the sulfonamide  $R^1-SO_2-NH_2$  and amine  $H_2N-R^2$ .

In the case of UR3, this hydrolysis route would lead to *p*-tolylsulfonamide and reform 2-aminoterephthalic acid (or its di-anion in basic solution). Yet, the NMR signals of H-1, H-2 and H-3 do not correspond to those of *p*-tolylsulfonamide. Therefore, we rule out a hydrolysis of the UR3 linker.

Sulfonylureas are weak acids with  $pK_a$  values generally ranging from 3 to 5 and exist as an equilibrium mixture of the neutral form and deprotonated form with the latter being much less subject to hydrolysis.



Thus, in the basic NaOD/D<sub>2</sub>O solution used for the decomposition of UR3-MIL-101(Cr), we find a hydrolysis even more unlikely. However, the organic UR3 linker will be present as a triply-deprotonated tri-anion, while UR1, UR2 and UR4 only exist as dicarboxylate di-anions. We suggest that this tri-anionic nature of UR3 is responsible for the differences in the NMR chemical shifts of H-1 to H-3 when compared to UR1, UR2 and UR4.

Finally, we note that a spectrum prediction of the UR3 linker with MestReNova reproduced the strong downfield shift of H-1. In the predicted spectrum in Figure S12b the proton H-1 is calculated at 8.52 ppm. In the above calibrating comparison between the experimental and predicted spectrum of the linker solution from NH<sub>2</sub>-MIL-101(Cr) in Figure S9a and S9b we had already noted that the actual chemical shifts are calculated too high by ~0.3 ppm to ~0.7 ppm. Thus, if we deduct 0.5 ppm from the calculated shift of 8.52 ppm of H-1, we obtain a chemical shift of 8.0 which matches the experimental shift in Figure S12a.



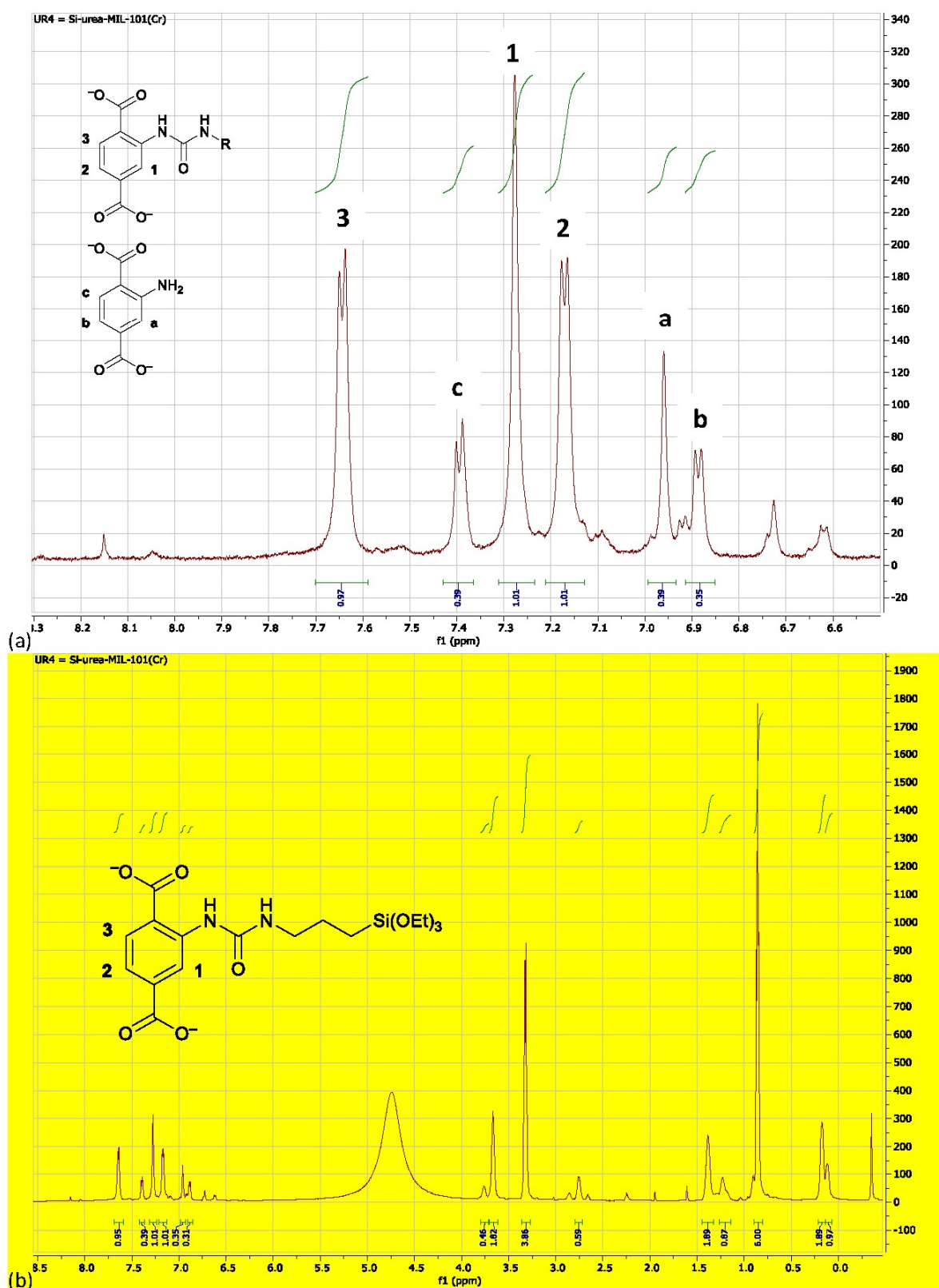


**Figure 13.** (a) Aromatic range and (b) full range in the  $^1\text{H}$ -NMR spectrum of the linker solution of UR4-MIL-101(Cr) after decomposition with  $\text{D}_2\text{O}/\text{NaOD}$ . The integrals for the ethoxy group protons at 0.86 ppm ( $-\text{CH}_3$ ) and 3.32 ppm ( $\text{Si}-\text{O}-\text{CH}_2-$ ) would have to be 9 and 6, respectively, relative to the integral of nearly 1 of the 1, 2 and 3 protons of the modified linker. Instead the integrals are only 6 and  $\sim 4$ , which indicates partial ( $\sim 1/3$ ) hydrolysis of the ethoxy groups. We note that the integrals of the  $-\text{CH}_2-$  groups of the propyl chain at 0.17, 1.39 and 3.67 ppm are  $\sim 2$  each (1.89, 1.89, 1.82).

## **S6. Nitrogen sorption experiments (T = 77 K)**

Apparent surface areas (BET) were determined by nitrogen (purity 99.999%) sorption experiments at 77 K using a *Quantachrome NOVA-4000e* instrument within a partial pressure range of  $10^{-3} < p/p_0 < 1$ . Each sample was degassed under vacuum ( $p/p_0 < 10^{-2}$ ) at 100 °C prior to measurement. All surface areas (BET) were calculated from five adsorption points in the pressure range  $0.05 < p/p_0 < 0.2$ .

### **Pressure ranges for BET calculations:**

#### **MIL-101(Cr)**

BET 5 data points,  $p/p_0 = 7.12 \cdot 10^{-2} - 1.45 \cdot 10^{-1}$

t-plot 7 data points,  $p/p_0 = 1.98 \cdot 10^{-1} - 3.98 \cdot 10^{-1}$

V-tag 1 data point at  $p/p_0 = 0.949$

#### **NH<sub>2</sub>-MIL-101(Cr)**

BET 5 data points,  $p/p_0 = 4.71 \cdot 10^{-2} - 1.48 \cdot 10^{-1}$

t-plot 6 data points,  $p/p_0 = 2.24 \cdot 10^{-1} - 4.07 \cdot 10^{-1}$

V-tag 1 data point at  $p/p_0 = 0.898$

#### **UR1-MIL-101(Cr)**

BET 5 data points,  $p/p_0 = 3.62 \cdot 10^{-2} - 1.26 \cdot 10^{-1}$

t-plot 7 data points,  $p/p_0 = 1.99 \cdot 10^{-1} - 4.05 \cdot 10^{-1}$

V-tag 1 data point at  $p/p_0 = 0.946$

#### **UR2-MIL-101(Cr)**

BET 5 data points,  $p/p_0 = 3.80 \cdot 10^{-2} - 1.26 \cdot 10^{-1}$

t-plot 7 data points,  $p/p_0 = 1.99 \cdot 10^{-1} - 3.99 \cdot 10^{-1}$

V-tag 1 data point at  $p/p_0 = 0.948$

#### **UR3-MIL-101(Cr)**

BET 5 data points,  $p/p_0 = 4.94 \cdot 10^{-2} - 1.49 \cdot 10^{-1}$

t-plot 5 data points,  $p/p_0 = 3.00 \cdot 10^{-1} - 4.99 \cdot 10^{-1}$

V-tag 1 data point at  $p/p_0 = 0.801$

#### **UR4-MIL-101(Cr)**

BET 7 data points,  $p/p_0 = 1.99 \cdot 10^{-2} - 1.33 \cdot 10^{-1}$

t-plot 5 data points,  $p/p_0 = 2.99 \cdot 10^{-1} - 5.01 \cdot 10^{-1}$

V-tag 1 data point at  $p/p_0 = 0.858$

### S7. SO<sub>2</sub> sorption experiments (T = 0 °C, 20 °C)

Sulfur dioxide sorption measurements were carried out on a *Quantachrome iQ MP* at 273 K (ice/water bath) and 293 K (active thermostating). The *iQ MP* was equipped with oil-free vacuum pumps ( $<10^{-8}$  mbar) and valves, which guaranteed contamination free measurements, moreover resistivity towards SO<sub>2</sub> by Viton<sup>®</sup> gaskets. Each sample was connected to the preparation port of the sorption analyzer and degassed under vacuum for 3 h at 150 °C. The purity of SO<sub>2</sub> was 99.98 % (N3.8) and the STP volumes are given at 273.15 K, 100.000 kPa. Helium gas was used for the determination of the cold and warm free space of the sample tubes.

SO<sub>2</sub> isotherms at T = 0 °C and 20 °C are shown in the main manuscript in Figure 5.

The *Quantachrome iQ MP* device was equipped with Viton<sup>®</sup> gaskets. SO<sub>2</sub> sorption experiments with these gaskets involve time limitations emerging from the corrosive nature of the SO<sub>2</sub> adsorptive. Hence, each SO<sub>2</sub> sorption run had to be completed within a maximal time of 10 h. This time limit was specified by the company Quantachrome to prevent damage to the gaskets. After this time, the system had to be regenerated by flushing with nitrogen. Irreversible swelling of the SO<sub>2</sub> adsorbing gaskets in the measurement device, which could cause leaks in the system, had to be prevented by setting the measurement time to this maximum (10 h) to meet safety precautions and to protect the device. Then, after each measurement the gas line was flushed with N<sub>2</sub> several times and remained under N<sub>2</sub> atmosphere for at least 12 h to regenerate the gaskets. The chemical compatibility of gasket materials is available in ref. [72]. All SO<sub>2</sub> sorption isotherms were measured up to a maximum of 0.9 bar, for safety reasons.

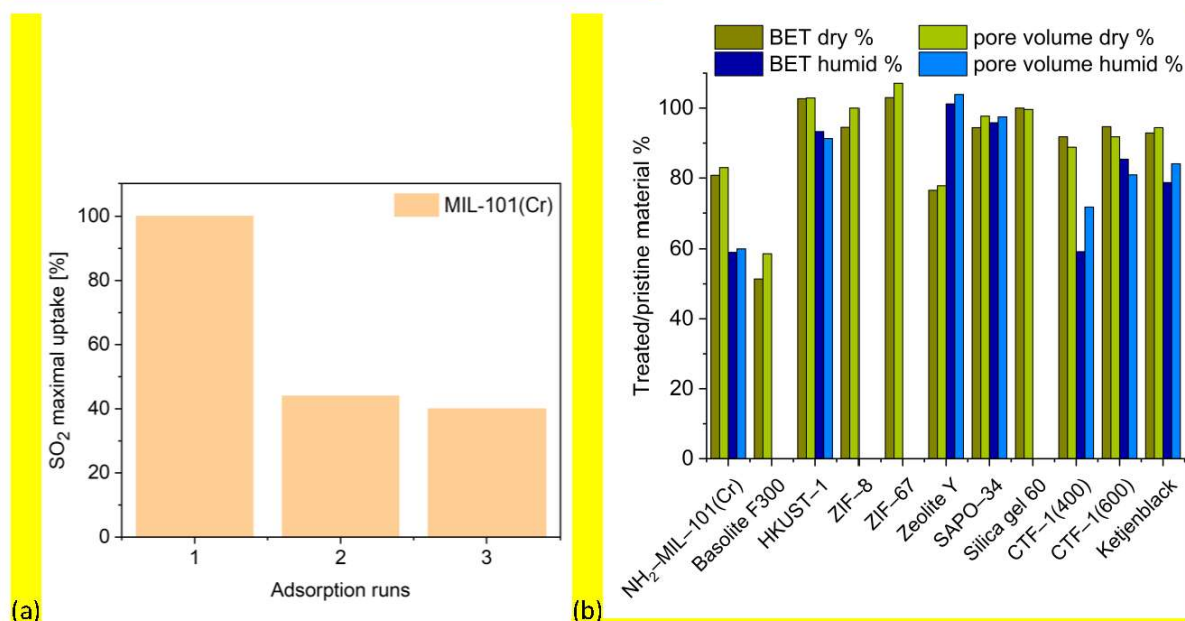


**Figure S14.** (a) Cycling SO<sub>2</sub> adsorption-desorption performance of MIL-101 at 293 K and 0.97 bar. (b) The relative (treated/pristine) BET surface area and total pore volume of investigated porous materials, including NH<sub>2</sub>-MIL-101(Cr) after dry and humid SO<sub>2</sub> exposure. Part (b) reprinted from ref. [73]. Copyright © 2021 The Authors. Advanced Sustainable Systems published by Wiley-VCH GmbH.

### **S8. CO<sub>2</sub> sorption experiments (T = 0 °C, 20 °C)**

Carbon dioxide sorption measurements were carried out on a *Quantachrome Autosorb iQ MP* at 273 K (ice/water bath) and 293 K (active thermostating). Each sample was connected to the preparation port of the sorption analyzer and degassed under vacuum for 3 h at 150 °C. Helium gas was used for the determination of the cold and warm free space of the sample tubes.

CO<sub>2</sub> sorption isotherms at T = 0 °C and 20 °C are shown in Figure 6 in the main manuscript.

### **S9. H<sub>2</sub>O vapor sorption experiments (T = 20 °C)**

Water vapor sorption was carried out on a *Quantachrome Autosorb iQ MP* at 293 K (active thermostating). Each sample was connected to the preparation port of the sorption analyzer and degassed under vacuum for 3 h at 150 °C. Helium gas was used for the determination of the cold and warm free space of the sample tubes.

Figure S15 displays the water vapor isotherms at T = 20 °C.

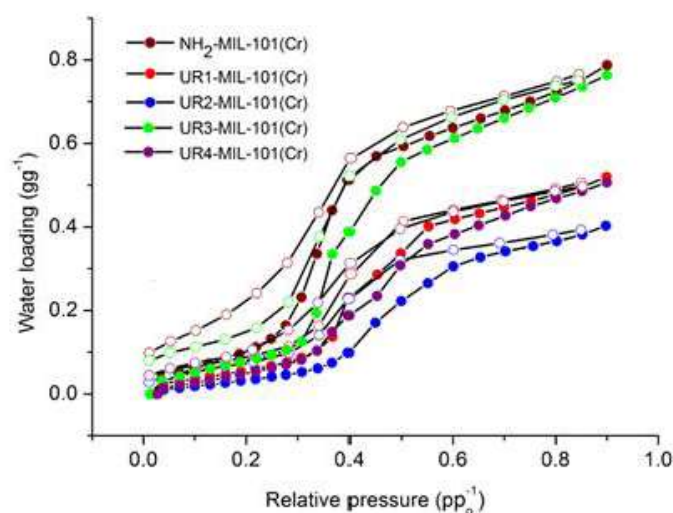


**Figure S15.** H<sub>2</sub>O sorption isotherms at 20 °C in comparison to NH<sub>2</sub>-MIL-101(Cr) (solid symbols: adsorption, hollow symbols: desorption).

## S11. References

- <sup>1</sup> T. Zhao, F. Jeremias, I. Boldog, B. Nguyen, S. K. Henninger, C. Janiak, *Dalton Trans.* **2015**, *44*, 16791-6801.
- <sup>2</sup> D. Jiang, L. L. Keenan, A. D. Burrows, K. J. Edler, *Chem. Commun.* **2012**, *48*, 12053-12055.
- <sup>3</sup> A. Khutia, C. Janiak, *Dalton Trans.* **2014**, *43*, 1338-1347.
- <sup>4</sup> G. Férey, C. Mellot-Draznieks, C. Serre, F. Millange, J. Dutour, S. Surblé, I. Margiolaki, *Science* **2005**, *309*, 2040-2042.
- <sup>5</sup> K. Brandenburg, Diamond Version 4, Crystal and Molecular Structure Visualization, Crystal Impact - K. Brandenburg & H. Putz GbR, Bonn, Germany, 2009-2020.
- <sup>6</sup> S. H. Jung, J. H. Lee, J. W. Yoon, C. Serre, G. Férey, J. S. Chang, *Adv. Mater.* **2007**, *19*, 121-124.
- <sup>7</sup> B. D.-Y. Hong, Y. K. Hwang, C. Serre, G. Férey, J.-S. Chang, *Adv. Funct. Mater.* **2009**, *19*, 1537-1552.
- <sup>8</sup> M. Latroche, S. Surblé, C. Serre, C. Mellot-Draznieks, P. L. Llewellyn, J.-H. Lee, J.-S. Chang, S. H. Jung, G. Férey, *Angew. Chem.* **2006**, *118*, 8407-8411.
- <sup>9</sup> J. Yang, Q. Zhao, J. Li, J. Dong, *Micropor. Mesopor. Mater.* **2010**, *130*, 174-179.
- <sup>10</sup> P. L. Llewellyn, S. Bourelly, C. Serre, A. Vimont, M. Daturi, L. Hamon, G. De Weireld, J.-S. Chang, D.-Y. Hong, Y. K. Hwang, S. H. Jung, G. Férey, *Langmuir* **2008**, *24*, 7245-7250.
- <sup>11</sup> D. Jiang, A. D. Burrows, K. J. Edler, *CrystEngComm* **2011**, *13*, 6916-6919.
- <sup>12</sup> H. C. Yoon, P. B. S. Rallapalli, H. T. Beom, S. S. Han, J.-N. Kim, *Energy & Fuels* **2018**, *32*, 1365-1373.
- <sup>13</sup> Q. Yan, Y. Lin, C. Kong, L. Chen, *Chem. Commun.* **2013**, *49*, 6873-6875.
- <sup>14</sup> P. Küsgens, M. Rose, I. Senkovska, H. Fröde, A. Henschel, S. Siegle, S. Kaskel, *Micropor. Mesopor. Mater.* **2009**, *120*, 325-330.
- <sup>15</sup> G. Akiyama, R. Matsuda, H. Sato, A. Hori, M. Takata, S. Kitagawa, *Micropor. Mesopor. Mater.* **2012**, *157*, 89-93.
- <sup>16</sup> A. Khutia, H. U. Rammelberg, T. Schmidt, S. K. Henninger, C. Janiak, *Chem. Mater.* **2013**, *25*, 790-798.
- <sup>17</sup> F. Jeremias, D. Fröhlich, C. Janiak, S. K. Henninger, *New J. Chem.* **2014**, *38*, 1846-1852.
- <sup>18</sup> J. Ehrenmann, S. K. Henninger, C. Janiak, *Eur. J. Inorg. Chem.* **2011**, *4*, 471-474.
- <sup>19</sup> A) N. C. Burtch, H. Jasuja, K. S. Walton, *Chem. Rev.* **2014**, *114*, 10575-10612; B) M. F. de Lange, K. J. F. M. Verouden, T. J. H. Vlught, J. Gascon, F. Kapteijn, *Chem. Rev.* **2014**, *20*, 10575-10612; C) M. F. de Lange, B. L. van Velzen, C. P. Ottevanger, K. J. F. M. Verouden, L.-C. Lin, T. J. H. Vlught, J. Gascon, F. Kapteijn, *Langmuir* **2015**, *31*, 12783-12796.
- <sup>20</sup> M. Hartmann, M. Fischer, *Micropor. Mesopor. Mater.* **2012**, *164*, 38-43.
- <sup>21</sup> A. Herbst, C. Janiak, *New J. Chem.* **2016**, *40*, 7958-7967.
- <sup>22</sup> M. Wickenheisser, C. Janiak, *Micropor. Mesopor. Mater.* **2015**, *204*, 242-250.
- <sup>23</sup> P. Horcajada, T. Chalati, C. Serre, B. Gillet, C. Sebrie, T. Baati, J. F. Eubank, D. Heurtaux, P. Clayette, C. Kreuz, J.-S. Chang, Y. K. Hwang, V. Marsaud, P.-N. Bories, L. Cynober, S. Gil, G. Férey, P. Couvreur, R. Gref, *Nature Mater.* **2010**, *9*, 172-178.
- <sup>24</sup> S. Wuttke, S. Braig, T. Preiß, A. Zimpel, J. Sicklinger, C. Bellomo, J. O. Rädler, A. M. Vollmar, T. Bein, *Chem. Commun.* **2015**, *51*, 15752-15755.
- <sup>25</sup> M. Wen, K. Mori, T. Kamegawa, H. Yamashita, *Chem. Commun.* **2014**, *50*, 11645-11648.
- <sup>26</sup> M. Lammert, S. Bernt, F. Vermoortele, D. E. De Vos, N. Stock, *Inorg. Chem.* **2013**, *52*, 8521-8528.
- <sup>27</sup> D. Jiang, L. L. Keenan, A. D. Burrows, K. J. Edler, *Chem. Commun.* **2012**, *48*, 12053-12055.
- <sup>28</sup> A. Klinkebiel, N. Reimer, M. Lammert, N. Stock, U. Lüning, *Chem. Commun.* **2014**, *50*, 9306-9308.
- <sup>29</sup> N. Ko, P. G. Choi, J. Hong, M. Yeo, S. S. Kyle E. Cordova, H. J. Park, J. K. Yang, J. Kim, *J. Mater. Chem. A* **2015**, *3*, 2057-2064.
- <sup>30</sup> K. K. Tanabe, S. M. Cohen, *Chem. Soc. Rev.* **2011**, *40*, 498-519.
- <sup>31</sup> S. M. Cohen, *J. Am. Chem. Soc.*, **2017**, *139*, 2855-2863.
- <sup>32</sup> Z. Yin, S. Wan, J. Yang, M. Kurmoo, M.-H. Zeng, *Coord. Chem. Rev.* **2019**, *378*, 500-512.
- <sup>33</sup> G. Akiyama, R. Matsuda, H. Sato, A. Hori, M. Takata, S. Kitagawa, *Micropor. Mesopor. Mater.* **2012**, *157*, 89-93.
- <sup>34</sup> H. Furukawa, K. E. Cordova, M. O'Keeffe, O. M. Yaghi, *Science* **2013**, *341*, 1230444.
- <sup>35</sup> K. Tan, P. Canepa, Q. Gong, J. Liu, D. H. Johnson, A. Dyevoich, P. K. Thallapally, T. Thonhauser, J. Li, Y. J. Chabal, *Chem. Mater.* **2013**, *25*, 4653-4662.
- <sup>36</sup> D. Britt, D. Tranchemontagne, O. M. Yaghi, *Proc. Natl. Acad. Sci. USA* **2008**, *105*, 11623-11627.



- <sup>37</sup> M. Ranjbar, M. A. Taher, *J. Porous Mat.* **2016**, *23*, 1249-1254.
- <sup>38</sup> H. Dathe, E. Peringer, V. Roberts, A. Jentys, J. A. Lercher, *C. R. Chim.* **2005**, *8*, 753-763.
- <sup>39</sup> G. L. Smith, J. E. Eyley, X. Han, X. Zhang, J. Li, N. M. Jaques, H. G. W. Godfrey, S. P. Argent, L. J. McCormick McPherson, S. J. Teat, Y. Cheng, M. D. Frogley, G. Cinque, S. J. Day, C. C. Tang, T. L. Easun, S. Rudić, A. J. Ramirez-Cuesta, S. Yang, M. Schröder, *Nature Mater.* **2019**, *18*, 1358-1365.
- <sup>40</sup> J. H. Carter, X. Han, F. Y. Moreau, I. da Silva, A. Nevin, H. G. W. Godfrey, C. C. Tang, S. Yang, M. Schröder, *J. Am. Chem. Soc.* **2018**, *140*, 15564-15567.
- <sup>41</sup> S. Yang, J. Sun, A. J. Ramirez-Cuesta, S. K. Callear, W. I. F. David, D. P. Anderson, R. Newby, A. J. Blake, J. E. Parker, C. C. Tang, M. Schröder, *Nat. Chem.* **2012**, *4*, 887-894.
- <sup>42</sup> M. Savage, Y. Cheng, T. L. Easun, J. E. Eyley, S. P. Argent, M. R. Warren, W. Lewis, C. Murray, C. C. Tang, M. D. Frogley, G. Cinque, J. Sun, S. Rudić, R. T. Murden, M. J. Benham, A. N. Fitch, A. J. Blake, A. J. Ramirez-Cuesta, S. Yang, M. Schröder, *Adv. Mater.* **2016**, *28*, 8705-8711.
- <sup>43</sup> J. A. Zárate, E. Sánchez- González, D. R. Williams, E. González-Zamora, V. Martis, A. Martínez, J. Balmaseda, G. Maurin, I. A. Ibarra, *J. Mater. Chem. A* **2019**, *7*, 15580-15584.
- <sup>44</sup> J. Zhang, P. Zhang, F. Han, G. Chen, L. Zhang, X. Wei, *Ind. Eng. Chem. Res.* **2009**, *48*, 1287-1291.
- <sup>45</sup> S. Yang, L. Liu, J. Sun, K. M. Thomas, A. J. Davies, M. W. George, A. J. Blake, A. H. Hill, A. N. Fitch, C. C. Tang, M. Schröder, *J. Am. Chem. Soc.* **2013**, *135*, 4954-4957.
- <sup>46</sup> R. Domínguez-González, I. Rojas-Léon, E. Martínez-Ahumada, D. Martínez-Otero, H. A. Lara-García, J. Balmaseda-Era, I. A. Ibarra, E. G. Percástegui, V. Jancik, *J. Mater. Chem. A* **2019**, *7*, 26812-26817.
- <sup>47</sup> C. A. Fernandez, P. K. Thallapally, R. K. Motkuri, S. K. Nune, J. C. Sumrak, J. Tian, J. Liu, *Cryst. Growth Des.* **2010**, *10*, 1037-1039.
- <sup>48</sup> P. K. Thallapally, R. K. Motkuri, C. A. Fernandez, B. P. McGrail, G. S. Behrooz, *Inorg. Chem.* **2010**, *49*, 4909-4915.
- <sup>49</sup> Y. Zhang, P. Zhang, W. Yu, J. Zhang, J. Huang, J. Wang, M. Xu, Q. Deng, Z. Zeng, S. Deng, *ACS Appl. Mater. Interfaces* **2019**, *11*, 10680-10688.
- <sup>50</sup> S. Hungerford, S. Bhattacharyya, U. Tulumuri, S. Nair, Z. Wu, K. S. Walton, *J. Phys. Chem. C* **2018**, *122*, 23493-23500.
- <sup>51</sup> T. J. Matemb Ma Ntep, H. Breitzke, L. Schmolke, C. Schlüsener, B. Moll, S. Millan, N. Tannert, I. El Aita, G. Buntkowsky, C. Janiak, *Chem. Mater.* **2019**, *31*, 8629-8638.
- <sup>52</sup> M. R. Tchalala, P. M. Bhatt, K. N. Chappanda, S. R. Tavarez, K. Adil, Y. Belmabkhout, A. Shkourenko, A. Cadiau, N. Heymans, G. De Weireld, G. Maurin, K. N. Salama, M. Eddaoudi, *Nature Commun.* **2019**, *10*, 1-10.
- <sup>53</sup> P. Brandt, A. Nuhnen, M. Lange, J. Möllmer, O. Weingart, C. Janiak, *ACS Appl. Mater. Interfaces* **2019**, *11*, 17350-17358.
- <sup>54</sup> L. Xia, Q. Cui, X. Suo, Y. Li, X. Cui, Q. Yang, J. Xu, Y. Yang, H. Xing, *Adv. Funct. Mater.* **2018**, *28*, 1704292.
- <sup>55</sup> Z. Chen, X. Wang, R. Cao, K. B. Idrees, X. Liu, M. C. Wasson, O. K. Farha, *ACS Mater. Lett.* **2020**, *9*, 1129-1134.
- <sup>56</sup> S. Glomb, D. Woschko, G. Makhoulfi, C. Janiak, *ACS Appl. Mater. Interfaces* **2016**, *9*, 37419-37434.
- <sup>57</sup> L. J. Barrios-Vargas, J. G. Ruiz-Montoya, B. Landeros-Rivera, J. Raziel Alvarez, D. Avarado-Alvarado, R. Vargas, A. Martínéz, E. González-Zamora, L. M. Cáceres, J. C. Morales, I. A. Ibarra, *Dalton Trans.* **2020**, *49*, 2786-2793.
- <sup>58</sup> J. Antonio-Zárate, E. Domínguez-Ojeda, E. Sánchez-González, E. Martínez-Ahumada, V. B. López-Cervantes, D. R. Williams, V. Martis, I. A. Ibarra, J. Alejandro, *Dalton Trans.* **2020**, *49*, 9203-9207.
- <sup>59</sup> D. Dietrich, C. Licht, A. Nuhnen, S.-P. Höfert, L. De Laporte, C. Janiak, *ACS Appl. Mater. Interfaces* **2019**, *11*, 19654-19667.
- <sup>60</sup> J. W. Long, J. M. Wallace, G. W. Peterson, K. Huynh, *ACS Appl. Mater. Interfaces* **2016**, *8*, 1184-1193.
- <sup>61</sup> S. Yun, H. Kim, H. Lee, H. S. Park, *Mater. Express* **2015**, *5*, 463-469.
- <sup>62</sup> H. Yi, Z. Wang, H. Liu, X. Tang, D. Ma, S. Zhao, B. Zhang, F. Gao, Y. Zuo, *J. Chem. Eng. Data* **2014**, *59*, 1556-1563.
- <sup>63</sup> I. Matito-Martos, A. Martín-Calvo, J. J. Gutiérrez-Sevillano, M. Haranczyk, M. Doblare, J. B. Parra, C. O. Ania, S. Calero, *Phys. Chem. Chem. Phys.* **2014**, *16*, 19884-19893.
- <sup>64</sup> H. Deng, H. Yi, X. Tang, Q. Yu, P. Ning, L. Yang, *Chem. Eng. J.* **2012**, *188*, 77-85.
- <sup>65</sup> X. Cui, Q. Yang, L. Yang, R. Krishna, Z. Zhang, Z. Bao, H. Wu, Q. Ren, W. Zhou, B. Chen, H. Xing, *Adv. Mater.* **2017**, *29*, 1606929.

- 
- <sup>66</sup> L. Wu, D. An, J. Dong, Z. Zhang, B.-G. Li, S. Zhu, *Macromol. Rapid Commun.* **2006**, *27*, 1949-1954.
- <sup>67</sup> L. Zhao, X. Li, C. Hao, C. L. Raston, *Appl. Catal. B Environ.* **2012**, *117-118*, 339-345.
- <sup>68</sup> Z. Zhang, L. Wu, J. Dong, B.-G. Li, S. Zhu, *Ind. Eng. Chem. Res.* **2009**, *48*, 2142-2148.
- <sup>69</sup> E. Martínez-Ahumada, M. L. Díaz-Ramírez, H. A. Lara-García, D. R. Williams, V. Martis, V. Jancik, E. Lima, I. A. Ibarra, *J. Mater. Chem. A* **2020**, *8*, 11515-11520.
- <sup>70</sup> D. Wang, B. Liu, S. Yao, T. Wang, G. Li, Q. Huo, Y. A. Liu, *Chem. Commun.* **2015**, *51*, 15287-15289.
- <sup>71</sup> R.-B. Lin, Y. He, P. Li, H. Wang, W. Zhou, B. Chen, *Chem. Soc. Rev.* **2019**, *48*, 1362-1389.
- <sup>72</sup> <https://www.coleparmer.com/chemical-resistance>, retrieved November 3rd 2020
- <sup>73</sup> P. Brandt, A. Nuhnen, S. Öztürk, G. Kurt, J. Liang, C. Janiak, *Adv. Sust. Mater.* **2021**, *in press*.  
<https://doi.org/10.1002/adsu.202000285>

## 4. Unpublished Results

Apart from the results presented in the preceding, cumulative part, additional work packages are covered in this thesis but remain unpublished for practical or patent reasons. These work packages are presented in the current chapter.

### 4.1. Unravelling Gas Sorption in Microporous Al-MOF CAU-23 – N<sub>2</sub>, Ar, CO<sub>2</sub>, H<sub>2</sub>, CH<sub>4</sub>, SO<sub>2</sub> and H<sub>2</sub>O Sorption and Mixed-Adsorptive Calculations

#### Introduction

The MOF CAU-23 was simultaneously found by researchers of *Christian-Albrechts-Universität* Kiel (CAU), nominal D. Lenzen, and *Heinrich-Heine-Universität* Düsseldorf, nominal N. Tannert. After early contacts between the two groups, especially to H. Reinsch (CAU Kiel) for Rietveld-refinements of MOF samples, both universities agreed on publishing in at least two literature contributions. The first contribution (D. Lenzen, J. Zhao, S.-J. Ernst, M. Wahiduzzaman, A. K. Inge, D. Fröhlich, H. Xu, H.-J. Bart, C. Janiak, S. Henninger, G. Maurin, X. Zou, N. Stock, *Nat. Commun.*, 2019, **10**, article no. 3025) introduced the novel MOF CAU-23 and its water sorption properties. The second contribution will be published prospectively. The manuscript will focus on gas sorption isotherms of N<sub>2</sub>, Ar, CO<sub>2</sub>, H<sub>2</sub>, CH<sub>4</sub>, SO<sub>2</sub> and H<sub>2</sub>O vapor isotherms, adsorption enthalpies, mixed-adsorptive calculations, moreover high-pressure CO<sub>2</sub> sorption. In sum, the manuscript will be a sophisticated evaluation of sorption properties of the new adsorbent CAU-23.

#### Experimental Section

We are currently working on a manuscript submission including all relevant data and results in a high-quality peer-reviewed journal (authors include: C. Jansen, N. Tannert, D. Lenzen, S. Millan, A. Goldmann, N. Stock and C. Janiak). The collected data and results will be published soon, the full manuscript content and thematic classification will be available in the dissertation of C. Jansen. Due to these facts this topic will not be discussed in detail any further within this dissertation.

Author's contribution of work include all analytical measurements, appreciable seventeen displayed sorption isotherms. Fifteen isotherms (except for N<sub>2</sub> and Ar) were considered for mixed-adsorptive calculations (using fitted isotherms and IAST theory) and determination of adsorption enthalpies for each adsorptive at two temperature pairs.

## 4.2. Evaluation of Al-sources in The Syntheses of MIL-53-type MOFs With [Al(OH)(linker)]-Structure

### Introduction

Until today, literature publications on predominantly water-stable MIL-53-type MOFs with [Al(OH)(linker)]-structure and V-shaped linkers, for example MIL-53, CAU-10-H, MIL-160, MIL-53-TDC, CAU-23 and many others, utilize several different Al-salt sources in the MOF syntheses. It is somehow unintelligible why different Al-sources are used for the same or a closely related MOF. Even more interesting, it is unclear what impact the Al-reactant has on the MOF properties, foremost porosity parameters. The outlined issue and uprising questions are still topical and have not been exactly enlightened any further in the literature. The following work has not been published, may nonetheless be considerable. Additional and supporting experiments and investigations were carried out by A. Nuhnen and for Al<sub>fum</sub> and CAU-10-H.

Within the manuscript introduced in chapter 3.2., the influence of applied Al-salt in the synthesis of MIL-53(Al)-TDC has descriptively been investigated in the example of four Al-sources. Hence, some of the results that were found in the realm of the presented issue have been published and can be found in the named literature contribution. The additional findings for CAU-23 and MIL-160 is summarized in the following.

### Experimental Section

The influence on Al-salts on the formation of MIL-53(Al)-TDC was investigated within the manuscript of chapter 3.2., revealing several trends. In this specific case, four different Al-source approaches (namely Al<sub>2</sub>(SO<sub>4</sub>)<sub>3</sub> · 18 H<sub>2</sub>O, AlCl<sub>3</sub> · 6 H<sub>2</sub>O, Al(OH)(acetate)<sub>2</sub> · x H<sub>2</sub>O and NaAlO<sub>2</sub> in combination with AlCl<sub>3</sub> · 6 H<sub>2</sub>O) resulted in fairly equal porosities around 1100 m<sup>2</sup> g<sup>-1</sup>. Considerable differences in crystallinity could not be observed in any case, however morphology and crystallite sizes differed with the utilized Al-salt (*cf.* manuscript and ESI of chapter 3.2. for more details). Table 2 lists the porosity parameters of CAU-23, MIL-53-TDC and MIL-160 in dependance of the applied Al-source in each synthesis.

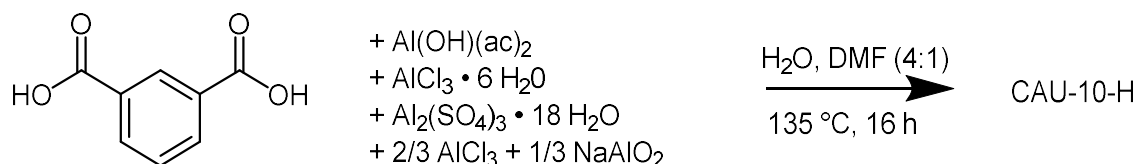


**Figure 15: Synthesis of Al-MOF (here exemplarily shown for CAU-10-H) with varying Al-source.**

**Table 2: Porosity parameters of Al-MOFs CAU-23, MIL-53-TDC, MIL-160 and CAU-10-H in dependency of the Al-source applied in the synthesis. Top value: BET surface area, bottom value: water vapor capacity.**

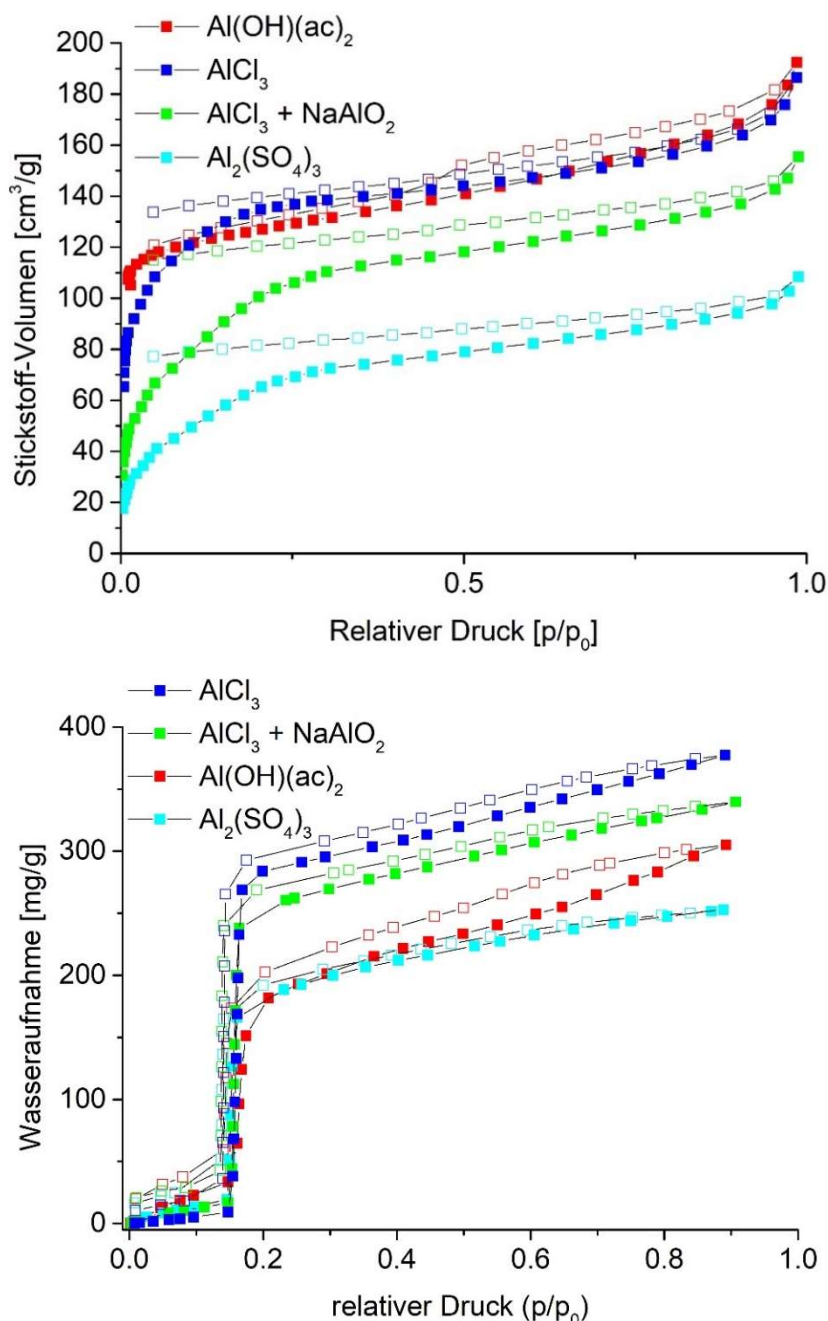
	CAU-23	MIL-53-TDC	MIL-160	CAU-10-H
AlCl <sub>3</sub>	202 m <sup>2</sup> /g	1080 m <sup>2</sup> /g	928 m <sup>2</sup> /g	664 m <sup>2</sup> /g
	0.11 mg/g	0.34 mg/g	0.27 mg/g	0.36 mg/g
Al <sub>2</sub> (SO <sub>4</sub> ) <sub>3</sub>	20 m <sup>2</sup> /g	1102 m <sup>2</sup> /g	880 m <sup>2</sup> /g	257 m <sup>2</sup> /g
	0.02 mg/g	0.37 mg/g	0.28 mg/g	0.24 mg/g
Al(OH)(ac) <sub>2</sub>	1027 m <sup>2</sup> /g	1027 m <sup>2</sup> /g	130 m <sup>2</sup> /g	491 m <sup>2</sup> /g
	0.22 mg/g	0.33 mg/g	0.07 mg/g	0.30 mg/g
NaAlO <sub>2</sub> +AlCl <sub>3</sub>	1. 686 m <sup>2</sup> /g 1. 0.28 mg/g 2. 1247 m <sup>2</sup> /g 2. 0.41 mg/g	/	1094 m <sup>2</sup> /g 0.33 mg/g	385 m <sup>2</sup> /g 0.33 mg/g
Literature (Al-source)	ref. 177 1250 m <sup>2</sup> /g (NaAlO <sub>2</sub> + AlCl <sub>3</sub> )	ref. 175 1150 m <sup>2</sup> /g 0.40 mg/g (AlCl <sub>3</sub> )	ref. 261 / 262 1098 / 1150 m <sup>2</sup> /g 0.41 / 0.48 mg/g (both Al(OH)(ac) <sub>2</sub> ) ref. 263 1070 m <sup>2</sup> /g 0.40 mg/g (AlCl <sub>3</sub> )	ref. 174, 264, 265 525-660 m <sup>2</sup> /g 0.30-0.35 mg/g (AlCl <sub>3</sub> )

Table 2 supports the introductorily mentioned uncertainties of Al-source use within the aqueous syntheses of MIL-53-like Al-MOFs in general. For example, AlCl<sub>3</sub> seems to be a very differing starting reagent in the syntheses of the isomorphous MOFs MIL-53-TDC and CAU-23. Another insight may be that CAU-10-H obtained from Al(OH)(ac)<sub>2</sub> adsorbs less water (0.30 mg/g) than the same MOF obtained from NaAlO<sub>2</sub>+AlCl<sub>3</sub> (0.33 mg/g), at the same time having significantly more surface area (491 m<sup>2</sup>/g vs. 385 m<sup>2</sup>/g, cf. Figure 16). Even MOF from AlCl<sub>3</sub> with highest BET



surface area ( $664 \text{ m}^2/\text{g}$ ) lifts only  $0.03 \text{ mg/g}$  more ( $0.36 \text{ mg/g}$ ) than CAU-10-H obtained from  $\text{Al}(\text{OH})(\text{ac})_2$ . The discrepancy between surface area and water vapor uptake is certainly correlating with pore volume, however, several insights into the influence on pore hydrophilicity of CAU-10-H could be gained.

Exemplarily for CAU-10-H, nitrogen and water sorption isotherms for samples obtained from the mentioned four Al-sources are graphically compared in Figure 16.



**Figure 16: Nitrogen sorption (top,  $T = 77.36 \text{ K}$ ) and water vapor sorption (bottom,  $T = 20 \text{ }^\circ\text{C}$ ) isotherms. Solid symbols depict adsorption points, hollow symbols depict desorption points.**

Numerous more details on CAU-10-H are given in the BSc thesis by M. Bengsch, which was supervised by the author.<sup>266</sup>

### 4.3. MOF composites

The appearance of MOFs is typically powdery. Hence, the shaping and forming of MOFs, which consequently goes along with prospective utilization of MOFs, has become a living sector of MOF research and development. Since the fabrication and evaluation of MOF composites has been one project goal of the OptiMat project (*cf.* chapter 2), several experiments of forming MOF composites were tried out, from which some have been published. Specifically, author's contributions to: S. Gökpınar, S.-J. Ernst, E. Hastürk, M. Möllers, I. El Aita, R. Wiedey, N. Tannert, S. Nießing, S. Abdpour, A. Schmitz, J. Quodbach, G. Földner, S. K. Henninger and C. Janiak, *Air-Con Metal-Organic Frameworks in Binder Composites for Water Adsorption Heat Transformation Systems*, *Ind. Eng. Chem. Res.*, 2019, **58**, 21493-21503; additionally Ü. Kökcam-Demir, N. Tannert, M. Bengsch, A. Spieß, C. Schlüsener, S. Nießing and C. Janiak, *Improving porosity and water uptake of aluminum metal-organic frameworks (Al-MOFs) as graphite oxide (GO) composites*, *Micropor. Mesopor. Mater.*, 2021, *submitted*; can be cited within this realm. Several other scientific articles have been published within the project OptiMat and in this context. Additional experiments and investigations that have not been published, but may nonetheless be considerable, are given in the following.

#### 4.3.1. Stabilized HIPEs with High MOF Fraction

##### Introduction

The nature of polycrystalline MOF powders from typical MOF syntheses requires for shaping techniques, as explained chapter 1.3.3.1. Hence, the shaping of MOFs into mechanically stable monoliths or coatings is one part of the puzzle called industrialization of MOFs. Besides various other strategies, one possibility of bringing MOFs into monolithic shapes are high-internal phase emulsions (HIPEs).<sup>267</sup> Previous research on water stable MIL-100(Fe,Cr) and MIL-101(Cr) embedded into polymer-HIPEs like poly(HEMA)HIPE (HEMA = 2-hydroxyethyl methacrylate) displayed an elegant route towards porous composites.<sup>203</sup> Zhang *et al.* demonstrated the formation of stable HIPEs from a mixture of water and diethylether in the presence of MOF particles. While the latter supported the stability of the HIPE, the approach resulted further in macroporous ultralight metal-organic aerogels (MOAs).<sup>268</sup> In general, the increase of MOF fraction in HIPE-derived MOF composites could be an elegant way to form highly loaded, hierarchical porous and gas or air stream permeable MOF composites that could also be utilized in AHTs and MOF-based applications in general.

##### Experimental Section

The following experiments were carried out in analogy to the principles demonstrated by Zhang *et al.*<sup>268</sup> In each case either 50 or 500 mg of AlFum, nano-sized MIL-101(Cr), CAU-10-H or

MIL-100(Fe) was mixed with 5 mL of water/cyclohexane (1:1) or water/diethyl ether (1:1) in a glass vial by a vortex mixer for 30 min. It could be observed that the only the facile mixture of nano-MIL-101(Cr) and water/cyclohexane (1:1) formed stable HIPEs, of which the viscosity increased rapidly upon mixing. Upon treatment of nano-MIL-101(Cr)@HIPEs in an ultrasonic bath for 30 Min all samples remained structurally stable. Remarkably, HIPEs loaded with nano-MIL-101(Cr) showed interesting structural stability, superior to other MOFs that have been undergone the same process (e.g. MIL-100(Fe), CAU-10-H or Al<sub>2</sub>um). No other tested MOF formed HIPEs that highly viscous and stable in shape (see Figure 17). It may be proposed that this phenomenon was evoked by the specific crystallite sizes of the MOF sample(s), supporting the formation of HIPE with nano-MIL-101(Cr). Other explanations include specific interactions of the chemical attributes of the nano-MOF particle surface(s).



**Figure 17: Stable nano-MIL-101(Cr)@HIPE from a water/cyclohexane mixture in a glass vial. After formation of the HIPE the glass vial was laid and kept structurally stable for at least 12 h.**

The considerate supercritical CO<sub>2</sub> drying (SCD) method consists of the slow exchange of solvent with ethanol and subsequently with supercritical CO<sub>2</sub>. As this method minimizes capillary forces during the drying process, it was tested to dry the obtained MOF-loaded HIPEs in a SCD device. Therefore, they were soaked with ethanol, upon which they maintained its structural integrity, and transferred to the SCD. However, only powdery materials could be obtained after SCD. Hence, these efforts can only be declared as pretest for further development of stable MOF bodies with MIL-101(Cr). Prospectively, small amounts of cross-linking agent could be added before the HIPE formation, to support the maintenance of macroporous framework after SCD. The product should preferably be comprised of interconnected MOF particles, resulting highly loaded MOF bodies. A precise control over the porous structure could be obtained by further efforts implying design of experiments (DoE) with varying either ratio of both phases, MOF portion, also potential addition and choice of monomers or surfactants, degree of cross-linking agent, temperature, curing time, drying method or several other conditions. These efforts could also give access to MOAs or more precisely macroporous bodies of highly loaded MOF composites.

### 4.3.2. Composites Obtained from Aerosil® and Aeroperl® with CAU-10-H

#### Introduction

The products Aeroperl® and Aerosil® (EVONIK, Essen, Germany) are pyrogenic (*i.e.* produced in a flame, also “fumed”) silica materials with hydrophilic properties.

The work was carried out in analogy to very recently published work by Ü. Kökcam-Demir, N. Tannert, M. Bengsch, A. Spieß, C. Schlüsener, S. Nießing and C. Janiak, *Improving porosity and water uptake of aluminum metal-organic frameworks (Al-MOFs) as graphite oxide (GO) composites*, *Micropor. Mesopor. Mater.*, 2021, *submitted*. Hence, various *in-situ* composites (*i.e.* MOF synthesis in the presence of Aeroperl® or Aerosil®) and *ex-situ* mixtures (*i.e.* MOF mixed with Aeroperl® or Aerosil®) obtained from CAU-10-H and Aeroperl® or Aerosil® were investigated and compared. Numerous more details on CAU-10-H composites are given in the BSc thesis by M. Bengsch, which was supervised by the author.<sup>266</sup>

#### Experimental Section

**Synthesis of CAU-10-H and *in-situ* composites:** CAU-10-H was synthesized by a previously developed protocol from Al(OH)(ac)<sub>2</sub> in aqueous solution.<sup>269</sup> For *in-situ* composites 25–55 mg of either Aeroperl® or Aerosil® was stirred into the MOF precursor solution before applying synthesis temperature. For *ex-situ* mixtures the same amount of either Aeroperl® or Aerosil® was mixed with CAU-10-H as-synthesized.

**Analytics:** Several analytical investigations including PXRD, N<sub>2</sub> and H<sub>2</sub>O sorption experiments were carried out with multiple samples. Summarizing, the following values give an overview on porosity parameters of such *in-situ* composites and *ex-situ* mixtures, as rather unsatisfying results allow for spacious shortening of experimental results and data, at this point. The surface area of obtained materials can be specified as follows:

- Aeroperl®: ca. **400 m<sup>2</sup> g<sup>-1</sup>**
- Aerosil®: ca. **275 m<sup>2</sup> g<sup>-1</sup>**
- CAU-10-H: **445–484 m<sup>2</sup> g<sup>-1</sup>** (depending on Al-source)
- *in-situ* composite of Aeroperl® with CAU-10-H: **421 m<sup>2</sup> g<sup>-1</sup>**
- *in-situ* composite of Aerosil® with CAU-10-H: **404 m<sup>2</sup> g<sup>-1</sup>**

In order to determine morphology of the composites and check to which extent the samples contained intergrown particles of both composite parts SEM images were collected. Figure 18-20 depict SEM images of neat CAU-10-H, Aeroperl®, Aerosil® and *in-situ* MOF composites of both pyrogenic silica materials.



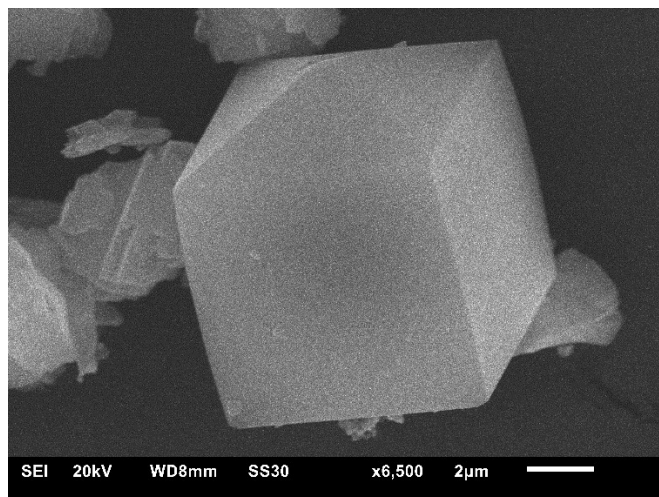


Figure 18: SEM image of a CAU-10-H crystallite as-synthesized from  $\text{AlCl}_3 + \text{NaAlO}_2$  (1:2).

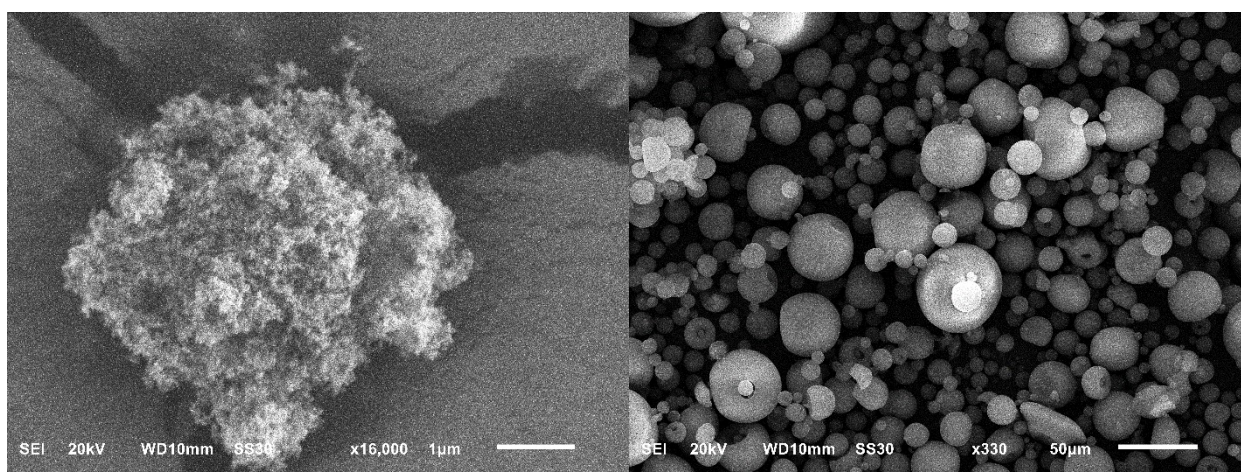


Figure 19: SEM images of neat Aerosil® (left) and Aeroperl® (right).

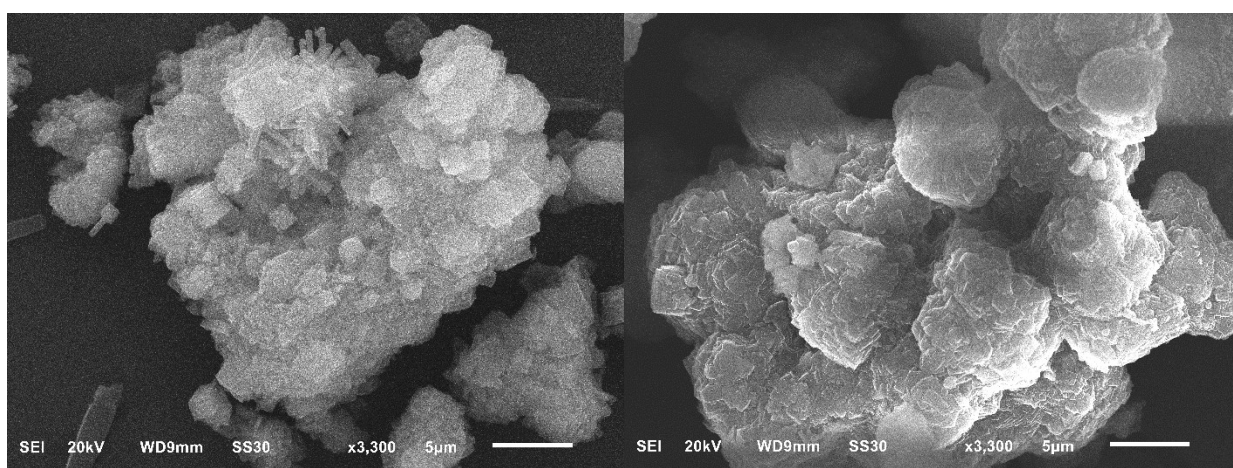


Figure 20: SEM images of *in-situ* composites of Aerosil® (left) and Aeroperl® (right) with CAU-10-H. The structures of Aerosil® and Aeroperl® are obviously intergrown with or coated by CAU-10-H (note the Aeroperl® shapes in the right SEM image).



Conclusively, the presented results did not lead to the intended increase of porosity or hydrophilicity and can only be valued as pretests or proof of concept for intergrown structures and differences between *in-situ* composites and *ex-situ* mixtures.

#### 4.4. Hydrothermal Long-term Cycling (6000 cycles) of NH<sub>2</sub>-MIL-125(Ti)

##### Introduction

The MOF NH<sub>2</sub>-MIL-125(Ti) is one more viable candidate for water sorption-based applications like AHP/TDC or water harvesting.<sup>270,271</sup> Although both MOFs MIL-125(Ti) and NH<sub>2</sub>-MIL-125(Ti) have been proposed for such applications and both were thoroughly investigated within this realm, there has been no long-term hydrothermal cycle stability investigated, to the best of the authors knowledge. Consequently, it was envisaged to carry out hydrothermal cycling experiments for multiple thousands of water sorption cycles.

##### Experimental Section

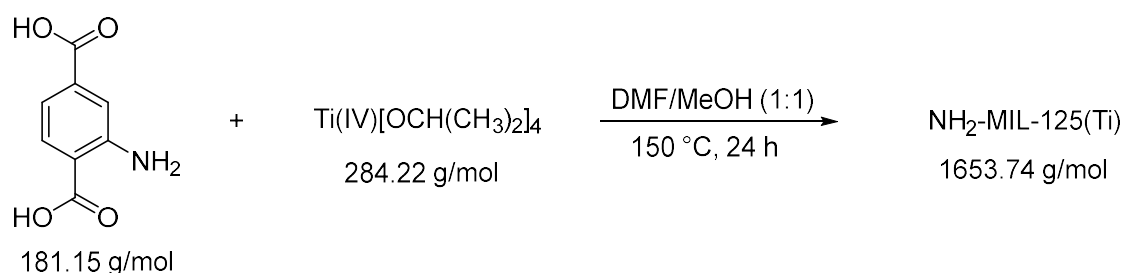


**Figure 21: Synthesis of NH<sub>2</sub>-MIL-125(Ti).** Molar masses are given below each species and synthetic conditions above/below the reaction.

**Synthesis of NH<sub>2</sub>-MIL-125(Ti):** Titanium(IV)isopropoxide (0.60 mL, 0.57 g, 2 mmol, 1.0 eq) and 2-aminoterephthalic acid (1.086 g, 6 mmol, 3.0 eq) in a mixture of DMF/methanol (5 mL / 5 mL) were stirred at room temperature until complete solution of the 2-aminoterephthalic acid. The reaction solution was transferred to a PTFE-liner and heated for 24 h at T = 150 °C with 1 h upward and downward ramping. After separation from the mother lye, the resulting powdery, yellow raw product was washed, centrifuged, and then separated from the washing liquids four times, using DMF (2 × 25 mL) and methanol (2 × 25 mL) respectively. In a final step, the precipitate was stirred in boiling methanol (25 mL) for 16 h. The final product was yielded upon drying at T = 80 °C under reduced pressure for 2 d as a yellow powder (325 mg, 0.2 mmol, 75%, Lit. 99%)<sup>270</sup>.

**Analytics:** PXRD, FTIR, TGA, N<sub>2</sub>-Sorption (BET-surface derived from 7 data points, range from  $9.73 \cdot 10^{-3} < pp_0^{-1} < 3.99 \cdot 10^{-2}$ ; t-plot with 7 data points, range from  $2.01 \cdot 10^{-1} < pp_0^{-1} < 3.99 \cdot 10^{-1}$ ; V-tag at  $pp_0^{-1} = 0.948$ ).

Satisfying crystallinity, thermal stability up to  $T = 320\text{ }^{\circ}\text{C}$  and typical IR spectroscopic bands were found. Exemplarily the  $\text{N}_2$  sorption isotherm is provided in Figure 22.

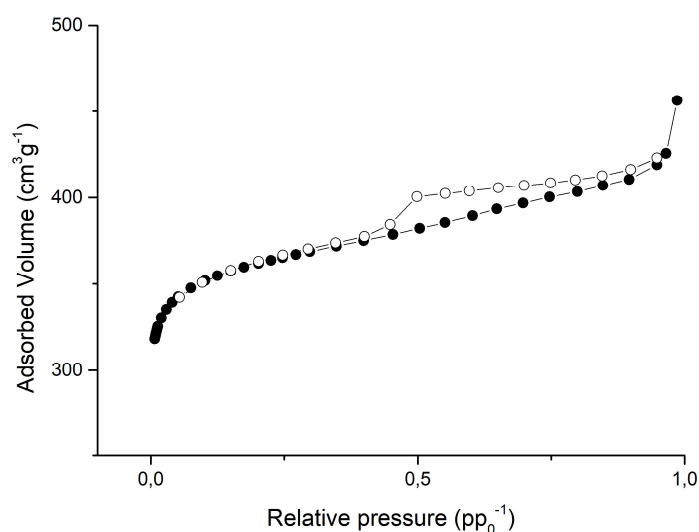


**Figure 22: Nitrogen sorption isotherm of  $\text{NH}_2\text{-MIL-125(Ti)}$ .**

From the  $\text{N}_2$  isotherm, the following porosity parameters could be derived (Table 3).

**Table 3: Porosity parameters of  $\text{NH}_2\text{-MIL-125(Ti)}$  from  $\text{N}_2$  sorption isotherm.**

	Experiment					Lit. <sup>272</sup>		
	$S_{\text{BET}}$	$S_{\text{micropore}}$	$V_{\text{micropore}}$	$V_{\text{pore}}$	$d_{\text{pore}}$	$S_{\text{BET}}$	$V_{\text{pore}}$	$d_{\text{pore}}$
	( $\text{m}^2/\text{g}$ )	( $\text{m}^2/\text{g}$ )	( $\text{cm}^3/\text{g}$ )	( $\text{cm}^3/\text{g}$ )	( $\text{\AA}$ )	( $\text{m}^2/\text{g}$ )	( $\text{cm}^3/\text{g}$ )	( $\text{\AA}$ )
<b><math>\text{NH}_2\text{-MIL-125(Ti)}</math></b>	1298	1273	0.49	0.65	12	1268	0.84	-

The as-synthesized MOF was subjected to 6000 cycles of water ad- and desorption. Subsequently collected PXRD pattern is given in Figure 23 in comparison to freshly synthesized MOF.

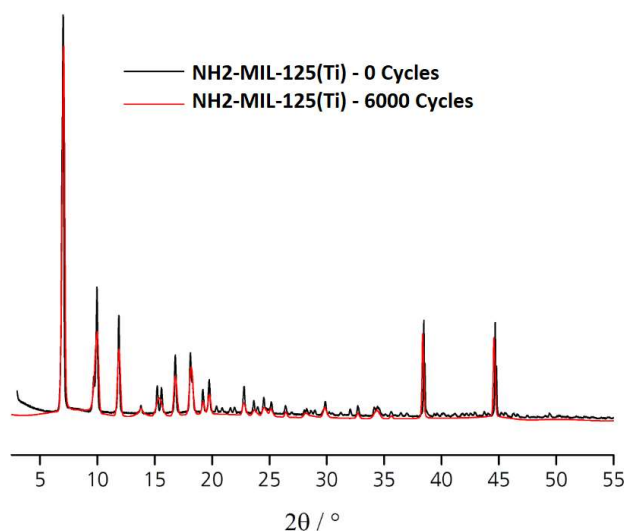


**Figure 23: PXRD pattern of NH<sub>2</sub>-MIL-125(Ti) before (black) and after (red) 6000 hydrothermal cycles.**

Figure 23 is a veritable proof for the hydrothermal stability of NH<sub>2</sub>-MIL-125(Ti). The structural integrity of NH<sub>2</sub>-MIL-125(Ti) after 6000 hydrothermal cycles renders the material an even more attractive candidate amongst the water stable MOFs. Subsequent investigations like retainment of porosity and water vapor sorption performance of cycled NH<sub>2</sub>-MIL-125(Ti) could not be carried out, due to time reasons. It can be concluded that the previously mentioned high valency of Ti<sup>4+</sup> obviously results in stable Ti-carboxylate bonds. Additionally, Ti would be the favorable metal ion in comparison to Cr from a toxicological point of view in any application. The obtained results may be regarded as an investigation towards prospective utilization of NH<sub>2</sub>-MIL-125(Ti) in applications like AHT or water-harvesting devices.

## 5. Conclusions

Within this thesis, numerous aspects of MOF syntheses and applications have been covered comprehensively, focusing on water-stable MOFs. Most of the results obtained were published in peer-reviewed scientific international journals and were presented in the form of conference contributions. The thesis' title claim of sustainability within MOF processes is compliant with all literature contributions, to the greatest possible extent.

Foremost, the environmentally friendly DGC synthesis was successfully employed to the important subclass of Al-MOFs for the first time. Specifically, the very prominent and water-stable MOFs Alfum, CAU-10-H and MIL-160 could be synthesized reproducibly in good yields, with satisfying crystallinities and high porosity parameters. Additionally, the previously only suggested solvent re-use within a DGC synthesis could be proven primarily within the synthesis of all the four Al-MOFs for three repeated synthesis runs in each case. The resulting DGCs contribute to valorized MOF syntheses in general, as it could be demonstrated for the very first time that solvent re-use is practicable in MOF synthesis in general, moreover that the accompanied solvent savings sum up to enormous amounts, when transferred to (pre-)industrial scale. Supportive calculations of solvent savings sustained the aspiration of DGCs of MOFs to highly environment-friendly synthesis. In conclusion, these significantly faster and energy-decreased syntheses, each with beneficial solvent re-use, pave the way towards enormously improved sustainability within the synthesis of Al-MOFs and other MOFs. These facts could be underlined by a fundamental comparison of both product properties and synthetic conditions of DGC, reflux syntheses and corresponding literature values.

In a next step towards substantially increased sustainability within the synthesis of MOFs, the novel method MW-DGC was firstly developed and subsequently showed to be a highly flexible, yet reliable method for the sophisticated synthesis of MOFs. Therefore, the DGC of the water-stable Fe-based MOF MIL-100(Fe) as described in the literature was optimized with respect to usage of non-fluoride Fe-source, with both drastic reduction of time and energy input. Then, the DGC of MIL-100(Fe) was successfully transferred into a microwave, resulting in novel MW-DGC. The further successful extension of both DGC and MW-DGC to the syntheses of Zr-based MOFs UiO-66 and MIL-140 underlined the robustness of both methods, also enabling for the assessment of synthetic conditions and product features with respect to metal ion (Al, Fe, Zr), yields, porosities and reproducibly. In each case, MW-DGC yielded reproducibly Alfum, MIL-100(Fe), UiO-66 and MIL-140A with solvent re-use. A thorough comparison of product features of MOFs from common synthesis routes that have been described in the literature with DGC, MW-DGC and additionally self-made aqueous routes revealed, that both DGC and MW-DGC can compete with hydrothermal and reflux-based routes in any MOF case. Interestingly, Alfum obtained by MW-DGC was shown to exhibit hierarchical porosity in the micro-meso-porous

range reproducibly. This unique feature has not been described before and it makes hierarchical porosity in *one* single Al-MOF accessible for the very first time.

Whilst AHT applications are gaining increasingly attention in the MOF community, it could be demonstrated that the rather new MOF MIL-53(Al)-TDC offers a unique working window for cooling purposes in the AHT context (*i.e.* the linker TDC). Water vapor sorption isotherms at three different temperatures enabled for determination of the materials' isosteric heat of adsorption  $\Delta_{ads}H$ . The findings were upvalued by graphic representation of dependencies of temperature levels within the targeted TDC application. In total, the combination of the considerable water loading lift, abundant and non-toxic metal-linker-combination, hydrothermal stability and, superficially, the energy-related boundary conditions characterize MIL-53(Al)-TDC as very promising material in a TDC device. Conclusively, it can be stated that Al-MOFs were thereby once again proven to be one of the most notable MOF subgroups when it comes to application.

In another literature contribution of this cumulative  $\text{NH}_2$ -MIL-101(Cr) was successfully converted with four different isocyanates to yield the corresponding urea-substituted MIL-101(Cr) derivatives. These urea-MOFs showed significant uptake of  $\text{SO}_2$  and altered water sorption compared to parental MOFs  $\text{NH}_2$ -MIL-101(Cr) and MIL-101(Cr). Thereby, it was found that the partially *p*-toluenesulfonyl-urea-modified  $\text{NH}_2$ -MIL-101(Cr) exhibits an outstanding  $\text{SO}_2$  uptake of  $823 \text{ cm}^3 \text{ g}^{-1}$ , which is the second highest  $\text{SO}_2$  uptake of any known material today.

As a final remark, it may be outlined, that especially the combination of enhanced sustainability within synthetic procedures *together* with the environmentally friendly utilizations of MOFs will facilitate the emergence of MOF-based applications and may support the entry of MOFs into industrial usage soon.



## 6. Outlook

After illuminating the subjects set up by the thesis' assignment of tasks the author wants to address the two most urgent at the same time promising developments of MOF chemistry that appear in the thematic area of this thesis. The following sections point out a personal view on challenges and opportunities that have come up during this thesis.

One aspect that must be mentioned in the realm of this thesis' outlook, however without a dedicated subchapter, is the shaping of MOFs (*cf.* chapter 1.3.5.1). Due to the typically powdery appearance of MOFs, their shaping (*e.g.* coating or other fixation on a heat exchanger, shaping into granules or into MMMs) remains a challenge that is constantly been tackled in MOF research contributions, also within the project OptiMat. Prospective developments towards incorporation of water-stable MOFs into devices will help pave the way for industrial utilization of MOFs in general. Even more, the insertion of MOFs into tailor-made, functional composites open additional potentials by the creation of hierarchical porosity, eventually going along with beneficial attributes.

### 6.1. Sustainable Syntheses of MOFs

The promising attributes of MOFs have been praised for centuries and it has now become clear that the upscaling of MOFs in economically and ecologically friendly syntheses displays a strong challenge for chemical engineers. Hence, sustainability within MOF syntheses can contribute to prospective utilization of MOFs in real applications.

Many chemical companies and start-ups have joined the field of MOF synthesis. Nowadays it is possible to request on-demand syntheses of MOFs, however mostly in exceedingly small amounts (< 1–100 g) and obviously for research purposes. Hence the industrialization of MOF production is yet to come. Quiet logically water-stable, facile, and robustly synthesizable MOFs with abundant, cheap, non-toxic metal ion will be favorable for applications and industrialization.

Consequently chapters 3.1. and 3.3. investigate thoroughly the potential of DGC and MW-DGC methods for the sustainable synthesis of water-stable MOFs. Both methods were new for the prominent group of hydrolytically stable Al-MOFs and accompanied by environmentally friendly solvent-savings and reduction of energy input. The continuous production of MOFs in a DGC or even MW-DGC setup would pave the way towards sustainable upscaling of MOF syntheses, at the same time it displays a great challenge for chemical researchers and engineers. The operational process is yet to be developed, nevertheless the step towards continuous, upscaled and sustainable syntheses of MOFs would be a key-step in enabling the chemical industry to large-industrial production. One further step would be the successful conversion of aluminum oxide or aluminum hydroxide into water-stable Al-MOFs, since those minerals are naturally abundant and highly inexpensive, hence the ecological footprint of the Al-salt would be

diminished. The demonstrated suitability of basic aluminum acetate for the synthesis of MIL-53(Al)-TDC is one step towards this direction, additional investigation of modifiers, such as benzoic acid, acidic acid or others, may also be helpful and may be seen prospectively.

Other synthetic processes, such as mechanochemical synthesis by extrusion techniques or ball milling, flow-reactors or other sophisticated synthesis methods may also play a crucial role for the sustainable production of MOFs on an industrial scale.

## **6.2. Water Sorption Applications**

Water sorption using MOFs as adsorbents seems intuitively right, as commonly applied adsorbents like silica, zeolites or carbon materials are widely outperformed by the characteristics of MOFs. The nearly infinite tailoring possibilities within MOF structures make them additionally highly flexible for each temperature and relative humidity level. Consequently this focus topic remains a hot topic in the MOF community.

Adsorption heat pumps (AHTs), thermally driven chillers (TDCs), thermal heat storage devices and related techniques require hydrothermally stable and highly porous adsorbent materials. In this context, the manifold opportunities of tailor-made MOF adsorbents are evident. It must not be underestimated that the global energy demand of heating and cooling sums up to immense amounts of energy and multiple industries rely on related businesses and techniques. The cost-effectiveness of products for a market launch of affiliated MOF-devices will be one key parameter that determines the emergence of such applications. However, the alluded amounts of energy could widely be saved, for example by sustainable TDCs, that utilize air humidity and sun light, respectively heat as driving forces to provide chilled air. Therefore, it can be assumed that the motivation of companies with research and development departments for the market launch of MOF-based AHT devices is high and that related devices will be seen soon. In conclusion the potential of MOFs for AHT processes is most likely realized now and there will be a constant and increasing evolution of MOF-based adsorbents in this thematic field.

The already mentioned subchapter of water harvesting is a flourishing field of MOF research, as one remarkably interesting aspect of hydrophilic and water-stable MOFs is their possible usage in water-harvesting from air humidity even at low relative humidity. This can give rise to drinking water production even in arid regions. There have been vivid descriptions of the potential of MOFs for such purposes, still the previously discussed issue of upscaled MOF syntheses and industrialization of MOF is prominent. As soon as there are cost-effective large-scale productions of applicable MOFs and related devices, there may arise a whole new possibility of drinking water production, additionally by water purification. Once again, this interconnection of sustainability in both MOF synthesis and applications underlines the motivation for the present thesis.

## 7. Experimental Part

### 7.1. Instrumentation and Equipment

**Argon sorption** (purity 99.999%, N5.0) was performed at  $T = 87\text{ K}$  using a *Quantachrome CryoCooler* (QUANTACHROME, Odelzhausen, Germany) for appropriate adjustment of  $T = 87\text{ K}$  and performing on a *Quantachrome Autosorb iQ MP* instrument with within a pressure range of  $pp_0^{-1} = 10^{-7} - 1\text{ bar}$ . Each sample was degassed under vacuum ( $pp_0^{-1} < 10^{-5}\text{ mbar}$ ) at  $T = 150\text{ °C}$  for ca. 3 h, prior to measurement. Helium gas (purity 99.999%, N5.0) was used for the determination of the cold and warm free space of the sample tubes. All surface areas (BET) were calculated from five adsorption points in the pressure range  $0.005 < pp_0^{-1} < 0.05$ . NLDFT calculations for the pore size distribution curves were done with the native *NovaWin 11.03* software using the 'Ar at 87 K on carbon, slit pore, NLDFT equilibrium' model. Micropore volumes were derived by *t-plot* method, De Boer model.

**Ball Milling** was performed using a *Retsch MM301* (RETSCH, Haan, Germany) applying 20 Hz for 20 min, except where other specified.

**Carbon dioxide sorption** (purity 99.995%, N4.5) was carried out on a *Quantachrome Autosorb iQ MP* (QUANTACHROME, Odelzhausen, Germany) at  $T = 195\text{ K}$  (dry ice/acetone bath),  $T = 273\text{ K}$  (ice/water bath) and  $T = 293\text{ K}$  (active thermostating). Each sample was connected to the preparation port of the sorption analyzer and degassed under vacuum for 3 h at  $T = 150\text{ °C}$ . Helium gas (purity 99.999%, N5.0) was used for the determination of the cold and warm free space of the sample tubes.

**Centrifugations** were done with devices *EBA 3S* and *Rotina 46* (HETTICH, Tuttlingen, Germany) applying 2000 rpm in each case, except where other specified.

**DGC and MW-DGC inlays and sieves (PTFE)** were self-built. The holes in DGC and MW-DGC sieves had 0.5 mm diameter. The ring inlays, shown in Figure 24 can have various heights for height adjustment. Special thanks to precision mechanics workshop of Heinrich-Heine-Universität Düsseldorf.

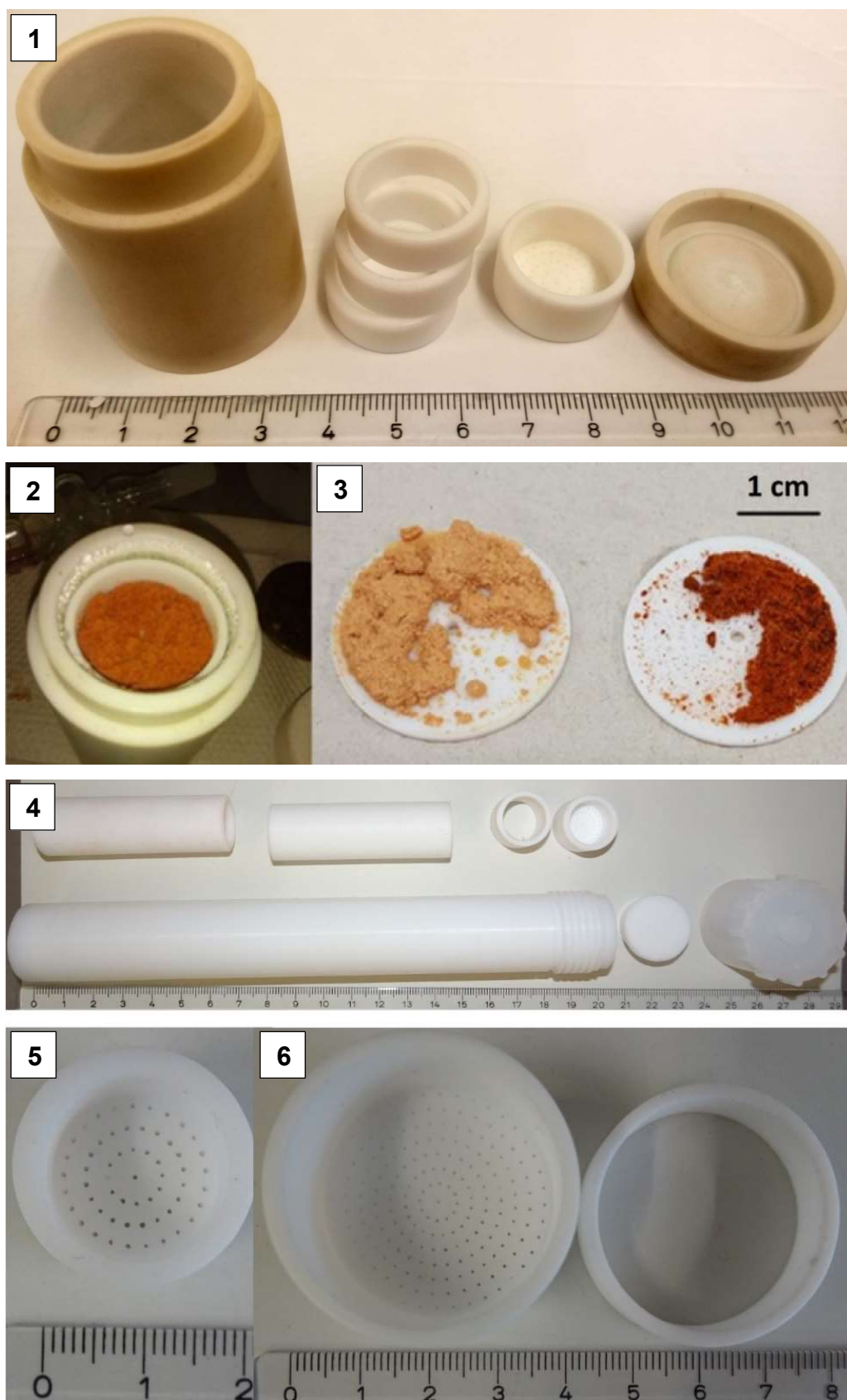


**Figure 24: PTFE parts for DGC and MW-DGC syntheses. 1: From left to right: DGC container, rings for height adjustment, sieve (with wall), and autoclave cap; 2: Assembled autoclave with detached cap, showing the MOF MIL-100(Fe) after reaction of metal precursor and btc linker; 3: DGC sieves (without wall) with MIL-100(Fe) obtained from different Fe-salt sources; 4: Complete set of MW-DGC; 5: MW-DGC sieve (with wall); 6: DGC sieve (with wall), and ring for height adjustment.**

**Elemental analysis** was acquired on a *vario MICRO cube* (ELEMENTAR ANALYSENSYSTEME, Langenselbold, Germany).

**Fourier transformed infrared spectra (FT-IR)** were acquired on a *Bruker Tensor 37 FT-IR* device at ambient temperature in a wavenumber region of 4000–500  $\text{cm}^{-1}$  using self-fabricated disks of KBr mixed with sample. For preparation of the KBr disks, the samples were well-ground with an excess of KBr (20–40-fold amount) in an agate mortar followed by pressure/vacuum treatment in a 30-ton press (Rüch, London, England), applying 10 tons. Evaluations of the spectra were done with the software 'OPUS 7.2'.

**High-pressure carbon dioxide adsorption** was collected with an *IsoSORP®-Hygra* (RUBOTHERM, Bochum, Germany) for the MOF CAU-23 (*cf.* chapter 4.1).

**$^1\text{H}$ -NMR** spectroscopy was carried out on a *Bruker FT-NMR AVANCE III – 300* (BRUKER, Billerica, US) at 300 K.  **$^{13}\text{C}$ -NMR** spectroscopy was carried out on a *Bruker FT-NMR AVANCE III – 600* (BRUKER, Billerica, US) at  $T = 300$  K. Deuterated solvents were constantly stored at  $T = 4$  °C. Reference for chemical shifts (in ppm) was always the solvent signal. Software for data handling was MestrelNova 14.1.

**Hydrogen sorption** (purity 99.999%, N5.0) was performed at  $T = 77$  K, 87 K and 100 K using a *Quantachrome CryoCooler* (QUANTACHROME, Odelzhausen, Germany) for appropriate adjustment of temperature and performing on a *Quantachrome Autosorb iQ MP* instrument with within a pressure range of  $10^{-7} < p_{\text{p}_0} < 1$  bar. Each sample was degassed under vacuum at  $p_{\text{p}_0} < 10^{-5}$  mbar and  $T = 150$  °C for ca. 3 h, prior to measurement. Helium gas (purity 99.999%, N5.0) was used for the determination of the cold and warm free space of the sample tubes.

**Karl-Fischer Titrations** were carried out on an *ECH AQUA 40.00* (ECH, Halle (Saale), Germany).

**Methane sorption** (purity 99.995%, N4.5) was performed using a *Quantachrome CryoCooler* (QUANTACHROME, Odelzhausen, Germany) for appropriate adjustment of temperature, performing on a *Quantachrome Autosorb iQ MP* instrument with within a range of  $10^{-7} < p_{\text{p}_0} < 1$  bar. Each sample was degassed under vacuum ( $p_{\text{p}_0} < 10^{-5}$  mbar) at  $T = 150$  °C for ca. 3 h, prior to measurement. Helium gas (purity 99.999%, N5.0) was used for the determination of the cold and warm free space of the sample tubes.

**Microwave reactions** were carried out in a *CEM MARS-5* (CEM CORPORATION, Matthews, US) microwave.

**Nitrogen sorption** (purity 99.999%, N5.0) was performed at  $T = 77.36$  K using liquid nitrogen and analyzing on a *Quantachrome NOVA-4000e* (QUANTACHROME, Odelzhausen, Germany)



instrument within a partial pressure range of  $10^{-3} < pp_0^{-1} < 1$  bar. Each sample was degassed under vacuum ( $pp_0^{-1} < 10^{-2}$  mbar) at  $T = 150$  °C for ca. 3 h, prior to measurement. Helium gas (purity 99.999%, N5.0) was used for the determination of the cold and warm free space of the sample tubes. All surface areas (BET) were calculated from five adsorption points in the pressure range  $0.005 < pp_0^{-1} < 0.05$  by applying Roquerol plots ( $r > 0.998$ ). Total pore volumes were calculated from the  $N_2$  sorption isotherm at  $pp_0^{-1} = 0.95$ . NLDFT calculations for the pore size distribution curves were done with the native *NovaWin 11.03* software using the 'N<sub>2</sub> at 77 K on carbon, slit pore, NLDFT equilibrium' model.

**Ovens** for heat supply in hydrothermal and solvothermal MOF syntheses were carried out in ovens of type *Memmert IN260* (MEMMERT, Schwabach, Germany).

**Powder X-ray diffraction (PXRD)** patterns were obtained at ambient temperature on a *D2 phaser* (BRUKER, Billerica, US) using Cu-K $\alpha$  radiation ( $\lambda = 1.54182$  Å) between  $5^\circ < 2\Theta < 50^\circ$  with a scanning rate of  $0.0125^\circ \text{ s}^{-1}$  (300 W, 30 kV, 10 mA). The diffractograms were obtained on a flat "low background sample holder", in which at low angle the beam spot is strongly broadened so that only a fraction of the reflected radiation reaches the detector, hence the low relative intensities measured at  $2\Theta < 7^\circ$ . Analyses of the diffractograms were carried out with *Match 3.11* software.

**Scanning electrode microscopy (SEM)** images were collected by a *JEOL JSM-6510 Advanced electron microscope* (JEOL, Akishima, Japan) with a LaB<sub>6</sub> cathode at 5 – 20 keV. The microscope was equipped with a *Xflash 410* (BRUKER, Billerica, US) silicon drift detector.

**Sulfur dioxide sorption** (purity 99.98%, N3.8) was carried out on a *Quantachrome Autosorb iQ MP* (QUANTACHROME, Odelzhausen, Germany) at  $T = 273$  K (ice/water bath) and  $T = 293$  K (active thermostating). The *Autosorb iQ MP* was equipped with oil-free vacuum pumps (pressure down to  $pp_0^{-1} < 10^{-8}$  mbar) and valves, which guaranteed contamination free measurements, moreover resistivity towards SO<sub>2</sub>. Each sample was connected to the preparation port of the sorption analyzer and degassed under vacuum for 3 h at  $T = 150$  °C. Helium gas (purity 99.999%, N5.0) was used for the determination of the cold and warm free space of the sample tubes. The STP volumes are given at  $T = 273.15$  K, 100.000 kPa.

**Supercritical CO<sub>2</sub> drying (SCD)** was done with a supercritical point dryer *EM CPD300* (LEICA MICROSYSTEMS, Wetzlar, Germany) with CO<sub>2</sub> (purity 99.999%, N5.0) driving out ethanol from the fully soaked sample during the SCD process.

**Thermogravimetric analysis (TGA)** measurements were carried out on a *Netzsch TG209 F3 Tarsus* (NETZSCH, Selb, Germany) device under nitrogen atmosphere, ramping with  $5 \text{ K min}^{-1}$  to target temperature ( $T = 600$  °C).

**Water sorption** was performed on a *Quantachrome VStar4* (QUANTACHROME, Odelzhausen, Germany) device within a partial pressure range of  $10^{-3} < pp_0^{-1} < 0.9$ . Each sample was degassed under vacuum ( $pp_0^{-1} < 10^{-5}$  mbar) at  $T = 150$  °C for ca. 3 h, prior to measurement. Helium gas (purity 99.999%, N5.0) was used for the determination of the cold and warm free space of the sample tubes. The acquired data were fit with native *VersaWin™ 1.0* software.

**Water cycling stabilities** were examined in a *Setaram™ TGA-DSC-111* (SETARAM, Caluire, France) on powdered samples. A humidified argon gas flow ( $T = 40$  °C, 76.3% relative humidity) was generated by a *Setaram™ WetSys* (SETARAM, Caluire, France) humidity controller and passed through the sample chamber, while the temperature of the sample was varied, and the mass of the adsorbent was monitored. For the multi-cycle ad-/desorption experiments, the temperature of the sample was varied between  $40$  °C  $< T < 140$  °C with a cycle time of 5 h.

**X-ray diffractograms under humid conditions** were acquired *in-situ* on a *Bruker D8 Advance* with *DaVinci™* (BRUKER, Billerica, US), using a Cu anode tube at 40 kV/40 mA, with a Ni filter and constant sample illumination spot size (broadness: 12 mm); step size  $0.02^\circ$ , 1.0 s/step, Cu- $K_\alpha$  radiation. *MRI Humidity Stage* (BRUKER AXS, Karlsruhe, Germany) was used for controlled humidity, where a humidified  $N_2$  gas flow was passed over the sample at atmospheric pressure. Before each scan, each sample was allowed to equilibrate for 90 min.

## 7.2. General Working Methods

All glassware was chemically cleaned in a KOH/Isopropanol bath for at least 24 h, then rinsed with water, fully neutralized in a HCl bath, then washed with distilled water thoroughly and dried for at least 12 h at  $T = 80$  °C in an oven, prior to each use.

All experiments and syntheses were carried out under atmospheric pressure, except where other specified.

In chapter 3.4., specifically for the PSMs of  $NH_2$ -MIL-101(Cr) with reactive isocyanate reagents, standard Schlenk-line techniques under inert nitrogen atmosphere were applied. Accordingly, all glassware was properly heated under vacuum prior to utilization and kept constantly inert during the syntheses (PSMs).

### 7.3. List of Chemicals and Solvents

All chemicals were used as received by suppliers (*cf.* Table 4). All solvents were additionally dried under molecular sieve (4 Å).

**Table 4: Utilized chemicals specified by supplier and purity as indicated on the label.**

Chemical	Supplier	Purity
Acetone	SIGMA ALDRICH	> 99.5%
Acetonitrile	SIGMA ALDRICH	99.8%
Aerosil®	EVONIK	not specified
Aeroperl®	EVONIK	not specified
$\text{AlCl}_3 \cdot 6\text{H}_2\text{O}$	JANSSEN CHIMICA	99%
$\text{Al}(\text{NO}_3)_3 \cdot 9\text{H}_2\text{O}$	ALFA AESAR	98.0%
$\text{Al}_2(\text{SO}_4)_3 \cdot 18\text{H}_2\text{O}$	APPLICHEM	not specified
$\text{Al}(\text{OH})(\text{acetate})_2 \cdot x\text{H}_2\text{O}$	ALFA AESAR	not specified
2-Aminoterephthalic acid	SIGMA ALDRICH	99%
Basolite® A520	SIGMA ALDRICH	not specified
Basolite® F300	SIGMA ALDRICH	not specified
Benzoic Acid	RIEDEL DE HAËN	99.5%
$\text{Cr}(\text{NO}_3)_3 \cdot 9\text{H}_2\text{O}$	ALFA AESAR	99%
Dichloromethane	SIGMA ALDRICH	> 99.8%
Diethylether	RIEDEL DE HAËN	99.8%
$\text{D}_2\text{O}$	SIGMA ALDRICH	99.9 atom% D
<i>N,N'</i> -Dimethylformamide	FISCHER CHEMICALS	> 99.0%
Ethanol	SIGMA ALDRICH	> 99.8%
Ethyl isocyanatoacetate	SIGMA ALDRICH	95%
$\text{FeCl}_3 \cdot 6\text{H}_2\text{O}$	SIGMA ALDRICH	97%
$\text{Fe}(\text{NO})_3 \cdot 9\text{H}_2\text{O}$	SIGMA ALDRICH	98%
Fumaric acid	ALFA AESAR	99%
2,5-Furandicarboxylic acid	OXCHEM	95%
Furfuryl isocyanate	SIGMA ALDRICH	97%
Hydrochloric acid, 37%	SIGMA ALDRICH	p.a.
Hydrofluoric acid, 48%	SIGMA ALDRICH	p.a.
Isophthalic acid	ALFA AESAR	99%
KBr (FT-IR grade)	SIGMA ALDRICH	> 99.0%
$\text{KMnO}_4$	SIGMA ALDRICH	> 99.0%
$\text{NaAlO}_2$	VWR CHEMICALS	not specified
NaF	SIGMA ALDRICH	99.99%

NaOD/D <sub>2</sub> O solution, 40 wt. %	SIGMA ALDRICH	99.5 atom% D
NaOH (microgranulate)	CHEM SOLUTE	not specified
Nitric acid, 65%	VWR CHEMICALS	not specified
Terephthalic acid	SIGMA ALDRICH	> 98.0%
Tetrabutylammonium fluoride, hydrate	SIGMA ALDRICH	96%
Tetrahydrofuran	RIEDEL DE HAËN	p.a.
Tetramethylammonium hydroxide (25 wt. % in H <sub>2</sub> O)	SIGMA ALDRICH	not specified
2,5-Thiophenedicarboxylic acid	SIGMA ALDRICH	99%
<i>p</i> -Toluenesulfonyl isocyanate	SIGMA ALDRICH	96%
3-(Triethoxysilyl)propyl isocyanate	SIGMA ALDRICH	95%
Trimesic acid	SIGMA ALDRICH	95%
ZrCl <sub>4</sub>	ALFA AESAR	> 99.5%

## 8. References

- <sup>1</sup> O. M. Yaghi and H. Li, *J. Am. Chem. Soc.*, 1995, **117**, 10401-10402.
- <sup>2</sup> O. M. Yaghi, G. Li and H. Li, *Nature*, 1995, **378**, 703-706.
- <sup>3</sup> O. M. Yaghi, H. Li, M. Eddaoudi and M. O'Keeffe, *Nature* 1999, **402**, 276-279.
- <sup>4</sup> O. M. Yaghi, M. J. Kalmutzki and C. S. Diercks, *Introduction to Reticular Chemistry. Metal-organic frameworks and covalent organic frameworks*, Wiley, Weinheim, 2019.
- <sup>5</sup> M. Eddaoudi, J. Kim, N. Rosi, D. Vodak, J. Wachter, M. O'Keeffe and O. M. Yaghi, *Science*, 2002, **295**, 469-472.
- <sup>6</sup> G. E. Stahl, *Stahlii, Experimenta, Observationes, Animadversiones, CCC Numero, Chymicae Et Physicae*, Berlin, 1731.
- <sup>7</sup> R. Alsfasser, T. M. Klapötke, C. Janiak and H.-J. Meyer, *Moderne Anorganische Chemie* (Ed.: E. Riedel), de Gruyter, Berlin / New York, 2007, p. 533.
- <sup>8</sup> F. Herren, P. Fischer, A. Ludi and W. Haelg, *Inorg. Chem.*, 1980, **19**, 956-959.
- <sup>9</sup> C. C. Scherb, *Controlling the Surface Growth of Metal-Organic Frameworks*, doctoral thesis, Ludwig-Maximilians-Universität München, 2009.
- <sup>10</sup> E. A. Tomic, *J. Appl. Polym. Sci.*, 1965, **9**, 3745-3752.
- <sup>11</sup> S. R. Batten, N. R. Champness, X.-M. Chen, J. Garcia-Martinez, S. Kitagawa, L. Öhrström, M. O'Keeffe, M. P. Suh and J. Reedijk, *Cryst. Eng. Comm.*, 2012, **14**, 3001-3004.
- <sup>12</sup> S. R. Batten, N. R. Champness, X.-M. Chen, J. Garcia-Martinez, S. Kitagawa, L. Öhrström, M. O'Keeffe, M. Paik Suh and J. Reedijk, *Pure Appl. Chem.*, 2013, **85**, 1715-1724.
- <sup>13</sup> S. M. Moosavi, A. Nandy, K. M. Jablonka, D. Ongari, J. P. Janet, P. G. Boyd, Y. Lee, B. Smit and H. J. Kulik, *Nature Commun.*, 2020, **11**, 1-10.
- <sup>14</sup> P. Z. Moghadam, A. Li, S. B. Wiggin, A. Tao, A. G. P. Maloney, P. A. Wood, S. C. Ward and D. Fairen-Jimenez, *Chem. Mater.*, 2017, **29**, 2618-2625.
- <sup>15</sup> Y. Chen and S. Ma, *Rev. Inorg. Chem.*, 2012, **32**, 81-100.
- <sup>16</sup> E. A. Dolgoplova, O. A. Ejagbavwo, C. R. Martin, M. D. Smith, W. Setyawan, S. G. Karakalos, C. H. Henager, H.-C. zur Loye and N. B. Shustova, *J. Am. Chem. Soc.*, 2017, **139**, 16852-16861.
- <sup>17</sup> D. J. Tranchemontagne, J. L. Mendoza-Cortés, M. O'Keeffe and O. M. Yaghi, *Chem. Soc. Rev.*, 2009, **38**, 1257-1283.
- <sup>18</sup> O. M. Yaghi, M. O'Keeffe, N. W. Ockwig, H. K. Chae, M. Eddaoudi and J. Kim, *Nature*, 2003, **423**, 705-714.
- <sup>19</sup> L. R. MacGillivray, *Metal-Organic Frameworks: Design and Application*, John Wiley & Sons, Inc., Hoboken, New Jersey, 2010.
- <sup>20</sup> C. Janiak and J. K. Vieth, *New J. Chem.*, 2010, **34**, 2366-2388.
- <sup>21</sup> S. Mukherjee and N. J. Zaworotko, *Trends Chem.*, 2020, **2**, 506-518.
- <sup>22</sup> O. K. Farha, I. Eryazici, N. C. Jeong, B. G. Hauser, C. E. Wilmer, A. A. Sarjeant, R. Q. Snurr, S. B. T. Nguyen, A. Ö. Yazaydin and J. T. Hupp, *J. Am. Chem. Soc.* 2012, **134**, 15016-15021.
- <sup>23</sup> I. M. Hönicke, I. Senkovska, V. Bon, I. A Baburin, N. Bönisch, S. Raschke, J. D. Evans and S. Kaskel, *Angew. Chem. Int. Ed.*, 2018, **57**, 13780-13783.
- <sup>24</sup> S. Biswas, S. Couck, D. Denysenko, A. Bhunia, M. Grzywa, J. F. M. Denayer, D. Volkmer, C. Janiak and P. Van Der Voort, *Micropor. Mesopor. Mater.*, 2013, **181**, 175-181.
- <sup>25</sup> S. K. Elsaidi, M. H. Mohamed, D. Banerjee and P. K. Thallapally, *Coord. Chem. Rev.*, 2018, **358**, 125-152.
- <sup>26</sup> S. S. Y. Chui, S. M. F. Lo, J. P. H. Charmant, A. G. Orpen and I. D. Williams, *Science*, 1999, **283**, 1148-1150.
- <sup>27</sup> W. Shang, X. Kang, H. Ning, J. Zhang, X. Zhang, Z. Wu, G. Mo, X. Xing and B. Han, *Langmuir*, 2013, **29**, 13168-13174.
- <sup>28</sup> S. Dissegna, K. Epp, W. R. Heinz, G. Kieslich and R. A. Fischer, *Adv. Mater.*, **2018**, 1704501.
- <sup>29</sup> O. V. Gutov, S. Molina, E. C. Escudero-Adán and A. Shafir, *Chem. - Eur. J.*, 2016, **22**, 13582-13587.
- <sup>30</sup> B. Van de Voorde, I. Stassen, B. Bueken, F. Vermoortele, D. De Vos, R. Ameloot, J.-C. Tan and T. D. Bennett, *J. Mater. Chem. A*, 2015, **3**, 1737-1742.
- <sup>31</sup> S. Canossa, A. Gonzalez-Nelson, L. Shupletsov, M. d. C. Martin and M. A. van der Veen, *Chem. - Eur. J.*, 2020, **26**, 3564-3570.



- <sup>32</sup> M. I. Severino Neves, E. Gkanatiatsou, F. Nouar, M. L. Pinto and C. Serre, *Faraday Discuss.*, accepted manuscript: <https://doi.org/10.1039/D1FD00018G>.
- <sup>33</sup> D. DeSantis, J. A. Mason, B. D. James, C. Houchins, J. R. Long and A. Veenstra, *Energ. Fuel.*, 2017, **31**, 2024-2032.
- <sup>34</sup> M. Li and M. Dincă, *J. Am. Chem. Soc.*, 2011, **133**, 12926-12929.
- <sup>35</sup> J. L. Hauser, M. Tso, K. Fitchmun and S. R. J. Oliver, *Cryst. Growth Des.*, 2019, **19**, 2358-2365.
- <sup>36</sup> F. Jeremias, S. K. Henninger and C. Janiak, *Chem. Commun.*, 2012, **48**, 9708-9710.
- <sup>37</sup> J. Liu and C. Wöll, *Chem. Soc. Rev.*, 2017, **46**, 5730-5770.
- <sup>38</sup> F. Jeremias, S. K. Henninger and C. Janiak, *Dalton Trans.*, 2016, **45**, 8637-8644.
- <sup>39</sup> H. Reinsch and N. Stock, *Dalton Trans.*, 2017, **46**, 8339-8349.
- <sup>40</sup> M. Taddei, D. A. Steitz, J. A. van Bokhoven and M. Ranocchiari, *Chem. - Eur. J.*, 2016, **22**, 3245-3249.
- <sup>41</sup> J. Klinowski, F. A. Almeida Paz, P. Silva and J. Rocha, *Dalton Trans.*, 2011, **40**, 321-330.
- <sup>42</sup> C. Echaide-Górriz, C. Clément, F. Cacho-Bailo, C. Téllez and J. Coronas, *J. Mater. Chem. A*, 2018, **6**, 5485-5506.
- <sup>43</sup> A. G. Márquez, A. Demessence, A. E. Platero-Plats, D. Heurtaux, P. Horcajada, C. Seree, J.-S. Chang, G. Férey, V. A. de la Peña-O'Shea, C. Boissière, D. Grosso and C. Sanchez, *Eur. J. Inorg. Chem.*, 2012, **32**, 5165-5174.
- <sup>44</sup> A. Laybourn, A. M. López-Fernández, I. Thomas-Hillman, J. Katrib, W. Lewis, C. Dodds, A. P. Harvey and S. W. Kingman, *Chem. Eng. J.*, 2019, **356**, 170-177.
- <sup>45</sup> D. Chen, J. Zhao, P. Zhang and S. Dai, *Polyhedron*, 2019, **162**, 59-64.
- <sup>46</sup> B. Szcześniak, S. Borysiuk, J. Choma and M. Jaroniec, *Mater. Horiz.*, 2020, **7**, 1457-1473.
- <sup>47</sup> C. Vaitsis, G. Sourkouni and C. Argiris, *Ultrason. Sonochem.*, 2019, **52**, 106-119.
- <sup>48</sup> W.-J. Son, J. Kim, J. Kim and W.-J. Ahn, *Chem. Commun.*, 2008, **47**, 6336-6338.
- <sup>49</sup> T. Stassin, I. Stassen, J. Marreiros, A. J. Cruz, R. Verbeke, M. Tu, H. Reinsch, M. Dickmann, W. Egger, I. F. J. Vankelecom, D. E. De Vos and R. Ameloot, *Chem. Mater.*, 2020, **32**, 1784-1793.
- <sup>50</sup> N. Campagnol, T. R. C. Van Assche, M. Li, L. Stappers, M. Dincă, J. F. M. Denayer, K. Binnemans, D. E. De Vos and J. Fransaer, *J. Mater. Chem. A*, 2016, **4**, 3914-3925.
- <sup>51</sup> X. Zhang, K. Wan, P. Subramanian, M. Xu, J. Luo and J. Fransaer, *J. Mater. Chem. A*, 2020, **8**, 7569-7587.
- <sup>52</sup> L. Garzon-Tóvar, M. Cano-Sarabia, A. Carné-Sánchez, C. Carbonell, I. Imaz and Maspoch, *React. Chem. Eng.*, 2016, **1**, 533-539.
- <sup>53</sup> J. Troyano, C. Çamur, L. Garzon-Tóvar, A. Carné-Sánchez, I. Imaz and Maspoch, *Acc. Chem. Res.*, 2020, **53**, 1206-1217.
- <sup>54</sup> N. Stock and S. Biswas, *Chem. Rev.*, 2012, **112**, 933-969.
- <sup>55</sup> S. Kumar, S. Jain, M. Nehra, N. Dilbaghi, G. Marrazza and K.-H. Kim, *Coord. Chem. Rev.*, 2020, **420**, 213407.
- <sup>56</sup> J. Chen, K. Shen and Y. Li, *ChemSusChem*, 2017, **10**, 3165-3187.
- <sup>57</sup> Q. Shi, Z. Chen, Z. Song, J. Li and J. Dong, *Angew. Chem. Int. Ed.*, 2011, **123**, 698-701.
- <sup>58</sup> H. Reinsch, *Eur. J. Inorg. Chem.*, 2016, **27**, 4290-4299.
- <sup>59</sup> H. Reinsch, S. Waitschat, S. M. Chavan, K. P. Lillerud and N. Stock, *Eur. J. Inorg. Chem.*, 2016, **27**, 4490-4498.
- <sup>60</sup> M. Abraham, *Environ. Prog.*, 2004, **23**, p. 266.
- <sup>61</sup> P. Coish, E. McGovern, J. B. Zimmermann and P. T. Anastas, The Value-Adding Connections Between the Management of Ecoinnovation and the Principles of Green Chemistry and Green Engineering. In: B. Torok and T. Dransfield, *Green Chemistry – An inclusive approach*, Elsevier Science Publishing Co Inc, 2017, 981-998.
- <sup>62</sup> S. Y. Tang, R. A. Bourne, R. L. Smith and M. Poliakoff, *Green Chem.*, 2008, **10**, 268-269.
- <sup>63</sup> G. Zhan and H. C. Zheng, *Chem. Commun.*, 2017, **53**, 72-81.
- <sup>64</sup> J. Ren, X. Dyosiba, N. M. Musyoka, H. W. Langmi, M. Mathe and S. Liao, *Coord. Chem. Rev.*, 2017, **352**, 187-219.
- <sup>65</sup> M. Rubio-Martinez, C. Avci-Camur, A. W. Thornton, I. Imaz, D. Maspoch and M. R. Hill, *Chem. Soc. Rev.*, 2017, **46**, 3453-3480.
- <sup>66</sup> M. J. Kalmutzki, N. Hanikel and O. M. Yaghi, *Sci. Adv.*, 2018, **4**, eaat9180.

- <sup>67</sup> F. Jeremias, A. Khutia, S. K. Henninger and C. Janiak, *J. Mater. Chem.*, 2012, **22**, 10148-10151.
- <sup>68</sup> S. Abednatanzi, P. G. Derakhshandeh, H. Depauw, F.-X. Coudert, H. Vrielinck, P. Van Der Voort and K. Leus, *Chem. Soc. Rev.*, 2019, **48**, 2535-2565.
- <sup>69</sup> M. Y. Masoomi, A. Morsali, A. Dhashinamoorthy and H. Garcia, *Angew. Chem. Int. Ed.*, 2019, **58**, 15188-15205.
- <sup>70</sup> M. Lalonde, W. Bury, O. Karagiari, Z. Brown, J. T. Hupp and O. K. Farha, *J. Mater. Chem. A*, 2013, **1**, 5453-5468.
- <sup>71</sup> C. Schlüsener, M. Xhinovci, N. Tannert, A. Schmitz and C. Janiak, *Chem. Mater.*, 2019, **31**, 4051-4062.
- <sup>72</sup> C. Schlüsener, D. N. Jordan, M. Xhinovci, T. J. Matemb Ma Ntep, A. Schmitz, B. Giesen and C. Janiak, *Dalton Trans.*, 2020, **49**, 7373-7383.
- <sup>73</sup> O. Karagiari, W. Bury, J. E. Mondloch, J. T. Hupp and O. K. Farha, *Angew. Chem. Int. Ed.*, 2014, **53**, 4530-4540.
- <sup>74</sup> R. Kitaura, K. Fujimoto, S.-i. Noro, M. Kondo and S. Kitagawa, *Angew. Chem. Int. Ed.*, 2002, **41**, 141-143.
- <sup>75</sup> H. Deng, C. J. Doonan, H. Furukawa, R. B. Ferreira, J. Towne, C. B. Knobler, B. Wang and O. M. Yaghi, *Science*, 2010, **327**, 846-850.
- <sup>76</sup> A. Helal, Z. H. Yamani, K. E. Cordova and O. M. Yaghi, *Natl. Sci. Rev.*, 2017, **4**, 296-298.
- <sup>77</sup> H. Jiang, J. Jia, A. Shkurenko, Z. Chen, K. Adil, Y. Belmabkhout, L. J. Weselinski, A. H. Assen, D.-X. Xue, M. O'Keeffe and M. Eddaoudi, *J. Am. Chem. Soc.*, 2018, **140**, 8858-8857.
- <sup>78</sup> Z. Yin, S. Wan, J. Yang, M. Kurmoo and M.-H. Zeng, *Coord. Chem. Rev.*, 2019, **378**, 500-512.
- <sup>79</sup> M. Ranjbar and M. A. Taher, *J. Porous Mat.*, 2016, **23**, 1249-1254.
- <sup>80</sup> Z. Akimbekov, A. D. Katsensis, G. P. Nagabhushana, G. Ayoub, M. Arhangelskis, A. J. Morris, T. Friščić and A. Navrotsky, *J. Am. Chem. Soc.*, 2017, **139**, 7952-7957.
- <sup>81</sup> M. Wickenheisser, F. Jeremias, S. K. Henninger and C. Janiak, *Inorg. Chim. Acta*, 2013, **407**, 145-152.
- <sup>82</sup> J. Gascon, A. Corma, F. Kapteijn and F. X. Llabrés i Xamena, *ACS Catal.*, 2014, **4**, 361-378.
- <sup>83</sup> S. Li and F. Huo, *Nanoscale*, 2015, **7**, 7482-7501.
- <sup>84</sup> Q.-L. Zhu, Q. Xu, *Chem. Soc. Rev.*, 2014, **43**, 5468-5512.
- <sup>85</sup> J. Fonseca, T. Gong, L. Liao and H.-L. Jiang, *J. Mater. Chem. A*, 2021, **9**, 10562-10611.
- <sup>86</sup> R. Gaillac, P. Pullumbni, K. A. Beyer, K. W. Chapman, D. A. Keen, T. D. Bennett and F.-X. Coudert, *Nature Mater.*, 2017, **16**, 1149-1154.
- <sup>87</sup> C. Healy, K. M. Patil, B. H. Wilson, L. Hermanspahn, N. C. Harvey-Reid, B. I. Howard, C. Kleinjan, J. Kolien, F. Payet, S. G. Telfer, P. E. Kruger and T. D. Bennett, *Coord. Chem. Rev.*, 2020, **419**, 213388.
- <sup>88</sup> Y. G. Chung, E. Haldoupis, B. J. Bucior, M. Haranczyk, S. Lee, H. Zhang, K. D. Vogiatzis, M. Milisavljevic, S. Ling, J. S. Camp, B. Slater, J. I. Siepmann, D. S. Sholl and R. Q. Snurr, *J. Chem. Eng. Data*, 2019, **64**, 5985-5998.
- <sup>89</sup> <https://mof-international.org/mof-structures/>; retrieved March 11<sup>th</sup>, 2021.
- <sup>90</sup> G. Avci, I. Erucar and S. Keskin, *ACS Appl. Mater. Interfaces*, 2020, **12**, 41567-41579.
- <sup>91</sup> Y. G. Chung, J. Camp, M. Haranczyk, B. J. Sikora, W. Bury, V. Krungleviciute, T. Yildirim, O. K. Farha, D. S. Sholl and R. Q. Snurr, *Chem. Mater.*, 2014, **26**, 6185-6192.
- <sup>92</sup> Y. He, E. D. Cubuk, M. D. Allendorf and E. J. Reed, *J. Phys. Chem. Lett.*, 2018, **9**, 4562-4569.
- <sup>93</sup> T. D. Burns, K. N. Pai, S. G. Subraveti, S. P. Collins, M. Krykunov, A. Rajendran and T. K. Woo, *Environ. Sci. Technol.*, 2020, **54**, 4536-4544.
- <sup>94</sup> M. Thommes, K. Kaneko, A. V. Neimark, J. P. Olivier, F. Rodriguez-Reinoso, J. Roquerol and K. S. W. Sing, *Pure Appl. Chem.*, 2015, **87**, 1051-1069.
- <sup>95</sup> R. T. Yang, *Gas Separation by Adsorption Processes*, Imperial College Press, London, 1997.
- <sup>96</sup> E. P. Barrett, L. G. Joyner and P. P. Halenda, *J. Am. Chem. Soc.*, 1951, **73**, 373-380.
- <sup>97</sup> T. J. Matemb Ma Ntep, H. Reinsch, B. Moll, E. Hastürk, S. Gökpınar, H. Breitzke, C. Schlüsener, L. Schmolke, G. Buntkowsky and C. Janiak, *Chem. Eur. J.*, 2018, **24**, 14048-14053.
- <sup>98</sup> A. Nuhnen and C. Janiak, *Dalton Trans.*, 2020, **49**, 10295-10307.
- <sup>99</sup> S. Krause, V. Bon, I. Senkovska, U. Stoeck, D. Wallacher, D. M. Töbrens, S. Zander, R. S. Pillai, G. Maurin, F.-X. Coudert and S. Kaskel, *Nature*, 2016, **532**, 348-352.

- <sup>100</sup> S. Krause, J. D. Evans, V. Bon, I. Senkovska, P. Iacomì, F. Kolbe, S. Ehrling, E. Troschke, J. Getzschmann, D. M. Többs, A. Franz, D. Wallacher, P. G. Yot, G. Maurin, E. Brunner, P. L. Llewellyn, F.-X. Coudert and S. Kaskel, *Nat. Commun.*, 2019, **10**, article no. 3632.
- <sup>101</sup> S. Krause, J. D. Evans, V. Bon, I. Senkovska, S. Ehrling, P. Iacomì, D. M. Többs, D. Wallacher, M. S. Weiss, B. Zheng, P. G. Yot, G. Maurin, P. L. Llewellyn, F.-X. Coudert and S. Kaskel, *Chem. Sci.*, 2020, **11**, 9468-9479.
- <sup>102</sup> S. Krause, J. D. Evans, V. Bon, I. Senkovska, F.-X. Coudert, D. M. Többs, D. Wallacher, N. Grimm and S. Kaskel, *Faraday Discuss.*, 2021, **225**, 168-183.
- <sup>103</sup> J. D. Evans, L. Bocquet and F.-X. Coudert, *Chem*, 2016, **1**, 873-886.
- <sup>104</sup> N. L. Rosi, J. Eckert, M. Eddaoudi, D. T. Vodak, J. Kim, M. O'Keefe and O. M. Yaghi, *Science*, 2003, **300**, 1127-1129.
- <sup>105</sup> G. Férey, M. Latroche, C. Serre, F. Millange, T. Loiseau and A. Percheron-Guégan, *Chem. Commun.*, 2003, **0**, 2976-2977.
- <sup>106</sup> M. Eddaoudi, J. Kim, N. Rosi, D. Vodak, J. Wachter, M. O'Keefe, O. M. Yaghi, *Science*, 2002, **295**, 469-472.
- <sup>107</sup> K. Konstantas, T. Osl, Y. Yang, M. Batten, N. Burke, A. J. Hill and M. R. Hill, *J. Mater. Chem.*, 2012, **22**, 16698-16708.
- <sup>108</sup> J. Lyu, X. Zhang, Z. Chen, R. Anderson, X. Wang, M. C. Wasson, P. Bai, X. Guo, T. Islamoglu, D. A. Gómez-Gualdrón and O. K. Farha, *ACS Appl. Mater. Inter.*, 2019, **45**, 42179-42185.
- <sup>109</sup> C. G. Piscopo, F. Trapani, A. Polyzoidis, M. Schwarzer, A. Pace and S. Loebbecke, *New J. Chem.*, 2016, **40**, 8220-8224.
- <sup>110</sup> P. Z. Moghadam, T. Islamoglu, S. Goswami, J. Exley, M. Fantham, C. F. Kaminski, R. Q. Snurr, O. K. Farha and D. Fairen-Jimenez, *Nature Commun.*, 2019, **9**, 1378.
- <sup>111</sup> D. M. Driscoll, D. Troya, P. M. Usov, A. J. Maynes, A. J. Morris and J. R. Morris, *Phys. Chem. Chem. Phys.*, 2019, **21**, 5078-5085.
- <sup>112</sup> L. Valenzano, B. Civalieri, S. Chavan, G. T. Palomino, C. T. Areán and S. Bordiga, *J. Phys. Chem. C*, 2010, **114**, 11185-11191.
- <sup>113</sup> D. F. Sava Gallis, D. J. Vogel, G. A. Vincent, J. M. Rimsza and T. M. Nenoff, *ACS Appl. Mater. Inter.*, 2019, **46**, 43270-43277.
- <sup>114</sup> A. H. Khan, K. Peikert, F. Hofmann, M. Fröba and M. Bertmer, *J. Phys. Chem. C*, 2019, **123**, 4299-4307.
- <sup>115</sup> X. Han, Y. Hong, Y. Ma, W. Lu, J. Li, L. Lin, A. M. Sheveleva, F. Tuna, E. J. L. McInnes, C. Dejoie, J. Sun, S. Yang and M. Schröder, *J. Am. Chem. Soc.*, 2020, **142**, 15235-15239.
- <sup>116</sup> G. W. Peterson, J. J. Mahle, J. B. DeCoste, W. O. Gordon and J. A. Rossin, *Angew. Chem.-Ger. Edit.*, 2016, **128**, 6343-6346.
- <sup>117</sup> E. Martínez-Ahumada, A. López-Olvera, V. Jancik, J. E. Sánchez-Bautista, E. González-Zamora, V. Martis, D. R. Williams and I. A. Ibarra, *Organometallics*, 2020, **7**, 883-915.
- <sup>118</sup> A. H. Assen, O. Yassine, O. Shekhah, M. Eddaoudi and K. N. Salama, *ACS Sens.*, 2017, **9**, 1294-1301.
- <sup>119</sup> S. Glomb, D. Woschko, G. Makhlofi and C. Janiak, *ACS Appl. Mater. Inter.*, 2017, **9**, 37419-37434.
- <sup>120</sup> Y. Chen, B. Shan, C. Yang, J. Yang, J. Li and B. Mu, *J. Mater. Chem. A*, 2018, **6**, 9922-9929.
- <sup>121</sup> J. A. Zárate, E. Sánchez-González, T. Jurado-Vázquez, A. Gutiérrez-Alejandre, E. González-Zamora, I. Castillo, G. Maurin and I. A. Ibarra, *Chem. Commun.*, 2019, **55**, 3049-3052.
- <sup>122</sup> J. G. Flores, J. A. Zárate-Colín, E. Sánchez-González, J. R. Valenzuela, A. Gutiérrez-Alejandre, J. Ramírez, V. Jancik, J. Aguilar-Pliego, M. C. Zorrilla, H. A. Lara-García, E. González-Zamora, G. Guzmán-González, I. González, G. Maurin and I. A. Ibarra, *ACS Appl. Mater. Inter.*, 2020, **16**, 18885-18892.
- <sup>123</sup> Y.-S. Bae, B. G. Hauser, Y. J. Colón, J. T. Hupp, O. K. Farha and R. Q. Snurr, *Micropor. Mesopor. Mater.*, 2013, **169**, 176-179.
- <sup>124</sup> L. Li, L. Guo, Z. Zhang, Q. Yang, Y. Yang, Z. Bao, J. Ren and J. Li, *J. Am. Chem. Soc.*, 2019, **141**, 9358-9364.
- <sup>125</sup> X.-L. Xiong, G.-H. Chen, S.-T. Xiao, Y.-G. Ouyang, H.-B. Li and Q. Wang, *J. Phys. Chem. C*, 2020, **27**, 14603-14612.
- <sup>126</sup> H. Bunzen, A. Kalytta-Mewes, L. van Wüllen and D. Volkmer, *Beilstein J. Nanotechnol.* 2019, **10**, 1851-1859.

- <sup>127</sup> C. Y. Chuah, K. Goh and T.-H. Bae, *J. Phys. Chem. C*, 2017, **12**, 6748-6755.
- <sup>128</sup> H. Wang, W. P. Lustig and J. Li, *Chem. Soc. Rev.*, 2018, **47**, 4729-4756.
- <sup>129</sup> X. Han, S. Yang and M. Schröder, *Nat. Rev. Chem.*, 2019, **3**, 108-118.
- <sup>130</sup> N. A. Khan, Z. Hasan and S. H. Jhung, *J. Hazard. Mater.*, 2013, **244-245**, 444-456.
- <sup>131</sup> E. Barea, C. Montoro and J. A. R. Navarro, *Chem. Soc. Rev.*, 2014, **43**, 5419-5430.
- <sup>132</sup> K. Tan, S. Zuluaga, Q. Gong, Y. Gao, N. Nijem, J. Li, T. Thonhauser and Y. J. Chabal, *Chem. Mater.* 2015, **27**, 2203-2217.
- <sup>133</sup> X. Liu, X. Wang and F. Kapteijn, *Chem. Rev.* 2020, **120**, 8303-8377.
- <sup>134</sup> S. M. T Abtab, D. Alezi, P. M. Bhatt, A. Shkurenko, Y. Belmabkhout, H. Aggarwal, Ł. J. Weseliński, N. Alsadun, U. Samin, M. N. Hedhili and M. Eddaoudi, *Chem*, 2018, **4**, 94-105.
- <sup>135</sup> M. Taddei, *Coord. Chem. Rev.*, 2017, **343**, 1-24.
- <sup>136</sup> J. Jin, P. Li, D. H. Chun, B. Jin, K. Zhang and J. H. Park, *Adv. Funct. Mater.*, 2021, 2102511.
- <sup>137</sup> Z. Fang, B. Bueken, D. E. De Vos, and R. A. Fischer, *Angew. Chem. Int. Ed.*, 2015, **54**, 7234-7254.
- <sup>138</sup> M. Zu, M. Qin and S. Ciu, *Renew. Sust. Energ. Rev.*, 2020, **133**, 110246.
- <sup>139</sup> M. F. De Lange, B. L. van Velzen, C. P. Ottevanger, K. J. F. M. Verouden, L.-C. Lin, T. J. H. Vlugt, J. Gascon and F. Kapteijn, *Langmuir*, 2015, **31**, 12783-12796.
- <sup>140</sup> C. Schlüsener, Dissertation, Heinrich-Heine-Universität Düsseldorf, Düsseldorf, Germany, 2020.
- <sup>141</sup> R.-B. Lin, S. Xiang, H. Xing, W. Zhou and B. Chen, *Coord. Chem. Rev.*, 2019, **378**, 87-103.
- <sup>142</sup> H. Daglar and S. Keskin, *Coord. Chem. Rev.*, 2020, **422**, 213470.
- <sup>143</sup> D. S. Sholl and R. P. Lively, *Nature*, 2016, **532**, 435-437.
- <sup>144</sup> H. B. Tanh Jeazet, C. Staudt and C. Janiak, *Dalton Trans.*, 2012, **41**, 14003-14027.
- <sup>145</sup> J. Zhang, S.-H. Chai, Z.-A. Qiao, S. M. Mahurin, J. Chen, Y. Fang, S. Wan, K. Nelson, P. Zhang and S. Dai, *Angew. Chem.*, 2015, **127**, 946-950.
- <sup>146</sup> S. Li, Y. G. Chung and R. Q. Snurr, *Langmuir* 2016, **32**, 10368-10376.
- <sup>147</sup> S.-C. Xiang, Z. Zhang, C.-G. Zhao, K. Hong, X. Zhao, D.-R. Ding, M.-H. Xie, C.-D. Wu, M. C. Das, R. Gill, K. M. Thomas and B. Chen, *Nature Commun.*, 2011, **2**, 204.
- <sup>148</sup> A. Hazra, S. Jana, S. Bonakala, S. Balasubramanian and T. K. Maji, *Chem. Commun.*, 2017, **53**, 4907-4910.
- <sup>149</sup> H. Yang, Y. Wang, R. Krishna, X. Jia, Y. Wang, A. N. Hong, C. Dang, H. E. Castillo, X. Bu and P. Feng, *J. Am. Chem. Soc.*, 2020, **142**, 2222-2227.
- <sup>150</sup> L. Li, R.-B. Lin, R. Krishna, H. Li, S. Xiang, H. Wu, J. Li, W. Zhou and B. Chen, *Science*, 2018, **362**, 443-446.
- <sup>151</sup> A. Cadiau, K. Adil, P. M. Bhatt, Y. Belmabkhout and M. Eddaoudi, *Science*, 2016, **353**, 137-140.
- <sup>152</sup> H. Wang, X. Dong, V. Colombo, Q. Wang, Y. Liu, W. Liu, X.-L. Wang, X.-Y. Huang, D. M. Proserpio, A. Sironi, Y. Han and J. Li, *Adv. Mater.*, 2018, **49**, 1805088.
- <sup>153</sup> L. Yang, S. Qian, X. Wang, X. Cui, B. Chen and H. Xing, *Chem. Soc. Rev.*, 2020, **49**, 5359-5406.
- <sup>154</sup> B. R. Barnett, M. I. Gonzalez and J. R. Long, *Trends Chem.*, 2019, **1**, 159-171.
- <sup>155</sup> M. Tatlier, *Appl. Therm. Eng.*, 2017, **113**, 290-297.
- <sup>156</sup> E. Hastürk, S.-J. Ernst and C. Janiak, *Curr. Opin. Chem. Eng.*, 2019, **24**, 26-36.
- <sup>157</sup> M. F. de Lange, K. J. F. M. Verouden, T. J. H. Vlugt, J. Gascon and F. Kapteijn, *Chem. Rev.* 2015, **115**, 12205-12250.
- <sup>158</sup> N. C. Burtch H. Jasuja and K. S. Walton, *Chem. Rev.*, 2014, **114**, 10575-10612.
- <sup>159</sup> F. Jeremias, Dissertation, Heinrich-Heine-Universität Düsseldorf, Düsseldorf, Germany, 2014.
- <sup>160</sup> F. Jeremias, D. Fröhlich, C. Janiak and S. Henninger, *New J. Chem.*, 2014, **38**, 1846-1852.
- <sup>161</sup> C. Janiak and S. K. Henninger, *Chimia*, 2013, **67**, 419-424.
- <sup>162</sup> F. Trapani, A. Polyzoidis, S. Loebbecke and C. G. Piscopo, *Micropor. Mesopor. Mater.*, 2016, **230**, 20-24.
- <sup>163</sup> H. Kim, S. Yang, S. R. Rao, S. Narayanan, E. A. Kapustin, H. Furukawa, A. S. Umans, O. M. Yaghi and E. N. Wang, *Science*, 2017, **356**, 430-434.
- <sup>164</sup> R. Service, *Science*, April 13<sup>th</sup>, 2017, <https://www.sciencemag.org/news/2017/04/new-solar-powered-device-can-pull-water-straight-desert-air>.
- <sup>165</sup> M. Kalmutzki, C. S. Diercks and O. M. Yaghi, *Adv. Mater.*, 2018, **30**, 1704304.

- <sup>166</sup> F. Fathieh, M. J. Kalmutzki, E. A. Kapustin, P. J. Waller, J. Yang and O. M. Yaghi, *Science Adv.*, 2018, **4**, eaat3198.
- <sup>167</sup> H. Kim, S. R. Rao, E. A. Kapustin, L. Zhao, S. Yang, O. M. Yaghi and E. N. Wang, *Nat. Commun.*, 2018, **9**, article no. 1191.
- <sup>168</sup> N. Hanikel, M. S. Prévot, F. Fathieh, E. A. Kapustin, H. Lyu, H. Wang, N. J. Diercks, T. G. Glover and O. M. Yaghi, *ACS Cent. Sci.*, 2019, **5**, **10**, 1699-1706.
- <sup>169</sup> J. Xu, T. Li, J. Chao, S. Wu, T. Yan, W. Li, B. Zhao and B. Wang, *Angew. Chem. Int. Ed.*, 2020, **59**, 5202-5210.
- <sup>170</sup> N. Hanikel, M. S. Prévot and O. M. Yaghi, *Nat. Nanotechnol.*, 2020, **15**, 348-355.
- <sup>171</sup> W. Xu and O. M. Yaghi, *ACS Cent. Sci.* 2020, **6**, 1348-1354.
- <sup>172</sup> H. Kummer, F. Jeremias, A. Warlo, G. Földner, D. Fröhlich, C. Janiak, R. Gläser and S. K. Henninger, *Ind. Eng. Chem. Res.*, 2017, **56**, 8393-8398.
- <sup>173</sup> F. Jeremias, D. Fröhlich, C. Janiak and S. K. Henninger, *RSC Adv.*, 2014, **4**, 24073-24082.
- <sup>174</sup> D. Fröhlich, S. K. Henninger and C. Janiak, *Dalton Trans.*, 2014, **43**, 15300-15304.
- <sup>175</sup> C. B. L. Tschense, N. Reimer, C.-W. Hsu, H. Reinsch, R. Siegel, W.-J. Chen, C.-H. Lin, A. Cadiau, C. Serre, J. Senker and N. Stock, *Z. Anorg. Allg. Chem.* 2017, **643**, 1600-1608.
- <sup>176</sup> N. Tannert, S.-J. Ernst, C. Jansen, H.-J. Bart, S. K. Henninger and C. Janiak, *J. Mater. Chem. A*, 2018, **6**, 17706-17712.
- <sup>177</sup> D. Lenzen, J. Zhao, S.-J. Ernst, M. Wahiduzzaman, A. K. Inge, D. Fröhlich, H. Xu, H.-J. Bart, C. Janiak, S. Henninger, G. Maurin, X. Zou and N. Stock, *Nature Commun.*, 2019, **10**, 3025.
- <sup>178</sup> J. Ehrenmann, S. K. Henninger and C. Janiak, *Eur. J. Inorg. Chem.*, 2011, **4**, 471-474.
- <sup>179</sup> M. V. Solovyeva, L. G. Gordeeva and Y. I. Aristov, *Energ. Convers. Manage.*, 2019, **182**, 299-306.
- <sup>180</sup> F. Jeremias, V. Lozan, S. K. Henninger and C. Janiak, *Dalton Trans.*, 2013, **42**, 15967-15973.
- <sup>181</sup> L. G. Gordeeva, M. Solovyeva, and Y. I. Aristov, *Energy*, 2016, **100**, 18-24.
- <sup>182</sup> H. Furukawa, K. E. Cordova, M. O'Keeffe and O. M. Yaghi, *Science*, 2013, **341**, 1230444.
- <sup>183</sup> A. Kirchon, L. Feng, H. F. Drake, E. A. Joseph and H.-C. Zhou, *Chem. Soc. Rev.*, 2018, **47**, 8611-8638.
- <sup>184</sup> M. H. Yap, K. L. Fow and G. Z. Chen, *Green Energy Environ.*, 2017, **2**, 218-245.
- <sup>185</sup> S. Kaskel, B. Böhlinger, J. Caro, M. Fröba, C. Göbbert, N. Klein, M. Hartmann, S. Henninger, S. Löbbecke, E. Schieferstein, R. Staudt and A. Lieb, ISBN: 978-3-89746-163-5.
- <sup>186</sup> M. Kalaj, K. C. Bentz, S. Ayala, J. M. Palomba, K. S. Barcus, Y. Katayama and S. M. Cohen, *Chem. Rev.*, 2020, **120**, 8267-8302.
- <sup>187</sup> J. Yu, C. Mu, B. Yan, X. Qin, C. Chen, H. Xue and H. Pang, *Mater. Horiz.*, 2017, **4**, 557-569.
- <sup>188</sup> J. Aguilera-Sigulat and D. Bradshaw, *Coord. Chem. Rev.*, 2016, **307**, 267-291.
- <sup>189</sup> P. D'Ans, E. Courbon, A. Permyakova, F. Nouar, C. Simonnet-Jégat, F. Bourdreaux, L. Malet, C. Serre, M. Frère and N. Steunou, *J. Energy Storage*, 2019, **25**, 100881.
- <sup>190</sup> M. Zeeshan, V. Nozari, M. B. Yagci, T. Isik, U. Unal, V. Ortalan, S. Keskin and A. Uzun, *J. Am. Chem. Soc.*, 2018, **140**, 10113-10116.
- <sup>191</sup> X.-W. Liu, T.-J. Sun, J.-L. Hu and S.-D. Wang, *J. Mater. Chem. A*, 2016, **4**, 3584-3616.
- <sup>192</sup> K. Ma, K. B. Idrees, F. A. Son, R. Maldonado, M. C. Wasson, X. Zhang, X. Wang, E. Shehayeb, A. Merhi, B. R. Kaafarani, T. Islamoglu, J. H. Xin and O. K. Farha, *Chem. Mater.*, 2020, **32**, 7120-7140.
- <sup>193</sup> Y. Peng, M. Zhao, B. Chen, Z. Zhang, Y. Huang, F. Dai, Z. Lai, X. Cui, C. Tan and H. Zhang, *Adv. Mater.*, 2017, **30**, 1705454.
- <sup>194</sup> S. Wu, G. Zhuang, J. Wei, Z. Zhuang and Y. Yu, *J. Mater. Chem. A*, 2018, **6**, 18234-18241.
- <sup>195</sup> C. S. L. Koh, H. Y. F. Sim, S. X. Leong, S. K. Boong, C. Chong and X. Y. Ling, *ACS Mater. Lett.*, 2021, **3**, 557-573.
- <sup>196</sup> S. Liu, J. Pan, Y. Ma, F. Qiu, X. Niu, T. Zhang and L. Yang, *Chem. Eng. J.*, 2016, **306**, 655-666.
- <sup>197</sup> M. S. Denny, M. Kalaj, K. C. Bentz and S. M. Cohen, *Chem. Sci.*, 2018, **9**, 8842-8849.
- <sup>198</sup> U. Betke, M. Klaus, J. G. Eggebrecht, M. Scheffler and A. Lieb, *Micropor. Mesopor. Mater.*, 2018, **265**, 43-56.
- <sup>199</sup> P. Vivekh, M. Kumja, D. T. Bui and K. J. Chua, *Appl. Energ.*, 2018, **229**, 778-803.
- <sup>200</sup> F. Lorignon, A. Gossard and M. Carboni, *Chem. Eng. J.*, 2020, **393**, 124765.
- <sup>201</sup> M. Wickenheisser, T. Paul and C. Janiak, *Micropor. Mesopor. Mater.*, 2016, **220**, 258-269.



- <sup>202</sup> M. Wickenheisser, A. Herbst, R. Tannert, B. Milow and C. Janiak, *Micropor. Mesopor. Mater.*, 2015, **215**, 143-153.
- <sup>203</sup> M. Wickenheisser and C. Janiak, *Micropor. Mesopor. Mater.*, 2015, **204**, 242-250.
- <sup>204</sup> E. Hastürk, S.-J. Ernst and C. Janiak, *Curr. Opin. Chem. Eng.*, 2019, **24**, 26-36.
- <sup>205</sup> S. Gökpınar, S.-J. Ernst, E. Hastürk, M. Möllers, I. El Aita, R. Wiedey, N. Tannert, S. Nießing, S. Abdpour, A. Schmitz, J. Quodbach, G. Földner, S. K. Henninger and C. Janiak, *Ind. Eng. Chem. Res.*, 2019, **58**, 21493-21503.
- <sup>206</sup> P. Yao, H. Yu, Z. Ding, Y. Liu, J. Lu, M. Lavorgna, J. Wu and X. Liu, *Front. Chem.*, 2019, **7**, 522.
- <sup>207</sup> Z. Wang, H. Tao and Y. Yue, *ChemElectroChem*, 2019, **6**, 5358-5374.
- <sup>208</sup> S. Sundriyal, H. Kaur, S. K. Bhardwaj, S. Mishra, K.-H. Kim and A. Deep, *Coord. Chem. Rev.*, 2019, **369**, 15-38.
- <sup>209</sup> Y. Xue, S. Zheng, H. Xue and H. Pang, *J. Mater. Chem. A*, 2019, **7**, 7301-7327.
- <sup>210</sup> Q.-L. Zhu and Q. Xu, *Chem. Soc. Rev.*, 2014, **43**, 5468-5512.
- <sup>211</sup> X.-M. Liu, L.-H. Xie and Y. Wu, *Inorg. Chem. Front.*, 2020, **7**, 2840-2866.
- <sup>212</sup> J. Dechnik, J. Gascon, C. J. Doonan, C. Janiak and C. J. Sumby, *Angew. Chem. Int. Ed.*, 2017, **56**, 9292-9310.
- <sup>213</sup> Q. Qian, P. A. Asinger, M. J. Lee, G. Han, K. M. Rodriguez, S. Lin, F. M. Benedetti, A. X. Wu, W. S. Chi and Z. P. Smith, *Chem. Rev.*, 2020, **120**, 8161-8266.
- <sup>214</sup> W.-G. Cui, G.-Y. Zhang, T.-L. Hu and X.-H. Bu, *Coord. Chem. Rev.*, 2019, **387**, 79-120.
- <sup>215</sup> M. Liu, J. Wu and H. Hou, *Chem. Eur. J.*, 2018, **25**, 2935-2948.
- <sup>216</sup> A. Bhunia, S. Dey, J. M. Moreno, U. Diaz, P. Concepcion, K. Van Hecke, C. Janiak and P. Van Der Voort, *Chem. Commun.*, 2016, **52**, 1401-1404.
- <sup>217</sup> T. A. Goetjen, J. Liu, Y. Wu, J. Sui, X. Zhang, J. T. Hupp and O. K. Farha, *Chem. Commun.*, 2020, **56**, 10409-10418.
- <sup>218</sup> Y.-H. Hu, J.-C. Wang, S. Yang, Y.-A. Li and Y.-B. Dong, *Inorg. Chem.*, 2017, **56**, 8341-8347.
- <sup>219</sup> S. Nießing, C. Czekelius and C. Janiak, *Catal. Commun.*, 2017, **95**, 12-15.
- <sup>220</sup> A. Herbst, A. Khutia and C. Janiak, *Inorg. Chem.*, 2014, **53**, 7319-7333.
- <sup>221</sup> J. Shi, A.-F. Yang, C.-S. Cao and B. Zhao, *Coord. Chem. Rev.*, 2019, **390**, 50-75.
- <sup>222</sup> I. I. Alkhatib, C. Garlisi, M. Pagliaro, K. Al-Ali and G. Palmisano, *Catal. Today*, 2020, **340**, 209-224.
- <sup>223</sup> N. Delaporte, E. Rivard, S. K. Natarajan, P. Benard, M. L. Trudeau and K. Zaghib, *Nanomaterials*, 2020, **10**, 1947.
- <sup>224</sup> S. Wu, J. Liu, B. Cui, Y. Li, Y. Liu, B. Hu, L. He, M. Wang, Z. Zhang, K. Tian and Y. Song, *Electrochim. Acta*, 2019, **299**, 231-244.
- <sup>225</sup> Y. Liu, D. Huang, M. Chen, Z. Liu, C. Lai, C. Zhang, C. Zhou, W. Xiong, L. Qin, B. Shao and Q. Liang, *Coord. Chem. Rev.*, 2020, **409**, 213220.
- <sup>226</sup> H. Konnerth, B. M. Matsagar, S. S. Chen, M. H. G. Precht, F.-K. Shieh and K. C.-W. Wu, *Coord. Chem. Rev.*, 2020, **416**, 213319.
- <sup>227</sup> A. Herbst and C. Janiak, *New J. Chem.*, 2016, **40**, 7958-7967.
- <sup>228</sup> A. Herbst and C. Janiak, *CrystEngComm*, 2017, **19**, 4092-4117.
- <sup>229</sup> Q. Wang and D. Astruc, *Chem. Rev.*, 2020, **120**, 1438-1511.
- <sup>230</sup> B. N. Bhadra, A. Vinu, C. Serre and S. H. Jhung, *Mater. Today*, 2019, **25**, 88-111.
- <sup>231</sup> C. Xu, R. Fang, R. Luque, L. Chen and Y. Li, *Coord. Chem. Rev.*, 2019, **388**, 268-292.
- <sup>232</sup> J. Dechnik, F. Mühlbach, D. Dietrich, T. Wehner, M. Gutmann, T. Lühmann, L. Meinel, C. Janiak and K. Müller-Buschbaum, *Eur. J. Inorg. Chem.*, 2016, **27**, 4408-4415.
- <sup>233</sup> F. Wang, Y. Pu, X. Zhang, F. Zhang, H. Cheng and Y. Zhao, *J. Lumin.*, 2019, **206**, 192-198.
- <sup>234</sup> S.-Y. Zhu and B. Yan, *Dalton Trans.*, 2018, **47**, 1674-1681.
- <sup>235</sup> A. Das, S. Das, V. Triwedi and S. Biswas, *Dalton Trans.*, 2019, **48**, 1332-1343.
- <sup>236</sup> X.-D. Zhu, K. Zhang, Y. Wang, W.-W. Long, R.-J. Sa, T.-F. Liu and J. Lü, *Inorg. Chem.*, 2018, **57**, 1060-1065.
- <sup>237</sup> J. M. Stangl, D. Dietrich, A. E. Sedykh, C. Janiak and K. Müller-Buschbaum, *J. Mater. Chem. C*, 2018, **6**, 9248-9257.
- <sup>238</sup> Y.-H. Han, C.-B. Tian, Q.-H. Li and S.-W. Du, *J. Mater. Chem. C*, 2014, **2**, 8065-8070.
- <sup>239</sup> V. Chernikova, O. Yassine, O. Shekkah, M. Eddauodi and K. N. Salama, *J. Mater. Chem. A*, 2018, **6**, 5550-5554.

- <sup>240</sup> J.-H. Wang, M. Li and D. Li, *Chem. Sci.*, 2013, **4**, 1793-1801.
- <sup>241</sup> Q. Zhang, J. Wang, A. M. Kirilov, W. Dou, C. Xu, C. Xu, L. Yang, R. Fang and W. Liu, *ACS Appl. Mater. Inter.*, 2018, **28**, 23976-23986.
- <sup>242</sup> J.-P. Ma, Y. Yu and Y.-B. Dong, *Chem. Commun.*, 2012, **48**, 2946-2948.
- <sup>243</sup> M. Gong, J. Yang, Y. Li, Q. Zhuang and J. Gu, *J. Mater. Chem. C*, 2019, **7**, 12674-12681.
- <sup>244</sup> X. Liao, H. Fu, T. Yan and J. Lei, *Biosens. Bioelectron.*, 2019, **146**, 111743.
- <sup>245</sup> B. Gil-Hernández, S. Savvin, G. Makhloufi, P. Núñez, C. Janiak and J. Sanchiz, *Inorg. Chem.*, 2015, **54**, 1597-1605.
- <sup>246</sup> S. Goswami, D. Ray, K.-i. Otake, C.-W. Kung, S. J. Garibay, T. Islamoglu, A. Atilgan, Y. Cui, C. J. Cramer, O. K. Farha and J. T. Hupp, *Chem. Sci.*, 2018, **9**, 4477-4482.
- <sup>247</sup> S. Pandey, B. Demaske, O. A. Ejegbavwo, A. A. Berseneva, W. Setyawan, N. Shustova and S. R. Phillpot, *Comp. Mater. Sci.*, 2020, **184**, 109903.
- <sup>248</sup> P. Tong, J. Liang, X. Jiang and J. Li, *Crit. Rev. Anal. Chem.*, 2020, **50**, 376-392.
- <sup>249</sup> A. Amini, S. Kazemi and V. Safarifard, *Polyhedron*, 2020, **177**, 114260.
- <sup>250</sup> I. Stassen, N. Burtch, A. Talin, P. Falcaro, M. Allendorf and R. Ameloot, *Chem. Soc. Rev.*, 2017, **46**, 3185-3241.
- <sup>251</sup> P. Kumar, V. Bansal, K.-H. Kim and E. E. Kwon, *J. Ind. Eng. Chem.*, 2018, **62**, 130-145.
- <sup>252</sup> S. Karmakar, J. Dechnik, C. Janiak and S. De, *J. Hazard. Mater.*, 2016, **303**, 10-20.
- <sup>253</sup> Q. Gao, J. Xu and X.-H. Bu, *Coord. Chem. Rev.*, 2019, **378**, 17-31.
- <sup>254</sup> S. Dhaka, R. Kumar, A. Deep, M. B. Kurade, S.-W. Ji and B.-H. Jeon, *Coord. Chem. Rev.*, 2019, **380**, 330-352.
- <sup>255</sup> M. Kadhom and B. Deng, *Appl. Mater. Today*, 2018, **11**, 219-230.
- <sup>256</sup> Y. Cai, D. Chen, N. Li, Q. Xu, H. Li, J. He and J. Lu, *ACS Sustain. Chem. Eng.*, 2019, **7**, 2709-2717.
- <sup>257</sup> M. Leloire, J. Dhainaut, P. Devaux, O. Leroy, H. Desjonqueres, S. Poirier, P. Nerisson, L. Cantrel, S. Royer, T. Loiseau and C. Volkringer, *J. Hazard. Mater.*, 2021, **416**, 125890.
- <sup>258</sup> J. Bedia, V. Muelas-Ramos, M. Peñas-Garzón, A. Gómez-Aviléz, J. J. Rodríguez and C. Belver, *Catalysts*, 2019, **9**, 52.
- <sup>259</sup> A. Elrasheedy, N. Nady, M. Bassyouni, A. El-SHazly, *Membranes*, 2019, **9**, 88.
- <sup>260</sup> B.-M. Jun, Y. A. J. Al-Hamadani, A. Son, C. M. Park, M. Jang, A. Jang, N. C. Kim and Y. Yoon, *Sep. Purif. Technol.*, 2020, **247**, 116947.
- <sup>261</sup> M. Wahiduzzaman, D. Lenzen, G. Maurin, N. Stock and M. T. Wharmby, *Eur. J. Inorg. Chem.*, 2018, **32**, 3626-3632.
- <sup>262</sup> A. Permyakova, O. Skrylnik, E. Courbon, M. Affram, S. Wang, U.-H. Lee, A. H. Valekar, F. Nouar, G. Mouchaham, T. Devic, G. De Weireld, J.-S. Chang, N. Stenou, M. Frère and C. Serre, *ChemSusChem*, 2017, **10**, 1419-1426.
- <sup>263</sup> A. Cadiau, J. S. Lee, D. Damasceno Borges, P. Fabry, T. Devic, M. T. Wharmby, C. Martineau, D. Fourcher, F. Taulelle, C.-H. Jun, Y. K. Hwang, N. Stock, M. F. De Lange, F. Kapteijn, J. Gascon, G. Maurin, J.-S. Chang and C. Serre, *Adv. Mater.*, 2015, **27**, 4775-4780.
- <sup>264</sup> H. Reinsch, S. Waitschat and N. Stock, *Dalton Trans.*, 2013, **42**, 4840-4847.
- <sup>265</sup> H. Reinsch, M. A. van der Veen, B. Gil, B. Marszalek, T. Verbiest, D. de Vos and N. Stock, *Chem. Mater.*, 2013, **25**, 17-26.
- <sup>266</sup> M. Bengsch, BSc thesis, Heinrich-Heine-Universität Düsseldorf, Düsseldorf, Germany, 2018.
- <sup>267</sup> M. S. Silverstein, *Prog. Polym. Sci.*, 2014, **39**, 199-234.
- <sup>268</sup> B. Zhang, J. Zhang, C. Liu, L. Peng, X. Sang, B. Han, X. Ma, T. Luo, X. Tan and G. Yang, *Sci. Rep.*, 2016, **6**, 21401.
- <sup>269</sup> N. Tannert, C. Jansen, S. Nießing and C. Janiak, *Dalton Trans.*, 2019, **48**, 2967-2976.
- <sup>270</sup> M. Sohail, Y.-N. Yun, E. Lee, S. K. Kim, K. Cho, J.-N. Kim, T. W. Kim, J.-H. Moon and H. Kim, *Cryst. Growth Des.*, 2017, **17**, 1208-1213.
- <sup>271</sup> M. W. Logan, S. Langevin and Z. Xia, *Sci. Rep.*, 2020, **10**, 1-11.
- <sup>272</sup> S. Hu, M. Liu, K. Li, Y. Zuo, A. Zhang, C. Song, G. Zhang, X. Guo, *CrystEngComm*, 2014, **16**, 9645-9650.